ASYMMETRIC PLANETARY NEBULAE 5

Proceedings of a conference held at
Bowness-on-Windermere, UK
20–25 June 2010

Edited by

Albert A. Zijlstra
Jodrell Bank Centre for Astrophysics, The University of Manchester, U.K.

Foteini Lykou
Jodrell Bank Centre for Astrophysics, The University of Manchester, U.K.

Eric Lagadec
European Southern Observatory, Garching bei München, Germany

Iain McDonald
Jodrell Bank Centre for Astrophysics, The University of Manchester, U.K.

Contents

Welcome to Asymmetric Planetary Nebulae 5

On behalf of the scientific organizing committee, it is a pleasure to present the proceedings of APN5.

The intricate structures shown by many planetary nebulae have for many years presented one of the most vexing problems in astrophysics. The origin and development of the asymmetries, both on large and small scales, is still not understood. Similar structures are now seen in a variety of circumstellar environments, including nova shells and SN1987A. Common physics act in these different classes of objects. The origin of the asymmetries has been sought in, amongst others, the interaction with binary companions and the effect of magnetic fields.

The rapid development of the field, and its application in many areas of astrophysics, have been the subject of a series of meetings, starting at Oranim, Israel, 1994. Subsequent meetings in the series were held at Boston, USA (1999), Mount Rainier, Seattle, USA (2004), and Los Cancajos, La Palma (Spain), 2007. This, the 5^{th} APN meeting, was held in Bowness-on-Windermere (UK), 2010.

Planetary nebulae meetings have often been associated with volcanoes. One can speculate why - perhaps an appreciation of natural beauty, or a wish to work away fom the madding crowd. APN3, APN4, and APN5 were all held next to - or on- volcanoes, although different from the previous two, the APN5 volcano was an ancient and safely extinct one. The Lake District volcano dates from the closure of an old ocean, Iapetus. Iapetus is in astronomy better known as the peculiar moon of Saturn, with one side 7 times brighter than the other - a bipolar if ever there was one. We now know that one side of Iapetus collects ice ejected by the cryo volcanoes of Enceladus, thus extending the link between asymmetry and volcanoes from Earth to space!

These proceedings contain evidence of rapid progress in the field, with some randomly chosen highlights: the detected expansion of nebulae in new HST images, the detection of compact dust disks around central stars, and the developing magnetic jet models, as well as the contributions by Martin Huarte-Espinosa and Cezary Szyszka for awarded prizes for the best talk and best poster by young researchers.

Some of the people who initiated the field are no longer with us. APN4 was dedicated to the memory of Hugo Schwarz. Franz Kahn, of the University of Manchester, who died in 1998, gave the summary of the first APN meeting. His talk is reproduced in these proceedings. John Dyson, also of Manchester (later moving to Leeds) died shortly before this meeting. An obituary written by Tom Hartquist is also included here. All are sorely missed; the work presented here is a tribute to their inspiration.

Finally, the series will not end at APN5. The next meeting, APN6, is expected to take place in Mexico. Whether it will again involve a volcano remains to be seen. That it will show progress far beyond APN5 is not. New facilities will reveal aspects of the stars and nebulae we do not even know about yet. The big questions are becoming clear: the problems of angular momentum, magnetic fields, interacting winds, the mutual interaction between star and circumstellar medium, all combine to create an astrophysics of complexity. We are lucky to be working in this world.

Albert A. Zijlstra
Chair

In memoriam
John Edward Dyson (7 January 1941 - 3 February 2010)

John was born in West Yorkshire and remained true to his roots during his entire life. He was proud that even while studying for his first degree in Kings College London, he never lived south of the Thames. He travelled extensively and from 1966 to 1967 worked at the University of Wisconsin and starting in 1977 made many extended visits to Max Planck Institutes in Munich and Garching. However, John spent the majority of his career in Manchester, where in February 1966 he completed his PhD under the supervision of Franz Kahn and from late 1967 until April 1996 was on the academic staff. He became Professor of Astronomy in 1993. John spent the rest of his full-time career as the Professor of Astronomy in Leeds where he became a Research Professor upon his formal retirement in 2006.

In his work John identified key pictures and processes, elucidated them, and then explained a wide variety of phenomena in terms of them. His work on wind-blown bubbles over more than three decades exemplified this characteristic. He and J. de Vries introduced similarity solutions for such bubbles in 1972 and were the first to compare the results of such models with observations. John applied similar models to a wide variety of phenomena including Herbig-Haro objects and other jet- related phenomena and to AGN line forming regions. His approach was that of a deep thinker who saw connections. His intuition and analytical skills were formidable, and he collaborated effortlessly with observers as well as other theorists and computational astrophysicists.

He published more than a dozen papers, not counting book reviews, with "planetary nebula", "planetary nebulae", or the names of specific planetary nebulae in the titles. He published many more papers on related problems. Before the use of High Performance Computing became common, many theorists modelled the dynamics of nebulae as though the nebulae are composed of smooth media or of two smooth media divided by a shock. John recognised that the media are clumpy and made many contributions to the study of the evaporation of clumps, the effects of evaporated material on global nebular flows, and the intermediate scale structures that develop around the clumps. In short, he was a theorist who was willing to deal with the complexities of reality. His first paper on the photoevaporation of clumps was published in 1968, and his final paper on the hydrodynamic destruction and shaping of clumps, to which he attributed many of the beautiful tails seen in planetary nebulae, was published in 2009. According to John, the existence of subsonic global flows in the cores of planetary nebulae and the properties of warmer transsonic flows in the haloes are due to the mass transfer between clumps and the more diffuse phase flowing between them. He also invoked mass transfer in his model of the jet formation of FLIERS. He was not content merely to accept that clumps exist in planetary nebulae and study the consequences. Rather, he tried to understand the origin of the clumps in terms of the magnetohydrodynamic instability of the outflows of evolved stars and wondered about the possible relationship to the formation of maser spots in AGB outflows.

John's selflessness and patience in collaborations provide an example to us all. He encouraged others and was free with his praise. He understood that one makes false starts and mistakes in creative scientific discussions, and made others comfortable when they thought out loud with him. John liked people and this made working with him very easy and delightful for his colleagues. He made friends and influenced science on six

continents. John's wit is famous. He made us all smile, laugh, and enjoy life much more.

Tom Hartquist, May 2010

Closing summary
of the Asymmetric Planetary Nebula 1 conference*

F. D. Kahn
Department of Physics & Astronomy, The University, Manchester M13 9PL, England

Abstract. It has always been known that planetary nebulae are not ideal smooth structures with spherical symmetry. The participants at this meeting have at last come to grips with this realisation. The summary talk explores a few of the implications.

1. Introduction

The consensus has taken some time to mature, but it is now generally agreed that planetary nebulae (PNe) develop at a late stage in the evolution of a star, that the material that they consist of was originally emitted by the star as a slow wind during a protracted mass loss phase, and that the complex structures that are seen in PNe form as a result of the interaction between the earlier slow wind and the later fast wind which overtakes it. The central stars, the planetary nebula nuclei (PPNi), are usually on the asymptotic giant branch (AGB) when the mass loss begins in earnest, and have evolved from main sequence stars of relatively low mass, less than about $8M_{\odot}$. Stars with larger main sequence mass end their evolution in a different way, and eventually become supernovae of Type II.

In most such supernovae the final explosion takes place while the central star is a red supergiant surrounded by the material emitted in a slow wind. But Supernova 1987A, the supernova explosion that we know best, was different. Here the central star was more compact at the time of outburst: its spectral type was B, rather than M, and the implication is that the circumstellar medium was not simply a featureless pool of cool stellar wind, but should have been sculpted into more interesting configurations by the interaction of the fast wind, emitted during the B star phase, with the preceding slow wind[1]. Since 1987 it has been possible to observe more distant parts of the remnant as the light from the explosion has reached them. It has become clear that ring structures are present in the wind, and as time passes they have revealed themselves as being more and more intricate[2].

Supernovae were not really on the agenda of this conference, and much of the physics that underlies is radically different from the physics of PNe. But the gas dynamics of the winds of their precursors looks very much like a scaled-up version of the gas dynamics governing the winds in PPNe, and it would be foolish for us to ignore the very useful lessons to be learnt from the study of the early evolution of supernova remnants. The remnant of 1987A, with its interlinked rings, is anything but spherically symmetrical. Nor are the majority of PNe that we know about.

---

*Reproduced with the kind permission of the Israeli Physics Society

2. Proto Planetary Nebulae

The gas that forms the PPN is emitted when the central star has reached an advanced state of evolution, with a compact core and an extended envelope that reaches out to a distance of the order of 1 AU. The escape velocity from the surface of the star is of the order of $30\,\mathrm{km\,s^{-1}}$. The slow wind carries away mass at a prodigious rate, around $10^{-4}M_{\odot}/yr^{-1}$, but the terminal velocity of the wind is low, only some $10\,\mathrm{km\,s^{-1}}$. It is not known how precisely the gas acquires the energy to escape from the star, but there have been numerous suggestions. They include radiation pressure on dust grains (Sun Kwok)[3], radiation pressure on molecules (Hollis Johnson)[4] and the passage of shock waves through the extended atmosphere of the star (Shimon Asida)[5]. This last proposal is particularly interesting, since it can lead quite naturally to an anisotropic wind. If the central star is rotating, then the escape velocity from the surface is smallest in the equatorial plane. The arrival of a pulse of shock waves from below gives extra energy to the material at the top of the atmosphere. In general the result will be that a fountain of gas will leave the surface of the star, and then fall back again because it has insufficient energy to escape. But occasionally the gas near the surface may be given enough energy by a pulse that is particularly strong. This will happen most easily near the equator, where the energy required is smallest, and the combined effect of all these pulses is to produce an outflow of gas which is strongest there. Most theoretical explanations for the shapes of PNe start with the assumption that the outflow of the superwind is biased in some such way.

Observations made by means of IRAS confirm that PPNe are indeed aspherical more often than not. Susan Trammel[6] has reported on the results of polarization measurements in the infra-red. She found that 24, out of a sample of 31 AGB stars that were observed, showed polarization in various spectral lines, and of course polarization implies anisotropy.

Departures from isotropy will necessarily be present in cases where the PPN is part of a binary. The evidence was reviewed by Howard Bond[7] and Zhenwen Han[8]. In some cases (15 are known) the PPNi belong to close binaries, and about half the pairs have orbital period less than 100 yr. An interesting speculation is that, at least in some cases, the formation of a common envelope releases sufficient energy to drive the superwind.

Any PPN that forms around a binary star may have a nested shell structure, for at least part of its existence. This effect has been described by Noam Soker[9]; his contribution was not explicitly on the programme of the meeting, but preprints are circulated, and the phenomenon is important enough to be discussed further here. So let the two stars have a combined mass M, let the primary have mass fM, and let the separation between the stars to be α. The angular velocity of the system is given by

$$\Omega^2 = \frac{GM}{a^3} \tag{1}$$

To pluck some figures from the air, set $f = 0.75$, $M = 1M_{\odot}$ and $\alpha = 10^{15}$cm, then $\Omega = 3.6 \times 10^{-10}\mathrm{s}^{-1}$, and the orbital period is 576 years. The orbital speed of the primary is $0.9\,\mathrm{km\,s^{-1}}$, and the terminal wind speed is $V = 10\,\mathrm{km\,s^{-1}}$. Shell formation occurs at axial distance

$$\omega = \frac{V^2}{(1-f)\,\alpha\Omega^2} - (1-f)\,\alpha, \tag{2}$$

here 3×10^{16} cm. The wind takes 1000 years to reach this distance in the equatorial plane, and longer away from the equator. Shell formation does not take place at high latitudes, at polar angles for which

$$\theta < \theta_e = \sin^{-1} \frac{\alpha\Omega}{V} \sim 5^o 10' \text{ (with the present values)}.$$

Eventually second, third and later shells form in any allowed direction; the spacing between them is

$$D = \frac{2\pi V}{\Omega} = 1.75 \times 10^{16}\text{cm}$$

here. Now the gas in the wind has a finite thermal speed c_s, say $0.2\,\mathrm{km\,s^{-1}}$ at a temperature of 10 K, and so that shells will expand again to fill the empty space around them, in a characteristic time

$$t_{exp} = \frac{D}{2c_s} = 4.4 \times 10^{11}\text{s} \sim 15000\text{yr}.$$

Under these conditions, the PPN may be expected to have a shell-like structure starting at distance 03×10^{16} cm and possibly extending to an outer distance $Vt_{exp} \sim 4.4 \times 10^{17}$cm(~0.15pc). In typical cases the superwind blows for a time of order 10^4 year and the PN that forms later has linear dimensions of order 0.1 pc.

Shell formation can only occur if the sound speed c_s is small enough, considerably less than the variation in speed brought by the orbital motion of the star that emits the wind. This same reason limits the allowable strength of any toroidal magnetic field present in the superwind if the shells are to survive. The Alfven speed v_A at radial distance r in the wind is related to the field strength B_ϕ by

$$v_A^2 = \frac{B_\phi^2}{4\pi\rho} = \frac{B_\phi^2 r^2 V}{\dot{M}}. \tag{3}$$

If v_A is to be smaller than $0.2\,\mathrm{km\,s^{-1}}$, say, then, with our present values, B_ϕ the magnetic field strength would have to be less than 1.5×10^{-4} or 1.5×10^{-5} gauss, at 10^{16} or 10^{17} cm, respectively. In general Alfven waves will remove any shell-like corrugations just as effectively as sound waves do, so that these shells cannot coexist with strong toroidal fields.

The creation of toroidal field structure in PPNe was described at the meeting by Roger Chevalier[10]. The same process has in the past been invoked to explain magnetic fields in the Crab Nebula, and will (possibly) apply also to any rotating star that has a bipolar magnetic field and undergoes mass loss.

The wind flows out radially and, as a star turns underneath, with angular velocity ω, the lines of force are distorted into the azimuthal direction. It is, of course, assumed that the wind material is a good conductor of electricity, so that the lines of force are frozen into the material. The radial component of the field will then vary inversely as r^2 at any given polar angle θ. The radial field component becomes

$$B_r = B(\theta)\left(\frac{r_*}{r}\right)^2 \tag{4}$$

at radial distance r, the azimuthal component is

$$B_\phi(r,\theta) = \frac{B_r \omega r \sin\theta}{V} = \frac{B(\theta)\omega r_*^2 \sin\theta}{Vr} \tag{5}$$

and eventually dominates the magnetic field, except in directions close to the rotation axis.

If the radial component B_* at the stellar surface changes over the azimuthal angle $\Delta\phi_*$, then the distant field along a given radial direction will change over a radial distance $V\Delta\phi_*/\omega$. The winding up of the lines of force might subsequently produce reversals in the toroidal field, but they will be removed by reconnection. Stretches of the wind can thus become field free and the gas density must increase there so as to support the magnetic pressure from the surrounding medium. John Dyson and Tom Hartquist[11] have frequently emphasised the great importance of clumps in cosmical gases; possibly the superwind acquires its clumpy structure like this.

The energy needed to create the toroidal field comes from the superwind. The magnetic energy required, in the conical shell between polar angles θ and $\theta + \Delta\theta$, is

$$\Delta W_{mag} = 2\pi \sin\theta \Delta\theta \int_{r_*}^{r_e} \frac{B_\phi^2}{8\pi} r^2 dr = \frac{B_*^2(\theta)\omega^2 r_*^4 \sin^3\theta (r_e - r_*)\Delta\theta}{4V^2}; \tag{6}$$

here r_e is the outer radial distance to which the field has been carried. The superwind transports energy into this shell at rate

$$2\pi \sin\theta \Delta\theta \frac{\rho V^3}{2} r_*^2$$

and in time r_e/V the total energy supplied is

$$\Delta W_{SW} = \pi \sin\theta \Delta\theta \rho V^2 r_*^2 r_e. \tag{7}$$

Clearly the process continues only if

$$\Delta W_{SW} \geq \Delta W_{mag}$$

or

$$\sin\theta \leq \frac{V^2(4\pi\rho_*)^{1/2}}{\omega r_* B_*(\theta)}, \tag{8}$$

and it follows that

$$B_\phi \leq (4\pi\rho_*)^{1/2} V r_*/r. \tag{9}$$

This description can really be trusted only if the magnetic energy that is needed remains much below the kinetic energy content of the wind. Departures from spherical symmetry will occur when these two quantities become comparable.

Magnetic fields have been detected in maser sources located in PPNe. Typical field strengths are of the order of 10^{-3} gauss corresponding to energy densities of order 4×10^{-8} erg cm^{-3}. With the values adopted here, the energy density in the superwind is 2.4×10^{-6} erg cm^{-3} at 10^{16} cm distance, and varies like r^{-2}. The toroidal field would be strong enough to explain any such source, out to a distance of a few times 10^{16} cm. If there were several such sources in the same PPN they would not show a consistent field direction, as seems to have been observed by Wang and Hu[12], of Beijing.

There is another possible configuration for the superwind and the magnetic field. Any star on the AGB has a very deep convective mantle. It has been known for a very long time that convection cells expel magnetic flux, and that the field lines are crowded into the space between the cells – see, for example, the classical paper by Weiss[13] on

the solar convection zone and its magnetic field structure. The superwind therefore takes off from the stellar surface which is largely free of magnetic field, and where the magnetic flux emerges along a network of well-defined lines. The wind will then pull the lines of force outwards, but because of field freezing the lines of force will be continued to sheets. If there is pressure equilibrium the field strength B at distance r from the star will be given by

$$\frac{B^2}{8\pi} = \frac{\dot{M}c_s^2}{4\pi r^2 V}. \tag{10}$$

With the usual values, and the (isothermal) sound speed c_s set equal to 0.2 km s^{-1}, as before, the field is found to be

$$B = 0.2\,\mathrm{mgauss}$$

and therefore too small to be of interest–unless the wind is very much warmer. Such a model cannot be used to explain the observations.

3. Shaping the Planetary Nebula

The superwind continues to blow until the envelope of the progenitor star is almost completely eroded. According to Detlev Schönberner[14] the central star (or PNN) begins to evolve away from the AGB when the mass of its envelope has been reduced to about $10^{-3}M_\odot$. It then moves to the left in the HR diagram, from low towards high surface temperatures, and the track is horizontal because the luminosity of any given PNN is determined only by the mass of its degenerate core. The release of nuclear energy ceases when the envelope becomes too sparse, below $10^{-4}M_\odot$, and so the luminosity drops. The life of a planetary nebula is therefore confined to the time t_{ev} taken by the journey of the central star from right to left in the HR diagram. In the standard model which seems t be favoured the central star has a core mass M_c of 0.61 $M_\odot$. The evolution time, t_{ev}, about 10^4 years in this case, depends sensitively on M_c; when $M_c = 0.84\,M_\odot$, t_{ev} is only 300 yr. Nature seems to operate a selection effect which picks out PNNi with a mass around 0.6 $M_\odot$. The dynamics of the evolution of a PN is driven by the fast wind from the central star, and the speed only really picks up when the PNN gets hot, with surface temperatures above 30000 K. A star with a core mass of 0.6 $M_\odot$ spends several thousand years in this range of temperatures, enough time for the fast wind to expand the PN to a diameter of order 0.1 pc. A PNN with a more massive core, say 0.84 $M_\odot$, would be more luminous and would have a faster wind, so the expansion would go faster, but the dependence of t_{ev} on M_c is very strong and the increase in speed cannot compensate for the reduction in the lifetime, by a factor 30, of the central star. As a result the PN grows only to an insignificant size before the central star fades. If, on the other hand, the core mass is rather smaller, then the star is significantly less luminous, and the fast wind much weaker. There is a marked reduction in the velocity difference $u - V$ between the hot shocked stellar wind and the superwind, so that the pressure in the shocked superwind also falls, by an even larger factor. The final consequence is that the shocked shell in the superwind – that is the planetary nebula as we observe it – becomes much less opaque to the Lyman continuum radiation from the central star. Instead of being ionization bounded, the PN soon becomes density bounded, and much less bright. These general properties apply, whether the PN is symmetrical or not.

The arguments used so far are based on a simple, perhaps too simple premise. It has been taken for granted here that only two kinds of wind are involved, that they have sharply different properties, and that the interaction between them will determine all the interesting dynamics that follows. In this way it can be argued that all the anisotropies and asymmetries are introduced through the superwind, which is cold and sluggish. The later fast wind will be much hotter once it has been shocked, and will therefore be more volatile. It follows that pressure waves will even out any density differences within it, in a period short compared with the evolution time of the PN. In reality the history of a PN is more complex; the wind speed does not change instantaneously, but increases from around $10\,\mathrm{km\,s^{-1}}$ to the order of $1000\,\mathrm{km\,s^{-1}}$ on the same time scale as the evolution of the PNN across the HR diagram. Meanwhile the mass loss rate drops by three or four orders of magnitude, and the mechanical luminosity of the wind rises by an order of magnitude or so. Finally there is a decrease, by one or two orders of magnitude, in the rate at which momentum is carried away from the star into any given solid angle.

Once again the flow pattern leads to the formation of a shell, because a faster wind behind tries to overtake a slower wind ahead. A shell can form in the wind at the time

$$t = \tau + V(\tau)/\dot{V}(\tau) \tag{11}$$

from gas emitted at time τ, with speed $V(\tau)$. The time t has a minimum with respect to τ when

$$0 = \frac{dt}{d\tau} = 2 - \frac{V\bar{V}}{\dot{V}^2}, \tag{12}$$

and let $\tau = \tau_s$ and $t = t_s$ then. The time t_s defines the earliest instant that shell can form. Any gas that was emitted earlier than or later than τ_s will eventually be wept up into a shell.

For an illustration let the wind speed depend on τ like

$$V = V_A + (V_B - V_A)(\tau/t_{ev})^n \tag{13}$$

where V_A and V_B are, respectively, the speeds of the superwind and the fast wind. It then follows that

$$\left(\frac{\tau_s}{t_{ev}}\right)^n = \frac{n-1}{n+1}\left[\frac{V_A}{V_B} + 0\left(\frac{V_A}{V_B}\right)^2\right]. \tag{14}$$

If the wind speed rises linearly with time, the shell forms immediately. Shell formation is delayed if the speed picks up more gradually, so that τ_s/t_{ev} equals 0.058 or 0.28, for $n = 2$ or 4 respectively. The speed of the fluid element where the shell first forms is $23.3\,\mathrm{km\,s^{-1}}$ or $16.1\,\mathrm{km\,s^{-1}}$ respectively, in these two cases. The ratio of wind speeds has been taken to be $V_B : V_A = 100 : 1$ for this illustration. In any case the shell begins to form long before the stellar wind has picked up full speed.

At first the shell remains thin: it is bounded inside and outside by low velocity shocks which do not heat the gas much. Any thermal energy is rapidly radiated away, so that the shocked gas is compressed to a small volume. Even later on the shell itself advances at only a few tens of $\mathrm{km\,s^{-1}}$ into the superwind, the outer shock remains well cooled throughout, but conditions gradually become different on the inner side, where the incident wind speed increases to hundreds of $\mathrm{km\,s^{-1}}$. Eventually the shocked gas there fails to cool radiatively and starts to expand back towards the centre. The PN

at this stage has approached a little closer to the idealised model. In this description there is an inner region where the stellar wind blows freely, until it runs into the inward facing shock. Beyond here the hot shocked stellar wind (HSSW) forms a bubble, which is more or less isobaric. The temperature in the HSSW decreases with increasing radial distance because the gas there was shocked earlier on, when the wind speed was lower. Eventually we reach the parts that were never heated much, have now cooled off entirely and have formed a shell. Outside this shell lies the primeval, untouched superwind. This picture has recognisable similarities with the primitive models which describe the expansion of a HSSW straight into a superwind, and where the shocked gas from the PPN forms a thin but massive shell.

An important physical process has been left out of this description: not a word has been said yet about photo-ionization, the dominant effect in all PNe. As the PPN grows progressively hotter, it changes the state of ionization of the gas in the nebula and naturally affects the spectrum of the radiation that the gas emits; but there are also dynamical consequences. Nothing much will change in the inner part of the evolving nebula, where the gas is hot and ionized anyway. But the Lyman continuum photons from the central star will start to ionize the shocked shell that has formed further out: the ionization takes place from inside and eats its way outward. The newly ionized gas is hotter than it was before and has to expand, and the outer shocked shell thickens as a result. It makes little difference whether the PN is spherically symmetrical or anisotropic: qualitatively the sequence of events is much the same in all cases.

Garrelt Mellema[15] reported to the conference on calculations done by himself and Adam Frank on a generalized interacting wind model (GIWM). As usual a hot shocked wind pushes its way outward, and the superwind that surrounds it is anisotropic. This process had previously been described in the simple treatment by Kahn and West[16], who had confined their attention to the dynamics of thin shells of shocked gas. Such an approach is not adequate, because the shell grows to a finite thickness on being ionized. Another complication is that the shell is no longer homogeneous, but now has cool dense gas on the outside and warm (10^4 K) gas of lower density inside. Finally the growing pressure in the ionized part tends to smooth out the jagged parts and to remove isotropy.

Are the theoretical constructs good enough to bear detailed comparison with observation? Bruce Balick[17] thought so several years ago and showed how many apparently different classes of nebulae could be accommodated within the same restricted set of dynamical models, given a little optimism and the eye of faith. There is no doubt that basically Bruce was on the right lines; some of the finer features probably need rather more attention, but he established his main point which was that a great deal depends on the angle from which PN is viewed.

In this connection it is interesting that Michael Bremer[18] has developed a method by which a 3-D model of a PN can be reconstructed from a 2-D image, given only that the nebula obeys some simple form of symmetry.

4. Further Asymmetries, as Observed

As time goes on the observational astronomers grow bolder and present ever more outrageous images of PNe. So Hugo Schwarz[19], for example, showed images of M2-9 in which there is a central star and an inner feature which at present lies to one side but rotates with a 35 year period. At greater distances from the centre there are two long arcs,

apparently stationary and symmetrically placed relative to the PNN. The temptation is to seek a model which explains such observations in terms of precessing jets, possibly jets that consist of fast moving material. Their only possible source would be the central star, yet Giora Shaviv[20] showed us clearly hot spots, which might be possible sources of such jets, disperse very rapidly on compact stars, unless there is a physical means to lock them into place. Matt Bobrowsky[21] produced a set of astonishing images. One of them, taken with HST, showed a PN with an outer bright shell which looked very much like the skin of a balloon that had just burst. Presumably the HSSW inside had pushed its way out through the cool gas of the PPN and compressed it into the shell which is observed; on one side the expanding shock must have reached the edge of the PPN, or at least a place where there was a steep decrease in density, and so the hot gas from the interior had begun to escape and torn open the shell. Another picture, also from HST, showed a nebula where two collimated flows moved in opposite directions, with a typical speed of $60\,\mathrm{km\,s^{-1}}$, and were surrounded close to the centre by a torus, also in a state of expansion but moving more slowly.

5. The Search for Plausible Models

It is obvious, in the light of such evidence, that some new ideas need to be explored in order to explain the observations. Various speakers, notably Mario Livio[22], emphasized that many properties of PNe could probably be traced back to the binary nature of their nuclei. For example the superwind would carry away angular momentum, after interacting with the secondary in the binary pair. Two effects follow: the transfer of angular momentum reduces the separation of the binary pair and perhaps ultimately releases an amount of energy which will be significant dynamically. The flow of the wind is also disturbed and the resulting redistribution of velocities will lead to the growth of interesting looking structures.

But here I want to return to Noam Soker's idea that a PPN will have a shell-like structure if its central star is one of a binary pair. How does the presence of shells affect the evolution from PPN to PN?

If the shells are not too widely spaced, then the evolution of the PN will be approximately the same as in a PPN with a smooth density distribution. In the simple model[23] the density in thePPN is given by

$$\rho = \frac{\mu}{4\pi r^2} \equiv \frac{\dot{M}_{SW}}{4\pi V r^2} \tag{15}$$

where $\dot{M}_{SW}$ is the mass loss rate into superwind and V the wind speed. The HSSW drives a blast wave into the PPN, with speed

$$u = \left(\frac{2L_W}{3\mu}\right)^{1/3} \tag{16}$$

and here $L_W = \frac{1}{2}\dot{M}_{SW}V^2$. Now keep the spherical symmetry to begin with, but distribute the gas into shells, each with mass $\Delta\mathcal{M}$, spaced distance Δr apart, so that

$$\Delta = \mathcal{M}\frac{\Delta r}{r}. \tag{17}$$

The blast wave picks up these shells one after another, and consolidates than into one, provided that spherical symmetry is preserved. When a new shell is added, the velocity change is

$$\Delta u = -u\frac{\Delta \mathcal{M}}{\mathcal{M}} = -u\frac{\Delta r}{r}. \tag{18}$$

Now in lowest order the speed u must be the same as it was for a PPN with a smooth distribution of density. This loss of speed must be made up before the blast wave hits the next shell on the way out. The available time is

$$\Delta t = \Delta r/u \tag{19}$$

to first order, and so the necessary outward acceleration is

$$\frac{|\Delta u|}{\Delta t} \equiv f = \frac{u^2}{r}. \tag{20}$$

In other words the shell bounding the hot bubble is accelerated outwards, for periods Δt at a time, and then suffers a recoil when a new shell is added from the PPN. The system is subject to the Kelvin-Helmholtz (KH) instability during the period of outward acceleration, because the HSSW, where the density is low, pushes on a gas of higher density in the shell and accelerates it outwards. In a real PN there will be an HII layer sandwiched between the hot wind bubble and the cool gas in the shell, but this circumstance does not affect the argument: the progression from low density yo high density is still in the same sense.

It can easily be shown that the thickness of the cold layer is

$$D \approx \frac{c_s^2}{u^2} r \tag{21}$$

as long as the shell is largely non-ionized, and c_s here is the sound speed in the neutral gas. The growth time of the KH instability is

$$t_{KH} = \left(\frac{D}{f}\right)^{1/2} = \frac{c_s r}{u^2}. \tag{22}$$

The shell will break up if

$$t_{KH} \ll \frac{\Delta r}{u} \equiv \Delta t$$

or

$$\frac{\Delta r}{r} \gg \frac{c_s}{u}. \tag{23}$$

In a realistic case

$$\frac{c_s}{u} = \frac{0.2\text{km s}^{-1}}{30\text{km s}^{-1}} = 0.015$$

so break up should occur unless the spacing of shells is extremely fine.

Up to this point the PPN has been treated as though it were spherically symmetrical. In the case described by Noam Soker[9], though, the shells form best in the equatorial regions and not at all along the axis of rotation of the binary system. The process of the break-up is modified as a result. The instability is driven by the excess pressure

which builds up when the main shell is suddenly retarded on picking up another new shell from the PPN. The excess pressure persists for a period of order Δr, and provokes the KH instability, as described before. But if the PPN has a shell structure, which is pronounced in the equatorial regions and absent near the poles, then the excess pressure in the HSSW will relieve itself in a time of order

$$t_{rel} \sim \frac{r}{c_h},$$

c_h being the sound speed in the HSSW. The KH instability will or will not have time to develop according as

$$\frac{r}{c_h} \sim t_{rel} \gtrless t_{KH} = \frac{c_s r}{u^2} \tag{24}$$

or

$$u^2 \gtrless c_s c_h. \tag{25}$$

Typical values to substitute here are

$$u = 30\,\mathrm{km\,s^{-1}},\ c_h = 500\,\mathrm{km\,s^{-1}},\ c_s = 0.2\,\mathrm{km\,s^{-1}}.$$

Given these parameters, the left hand side is larger in relation (25), the instability persists and the nebular material breaks up into clumps.

What is the effect of this disruption on the overall structure of the PN? There seem to be two possibilities.

The HSSW largely sweeps past the clumps and therefore accelerates less material in the equatorial regions than near the poles. The PN therefore expands outwards at higher speed in the equatorial region and develops a butterfly shape.

However there is an alternative. The HSSW ablates enough cooler gas from the clumps and reduced its specific entropy so much that radiative cooling sets in in earnest. The equatorial regions of the PN will therefore be momentum driven and will lag behind while the polar regions are still energy driven. The PN should then evolved into the composite shape, shown us by Matt Bobrowsky[21], and look rather like a bagel, with a Frankfurter stuck through the hole.

There will clearly have to be another conference on this subject.

References[†]

1. L. Wang and P. A. Massali: Nature **355**, 58, 1992
2. C. Burrows *et al*: ApJ **452**, 680, 1995
3. Sun Kwok: AnIPS **11**, 123, 1995
4. Hollis Johnson: AnIPS **11**, 98, 1995
5. S. Asida: AnIPS **11**, 108, 1995

[†]Original citations have been replaced with the current versions.

6. S. Trammell: AnIPS **11**, 37, 1995
7. H. Bond: AnIPS **11**, 61, 1995
8. Z. Han: AnIPS **11**, 66, 1995
9. N. Soker: MNRAS **270**, 774, 1994
10. R. Chevalier: AnIPS **11**, 240, 1995
11. J. E. Dyson and T. W. Hartquist: in *Circumstellar Media in the Late Stages of Stellar Evolution*, 34th Herstmonceaux Conference, R. E. S. Clegg, I. R. Stevens and W. R. S. Meike (eds.), Cambridge Univ. Press, p.52, 1994
12. L. Wang and J. Y. Hu: private communication
13. N. O. Weiss: Proc. Poy. Soc. A **293**, 310, 1966
14. D. Schönberner: AnIPS **11**, 81, 1995
15. G. Mellema: AnIPS **11**, 229, 1995
16. F. D. Kahn and K. West: MNRAS **212**, 837, 1985
17. B. Balick: Astron. J. **94**, 671, 1987
18. M. Bremer: AnIPS **11**, 183, 1995
19. H. Schwarz: AnIPS **11**, 292, 1995
20. G. Shaviv: in discussion at this meeting
21. M. Bobrowsky: AnIPS **11**, 178, 1995
22. M. Livio: AnIPS **11**, 51, 1995
23. F. D. Kahn: in *Planetary Nebulae*, IAU Symposium 103, D. R. Flower (ed.), D. Reidel Publ Co., Dordrecht, p.305, 1983

Asymmetric Planetary Nebulae V
A. A. Zijlstra, F. Lykou, E. Lagadec and I. McDonald
Jodrell Bank Centre for Astrophysics, Manchester, UK © 2011

The Rochester White Paper: A Roadmap for Understanding Aspherical Planetary Nebulae

O. De Marco[1], A. Frank[2], J. Kastner[3], R. Sahai[4], B. Balick[5], E. Blackman[2], J. Carroll[2], O. Chesneau[6], Y.-H. Chu[7], M. Claussen[8], Y. Gomez[9], L. Guazzotto[2], C. Haig[2], B. Hrivnak[10], P. Huggins[11], A. Lopez[12], J. L. Sokoloski[13], B. Miszalski[14], R. Montez[3], M. Morris[15], J. Nordhaus[16], Y. Sam Yu[3], E. Schester[2], B. Shroyer[2], A. Speck[17], W. Steffen[12], R. Szczerba[18], S. Tanny[2], T. Ueta[19], H. Van Winckel[20], P. F. Velasquez[21], W. Vlemmings[22], K. Yirak[2]

[1]*Macquarie University,* [2]*University of Rochester,* [3]*Rochester Institute of Technology,* [4]*Jet Propulsion Laboratory,* [5]*University of Washington,* [6]*Observatoire de la Côte d'Azur,* [7]*University of Illinois,* [8]*NRAO,* [9] *Universidad Nacional Autonoma de Mexico,* [10]*Valparaiso University,* [11]*New York University,* [12]*Instituto de Astronomia, UNAM,* [13]*Columbia University,* [14]*University of Hertfordshire,* [15]*University of California Los Angeles,* [16]*Princeton University,* [17]*University of Missouri,* [18]*N. Copernicus Astronomical Center,* [19]*University of Denver,* [20]*Institut voor Sterrenkunde, KULeuven,* [21]*Instituto de Ciencias Nucleares, UNAM,* [22]*Argelander Institut for Astronomy, Bonn University*

Abstract. On June 17-19, 2009 a workshop took place in Rochester, NY, USA, to define key problem areas in the field of planetary nebulae and the evolution of intermediate mass stars. The overarching aim was to determine groups of projects that could be achieved with current and next generation of observational and computational facilities. A second aim was to seed medium and large collaborations that could develop, propose and carry out these projects. This white paper is designed to stimulate conversations in view of the forthcoming meeting on Asymmetric Planetary Nebulae 5, which will take place in June 2010*. In this document we summarise the discussions of three panels, each involved in one of the areas of AGB, post-AGB/PPN and PN research.

1. Background and introduction

Stars between ∼1 and 10 $M_\odot$ undergo two phases of expansion, one after core hydrogen runs out, called the red giant branch (RGB), and a second following core helium burning, called the asymptotic giant branch (AGB). At the end of the AGB phase the stellar wind (with speeds of 10–15 km s^{-1} and mass-loss rates $\sim 10^{-7}$ $M_\odot\,yr^{-1}$) unexpectedly increases in intensity with mass-loss rates surging to as much as 10^{-4} $M_\odot\,yr^{-1}$ (11). This superwind phase quickly depletes the AGB envelope until the envelope mass falls below 10^{-3}–10^{-4} $M_\odot$. At this point the star's structure changes as the photospheric radius shrinks and stellar effective temperature rises. The mass-loss rate of the star drops

*This treatise was revised after the end of the APN5 conference.

to $\sim 10^{-8}$ $M_\odot$ yr^{-1} while the wind speed increases to ~200–2000 km s^{-1}. The evolving wind parameters should lead to violent circumstellar gas dynamics as fast wind plows up the material ejected during the super- wind phase. The resulting sculpted circumstellar gas distribution is then ionised by the heating central star, at which point we call it a planetary nebula (PN; 14).

The range of PN shapes are explained by the interactive wind model (IWM; 20). The superwind is assumed to depart from spherical symmetry so that the resulting nebula should not be spherical. Later modifications, known under the name of Generalised ISW (GISW; for a review see Balick & Frank 2002) has achieved some success in terms of modelling PN gas density structures, kinematics and morphology (at least for the main body of the PN). However, these models assume both superwind triggering and superwind geometry both of which are key features that a complete model would explain. We can all agree that a complete model for the evolution and shaping of PN needs to explain the surge in mass-loss rate called the superwind, and the origin of AGB and post-AGB mass-loss geometries, rather than assume them. The question then becomes what mechanisms lead to a consistent model of both stellar and nebular evolution.

For the last two decades the community has debated whether stellar rotation and global magnetic fields can be sustained in single AGB stars and thus confer non-spherical morphologies to PN (e.g., 28; 52; 50; 7; 8; 59, but see also Bond et al. 1). Recently, the debate has been rekindled (51; 29) by the argument that in a large majority of cases, single AGB stars are unlikely to be able to sustain large-scale magnetic fields for long enough to affect shaping. This time limit comes because the field drains the star of angular momentum on short time scales and quenches its own growth. As the models of, e.g., Garcia-Segura and collaborators have shown, magnetic fields can be an effective ingredient in shaping many PN, but in those models the magnetic field strength was assumed constant and did not include feedback of the field on the stellar envelope and envelope on the field. When one includes the feedback it appears that, without an additional source of angular momentum, the field would vanish before the post-AGB phase. An angular momentum source could effectively be provided by a stellar or sub-stellar companion. To these theoretical concerns, we add a long list of observational conundrums, which will be explained in detail in Sections 2, 3 and 4.

An overarching issue that has plagued all research in PN and adjacent evolutionary phases has been the lack of homogeneous samples. This has in part been due to the notorious difficulty to determine distances to PN. Today, thanks to surveys such as the MASH surveys, PN samples have not only been incremented and completed with fainter specimen, but a new distance method has been calibrated that can determine distances with precisions of ~20%. This new method has allowed the creation of volume limited samples, a tremendous new asset in studying PN. In addition, the techniques used to vet PN for inclusion in the new distance scale, have allowed to generate new ways of excluding PN mimics from the sample, increasing the purity of the samples to be used in further studies.

These difficulties and the increasing competitiveness of major observational platforms, dictate a need to form medium-to-large collaborative efforts to tackle problems via concerted observational programs. Below we summarise the recommendations of three panels, each reviewing issues and solutions in three separate evolutionary phases: the AGB phase, the post-AGB (pAGB) or pre-PN (PPN) phase and the PN phase proper. Most of these efforts will be the most productive provided that they are executed by co-

ordinated teams of people with a wide range of perspectives and skills. This balanced team approach is not only synergistic, it also is essential if large amount of scarce telescope time is to be obtained at key facilities and funds are to be found for capital investments in computers. Wherever possible the foundations of the research programs should be built on surveys conducted by students on smaller telescopes equipped with modern IR and optical cameras, narrow- or medium-band filters or good spectrographs, and adequate available time to take risks. The engagement of students and a multi-faceted community in research initiatives are key investments for continued vitality in this field.

2. The AGB panel

The key mechanisms responsible for PN shapes has roots in the AGB. The key unresolved issues for AGB stars is how their superwinds are triggered and what mechanisms change their mass-loss geometries.

2.1. Major unsolved problems in the AGB phase

AGB superwinds: if AGB star progenitors are more massive than 2.5 $M_{\odot}$, it is possible that a simple Reimers-type mass loss (31) can eject the required amount of mass in a relatively short time at the end of the AGB phase. However, on average, most PN evolve from less massive progenitors even in the younger Galactic thin disc (25). As a result we are still in need of a mechanism that can initiate the superwind for the bulk of the population. It is possible that the mass necessary for a single star to initiate its own superwind might be chemistry and metallicity dependant. If so, carbon-rich AGB stars would have a greater ease in promoting the superwind (and could do so at lower mass) than oxygen-rich ones, and Magellanic Clouds stars would always find it more difficult to promote the superwind and would only do so at larger mass (22). While it is hard to imagine that binary interactions are the only way to enhance AGB mass loss, common envelopes and other types of close binary interactions have the capability of initiating a superwind phase and remove the AGB envelope.

AGB superwind geometry: for a long time it was thought that the AGB mass-loss geometry was spherical (30, and references therein) with very few systems deviating from sphericity (e.g., V Hya, X Her 18; 17). The change to axi- or multi-symmetric mass loss happened at some point during the post-AGB evolution. Now we are finding that many AGB stars already possess a non-spherical mass loss (5). Future work will reveal how many and what types of AGB stars have non spherical mass loss and the relationship between asymmetries in mass loss and the presence of a binary companion.

AGB binaries. AGB star binaries of interest to the current problem are those where a companion is close enough so that Roche Lobe overflow, tidal capture or wind accretion are likely to take place upon further expansion of the stellar envelope. However, the difficulty of detecting faint companions directly in the proximity of very bright, windy and dusty AGB stars has limited the number of systems known (see also Jorissen & Frankowski (16) for a review of how to detect binary AGB stars). RV surveys (9) have shown that of 1500 F-K IV-II stars, 11-24% are spectroscopic binaries, while for the KII stars alone, which are more likely to be on the AGB, the fraction is 7-18%. Some AGB stars in binaries have been known for a while (most notably, Mira; 19; 58), others are suspected from secondary indicators (e.g. BM Gem; 15). Recently Sahai et al. (44) has

demonstrated that a large majority of AGB stars with Hipparcos astrometry containing a "multiplicity" flag, do actually contain a hot companion. It therefore appears that we are making progress on a full characterisation of AGB binarity.

Homogeneous AGB samples. How can we design observing projects to answer the questions above that are free from biases? AGB stars being probed today for asymmetric structures seem to always be special: they are either the brightest or those already selected because of some other characteristic. Some techniques, such as maser detection, only work in the brightest objects. How do we select the next samples of AGB stars that can be probed for the onset of asymmetry? What new techniques will allow us to push the envelope of delectability for structures, companions, and magnetic fields in AGB stars?

2.2. Projects: AGB panel

- AGB companion detection and detection of past mergers: the determination of companions near the AGB stars down to the planetary limit is needed. What is the AGB binary fraction, period and mass ratio distribution? How many AGB stars have swallowed a companion?

  1. Can pulsations tell us about companions?
  2. Huggins et al. (2009) has shown a method to detect companions by measuring the shapes of AGB star halos.
  3. Radio/LOFAR: detection of Jupiter/brown dwarf planetary magnetospheres around early AGB stars.
  4. Radio/ALMA: imaging to detect companions and polarisation of sources with the intention of detecting structures.
  5. NIR interferometry : detection of companions and structures.
  6. Adaptive optics (AO) imaging and coronography: companion detection.
  7. Optical spectroscopy: radial velocity (RV) survey for companions to AGB stars.
  8. Optical photometry to detect transitting companions to AGB stars
  9. Optical astrometry: detection of companions.
  10. UV spectroscopy; COS on HST: excess UV to detect hot companions to AGB stars.
  11. X-rays/XMM/Chandra: detection of X-rays in AGB stars as proxies for magnetic fields?

- **Detection of magnetic fields**. Those stars with fields need to be mapped at high resolution in order to determine field configurations and strengths. While current observations of masers show a consistent magnetic field geometry from close to the stellar surface to the outer envelope, the observation sample is still small and potentially biased. Observations are thus needed to extend the sample and combine both maser and other molecular line magnetic field tracers to confirm that the masers probe the large scale magnetic field geometry. Simultaneously, the link between fields detected via the masers and/or other field probes and the properties of the circumstellar environment as a whole must be determined. In view of the likely required source of angular momentum to maintain magnetic fields, those stars with strong magnetic fields should be specifically searched for the possible existence of a companion.

1. X-rays; XMM/Chandra: detection of X-rays in AGB stars as proxies for magnetic fields.
2. Radio; VLA/VLBA/Merlin ALMA (archival): detect magnetic fields via mm-size grain alignment. Zeeman splitting on CN lines by the Goldreich & Kylafis (13) method.

- **A survey of rotation rates in AGB stars**, using modest sizes telescopes with good spectrographs, should be carried out by looking for broadening of photospheric absorption lines (as, e.g., was done for V Hya, where the equatorial rotation speed was found to be 23 km s^{-1}). A study of 67 AGB stars only found V Hya as a case of rotational broadening (probably an observational limitation as it is difficult to detect rotational broadening of $\lesssim 10$ km s^{-1}).

- **The onset of axisymmetry**: catching the change. We need to detect the earliest moments of when mass loss becomes axisymmetric. What are the first structures that appear in the early transition phase (wide cones, jetlets, tori)? Early structures would be small and would typically happen in the midst of the AGB dusty envelope. What are the first signs of interaction with a companion? What are the techniques to carry out these observations?

- **Miras**. We should carry forward a particularly intensive area of study of Miras, because these objects are at the end of the AGB evolution when the superwind takes place. In particular, objects such as V Hya, π Cru and AFGL3068 should have dedicated observing campaigns with matching theoretical efforts that integrate missing data/knowledge into what we know. What is the role of OH/IR stars in these studies?

- **Circular rings and arcs** (AGB and PPN): We know these rings are not explained by thermal pulses, so what is the explanation? Could they derive from shocks driven by an orbiting companion? Can magneto hydrodynamics (MHD) models generate a list of probable mechanisms? Would adaptive optics (AO) observations of the arks add critical information (asymmetric rarefaction/kinematic structures, local instability driven sub arcs, arc width variations). Arc characteristics such as expansion, spacing as a function of stellar distance, statistics, lifetimes, evolution, have never been systematically probed. What is the relationship between arcs and binarity (is there a difference between arcs detected around known AGB binaries and those around other AGB stars)?

- **Dust**: the interplay of carbon and oxygen-rich dust types, or hydrogenated vs. non hydrogenated carbon dusts should be used as a way to connect to the evolution of the object. Dust evolution is unfortunately more complex and small changes in the dust environment lead to large changes in the dusts observed. Can dust type be meaningfully connected to stellar classes or to classes of other characteristics? For example, we know that some central stars of PN (mostly of the [WR] type) have dual dust chemistry. What can AGB stars tell us about this? What is the relationship between PAH and a companion presence? Why do carbon stars have silicates only sometimes and why do some carbon-rich AGB stars fail to show PAHs? Can we compare the dust chemistry of AGB stars with and without discs?

3. The post-AGB and pre-PN panel

The circumstellar envelopes (CSEs) of the vast majority of AGB stars are largely spherical and expanding slowly (5–15 km s^{-1}), whereas HST surveys have shown that the vast majority of young PN are aspherical, and likely to possess fast outflows ($\gtrsim$ 100 km s^{-1}) directed along one or more axes. PPN are transition objects between the AGB and PN phases, and HST surveys of PPN show that these already possess, to a very large degree, the basic geometrical shapes and symmetries seen in PN. Hence, in order to understand the formation of asymmetrical PN, we must first understand the formation of asymmetrical PPN.

3.1. Major unsolved problems in the pAGB and PPN phases

Aspherical PPN morphologies & jets. The significant changes in the circumstellar envelope (CSE) morphology during the evolutionary transition from the AGB to the post-AGB (pAGB) phase require a primary physical agent or agents which can break the spherical symmetry of the radiatively-driven, dusty, mass-loss phase on the AGB. In the GISW model, a fast (>1000 km s^{-1}) isotropic wind from the PN central star expands within an equatorially-dense AGB CSE, and hydrodynamic simulations reproduce a variety of axisymmetric shapes. But the complexity, organisation and frequent presence of point symmetry in the morphologies of young PN, strongly suggests that the primary agent for breaking spherical symmetry are jets or high-speed collimated fast winds (CFW), operating during the early post-AGB or late AGB evolutionary phase (36). The CFWs are likely to be episodic, and either change their directionality (i.e., wobbling of axis or precession) or have multiple components operating in different directions (quasi)simultaneously.

Direct evidence for CFWs during the PPN phase has come from sensitive molecular line observations which reveal the presence of very fast (few×100 km s^{-1}) molecular outflows in PPN, with huge momentum excesses which showed that these winds are not radiatively driven (3). In a few cases, the collimated wind is seen in stars which are bona fide AGB stars: e.g., the extreme carbon star, V Hya, have been "caught in the act" of ejecting a very fast (250 km s^{-1}), highly collimated blobby outflow (40). An HST survey for such "nascent PPN" has revealed several new candidates with collimated structures (34).

Thus, the primary shaping of PN must begin *prior* to the PN phase (43), and it is plausible that the variety of PN shapes and structure may be explained by variations of the properties of the CFW (direction, strength, opening angle, temporal history) interacting with a spherical AGB envelope. However, assuming this plausibility is borne out by simulations, we still have to address the question: what is the engine for producing CFW's? Can CFW's be produced by single stars or is a binary companion essential? If point-symmetric shapes result from the flow collimator precessing or becoming unstable, then what causes the destabilisation? Single-star models for CFWs have invoked stellar rotation, strong magnetic fields, or both, and binary models have invoked the angular momentum and/or the gravitational influence of a companion.

Equatorial waists & discs. Most bipolar or multipolar PPN and PN harbour overdense, dusty equatorial waists. In PPN, the waists display convex (relative to the nebular centre) sharp outer (radial) edges in absorption, with radii typically $\gtrsim$ 1000 AU. Very infrequently, the waist appears as a disc with a sharp outer boundary seen in emission

at few×100 AU (e.g., 32; 21). The waist region can show complex symmetries: e.g., complex (double?) torii in He 2-113 and IRAS 19024-0044 (38; 41); point-symmetric microstructure in He 2-47 (33); central star offset by few×100 AU from the symmetry centre in MyCn 18 (37).

Significantly smaller equatorially-flattened structures or discs (∼50 AU) are found in a large sub-class of young pAGB stars (hereafter disc-prominent pAGB stars, 10), many of which are RV Tauri stars, and show photospheric depletion patterns similar to those seen in the ISM. The depletion is believed to result from a poorly understood process in which the circumstellar dust is trapped in a disc, and the dust-depleted gas is accreted back onto the star. Mid-IR spectroscopy with ISO and Spitzer has shown the ubiquitous presence of abundant crystalline silicates in these objects implying the presence of dust processing in long-lived discs with composition very similar to that seen in planet-forming discs around young stars and in comet Hale-Bopp (e.g., 12). But direct support for the disc being bound is limited to one pAGB object: the Red Rectangle (closest known PPN with a binary central star 4).

The origin of the small, likely Keplerian, discs and the larger, dusty waists in pAGB objects is a mystery, and the connection between these two (if any) is unknown. Compression of the AGB wind towards the equatorial plane by a fast wind with a relatively large opening angle (49) is unlikely to work in most bipolar nebulae which appear to be highly-collimated, momentum-driven shells. Although compact ($\lesssim 1$ AU) discs form readily around a companion via Bondi-Hoyle accretion of the primary AGB star's dusty wind (23), these simulations have so far not been able to produce the much larger circumbinary discs or the dusty waists which we observe in pAGB objects.

A large fraction of PPN and some PN show Hα emission lines with a narrow, intense emission core and very broad weak wings (extending up to few×1000km s^{-1}on each side of the centre); the observational evidence suggests that these arise in or around the central star (47). No profound explanation has yet been proposed for these very broad wings, although possible mechanisms include emission from a very high velocity outflow, Raman scattering and/or Keplerian rotation in a dense disc. Thus an improved understanding of this emission is likely to provide us new insights into the otherwise difficult to probe central regions of PPN, which are the likely launch sites of the CFWs (35).

Finally, a new puzzle has arisen with the discovery of large sub-millimetre excesses in both the disc-prominent pAGB objects as well as a few PPN (10), which imply the presence of fairly substantial masses of very large (∼few×100 − 1000 micron) grains (42; 46). This discovery also opens up a new opportunity: namely the study of important physical processes related to dust grain evolution such as coagulation in an environment similar to, but much simpler than proto-stellar discs. Post-AGB discs will allow us to probe the very early stages of grain coagulation, i.e. on time-scales (1000 years), not possible with studies of planet-forming discs which are typically $\gtrsim 10^6$ yr old.

Binarity: mass loss & evolution. Binarity can strongly influence mass loss in evolved stars. Perhaps all asymmetric PN and PPN involve binaries (25; 26; 51) but testing such a hypothesis requires a far better knowledge of the incidence of binarity in these objects than available currently. Direct observational evidence of binarity has been very hard to come by due to observational limitations. In the case of PPN, optical radial-velocity measurements have not been successful so far due to pulsational stellar variability; new techniques are needed.

Binarity may cut short the primary's AGB evolution as appears to be the case for disc-prominent pAGB stars, where the primary and companion stars are presently not in contact, but show orbits which are too small to accommodate a full-grown AGB star, and the disc sizes are large enough that they must be circumbinary. But no theoretical models exist to explain the formation of these systems.

3.2. Projects: post-AGB and PPN panel

- **New surveys of PPN and nascent PPN** should be carried out, which will remain unsurpassed in providing large field-of-view images with very high dynamical range because of their very stable PSFs, at ~100 mas resolution (crucial for detecting faint circumstellar structures next to bright central stars). Current surveys (55; 43) have provided a modest sample of resolved objects ($\lesssim$ 50); significantly better statistics are needed to determine the fraction of objects with morphologies which are likely to provide the strongest tests for theoretical formation and shaping models. These include objects with, e.g., multipolar shapes (e.g., IRAS19024+0044), quadrupolar shapes (e.g., IRAS19475+3119), truncated outer waists (e.g., IRAS17106-3046), haloes with circular arcs and/or searchlight beams (e.g., Egg Nebula) (41; 45; 21; 36). These surveys will require optical and NIR imaging with HST and JWST.

- **Multi-epoch high-resolution images of PPN**, spaced by $\gtrsim$ 5-10 yr should be used to trace nebular proper motions in well-resolved PPN. Both STIS/HST and ground-based observations in the NIR with integral-field (e.g., OSIRIS/Keck) or long-slit spectrographs (e.g., NIRSPEC/Keck) behind AO should be used to probe radial velocities. Combining the radial velocity and proper motion data will enable us to map the 3-dimensional kinematics in PPN at high spatial resolution – such data are crucial for probing jet acceleration and kinematics close and far from the launch sites. These surveys will require optical and NIR imaging with HST and JWST.

- **Probe the launch regions of fast collimated outflows in nascent PPN**. Near-IR and mid-IR interferometry; specially those which provide closure-phase data (VLTI/ AMBER, ISI/Mt.Wilson), low-resolution (R~530) spectral data (VLTI/ MIDI), and real images (upcoming 6-element reconfigurable Magdalena Ridge Observatory Interferometer [MROI], New Mexico), with resolutions ranging from 0.1 to 100, should be used determine in particular the disc temperature, geometry and density structure.

- **Search for binaries in edge-on PPN**. It is possible that objects with optically bright central stars which have been the subjects of existing studies, are being viewed along/near an unfavourable (for detecting RV variations) polar line-of-sight. For PPN with edge-on waists where the central stars are obscured or heavily extinct in the optical, but for which the RV variation signal is maximum, a feasibility study should be carried out to see if near-IR metallic lines can be used for RV monitoring.

- **A spectroscopic survey of a distance-specific sample of pAGB objects** (i.e., in the LMC and SMC) should be carried out: high-resolution optical, near-IR and mid-IR spectra are needed. We note that mid-IR to far-IR spectra/spectral energy

distributions (SEDs) of some objects already available via IRS/Spitzer observations of the LMC and SMC via the SAGE Legacy and various GO programs (e.g.; 56; 57; 2).

- **A pilot survey of spectroscopic monitoring of the broad Hα emission lines in PPN** should be carried out - a few observations indicate that the line shapes do vary significantly. If the peak of the emission component is found to show periodic radial velocity variations, that would suggest a Keplerian disc origin for the Hα emission.

- **Studies of key objects such as the "water-fountain" PPN**, which are distinguished by the presence of very high-velocity red- and blue-shifted H_2O and/or OH maser features should be carried out at radio, millimetre and sub-millimetre wavelengths. These are arguably amongst the youngest PPN and therefore most likely to show active jet sculpting: e.g., IRAS16342-3814 shows H_2O maser features with radial velocities separated by more than 250 km s^{-1}(6) and the telltale "corkscrew" signature of a precessing jet in near-IR AO/Keck images (41). The H_2O masers in these sources lie on the opposite sides of a bipolar jet, and being very bright and compact, are unsurpassed tracers of the jet proper motions. Such proper motion measurements (together with radial velocity data) obtained with the NRAO Very Long Baseline Array (VLBA) over several epochs can (a) determine the geometric parallax of sources with unparalleled accuracy to ~10 kpc, and (b) determine the high-velocity jet's 3-D motions (e.g., whether or not the jet is precessing). High spectral resolution monitoring using the Green Bank Telescope can accurately determine accelerations and decelerations in the jet radial velocity. Such measurements will greatly constrain theoretical models of how these high velocity jets sculpt the circumstellar medium in the evolution of these objects to PN.

  Upgrades to the sensitivity of the VLBA will enhance the continuum sensitivity to extragalactic sources as fiducial markers for the the measurement of proper motions, and allow geometric parallaxes to be measured to 10 or 15 kpc over a 1-year period. This improvement will not only facilitate parallax measurements for water-fountain PPN, but for optically invisible dust-obscured AGB stars as well, which harbour masers in their shells.

- **Surveys of thermal molecular gas emission in the outflows of PPN and disc-prominent pAGB** objects should be carried out in ^{12}CO and ^{13}CO J=2-1 lines with ALMA, which will provide an unprecedented dynamic range with the ability to produce 0.1 arcsec resolution images of all features above 0.1% peak intensity. Measurements of the ^{13}C/^{12}C ratio in the nebular material will help to distinguish between different origins – ratio would be significantly enhanced if material comes from the evolved primary, but typical of interstellar values if due to planet/main-sequence companion material. At 100 mas resolution in mm-wave molecular transitions of high-density tracers, we should see evidence for the high-velocity jet's interaction with the remnant AGB gas at ~100 AU (or better, depending upon the distance) from the star. Such imaging is needed to separate the disc/torus and outflow components, and determine the kinematics of the former" expansive or Keplerian rotation (or a combination).

- **Surveys of high-*J* emission lines of CO and other molecules in PPN** with HIFI/Herschel should be carried out to probe the physical conditions (kinematics, density, temperature) of the outflows close to the central source. Such observations coupled with low-*J* observations from ground based telescopes can help trace the mass loss history in PPN and nascent PPN.

- **An EVLA survey of PPN and disc-prominent pAGB objects** should be used to detect radio/millimetre/sub-millimetre continuum emission from the large grain component in these objects, which is likely to be present in the discs/torus regions.

- **Characterisation of magnetic fields in discs and outflows of well-resolved PPN** using the full polarisation measurement capability of ALMA via (a) polarisation of the sub-millimetre dust continuum resulting from aligned grains (e.g., detected via large-beam observations in a few objects), and (b) polarisation of molecular line emission resulting from the Goldreich-Kylafis effect.

- **Surveys of X-ray emission towards the central stars in PPN** can provide us with a unique probe (a) of magnetic fields in the outflow engine vicinity (dissipation of a solar analog dynamo-generated field should result in a non-thermal X-ray luminosity of 10^{32} erg s^{-1} from the central stars in very young PPN), and (b) the shock-interaction physics which shapes these objects. In contrast to PN, only one PPN (Hen 3-1475) has been detected so far (39); the emission results from shocked gas. The lack of PPN detections in X-rays is most likely due to the rapid cooling of the shocked, dense regions produced by the CFWs operating during the PPN phase leading to relatively small emission measures. An increased sensitivity mini-survey, i.e., with long integration times (>50 ksec) using current facilities such as Chandra and XMM-Newton need to be carried out are needed to study the physics of the shocks interactions in PPN which are involved in the shaping. These can later be followed up by bigger surveys using the International X-ray Observatory.

4. The PN panel

4.1. Major unsolved problems in the PN phase

The PN panel concluded that it is time to go "back to the star" — i.e., a coordinated, multi-wavelength observational campaign targeting the central stars of planetary nebulae (CSPN) is necessary, if we are to make further progress in our understanding of the mechanisms that shape planetary nebulae.

How do we connect the PPN to PN phase? What happens to the morphologies when photoionisation starts. What is the relationship between stellar classes (stellar parameters, chemical abundances, state of their winds) and nebular parameters? At first glance it appears that PN morphology and class does not depend on the type of central star. However a closer look reveals trends and relations between stellar type and PN type (e.g., 24). The lack of systematic surveys which can relate a sufficient number of PN type to central star parameters limits our ability to connect the star and the nebula.

How do the main features of PNe originate and evolve. At what stage in the post-AGB evolution of the star, do all the various PN components form (e.g. low-ionisation

structures). Which (if any) arise because of a binary interaction that took place during the AGB phase of the star? It has been demonstrated that connecting nebular kinematics to stellar (and binary) parameters of the CSPN is an effective way to link the nebular material to the stellar evolution. However there are only a handful of nebulae with sufficient data to complete a kinematic study, limiting the usability of this method.

The role of binarity. What is the binary fraction and period distribution of CSPN. What is the post-common envelope (very short period) binary fraction and why does it appear that the period distribution known today is too short compared to the predictions of common-envelope models?

4.2. Projects: PN panel

- **A multi-epoch blue/UV photometric and spectroscopic survey of a large sample of CSPN**, at moderate resolution, that will enlarge the database on physical characteristics of CSPN and their possible binarity. There is a considerable lack of high quality and consistent photometric and spectroscopic information on CSPN in the wavelength regimes where CSPN fluxes peak. A comprehensive blue/UV spectroscopic survey would provide basic stellar parameters such as luminosities, *log g* values, C/O abundance ratios,and reddening. Ideally these data would be obtained at multiple epochs for each object. These spectroscopic data are essential in order to better understand the photospheric and wind characteristics of WR-type , PG1159 and "normal" CSPN at different evolutionary stages. At the same time, dedicated programs of photometric monitoring are needed so as to establish a much larger sample of close binary central stars and thereby relate binary parameters and PN characteristics.

  A key resource for the UV spectroscopic observations of CSPN is the new COS spectrograph on HST. It reaches a magnitude faster than STIS for point sources that are not embedded in bright nebulosity. Whether STIS or COS, HST is the only UV facility to be in routine use for the next decade or until HST's demise, whichever is first. The next UV facility is in the early planning stages and may not be in use until 2030. Thus the next decade is a unique window of opportunity for insights into CSPN through UV observations. Telescope time will be fiercely competitive, so an expert team of observers and stellar modellers must be formed within our community with urgency.

  The panel suggests that (e.g., at the APNV meeting) a request be issued for existing spectra of CSPN to be made available in a public archive. A depository and curator for this potential data archive is needed. In addition, a team with clear long-term objectives is needed to assure that stellar monitoring programs will be conducted systematically so that the archive becomes rich in key data.

- **An imaging/photometry survey to detect and characterise dusty debris or accretion discs surrounding CSPN**. The discovery of a mid-to-far-IR excess at the central star of the Helix (54) opens up a new means to probe for the presence of discs within PN. In the case of the Helix, the disc is most likely a residual debris disc that orbited the PN progenitor star and survived the star's post-main sequence evolution. Such a "primordial" debris disc may or may not have influenced the Helix PN's shaping, and would be very different in origin and structure from the accretion discs that are thought to be generated via CSPN binary inter-

actions and are invoked to explain the formation of collimated outflows and jets in PPN and PN.

Telescopes such as Gemini – particularly those with wave-front correction – provide ground-based opportunities for this sort of a comprehensive imaging survey in the mid and near IR where the CSPNe are likely to be easily visible. Many of these telescopes also have complementary imaging systems in various bright recombination and forbidden lines from complementary volumes of low (He^{o}), moderate (He^{+}), and high (He^{++}) ionisation. Studies of shocks are possible with these and [Fe II] lines at 1.3 and 1.6 microns.

The unprecedented mid-IR (~10 micron) to sub-millimetre imaging photometry capabilities of the forthcoming SOFIA, JWST, and ALMA facilities loom as important tools to establish the prevalence and, eventually, the origin and evolution of such dusty discs around CSPN. A comprehensive mid-IR to sub-millimetre survey of CSPN would detect dusty discs and characterise their SEDs, so as to distinguish between unresolved, lightweight, gas-poor debris discs and the larger-scale, massive and gas-rich, (perhaps) spatially extended dusty discs and tori resulting from binary interactions. Time on these facilities will be scarce, so proposals from coordinated teams of expert users and students will have distinct advantages. In addition, theoretical work on 3-dimensional radiation transfer in dusty media is necessary to connect and interpret the radio / IR / optical observations. Such expertise is becoming widely available around the world, and PN are an ideal application of the technology.

- **An X-ray imaging spectroscopic survey of PN[†]:** We seek to obtain a complete, volume-limited X-ray emission survey of PNe that will sample both the thin and thick Galactic discs and therefore will represent a wide progenitor mass range. We estimate such a survey (e.g., of all PNe within ~ 2 kpc) will require an eventual total time allocation of ~ 5 Msec on contemporary X-ray observatories. The resulting suite of high-energy spectral and temporal diagnostics for a representative sample of CSPNe will provide unique constraints on circumstellar magnetic fields, accretion discs, wind shocks, and/or binary companions at PN cores, thereby relating CSPN binaries to (potentially) related systems such as symbiotic stars and SN Ia progenitor binaries. Specifically, hard but "flickering" point-like X-ray sources would be indicative of the presence of accretion discs (53); soft and constant point-like X-ray sources would be indicative of shocked CSPN winds; and strongly time-variable (flaring) point sources would most likely originate in the coronae of late-type companions (27). Such detections of X-rays from the cores of the PN, in combination with future characterisation of binary CSPN as described in this document, would open a new era in the study of common envelope evolution, would inform studies of magnetically active binaries in general, and would provide motivation for and constraints on future models of X-ray production from main sequence stars.

[†]As this article was nearing completion, a team that formed at the Rochester meeting was awarded a Cycle 12 Chandra Large Project (570 ks) to survey 21 high-excitation planetary nebulae within ~ 1 kpc. A second (overlapping) team then was awarded a Herschel Large Project (711 ks) to perform far-IR imaging and spectroscopy of a subset of the nebulae targeted by the Chandra survey during initial Herschel open time observing.

- **An HST/WFC3 snapshot survey of low ionisation, very young PN** in various narrow band and broad band filters, to assess the timescales of stellar ejection and subsequent flow collimation processes. Recent morphological studies of PPN imply that the shapes of stellar ejecta morph into simpler shapes with time perhaps abetted by the onset of the disruptive shocks preceding ionisation fronts and rapid local pressure changes that follows the passage of the ionisation front. Theoretical models need to be generalised from one dimension using sophisticated numerical schemes for shocks and radiation transfer of stellar photons. Systematic imaging and kinematic/proper motion surveys of PPN and newly ionised PN are needed to guide and constrain the models. These efforts will require large teams that contain within them the many types of expertise needed to move the field forward, and to justify scarce time on key facilities. At the same time, small telescopes and strategic student projects can lay a firm foundation for the more challenging observations.

- **High-resolution imaging of young and compact PN** need the highest possible spatial and spectral resolution at visible wavelengths. The newly installed Wide-Field Camera 3 on HST is ideal since it has a large complement of narrow-band filters that isolate key emission lines for mapping ionisation structures, such as [OI], [OII], and [OIII]. The camera also has filters that isolate key "diagnostic" lines such as [NII] $\lambda\lambda$5755,6583 and [SII] $\lambda\lambda$6717,6731, so that physical conditions can be mapped in detail at pressure "boundaries" where temperatures, densities, and streamline vectors my change precipitously. In this way the models of the origin and persistence of collimated outflows and the roles of binary-companion tidal effects can be very usefully constrained.

- **Mapping the internal kinematics of young PN** in order to identify the types and locations of forces that act on the outflowing gas. This complementary and coordinated program of ground-based, high-dispersion spectroscopy (preferably with integral field units) should go alongside the imaging campaigns.

- **Early reconnaissance surveys**. Prior ground-based spectroscopy or narrow-band photometry may be needed to uncover many more compact and low-ionisation (presumably nascent) PN targets. This survey is ideal for smaller telescopes and student projects.

- **Mapping nebular interfaces**. It is clear that young PN are richer in complex symmetries than their evolved counterparts. In particular, many or possibly most are bipolar, and the bipolar lobes are associated with H_2 emission. The excitation of H_2 implies that the H_2 is found in shocks associated with photo-dissociation fronts at boundaries between the ionised nebula and a molecular medium. Thus careful studies of H_2 kinematics will reveal the nature of nebular interactions with the surrounding but largely invisible medium. Large ground-based telescopes operating at their diffraction limit are an exciting possibility for mapping H_2 flows in the next decade.

5. All panels: Theory

- **Binary population synthesis:** what can we expect from the population of PN as a whole if certain evolutionary channels prevail over others? In particular what are chemical markers of binary evolution?

- **Binary theory:** what can hydro/magneto-hydro simulations supported by analytical theory tell us about the evolution of these complex systems? What observable effects can we expect from early interaction between an AGB star and a companion? How do companions alter the rotation and mass loss properties of AGB stars? What is the time evolution of an AGB star + close companion?

- **Central engines & fast collimated outflows:** several observational challenges are in need of detailed simulations for their interpretation. Examples include the launching mechanisms that can account for the huge momentum 'excesses' in molecular outflows, how mass transfer systems might provide the shears and stresses that generate strong magnetic collimators, stellar rotation might create the dusty discs that are so frequently seen in PPNe, and dynamo fields might appear briefly at the stellar surface to launch brief jets or clumps.

- **The creation of dusty discs near the AGB tip:** dusty discs, many with sharp outer edges, are so common in PPNe that a theoretical understanding of their formation and launching is urgently needed. Whether single stars can create these discs from surface rotation or field emergence is problematic and must be resolved. The binary environment offers tantalising advantages for disc formation; however, models that can follow the growth and dynamics of AGB envelopes in a close binary environment will need to be very sophisticated. Can orbiting companion objects shape the disc after its formation?

- **Impacts of the onset of ionisation on realistic PPN geometries:** GISW models have provided a firm ground for much more complex radiation hydro modelling with ionisation dynamics. Ionisation physics has been incorporated into 1-D hydro models by M. Steffen and his colleagues. Their models have shown that reverberating pressure waves rearrange and greatly complicate simple wind outflows. The extension of radiation hydro into 3 dimensions will permit a study of the impact of ionisation fronts and the shocks that precede them on realistic PPN morphologies. Does radiation heating of the nebular interior drastically soften PPNe? What are the observable consequences of the expanding wind-heated interior bubble on the nebula shell? What happens when the hot bubble pierces the edge of he PN?

References

Bond, H. E., Liller, W., & Mannery, E. J. 1978, ApJ, 223, 252
Buchanan, C. L., Kastner, J. H., Hrivnak, B. J., & Sahai, R. 2009, AJ, 138, 1597
Bujarrabal, V., Castro-Carrizo, A., Alcolea, J., & Sánchez Contreras, C. 2001, A&A, 377, 868
Bujarrabal, V., Castro-Carrizo, A., Alcolea, J., & Neri, R. 2005, A&A, 441, 1031
Castro-Carrizo, A., Neri, R., Winters, J. M., Bujarrabal, V., Quintana-Lacaci, G., Alcolea, J., Schïer, F. L., Olofsson, H., & Lindqvist, M. 2007, in Why Galaxies Care About AGB Stars: Their Importance as Actors and Probes, edited by F. Kerschbaum, C. Charbonnel, & R. F. Wing, vol. 378 of Astronomical Society of the Pacific Conference Series, 199

Claussen, M. J., Sahai, R., & Morris, M. R. 2009, ApJ, 691, 219
De Marco, O. 2006, in Planetary Nebulae in our Galaxy and Beyond, edited by M. J. Barlow, & R. H. Méndez, vol. 234 of IAU Symposium, 111
De Marco, O. 2009, PASP, 121, 316
de Medeiros, J. R., & Mayor, M. 1999, A&AS, 139, 433
de Ruyter, S., van Winckel, H., Dominik, C., Waters, L. B. F. M., & Dejonghe, H. 2005, A&A, 435, 161
Delfosse, X., Kahane, C., & Forveille, T. 1997, A&A, 320, 249
Gielen, C., van Winckel, H., Min, M., Waters, L. B. F. M., & Lloyd Evans, T. 2008, A&A, 490, 725
Goldreich, P., & Kylafis, N. D. 1982, ApJ, 253, 606
Iben, I. 1995, Physics Reports, 250, 2
Izumiura, H., Noguchi, K., Aoki, W., Honda, S., Ando, H., Takada-Hidai, M., Kambe, E., Kawanomoto, S., Sadakane, K., Sato, B., Tajitsu, A., Tanaka, W., Okita, K., Watanabe, E., & Yoshida, M. 2008, ApJ, 682, 499.
Jorissen, A., & Frankowski, A. 2008, in American Institute of Physics Conference Series, edited by P. Pellegrini, S. Daflon, J. S. Alcaniz, & E. Telles, vol. 1057 of American Institute of Physics Conference Series, 1
Kahane, C., Audinos, P., Barnbaum, C., & Morris, M. 1996, A&A, 314, 871
Kahane, C., & Jura, M. 1996, A&A, 310, 952
Karovska, M., Hack, W., Raymond, J., & Guinan, E. 1997, ApJ, 482, L175+
Kwok, S., Purton, C. R., & Fitzgerald, P. M. 1978, ApJ, 219, L125
Kwok, S., Hrivnak, B. J., & Su, K. Y. L. 2000, ApJ, 544, L149
Lagadec, E., & Zijlstra, A. A. 2008, MNRAS, 390, L59.
Mastrodemos, N., & Morris, M. 1998, ApJ, 497, 303
Miszalski, B., Acker, A., Parker, Q. A., & Moffat, A. F. J. 2009, A&A, 505, 249.
Moe, M., & De Marco, O. 2006, ApJ, 650, 916.
Moe, M., & De Marco, O. 2010, in Asymmetric Planetary Nebulae 5, edited by A. A. Zijlstra, F. Lykou, I. McDonald and E. Lagadec (Manchester, UK: Jodrell Bank Centre for Astrophysics), A107
Montez, R., De Marco, O., Kastner, J. H., & Chu, Y. 2010, ApJ, 721, 1820.
Morris, M. 1987, PASP, 99, 1115
Nordhaus, J., Blackman, E. G., & Frank, A. 2007, MNRAS, 376, 599.
Olofsson, H. 1999, in Asymptotic Giant Branch Stars, edited by T. Le Bertre, A. Lebre, & C. Waelkens, vol. 191 of IAU Symposium, 3
Reimers, D. 1975, Memoires of the Societe Royale des Sciences de Liege, 8, 369
Sahai, R. 1999, ApJ, 524, L125
— 2000, ApJ, 537, L43
— 2007, in Asymmetrical Planetary Nebulae IV
— 2010, in Asymmetric Planetary Nebulae 5, edited by A. A. Zijlstra, F. Lykou, I. McDonald and E. Lagadec (Manchester, UK: Jodrell Bank Centre for Astrophysics), 11
Sahai, R., Trauger, J. T., Watson, A. M., Stapelfeldt, K. R., Hester, J. J., Burrows, C. J., Ballister, G. E., Clarke, J. T., Crisp, D., Evans, R. W., Gallagher, J. S., III, Griffiths, R. E., Hoessel, J. G., Holtzman, J. A., Mould, J. R., Scowen, P. A., & Westphal, J. A. 1998, ApJ, 493, 301
Sahai, R., Dayal, A., Watson, A. M., Trauger, J. T., Stapelfeldt, K. R., Burrows, C. J., Gallagher, J. S., III, Scowen, P. A., Hester, J. J., Evans, R. W., Ballester, G. E., Clarke, J. T., Crisp, D., Griffiths, R. E., Hoessel, J. G., Holtzman, J. A., Krist, J., & Mould, J. R. 1999, AJ, 118, 468
Sahai, R., Nyman, L., & Wootten, A. 2000, ApJ, 543, 880
Sahai, R., Kastner, J. H., Frank, A., Morris, M., & Blackman, E. G. 2003, ApJ, 599, L87
Sahai, R., Morris, M., Knapp, G. R., Young, K., & Barnbaum, C. 2003, Nat, 426, 261
Sahai, R., Sánchez Contreras, C., & Morris, M. 2005, ApJ, 620, 948
Sahai, R., Young, K., Patel, N. A., Sánchez Contreras, C., & Morris, M. 2006, ApJ, 653, 1241
Sahai, R., Morris, M., Sánchez Contreras, C., & Claussen, M. 2007, AJ, 134, 2200

Sahai, R., Findeisen, K., Gil de Paz, A., & Sánchez Contreras, C. 2008, ApJ, 689, 1274.
Sahai, R., Sánchez Contreras, C., Morris, M., & Claussen, M. 2007, ApJ, 658, 410
Sánchez Contreras, C., Le Mignant, D., Sahai, R., Gil de Paz, A., & Morris, M. 2007, ApJ, 656, 1150
Sánchez Contreras, C., Sahai, R., Gil de Paz, A., & Goodrich, R. 2008, ApJS, 179, 166
Soker, N. 2006, ApJ, 645, L57
Soker, N., & Rappaport, S. 2000, ApJ, 538, 241
Soker, N. 1997, ApJS, 112, 487
— 2006, PASP, 118, 260.
Soker, N., & Livio, M. 1989, ApJ, 339, 268
Sokoloski, J. L., & Bildsten, L. 2010, ApJ, 723, 1188
Su, K. Y. L., Chu, Y.-H., Rieke, G. H., Huggins, P. J., Gruendl, R., Napiwotzki, R., Rauch, T., Latter, W. B., & Volk, K. 2007, ApJ, 657, L41.
Ueta, T., Meixner, M., & Bobrowsky, M. 2000, ApJ, 528, 861
van Loon, J. T., Oliveira, J. M., Gordon, K. D., Meixner, M., Shiao, B., Boyer, M. L., Kemper, F., Woods, P. M., Tielens, A. G. G. M., Marengo, M., Indebetouw, R., Sloan, G. C., & Chen, C. 2010, AJ, 139, 68
van Loon, J. T., Oliveira, J. M., Gordon, K. D., Sloan, G. C., & Engelbracht, C. W. 2010, AJ, 139, 1553
Wood, B. E., & Karovska, M. 2006, ApJ, 649, 410.
Zijlstra, A. A. 2007, Baltic Astronomy, 16, 79.

Participants

E. van Aarle, KU Leuven, Leuven, BE
J. Alcolea Jimanez, Observatorio Astronomico Nacional, Madrid, ES
I. Aleman, JBCA, Manchester, UK
N. Amiri, Sterrewacht Leiden, Leiden, NL
I. Bains, Swinburne University of Technology, Melbourne, AU
B. Balick, Univ. of Washington, Seattle, USA
M. Barlow, UCL, London, UK
P. Bendjoya, Obs. de la Côte Azur, Nice, FR
J. Bilikova, Univ. of Illinois at Urbana-Champaign, Urbana, USA
M. Bode, Liverpool John Moores University, Liverpool, UK
S. N. Bright, Macquarie Univ., Sydney, AU
Z. Carikova, Astronomical Institute, Tatranska Lomnica, SK
O. Chesneau, Obs. de la Côte Azur, Grasse, FR
Y.-H. Chu, Univ. of Illinois at Urbana-Champaign, Urbana, USA
D. Clark, UNAM, Ensenada, MX
M. Claussen, VLA, Socorro, USA
G. Clayton, Louisiana State Univ., Baton Rouge, USA
N. Clementel, Sterrewacht Leiden, Leiden, NL
R. Corradi, Instituto de Astrofisica de Canarias, Tenerife, ES
R. Costa, Univ. Sao Paulo, Sao Paulo, BR
S. Dalnodar, Institute of Astro- and Particle Physics, Innsbruck, AT
F. Day, Univ. of New Mexico, Albuquerque, USA
O. De Marco, Macquarie Univ., Sydney, AU
J.-F. Desmurs, , Madrid, ES
G. Delgado-Inglada, Instituto Nacional de Astrofisica, Puebla, MX
K. DePew, Macquarie Univ., Sydney, AU
H. Dinerstein, Univ. of Texas, Austin, USA
J. Drew, Univ. of Hertfordshire, Hatfield, UK
N. Evans, Keele Univ., Keele, UK
K. Exter, KU Leuven, Leuven, BE
S. Eyres, Univ. Lancashire, Preston, UK
C. R. Fierro, Instituto de Astronomia, Mexico City, MX
B. Fitzpatrick, Univ. of Oxford, Oxford, UK
K. Forde, Univ. of Hertfordshire, Hatfield, UK
A. Frank, Univ. of Rochester, Rochester, USA

D. Frew, Macquarie Univ., Sydney, AU
F. Friederich, Eberhard Karls University, Tuebingen, DE
K. Gesicki, Centrum Astronomii, Torun, PL
C. Gielen, KU Leuven, Leuven, BE
T. Gledhill, Univ. of Hertfordshire, Hatfield, UK
D. R. Gonalves, Obs. do Valongo, Rio de Janeiro, BR
N. Gorlova, KU Leuven, Leuven, BE
Ma. T. Gracia-Diaz, UNAM, Ensenada, MX
M. Gromadzki, Nicolaus Copernicus Astronomical Center, Warszawa, PL
L. Guzman Ramirez, JBCA, Manchester, UK
M. Hajduk, Nicolaus Copernicus Astronomical Center, Torun, PL
A. Hart, Harvard Univ., Cambridge, USA
K. Hebden, JBCA, Manchester, UK
T. Hillwig, Valparaiso Univ., Valparaiso, USA
P. van Hoof, Royal Observatory, Brussels, BE
B. Hrivnak, Valparaiso Univ., Valparaiso, USA
M. Huarte-Espinosa, Univ. of Rochester, Rochester, USA
P. Huggins, New York University, New York, USA
V. Icke, Sterrewacht Leiden, Leiden, NL
R. Izzard, Vrije Universiteit, Brussels, BE
H. Izumiura, NAO, Tokyo, JP
D. Jones, JBCA, Manchester, UK
A. Karakas, Mount Stromlo Observatory, Weston Creek, AU
J. Kastner, Rochester Institute of Technology, Rochester, USA
S. Kimeswenger, Institute of Astro- and Particle Physics, Innsbruck, AT
N. Koning, Univ. of Calgary, Calgary, CA
A. Kovacevic, Macquarie Univ., Sydney, AU
S. Kwok, The University of Hong Kong, Hong Kong, HK
E. Lagadec, ESO, Garching, DE
H. van Langevelde, ASTRON, Dwingeloo, NL
M. Leal-Ferreira, Argelander-Institut für Astronomie, Bonn, DE
M. Lloyd, JBCA, Manchester, UK
J. A. Lopez, UNAM, Ensenada, MX
S. Lorenz-Martins, Obs. do Valongo, Rio de Janeiro, BR
F. Lykou, JBCA, Manchester, UK
W. Maciel, Univ. Sao Paulo, Sao Paulo, BR
A. Markwick, JBCA, Manchester, UK

M. Matsuura, UCL, London, UK
I. McDonald, JBCA, Manchester, UK
B. Miszalski, Univ. of Hertfordshire, Hatfield, UK
M. Moe, Harvard, Cambridge, USA
S. Mohamed, Argelander-Institut für Astronomie, Bonn, DE
R. Montez, Rochester Institute of Technology, Rochester, USA
C. Morisset, UNAM, Ensenada, MX
K. Murakawa, MPIFR, Bonn, DE
C. Nicholls, Mount Stromlo Observatory, Weston Creek, AU
J. Nordhaus, Princeton Univ., Princeton, USA
T. O'Brien, JBCA, Manchester, UK
Q. Parker, Macquarie Univ., Sydney, AU
M. Peña, UNAM, Ensenada, MX
J. Pittard, Univ. of Leeds, Leeds, UK
J. Prieto, JPL, Pasadena, USA
A. Raga, UNAM, Ensenada, MX
S. Ramstedt, Argelander-Institut für Astronomie, Bonn, DE
T. Rauch, Eberhard Karls University, Tuebingen, DE
B. Rees, JBCA, Manchester, UK
W. Reid, Macquarie Univ., Sydney, AU
V. A. R. M. Ribeiro, Liverpool John Moores University, Liverpool, UK
A. Richards, JBCA, Manchester, UK
A. Riera, Universitat Politechnica de Catalunya, Barcelona, ES
E. Ringat, Eberhard Karls University, Tuebingen, DE
A. Ruiz Velasco, ESO, Garching, DE
L. Sabin, UNAM, Ensenada, MX
R. Sahai, JPL, Pasadena, USA
C. Sanchez-Contreras, CSIC-INTA, Madrid, ES
C. Sandin, AIP, Potsdam, DE
M. Santander-García, Instituto de Astrofisica de Canarias, Tenerife, ES
M. Sekeras, Astronomical Institute, Tatranska Lomnica, SK
A. Skopal, Astronomical Institute, Tatranska Lomnica, SK
N. Soker, Technion, Haifa, IL
J. Sokoloski, Columbia Univ., New York, USA
A. Speck, University of Missouri, Columbia, USA
L. Stanghellini, NOAO, Tucson, USA
G. Van de Steene, Royal Observatory, Brussels, BE

W. Steffen, UNAM, Ensenada, MX
N. Sterling, Michigan State Univ., East Lansing, USA
O. Suarez, Obs. de la Côte Azur, Nice, FR
K. Su, Steward Observatory, Arizona, USA
R. Szczerba, Nicolaus Copernicus Astronomical Center, Torun, PL
C. Szyszka, JBCA, Manchester, UK
D. Tafoya, Kagoshima Univ., Kagoshima, JP
S. Torres-Peimbert, UNAM, Ensenada, MX
R. Townsend, Univ. of Wisconsin-Madison, Madison, USA
A. Tyndall, JBCA, Manchester, UK
N. Vaytet, Obs. de Paris Meudon, Gif-sur-Yvette, FR
T. Verhoelst, KU Leuven, Leuven, BE
E. Villaver, UAM, Madrid, ES
W. Vlemmings, Argelander-Institut für Astronomie, Bonn, DE
C. Wareing, JBO, Manchester, UK
R. Wesson, UCL, London, UK
S. Weston, Univ. of Hertfordshire, Hatfield, UK
H. Van Winckel, KU Leuven, Leuven, BE
M. Wittkowski, ESO, Garching, DE
P. Wood, Mount Stromlo Oservatory, Weston Creek, AU
A. A. Zijlstra, JBCA, Manchester, UK

Conference participants in the garden of Burnside Hotel.

Asymmetric Planetary Nebulae V
A. A. Zijlstra, F. Lykou, E. Lagadec and I. McDonald
Jodrell Bank Centre for Astrophysics, Manchester, UK © 2011

Planetary Nebula Surveys: Past, Present and Future

Quentin A. Parker[1,2] and David J. Frew[1]

[1]*Department of Physics and Astronomy, Macquarie University, NSW 2109, Australia*

[2]*Australian Astronomical Observatory, PO Box 296, Epping, NSW 1710, Australia*

Abstract. In this review we cover the detection, identification and astrophysical importance of planetary nebulae (PN). The legacy of the historic Perek & Kohoutek and Acker et al. catalogues is briefly covered before highlighting the more recent but significant progress in PN discoveries in our Galaxy and the Magellanic Clouds. We place particular emphasis on the major MASH and IPHAS catalogues, which, over the last decade alone, have essentially doubled Galactic and LMC PN numbers. We then discuss the increasing role and importance that multi-wavelength data is playing in both the detection of candidate PN and the elimination of PN mimics that have seriously biased previous PN compilations. The prospects for future surveys and current efforts and prospects for PN detections in external galaxies are briefly discussed due to their value both as cosmic distance indicators and as kinematical probes of galaxies and dark matter properties.
Keywords. Stars: post-AGB – planetary nebulae: general – surveys: general

1. Introduction: the astrophysical value of planetary nebulae

Planetary nebulae (PN) are amongst the most photogenic and complex of celestial phenomena but are also amongst the most important to properly understand. This is because their brief flowering provides a unique window into the late-stage evolution of low- to intermediate-mass stars. They are important probes of nucleosynthesis processes, mass-loss physics and Galactic abundance gradients, and, because their progenitor stars dominate all stars above one solar mass, PN are responsible for a large fraction of the chemical enrichment of the interstellar medium, including the seeding of pre-biotic carbon between the stars.

Furthermore, their rich emission-line spectra enable detection to large distances. These emission lines allow the determination and analysis of chemical abundances and permit the estimation of shell expansion velocities and ages, and so probe the physics and timescales of stellar mass loss (e.g. Iben 1995). The measured radial velocities can trace the kinematic properties of observed PN, enabling us to decide if they belong to a relatively young or old stellar population. The kinematic properties of PN in galaxy halos also give strong constraints both on the mass distributions and formation processes of giant elliptical galaxies (e.g. Bekki & Peng 2006; Douglas et al. 2007), making them useful kinematical probes for understanding the structure of galaxies, and to test

whether a galaxy contains a substantial amount of dark matter (e.g. Romanowsky et al. 2003; Herrmann & Ciardullo 2009).

The PN formation rate also gives the death rate of stars born billions of years ago. They thus directly probe Galactic stellar and chemical evolution (Maciel & Costa 2003). Their beautiful, complex morphologies provide clues to their formation, evolution, mass-loss processes, and the shaping role that may be played by magnetic fields, binary central stars (e.g. Moe & De Marco 2006; Frew & Parker 2007; De Marco, Hillwig & Smith 2008; De Marco 2009; Miszalski et al. 2009a,b) or massive planets (e.g. Soker & Subag 2005). As the central star fades to become a white dwarf and the nebula expands, the integrated flux, surface brightness and radius change in ways that can be predicted by current stellar and hydrodynamic theory (e.g. Perinotto et al. 2004).

Importantly, the ensemble PN luminosity function (PNLF; Ciardullo 2010) in a given galaxy is sufficiently well behaved that it can act as a powerful distance calibrator, or standard candle, to determine the scale of the Universe to better than 10% (e.g. Ciardullo et al. 2002; Feldmeier, Jacoby & Phillips 2007), but how and why it works so well is not properly understood. Unravelling the detailed form of the PNLF in resolvable populations of different metallicity in the Galactic Bulge (Kovacevic et al. 2010), LMC (Reid & Parker 2010) and the local Galactic disk (Frew 2008) is helping to address this issue. In all these ways PN are powerful astrophysical tools making them valuable targets for discovery in our own Galaxy, the Local Group, and beyond.

2. The first PN discoveries 1764–1999: from Herschel to Acker and Kohoutek

The first known observation of a PN, the now famous "Dumbbell" nebula or M 27, was undertaken by Charles Messier in 1764. By 1800, a further 33 PN had been added, primarily by William Herschel, and thereafter the class was incrementally added to in a largely ad-hoc manner over the next two centuries. The seminal catalogue of Perek & Kohoutek (1967), followed by the ESO PN catalogues of Acker et al. (1992, 1996) and the essentially equivalent catalogue of Kohoutek (2001), compiled these heterogeneous samples of principally optical discoveries into catalogues of between ∼1000 and ∼1900 "true" and candidate PN, assembled from all sources of discovery going back to Messier. They include the bright PN found in the NGC and IC catalogues, plus major samples from Minkowski (1946, 1947), Haro (1952), Abell (1966), Wray (1966), Henize (1967), Longmore (1977) and Lauberts (1982), amongst others, found either from objective-prism surveys or Schmidt telescope direct broad-band imaging photographic surveys in B (and R). The B-band includes not only the strong Hβ line 4861Å but the key [O III] 5007Å emission line in the filter wing which is the strongest optical line in unreddened PN spectra, resulting in the bulk of the early discoveries.

These discovery papers have been supplemented by numerous investigations over the period between 1980 and 1999 that uncovered small samples, or even individual PN (e.g. Dengel, Hartl & Weinberger 1980; Cappellaro et al. 1994; Kraan-Korteweg et al. 1996). These lists were supplemented by small but targeted narrow-band surveys at longer wavelengths such as Hα (Beaulieu, Dopita & Freeman 1999) which has the advantage of partly alleviating the effects of dust when searching in high-value discovery zones such as the Galactic Bulge. The scientific legacy of the Perek & Kohoutek and Acker et al. catalogues is reflected in the 650 and 500 citations each has currently received in the literature, powerfully demonstrating the utility that the provision

of consolidated object catalogues can have for facilitating investigations by others. We also note the parallel discoveries of pre-PN and post-AGB stars over the same period, especially following the IRAS mission, as summarised by Szczerba et al. (2007).

3. A new golden age of PN discoveries: 2000–2010

Modest PN discovery programmes continued after the release of the updated Kohoutek catalogue such as the [O III] CCD surveys of Boumis et al. (2003, 2006) and the [S III] survey of Jacoby & Van de Steene (2004). This latter survey uncovered 94 candidate PN, with identifications assisted via follow-up 6 cm radio and Hα observations. The painstaking work of scrutinising the extant wide-field Schmidt surveys for faint PN has also continued until quite recently, though with diminishing returns (e.g. Kerber et al. 2000, and references therein), assisted via the serendipitous PN discoveries of Whiting et al. (2002, 2007) in searches for dwarf galaxies. Such careful scrutiny of wide-field legacy Schmidt surveys has enjoyed a more recent renaissance through the work of the so-called Deep Sky Hunters (Jacoby et al. 2010) where a valuable new sample of ~100 new PN has been uncovered. The online availability of survey imaging data has enabled teams of amateur astronomers to combine efforts to search for very low-surface brightness PN at higher galactic latitudes not covered by the recent Hα surveys. Miszalski et al. (in preparation) is also applying semi-automated search techniques to these legacy surveys with some modest success via the so-called Extremely Turquoise Halo Objects Survey (ETHOS), while Gomez et al. (2010) are utilising SDSS data to look for halo PN. These are all valuable additions.

However, it is the recent advent of powerful, high-resolution, narrow-band Hα surveys that has led to a new golden age of PN discovery that is still ongoing. To date, most of these new PN discoveries have been made from the SuperCOSMOS Hα Survey (SHS) covering 4000 square degrees of the Southern Galactic Plane and Magellanic Clouds (Parker et al. 2005), undertaken on the Australian Astronomical Observatory's UK Schmidt telescope. This survey opened up significant new discovery space for both compact and extended low-surface brightness PN thanks to a spatial resolution of ~1″ and a sensitivity to ionized hydrogen of ~2–5 Rayleighs. The discoveries are described in the Macquarie/AAO/Strasbourg Hα catalogues of Parker et al. (2006a; MASH-I) and Miszalski et al. (2008; MASH-II) which list ~900 and ~350 spectroscopically confirmed Galactic PN respectively. Equivalent discoveries of ~500 PN in the LMC are described by Reid & Parker (2006a,b). The success of the SHS directly inspired the similar INT Photometric Hα Survey in the northern hemisphere (IPHAS; Drew et al. 2005) which is also providing a rich seam of ongoing PN discoveries (e.g. Mampaso et al. 2006; Sabin 2008; Viironen et al. 2009a,b; Sabin et al. 2010), so that the total number of Galactic PN is now nearly 3000 (Frew & Parker 2010a).

The MASH catalogues alone represent the culmination of a 10 year programme of survey searches, candidate identification, and subsequent confirmatory spectroscopy from 350 nights won on 2-, 4- and 8-m optical telescopes, supplemented by radio and space telescope data. Note that the PN identification criteria described by Frew & Parker (2010a,b) were widely applied during generation of the MASH catalogues. Ongoing refinement of these data sets continues such that overall contamination in MASH by non-PN is low. Furthermore, both MASH and now IPHAS PN catalogues contain samples that are generally more evolved, of lower surface brightness, and are more

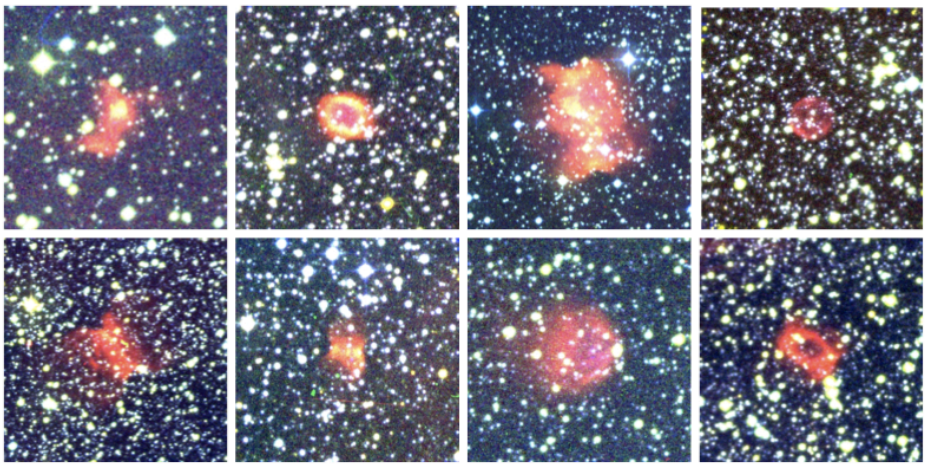

Figure 1. A montage of selected MASH-I PN presented as a combined SuperCOSMOS data colour composite. Red: Hα, Green: SR and Blue: B_J

obscured than those listed in the previous compilations. Consequently, a more representative sample of the true, underlying Galactic PN population across a broader range of evolutionary state is provided. Important samples of local (<2 kpc) but extremely low-surface brightness evolved PN have been identified (e.g. Pierce et al. 2004; Frew, Madsen & Parker 2006; Frew 2008) while the true PN nature of other faint nebulae has been revealed (e.g. Frew, Parker & Russeil 2006).

Furthermore, the Perek & Kohoutek and Acker et al. compilations comprise many PN samples from data with widely varying sensitivity, selection technique, detection efficiency, and spatial coverage. Our inability to fully understand the complex selection effects of these heterogeneous samples renders them problematic for generating a reliable PN luminosity function, for proper kinematical modelling, or for the estimation of key parameters necessary to understand their detailed evolution. Such problems are greatly reduced in the MASH and IPHAS samples, which provide the largest, least biased and most homogeneous samples of PN currently available in our Galaxy and the LMC. It is essential that any statistical study of the properties of Galactic PN (e.g. Stanghellini & Haywood 2010) incorporate MASH and IPHAS PN.

3.1. The importance of pure and representative PN samples

A key point to appreciate is that the utility of PN as astrophysical tools, as elucidated earlier, is predicated on correct identification (e.g. Acker & Stenholm 1990; Zijlstra, Pottasch & Bignell 1990). As we show in detail in Frew & Parker (2010a, and 2010b, these proceedings) it has become increasingly clear that many object types can mimic PN. The availability of wide-field imaging surveys of high resolution and sensitivity across different wavelength regimes in the optical, MIR and radio in particular, not only provide new discovery media but also give enhanced opportunities to explore the broader multi-wavelength properties of PN and their mimics than hitherto possible (e.g. Parker et al. 2006a; Cohen et al. 2007). This has enabled more powerful diagnostic tools to be developed to discriminate between bona-fide PN and interlopers. Again, the

reader is referred to the recent review by Frew & Parker (2010a) where such mimics and the improved tools to identify them are discussed in depth.

We are now unearthing significant numbers of contaminants in previously existing catalogues. This somewhat undermines the integrity and scientific value of studies based on these previous heterogeneous compilations. As an example, Cohen et al. (2010) use MIR data from GLIMPSE to explore previously known and MASH PN at low Galactic latitude where the selection criteria of Frew & Parker (2010a) were broadened to incorporate GLIMPSE data. This led to only a 5% fraction of MASH PNe being eliminated as contaminants, compared to ∼45% culled from the previously known PNe across the same survey region. This illustrates the uneven nature of the pre-MASH catalogues whose entries were not always subjected to robust diagnostic techniques. It is extremely important that these new selection criteria are brought to bear on the pre-MASH catalogues, to avoid biasing the interpretations and analyses performed on these data. For example, Kwok et al. (2008) base a detailed MIR analysis on 30 PN, taking their PN identifications as given. However, application of our new discriminatory tools reveal 16 to be H II region contaminants (Cohen et al. 2010). Furthermore, in the construction of a carefully evaluated sample of PN within a nearby 1.0 kpc local volume, Frew (2008) found that a significant number of objects, perhaps up to 20%, are, in fact Strömgren spheres around hot pre-white dwarf or subdwarf stars. These stars are simply ionizing the surrounding ambient ISM through which they are passing; see Frew & Parker (2006), Madsen et al. (2006), and Frew et al. (2010) for specific examples.

An important goal is the determination of the total PN population in our Galaxy. Estimates of this number have a direct bearing on our understanding of stellar evolution theory, Galactic chemical enrichment rates, and Galactic ecology. Important related questions concern the formation mechanisms of PN. For example, is a common envelope origin (Moe & De Marco 2006, De Marco 2009, and these proceedings) a pre-requisite for generating most PN? Are different evolutionary pathways to PN-like nebulae possible (Frew & Parker 2010a)? Although the current number of Galactic PN is only around 3000, this is double what it was just a decade ago as a result of the MASH surveys in the southern hemisphere (Parker et al. 2006a; Miszalski et al. 2008), and now from the equivalent IPHAS survey in the north (Sabin et al. 2010; Viironen et al. 2009a, b). However, this is still far short of our best estimates of the expected Galactic PN population based on population synthesis models or extrapolations from local space densities (see Jacoby et al. 2010). We still urgently need to improve the detection completeness for Galactic PN. Progress is being made (e.g. refer to the previous review of Parker et al. 2006b) and with new results and surveys coming on stream, the diversity of pathways to PN formation may be finally revealed.

4. The power of multi-wavelength observations: refining existing samples and uncovering hidden populations

The large majority of Galactic and Magellanic Cloud PNe have been historically discovered in the optical domain, first with broadband imaging and objective prism techniques, then using [O III] narrow-band imaging. More recently, as illustrated by the large numbers of MASH and IPHAS discoveries, deep Hα narrow-band imaging has been used to isolate what is normally the second most intense optical emission line in

unobscured PNe. The success of these surveys is due to the ability to find PN in more dusty regions where this line can be much stronger.

Kistiakowsky & Helfand (1993) were the first to conduct searches for PN in obscured regions using narrow-band filters to isolate lines further to the NIR so as to be less affected by dust with later important work also conducted by Jacoby & Van de Steene (2004). Large numbers of candidate PN have also been selected via IRAS mid-infrared colours (e.g. Preite-Martinez 1988; Pottasch et al. 1988; Ratag et al. 1990; García-Lario et al. 1997) but success rates for confirming these as PN via follow-up spectroscopy have been quite modest to date (e.g. Súarez et al. 2006). The availability of large-scale, wide-field Galactic surveys at high angular resolution in several optical and near/mid-infrared and radio passbands (e.g. SHS, IPHAS, SDSS, 2MASS, UKIDSS, GLIMPSE, MIPSGAL, MSX, AKARI, MOST, NVSS) provides unprecedented opportunities to combine multi-wavelength detections to refine selection techniques to effectively eliminate contaminants (Frew & Parker 2010a).

4.1. The value of mid-IR surveys

Mid-IR imagery allows the detection of extremely reddened PN invisible at optical wavelengths (e.g. Cohen et al. 2005; Phillips & Ramos-Larios 2008). Such new data allow us to investigate quantitative differences in PN multi-wavelength characteristics (e.g. Cohen et al. 2007, 2010) and relate these to the PN age, type and chemistry. Accounting for the non-ionised component of PN via MIR data also improves the derivation of mass-loss estimates and other key physical parameters, helping us to better understand the role of PN in the chemical evolution of our Galaxy. Recently, Carey et al. (2009) and Mizuno et al. (2010) have noted over 400 compact ($<1'$) ring, shell, and disk-shaped sources in the Galactic plane at 24μm in *Spitzer* MIPSGAL images. We believe that many of these will turn out to be strongly reddened, high-excitation PN with only a minority being circumstellar nebulae around massive stars (cf. Gvaramadze, Kniazev & Fabrika 2010; Wachter et al. 2010). PN can be strong mid-IR sources because of PAH emission, fine-structure line emission, and molecular and thermal dust emission within the PN shells, and in any circumnuclear disks. Cohen et al. (2010) analysed 136 optically detected PN and candidates from the GLIMPSE-I survey with the goal of developing robust, multi-wavelength classification criteria to augment existing diagnostics and provide pure PN samples. The ultimate goal is to recognise PN using only MIR and radio characteristics. This will then enable us to trawl for PN effectively even in highly obscured regions of the Galaxy that are impossible to access using traditional techniques. We expect to uncover a rich population of hidden PN.

5. The future of PN surveys and key science projects

Despite the recent significant progress in PN surveys much work still remains to be done in realising the full astrophysical potential of this fascinating phenomenon across different galaxies and environments. This can only be done in an unbiased way when truly representative samples are available. Many outstanding problems remain, such as resolving the role and importance of binary central stars and establishing clear links between central star properties and their PN — currently only ~25% of PN central stars have been unequivocally identified, while the proportion with spectra is even less

(e.g. Weidmann & Gamen 2010). Additionally, the importance and evolutionary role of the [WR] class remains elusive — see DePew et al. (2010, and these proceedings). Furthermore, only ~150 Galactic PN have accurate abundances, while the origin and development of the complex morphologies and asymmetries, on both large and small physical scales, is poorly known. A more complete inventory of Galactic PN is urgently needed as our current best estimates of the Galactic PN population range from 6000 to 30,000, still way in excess of those actually discovered, although the known LMC sample is now getting close to the best population estimates (see Reid & Parker 2006b). Immediate progress will come from the essentially complete IPHAS Hα survey where large numbers of PN candidates are now being followed-up spectroscopically. Confirmatory spectroscopy is also needed for the newly found DSH, SDSS, ETHOS and other candidate objects. However, infrared spectroscopy will be needed for most of the new GLIMPSE and MIPSGAL discoveries which have no optical counterparts, though some of the less reddened examples can be identified in the optical (e.g. Fesen & Milisavljevic 2010). The honing of MIR identification techniques (e.g. Cohen et al. 2010) offers prospects for finding PN in external galaxies at greater distances with the James Webb Space Telescope. Finally, future narrow-band and multi-waveband surveys of the Galactic plane (VPHAS+, VVV, etc.) and out-of-plane regions (e.g. SkyMapper) will provide excellent additional discovery capability. The future is bright.

Acknowledgments. QAP thanks the SOC for an Invited Review, and Macquarie University and the Australian Astronomical Observatory for travel funding.

References

Abell, G.O. 1966, ApJ, 144, 259
Acker, A., et al. 1992, Strasbourg-ESO Catalogue of Galactic Planetary Nebulae (Garching)
Acker, A., Marcout J. & Ochsenbein F. 1996, First Supplement to the SECPGN (Strasbourg)
Acker, A. & Stenholm, B. 1990, A&AS, 86, 219
Beaulieu, S.F., Dopita, M.A. & Freeman, K.C. 1999, ApJ, 515, 610
Bekki, K. & Peng, E.W. 2006, MNRAS, 370, 1737
Boumis, P., Paleologou, E.V., Mavromatakis, F. & Papamastorakis, J. 2003, MNRAS, 339, 735
Boumis, P., et al. 2006, MNRAS, 367, 1551
Cappellaro, E., Sabbadin, F., Salvadori, L., Turatto, M. & Zanin, C. 1994, MNRAS, 267, 871
Carey, S.J., et al. 2009, PASP, 121, 76
Ciardullo, R., et al. 2002, ApJ, 577, 31
Ciardullo, R. 2010, PASA, 27, 149
Cohen, M.C., et al. 2005, ApJ, 627, 446
Cohen, M.C., et al. 2007, ApJ, 669, 343
Cohen, M.C., et al. 2010, MNRAS, submitted
De Marco, O. 2009, PASP, 121, 316
De Marco, O., Hillwig, T.C. & Smith, A.J. 2008, AJ, 136, 323
Dengel, J., Hartl, H. & Weinberger, R. 1980, A&A, 85, 356
DePew, K., et al. 2010, MNRAS, submitted
Douglas, N.G., et al. 2007, ApJ, 664, 257
Drew, J.E., et al. 2005, MNRAS, 362, 753
Feldmeier, J.J., Jacoby, G.H. & Phillips, M.M. 2007, ApJ, 657, 76
Fesen, R.A. & Milisavljevic, D. 2010, AJ, 139, 2595
Frew, D.J. 2008, PhD thesis, Macquarie University
Frew, D.J. & Parker, Q.A. 2006, IAUS, 234, 49
Frew, D.J. & Parker, Q.A. 2007, APN4 Proceedings (IAC Elec. Pub), p. 475

Frew, D.J. & Parker, Q.A. 2010a, PASA, 27, 129
Frew, D.J. & Parker, Q.A. 2010b, *Asymmetric Planetary Nebulae 5*, Eds. A.A. Zijlstra, F. Lykou,
I. McDonald & E. Lagadec, p. 33
Frew, D.J., Madsen, G.J. & Parker, Q.A. 2006, IAUS, 234, 395
Frew, D.J., Parker, Q.A. & Russeil, D. 2006, MNRAS, 372, 1081
Frew, D.J., Madsen, G.J., O'Toole, S.J., & Parker Q.A. 2010, PASA, 27, 203
García-Lario, P., Manchado, A., Pych, W. & Pottasch, S.R. 1997, A&AS, 126, 479
Gomez, T., et al. 2010, BAAS, 42, 472
Gvaramadze, V.V., Kniazev, A.Y. & Fabrika, S., 2010, MNRAS, 405, 1047
Haro, G. 1952, Boletín de los Observatorios de Tonantzintla y Tacubaya, 1, 1
Henize, K.G. 1967, ApJS, 14, 125
Herrmann, K.A. & Ciardullo, R. 2009, ApJ, 705, 1686
Iben, I., Jr. 1995, Phys. Reports, 250, 2
Jacoby, G.H. & Van de Steene, G. 2004, A&A, 419, 563
Jacoby, G.H. et al. 2010, PASA, 27, 156
Kerber, F., Furlan, E., Roth, M., Galaz, G. & Chanamé, J.C. 2000, PASP, 112, 542
Kistiakowsky, V., & Hefland, D.J., 1993, AJ, 105, 2199
Kohoutek, L. 2001, A&A, 378, 843
Kovacevic, A. et al. 2010, MNRAS, submitted
Kraan-Korteweg, R., et al. 1996, A&A, 315, 549
Kwok, S., Zhang, Y., Koning, N., Huang, H.-H. & Churchwell, E. 2008, ApJS, 174, 426
Lauberts, A. 1982, The ESO/Uppsala Survey of the ESO (B) Atlas (Garching: ESO)
Longmore, A.J. 1977, MNRAS, 178, 251
Maciel, W.J. & Costa, R.D.D. 2003, IAUS, 209, 551
Madsen, G.J., Frew, D.J., Parker, Q.A., Reynolds, R.J. & Haffner L.M. 2006, IAUS, 234, 455
Mampaso, A., et al. 2006, A&A, 458, 203
Minkowski, R. 1946, PASP, 58, 305
Minkowski, R. 1947, PASP, 59, 257
Miszalski, B., et al. 2008, MNRAS, 384, 525 (MASH-II)
Miszalski, B., Acker, A., Moffat, A.F.J., Parker, Q.A. & Udalski, A. 2009a, A&A, 496, 813
Miszalski, B., Acker, A., Moffat, A.F.J., & Parker, Q.A. 2009b, A&A, 505, 249
Mizuno, D.R., et al. 2010, AJ, 139, 1542
Moe, M. & De Marco, O., 2006, ApJ, 650, 916
Parker, Q.A. et al. 2005, MNRAS, 362, 689
Parker, Q.A. et al. 2006a, MNRAS, 373, 79 (MASH-I)
Parker, Q.A., Acker, A., Frew, D.J. & Reid, W.A. 2006b, IAUS, 234, 1
Perek, L. & Kohoutek, L. 1967, Catalogue of Galactic Planetary Nebulae (Prague)
Perinotto, M., Schönberner, D., Steffen, M. & Calonaci, C. 2004, A&A, 414, 993
Phillips, J.P. & Ramos-Larios, G. 2008, MNRAS, 386, 995
Pierce, M.J., Frew, D.J., Parker Q.A. & Köppen, J. 2004, PASA, 21, 334
Pottasch, S.R., Olling, R., Bignell, C. & Zijlstra, A.A. 1988, A&A, 205, 248
Preite-Martinez, A. 1988, A&AS, 76, 317
Ratag, M.A., Pottasch, S. R., Zijlstra, A.A. & Menzies, J. 1990, A&A, 233, 181
Reid, W.A. & Parker, Q.A. 2006a, MNRAS, 365, 401
Reid, W.A. & Parker, Q.A. 2006b, MNRAS, 373, 521
Reid, W.A. & Parker, Q.A. 2010, MNRAS, 405, 1349
Romanowsky, A.J., et al. 2003, Science, 301, 1696
Sabin, L. 2008, PhD thesis, University of Manchester

Sabin, L. et al. 2010, PASA, 27, 166
Soker, N., & Subag, E. 2005, AJ, 130, 2717
Stanghellini, L. & Haywood, M. 2010, ApJ, 714, 1096
Suárez, O., et al. 2006, A&A, 458, 173
Szczerba, R., Siódmiak, N., Stasińska, G. & Borkowski, J. 2007, A&A, 469, 799
Viironen, K. et al. 2009a, A&A, 502, 113
Viironen, K. et al. 2009b, A&A, 504, 291
Wachter, S., et al. 2010, AJ, 139, 2330
Weidmann, W.A. & Gamen, R. 2010, A&A, in press, arXiv:1010.5376
Whiting, A.B., Hau, G.K.T. & Irwin, M. 2002, ApJS, 141, 123
Whiting, A.B., Hau, G.K.T., Irwin, M. & Verdugo, M. 2007, AJ, 133, 715
Wray, J.D. 1966, PhD thesis, Northwestern University
Zijlstra, A., Pottasch, S. & Bignell, C., 1990, A&AS, 82, 273

Asymmetric Planetary Nebulae V
A. A. Zijlstra, F. Lykou, E. Lagadec and I. McDonald
Jodrell Bank Centre for Astrophysics, Manchester, UK © 2011

Hunting for Shaping Mechanisms in the Progenitors of Aspherical Planetary Nebulae

R. Sahai[1], C. Sánchez Contreras[2], M. R. Morris[3], & M. Claussen[4]

[1]*Jet Propulsion Laboratory, Caltech, Pasadena, CA 91109*

[2]*Astrobiology Center (CSIC-INTA), ESAC campus, P.O. Box 78, E-28691 Villanueva de la Canada, Madrid, Spain*

[3]*Division of Astronomy, Department of Physics and Astronomy, UCLA, Los Angeles, CA 90095*

[4]*National Radio Astronomy Observatory, 1003 Lopezville Road, Socorro, NM 87801*

Abstract. Pre-Planetary Nebulae (PPNe) are believed to represent a relatively short, intermediate evolutionary phase in the evolution of AGB stars to Planetary Nebulae (PNe). Our unbiased, high-resolution imaging surveys with HST of young PNe and PPNe show very strong morphological similarities between these classes. We therefore extend our morphological scheme for PPN classification to young PNe, preserving virtually all of the primary and secondary descriptors, and adding a few new ones. These morphological surveys tell us that the primary shaping of PNe begins during the PPNe and/or late-AGB phase – we have therefore been searching for the clues to PNe shaping mechanisms in these latter objects. Amongst the clues which we have uncovered in our multiwavelength studies, we discuss the following: (i) FUV excesses in cool AGB stars as indicators of binarity (ii) Hα emission with very broad wings and P-Cygni profiles as probes of the region where the fast post-AGB outflows that do the shaping are most likely launched from, and (iii) equatorial waists with large-sized dust grains and large masses in PPNe.
Keywords. Planetary nebulae – Pre-Planetary nebulae – Stars: AGB

1. Introduction

The interaction of collimated (episodic) fast winds (CFWs) or jets, operating during the pre-planetary nebula (PPN) or very late-AGB phase, with the surrounding AGB circumstellar envelope, is most likely the primary mechanism whereby most planetary nebulae (PNe) acquire their aspherical shapes (Sahai & Trauger 1998). The formation of the dense waists seen in PNe likely occurs during the early PPN or late-AGB phase. Waists and lobes are perhaps formed nearly simultaneously, as suggested by Huggins (2007) from a study of a small sample, with waists forming a bit earlier (the expansion timescales are $\sim$ *few* $\times$ 100 to 1000 yr). We need to focus our attention on the PPN and very late-AGB phases if we are to successfully resolve fundamental issues in the formation of aspherical PNe. These issues are (i) the origin and properties of the

fast outflows ($\sim$ *few* $\times$ 100 km s^{-1}) which carry out the shaping, (ii) the origin and properties of equatorially-dense structures, i.e., the waists (bound/ expanding), (iii) the role of magnetic fields (e.g., in launching, accelerating and collimating outflows), and (iv) the role of binarity, which is widely believed to be the underlying cause (e.g., de Marco 2009), as it can induce stellar rotation and generate magnetic fields, lead to the formation of accretion disks, and result in common envelope ejection.

2. Clues to Shaping Mechanisms

We report here on a multi-wavelength program of studying the early evolutionary phases – namely the PPN and late AGB phases – where the transformation to asphericity begins, in order to uncover clues to the shaping mechanisms. As part of this program, a systematic characterization of the observed morphologies of PPNe using HST imaging was presented by Sahai et al. (2007a) using a scheme with 4 primary classes (B: bipolar, M: multipolar, E: elongated, and I: irregular), and a number of secondary descriptors, relating to, e.g., the presence of point-symmetry, ansae, halos, etc. We have now shown that this scheme can be adapted to the morphological classification of young PNe as well (Sahai, Morris & Villar 2010), by adding 3 new primary classes – R (round), L (collimated lobe pair, but not pinched-in at the waist), and S (spiral arm), and additional secondary descriptors (Sahai, Villar & Morris 2010, Sahai, Morris & Villar 2010). Many of the latter are related to the central region: the differences in this region between PNe and PPNe may be explained as an evolutionary effect due to (i) the ionizing flux and (ii) hydrodynamic action of the fast radiative wind from the PNe central star on this region. In contrast, the morphologies seen during the nascent PPN phase, based on our HST imaging survey, are rather different, with compact ($\lesssim$ *few* $\times$ 0.1″), one-sided collimated structures being predominant, suggesting that the collimated-outflow phase has just begun (Sahai 2009, Sahai et al. 2010).

2.1. Binarity in Cool AGB Stars

The search for binarity in AGB stars is of critical importance for our understanding of how planetary nebulae acquire the dazzling variety of aspherical shapes which characterises this class. However, detecting binary companions in such stars has been severely hampered due to their extreme luminosities and pulsations. We have carried out a small imaging survey of AGB stars in ultraviolet light (using GALEX) where these cool objects are very faint, in order to search for hotter companions. We discovered significant far-ultraviolet excesses towards nine of these stars, and concluded that the far-ultraviolet excess most likely results either directly from the presence of a hot binary companion, or indirectly from a hot accretion disk around the companion (Sahai et al. 2008). In 3 out of the 4 stars modelled, the companion luminosities were found to be too low for main-sequence stars with the derived effective temperatures, implying that the FUV emission likely came from hot accretion regions around the companion stars. We are carrying out a Cycle 5 GALEX program to obtain UV spectroscopy of these stars and determine the nature of the FUV excess (emission lines and/or continuum). Amongst the detected objects, V Hya, which has the largest FUV flux, as well as the highest FUV-to-NUV flux ratio amongst all our targets, is well known for its collimated, high-velocity, outflows , an extended dusty torus, and an inner hot disk (Sahai et al. 2003, Hirano et al. 2004), and is thus the best example to date of an evolved star with an

active, collimated outflow, dense equatorially-flattened structures possibly related to a central accretion disk, and an inferred binary companion from our UV excess measurements.

2.1.1. Survey for High-Velocity Outflows in FUV-Excess Binary Stars

With the goal of searching for objects in which the mass-loss process may have been affected by binarity, we have carried out CO J=2-1 and 1-0 observations of our sample of candidate binary AGB stars. Specifically, the accretion disk around a binary companion can drive a high-velocity collimated outflow. However, evidence for such outflows is indirect; this phase is so short that few nearby AGB stars are likely to be caught in the act (Sahai et al. 2003), V Hya being one of these. Our sample of 22 objects included, in addition to our 9 GALEX survey objects, new cool AGB stars with far-UV fluxes from the GALEX archive. We found 2 objects, RW Boo and RU Her, with CO J=2-1 line profiles that show intriguing evidence of high-velocity outflows from the presence of extended emission in the wings of the lines (Fig. 1). For example, in RW Boo, the double-peaked CO J=2-1 line shape, the sloping wings extend about (10–14) km s^{-1} beyond these peaks, bear a remarkable resemblance to the CO single-dish profile for V Hya (Kahane et al. 1996).

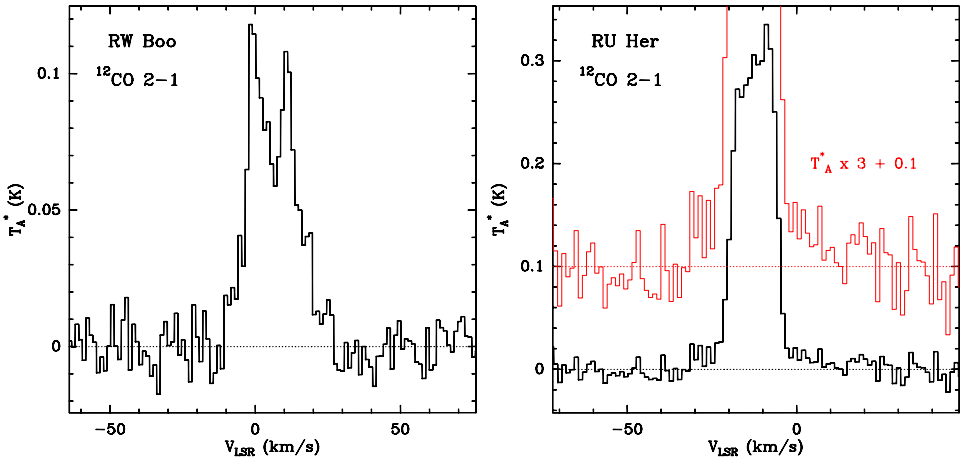

Figure 1. CO J=2-1 spectra of 2 targets from our survey, RW Boo and RU Her, which show the presence of weak (likely sensitivity-limited) emission in the wings of the lines – intriguing evidence of high-velocity outflows in these objects.

2.2. Dusty Equatorial Waists/ Disks and Large Grains

Dusty equatorial components are an important morphological feature of aspherical PPNe and PNe. Observationally, there appear to be two manifestations of an equatorial dust component around pAGB stars, namely (1) as waists of bipolar/multipolar PPNe with sizes of about 1000 AU, and (2) as medium-sized (50 AU) "circumbinary" disks in binary pAGB stars (e.g., Van Winckel et al. 2009). The origin of these circumbinary disks and large dusty waists remains a mystery. Current models based on Bondi-Hoyle accretion from an AGB wind around a companion only produce small-sized (~1 AU), relatively low-mass accretion disks (Mastrodemos and Morris 1998), whereas common

envelope ejection will likely result in significantly larger masses and overall expansion motion.

PPNe appear to be different in their morphologies, compared to the binary pAGB objects, which generally appear to lack extended nebulae – except for HD44179 or 89 Her (Cohen et al. 2004, Bujarrabal et al. 2007), no extended nebulosity is seen optically, or in mm-wave continuum/CO emission (e.g., AC Her, U Mon, RV Tau are unresolved in our CARMA observations with sizes $< (1-2)''$, Sahai & Schnee 2010). But the waist regions of PPNe share observational similarities with the disks in binary pAGBs: both show (i) large submm excesses (de Ruyter et al. 2005, Sahai et al. 2006, Sánchez Contreras et al. 2007), which have been inferred to arise from large (mm-sized) grains, and (ii) crystalline silicate features (Gielen et al. 2008, Sahai et al. 2009). Both the mineralogy and grain sizes show that dust is highly processed, implying that the age of this component should be larger than that needed for such processing and grain growth ($\gtrsim 2000$ yr; Jura 2001). We thus need to probe the mass, kinematics and structure of the disk/waist regions in order to test formation models.

We have therefore begun a pilot study of these large-grain disks/waists with the EVLA, using multi-band observations (X: 3.6 cm, Ka: 0.9 cm, Q: 0.7cm) with the goal of defining the long-wavelength SED in order to robustly characterize the large-grain component, and constraining any contribution of free-free emission to the submm fluxes. The 11 objects selected for this study include both PPNe and binary post-AGB stars with detected submm and/or mm-wave continuum fluxes; several of which have been detected for the first time in our 3 mm OVRO SNAPshot survey of PPNe (Sánchez Contreras & Sahai 2010). Preliminary analysis of the recently acquired X-band data show no X-band flux (with 1σ upper limits 18–32 μJy) from the PPNe IRAS 22036, IRAS 19548, IRAS 20000, and the binary pAGB star AC Her, suggesting that free-free emission is unlikely to be the main contributor to the submm emission. E.g., for IRAS22036, $F(3.6cm) < 96\mu$Jy (3σ), setting an upper limit of 160 mJy for free-free emission at 0.88 mm, compared to an observed flux of 290 mJy.

2.3. Broad Hα emission

There are no direct probes of the central regions of PPNe, from where the high-velocity outflows are presumably launched. Our optical spectroscopic survey of a sample of young PPNe (Sánchez Contreras et al. 2008) has revealed the widespread presence of very broad Hα emission, often with blue-shifted (P-Cygni type) absorption features (e.g., Fig. 2). The Hα line-shape is most simply interpreted in terms of the following model – the broad emission profile arises from a compact central source; this emission (and stellar continuum) is scattered by dust in the walls of the nebular lobes, and the blue-shifted absorption is due to neutral or partially ionised outflowing gas in the lobes absorbing the scattered photons. Such a model has been successful in producing a detailed fit to the spatio-kinematic distribution of the blue-shifted absorption in the Hα line profiles observed with STIS/HST in the PPN Hen 3-1475 (Sánchez Contreras & Sahai 2001). Thus the broad Hα emission feature is a potential probe of the central region and we are carrying out similar STIS observations of a small sample of PPNe (GO 11634, PI: Sánchez Contreras) – *but we need to understand the mechanism which produces it*.

Such profiles had already been observed in young PNe, and Raman scattering of Lyβ (which leads to Hα with a width a factor 6.4 larger than the Lyβ width and

a λ^{-2} wing profile) was proposed as the best mechanism to explain them (Arrieta & Torres-Peimbert 2003; ATP03). However, it is not possible to conclude that this is the mechanism for our PPN sample (see Sánchez Contreras et al. 2008 for details). The main difficulty is that a necessary condition for the Raman scattering mechanism is the availability of a relatively strong Lyβ flux, which is not expected in PPNe with relatively late-type central stars (A-G spectral types: IRAS 08005, 22036, 22574), yet these objects show broad wings. Other line-broadening mechanisms include electron scattering and emission from a rotating disk or a fast stellar wind. Rotating disks around the central stars of young PNe which have masses in the range M=0.6–0.83$M_{\odot}$, and radii R=(1–18)$R_{\odot}$ produce velocities, $V_{max} < 400(M\,R)^{1/2}$ km s^{-1} (ATP03), which are too low to account for the broad line-widths. Since PPN central stars are much cooler, they are significantly larger, hence V_{max} is even lower! The extreme densities required for electron scattering (e.g., $n_e > 10^{12}$ cm^{-3} in M 2-9; ATP03) also make that an implausible mechanism. Outflow models are attractive because they have also been proposed for explaining Hα profiles with broad emission wings in other stellar objects with (i) companions: symbiotic stars (e.g. Skopal 2006), or (ii) disks: T Tauri stars (Edwards et al. 1987). Similarly, for the young PN Hen2-90, which also has an Hα profile with very broad wings, as well as an extended, linear, knotty jet (Sahai & Nyman 2000), Costa et al. (1993) propose a fast outflow model. The very high outflow speeds observed in most of these objects then require the presence of a compact stellar companion such as a white dwarf.

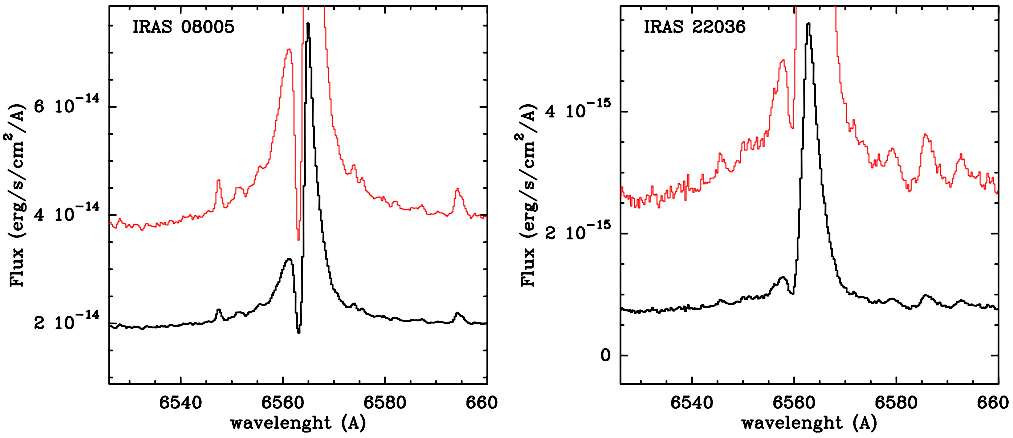

Figure 2. Hα line profiles towards the PPNe, (*left*) IRAS 08005, and (*right*) IRAS 22036, showing borad wings and blue-shifted absorption (adapted from Sánchez Contreras et al. 2008).

We conjecture that the broad wings might arise as a result of Lyβ emission from a compact, hot ionized region around the central star, which is then Raman-scattered off the neutral fast outflow (the signature of the latter is the blue-shifted absorption feature in the Hα profiles, Fig. 2). In this case, the mass-loss rate needed in this neutral outflow has to be substantial. Scaling from the scattering column density, $N_s = 10^{20}$ cm^{-2} required to achieve the Raman conversion efficiency needed to produce the very broad observed line-widths (see Fig. 1 of Lee & Hyung 2000), we find that $dM_s/dt = 0.9 \times 10^{-6}M_{\odot}$ yr^{-1}(0.1″/θ) (D/3 kpc) (V_{exp}/250 km s^{-1}) (N_s/10^{20}cm^{-2}), where θ is the size of the ionized region, and V_{exp} is the outflow velocity. Although we do not know the nature or origin of such an ionized region in PPNe, it may already be produced

during or before the late-AGB phase: Sahai et al. (2003) found such a region in V Hya, which they modelled as an expanding disk.

3. Concluding Remarks

We are still far from understanding the mechanisms which produce aspherical PNe, and we need to focus our efforts as a community on PPNe and nascent PPNe, both observationally and theoretically. One of the least understood, but potentially most exciting clues of the launch site of the fast post-AGB outflows that do the shaping, is the broad-wing Hα emission which we find in PPNe. Observational surveys of Hα in PPNe and young PN with class-E and R morphologies, as well as in nascent PPN, will be helpful in understanding its origin. High angular resolution ($< 0.3''$) interferometric mapping (e.g., in the submm with ALMA, or cm-wavelengths with the EVLA) of the large-grain emission will help in understanding the origin of equatorial waists in these objects.

References

Arrieta, A., & Torres-Peimbert, S. 2003, ApJS, 147, 97
Bujarrabal, V., Van Winckel, H., Neri, R., Alcolea, J., Castro-Carrizo, A., & Deroo, P. 2007, A&A, 468, L45
Cohen, M., Van Winckel, H., Bond, H. E., & Gull, T. R. 2004, AJ, 127, 2362
Costa, R. D. D., de Freitas-Pacheco, J. A., & Maciel, W. J. 1993, A&A, 276, 184
de Marco, O. 2009, PASP, 121, 316
de Ruyter, S. et al. 2005, A&A, 435, 161
Edwards, S. et al. 1987, ApJ, 321, 473
Gielen, C. et al. 2008, A&A, 490, 725
Hirano, N., et al. 2004, ApJ, 616, L43
Huggins, P. J. 2007, ApJ, 663, 342
Jura, M., Webb, R. A., Kahane, C. 2001, ApJ, L71
Kahane, C., Audinos, P., Barnbaum, C., & Morris, M. 1996, A&A, 314, 871
Lee, H.-W., & Hyung, S. 2000, ApJ, 530, L49
Mastrodemos, N., & Morris, M. 1998, ApJ, 497, 303
Sahai, R. 2009, *Asymmetrical Planetary Nebulae IV*, eds. R.L.M. Corradi, A. Manchado & N. Soker, I.A.C. electronic publication
Sahai, R. & Trauger, J.T. 1998, AJ, 116, 1357
Sahai, R., Morris, M., Knapp, G. R., Young, K., & Barnbaum, C. 2003, Nat, 426, 261
Sahai, R., & Nyman, L.-Å. 2000, ApJ, 538, L145
Sahai, R., Young, K., Patel, N. A., Sánchez Contreras, C., & Morris, M. 2006, ApJ, 653, 1241
Sahai, R., Morris, M., Sánchez Contreras, C., & Claussen, M. 2007a, AJ, 134, 2200
Sahai, R., Rubin, M., Sánchez Contreras, C., & Claussen, M. 2009, *Asymmetrical Planetary Nebulae IV*, eds. R.L.M. Corradi, A. Manchado & N. Soker, I.A.C. electronic publication
Sahai, R., Findeisen, K., Gil de Paz, A., & Sánchez Contreras, C. 2008, ApJ, 689, 1274
Sahai, R., Morris, M., & Villar, G. 2010, AJ, (in press)
Sahai, R., & Villar, G., & Morris, M., 2010, this proc.
Sahai, R. & Schnee, S. 2010, in preparation
Sahai, R., Blumenfeld, C., Morris, M., Sánchez Contreras, C., & Claussen, M. 2010, Bulletin of the American Astronomical Society, 42, 471
Skopal, A. 2006, A&A, 457, 1003
Sánchez Contreras, C., & Sahai, R. 2001, ApJ, 553, L173

Sánchez Contreras, C., Le Mignant, D., Sahai, R., Gil de Paz, A., & Morris, M. 2007, ApJ, 656, 1150
Sánchez Contreras, C., Sahai, R., Gil de Paz, A., & Goodrich, R. 2008, ApJS, 179, 166
Sánchez Contreras & Sahai 2010, in prep
Van Winckel, H., et al. 2009, A&A, 505, 1221

Asymmetric Planetary Nebulae V
A. A. Zijlstra, F. Lykou, E. Lagadec and I. McDonald
Jodrell Bank Centre for Astrophysics, Manchester, UK © 2011

Proto-Planetary Nebulae with the Spitzer Space Telescope

Alexa Hart[1,2], Joe Hora[2], Luciano Cerrigone[3], Grazia Umana[4], Corrado Trigilio[4], Martin Cohen[5] and Massimo Marengo[6]

[1]*Department of Physics & Astronomy, University of Denver, 2112 E. Wesley Avenue, Denver, CO 80208, USA*

[2]*Harvard-Smithsonian Center for Astrophysics, 160 Garden Street, Cambridge, MA 02138, USA*

[3]*Max-Planck-Institut fuer Radioastronomie, Auf dem Huegel 69, 53121 Bonn, Germany*

[4]*INAF-Osservatorio Astrofisico di Catania, Via S. Sofia 75, 95123 Catania, Italy*

[5]*Astronomy Department, University of California at Berkeley, 601 Campbell Hall, Berkeley, CA 94720 USA*

[6]*Department of Physics & Astronomy, Iowa State University, A313E Zaffarano, Ames, IA 50011 USA*

Abstract. The transition from Asymptotic Giant Branch star to Planetary Nebula is short-lived and mysterious. Though it lasts only a few thousand years, it is thought to be the time when the asymmetries observed in subsequent phases arise. During this epoch, the star is shrouded in thick clouds of dust and molecular gas; infrared observations are needed to reveal these objects at their most pivotal moment. I present preliminary results of a Spitzer study of targets spanning the range from post-AGB stars to Planetary Nebulae with the goal of determining the genesis of asymmetry in these objects.
Keywords. Planetary Nebulae – stars: AGB and post-AGB – infrared: stars

1. The Evolution of Intermediate-Mass Stars

The life cycle of a star and the manner of its ultimate demise depends on its mass. Intermediate-mass stars gradually fling their outer layers into space, forming planetary nebulae.

At the end of the Giant phase, the envelope of intermediate mass stars (defined as 0.8–8$M_{\odot}$) expands and the core contracts, resulting in a degenerate C/O core. This is the beginning of the Asymptotic Giant Branch (AGB) phase; the star will start to burn nuclear fuel in shells surrounding the spent core. During this stage, there is a slow, dense and (presumably) spherically symmetric stream of material leaving the star

called the AGB wind. This wind is interspersed with shells of enhanced density due to pulsation. These shells have been observed in many Planetary Nebulae such as the Cat's Eye Nebula (Balick et al., 2001).

As the mass loss process continues, the thick cloud of dust and gas it creates begins to obscure the star itself in visible wavelengths (García-Lario, 2006). Eventually, the central star will have lost so much mass that the AGB wind will cease; this marks the beginning of the post-AGB phase (Kwok et al. 1993). Though we can conjecture about what happens next, observations are difficult due to the obscuration of the central star. However, post-AGB stars observed in the mid-infrared with IRAS apparently fit into an evolutionary sequence with effective temperatures steadily increasing until the star is hot enough to ionize its envelope (spectral types marching from K, G, F, A to B). Near the earliest onset of ionization, the star becomes a Transition Object, sometimes called a proto-Planetary Nebula. The transition phase lasts mere thousands of years.

The planetary nebula phase commences when the star ionizes its envelope. The ionized material is optically thin, so the central star re-emerges in visible wavelengths once the ionization front has traveled sufficiently far out into the envelope. Morphologies of these young PNe are diverse: bipolar, elliptical, point-symmetric and spherical.

Though few AGB stars have been spatially resolved, they are generally assumed to have spherically symmetric outflows (as long as they are single). Yet when the star emerges just a short time later, it is suddenly the central star of a spectacular, and often highly asymmetric, Planetary Nebulae. Somehow, during this phase of mere thousands of years, the structure of the winds, and perhaps the star itself, change fundamentally. What happens behind that dark cloud of dust and gas is revealed in infrared observations with the Spitzer Space Telescope.

2. The Sample

A sample of targets was chosen to span the entire temporal sequence from star to nebula. This sequence was divided into three constituent epochs: post-AGB stars, true Transition Objects, and Planetary Nebulae. Each of these epochs were the subject of an observational program on *Spitzer*, divided as follows: 26 post-AGB stars, 36 Transition Objects, and 18 Planetary Nebulae.

The post-AGB sample was designed to catch stars that are nearing the end of the post-AGB phase, that is, stars that are on the brink of ionizing their envelopes. To find such stars, we started from targets that were characterized as post-AGB candidates based on their IRAS colors (Suarez et al. 2006) and then further constrained them to have a central star of spectral type A and a far-IR excess typical of PNe (Parthasarathy 2000). The spectral type condition should limit the sample to objects with very hot central stars, which should be those that are at the very end of the post-AGB phase. Type A stars should not generally be hot enough to ionize surrounding material.

To isolate true Transition Objects, i.e. stars that have just begun to ionize their circumstellar envelopes, a sample of post-AGB candidate (again selected based on IRAS colors and infrared excess) with slightly hotter spectral type B central stars were chosen. These stars should be just hot enough to emit ionizing radiation. As an independent measure of ionization, these objects were observed with the VLA; 16 of the 36 were

detected, confirming the presence of ionized shells (Umana et al. 2004; Cerrigone et al. 2008).

The chosen Planetary Nebulae all have H-deficient central stars of late, carbon-rich Wolf-Rayet spectral type ([WC 8–12]). These PNe may also have in common a peculiar spectroscopic property: simultaneous evidence for both oxygen-based crystalline silicates and carbon-based PAHs in their dust.

3. Dust Chemistry

An important observational aspect of these stars is their dust chemistry, that is, if the dust around them is Oxygen-rich or Carbon-rich. This distinction is a consequence of the high binding energy of CO; since the CO molecule will form first, only the more abundant of C or O will be left to form other dust grains. All AGB stars start out O-rich; stars with roughly 1.5–4$M_{\odot}$ can become C-rich via the Third Dredge Up.

In Carbon-rich sources, we see Polycyclic Aromatic Hydrocarbon (PAH) features at 3.3, 6.2, 7.7, 8.6 and 11.3 μm (Hrivnak et al. 2007), as well as an SiC feature at 11.3 μm (Speck et al. 2009). Oxygen-rich sources have silicate features at ~10-18 μm and show evidence for water ice. A small minority of stars show evidence of both PAHs and silicates in their dust (called dual-dust objects), a phenomena which has yet to be understood. These dual dust spectra could be indicative of either an O-rich environment preserved in a disk while the rest of the envelope transformed to C-rich or simply the formation of PAHs in a C-rich environment as a result of the photo-dissociation of CO molecules.

Interestingly, Cerrigone et al. 2009 found that approximately 40% of the Transition Object sample were dual-dust objects, a striking contrast to the global occurrence of $\sim$ 10% among PNe. The authors noted that this might be due to a selection effect, in particular the choice of objects with a far-IR excess which may be indicative of the presence of a disk. Additionally, 70% of those dual-dust objects were radio-detected in free-free emission, hinting at a potential correlation between ionization and the dual-dust phenomenon. Modeling of the PAH features resulted in the conclusion that the PAH molecules are located in the outflows, far from the central star. For the detailed analysis, see Cerrigone et al. 2009.

The PNe sample was chosen with this peculiarity in mind: Cohen et al. 2002 found that four out of six PNe with central stars of type [WCL] in their study were dual-dust objects; the PNe sample was designed to further explore this apparent connection.

4. Observations & Results

The sample of 80 targets were first observed with *Spitzer*; follow-up observations of 30 targets were performed using the Magellan I & II Telescopes at Las Campanas Observatory in Chile.

The three programs that were taken with *Spitzer* (Werner et al. 2004) that form the basis of this project were completed in 2009. The sample comprises about 75 targets in total. All have infrared spectra covering 5–40 μm measured on the Infrared Spectrograph (IRS) (Houck et al. 2004) and were also observed with the Infrared Array

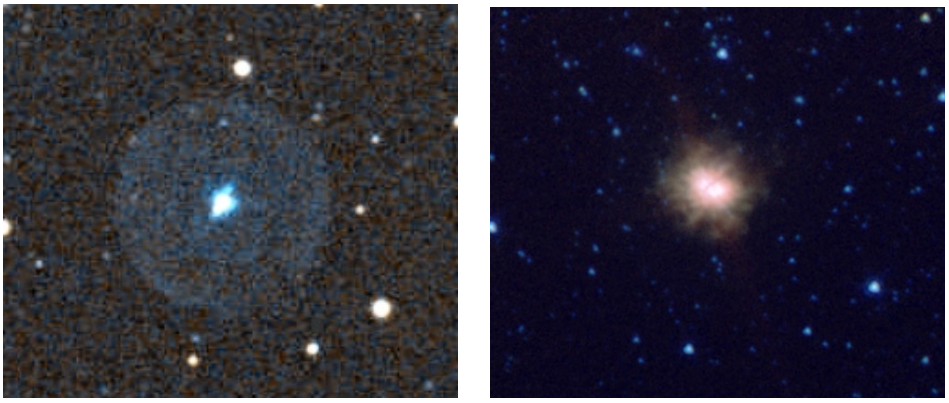

Figure 1. Planetary Nebula Abell 30 in optical taken at Kitt Peak (left) and with IRAC (right). Optical image credit: Allan Cook/Adam Block/NOAO/AURA/NSF

Camera (IRAC) imager (Fazio et al. 2004), which images each object in four broad-band channels centered at 3.6, 4.5, 5.8, and 8.0 μm .

The Magellan Clay telescope with the MMIRS (McLeod et al. 2004) was used to obtain near-infrared (H and K band) spectra of the observable subset of the *Spitzer* sample. In addition, the Magellan Baade telescope was used to image the subset of sources in the *Spitzer* sample that have extended emission using near-Infrared narrow-band filters that isolate H_2 and $Br\gamma$ emission with PANIC (Martini et al. 2004).

Results of the Transition Object program have been published by Cerrigone et al. 2009. The imaging search (with IRAC and PANIC) for faint, extended emission around the post-AGB sample yielded a null result in most cases; SED and spectral analysis of the data is underway. A sample IRAC image from the Planetary Nebula program is shown in Figure 1.

References

Balick, B., Wilson, J., & Hajian, A. R. 2001, AJ, 121, 354

Cerrigone, L., Hora, J. L., Umana, G., & Trigilio, C. 2009, ApJ, 703, 585

Cerrigone, L., et al. 2008, MNRAS, 390, 363

Cohen, M., Barlow, M. J., Liu, X.-W., & Jones, A. F. 2002, MNRAS, 332, 879

Fazio, G. G., et al., 2004, ApJS 154,10

García-Lario, P. 2006, Planetary Nebulae in our Galaxy & Beyond, 234, 63

Habing, H. J., & Olofsson, H. 2003, Asymptotic giant branch stars, Astronomy & Astrophysics library: Springer

Houck et al., 2004, ApJS 154, 18

Hrivnak, B. J., Geballe, T. R., & Kwok, S. 2007, ApJ, 662, 1059

Kwok, S. 1993, ARA&A, 31, 63

Martini, P. et al., 2004, Proc. SPIE, 5492, 1653

McLeod, B. A. et al., 2004, Proc. SPIE, 5492, 1306

Nenkova, M., Ivezić, Ž., & Elitzur, M. 2000, Thermal Emission Spectroscopy and Analysis of Dust, Disks, & Regoliths, 196, 77

Parthasarathy, M., Vijapurkar, J., & Drilling, J. S. 2000, A&AS, 145, 269
Speck, A. K. et al. 2009, ApJ, 691, 1202
Suárez, O. et al. 2006, A&A, 458, 173
Umana, G., Cerrigone, L., Trigilio, C., & Zappalà, R. A. 2004, A&A, 428, 121
Werner et al., 2004, ApJS 154, 1

Asymmetric Planetary Nebulae V
A. A. Zijlstra, F. Lykou, E. Lagadec and I. McDonald
Jodrell Bank Centre for Astrophysics, Manchester, UK © 2011

Imaging Planetary Nebulae with Herschel-PACS and SPIRE *

P.A.M. van Hoof[1], K.M. Exter[3], G.C. Van de Steene[1], M.J. Barlow[2], T.L. Lim[8], B. Sibthorpe[4], M.A.T. Groenewegen[1], T. Ueta[5], M. Matsuura[2], J.A.D.L. Blommaert[3], M. Cohen[6], W. De Meester[3], W.K. Gear[7], H.L. Gomez[7], P.C. Hargrave[7], E. Huygen[3], R.J. Ivison[4], C. Jean[3], S.J. Leeks[8], G. Olofsson[9], E.T. Polehampton[8,10], S. Regibo[3], P. Royer[3], B.M. Swinyard[8], B. Vandenbussche[3], H. Van Winckel[3], C. Waelkens[3], R. Wesson[2]

[1]*Royal Observatory of Belgium, Ringlaan 3, B-1180 Brussels, Belgium*

[2]*Dept. of Physics & Astronomy, UCL, Gower St, London WC1E 6BT, UK*

[3]*IvS, Katholieke Univ. Leuven, Celestijnenlaan 200 D, Leuven, Belgium*

[4]*UK Astronomy Technology Centre, ROE, Blackford Hill, Edinburgh, UK*

[5]*Dept. of Physics and Astronomy, Univ. of Denver, Denver, CO 80208, USA*

[6]*Radio Astronomy Laboratory, Univ. of California at Berkeley, CA 94720, USA*

[7]*School of Physics and Astronomy, Cardiff University, Cardiff, Wales, UK*

[8]*Rutherford Appleton Laboratory, Oxfordshire, OX11 0QX, UK*

[9]*Dept. of Astronomy, Stockholm University, Stockholm, Sweden*

[10]*Department of Physics, Univ. of Lethbridge, Alberta, T1J 1B1, Canada*

Abstract. In this paper we will discuss the images of Planetary Nebulae that have recently been obtained with PACS and SPIRE on board the Herschel satellite. This comprises results for NGC 650 (the little Dumbbell nebula), NGC 6853 (the Dumbbell nebula), and NGC 7293 (the Helix nebula).
Keywords. Planetary Nebulae

1. Introduction

We have obtained Herschel PACS and SPIRE images of planetary nebulae (PNe) as part of the MESS (Mass loss of Evolved StarS) guaranteed time key program. The aims of this program are threefold: (1) study the time dependence of the mass loss process via a search for shells and multiple shells, (2) study the dust and gas chemistry as a function of progenitor mass, and (3) study the properties and asymmetries of a representative sample of evolved objects. This program will be discussed in more detail

* Herschel is an ESA space observatory with science instruments provided by European-led Principal Investigator consortia and with important participation from NASA.

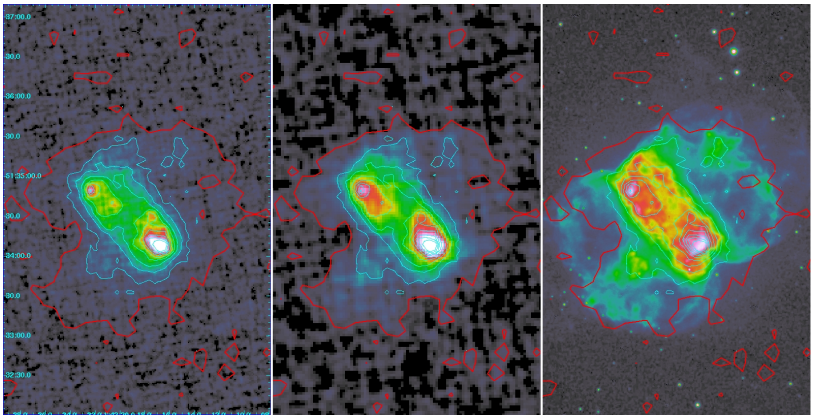

Figure 1. NGC 650. Left: PACS 70 μm, middle PACS 160 μm, right: ground-based Hα image (Lars Ø. Andersen, Lars Malmgren, Frank R. Larsen, NOT). A manual shift of 4.5″ was applied to the WCS of the PACS images.

in a forthcoming paper (94). During the science demonstration phase of Herschel we obtained PACS and SPIRE images of NGC 6720, which have been discussed in van Hoof et al. (98). The detailed match between the H_2 and dust emission in this object appears to be the first observational evidence that H_2 forms on oxygen-rich dust. The most plausible scenario is that the H_2 resides in high density knots that were formed after the recombination of the gas started when the central star entered the cooling track. Models indicate that a substantial amount of H_2 could have formed since that time and that the formation may still be ongoing at this moment.

Below we will present preliminary reductions of PACS and SPIRE data of 3 other PNe that we obtained during the routine phase.

2. Data Reduction

Poglitsch et al. (96) describe the standard data reduction scheme for PACS scan maps from so-called "Level 0" (raw data) to "Level 2" products. The level 1 and 2 products that are part of the data sets from the Herschel science archive have been produced by execution of these standard pipeline steps. We do not use the standard products, but use an adapted and extended version of the pipeline script suited to our needs starting from the raw data. In particular the deglitching step(s), and the "high pass filtering" need special care.

When the central source is bright, the deglitching task incorrectly masks a significant number of frames of the source as glitches. A second pass (called "2nd level deglitching" is needed to remedy this. The purpose of the high pass filter is to remove the $1/f$ noise from the images. At the moment the task is using a median filter, which subtracts a running median from each readout. This works well for point sources, but causes significant problems for extended sources (resulting in negative "shadows" in the image). To prevent the artefacts, any part of the source needs to be masked from the median filter. We are currently still experimenting with various algorithms to achieve this in an optimal way. We are also looking into using MadMap as an alternative al-

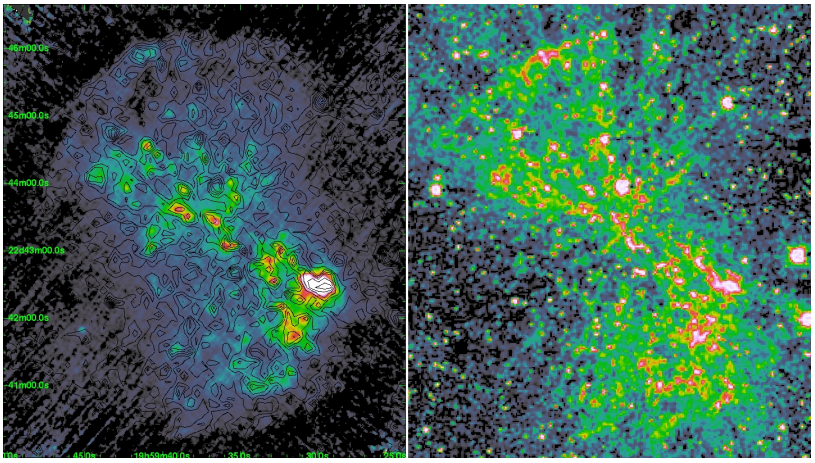

Figure 2. NGC 6853. Left: PACS 70 μm with H_2 contours overlaid, right: ground-based H_2 2.12 μm image (I. Gatley, M. Merrill, NOAO).

gorithm. In addition, as the standard pipeline script operates on a single Astronomical Observation Request (AOR), while our observations are always the concatenation of 2 AORs (a scan and a cross-scan) an additional step is also needed to combine the two scans. The pointing accuracy of Herschel is within specifications, but is however not negligible compared to the PACS beam size. Hence manual adjustments of the world coordinate system (WCS) may also be necessary when comparing with other (ground-based) images. A more in-depth discussion of the PACS data reduction will be given in Groenewegen et al. (94).

The standard SPIRE photometer data processing pipeline, described by Griffin et al. (92, 93), is sufficient to reduce our SPIRE photometric imaging data. The calibration steps for these data are described by Swinyard et al. (97).

In Figs. 1, 2, and 3 we present preliminary reductions of the PACS scan maps of NGC650, NGC 6853, and NGC 7293. The reduction of the SPIRE maps of NGC 7293 is final.

3. Outlook

Both NGC 7293 and NGC 6853 are well evolved PNe with central stars that are currently on the cooling track (95). So both nebulae are in a similar evolutionary state compared to NGC 6720. Especially NGC 7293 is almost an "older twin". Also in these objects we see that the distribution of the H_2 closely follows the dust. This suggests that in these objects the H_2 has also been formed in high density knots. We will model these PNe in detail to test whether the scenario that we proposed in van Hoof et al. (98) can also explain the H_2 formation in these objects. Also in NGC 650 we see that the gas and dust show a very similar distribution. It is not yet clear however if this H_2 formed in a similar fashion, or whether it is leftover AGB material.

In addition to the scan maps presented in van Hoof et al. (98) and this paper, we will also obtain Herschel images of NGC 650 (SPIRE), NGC 3587 (PACS, SPIRE),

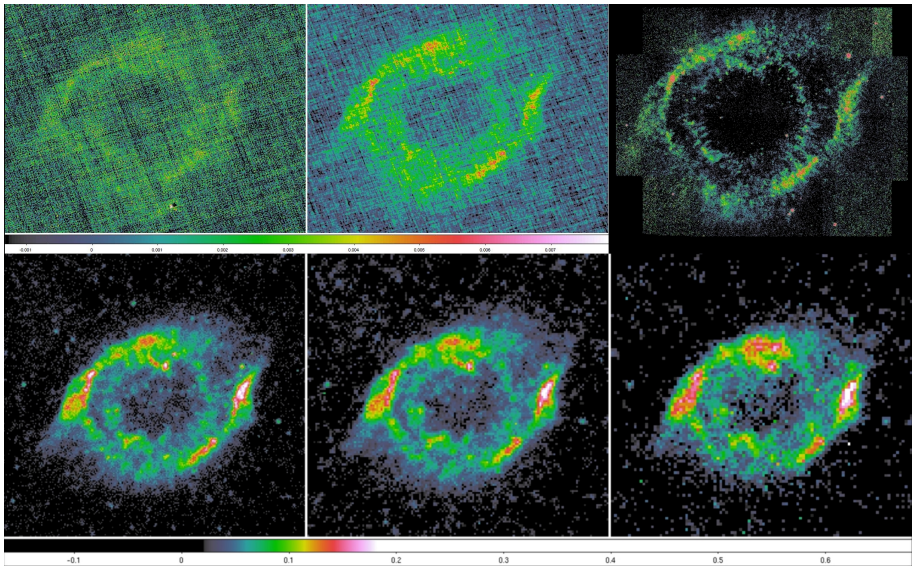

Figure 3. NGC 7293. Top row: PACS 70 & 160 μm, H_2 2.12 μm (courtesy A. Speck, KPNO), bottom row SPIRE 250, 350 & 500 μm.

NGC 6543 (PACS, SPIRE), NGC 6853 (SPIRE), NGC 7027 (PACS), IRAS 22036+5306 (PACS). For all targets we will obtain PACS images in the 70 and 160 μm bands, while SPIRE images will be obtained in all 3 bands: 250, 350, and 500 μm. The final goal of the program is to study the structures of their dust shells in order to learn about the (post-) AGB mass loss processes.

Acknowledgments. PvH, KE, GVdS, MG, JB, WDM, RH, CJ, SR, PR, and BV acknowledge support from the Belgian Federal Science Policy Office via the PRODEX Programme of ESA. PACS has been developed by a consortium of institutes led by MPE (Germany) and including UVIE (Austria); KU Leuven, CSL, IMEC (Belgium); CEA, LAM (France); MPIA (Germany); INAFIFSI/ OAA/OAP/OAT, LENS, SISSA (Italy); IAC (Spain). This development has been supported by the funding agencies BMVIT (Austria), ESA-PRODEX (Belgium), CEA/CNES (France), DLR (Germany), ASI/INAF (Italy), and CICYT/MCYT (Spain). SPIRE has been developed by a consortium of institutes led by Cardiff Univ. (UK) and including Univ. Lethbridge (Canada); NAOC (China); CEA, LAM (France); IFSI, Univ. Padua (Italy); IAC (Spain); Stockholm Observatory (Sweden); Imperial College London, RAL, UCL-MSSL, UKATC, Univ. Sussex (UK); Caltech, JPL, NHSC, Univ. Colorado (USA). This development has been supported by national funding agencies: CSA (Canada); NAOC (China); CEA, CNES, CNRS (France); ASI (Italy); MCINN (Spain); SNSB (Sweden); STFC (UK); and NASA (USA). Data presented in this paper were analysed using "HIPE", a joint development by the Herschel Science Ground Segment Consortium, consisting of ESA, the NASA Herschel Science Center, and the HIFI, PACS and SPIRE consortia. This research made use of tools provided by Astrometry.net.

References

Griffin, M., Dowell, C. D., Lim, T., & others 2008, Proc. of the SPIE, Vol. 7010, 70102Q
Griffin, M. J., Abergel, A., Ade, P. A. R., & others 2010, A&A, 518, L3
Groenewegen, M. A. T., Waelkens, C., Barlow, M. J., & others 2010, A&A, submitted
O'Dell, C. R., Sabbadin, F., & Henney, W. J. 2007, AJ, 134, 1679
Poglitsch, A., Waelkens, C., Geis, N., & others 2010, A&A, 518, L2
Swinyard, B. M., Ade, P. A. R., Baluteau, J.-P., & others 2010, A&A, 518, L4
van Hoof, P. A. M., Van de Steene, G. C., Barlow, M. J., & others 2010, A&A, 518, L137

Asymmetric Planetary Nebulae V
A. A. Zijlstra, F. Lykou, E. Lagadec and I. McDonald
Jodrell Bank Centre for Astrophysics, Manchester, UK © 2011

Origin of Morphological Structures of Planetary Nebulae

Sun Kwok

Faculty of Science, The University of Hong Kong, Hong Kong, China

Abstract. Infrared and submm observations have revealed that for many bipolar and multipolar planetary nebulae, most of the masses reside in the equatorial region and the spherical envelope. It is suggested that the optically bright lobes are in fact low-density cavities cleared out by fast outflows and photoionized by UV photons leaked from the torus.
Keywords. Planetary nebulae – Infrared

1. Introduction

Planetary nebulae (PNs) are classified according to their apparent morphology (107; 99; 105) and such classifications are used to infer their 3-D intrinsic structure (102). In the previous ASPN meetings, the question of fraction of bipolar nebulae has been extensively debated. Although the number of PNs with apparent bipolar morphology is small, their actual numbers can be much higher due to limitation of sensitivity and dynamic range. For example, the equatorial region of a bipolar nebula is often much brighter than the lobes, and in a sensitivity-limited image, the bipolar nature would be missed. The invention of CCDs has led to the realization that some elliptical PNs are in fact bipolar (e.g., NGC 650-1). The effect of orientation is another problem. Near face-on equatorial rings would appear to be elliptical, even though the intrinsic structure of the PN is bipolar (e.g., NGC 6720, NGC 7293).

Our recently acquired ability to image PNs in the infrared has also led to the discovery of some hidden bipolars. Figure 1 shows the *Spitzer IRAC* 8 images of IRAS 17351−3130 and M1−41. The bipolar morphology of these objects is revealed by dust emission in the lobes. Without the infrared image, this object would be classified as having a ring morphology, but actually the ring is the equatorial region of the bipolar.

2. Revelation of "Dark Matter"

Although the optical lobes of bipolar nebulae are bright and spectacular, they are not where the majority of the nebular masses lie. From the optical images of many bipolar nebulae (e.g., NGC 2346, NGC 6302), it is clear that the equatorial region is confined by unseen external material. Molecular hydrogen images of bipolar PNs suggest that the lobes are ionization bounded and H_2 emission can trace the boundaries through shock excitation (103). Mid-infrared and submm observations have revealed that most

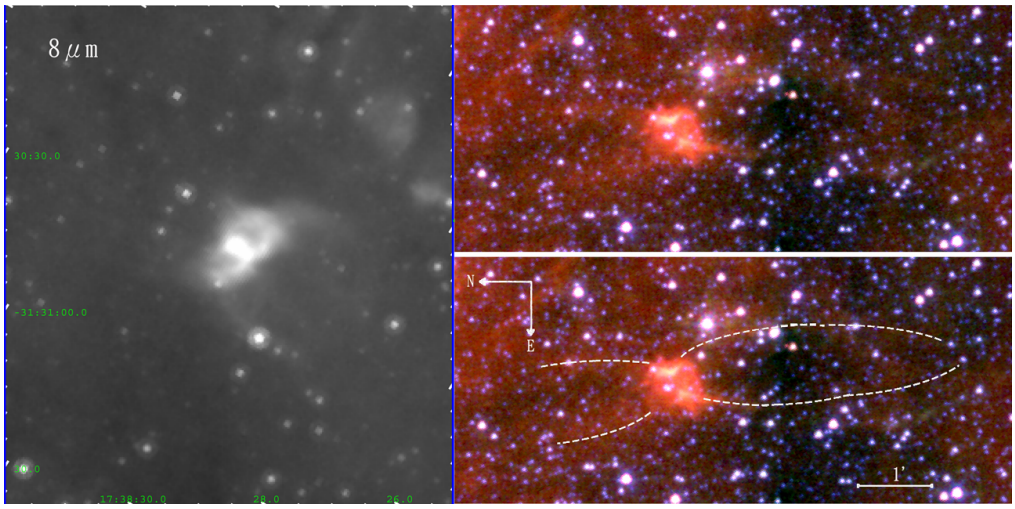

Figure 1. GLIMPSE 8 μm image of IRAS 17351-3130 (left) and composite color image of the PN M1-41. Bipolar lobes can clearly be seen in both objects. Images made by C.H. Hsia.

of the mass is in fact hidden in the equatorial region in the form of neutral (molecular) matter. Figure 2 shows that the mid-infrared image of the bipolar nebula NGC 6302 has a very different morphology from its optical image. Most of the infrared light is emitted from the equatorial region. Molecular mapping of NGC 6302 shows that it has a massive expanding molecular torus (100). In NGC 2346, the equatorial region manifests itself in the mid-IR and dominates emissions in the 24 and 70 μm images whereas the spherical AGB remnant dominates the emission at 160 μm (108).

The role played by the equatorial torus in the collimation of the fast outflow is of particular interest. Figure 3 shows the 18 μm image of the multipolar proto-planetary nebulae (PPN) IRAS 16594−4656 (109). Dust emission is seen predominantly in the equatorial region and along the edges of the lobes. We see that the lobes are still closed (unlike most bipolar PN which have open ends), indicating that the fast outflow has not yet broken through the circumstellar envelope. Also shown in Fig. 3 is the PPN IRAS 17441−2411. The bright torus in the infrared image corresponds to the dark lane in the optical image of this object (110).

3. Kinematic Components of PN

From optical, infrared, and mm molecular line observations, we have learned that a PN system consists of several kinematic components. There is an extended, spherical component (remnants of the AGB wind) which is expanding at ~10 km s^{-1}. The dynamical age of this component is $\sim 10^4$ yr. A later-developed equatorial outflow has velocities of $\sim 10^2$ km s^{-1} and has a dynamical age of $\sim 10^3$ yr. Directional outflows, possibly collimated by the torus, have velocities of $\sim 10^3$ km s^{-1} interact with the AGB remnants and sweeps up the material leaving behind a low-density cavity. Depending on the evolutionary stage of the nebula, some of these kinematic components may be ionized. The first to be ionized are the lobes, and then the ionization will gradually

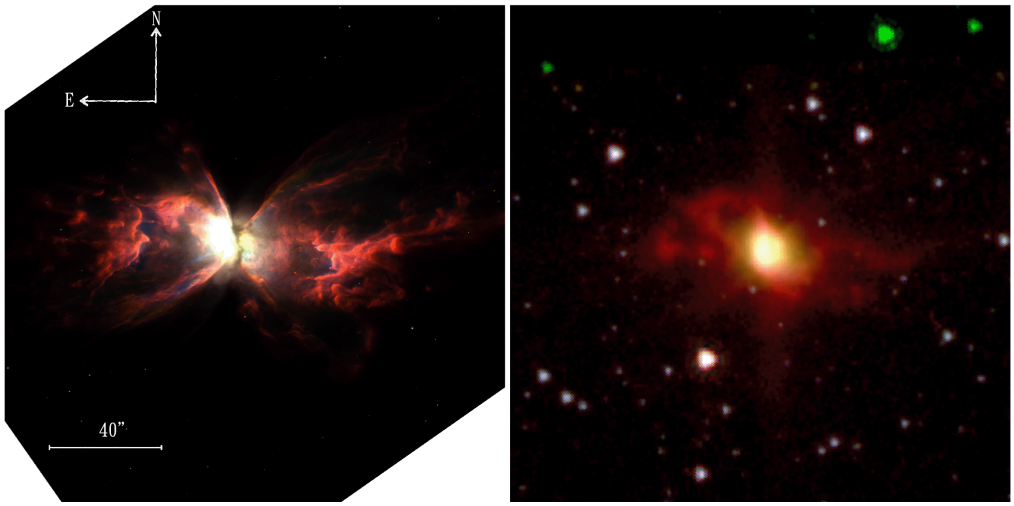

Figure 2. Comparison between the optical (left) and the infrared (right) images of NGC 6302. The color image on the right is a composite of 3.6, 5.8, and 8 μm IRAC images from *Spitzer* observations. Images made by C.H. Hsia.

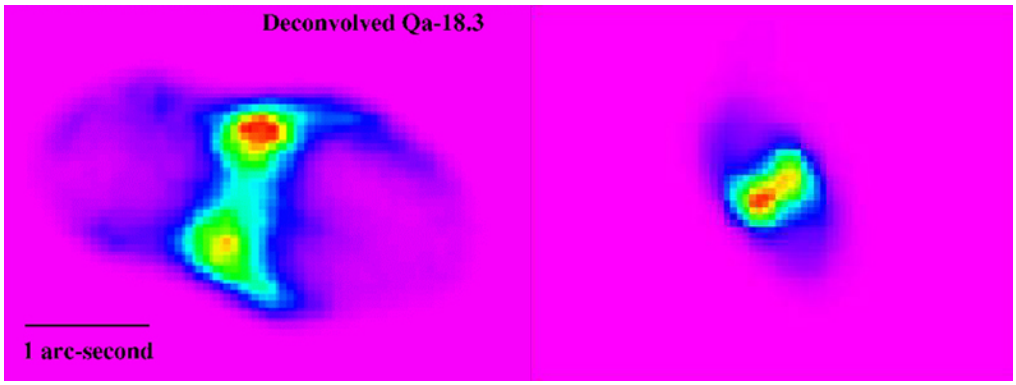

Figure 3. Gemini 18.3 μm image of the PPN IRAS 16594-4656 (left) and Gemini 11.7 μm image of the PPN IRAS 17441-2411 (right). See Volk et al. (2006, 2007) for details.

propagate through the torus. The high density of the torus makes it bright in the visible. A complete mapping of the kinematic structure of PN therefore requires integral field spectroscopy in the optical (for the ionized components) and interferometric molecular mapping for the neutral components.

4. A Model of Multipolar PN

One of the mysteries of multipolar nebulae is that the lobes are of approximately the same size (for examples see He 2-47 and M1-37 in Sahai (106) and NGC 2440 in Kwok (104)). This is difficult to understand in a multi-ejection model as the ejection has to happen almost simultaneously in multiple directions. An alternative hypothesis was proposed by Kwok (104) which the multiple lobes are not regions of high density but rather cavities carved out by high-velocity outflows. In this picture, most of the masses are contained in a spherical envelope. A later-developed equatorial torus channels the fast outflows through the poles and create bipolar cavities. When the central star is hot enough, UV photons that leak out from the poles will photoionize the cavities, making them optically bright. However, if the torus has holes, then there can be multiple pairs of lobes. A theory on how such holes can be developed from instabilities in dissociation fronts was recently developed by García-Segura (101).

5. Conclusions

Although we have traditionally classified PNs by their optical morphology, we have learned from observations in the infrared and submm wavelengths that the optical images may not correspond to the distribution of matter density. A full understanding of the morphology of PNs has to come from multi-wavelength observations so that the ionized, molecular, and solid-state components can all be mapped. These images have to be supplemented by spectral data so that the true 3-D structure can be reconstructed from kinematic models.

Acknowledgments. I would like to thank Yong Zhang and Chih-Hao Hsia for helpful discussions. This work was partially supported by the Research Grants Council of the Hong Kong Special Administrative Region, China (project no. HKU 7031/10P.)

References

Aaquist, O. B., & Kwok, S. 1996, ApJ, 462, 813
Dinh-V-Trung, Bujarrabal, V., Castro-Carrizo, A., Lim, J., & Kwok, S. 2008, ApJ, 673, 934
García-Segura, G. 2010, A&A, in press
Khromov, G. S., & Kohoutek, L. 2007, in Planetary Nebulae, vol. 34, 227
Kwok, S. 2007, in Asymmetric Planetary Nebulae IV, edited by R.L.M. Corradi, A. Manchado, N. Soker, p. 11
— 2010, PASA, 27, 174
Parker, Q. A., et al. 2006, MNRAS, 373, 79
Sahai, R. 2000, ApJ, 537, L43
Stanghellini, L., Corradi, R. L. M., & Schwarz, H. E. 1993, A&A, 279, 521
Su, K. Y. L., et al. 2004, ApJS, 154, 302

Volk, K., Hrivnak, B. J., Su, K. Y. L., & Kwok, S. 2006, ApJ, 651, 294
Volk, K., Kwok, S., & Hrivnak, B. J. 2007, ApJ, 670, 1137

Asymmetric Planetary Nebulae V
A. A. Zijlstra, F. Lykou, E. Lagadec and I. McDonald
Jodrell Bank Centre for Astrophysics, Manchester, UK © 2011

A view of the solar neighbourhood: the local population of planetary nebulae and their mimics

David J. Frew[1] and Quentin A. Parker[1,2]

[1]*Department of Physics and Astronomy, Macquarie University, NSW 2109, Australia*

[2]*Australian Astronomical Observatory, PO Box 296, Epping, NSW 1710, Australia*

Abstract. We have, for the first time, compiled a nearly complete census of planetary nebulae (PNe) centred on the Sun. Our goal is the generation of an unbiased volume-limited sample, in order to answer some long-standing statistical questions regarding the overall population of Galactic disk PNe and their central stars. Much improved discrimination of classical PNe from their mimics is now possible based on the wide variety of high-quality multiwavelength data sets that are now available. However, we note that evidence is increasing that PNe are heterogeneous, and probably derived from multiple evolutionary scenarios. We give some preliminary data on the relative frequencies of different types of PNe in the local Galactic disk.
Keywords. Stars: AGB and post-AGB – planetary nebulae: general

1. Introduction

Planetary nebulae (PNe) are an important, albeit brief, evolutionary phase in the lifetimes of a significant fraction of Milky Way stars. While their formation is broadly understood (e.g. Balick & Frank 2002), the exact mechanism(s) required to manufacture the multitude of PN morphologies remains unclear, as does the ultimate fate of our own Sun. To help answer these questions, we have compiled the most complete volume-limited census of PNe out to 2.0 kpc from the Sun ever compiled (Frew & Parker 2006, Frew 2008), containing 210 PNe. We have recently extended the census out to 3.0 kpc (Frew & Parker 2010b) which doubles the number to over 420 PNe, though this enlarged sample is less complete at the faint end of the PN luminosity function (Ciardullo 2010). This number can be compared to the known Galactic population which currently totals nearly 3000 PNe (Frew & Parker 2010; Jacoby et al. 2010).

Volume-limited samples are fundamental in astronomy, but not easy to produce. The ability to generate this PN census rests, in large part, on the application of our new, empirical Hα surface brightness – radius (SB-r) relation which we have shown can provide distances accurate to 20–30% (Frew & Parker 2006; Frew 2008). Our technique is currently the only statistical method that is applicable to the very faintest, senile PNe, which are selected against in extant radio surveys. Such faint PN numerically dominate any volume-limited sample, so it is crucial to include them in order to generate an unbiased census which can then be used to answer some long-standing statistical

questions regarding the overall population of Galactic disk PNe and their central stars (CSPN). Estimates of the local volume density, scale height, and total number of PN in the Galaxy also rest on having an accurate census of nearby nebulae (see Frew & Parker 2007, for a discussion).

Surprisingly, and somewhat distressingly, there remains a lack of consensus over the precise definition of a PN, a situation that lingers even after several decades of intensive effort* (for a fuller discussion of this problem, see Frew & Parker 2010a). It is commonly argued that the 'planetary nebula' moniker has a distinct physical meaning, and should be restricted to the ionized shell ejected at the end of the AGB phase, or by a common-envelope ejection (De Marco 2009, and references therein). This is an important point, as in many symbiotic systems, which are often confused with PNe, the gas is thought to be donated by a companion giant, and not derive from the precursor of the white dwarf (WD) which is usually present in these systems (Corradi 2003).

Besides our development of the Hα SB-r relation, we have also refined a range of multiwavelength classification tools to weed out the many mimics that have contaminated both Galactic and extragalactic PN catalogues in the past. We have recently used mid-IR and radio diagnostics to identify contaminants (Cohen et al. 2007, 2010). Based on an overview of the literature, extensive experience in the compilation of the MASH catalogues (Parker et al. 2006; Miszalski et al. 2008), as well as insights from the solar neighbourhood PN census, Frew & Parker (2010a) provided a phenomenological definition, listing a summary of the various observable properties manifested by PNe.

2. Identifying PNe

A review of the history of PN surveys is presented by Parker & Frew (2010, these proceedings). PNe have been confused with many different types of objects, as diverse as HII regions, massive star ring nebulae, Herbig-Haro objects, B[e] stars, reflection nebulae, supernova remnants, symbiotic outflows, and galaxies. We recommend that the following diagnostic criteria be examined, the exact combination depending on whether the candidate nebula is compact or extended. These criteria have been rigorously applied to our local volume sample (as discussed by Frew & Parker 2010a). They include:

- Presence of a hot (bluish) star that is relatively faint compared to the nebular flux. Non-blue stars may be either reddened single stars or binary stars with a cooler companion; in the latter case, a UV excess can provide evidence for the true ionizing star (e.g. Frew et al. 2010b). The properties of the ionizing star, if known, should be examined, including its evolutionary age and position in the HR diagram.
- Nebular morphology and the ionization structure, including the consistency of any ISM interaction with the proper-motion vector of the ionizing star.
- Nebular emission-line ratios, using diagnostic plots where applicable (see Frew & Parker 2010a).
- Near-IR and mid-IR colours; use a range of diagnostic plots (Schmeja & Kimeswenger

*During the 1967 IAU PN symposium, R. Minkowski responded to a query from D.S. Evans, stating: *As to the question of how to define a planetary nebula, there is no better way than to accept any object in a catalogue of planetary nebulae if nobody has serious objections* (Osterbrock & O'Dell 1968: 290).

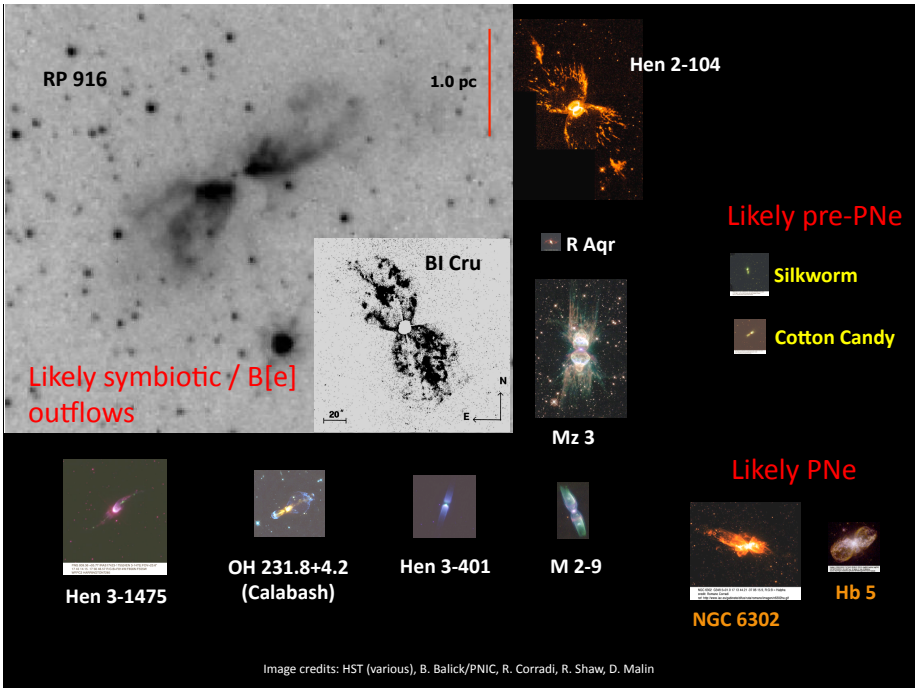

Figure 1. A montage of selected "PNe" from the literature, all presented at the same physical size; the scale bar represents 1 pc. We find that size appears to be a simple, but powerful discriminant between pre-PNe and most bona fide symbiotic outflows like BI Cru and He 2-104.

2001; Corradi et al. 2008; Cohen et al. 2007, 2010).

• Available time-domain photometric data to search for variability of the ionizing star, exhibited by close-binary CSPN or symbiotic stars.

• Strength of the radio and mid-IR flux densities (especially useful if a constraint on the distance is available).

• Systemic radial velocity of the nebula (does it differ from the RV of the ionizing star?) and the line width — is the nebula expanding or is the line width consistent with an HII region or static ISM? Alternatively, are broad Hα wings seen in compact objects, as this may be indicative of a symbiotic or B[e] star.

• Physical nebular diameter, which should be $\leq$5 pc, but a distance estimate is required. While there is overlap in the sizes of PNe, Population I ring nebulae, and resolved symbiotic outflows, we find bona-fide pre-PNe (Sahai et al. 2007; Szczerba et al. 2007) to be generally smaller than symbiotic outflows (Figure 1).

• Ionized mass, which should be between 0.005 and 3$M_{\odot}$, but the distance needs to be known.

• Local environment. For example, YSOs, and T Tauri stars are usually associated with HII regions, molecular clouds, and areas of heavy obscuration or dark lanes.

• Galactic latitude. PNe have a larger scale height than HII regions, SNRs, and massive

stars, and are more likely to be found away from the Galactic plane.
• Abundances of the nebular gas – check for N enrichment, which would indicate either a PN, a nova shell, or massive star ejecta.

No one criterion is generally enough, so we use the overall body of evidence to define the status of a candidate nebula (see Frew & Parker 2010a, for further details). As an illustrative example of our multiwavelength approach, the emission nebula around the sdOB star PHL 932 is detailed by Frew et al. (2010a), and convincingly shown to be a HII region; it should be expunged from current catalogues of PNe. We have discarded another dozen objects from the 1.0 kpc census (e.g. Sh 2-174 and Abell 35, amongst others; Frew 2008). The reader is also referred to Frew & Parker (2006), Parker et al. (2006) and Madsen et al. (2006) for other examples of nearby PN impostors.

3. Do PNe Form a Heterogeneous Class?

Even after removal of the obvious contaminants from PN catalogues, there is increasing evidence that the class itself is a 'mixed bag' (Frew & Parker 2010a), and that several stellar evolutionary pathways may produce nebulae best catalogued as PNe. Current work suggests that PN-like nebulae may arise from the following channels:

• Post-AGB evolution of a single star (or member of a wide, non-interacting binary), producing a conventional or classical PN.
• Short-period binaries that have passed through a common-envelope (CE; De Marco 2009). Their PNe appear to have distinct observational properties (Bond & Livio 1990; Frew & Parker 2007; Miszalski et al. 2009b, 2010). Some post-CE PNe seem to contain two hot subdwarfs (Hillwig 2010); the formation mechanism(s) of these, and the putative PNe around the classical novae V458 Vul and GK Per remain unclear (Wesson et al. 2008; Rodríguez-Gil et al. 2010). Also noteworthy is the re-interpretation of V605 Aql (in Abell 58) by Lau, De Marco & Liu (2010) as a possible nova in a PN.
• Longer-period interacting binaries, a subset of which appear to be related to the family of highly-collimated bipolar nebulae which host central stars exhibiting the B[e] phenomenon, with or without symbiotic characteristics.
• The so-called 'born-again' phenomenon, where a final helium flash produces a H-deficient star and surrounding knots inside a pre-existing, old PN (Zijlstra 2002), however there seem to be problems with this scenario (Lau et al. 2010).
• Scenarios that produce the rare O(He) stars; K 1-27 is the archetype of the class. They are possibly the long-sought successors of the R CrB stars (Rauch et al. 2008), which may result in turn from a double-degenerate merging process (Clayton et al. 2007).
• Evolution of a super-AGB star (Poelarends et al. 2008), but there are no confirmed examples known.

There is also great variation in the spectral types of CSPN. Up to 20% are H-deficient, including those where Wolf-Rayet features are present — these are denoted [WR] to differentiate them from their Population I cousins. Almost all [WR] CSPN belong to the [WC]/[WO] sequence except for the rare [WN] objects N 66 in the LMC (Peña et al. 1995; Hamann et al. 2003), PM 5 in the Galaxy (Morgan, Parker & Cohen 2003), and two recently discovered Galactic CSPN belonging to a proposed new [WN/WC] class: PB 8 (Todt et al. 2010) and Abell 48 (DePew et al. 2010); the

origin of these peculiar stars is unclear. N 66 surrounds a [WN4-5] star and has been suggested to be the product of a high-mass progenitor, but a binary evolution channel may be more likely (see Hamann et al. 2003, for a discussion).

4. Relative Numbers

It is difficult to ascertain the relative contributions of these various evolutionary pathways to the PN population until a complete spectroscopic survey of all nearby CSPN has been undertaken. Based on a preliminary 1.0 kpc volume-limited sample, Frew & Parker (2007) found 22 ± 9% of local CSPN are close binaries and are presumably derived from a post-CE evolutionary channel (De Marco 2009). We find the fraction of [WR] CSPN to be 7 ± 3%, and H-deficient CSPN to be about 20% of the total. Some nearby PNe possess unresolved high-density cores, which we have termed 'EGB 6-like' CSPN (Frew & Parker 2010a). Two are known within 1.0 kpc, so the fraction is ~2/55 or 4 ± 2%. This is a lower limit, as not all local CSPN have adequate spectroscopy.

Within a larger sample of 210 PNe within 2.0 kpc (Frew 2008), some rarer subclasses make an appearance. There are but one or two born-again objects (Abell 30 and Abell 78), one PN with an O(He) nucleus (K 1-27), one putative PN with a [WN] CSPN (PM 5), another with a [WN/WC] nucleus (Abell 48; DePew et al. 2010), and one or two highly collimated outflows associated with [Be] stars (which may not be true PNe), e.g. M 2-9. More robust estimates of these relative proportions will follow from a more detailed analysis of our enlarged 2.0 and 3.0 kpc samples.

5. Future Work

The total number of Galactic PNe is now nearly 3000, with the potential to grow more over the next few years (Parker & Frew 2010a; Jacoby et al. 2010). New discoveries from IPHAS (Viironen et al. 2009; Sabin et al. 2010) plus new candidates found at mid-IR wavelengths (e.g. Mizuno et al. 2010) should substantially add to the total. It is important that newly discovered nebulae be correctly classified, and it pays for the specialist to be cognisant of the full zoo of potential mimics. Much improved discrimination of true PN from their mimics is now possible based on the range of online UV, optical, near-IR, mid-IR, and radio data-sets that are available. While data-mining has its place, we caution that unusual objects be classified on a case-by-case basis.

One outstanding question from the two most recent APN meetings is the role of binarity in the formation and shaping of PNe (De Marco 2009, 2010), so we intend to carefully survey our samples for new close binaries to better ascertain the proportion of post-CE PNe in the local Galactic disk. This number can then be confronted with model predictions made by other authors (e.g. Soker 1997; Moe & De Marco 2006). Our preliminary disk post-CE estimate of ~22% is in agreement with the estimate of 17 ± 5% for a large, but flux-limited sample of Galactic bulge CSPN (Miszalski 2009a). We lastly note a surprising diversity of emission-line stars in PN-like nebulae, but the links between these nuclei and some symbiotic and B[e] stars is still unclear. A complete spectroscopic survey of all local CSPN is needed to better quantify the observed diversity of spectra. In particular, multiwavelength follow-up of unusual CSPN is required to confront evolutionary theory, and in this sense, they are much more valuable

than the more routine objects. We look forward to the day when a precise taxonomy of the 'PN phenomenon' is attained, but a consensus appears elusive at this point in time.

Acknowledgments. DJF would like to thank the SOC for the opportunity to present an invited talk, and we thank Macquarie University for travel funding.

References

Balick, B. & Frank, A. 2002, ARA&A, 40, 439
Bond, H.E. & Livio, M. 1990, ApJ, 355, 568
Ciardullo, R. 2010, PASA, 27, 149
Clayton, G.C., Geballe, T.R., Herwig, F., Fryer, C. & Asplund, M. 2007, ApJ, 662, 1220
Cohen, M.C., et al. 2007, ApJ, 669, 343
Cohen, M.C., et al. 2010, MNRAS, submitted
Corradi, R.L.M. 2003, ASPC, 303, 393
Corradi, R.L.M., et al. 2008, A&A, 480, 409
De Marco, O. 2009, PASP, 121, 316
De Marco, O. 2011, *in Asymmetric Planetary Nebulae 5*, Eds. A.A. Zijlstra, F. Lykou, E. Lagadec, I. McDonald, p. 252
DePew, K., et al. 2010, MNRAS, submitted
Frew, D.J. 2008, PhD thesis, Macquarie University
Frew, D.J. & Parker, Q.A. 2006, IAUS, 234, 49
Frew, D.J. & Parker, Q.A. 2007, APN4 Proceedings, IAC Electronic Pub., 475
Frew, D.J. & Parker, Q.A. 2010a, PASA, 27, 129
Frew, D.J. & Parker, Q.A. 2010b, in preparation
Frew, D.J., Madsen, G.J., O'Toole, S.J., & Parker Q.A. 2010a, PASA, 27, 203
Frew, D.J., et al. 2010b, PASA (in press), eprint: arXiv:1009.5914
Hamann, W.-R., Peña, M., Gräfener, G. & Ruiz, M.T. 2003, A&A, 409, 969
Hillwig, T. 2011, *in Asymmetric Planetary Nebulae 5*, Eds. A.A. Zijlstra, F. Lykou, E. Lagadec, I. McDonald, p. 276
Jacoby, G.H., et al. 2010, PASA, 27, 156
Lau, H.H.B., De Marco, O. & Liu X.-W. 2010, MNRAS (in press), eprint: arXiv:1009.3138
Madsen, G.J., Frew, D.J., Parker, Q.A., Reynolds, R.J. & Haffner L.M. 2006, IAUS, 234, 455
Miszalski, B., et al. 2008, MNRAS, 384, 525
Miszalski, B., Acker, A., Moffat, A.F.J., Parker, Q.A. & Udalski, A. 2009a, A&A, 496, 813
Miszalski, B., Acker, A., Parker, Q.A. & Moffat, A.F.J. 2009b, A&A, 505, 249
Miszalski, B., et al. 2011, *in Asymmetric Planetary Nebulae 5*, Eds. A.A. Zijlstra, F. Lykou, E. Lagadec, I. McDonald, p. 330
Mizuno, D.R., et al. 2010, AJ, 139, 1542
Moe, M. & De Marco, O. 2006, ApJ, 650, 916
Morgan, D.H., Parker, Q.A. & Cohen, M. 2003, MNRAS, 346, 719
Osterbrock, D.E. & O'Dell, C.R. (eds) 1968, Planetary Nebulae, IAUS, 34 (Reidel: Dordrecht)
Parker, Q.A. & Frew, D.J. 2011, *in Asymmetric Planetary Nebulae 5*, Eds. A.A. Zijlstra, F. Lykou, E. Lagadec, I. McDonald, p. 1
Parker, Q.A., et al. 2006, MNRAS, 373, 79
Peña, M., Peimbert, M., Torres-Peimbert, S., Ruiz, M.T. & Maza, J. 1995, ApJ, 441, 343
Poelarends, A.J.T., Herwig, F., Langer, N. & Heger, A. 2008, ApJ, 675, 614
Rauch, T., Reiff, E., Werner, K. & Kruk, J.W. 2008, ASPC, 391, 135

Rodríguez-Gil, P., et al. 2010, MNRAS, 407, L21
Sabin, L., et al. 2010, in preparation
Sahai, R., Morris, M., Sánchez Contreras, C. & Claussen, M. 2007, AJ, 134, 2200
Schmeja, D. & Kimeswenger, S. 2001, A&A, 377, L18
Soker, N. 1997, ApJS, 112, 487
Szczerba, R., Siódmiak, N., Stasińska, G. & Borkowski, J. 2007, A&A, 469, 799
Todt, H., Peña, M., Hamann, W.-R. & Gräfener, G. 2010, A&A, 515, 83
Viironen, K., et al. 2009, A&A, 504, 291
Wesson, R., et al. 2008, ApJ, 688, L21
Zijlstra, A.A. 2002, Ap&SS, 279, 171

Asymmetric Planetary Nebulae V
A. A. Zijlstra, F. Lykou, E. Lagadec and I. McDonald
Jodrell Bank Centre for Astrophysics, Manchester, UK © 2011

Iron Depletion into Dust Grains in Galactic Planetary Nebulae

G. Delgado-Inglada and M. Rodríguez

Instituto Nacional de Astrofísica, Óptica y Electrónica (INAOE), Apdo Postal 51 y 216, 72000 Puebla, Pue. Mexico

Abstract. We present preliminary results of an analysis of the iron depletion factor into dust grains for a sample of 20 planetary nebulae (PNe) from the Galactic bulge. We compare these results with the ones we obtained in a prior analysis of 28 Galactic disk PNe and 8 Galactic H II regions. We derive high depletion factors in all the objects, suggesting that more than 80% of their iron atoms are condensed into dust grains. The range of iron depletions in the sample PNe covers about two orders of magnitude, and we explore here if the differences are related to the PN morphology. However, we do not find any significant correlation.
Keywords. Planetary Nebulae – Dust

1. Introduction

Asymptotic giant branch (AGB) stars suffer mass loss episodes during the late stages of their evolution. The combination of high densities with relatively low temperatures makes the atmospheres of these stars favourable sites for grain formation, and in fact they are considered one of the most efficient sources of dust in the Galaxy (see, e.g., 127). Planetary nebulae (PNe) are created when AGB stars reach temperatures high enough to ionize the material previously ejected. Several authors have studied the dust present in PNe, but it is not clear how much dust they have and whether it is destroyed or modified during their lifetimes (119; 116; 125).

We study the dust in PNe through the analysis of the iron depletion factor, the ratio between the expected abundance of iron and the one measured in the gas phase. The abundances of refractory elements like iron have been calculated from ultraviolet absorption lines in several interstellar clouds toward different lines of sight, and the low values obtained, compared to the solar ones, are generally interpreted as due to depletion into dust grains (see, e.g., 118). Iron is mostly condensed into grains and has a relatively high cosmic abundance. Those two facts together make iron an important contributor to the mass of refractory grains (121), and hence the iron depletion factor is likely to reflect the abundance of refractory elements in dust grains. Besides, in ionized nebulae iron is the refractory element with the strongest lines in the optical range of the spectrum.

In a previous work (113), we performed a homogeneous analysis of the iron abundance in a sample of 28 Galactic disk PNe and 8 Galactic H II regions. We obtained very low iron abundances in all the objects, implying that more than 90% of their total

iron abundance is condensed into dust grains. This suggests that iron depletes very efficiently in AGB stars and molecular clouds, whereas refractory dust is barely destroyed in the ionized gas of PNe and H II regions. Here, we extend our analysis to include 20 Galactic bulge PNe (observed by Wang & Liu 126), and study the dependence of the results on PN morphology.

2. The analysis

In H II regions and low ionization PNe, Fe^{++} and Fe^{+3} are the dominant ionization stages of iron. Due to the faintness of [Fe IV] lines, the gaseous iron abundance is usually calculated from the Fe^{++} abundance and an ionization correction factor (ICF) derived from photoionization models. However, for the handful of objects with measurements of [Fe III] and [Fe IV] lines, a discrepancy has been found between the abundance calculated with the aforementioned method and the one found by adding the abundances of Fe^{++} and Fe^{+3}. Rodríguez & Rubin (120) studied this discrepancy and derived three correction schemes that take into account what changes in all the atomic data involved in the calculations would solve the discrepancy: (1) a decrease in the collision strengths for Fe^{+3} by factors of ∼2–3, (2) an increase in the collision strengths for Fe^{++} by factors of ∼2–3, or (3) an increase in the total recombination coefficient or the rate of the charge-exchange reaction with H^0 for Fe^{+3} by a factor of ∼10. Since these three possibilities are equally plausible, and since the discrepancy could be due to some combination of them, the real value of the iron abundance will be intermediate between the extreme values derived with the three correction schemes.

As in our previous work, we select PNe with a relatively low degree of ionization ($I(\text{He II}\,\lambda4686)/I(\text{H}\beta) \lesssim 0.3$, see Delgado-Inglada et al. 113), and with moderate electron density (below 25 000 cm^{-3}), since high densities can be associated with large density gradients that introduce large uncertainties in the calculations. Besides, the objects have spectra with all the lines we need to calculate the physical conditions and the abundances of Fe^{++}, O^+, and O^{++}. We calculate a mean electron density and two electron temperatures (using the usual [N II] and [O III] diagnostic line ratios) for the low and high ionization regions; and with them we derive the O^+, O^{++}, and Fe^{++} abundances. To derive the total oxygen abundances we use the ICF from Kingsburgh & Barlow (115) and for iron the three ionization schemes of Rodríguez & Rubin (120). See Delgado-Inglada et al. (113) for more details on the procedure and on the atomic data we use. The uncertainties in all the quantities were estimated via Montecarlo simulations (Delgado-Inglada & Rodríguez, in prep.).

3. Results

Figure 1 shows the values of the Fe/O abundance ratio (left axis), and the depletion factors (right axis) for Fe/O: $[\text{Fe/O}] = \log(\text{Fe/O}) - \log(\text{Fe/O})_\odot$. We use the solar abundance from Lodders 117, $\log(\text{Fe/O})_\odot = -1.22 \pm 0.06$, as the expected total abundance. Filled symbols in this figure indicate the values derived using the correction scheme defined by point (3) above, while empty symbols represent the values obtained with the other two correction schemes. The real values are expected to be in the range defined by these three values. We find that both PNe and H II regions have consistently high

depletions factors, with more than 80% of their iron atoms condensed into dust grains. The differences between the Fe/O values derived with the three correction schemes depend on the degree of ionization of the objects: the higher the degree of ionization, the greater the difference in Fe/O values. Hence, the iron abundance is better constrained for the objects with $\log(O^+/O^{++}) \gtrsim -1.0$, where the differences between the correction schemes are $\leq$0.5 dex. No matter which correction scheme we consider, the range of depletions is wide in this region, with a difference in the iron abundance of a factor of ~100 between the objects with the lowest and the highest value. Although these variations should be reflecting real differences between the objects, we do not find any clear correlation between the iron abundances and parameters related to the nebular age (such as the electron density or the surface brightness of the PN) or with the dust chemistry (Delgado-Inglada & Rodríguez, in prep.). The first result suggests that no significant destruction of dust grains is taking place in these objects, and the second one argues for a similar efficiency of iron depletion in C-rich and O-rich environments.

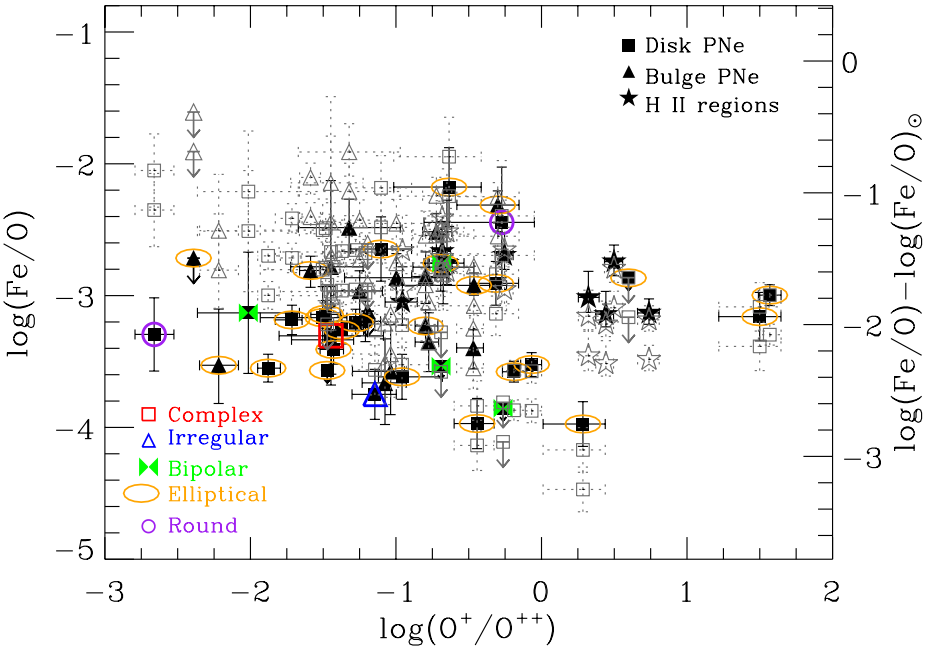

Figure 1. Values of Fe/O (left axis) and the depletion factors for Fe/O ([Fe/O] = log(Fe/O) – $\log(Fe/O)_\odot$, right axis) as a function of the degree of ionization. Three values of Fe/O are shown for each object, derived using the three correction schemes of Rodríguez & Rubin (120). The PNe are classified according to their origin (disk or bulge) and their morphology. See the text for more explanations.

Here, we explore the relation between the iron abundances of the sample PNe and their morphological types. There is some observational evidence that the morphological type of a PN is related to the progenitor mass. Symmetric PNe (round or elliptical nebulae) might descend from low mass progenitors, and asymmetric PNe (bipolar or more complex objects) might have the most massive progenitor stars (see, e.g., 111; 123). Asymmetric PNe have also been associated with binary systems (see, e.g., 111;

122; 112), and with stellar rotation and/or magnetic fields (see, e.g., 114). Although the reasons behind the shaping of PNe are still a matter of debate, we study here if there is a correlation between the morphologies and the iron depletion factors. Figure 1 shows the PNe morphologies given by the Planetary Nebula Image Catalog of Bruce Balick (PNIC*) and by Stanghellini et al. (124) for the 34 objects with available images. Two of them are classified as round, 26 as elliptical, four as bipolar, one as irregular, and one more as complex. This figure shows that there is no obvious trend relating the morphological type and the amount of iron condensed in dust grains. For example, elliptical and bipolar PNe are distributed in the whole range of depletions. The three correction schemes used in the abundance determination give consistent results on this issue.

4. Conclusions

We derive the iron abundance in a sample of 20 Galactic bulge PNe, and compare the results with the ones previously obtained for 28 Galactic disk PNe and 8 Galactic H II regions. We find high depletion factors in all the objects: less than 20% of their expected total number of iron atoms are measured in the gas phase. This result suggests that iron depletion into dust grains is an efficient process in AGB stars, whereas dust destruction is not very efficient in the subsequent PN phase. Although the range of depletions in the sample PNe is wide, covering around two orders of magnitude, we do not find any correlation between the iron depletion factors and the morphology of the PNe. Further details of the analysis will we presented in Delgado-Inglada & Rodríguez (in prep.).

Acknowledgments. We acknowledge support from Mexican CONACYT project 50359-F.

References

Corradi, R. L. M., & Schwarz, H. E. 1995, A&A, 293, 871
de Marco, O. 2009, PASP, 121, 316
Delgado-Inglada, G., Rodríguez, M., Mampaso, A., & Viironen, K. 2009, ApJ, 694, 1335
García-Segura, G., Langer, N., Różyczka, M., & Franco, J. 1999, ApJ, 517, 767
Kingsburgh, R. L., & Barlow, M. J. 1994, MNRAS, 271, 257
Lenzuni, P., Natta, A., & Panagia, N. 1989, ApJ, 345, 306
Lodders, K. 2003, ApJ, 591, 1220
Morton, D. C. 1974, ApJ, 193, 35
Pottasch, S. R., Baud, B., Beintema, D., Emerson, J., Harris, S., Habing, H. J., Houck, J., Jennings, R., & Marsden, P. 1984, A&A, 138, 10
Rodríguez, M., & Rubin, R. H. 2005, ApJ, 626, 900
Sofia, U. J., Cardelli, J. A., & Savage, B. D. 1994, ApJ, 430, 650
Soker, N. 1998, ApJ, 496, 833
Stanghellini, L., Guerrero, M. A., Cunha, K., Manchado, A., & Villaver, E. 2006, ApJ, 651, 898
Stanghellini, L., Villaver, E., Manchado, A., & Guerrero, M. 2002, ApJ, 576, 285
Stasińska, G., & Szczerba, R. 1999, A&A, 352, 297

*http://www.astro.washington.edu/users/balick/PNIC/

Wang, W., & Liu, X.-W. 2007, MNRAS, 381, 669
Whittet, D. C. B. 2003, Dust in the Galactic Environment (Bristol:IoP), 2nd ed.

Asymmetric Planetary Nebulae V
A. A. Zijlstra, F. Lykou, E. Lagadec and I. McDonald
Jodrell Bank Centre for Astrophysics, Manchester, UK © 2011

A new [OIII] λ5007 Å Galactic Bulge Planetary Nebula Luminosity Function

A. V. Kovacevic[1], Q. A. Parker[1,2], G. H. Jacoby[3] and B. Miszalski[4]

[1]*Macquarie University, Sydney, Australia*

[2]*Anglo-Australian Observatory, Sydney, Australia*

[3]*GMTO Corporation, CA, USA*

[4]*University of Hertfordshire, Hatfield, UK*

Abstract. The Planetary Nebulae Luminosity Function (PNLF) describes the collective luminosity evolution for a given population of Planetary Nebulae (PN). A major paradox in current PNLF studies is in the universality of the absolute magnitude of the brightest PNe with galaxy type and age. The progenitor central-star mass required to produce such bright PNe should have evolved beyond the PNe phase in old, red elliptical galaxies whose stellar populations are ∼10 Gyr. Only by dissecting this resolved population in detail can we attempt to address this conundrum. The Bulge of our Galaxy is predominantly old (150) and can therefore be used as a proxy for an elliptical galaxy, but with the significant advantage that the population is resolvable from ground based telescopes. We have used the MOSAIC-II camera on the Blanco 4-m at CTIO to carefully target ∼80 square degrees of the Galactic Bulge and establish accurate [OIII] fluxes for 80% of Bulge PNe currently known from the Acker and MASH catalogues. Construction of the [OIII] Bulge PNLF has allowed us to investigate placement of PNe population sub-sets according to morphology and spectroscopic properties the PNLF and most importantly, whether any population subset might constitute the bright end of the LF. Our excellent, deep data also offers exciting prospects for significant new PNe discoveries and [OIII] morphological studies.
Keywords. Planetary nebulae – Luminosity function

1. Introduction

For the past ∼20 yrs, the [OIII] PNLF has developed into a well-established and widely used reliable extra-galactic distance indicator, permitting accurate distance measurement for galaxies out to the Fornax and Virgo clusters (136; 133; 134). Ciardullo, Jacoby, & Ford (129) published the refined fit to the luminosity function:

$$N(M) \propto e^{0.307M}(1 - e^{3(M^*-M)}) \tag{1}$$

When the distance to the population is accounted for, the fit to the bright-end cut-off is found to have a precisely defined absolute magnitude of $M^* = -4.47^{+0.02}_{-0.03}$ (128). Except for a weak metallicity dependence (132), this bright-end cut-off is found

to be invariant to galaxy type or age. This fundamental inconsistency was outlined by Ciardullo et al. (130).

The central stars of the brightest planetaries have luminosities of ~6000 $L_{\odot}$, which infers masses of >0.6 $M_{\odot}$ (140) and consequently that they evolved through the main-sequence with a mass >2 $M_{\odot}$ (149). Stars with these relatively high masses only live for ~1-2 Gyr and therefore we do not expect to detect such stars in old populations such as elliptical galaxies that are ~10 Gyr old and have undergone no recent star formation. However, they are nonetheless observed in such old populations (for a more detailed discussion see Jacoby 135).

This paradox has seriously inhibited our understanding and interpretation of the observed invariability of the PNLF bright-end cut-off to population age. We propose to address this problem via construction of a new, significantly deeper Bulge PNLF to identify whether the bright-end of the luminosity function is comprised of PN that have evolved from old, population-II stars via some peculiar path to enhanced luminosity, e.g. through binarity (130), or whether it is primarily populated by younger, higher mass, bipolar nebulae of Type-I (148).

2. Optical observations and correcting for extinction

We obtained [OIII] photometry for 435 previously known and MASH PN (146; 141) in a $10^{\circ} \times 10^{\circ}$ region toward the Galactic Bulge (138). From these data, we measured [OIII] fluxes and angular diameters, both of which were in agreement to within the errors of the most trusted literature sources. Previously, only 48 PN in this region had published [OIII] fluxes, so we are increasing the number of PN with fluxes by a factor of eight. These data provide accurate fluxes and diameters for the largest sample of PN towards this region of the Bulge ever published.

Optical observations made toward the Galactic Bulge are subject to a large amount of patchy and highly variable interstellar absorption and scatter due to dust along the line-of-sight. It is therefore important to ascertain the magnitude of extinction towards PN individually. We note that by correcting for the amount of dust towards each PN, we are also correcting for the dust internal to the nebula shell. This is not done for extragalactic PNLF studies, where a singular global extinction correction is applied to all PN. Accounting for this in PN that have evolved from high-mass central stars, where their inherently large dust content would usually act to self-extinct their bright [OIII] emission, may prove detrimental and place them at a significantly higher value than M^{*}. This has also been observed when correcting the extinction towards individual PN for PNLF construction in the Bulge of M31.

To deredden our fluxes we undertook spectroscopic observation of ~400 PN towards the Galactic Bulge (see Miszalski et al., 2009a). For ~350 of these objects which also had [OIII] photometry, we obtained Balmer decrement measurements with which to derive extinction estimates. These data are given in Kovacevic et al. (139).

3. The new Galactic Bulge [OIII] PNLF

Previously defined criteria to identify and exclude disc PN from any Bulge PNLF construction are more assumption than fact, having never undergone rigorous testing. We re-evaluate and re-define the criteria required for PN Bulge membership in terms of

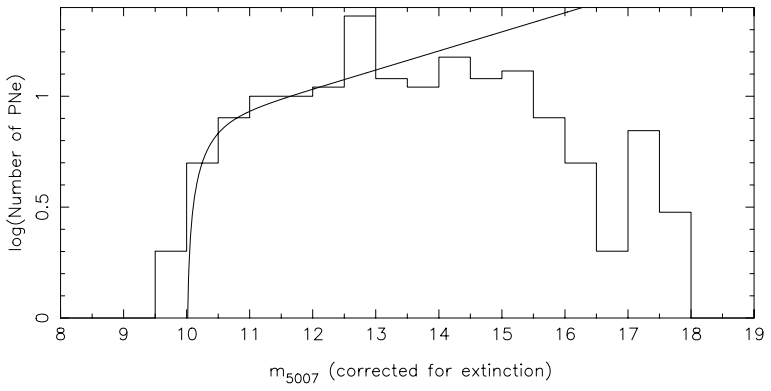

Figure 1. The [OIII] luminosity function for Galactic Bulge Planetary Nebulae.

location, radio flux, radial velocity, surface brightness and radio and optical angular diameters.

With this disc-cleaned sample, we present a new, preliminary version of the [OIII] PNLF (Fig. 1). After fitting equation 1 to the distribution, we calculate the bright-end cut-off has an absolute magnitide of -4.38 ± 0.13, assuming a distance to the Galactic Centre of 7.52 kpc (144). This agrees, to within the errors, with the canonical value of $M^* = -4.47^{+0.02}_{-0.03}$ (128). The high-resolution of the MOSAIC-II Imaging has permitted preliminary elucidation of morphology of some Bulge PN for the first time. This, together with SHS Hα images (145) and other imagery where it exists in the literature, will enable us to assign more conclusive morphological classifications from a multi-wavelength approach.

Interestingly, within our sample, we find that neither Type I nor bipolar PN populate the bright-end in agreement with Jacoby & De Marco (137). Instead they dominate the faint end of the SMC PNLF, perhaps as a consequence of fast evolution and a high amount of dust present.

4. Future work

Our [OIII] data not only allows for accurate measurement of fluxes, diameters and identifcation of morphologies of PN, but also, the sensitivity attained has permitted the discovery of faint nebular extensions pertaining to previous periods of mass loss in some PN. This is exemplified by the case of IC 4673 (see Fig. 2), where a halo surrounds the PN (131) together with external east-west arcs which could signifiy the presence of a binary central star (143). The depth of the survey data has also allowed for discovery of numerous faint new PN candidates. The [OIII] images of PN and extensions around PN will be made available online in the near future.

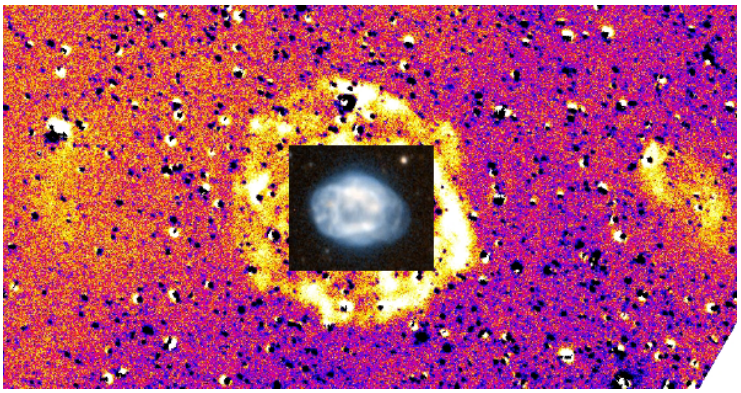

Figure 2. A faint halo of emission and external arcs detected around IC 4673. Inset image taken from Schwarz, Corradi, & Melnick (147).

5. Conclusions

We provide accurate [OIII] fluxes and angular diameters for the largest sample of PN in the 10° ×10° region toward the Galactic Bulge ever obtained. We obtained optical spectroscopy to provide accurate measurement and derivation of the reddening corrections towards ~350 of the PN with [OIII] fluxes. The general criteria considered for Bulge membership was re-defined, and implemented to exclude any disc PN. This cleaned sample was then used to construct our preliminary new Galactic Bulge PNLF.

This is the deepest Bulge PNLF ever constructed, ranging over 8 orders of magnitude and is complete to 4 magnitudes below M^*. The fit to the bright-end cut-off has an absolute magnitude of $M^* = -4.38 \pm 0.13$, using a distance of 7.52 kpc. After a brief analysis of high quality spectra from the literature, the PN constituents residing in the brightest bins are not found to be of Type-I or have bi-polar morphology.

Acknowledgments. AVK acknowledges Macquarie University for a PhD scholarship and the Astronomical Society of Australia for travel assistance.

References

Ciardullo R. et al., 2002, ApJ, 577, 31
Ciardullo R., Jacoby G. H., Ford H. C., 1989, ApJ, 344, 715
Ciardullo R., Sigurdsson S., Feldmeier J. J., Jacoby G. H., 2005, ApJ, 629, 499
Corradi R. L. M., Schönberner D., Steffen M., Perinotto M., 2003, MNRAS, 340, 417
Dopita M. A., Jacoby G. H., Vassiliadis E., 1992, ApJ, 389, 27
Feldmeier J. J., Jacoby G. H., Phillips M. M., 2007, ApJ, 657, 76
Gerhard O. et al., 2007, A&A, 468, 815
Jacoby G. H., 1997, IAUS, 180, 448
Jacoby G. H., Ciardullo R., Ford H. C., 1990, ApJ, 356, 332
Jacoby G. H., De Marco O., 2002, AJ, 123, 269
Kovacevic, A. V. et al., 2010, MNRAS, submitted.
Kovacevic, A. V. et al., 2010, in prep.
Marigo P., Girardi L., Weiss A., Groenewegen M. A. T., Chiosi C., 2004, A&A, 423, 995
Miszalski B. et al., 2008, MNRAS, 384, 525
Miszalski B., Acker A., Moffat A. F. J., Parker Q. A., Udalski A., 2009a, A&A, 496, 813

Miszalski B., Acker A., Parker Q. A., Moffat A. F. J., 2009b, A&A, 505, 249
Nishiyama S., et al., 2006, ApJ, 647, 1093
Parker Q. A., et al., 2005, MNRAS, 362, 689
Parker Q. A., et al., 2006, MNRAS, 373, 79
Schwarz H. E., Corradi R. L. M., Melnick J., 1992, A&AS, 96, 23
Torres-Peimbert S., Peimbert M., 1997, IAUS, 180, 175
Weidemann V., 2000, A&A, 363, 647
Zoccali M., et al., 2003, A&A, 399, 931

Asymmetric Planetary Nebulae V
A. A. Zijlstra, F. Lykou, E. Lagadec and I. McDonald
Jodrell Bank Centre for Astrophysics, Manchester, UK © 2011

A New Luminosity Function for PNe in the Large Magellanic Cloud

Warren A. Reid & Quentin A. Parker

Macquarie University, Sydney, Australia

Abstract. A deep AAO/UKST Hα multi-exposure stack of the LMC's central 25deg^2 was used to uncover several thousand candidate emission line sources. Follow-up confirmatory spectroscopy by the 2dF and FLAMES multi-object spectroscopy systems on the AAT and ESO VLT led to the discovery of 460 new LMC PNe while independently recovering all 169 previously known PNe in the LMC's central area.

This work is now being extended to the outer regions of the LMC through access to the Magellanic Cloud Emission Line Survey (MCELS) data where several thousand additional compact emission candidates have been found. Subsequent preliminary follow-up spectroscopy on the 2dF AAOmega system on the AAT has so far led to a further 90 new faint PNe being discovered from the first half of our observing program which aims to cover 56 deg^2 of the outer LMC. Again all 68 previously known PNe in the region surveyed so far were independently recovered.

Our new LMC planetary nebula luminosity function (PNLF), complete to 7 mag below the brightest and based on PNe within the central 25 deg^2 region, will be extended to include the new discoveries in the outer LMC. This will provide a unique probe into the LMC's chemical and dynamical evolution. The shape of the function depends on the central star mass and on the variation of the nebula optical depth with time. This makes the overall shape of the [O III] 5007 PNLF an important diagnostic for galactic chemical evolution. In particular, the faint end of the function reflects core stellar evolution. For the first time we present and compare the [O III] 5007 PNLF corrected for foreground reddening with the same objects corrected for internal extinction.
Keywords. Planetary nebulae – Luminosity function

1. PNe survey extended to the outer LMC

Reid & Parker (2006b)[RPb] previously used their deep AAO/UKST Hα multi-exposure stack of the LMC's central 25 deg^2 (Reid & Parker 2006a, RPb) to discover 460 new PNe confirmed by 2dF while independently recovering all 169 previously known PNe in the central area. A large fraction of new LMC PNe are $\geq 3\times$ fainter than those previously known, tripling numbers accrued from all surveys over the last 80 years. These data have led to significant advances in our understanding of the kinematical sub-structure of the central LMC including improved determination of LMC rotation, inclination and transverse velocity (RPb) as well as better elucidation of the old stellar population and a significantly improved PNLF (Reid & Parker 2010). Crucially, however, these data refer only to the LMC's central zone which may not be representative

of outer regions. The Magellanic Cloud Emission-line Survey (MCELS)*, provides the base data for significantly improved, more complete results across the entire LMC as it incorporates the outer ~56 deg^2 not previously covered.

Using the UM/CTIO Curtis Schmidt telescope coupled to a 2K x 2K CCD, the MCELS data consists of an Hα, [SII] 6716-6731 and [OII] 5007 map of the LMC. Despite relatively large 3 arcsec pixels, MCELS has a good capability to detect faint Hα emitters. In the combined images (shown in Figure 1) the Hα map is coloured red, the [SII] map is coloured green and the [O III] map is coloured blue. Careful matching of intensities allows candidate planetary nebulae to appear pink. A white centre indicates a bright candidate.

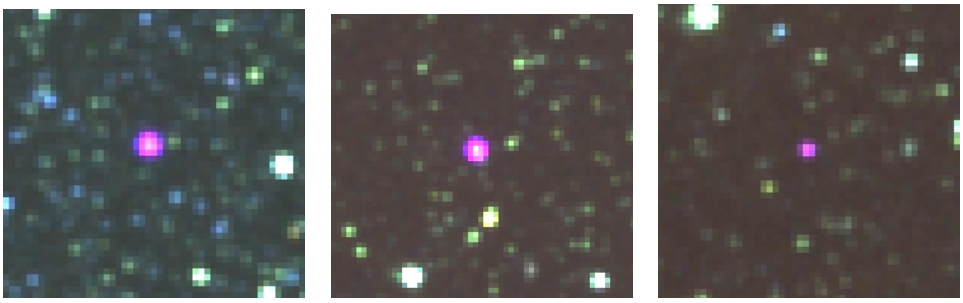

Figure 1. *Left to right:* Discovery images of RP2243, RR2110 and RP6291.

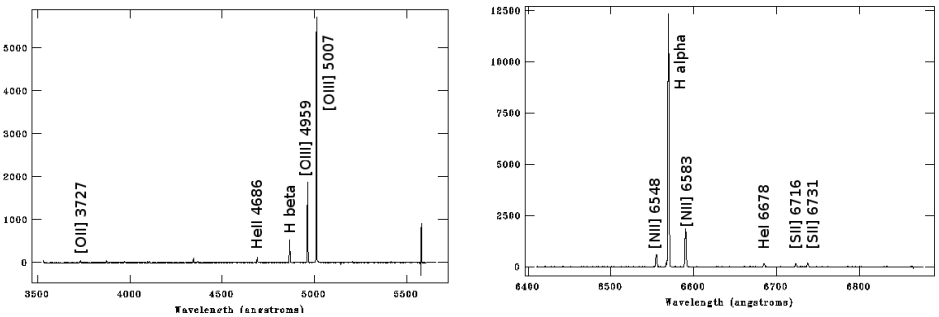

Figure 2. AAOmega B-band (left) and R-band (right) spectroscopic confirmations of PN RP2243.

Spectroscopic confirmation of the entire MCELS candidate PNe sample, uncovered by our processing techniques (RPb) for zones outside the original AAO/UKST survey region (see Figure 2) will allow precise determination of the PN distribution and kinematics across the entire LMC, never possible before for a whole galaxy. Following our initial confirmatory spectroscopy, we have already been able to confirm more than 90 new LMC PNe together with hundreds of other new emission sources.

*see http://www.ctio.noao.edu/mcels/

2. A new deep PNLF for the central 25 deg^2 of the LMC

We have been able to provide the most complete, deep and accurate PNLF ever assembled for an outer galaxy. This can be used to accurately predict the number of stars in the PN evolutionary stage in each luminosity bin compared to the luminosity and mass of the whole galaxy. This is not currently possible for any galaxy other than the LMC/SMC, as dust obscures too much of our own Galaxy and other galaxies are too distant to identify faint PNe. The well determined 49.2 Kpc LMC distance (Reid & Parker 2010), modest, 35 degree inclination angle and disk thickness (~500pc van der Marel & Cioni 2001), mean that LMC PNe are effectively co-located. With low extinction, we can better estimate absolute line fluxes.

The PNLF for the central 25 deg^2 of the LMC (shown in Reid & Parker 2010) is derived from an homogeneous sample of previously known and new RP LMC PNe. To use the PNLF for distance determination, the data have only been corrected for line of sight reddening, binned into 0.2 mag intervals and plotted in log space.

Only foreground reddening is used to determine extragalactic distances. This is because none of the measured PNLFs and simulations to date have included the effects of circumstellar dust which plays a large part in determining the observed brightness of the PNLF bright end. In order to make the correct comparison, our PNLF (see Figure 9 in Reid & Parker 2010) for distance determination has only been corrected for foreground reddening. The contribution of Galactic dust was removed assuming a foreground reddening value of E(B-V) = 0.074 (Caldwell & Coulson, 1986).

The [O III] 5007 PNLF may be represented by an exponential curve with a sharp truncation designed to accommodate the bright end (Ciardullo et al. 1989):

$$N(M) \propto e^{0.307M}\{1 - e^{3(M^*-M)}\} \quad (1)$$

In this equation, the key parameter M^* is the absolute magnitude of the brightest possible PN in the system. The limit to the high luminosity of the [O III] 5007 line is mainly due to the initial mass of the progenitor star and its evolution to a white dwarf as a function of time in the ranges of 3-11 Gyrs (Jacoby, 1989). This PNLF model has been demonstrated as an excellent standard candle when compared to other distance indicators (Ciardullo, 2006). In order to reveal the effects of dust, internal to the LMC and the environment of each individual PN, we include another PNLF (Figure 3) where the same objects have been corrected for what we will refer to as 'internal extinction' using the Balmer decrement. Both functions have been plotted on the same scale in order to clearly demonstrate the offset caused by extinction.

With most external galaxies, it is almost impossible to correct each observed PN for the effects of internal extinction. Remarkably however, Figure 3 implies that the one dimensional PNLF of external galaxies can be modeled by simply applying a mean offset, since the shape of the observed and de-reddened PNLFs are essentially identical. This result is rather surprising since although individual object extinctions vary between $0 < c\mathrm{H}\beta < 1.3$ (0 - 2 mag), the PNLF responds as though each PN has $c\mathrm{H}\beta = 0.4$.

PNe in the brightest 4 magnitudes have low to medium extinction (0 to 0.6) while PNe with medium to high extinction (>0.6) are only found > 4 magnitudes below the brightest. These highly reddened faint PNe probably have intrinsically fainter cores, evolving over a longer timescale. It is therefore possible that the dust properties of these objects may be rather different to those of the higher-core mass objects. Most of the

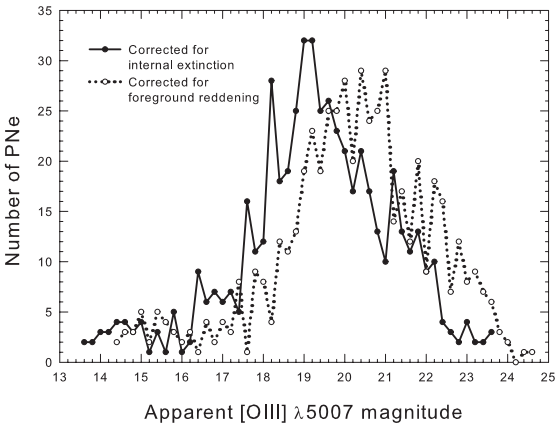

Figure 3. Comparison of the LMC PNLF corrected for foreground reddening and then corrected for internal extinction. Despite variations in $c\mathrm{H}\beta$ ranging between 0 and 1.4 for individual objects, the overall PNLF simply shifts 1 magnitude brighter after correction for internal extinction.

PNe are located in the low to medium extinction range. This suggests that, regardless of the diminishing intrinsic luminosity as a consequence of age, a large proportion of these PNe with high-mass cores have evolved fairly rapidly and their surrounding circumstellar envelope, which provides the extinction, have remained of similar opacity.

A new updated PNLF covering the entire LMC using our new discoveries, complete to 7 mag below the brightest, will provide a unique probe into the LMC's chemical and dynamical evolution. The mass and metallicity of the progenitor star largely determines the maximum [O III] line luminosity of the PN (Dopita et al. 1992). This makes the overall shape of the [O III] PNLF an important diagnostic for galactic chemical evolution. The bright end does not carry information about the underlying stellar populations. The faint end should reflect core evolution as well. With confirmatory spectroscopy for over a hundred newly discovered and 130 previously known PNe in the LMCs outer structure, we now have the kinematic and abundance data required to probe the structure and origin of the entire LMC system (e.g. Jacoby 1999).

3. Bibliography

Caldwell J.A.R. & Coulson I.M., 1986, MNRAS, 218, 223
Ciardullo R., Jacoby G., Ford H.C., Neill J.D., 1989, ApJ., 339, 53
Ciardullo R., 2006, proceedings ESO Workshop "Planetary Nebulae beyond the Milky Way", (eds.) L. Stanghelini, J. Walsh, N.G. Douglas, ESO astrophysics symposia, 91
Dopita M.A., Jacoby G.H., Vassiliadis E., 1992 ApJ 389, 27
Jacoby G.H., 1989, ApJ, 339, 39
Jacoby, G.H., Ciardullo R., Feldmeier John J., 1999 ASP Conf. Series, vol.167, p.175
Reid W.A. and Parker Q.A., 2006a, MNRAS, 365, 401
Reid W.A. and Parker Q.A., 2006b, MNRAS, 373, 521

Reid W.A. and Parker Q.A., 2010, MNRAS, 405, 1349
van der Marel R.P., et al. 2001 ApJ 122, 1827

Asymmetric Planetary Nebulae V
A. A. Zijlstra, F. Lykou, E. Lagadec and I. McDonald
Jodrell Bank Centre for Astrophysics, Manchester, UK © 2011

Symmetric vs. asymmetric planetary nebulae: morphology and chemical abundances

W. J. Maciel and R. D. D. Costa
Astronomy Department, University of São Paulo, Rua do Matão 1226, 05508-090 São Paulo SP, Brazil

Abstract. We analyse a large sample of galactic planetary nebulae based on their chemical composition and morphology. A recent morphological classification system is adopted, and several elements are considered, namely He, N, O, S, Ar, Ne, and C in order to investigate the correlations involving these elements and the different PN types. Special emphasis is given to the differences between symmetric (round or elliptical) nebulae and those that present some degree of asymmetry (bipolars or bipolar core objects). The results are compared with previous findings both for PN in the Galaxy and in the Magellanic Clouds.

Keywords. Planetary Nebulae – Abundances – Morphology

1. Introduction

Planetary nebulae (PN) may have different morphological aspects, as made evident by many classification schemes proposed since the pioneering work of Curtis (1918). Different morphologies are probably related to different physical origins, which may include the effects of different stellar masses, binary evolution, magnetic fields, etc. As a consequence, the observed variety of PN morphologies is associated with different physical properties, which include their chemical abundances. In this work, we consider a large sample of PN in the Galaxy for which high resolution optical images and accurate abundances are available, and investigate the relationship between the morphological characteristics and the chemical abundances, especially concerning symmetric and asymmetric nebulae.

2. Morphology, abundances, and stellar evolution

Generally speaking, the observed morphologies of PN can be interpreted either as the result of projection effects on a basic tridimensional structure or as a result of different physical processes affecting the PN origin and evolution. Recent work seems to favour the second approach, so that we will adopt the scheme proposed by Stanghellini et al. (1993) and later updates, and look for correlations involving the morphologies and the nebular chemical abundances. The PN types are: Round (R), Elliptical (E), Bipolar (B), Bipolar-core (BC), and Point symmetric (P). Although some nebulae do not fit exactly

in this scheme, most objects for which detailed high-resolution images are available can be classified in one of these types.

According to some previous results on the relationship between the morphology and the evolution of intermediate mass stars (IMS) that originate the planetary nebulae, bipolar nebulae seem to be formed by relatively massive progenitor stars, those closer to the high mass limit of the IMS. This is consistent with some characteristics of these nebulae, such as a lower scale height relative to the galactic plane or higher helium and nitrogen abundances. The He and N enhancements can be expected in bipolar nebulae if they are originated from the higher mass IMS, for which the dredge-up and Hot Bottom Burning (HBB) processes lead to a reduction in the C abundances, while the He/H and N/O ratios are enhanced. On the other hand, most elliptical and round PN seem to be formed by lower mass stars, those closer to one solar mass on the main sequence.

3. The sample

In this project we take into account elements that are manufactured by the PN progenitor stars (He, N, and C), as well as some elements that are not (O, Ne, S, and Ar). We have inspected many high resolution images and compared our results with previous classifications in the literature. The results reported here refer to two samples of galactic PN, which are probably the largest samples for which *both* the morphology *and* chemical abundances have been analysed: Sample A, with 234 nebulae, includes PN in the Milky Way disk, as recently analysed by Maciel et al. (2003) [see also Maciel et al. (2010) and references therein], and Sample B, which includes the PN of Sample A, supplemented by several galactic objects for which recent abundances have been determined in the literature. This sample is in principle less accurate than Sample A, but is considerably larger, presently including 372 nebulae.

4. Results

The main results are shown in Tables 1 and 2, and in Figure 1. For the sake of completeness, we have included the less accurate C/H data from the literature, in view of its importance in reflecting the nucleosynthesis of PN progenitor stars. From Table 1 we note that symmetrical PN (R, E) are more frequent in the Milky Way than asymmetric (B, BC, P) objects, both for Sample A and B. From these samples, bipolars correspond to approximately 25% of all galactic nebulae. As a comparison, the corresponding numbers for the Magellanic Clouds from Stanghellini (2009) are 46% (S) and 54% (A) for the LMC and 64% (S) and 36% (A) for the SMC. However, it should be mentioned that the samples considered are not complete, which also applies to the Magellanic Clouds.

Table 2 shows the elemental abundances defined as usual, $\epsilon(X) = \log (X/H) + 12$. It can be seen that both samples A and B reveal the same trends, that is (i) there is a continuous increase in the He/H abundances in the sequence *Symmetric – All – Asymmetric* PN, that is, asymmetric nebulae have systematically larger He/H abundances than symmetric objects; (ii) the same is true for the N/H and N/O ratios, and (iii) the inverse is true for the C/H ratio. Exactly the same trends are observed in Magellanic Cloud nebulae for the ratios C/H, N/H, and N/O, according to Stanghellini (2009). Therefore, these trends appear to hold for objects of different metallicities. These results confirm

Table 1. Distribution of the galactic PN according to the morphological types

Type	Sample A	Sample B
Round = R	24.8	21.2
Elliptical = E	31.2	30.1
Bipolar = B	16.2	16.7
Bipolar Core = BC	6.4	7.0
Point-symmetric = P	3.0	1.9
Unclassified = U	18.4	23.1
Symmetric = S	56.0	51.3
Asymmetric = A	25.6	25.5

Table 2. Average abundances of symmetric and asymmetric galactic PN

	Sample A	Sample B
He/H: All	0.114 ± 0.024	0.113 ± 0.025
Symmetric	0.107 ± 0.018	0.104 ± 0.019
Asymmetric	0.129 ± 0.027	0.132 ± 0.027
O/H: All	8.63 ± 0.26	8.59 ± 0.28
Symmetric	8.60 ± 0.26	8.55 ± 0.28
Asymmetric	8.66 ± 0.27	8.64 ± 0.25
S/H: All	6.88 ± 0.35	6.87 ± 0.37
Symmetric	6.82 ± 0.29	6.82 ± 0.24
Asymmetric	6.92 ± 0.40	6.92 ± 0.38
Ar/H: All	6.39 ± 0.31	6.37 ± 0.33
Symmetric	6.33 ± 0.29	6.30 ± 0.31
Asymmetric	6.48 ± 0.31	6.47 ± 0.32
N/H: All	8.14 ± 0.44	8.10 ± 0.46
Symmetric	8.02 ± 0.39	7, 94 ± 0.43
Asymmetric	8.34 ± 0.42	8.37 ± 0.40
Ne/H: All	7.96 ± 0.26	7.94 ± 0.31
Symmetric	7.95 ± 0.24	7.91 ± 0.28
Asymmetric	8.01 ± 0.28	8.02 ± 0.30
C/H: All	8.67 ± 0.37	8.66 ± 0.39
Symmetric	8.74 ± 0.28	8.71 ± 0.34
Asymmetric	8.47 ± 0.47	8.51 ± 0.45

that the asymmetric nebulae are probably originated from the higher mass IMS, while the symmetric objects come from progenitor stars with lower masses.

Figure 1 shows the differences $\Delta\epsilon = \epsilon - \epsilon(\text{all})$ for all elements for Sample A. It can be seen more clearly that the He and N abundances increase for asymmetric PN, while the opposite is true for C. A similar behaviour occurs for the elements that are not produced by the PN progenitor stars (O, S, Ne, and Ar). However, the abundance variations of these elements are relatively small, and probably reflect the fact the asymmetric nebulae are formed by more massive, younger stars, which are themselves formed out of an enriched interstellar medium. In the case of He, it should be recalled that the

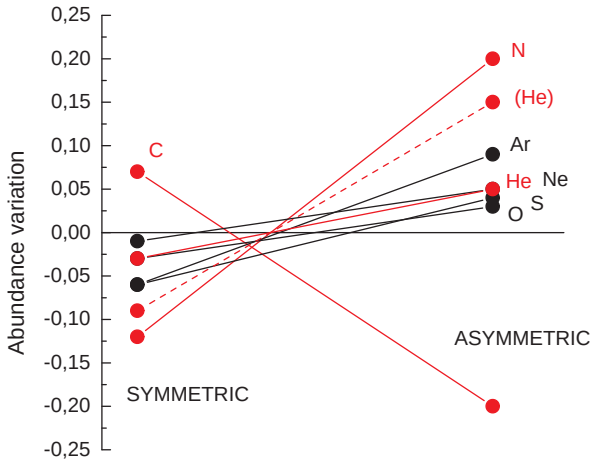

Figure 1. Abundance variations between symmetric and asymmetric PN.

abundance uncertainties are about a factor 3 smaller than for the heavier elements, so that in practice the variation in the He abundances in Figure 1 could be better represented by the dashed line shown in the figure. These trends are in good agreement with recent theoretical models by Marigo (2001) and Karakas & Lattanzio (2007).

It should be noted that some bipolar nebulae do not show He or N enhancements, which may be explained by their origin being related to common envelope as a consequence of binary star evolution. The fact that there is some measurable He and N enhancements in most B or BC nebulae suggests that common envelope evolution is probably a secondary aspect of PN formation. For example, in Sample A, 72% of the B/BC nebulae have enhanced He/H abundances (He/H > 0.120), while for 28% of the objects the He/H ratio is normal, that is He/H < 0.120, suggesting that about one third of the bipolar nebulae have common envelope origin.

Acknowledgments. This work was partially supported by FAPESP/CNPq.

References

Curtis, H. D. 1918, Publ. Lick Obs. Vol. XIII, Part III, 57
Karakas, A., Lattanzio, J. C. 2007, PASA 24, 103
Maciel, W. J., Costa, R. D. D., Idiart, T. E. P. 2010, A&A 512, A19
Maciel, W. J., Costa, R. D. D., Uchida, M. M. M. 2003, A&A 397, 667
Marigo, P. 2001, A&A 370, 194
Stanghellini, L. 2009, IAU Symp. 256, ed. J. T. van Loon, J. M. Oliveira, CUP, 421
Stanghellini, L., Corradi, R. L. M., Schwarz, H. E. 1993, A&A 279, 521

Asymmetric Planetary Nebulae V
A. A. Zijlstra, F. Lykou, E. Lagadec and I. McDonald
Jodrell Bank Centre for Astrophysics, Manchester, UK © 2011

Mass loss at the AGB and beyond and the asymmetry conundrum

Javier Alcolea

Observatorio Astrómico Nacional (I.G.N., M. Fomento, Spain)

Abstract. In this review I will summarize what the observations of the molecular envelopes around AGB and early post-AGB stars tell us about the way these objects loose mass. Although there is growing observational evidence of the effects of the binarity on the the mass loss at the AGB, the problem of explaining the shapes and dynamics of pPNe still persists, at least from a statistical point of view.

Keywords. Planetary Nebulae – Stars: AGB and post-AGB

1. Introduction: molecules in the envelopes of AGB and early post-AGB sources

One of the yet most intriguing aspects of stellar evolution is how stars like our Sun can lead to the formation of Planetary Nebulae (PNe), which probably are amongst the most bizarre objects we can find in Space. Our current understanding is that PNe are the result of the (post-AGB) evolution of the circumstellar envelopes (CSEs) around red giant and super-giant stars, which in turn are the result of the heavy mass loss that these stars undergo while at the AGB and red super-giant (RSG) phases. In addition, this mass loss process is the main agent driving the ultimate evolution of low/intermediate mass stars, specially at the very end of the AGB, where mass loss rates as high as several $10^{-5}\,M_{\odot}\,yr^{-1}$ can be attained. Furthermore, when these CSEs are lost in the ISM, modify the chemical composition of the latter, resulting and increasing metallicity. These envelopes are also the main factories for the formation of space dust grains.

The evolution of these nebulae/envelopes includes a drastic transformation both in shape and kinematics, from the simple spherical and radially expanding CSEs, to the full variety of forms and velocity fields displayed in the PN zoo. It is believed that this metamorphosis is due to a mechanism that either starts operating at the late AGB or early post-AGB phases, or, if present before, it does not reveal itself till these stages of late stellar evolution.

To better study this transformation process and the mechanism behind, we must target nebulae around AGB stars, i.e., regular CSEs, or early post-AGB stars, the so called pre-Planetary Nebulae (pPNe). In either case, the central stars are still too cool to ionize the nebulae around them, and so CSEs and pPNe mostly consist in molecular gas and a just bit (1% or even less) of dust grains. This is only true for distances to the central object smaller than the photo-dissociation radius, and may not hold for stars with very hot companions. Due to this composition, the best way to study these objects is by means of molecular line observations, since they trace the most abundant component of the envelopes. In fact, by observing the molecular gas, we can not only know about the

mass of the envelope (and its gravitational energy), but also about its dynamics (linear momentum and kinetic energy), temperature (by studying and modeling the excitation of the gas), and chemical composition. Some molecules can also tell us about the properties of the magnetic field in these objects and their central stars (see contribution by W. Vlemmings in this volume). As compared with dust studies, molecular line observations of CSEs and pPNe are less affected by extinction problems (and when they exist it can be easily modeled), and can provide high spatial (sub-arcsecond) and spectral (better than $1\,\mathrm{km\,s^{-1}}$) resolution images of these objects.

The best tracer of the molecular gas is CO. This is the most abundant circumstellar molecule, apart from H_2, regardless of the chemical composition. In addition, CO has the largest photo-dissociation radius, and can probe the CSE up to distances of several 10^{16} cm (and the mass loss history for the latest several thousand yr) for high mass loss rates. Furthermore, CO is very easy to interpret and model, allowing a very reliable determination of the parameters of the envelope from the observations. I will mainly focus on CO observation in this review.

These observations reveal that, although inhomogeneities are present at small scales, envelopes around AGB stars are in general quite spherically symmetric at larger scales. Quasi-periodic variations in the mass loss rate are also detected, but yet preserving the overall roundish shape of these envelopes. This may not be case of semiregular variables and symbiotic systems, were a significant prevalence of aspherical structures is being detected. On the contrary, pPNe appear as much bizarre as PNe, displaying a large variety of shapes and kinematics: self-similar structures in which the expansion velocity is proportional to the distance to the central stars, hour-glass structures, Keplerian rotating disks, jets working their way out inside fossil AGB CSEs, multipolar winds, etc. In summary, from the point of view of the molecular line observations, the enigma of the AGB-CSE $\Rightarrow$ pPN $\Rightarrow$ PN transformation is still present.

2. Are the CSEs of AGB stars indeed round ?

On first place, we should address the question of whether CSEs around normal AGB stars are really round, as opposite to those of post-AGB sources. Based on the results from the large sample mapped by Neri et al. (179) more than 10 yr ago, the answer would be definitively yes. However these observations have just $5''$ to $12''$ resolution, and we may wonder what would happen if we had a closer look at these objects. Let's take for example the case of IRC +10216 (a.k.a. CW Leo). This is by far the best studied AGB envelope, and the prototype of a massive C-rich CSE. If we have a look very close to the star, in the layers were the envelope is affected by the periodic pulsations, K-band Speckle interferometry shows an evolving clumpy structure, far from being spherically symmetric but showing no other particular symmetry: the result of a random ejection of blobs of matter (see 183).

If we move farther out, where the final expansion velocity has been reached, the envelope displays a set of (disrupted) concentric arcs both in the light reflected by the circumstellar dust (174) and in the emission of some molecules (Dinh-V-Trunh & Ling, 2008). A roughly spherical symmetry dominates the envelope, though the presence of these rings speaks in favor of episodes of enhanced mass loss, or rather of the presence of a companion (see review by A. Raga in this volume). The CSE is mostly isotropic even chemically (as several cyanopolynes show ring link distributions), im-

plying a fairly good spherical symmetry in density, temperature, and even chemical abundances. Yet farther out, where molecules become destroyed and the CSE interacts with the ISM, images still show the signatures of an envelope that is round at a large scale (180). We can also map the cold dust in the outskirts of the envelope, since this solid phase survives beyond the photo-dissociation radius. A recent APEX/LABoCa image of IRC 10216 at 870 μm by (173) reveals a quite round structure at scales of 100″.

Another well studied example is the O-rich envelope around WX Psc (a.k.a. IRC +10011). Again, close to the star, where pulsation affects the CSE layers, the dust is not fully formed, and the expansion of envelope has not yet attained its terminal velocity, high resolution VLBA images of SiO masers show an evolving clumpy structure, far from being perfectly spherically symmetric, but showing no other permanent symmetry (see 182). More examples can be found in the works by Cotton, Boboltz, Diamond, Wittkowski and others using the VLBA (sometimes in combination with the ESO/VLTI), and more recently by Kamohara, Rioja, Kobayashi and others using the Japanese VERA array (see review by M. Wittkowski in this conference).

Farther out, when the final expansion has been reached, the bulk of the envelope can be studied by high (spatial and spectral) resolution images of low-J rotational transitions of CO, as Castro-Carrizo et al. (164) have done using the IRAM telescopes in the COSAS program. Results for WX Psc show an envelope quite round at the center but displaying some less regular structure in the outer shells. Once again, the APEX/LABoCa map of the cold dust in the sub-mm wavelength by Ladjal et al. (173) looks very round too.

Obviously just a few examples is not enough. What we need is a statistical approach to the problem, and this is the main objective of the COSAS program, a *CO Survey of AGB (and beyond) Stars*. This is an IRAM large program aiming to map the ^{12}CO J=1–0 and 2–1 emission in a sample of 45 evolved stars, with spatial resolutions of about 1″–2″. Somehow it is an improved version of the work by Neri et al. COSAS combines the high spatial resolution of the IRAM Plateau de Bure Interferometer (PdBI), with the ability of mapping large structures of the IRAM 30 m Millimeter Radio Telescope (30m-MRT). All the flux lost by the PdB interferometer is recovered by the addition of the maps from the 30m-MRT, so both the details and the large structures in the envelopes are present in the maps. The results of the survey will be published in 3 papers, the first of which is already in press (see 164). This first paper includes the results from a total of 9 regular variables (i.e. Mira and OH/IR stars), namely: IK Tau, TX Cam, CRL 2362, χ Cyg, V Cyg, S Cep, R Cas, OH 104.9+2.4, and the aforementioned WX Psc. These stars show envelopes that are round or just slightly elongated, but other features like rings, arcs, spirals, inner winds are also present. In all cases, the expansion velocities are standard for AGB envelopes, and the associated mass loss can be simply explained by photon pressure on the basis of linear momentum conservation.

For example, for IK Tau a roundish shape is found both in the inner and outer parts of the envelope. The outer halo is very clumpy and a strong self-absorption is seen in the blue end of the line, that could be due to a slightly faster wind present in the inner shells of the envelope (although radiative transfer effects could also explain it). A similar feature is also detected in the CSE around χ Cyg. In R Cas the envelope is round and very clumpy, but azimuthal averaged profiles reveal the existence of two

rings of enhanced emission, very similar to the ones detected in some AGB and post-AGB sources in dust scattered light. TX Cam also displays a very round envelope, but a hook-like feature is detected at the center of the nebula. This feature could be a spiral structure similar to the one detected in CRL 3068 (177). These two types of structures (rings and spirals) can be produced by the presence of long period companions in the system (see Raga in this proceedings). The carbon star V Cyg has a CSE that shows a triangular shape in its outer layers, but note that in this case there is some degree of interstellar contamination in the maps.

2.1. The case of semi-regular variables

Special attention should be given to giant semi-regular variables (SRs). These are AGB stars showing a regular variation in the optical, but with less amplitude than Miras (< 2.5 mag), SRa variables, or slightly irregular variations, SRb, SRc and SRd variables. A priory this difference should not affect the mass loss geometry and kinematics, though it may be the case that slow amplitude pulsators drive less powerful winds. However, the CSEs around SR variables show a very distinct characteristic. So far, all these CSEs mapped in CO using mm-wave interferometry display a clear axial symmetry; a very striking result.

In the first COSAS paper there are two SRb's, RX Boo and X Her. In both cases, a hour-glass structure, expanding at moderate velocities, is found, very much like the one detected in the post-AGB low mass source 89 Her (Bujarrabal et al. 2005). In RX Boo, this bipolar structure is surrounded by a larger spherical halo, but in X Her this standard CSE component is absent. A similar result has been found for the SRb IRC +50049, to be included in the second COSAS paper (Castro-Carrizo, private communication). Other three SRb's, BM Gem, UU Aur and RT Vir, are also included in the COSAS sample, but their maps remain yet to be analyzed.

Hirano et al. (170) mapped the envelope around the SRa V Hya, and they found that it consists in a rotating disk plus a bipolar outflow expanding at relative high velocities. A similar structure was also found in the case of the SRb π^1 Gru by Chiu et al. (165). Bergman et al. (161) claimed the detection of a Keplerian rotating disk in the SRb RV Boo, and Winters et al. (184) and Libert et al. (175) have reported the detection of slowly expanding hour-glass components in the envelopes of the SRb EP Aqr and the SRc RS Cnc respectively.

The sample is starting to be statistically significant; we already have results for 8 sources, and 3 more are awaiting data reduction. There is a striking large prevalence of bipolar nebulae and/or equatorial disks, however I would not dare to conclude on whether this axis-symmetry is an intrinsic characteristic of the CSEs of SR variables, or if this result is contaminated by a strongly biased sample (sometimes authors prefer to map sources with known peculiar CO line profiles resulting in peculiar CO maps). As for the origin of the axial-symmetry in these envelopes, I must recall that at least for V Hya we know that there is a 17 yr secondary variability period that has been attributed to the presence of a (common envelope) binary system (160).

2.2. The case of bona fide binaries: *o* Cet and symbiotic systems

Speaking of binaries in AGBs, we can not forget the case of symbiotic and alike systems (composed by a Mira and a hot secondary companion), since they are obvious test

beds for the influence of binarity on the mass loss of the red giant. We have very different scenarios regarding the molecular CSE in binaries: there are cases in which the companion does not destroy the molecular gas, as in *o* Cet (Mira), and where the secondary is so hot that molecules can only survive very close to the AGB star and do no form a fully developed CSE (at least not a standard one), such as in the case of true symbiotics. *o* Cet was mapped in CO by Josselin et al. (172), who found that the molecular envelope is rather small and shows a clear axis-symmetric structure, with a thick equatorial disk and two emptied lobes, i.e. a sort of hour-glass shape. On the contrary, Bujarrabal et al. (163) have studied the two true symbiotic systems with stronger IR excess, R Aqr and CH Cyg, founding that the line is so weak that it must arise from a molecular envelope with a size similar to that of the orbit of the secondary, or even somewhat smaller: i.e., apparently molecules do not survive in these systems beyond the orbit of the hot component.

In spite of this, *o* Cet and R Arq show a strong similitude. In both cases, the very inner layers of the molecular CSE are very similar to those of normal AGB stars. This is shown by the VLBI observations of SiO masers in these sources (Cotton et al. 2004), which display the typical ring of knots, and where the presence of the companion does not show up conspicuously. Also in the two cases, a large scale bipolar structure can be seen in the optical, proving that the presence of the companion is really influencing the way these systems lose mass at larger scales in a similar way (176; 171).

3. CO observations of pPNe

In 2007, at the previous APN conference in La Palma, I already reviewed the status of the molecular line observations of post-AGB sources (158). I must admit that the scenario has not changed significantly in the last three years. I will update the list of post-AGB sources with CO interferometric maps, commenting on the observations of new sources, of new improved maps, and on the observations of the warm molecular gas, a piece of information that is sorely needed, and that is being collected right now by means of the observations of higher-J CO rotational transitions.

As of APN IV, the compilation of post-AGB stars with detailed maps of their molecular nebular content consisted in 37 sources, including low-mass objects, that might not result in the formation of a true PNe (such as the Red Rectangle), and yellow hyper-giants (which are really post red super-giants). By that time other sources such V Hya and π^1 Gru were also considered as pPNe because of their bipolar nature, but I have removed them from the list in view of the results being obtained for other SR variables. Including the only new addition, IRAS 08544−4431, and the sources removed, the updated list of sources contains 36 entries and it is presented in Table 1.

The only really new addition to the list, IRAS 08544−4431, has been observed in CO by Dinh-V-Trung (167). The observations lack of resolving power because the envelope is rather compact, and so the author concentrates on the study of the line profile. From this profile it is claimed that source would very similar to 89 Her, i.e. consisting in low velocity bipolar lobes plus a slowly expanding equatorial component, and maybe a central rotating component. Let me also record a new improved CO map of IRAS 07134−1005 by Nakashima et al. (2009), and new VLA maps of HC_3N J=5–4 and NH_3 in CRL 2688, by Dinh-V-Trung & Lim (169) and Dinh-V-Trung et al. (168)

Table 1. List of early post-AGB (pPNe) and post-RSG (YHG) sources for which interferometric CO maps have been performed (though not all the maps have been published).

IRAS name	AFGL/CRL	HD number	GCVS	other names
IRAS 04296+3429				
IRAS 04395+3601	CRL 618		V353 Aur	Westbrook Nebula
IRAS 06176–1036	CRL 915	HD 44179	V777 Mon	Red Rectangle
IRAS 07134–1005		HD 56126	CY CMi	
IRAS 07399–1435	CRL 5237		QX Pup	OH 231.8+4.2
IRAS 08544–4431			V390 Vel	
IRAS 09371+1212				Frosty Leo
IRAS 16342–3814				OH 344.1+5.8
IRAS 17423–1755				Hen 3–1475
IRAS 17436+5003	CRL 5384	HD 161796	V814 Her	
IRAS 17534+2603				89 Her
	CRL 2688		V1610 Cyg	Egg Nebula
IRAS 18276–1431	CRL 5497		V445 Sct	OH 17.68–2.03
IRAS 18448–0545	CRL 5296S	HD 173819	R Sct	
IRAS 18450–0148			W43A	OH 31.0+0.0
IRAS 18560+0638	CRL 2290		V1366 Aql	OH 39.7+1.5
IRAS 19024+0044				M 2–39, Starfish Nebula
IRAS 19114+0002	CRL 2343			
IRAS 19134+2131				
IRAS 19244+1115	CRL 2340		V1302 Aql	IRC +10420
IRAS 19255+2123				K 3–35
IRAS 19292+1806				
IRAS 19343+2926				M 1–92, Minkowski's Footprint
IRAS 19374+2359				
IRAS 19475+3119		HD 331319		M 2–42
IRAS 19500–1709	CRL 5568	HD 187885	V5112 Sgr	
IRAS 19520+2759				
IRAS 19548+3035	CRL 2477			
IRAS 20028+3910				M 2–43
IRAS 21282+5050				
IRAS 22223+4327			V448 Lac	
IRAS 22036+5306				
IRAS 22272+5435		HD 235858		
IRAS 23304+6147				M 2–47
IRAS 23321+6545				M 2–48
IRAS 23541+7031	CRL 3181			M 2–56

respectively. However, these observations do not change our previous understanding of these sources.

Other CO observations that have just become available, but that were included in my APN IV list, are those corresponding to the first release of the COSAS program, which include CRL 2477, IRAS 19475+3119, IRAS 20028+3910, IRAS 21282+5050, and IRAS 23321+6545 (164). Four more post-AGB sources (that I have already included in my list) will be released in the following papers; namely Hen 3–1475, OH 17.68–2.03, IRAS 19500–1709, and IRAS 22223+4327 (the data is already collected but the analysis is not yet finished). 4 out of these 5 pPNe in this COSAS I paper display signatures of axis-symmetry. In the remaining source, CRL 2477, the molecular nebula

consists in a round envelope with no signs of high velocity winds; i.e., in this case we are just observing the fossil AGB envelope.

IRAS 21282+5050 is a C-rich pPN displaying a rounded AGB-like halo and a barrel-shaped inner cavity, very probably excavated by a bipolar post-AGB flow. IRAS 19475+3119 is a highly bipolar pPN showing an axial linear velocity gradient, very much resembling the case of M 1–92 (159), but lacking the equatorial flat component dividing the two lobes. IRAS 23321+6545 is an O-rich pPN displaying a rounded halo and a high velocity bipolar outflow running inside, which results in a strong self-absorption in the blue wing of the CO lines. This is also the case of the last target in this COSAS I pPN sample, IRAS 20028+3910, another O-rich pPN displaying a rounded outer halo with a central high velocity bipolar outflow.

These strong self-absorption features, also present in IRAS 17436+5003 and IRAS 19500–1709 (Alcolea, private communication), are interpreted as due to the presence of fast outflows that are still making its way through the slower and colder AGB CSE remnant, as it is also the case of the well studied envelopes CRL 618 and CRL 2688 (see 181; 166, respectively). In these cases it is expected the presence of active shocks as the fast bipolar flow carves holes in the fossil AGB envelope, which should be be better probed by higher-J CO transitions. Interestingly, Nakashima et al. (178) have mapped the CO J=6–5 line in CRL 618 using the SMA, finding that the warm regions probed by this line are simply those closer to the central star.

The study of the existence and properties of these regions of warm gas in pPNe (and also in AGB envelopes) is a long standing issue, since they are very difficult to observe from the ground due to the relatively high opacity of the atmosphere in the sub-mm and far-IR ranges (where the high-J rotational lines of CO lie). This is one of the major topics addressed by two key programs being carried out with Herschel/HIFI, HIFIStars and SUCCESS (by V. Bujarrabal et al. and D. Teyssier et al. respectively). First HIFIStars results on CRL 618 by Bujarrabal et al. (162) demonstrate that the inner layers of this pPN are indeed hotter than what it was thought before. Other pPNe, as it seems to be the case of OH 231.8+4.2, lack this warm component of the envelope (see poster 3 by Alcolea et al.). It is expected that results on the full pPNe sample included in these two programs will become available in the next two years.

3.1. Some statistics

If from table 1 we only select those post-AGB sources (i.e., we exclude YHGs) for which the available CO mapping is of relatively good quality (20 sources in total), we note that just $\lesssim 10\%$ of the sources are simply spherical balls of gas with no traces of post-AGB high velocity winds, and hence do not present *momentum excess problem*. In these sources the envelope would just be the the former AGB CSE, still in expansion.

About 25% of pPNe do not display high velocity CO emission but show axial symmetry, as in the cases of 89 Her, the Red Rectangle, IRAS 08544–4431, Hen 3−1475, and IRAS 07134–1005. These sources have a dominant equatorial disk component, and sometimes a hourglass-like extended envelope. In another 25% of the sources, the molecular envelope is dominated by a high velocity gas component, characterized by a (Hubble-like) linear velocity gradient (i.e. self-similar structures), testifying in favor of a rapid formation of the nebula, and the absence of strong interaction between the AGB and post-AGB winds at present. Examples are M 1−92, OH 231.8+4.2,

M 2−56, Frosty Leo, and IRAS 19475+3119. Here, almost the whole CO nebula has *momentum excess*. Finally, the remaining 40% of the sources appear to be envelopes in which the fast bipolar post-AGB flow (also showing the *momentum problem*) its presently carving its way through the fossil AGB envelope, as in CRL 618. This would also be the case of IRAS 17436+5003, IRAS 23321+6545, IRAS 21282+5050, IRAS 20028+3910, 1RAS 19500−1709, CRL 2688, and IRAS 22036+5306.

As we can see, most pPNe are axially symmetric, contrarily to what happens for AGB envelopes in general, though there are exceptions such as some well known binaries and at least some SR variables. Although these connections should be further explored, I still believe that at present we have problems in explaining the main characteristics of the pPN population from the simple evolution of the envelopes around AGB stars.

References

Alcolea, J. 2007, in Asymmetrical Planetary Nebulae IV
Alcolea, J., Neri, R., & Bujarrabal, V. 2007, A&A, 468, L41
Barnbaum, C., Morris, M., & Kahane, C. 1995, ApJ, 450, 862
Bergman, P., Kerschbaum, F., & Olofsson, H. 2000, A&A, 353, 257
Bujarrabal, V., Alcolea, J., Soria-Ruiz, R., Planesas, P., Teyssier, et al. 2010, A&A, 521, L3
Bujarrabal, V., Mikołajewska, J., Alcolea, J., & Quintana-Lacaci, G. 2010, A&A, 516, A19
Castro-Carrizo, A., Quintana-Lacaci, G., Neri. R., Bujarrabal, V., Schöier, F. L., et al. 2010, A&A, in press, DOI: 10.1051/0004-6361/201014755
Chiu, P., Hoang, C., Dinh-V-Trung, Lim, J., Kwok, S., Hirano, N., & Muthu, C. 2006, ApJ, 645, 605
Cox, P., Lucas, R., Huggins, P. J., Forveille, T., Bachiller, R., Guilloteau, S., Maillard, J. P., & Omont, A. 2000, A&A, 353, L25
Dinh-V-Trung 2009, ApJ, 692, 1382
Dinh-V-Trung, Chiu, P. J., & Lim, J. 2009, ApJ, 700, 86
Dinh-V-Trung, & Lim, J. 2009, ApJ, 698, 439
Hirano, N., Shinnaga, H., Dinh-V-Trung, Fong, D., Keto, E., Patel, N., Qi, C., Young, K., Zhang, Q., & Zhao, J. 2004, ApJ, 616, L43
Hollis, J. M., Bertram, R., Wagner, R. M., & Lampland, C. O. 1999, ApJ, 514, 895
Josselin, E., Mauron, N., Planesas, P., & Bachiller, R. 2000, A&A, 362, 255
Ladjal, D., Justtanont, K., Groenewegen, M. A. T., Blommaert, J. A. D. L., Waelkens, C., & Barlow, M. J. 2010, A&A, 513, A53
Leão, I. C., de Laverny, P., Mékarnia, D., de Medeiros, J. R., & Vandame, B. 2006, A&A, 455, 187
Libert, Y., Winters, J. M., Le Bertre, T., Gérard, E., & Matthews, L. D. 2010, A&A, 515, A112
Meaburn, J., López, J. A., Boumis, P., Lloyd, M., & Redman, M. P. 2009, A&A, 500, 827
Morris, M., Sahai, R., Matthews, K., Cheng, J., Lu, J., Claussen, M., & Sánchez-Contreras, C. 2006, in Planetary Nebulae in our Galaxy and Beyond, edited by M. J. Barlow & R. H. Méndez, vol. 234 of IAU Symposium, 469
Nakashima, J., Fong, D., Hasegawa, T., Hirano, N., Koning, N., Kwok, S., Lim, J., Dinh-Van-Trung, & Young, K. 2007, AJ, 134, 2035
Neri, R., Kahane, C., Lucas, R., Bujarrabal, V., & Loup, C. 1998, A&AS, 130, 1
Sahai, R., & Chronopoulos, C. K. 2010, ApJ, 711, L53
Sánchez Contreras, C., Bujarrabal, V., Castro-Carrizo, A., Alcolea, J., & Sargent, A. 2004, ApJ, 617, 1142
Soria-Ruiz, R., Alcolea, J., Colomer, F., Bujarrabal, V., Desmurs, J., Marvel, K. B., & Diamond, P. J. 2004, A&A, 426, 131

Weigelt, G., Balega, Y. Y., Blöcker, T., Hofmann, K., Men'shchikov, A. B., & Winters, J. M. 2002, A&A, 392, 131
Winters, J. M., Le Bertre, T., Pety, J., & Neri, R. 2007, A&A, 475, 559

Asymmetric Planetary Nebulae V
A. A. Zijlstra, F. Lykou, E. Lagadec and I. McDonald
Jodrell Bank Centre for Astrophysics, Manchester, UK © 2011

Structure and shaping processes within the extended atmospheres of AGB stars

M. Wittkowski[1], D. A. Boboltz[2], I. Karovicova[1], K. Ohnaka[3], A. E. Ruiz-Velasco[1,4], M. Scholz[5,6], and A. A. Zijlstra[7]

[1] *ESO, Karl-Schwarzschild-Str. 2, 85748 Garching bei München, Germany*

[2] *US Naval Observatory, 3450 Massachusetts Avenue, NW, Washington, DC 20392-5420, USA*

[3] *Max-Planck-Institut für Radioastronomie, Auf dem Hügel 69, 53121 Bonn, Germany*

[4] *Departamento de Astronomía, Universidad de Guanajuato, Apartado Postal 144, 36000 Guanajuato, Mexico*

[5] *Zentrum für Astronomie der Universität Heidelberg (ZAH), Institut für Theoretische Astrophysik, Albert-Ueberle-Str. 2, 69120 Heidelberg, Germany*

[6] *Sydney Institute for Astronomy, School of Physics, University of Sydney, Sydney, NSW 2006, Australia*

[7] *Jodrell Bank Centre for Astrophysics, School of Physics and Astronomy, University of Manchester, Manchester M13 9PL, UK*

Abstract. We present recent studies using the near-infrared instrument AMBER of the VLT Interferometer (VLTI) to investigate the structure and shaping processes within the extended atmosphere of AGB stars. Spectrally resolved near-infrared AMBER observations of the Mira variable S Ori have revealed wavelength-dependent apparent angular sizes. These data were successfully compared to dynamic model atmospheres, which predict wavelength-dependent radii because of geometrically extended molecular layers. Most recently, AMBER closure phase measurements of several AGB stars have also revealed wavelength-dependent deviations from 0/180 deg., indicating deviations from point symmetry. The variation of closure phase with wavelength indicates a complex non-spherical stratification of the extended atmosphere, and may reveal whether observed asymmetries are located near the photosphere or in the outer molecular layers. Concurrent observations of SiO masers located within the extended molecular layers provide us with additional information on the morphology, conditions, and kinematics of this shell. These observations promise to provide us with new important insights into the shaping processes at work during the AGB phase. With improved imaging capabilities at the VLTI, we expect to extend the successful story of imaging studies of planetary nebulae to the photosphere and extended outer atmosphere of AGB stars.
Keywords. Planetary Nebulae – Stars: AGB and post-AGB

1. Introduction

Asymptotic Giant Branch (AGB) stars are low- and intermediate-mass stars, such as our Sun, in their final phase of evolution that is driven by nuclear burning. Mass-loss becomes increasingly important toward the tip of the AGB evolution, when the "superwind" phase occurs. The superwind mass-loss reduces the convective stellar envelope until the star starts to shrink. Then the star evolves at almost constant luminosity to higher effective temperatures, passes the post-AGB phase, and becomes a planetary nebula (PN). In this phase the now hot inner star ionizes its envelope, which is a remnant of the superwind mass-loss during its AGB and post-AGB phases (e.g. 190).

While the mass-loss process during the AGB phase is the most important driver for the further stellar evolution toward the PN phase, the details of the mass-loss process and its connection to the structure of the extended atmospheres and the stellar pulsation are not well understood and are currently a matter of debate, in particular for oxygen-rich AGB stars (e.g. 209; 191).

In the past decade, imaging studies of PNe and protoplanetary nebulae (pPNe) have revealed a great diversity of morphologies. This variety of shapes of pPNe and PNe is seemingly caused by processes at the end of the AGB evolution, but the details of the shaping processes are not well understood (e.g. 185).

Interferometric techniques at optical and radio wavelengths have proven their ability to provide important observational constraints on the atmosphere and mass-loss process of AGB stars by resolving the stellar disk and the circumstellar environment (e.g. 201; 203; 195; 200). Deviations from circular symmetry have been detected in the circumstellar environment (CSE) of AGB stars at radio as well as optical wavelengths (e.g. 204; 202).

Most recent studies using the near-infrared (AMBER) and mid-infrared (MIDI) instruments of the VLT Interferometer (VLTI) have added important information to our understanding of the pulsation and mass-loss of AGB stars thanks to their spectro-interferometric capabilities (197; 198; 199; 208; 207; 196; 186).

Here, we describe our most recent observations of the structure and morphology of the extended atmosphere of AGB stars using the VLTI/AMBER instrument, and their implication on the mass-loss process and the onset of asymmetric shapes during the AGB evolution.

2. Observations

The first AMBER observations of an AGB star were obtained on 12 October 2007 on the Mira variable S Ori (period 414 days 205), and are described in (207). These observations used the low resolution mode of AMBER with a spectral resolution of ∼35 and utilized the fringe tracker FINITO and three VLTI Auxiliary Telescopes (ATs) positioned on stations E0, G0, and H0 with ground baselines of 16 m, 32 m, and 48 m. Since then, we have obtained additional AMBER observations of the Mira variables S Col (325 d), T Col (225 d), W Vel (394 d), RW Vel (443 d), R Cnc (361 d), X Hya (301 d), and RR Aql (394 d) between September 2008 and June 2010. These observations used in addition to the low resolution mode the medium resolution modes of AMBER with a spectral resolution of ∼1500 in the near-infrared H and K bands, and also

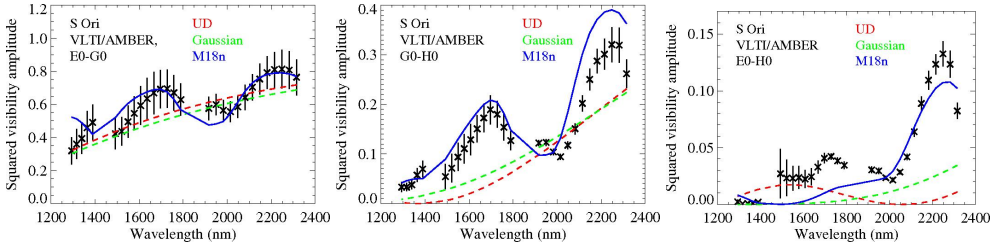

Figure 1. VLTI/AMBER visibility function of S Ori compared to simple models of a uniform disk and a Gaussian disk, as well as compared to the dynamic atmosphere model (207).

utilized additional AT configurations. These observations will be described in detail in forthcoming papers. Some of these observations were coordinated with concurrent VLBA observations of the SiO and H_2O maser emission. In addition to Mira variables, AMBER data on OH/IR stars have been obtained in April 2008 (Ruiz Velasco et al., these proceedings).

3. Modeling

Few dynamic atmosphere models for oxygen-rich Mira stars are available. The P and M model series (194; 193) are complete self-excited dynamic model atmospheres of Mira stars designed to match the prototype oxygen-rich Mira stars *o* Cet and R Leo. They have been used successfully compared to VLTI/VINCI broadband interferometric data of *o* Cet and R Leo (210; 187). Compared to *o* Cet and R Leo, our target stars have slightly different periods, masses, and radii. However, the general model results are not expected to be dramatically different for our target stars compared to *o* Cet and R Leo (cf. the discussion in 208). As a result, the P and M model series were chosen as the currently best available option to describe Mira star atmospheres. Wittkowski et al. (208) have added an ad-hoc radiative transfer model to these model series to describe the dust shell as observed by the mid-infrared interferometric instrument MIDI. However, at near-infrared wavelengths, the contribution of the dust shell can be neglected for our target stars. Gray et al. (189) have combined these hydrodynamic atmosphere models with a maser propagation code in order to describe the SiO maser observations that have been coordinated for some of our target stars.

4. Results

Fig. 1 shows the AMBER visibility data of S Ori (from 207). The visibility data of S Ori show significant wavelength-dependent features clearly deviating from uniform disk (UD) and Gaussian models of constant diameter on all three baselines. This indicates variations in the apparent angular diameter. For comparison, γ Eri, a regular M giant, was observed during the same night with the same instrument settings, and did not show such deviations from a UD curve, confirming that the features seen for S Ori are not instrumental or atmospheric effects.

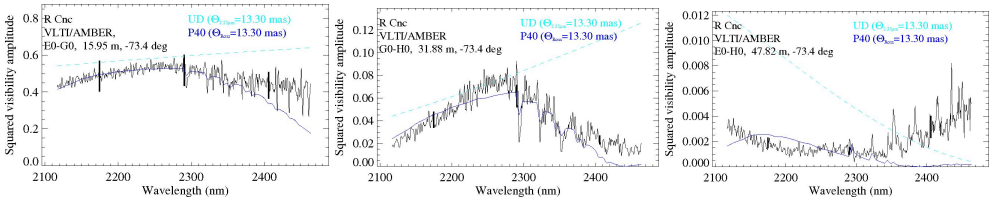

Figure 2. VLTI/AMBER visibility function of R Cnc compared to a simple model of a uniform disk, as well as compared to a dynamic atmosphere model.

Model M18n provided the best formal fit to our S Ori visibility data out of the available phase and cycle combinations of the M series. The synthetic visibility values based on the M18n model compared to our AMBER observation are also indicated in Fig. 1, showing that our AMBER visibility data could be described well by the dynamic atmosphere model series. The deviations of the model visibilities from a uniform disk of constant diameter is caused by molecular layers (most importantly CO and H_2O) lying above the continuum-forming layers. At spectral channels, where the molecular opacity is low, we see a larger contribution from the photosphere, and the target appears smaller. At spectral channels where the molecular opacity is larger, we see a larger contribution from the extended atmospheric molecular layers, and the target appears larger.

In summary, our AMBER observations of S Ori generally confirmed the predictions by the M model series and we found that the observed variation of diameter with wavelength can be understood as the effect of phase-dependent water vapor and CO layers lying above the photosphere. We also concluded that more such observations on more targets and at more phases were needed to confirm and constrain the model predictions in more detail.

Since the work described in Wittkowski et al. (207), we have obtained additional AMBER data of more targets and at more phases, as described in Sect. 2. Fig. 2 shows as an example the visibility function of the Mira variable R Cnc obtained with the medium resolution model of the AMBER instrument (spectral resolution ∼1500). These data confirm the conclusion from (207) that Mira variables show wavelength-dependent angular diameters when observed with spectro-interferometric techniques that can be explained by molecular layers lying above the continuum- forming photosphere, and that are consistent with predictions by dynamic model atmospheres. In addition to these AMBER observations, Chiavassa et al. (186) have obtained AMBER data of the very cool late-type star VX Sgr, and Ruiz Velasco et al. (these proceedings) have obtained AMBER data of three highly evolved AGB stars of OH/IR type. All these data show similar characteristics of the AMBER visibility function. The characteristic 'bumpy' AMBER visibility curves indicating the presence of molecular layers, thus seems to be a common feature of evolved oxygen-rich stars.

5. Shaping processes

Fig. 3 shows the AMBER closure phase measurement corresponding to the visibility curves of Fig. 2. The interferometric closure phase is a measure of the point symmetry of a source. Values of 0° and 180° indicate point symmetry, other values deviations

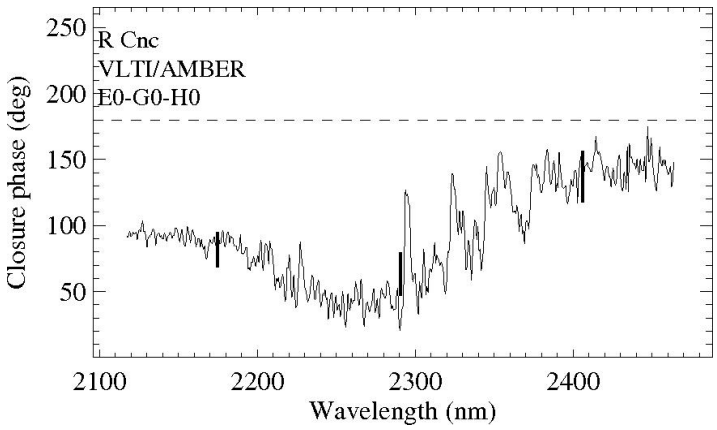

Figure 3. VLTI/AMBER closure phase of R Cnc.

from point symmetry. R Cnc shows closure phase values that are significantly different from 0°and 180°, thus indicate a significant deviation from point symmetry. The R Cnc closure phases vary with wavelength. At wavelengths around 2.25μm, where the visibility values show a maximum corresponding to a small angular diameter, the closure phase shows values of about 40°. Shortward of 2.25μm, where the visibility decreases and where the water vapor opacity becomes larger, the closure phase increases to 90°. Longward of 2.25μm, where the visibility decreases both due to CO and water vapor, the closure phase increases to 150°, with closure phase peaks marking the peaks of the CO bandheads. A similar characteristic signal of the closure phases are seen for other targets of our sample.

The interpretation of the closure phase measurements is work in progress. They might indicate a complex non-spherical stratification of the photosphere and extended atmosphere, and may reveal whether observed asymmetries are located near the photosphere or in the outer molecular layers. These observations thus promise to lead to new insights into the shaping processes at work during the AGB phase. As an example, the detection of photospheric convection cells and corresponding clumps in the molecular layer that have characteristics as those predicted by 3D atmosphere models (e.g. 188) would point to a process of large-scale photospheric convection. Random clumps in the molecular shell may point to highly temporally and also spatially variable chaotic mass ejections caused by perturbations in the oscillations (192) or by magnetic fields (e.g. 206).

6. Summary

AMBER spectro-interferometry shows wavelength-dependent apparent sizes of AGB stars, including Mira variables and OH/IR stars. These observations are generally consistent with dynamic model atmosphere predictions that include molecular layers, in the infrared most importantly CO and H_2O, lying above the continuum-forming photosphere. AMBER closure phase measurements of a sample of resolved Mira variables indicate deviations from point symmetry. A characteristic wavelength dependence of the closure phase values indicates a complex non-spherical stratification of the extended

atmosphere. A detailed interpretation of these measurements is needed, and may reveal whether asymmetric structures originate at the photosphere or at more extended layers, and how they develop from smaller to larger scales. Advanced imaging capabilities with the VLTI thanks to improved baseline configurations and 2nd generation instruments combining a larger number of beams will allow us to obtain model independent images of the extended atmospheres of AGB stars. We are thus at a turning point in the history of knowledge of AGB stars, where imaging studies can be extended from pPNe and PNe to layers of AGB stars at the photosphere and at molecular layers close to the photosphere, and thus reveal the shaping processes at work during the AGB phase.

References

Balick, B., & Frank, A. 2002, ARA&A, 40, 439
Chiavassa, A., Lacour, S., Millour, F., Driebe, T., Wittkowski, M., Plez, B., Thiébaut, E., Josselin, E., Freytag, B., Scholz, M., & Haubois, X. 2010, A&A, 511, A51+
Fedele, D., Wittkowski, M., Paresce, F., Scholz, M., Wood, P. R., & Ciroi, S. 2005, A&A, 431, 1019
Freytag, B., & Höfner, S. 2008, A&A, 483, 571
Gray, M. D., Wittkowski, M., Scholz, M., Humphreys, E. M. L., Ohnaka, K., & Boboltz, D. 2009, MNRAS, 394, 51
Habing, H. J., & Olofsson, H. (eds.) 2003, Asymptotic giant branch stars
Höfner, S., & Andersen, A. C. 2007, A&A, 465, L39
Icke, V., Frank, A., & Heske, A. 1992, A&A, 258, 341
Ireland, M. J., Scholz, M., Tuthill, P. G., & Wood, P. R. 2004, MNRAS, 355, 444
Ireland, M. J., Scholz, M., & Wood, P. R. 2004, MNRAS, 352, 318
Kemball, A. J., & Diamond, P. J. 1997, ApJ, 481, L111+
Le Bouquin, J., Lacour, S., Renard, S., Thiébaut, E., Merand, A., & Verhoelst, T. 2009, A&A, 496, L1
Ohnaka, K., Bergeat, J., Driebe, T., Graser, U., Hofmann, K., Köhler, R., Leinert, C., Lopez, B., Malbet, F., Morel, S., Paresce, F., Perrin, G., Preibisch, T., Richichi, A., Schertl, D., Schöller, M., Sol, H., Weigelt, G., & Wittkowski, M. 2005, A&A, 429, 1057
Ohnaka, K., Driebe, T., Hofmann, K., Leinert, C., Morel, S., Paresce, F., Preibisch, T., Richichi, A., Schertl, D., Schöller, M., Waters, L. B. F. M., Weigelt, G., & Wittkowski, M. 2006, A&A, 445, 1015
Ohnaka, K., Driebe, T., Weigelt, G., & Wittkowski, M. 2007, A&A, 466, 1099
Perrin, G., Ridgway, S. T., Mennesson, B., Cotton, W. D., Woillez, J., Verhoelst, T., Schuller, P., Coudé du Foresto, V., Traub, W. A., Millan-Gabet, R., & Lacasse, M. G. 2004, A&A, 426, 279
Quirrenbach, A., Mozurkewich, D., Armstrong, J. T., Johnston, K. J., Colavita, M. M., & Shao, M. 1992, A&A, 259, L19
Ragland, S., Le Coroller, H., Pluzhnik, E., Cotton, W. D., Danchi, W. C., Monnier, J. D., Traub, W. A., Willson, L. A., Berger, J., & Lacasse, M. G. 2008, ApJ, 679, 746
Reid, M. J., & Menten, K. M. 1997, ApJ, 476, 327
— 2007, ApJ, 671, 2068
Samus, N. N., Durlevich, O. V., & et al. 2009, VizieR Online Data Catalog, 1, 2025
Suzuki, T. K. 2007, ApJ, 659, 1592
Wittkowski, M., Boboltz, D. A., Driebe, T., Le Bouquin, J., Millour, F., Ohnaka, K., & Scholz, M. 2008, A&A, 479, L21
Wittkowski, M., Boboltz, D. A., Ohnaka, K., Driebe, T., & Scholz, M. 2007, A&A, 470, 191
Woitke, P. 2006, A&A, 460, L9
Woodruff, H. C., Eberhardt, M., Driebe, T., Hofmann, K., Ohnaka, K., Richichi, A., Schertl, D., Schöller, M., Scholz, M., Weigelt, G., Wittkowski, M., & Wood, P. R. 2004, A&A, 421, 703

Asymmetric Planetary Nebulae V
A. A. Zijlstra, F. Lykou, E. Lagadec and I. McDonald
Jodrell Bank Centre for Astrophysics, Manchester, UK © 2011

Measuring and modeling massive stellar winds at the tip of the asymptotic giant branch

Christer Sandin

AIP, An der Sternwarte 16, D-14482 Potsdam, Germany

Abstract. Planetary nebulæ (PNe) form in the remains of the final stages of mass-loss on the preceding asymptotic giant branch (AGB). In order to understand the stellar evolution and the formation and evolution of PNe, it is important to treat the AGB wind properly. I here present the key concepts of our unique approach of measuring the mass-loss evolution of the AGB wind, using observations of faint halos of PNe. Both densities and kinematics can hereby be measured. In comparison to more commonly used methods we measure the gas directly, and thereby avoid the need for supplementary models. I also present an approach to extend stellar wind models to allow the formation of the massive winds that we observe.
Keywords. Planetary Nebulae

1. Introduction

Low- to intermediate-mass stars, with a main-sequence mass of $0.8\,M_{\odot} \lesssim M \lesssim 8\,M_{\odot}$, lose most of their envelopes during the time on the thermally pulsing asymptotic giant branch (TP-AGB). The increasing rate of mass loss dominates time scales of stellar evolution as the stellar wind changes the star more rapidly than nuclear burning in the stellar core does. The matter of the stellar wind is enriched with synthesized elements, which are dredged up from the core during the evolution. These winds are also sites of strong dust formation and determine properties of the physical environment where planetary nebulæ (PNe) form subsequently. Because most stars pass through this phase mass loss from AGB stars contribute significantly to the chemical evolution of the interstellar medium (ISM) and the galaxy. Recent reviews of mass loss from cool stars are given by, e.g., Willson (240), Höfner (222), Zijlstra (242), and van Loon (237).

When the (central) star is not concealed by a massive envelope anymore it heats up and can, under the right circumstances, ionize the matter of the AGB wind. The shape of the then formed and ionized PN shows a variety of geometries (see e.g. 211). PNe with a spherical or elliptical geometry consist of a central part with a relatively bright rim and a fainter attached shell, where both are built-up in an interplay between photoionization and wind interaction (see, for example, 218; 225; 217; 226; 228). The matter in the central parts of these objects has been restructured during their formation and this mass can therefore not be used to measure properties of the last period of more spherically symmetric mass loss on the AGB. As the PN evolves the region outside the PN proper is eventually ionized, and an AGB halo forms (see e.g. 235). Such a halo is relatively unaffected by the PN formation processes, and therefore still contains directly

accessible information of mass loss on the previous AGB. The least affected region of mass loss in the halo is, moreover, the inner part. In the outer halo it is expected that wind interaction, between periods of (the last) thermal pulse(s) and intermediate periods of mass loss, has modified the flow.

AGB halos of old PNe are very faint; the halo of these objects must not be confused with the faint recombining shell, where the degree of ionization is also unknown. Furthermore, for example Villaver et al. (238) and Wareing et al. (239) study the interaction between the outer parts of the PN and the ISM (also see the contributions of either author in these proceedings). They find that the nebula can become asymmetric when the spherically symmetric structure of an AGB wind moves through the ISM. For such objects (which fraction is about 20% of all objects, 239) it is important to measure the mass loss in the wake of the interaction. Soker (234) discusses the transition from more spherically symmetric outflow on the AGB to axisymmetric outflow that is often observed in the central parts of PNe, and Huggins et al. (223) study the role and properties of asymmetries in envelopes of AGB stars – and PN halos – to detect binary systems.

Studies of the mass-loss evolution on the AGB through observations of PN halos can provide accurate density structures that can be used to improve other studies, which depend on the mass distribution at the tip of the AGB. They are also useful to evolutionary studies of the star and galaxies, which depend on the final, and most massive, stages of mass loss. In this paper I present some of the key concepts of our observational method to measure the mass-loss evolution in PN halos in § 2. In § 3 I present an approach to model the formation of the most massive winds on the AGB, which are seen in these observations.

2. Measuring the mass-loss evolution using observations of halos of PNe

Sandin et al. (232) study four halos of Galactic Disk PNe and measure the mass-loss evolution and other properties after the last thermal pulse at the tip of the AGB. Our new approach uses the novel method of integral field spectroscopy (IFS). Based on the approach of Plait & Soker (229) this method allows the radial gas-density structure – i.e. the mass-loss evolution – to be measured directly. No fitting procedure is necessary using supplementary models, with additional assumptions, as is the case with the other two spectroscopic methods, which instead make use of the spectral energy distribution of the dust (cf., for example, the review of 236, and references therein) and high-resolution measurements of carbon monoxide (cf., for example, the review of 233, and references therein). A limitation of the PN-halo method is that it only works when observing the final stages of AGB mass loss, since the matter only becomes ionized during the PN phase. It obviously also only works with stars that form a PN (and later also a halo).

Since the PN forms in the AGB wind, it seems realistic to assume that every PN is, eventually, surrounded by a halo; although, this is not what is observed. Corradi et al. (215, 214) find 24 Galactic Disk AGB halos, which are either circular, slightly elliptical, or highly asymmetric. This is about 60% of the sample of elliptical objects in their study. Sandin et al. (232) find two additional halos; Corradi et al. (215) mark one of these objects, IC 3568, to not have a halo. Reid & Parker (230, SMP27) identify one

additional AGB halo in the Magellanic clouds. Although relatively few AGB halos are known it appears that they are a common phenomenon, where their detection is mainly limited by their brightness.

Sandin et al. (232) assume a constant outflow velocity of 10 $\mathrm{km\,s^{-1}}$, when they calculate a mass-loss history from the density structure. These estimates would be more accurate if a radial outflow velocity structure is measured also throughout the halo. The resulting Doppler line broadening, due to the low velocities, is moderate, which is why such work is tricky. Nevertheless, Guerrero et al. (221, who also summarize previous kinematic measurements) present an approach that can be used to make such measurements. Radial density and temperature structures, which are both provided from measurements of the PN halo, are required to deconvolve the kinematic measurements when determining the radial velocity structure.

3. Modeling the formation of massive stellar winds at the tip of the AGB

In order to model the formation of massive stellar winds at the tip of the AGB it is necessary to enhance current models of dust-driven winds. Normally these models use a radial domain that extends from above the region where pulsations form (at about 0.8–0.9 stellar radii) out to 10–60 stellar radii (see the discussion in, e.g., 231). The amount of mass present in the model within this domain – about 10^{-3}–$10^{-2}\,M_{\odot}$, using gray or frequency-dependent opacities, respectively* – is not enough to calculate mass-loss rates of the order $\gtrsim 10^{-5}\,M_{\odot}\,yr^{-1}$ with any reliability. For example, it normally takes about 10^2 years of evolution to start a dynamic model from a hydrostatic initial model. A sketch of the radial structure of the extended AGB star is shown in Fig. 1, which illustrates that the radial domain of wind formation models merely include a small part of the star.

By including more of the central parts of the star in the wind-formation model it becomes possible to model also the highest mass-loss rates – and thereby provide a mean to understand observations at the tip of the AGB. The inclusion of the convective envelope in the model requires the use of either a three-dimensional approach (such as is presented in the first-time study of 219) or a description of turbulent energy (see e.g. 224; 220; 213; 241; 216), which implies three free parameters (227) that replace the two free parameters of the piston (i.e. the moving inner boundary) of current models. It may turn out that dust cannot itself drive the strongest winds observed, in this case it may be necessary to find and include another, complementary, driving mechanism in the models.

Acknowledgments. C.S. is supported by the DFG, grant SCHO 394/29-1.

References

Balick, B., & Frank, A. 2002, ARA&A, 40, 439
Bowen, G. H. 1988, ApJ, 329, 299

*In comparison most of the stellar mass is placed in the envelope in models that use a constant gas opacity, and the standard value $\kappa_g = 2\times10^{-4}\,cm^2\,g^{-1}$ (that is introduced in the pioneering work of 212).

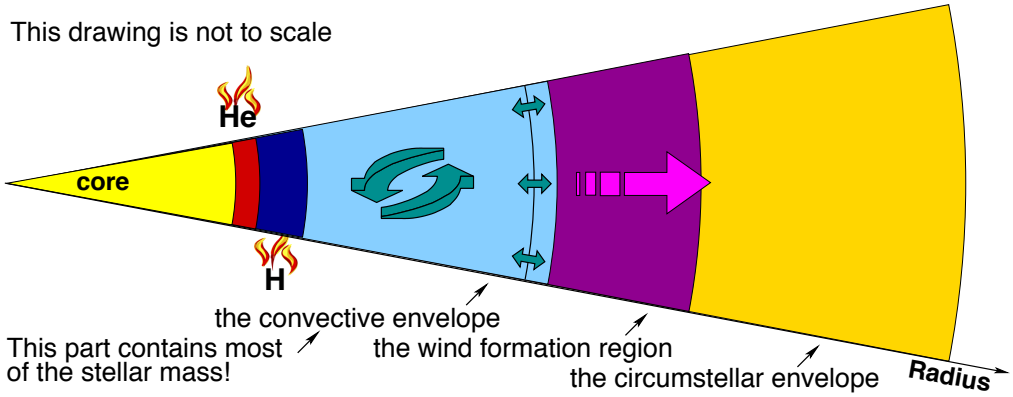

Figure 1. A sketch of the AGB star that divides it into separate radial domains. Starting from the outside with the circumstellar envelope (CSE; on the right-hand side) it encloses the wind formation region, the convective envelope, the periodically active hydrogen- and helium-burning shells, and the inert core. Long-period pulsations form in the outer parts of the convective envelope, and dust forms in the wind-formation region. The star ends with the ISM on the outside of the CSE.

Canuto, V. M., & Dubovikov, M. 1998, ApJ, 493, 834
Corradi, R. L. M., Sánchez-Blázquez, P., Mellema, G., et al. 2004, A&A, 417, 637
Corradi, R. L. M., Schönberner, D., Steffen, M., & Perinotto, M. 2003, MNRAS, 340, 417
Feuchtinger, M. U. 1999, A&AS, 136, 217
Frank, A. 1994, AJ, 107, 261
Frank, A., Balick, B., & Riley, J. 1990, AJ, 100, 1903
Freytag, B., & Höfner, S. 2008, A&A, 483, 571
Gehmeyr, M., & Winkler, K.-H. A. 1992, A&A, 253, 92
Guerrero, M. A., Villaver, E., & Manchado, A. 1998, ApJ, 507, 889
Höfner, S. 2005, in ESASPB, 560, 335
Huggins, P. J., Mauron, N., & Wirth, E. A. 2009, MNRAS, 396, 1805
Kuhfuß, R. 1986, A&A, 160, 116
Marten, H., & Schönberner, D. 1991, A&A, 248, 590
Mellema, G. 1994, A&A, 290, 915
Olivier, E. A., & Wood, P. R. 2005, MNRAS, 362, 1396
Perinotto, M., Schönberner, D., Steffen, M., & Calonaci, C. 2004, A&A, 414, 993
Plait, P., & Soker, N. 1990, AJ, 99, 1883
Reid, W. A., & Parker, Q. A. 2006, MNRAS, 365, 401
Sandin, C., Roth, M. M., & Schönberner, D. 2010, PASA, 27, 214
Sandin, C., Schönberner, D., Roth, M. M., et al. 2008, A&A, 486, 545
Schöier, F. L. 2007, ASPC, 378, 216
Soker, N. 2006, New Astronomy, 11, 396
Steffen, M., & Schönberner, D. 2003, IAUS, 209, 439
van Loon, J. T. 2007, ASPC, 378, 227
— 2008, MmSAI, 79, 412
Villaver, E., García-Segura, G., & Manchado, A. 2003, ApJ, 585, L49
Wareing, C. J., Zijlstra, A. A., & O'Brien, T. J. 2007, MNRAS, 382, 1233
Willson, L. A. 2000, ARA&A, 38, 573
Wuchterl, G., & Feuchtinger, M. U. 1998, A&A, 340, 419
Zijlstra, A. A. 2006, IAUS, 234, 55

Asymmetric Planetary Nebulae V
A. A. Zijlstra, F. Lykou, E. Lagadec and I. McDonald
Jodrell Bank Centre for Astrophysics, Manchester, UK © 2011

Unexpected AGB Asymmetries

A M S Richards[1], K A Assaf[1], I Bains[2], P Diamond[1], S Etoka[1], M D Gray[1], E A Humphreys[3] K Murakawa[4], H J van Langevelde[5], J A Yates[6]

[1]*JBCA, School of Physics & Astronomy, Manchester University, M13 9PL, UK*

[2]*Swinburne University of Technology, Victoria, Australia*

[3]*ESO, D-85748 Garching-bei-München, Germany*

[4]*MPIfR, 53121 Bonn, Germany*

[5]*Leiden University & JIVE, PO Box 2, NL-7990 AA Dwingeloo, NL*

[6]*Department of Physics and Astronomy, UCL, London WC1E 6BT, UK*

Abstract. Maps of water and hydroxyl masers in the winds of AGB stars reveal subtle asymmetries. Multi-epoch observations show that most circumstellar envelopes supporting bright masers are close to spherical but with uneven filling. The dominant wind direction is radial and there is no significant rotation or other signs of companions at a velocity resolution ≤ 0.2 km s^{-1}. The stars do appear to possess dynamically significant magnetic fields but the origin of these is not fully understood. Future observations will test the suggestions from current data, that clumping scales and asymmetries are determined at the origin of mass loss, from the stellar surface itself.

Keywords. Planetary nebulae – Stars: AGB and post-AGB

1. Introduction

The most extreme bipolar PN undoubtedly require companions for shaping but not all stars are in binary systems. AGB (and more massive) stars with no detectable companions, and stringent upper limits on rotation, also have asymmetric winds. We present observational evidence for this and discusses possible causes and future investigations.

2. Maser observations

We have monitored H_2O and OH masers in six AGB stars, RT Vir, U Ori, U Her, IK Tau, R Crt and W Hya, between 1993-2002. MERLIN* has a resolution of 10–20 mas at the H_2O frequency of 22 GHz, and 150–250 mas at the OH mainline frequencies of 1.665

*The UK radio interferometer, operated by the University of Manchester on behalf of STFC

and 1.667 GHz, and detects all the emission. The EVN (European VLBI Network) has a resolution around 20 mas at 1.6 GHz, but some extended OH is resolved out. Between a few tens and a couple of hundred H_2O maser clumps are identified in each circumstellar envelope, each spanning about 1–2 km s^{-1} and a few AU. They form a shell between about 5 and 50 stellar radii (the stellar radius is typically one or two AU) with a volume filling factor of a few percent or less. The OH mainlines are expected to appear further out but in some cases overlap the H_2O maser region, probably interleaving the denser H_2O maser clouds.

3. Accelerating expansion

In many cases some of the H_2O maser clumps can be identified at more than one epoch not more than 18 months apart. This provides proper motion measurements, such as the example shown for RT Vir in Fig. 1. Compared with the Doppler velocities this provides a 3D picture of the circumstellar envelope velocity field. These show that the wind is accelerating radially away from the star but there is no sign of any systematic rotation above a limit of a few tenths of a km s^{-1}, giving a limit of about 1 km s^{-1} at the stellar surface. The east side of the CSE in Fig. 1 has more red-shifted emission than the west side, but the most extreme red- and blue-shifted emission comes from closer to the line of sight towards the star at the centre, and the velocity asymmetry is probably due to the shell being elongated, i.e. spheroidal rather than spherical.

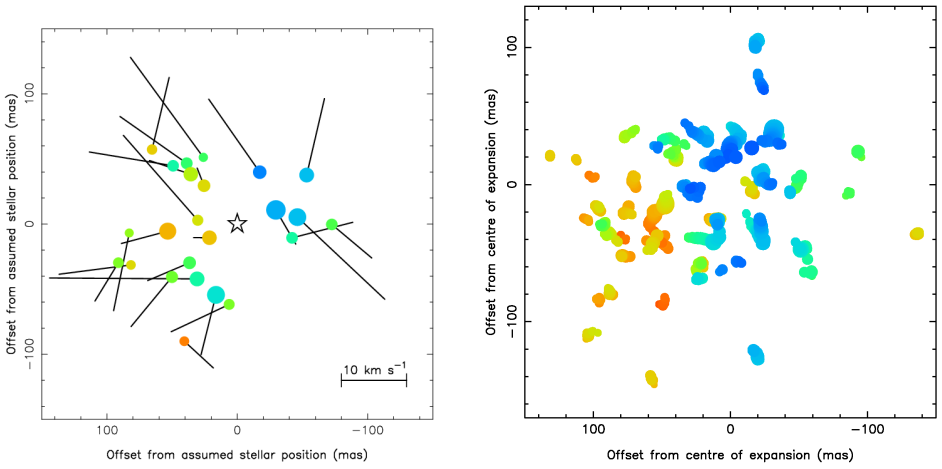

Figure 1. Proper motion vectors measured from six observations of RT Vir H_2O masers during 10 weeks (247) are shown on the left. A single epoch (243) is shown on the right.

4. Asymmetries – transient or persistent

The exponential nature of maser amplification exaggerates small changes in physical conditions. Fig. 2 shows that U Ori H_2O maser emission has a roughly elliptical distribution but the direction of elongation changes. The brightest emission is at a similar

distance from the centre but a different position angle. Some clumps of OH masers persist for at least a year. More extended emission is seen in the more sensitive 1998 MERLIN+EVN data, whilst the 1999 data are EVN only. It is often the case that VLBI hot-spots show an elongated distribution within a more spherical shell detected by MERLIN observations with higher surface-brightness sensitivity.

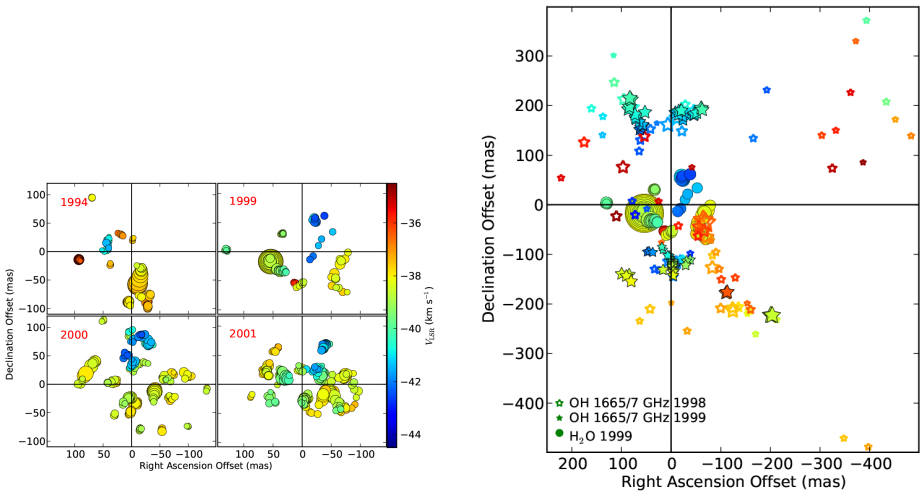

Figure 2. Four epochs of H_2O maser observations of U Ori are shown on the left. One epoch is overlaid on two epochs of OH mainline observations on the right.

The aim of our project is to use multi-epoch monitoring to investigate whether any asymmetries are persistent, and consistent with the CSE velocity field as deduced from Doppler and proper motions. This has been seen in supergiants (e.g. Etoka & Diamond 245, Murakawa et al. 246) but we can't be sure whether this is also the case in AGB stars until all epochs of data have been reduced fully. The H_2O maser shell of IK Tau is fairly spherical (Yates & Cohen 253, Bains et al. 243) but the OH mainline masers (Fig. 3) have a morphology suggesting a biconical outflow seen close to face-on.

These results suggest that AGB CSEs have a modest equatorial density enhancement where H_2O masers and strong acceleration are favoured by a denser, dustier environment. OH seems initially to have a spherical distribution but is more likely to develop asymmetries whilst still on the AGB; IK Tau, for example, seems to resemble the models of Zijlstra et al. (254).

5. Origins of asymmetry and future work

Zeeman splitting of the OH lines (249; 250) and H_2O (252) has been measured in several AGB stars, demonstrating the presence of magnetic fields strong enough to shape the outflow. However, the origin of such a field remains controversial in the absence of significant stellar surface rotation, although local enhancement of a weak dynamo looks promising (Soker & Zoabi 248; Thirumalai & Heyl 251). One possibility is the interplay between a rotating, degenerate core and large surface convection cells. The size of H_2O maser clouds varies with the stellar size, corresponding to a birth size

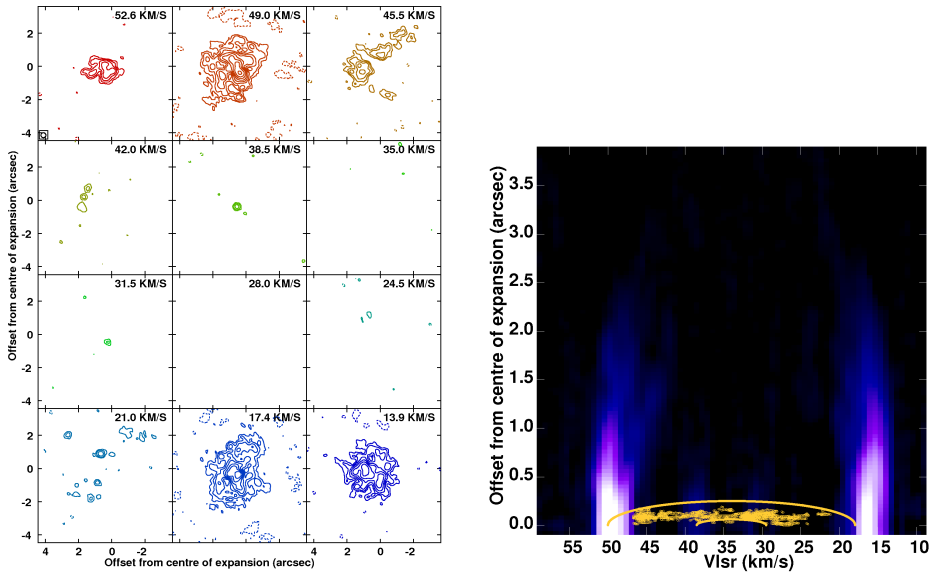

Figure 3. MERLIN observations of IK Tau at 1667 MHz (left) show surprisingly extended emission at the extreme velocities, incompatible with a uniform spherical shell. Traces of an inner shell are seen, also shown on the right (OH in purple scale), overlapping the H_2O masers (yellow components).

roughly 10% of the stellar diameter, consistent with convection models (albeit mostly tailored to RSG stars, e.g. Chiavassa et al. 244).

We are planning to continue investigations by a series of linked monitoring proposals. Combinations of e-MERLIN, EVLA, ALMA and VLTI data will resolve the radio photosphere at increasing radii with increasing frequency, i.e. deeper layers of the star are seen at mm wavelengths than at cm wavelengths. Appropriately timed observations will track disturbances through the stellar surface (as well as yielding temperature maps). A persistent axis of symmetry would suggest a magnetic dipole, whilst localised variations could be used to distinguish between convection and complex pulsation modes. We can then use coordinated SiO (VLBA), H_2O (e-MERLIN) and OH (e-MERLIN and EVN) maser observations to track individual clumps as they cross the crucial transition zones e.g. dust formation, eventually supplemented by ALMA images of dust and thermal lines as well as high-frequency masers.

References

Bains, I., Cohen, R. J., Louridas, A., Richards, A. M. S., Rosa-Gonzaléz, D., & Yates, J. 2003, MNRAS, 342, 8

Chiavassa, A., Plez, B., Josselin, E., & Freytag, B. 2009, A&A, 506, 1351

Etoka, S., & Diamond, P. 2004, MNRAS, 348, 34

Murakawa, K., Yates, J. A., Richards, A. M. S., & Cohen, R. J. 2003, MNRAS, 344, 1

Richards, A. M. S., Yates, J. A., Cohen, R. J., & Bains, I. 1999, in IAU Symp. 191: Asymptotic Giant Branch Stars, edited by T. Le Bertre, A. Lèbre, & C. Waelkens (ASP), 315

Soker, N., & Zoabi, E. 2002, MNRAS, 329, 204

Szymczak, M., Cohen, R. J., & Richards, A. M. S. 1998, MNRAS, 297, 1151

— 1999, MNRAS, 304, 877
Thirumalai, A., & Heyl, J. S. 2010, MNRAS, 1403
Vlemmings, W. H. T., Diamond, P. J., & van Langevelde, H. J. 2002, A&A, 394, 589
Yates, J. A., & Cohen, R. J. 1994, MNRAS, 270, 958
Zijlstra, A. A., te Lintel Hekkert, P., Chapman, J. M., Likkel, L., Comeron, F., Norris, R. P., Molster, F. J., & Cohen, R. J. 2001, MNRAS, 322, 280

Asymmetric Planetary Nebulae V
A. A. Zijlstra, F. Lykou, E. Lagadec and I. McDonald
Jodrell Bank Centre for Astrophysics, Manchester, UK © 2011

W43A: magnetic field and morphology

Nikta Amiri[1,2], Huib Jan van Langevelde[1,2], and Wouter Vlemmings[3]

[1] *Joint Institute for VLBI in Europe (JIVE), The Netherlands*

[2] *Leiden Observatory, Leiden University, The Netherlands*

[3] *Argelander Institute for Astronomy, University of Bonn, Germany*

Abstract. Water fountain sources are a class of post-AGB stars that exhibit highly collimated H_2O maser jets. These jets are likely associated with the origin of asymmetric PNe. Magnetic fields are found to play an important role in collimating these jets. We measured the Zeeman splitting of the 1612 MHz OH masers in W43A, which is an archetype of this class of objects. A magnetic field of 100μG was derived for the OH maser region of this source. Additionally, we performed kinematical re-construction of the OH maser region of this source. Our results show that the OH masers are most likely distributed in the equatorial region of the circumstellar envelope . The equatorial enhancement of the OH masers could be due to the presence of a binary companion.
Keywords. Planetary nebulae – Magnetic fields – Post-AGB stars

1. Introduction

Water fountain sources are a class of post-AGB objects where the H_2O maser velocity range exceeds that of OH maser in the CSE (258). High resolution H_2O maser observations trace highly collimated jets in the inner envelope of these objects. Therefore, these objects can not be understood by the standard expanding shell model. The origin of these jets is not clearly understood. Theoretical models show that magnetic fields can have an important role in collimating these jets (261). An archetype of this class is W43A, for which interferometric observations showed highly collimated H_2O maser jets, with a 3D outflow velocity of 145 km/s (257). Polarization observations of the H_2O masers of W43A revealed a strong magnetic field apparently collimating the jet (263).

The bipolar jets observed in water fountain sources are thought to explain the onset of asymmetric planetary nebulae (PNe) (262). This is significant because the majority of the observed planetary nebulae show elliptical or bipolar structures (259). During the post-AGB phase, the jet-like outflows, carve out polar cavities in the AGB wind. These cavities provide the morphological signature to produce the a-spherical PNe.

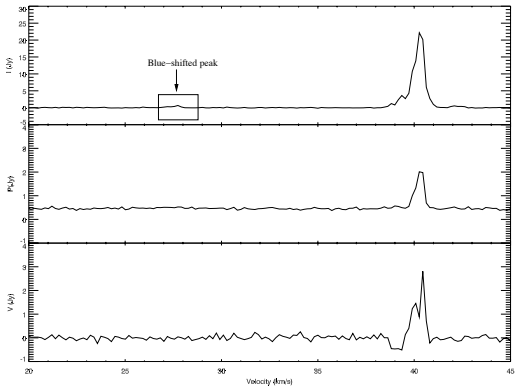

Figure 1. The 1612 MHz spectra of W43A.

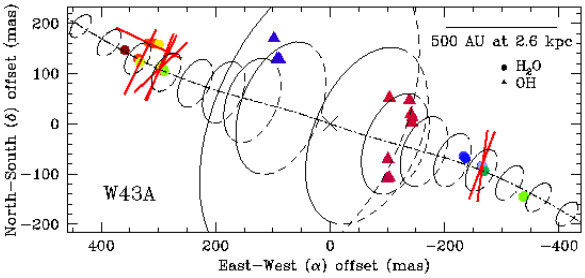

Figure 2. The spatial distribution of the OH and H_2O maser features of W43A. OH maser positions are overlaid on H_2O maser features (263).

2. The magnetic field of the 1612 MHz OH masers of W43A

We performed polarization observations of the 1612 MHz OH masers of W43A with MERLIN. Fig. 1 shows the total intensity, polarization intensity and circular polarization profiles. The brightest peak is red-shifted and the blue-shifted peak has a much lower brightness; ~ 30 times weaker. The peaks in the polarization intensity and circular polarization profiles show 12% linearly and 10% circularly polarization.

Fig. 2 shows the spatial distribution of the OH maser features of W43A together with H_2O maser positions. The offset positions are with respect to the reference feature. H_2O maser features are indicated by filled circles and OH maser features are shown as triangles. Red and blue colors indicate the red-shifted and blue-shifted features. This map clearly shows that H_2O maser occurs at the tips of a jet and the OH masers occur at a projected distance much closer to the star.

The actual measurement of the magnetic field strength may depend on a number of conditions, but is estimated to be 100 μG (255). This value is consistent with the

expected magnetic field strength of 70 μG extrapolated from H_2O maser observations (263).

3. Kinematical re-construction of the OH maser region of W43A

The spatial distribution of the OH and H_2O maser region of W43A (Fig. 2) reveal that the CSE of this source has deviation from spherical symmetry. We performed kinematical reconstruction to investigate the morphology of the OH maser region of this source. We wanted to understand why the OH maser features are offset from each other and in particular why this offset is reversed compared to that of the red- and blue-shifted H_2O masers.

The H_2O maser jet of W43A is located in a bipolar outflow with 39° inclination from the plane of the sky (257). The expansion velocity of the OH maser region of W43A is $\sim$ 18 km/s (255). This implies that the OH maser region is not entrained by the fast post-AGB wind. We considered two scenarios of an equatorial distribution and a bi-conical outflow for the OH maser region of W43A. We determined the velocity coherent path length along the line of sight for various opening angles in the equatorial region or bi-conical outflow.

We applied isotropic or latitudinal dependent velocity fields increasing towards the equatorial plane or the polar region. Fig. 3 displays the offset between the blue-shifted and red-shifted peaks assuming a shell radius of $3{\times}10^{16}$ cm (256). Our results show that if the masers are confined within $\sim 30°$ from the equatorial plane, separation between the red- and blue-shifted masers can reproduce the 650 AU observed for the OH maser region of W43A (Fig. 3). The velocity fields in this scenario must be either isotropic or latitudinal dependent enhanced towards the equatorial region.

The distribution of the OH masers in an equatorial outflow could be due to the presence of a binary companion. (260) show that the common envelope evolution of a low mass companion can produce the equatorial outflow. Additionally, in this scenario the bipolar H_2O maser outflow of W43A, can be explained by the dynamo-driven magnetic field caused by the in-spiral of the companion into the envelope.

4. Conclusions

We presented the detection of the magnetic field of $\sim$ 100 μG in the OH maser region of W43A surrounding the collimated jet. This confirms that a large scale magnetic field is present in W43A, which likely plays a role in collimating the jet.

The OH maser distribution of W43A shows non-spherical morphology. We suggest that there is an equatorial distribution for the OH maser region of W43A. This could have been caused by the presence of a binary companion close to the CSE of W43A.

References

Amiri, N., Vlemmings, W., & van Langevelde, H. J. 2010, A&A, 509, A26
Chapman, J. M., & Cohen, R. J. 1986, MNRAS, 220, 513

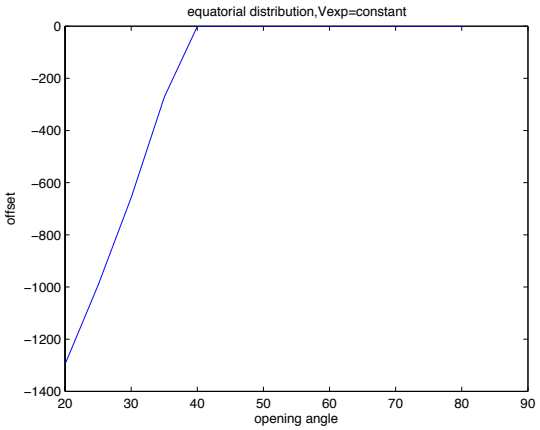

Figure 3. The offset between the most blue-shifted and red-shifted peaks vs. the opening angle in the equatorial plane. The maser shell is supposed to have a constant expansion velocity of 18 km/s in all directions.

Imai, H., Obara, K., Diamond, P. J., Omodaka, T., & Sasao, T. 2002, Nat, 417, 829
Likkel, L., Morris, M., & Maddalena, R. J. 1992, A&A, 256, 581
Manchado, A., Villaver, E., Stanghellini, L., & Guerrero, M. A. 2000, in Asymmetrical Planetary Nebulae II: From Origins to Microstructures, edited by J. H. Kastner, N. Soker, & S. Rappaport, vol. 199 of Astronomical Society of the Pacific Conference Series, 17. arXiv:astro-ph/0002073
Nordhaus, J., & Blackman, E. G. 2006, MNRAS, 370, 2004
Nordhaus, J., Blackman, E. G., & Frank, A. 2007, MNRAS, 376, 599
Sahai, R., & Trauger, J. T. 1998, AJ, 116, 1357
Vlemmings, W. H. T., Diamond, P. J., & Imai, H. 2006, Nat, 440, 58

Asymmetric Planetary Nebulae V
A. A. Zijlstra, F. Lykou, E. Lagadec and I. McDonald
Jodrell Bank Centre for Astrophysics, Manchester, UK © 2011

Morphology of Planetary Nebulae with Water Maser Emission

Tafoya, D.[1], Goméz Y.[2], Patel, N. A.[3], Torrelles J. M.[4], Anglada G.[5] and Miranda, L. F.[6,7]

[1]*Department of Physics and Astronomy, Graduate School of Science and Engineering, Kagoshima University, 1-21-35 Korimoto, Kagoshima 890-0065, Japan.*

[2]*Centro de Radioastronomía y Astrofísica, Universidad Nacional Autónoma de México, 58089 Morelia, Michoacán, México.*

[3]*Harvard-Smithsonian Center for Astrophysics, 60 Garden Street, Cambridge, MA 02138, USA.*

[4]*Instituto de Ciencias del Espacio (CSIC)-UB/IEEC, Facultat de Física, Universitat de Barcelona, Martí i Franquès 1, E-08028 Barcelona, Spain.*

[5]*Instituto de Astrofísica de Andalucía, CSIC, Apartado Correos 3004, E-18080 Granada, Spain.*

[6]*Instituto de Astrofísica de Andalucía - CSIC, C/ Glorieta de la Astronomía s/n, E-18008 Granada, Spain.*

[7]*Departamento de Física Aplicada, Facultade de Ciencias, Universidade de Vigo E-36310 Vigo, Spain (present address).*

Abstract. In order to better understand the formation of asymmetric structures in planetary nebulae (PNe), we have studied two of the three planetary nebulae that are known to harbor water maser emission: K 3−35, IRAS 17347−3139. These objects show a clear bipolar morphology with a narrow waist; the water maser emission arises from the central region and in the case of K 3−35 it is also found located at the surprisingly large distance of 4000 AU from the central star (near the tips of the bipolar lobes). Several mechanisms have been proposed to explain the bipolar morphology of PNe. In the case of K 3−35 we believe that we may be observing some of them at the same time: (i) a disk-like structure traced by the H_2O masers, (ii) a precessing bipolar jet probably due to the presence of a binary companion and (iii) circular polarization in the OH 1665 MHz masers, which suggests the presence of a magnetic field. A detailed modeling of all these observational results might shed light on the formation of asymmetric structures in planetary nebula. On the other hand, we also present the first high angular resolution images of the ionized gas (in radio continuum at λ = 1.3 and 0.7 cm) of IRAS 17347−3139. The results support the presence of a collimated wind which might be shaping the bipolar lobes. Additionally, the 0.7 cm images show an equatorial structure that has been interpreted as a high density ionized torus in which the water maser emission would be arising.
Keywords. Planetary Nebulae

1. Introduction

The mechanisms that lead to the formation of collimated outflows in PNe and their role in the global shaping of these objects are still a matter of debate. Magnetic forces and binary systems have been invoked to explain jets and bipolar morphologies in PNe (see review by 264). However, due to the short time scale of the phase in which the asymmetries are developed (∼1000 years) and to the high degree of absorption of light in the circumstellar envelopes (CSEs) in these objects, the observations necessary to test the models are generally difficult and consequently scarce. In this regard, the maser emission has proven to be a very powerful tool to study the CSEs of AGB, post-AGB stars and PNe. It traces regions that are located just tens of AU from the star to regions in the outer parts of the CSE at $\sim 10^4$ AU. Furthermore, the polarization of the maser emission can reveal the presence of magnetics fields that permeate the CSE. While maser emission of SiO, H_2O and OH has been commonly observed toward the oxygen-rich CSEs of AGB and post-AGB stars, only H_2O and OH maser emission has been found in PNe. Particularly, the H_2O maser emission was not expected to be present in PNe due to the lower density of the circumstellar gas and the high degree of ionization. However, (266) discovered water masers for the first time toward the young PN K 3−35. These authors also found that the OH 1665 MHz maser emission in this source, which seems to be tracing an equatorial torus, shows a high degree of circular polarization ($\gtrsim$50%). This suggests the presence of a magnetic field in the equatorial region of this nebula. However, the spatial and spectral resolution of their observations did not allow to draw clear conclusions. After the discovery of water masers in K 3−35, a survey toward highly obscured young PNe was carried out by (265). They observed 27 objects and found one positive detection toward the PN IRAS 17347−3139. The water masers in this source appeared distributed in a ring-like structure whose center is offset ∼0.″15 from the peak of the radio continuum at 1.3 cm. These authors proposed the possibility that these masers could be arising in one member of a binary system while the radio continuum would be associated to the other member. In addition, the spectral index of the radio continuum of IRAS 17347−3139 was found to be very similar to that of an ionized expanding wind. However, the observations did not have enough angular resolution to clearly determine the parameters of such wind.

In this work we present higher angular and spectral resolution VLA observations of the OH 1665 MHz maser emission toward the PN K 3−35 (§2). We also present VLA radio continuum images of the PN IRAS 17347−3139 (§3) in which we resolve for the first time the ionized component of this nebula.

2. Zeeman pair in the PN K 3−35

On 2002 March 31 we carried VLA observations of the four OH transition at λ∼18 cm in the A configuration, achieving an angular and spectral resolution of ∼1″ and 0.14 km s^{-1}, respectively. Both right circular polarization (RCP) and left circular polarization (LCP) were observed simultaneously. Then, we created the Stokes $I = (I_{\rm RCP} + I_{\rm LCP})/2$ and Stokes $V = (I_{\rm RCP} - I_{\rm LCP})/2$ data sets, where $I_{\rm RCP}$ and $I_{\rm LCP}$ are the intensities in the right and left circular polarizations, respectively. Figure 1 shows the spectra and distribution of the OH 1665 MHz masers spots toward the K 3−35. The circles and triangles indicate the LCP and RCP maser spots, respectively. These maser spots ap-

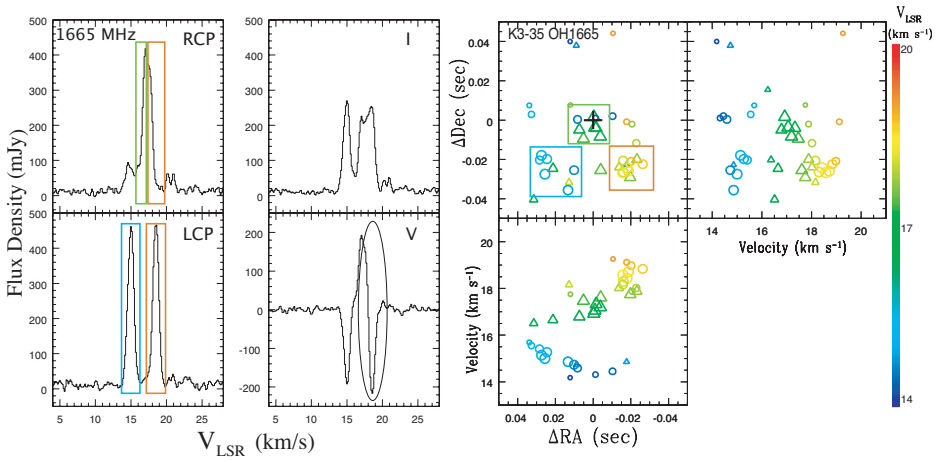

Figure 1. Spectra, spatial distribution and position-velocity diagrams of the OH 1665 MHz masers toward K 3-35. The OH maser spots have been plot with a color-coded velocity shown on the right of the Figure. The circles represent the left circular polarization (LCP) and the triangles the right circular polarization (RCP) features. Three different groups of masers been marked with colored squares in both, the spectra and the maser distribution plot. The orange square marks the region where we suggest there is a Zeeman pair (see §2). The oval in the Stokes *V* spectrum shows the typical "S" shape fingerprint of the Zeeman splitting. The black cross indicates the position of the peak of radio continuum at 1.3 cm.

pear grouped in three spatial regions with different characteristic velocities: one close to the 1.3 cm continuum emission peak ($\sim$ 17.1 km s^{-1}, marked with a green square), and the other two located toward the southeast ($\sim$ 15.0 km s^{-1}, blue square) and southwest ($\sim$ 18.6 km s^{-1}, red square) of the peak of the radio continuum. We notice that the positions of the RCP and LCP maser spots with velocities $\sim$ 17.5 to 18.0 km s^{-1} overlap each other (within 0.″01). Moreover, Stokes *V* spectrum exhibits the typical "S" shape of the Zeeman splitting in that same velocity range (marked with an oval in Figure 1). Assuming that this is indeed a Zeeman pair, we used the following expression to obtain the magnetic field along the line of sight ($B_{\rm LOS}$): $V = b\ c/\nu_0\ dI/dv\ B_{\rm LOS}$ Hz μG^{-1} (267), where dI/dv is the velocity derivative of the Stokes *I* spectrum, ν_0 is the frequency of the transition, c is the speed of light, and b is the splitting coefficient (b = 3.270 for the OH 1665 MHz transition). By computing dI/dv we find that $B_{\rm LOS} \simeq$ 0.9 $\pm$ 0.1 mG, at a distance $\sim$ 0.″03 from the 1.3 continuum peak. When this value is plotted in a *B* - *r* diagram, as that presented by (268), we find that the value of the magnetic field in K 3−35 is in agreement with a $B \propto r^{-2}$ dependance, i.e. a solar-type model.

3. Ionized torus and bipolar lobes in IRAS 17347−3139

On 2005 January 27, we used the VLA in the hybrid configuration BnA, to carry out continuum observations of the PN IRAS 17347−3139 at λ = 3.6, 1.3 and 0.7 cm. The radio continuum emission at 3.6 and 1.3 cm shows a bright central region and a fainter

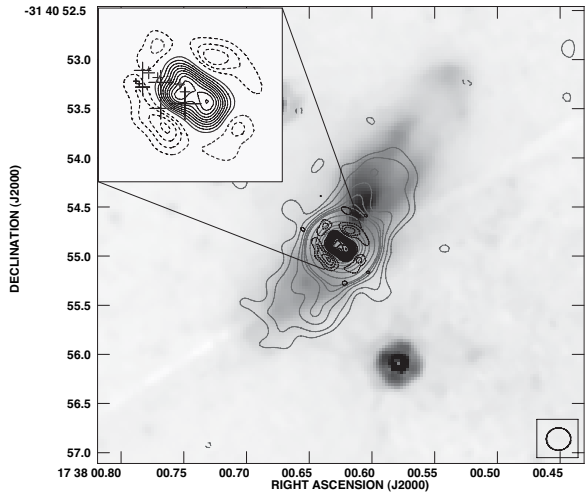

Figure 2. Grey contours: radio continuum emission of IRAS 17347−3139 at wavelength 1.3 cm. Contours are −0.53, 0.53, 1, 2, 3, 4, 5, 10, 20, 30, 40, 50, 60, 70, 80, 90 and 99 per cent of 1.1 $\times 10^{-1}$ Jy/beam. Black contours: radio continuum emission at wavelength 0.7 cm obtained restricting the visibilities to those with a *uv* baseline longer than 500 kλ. Contours are −40, −30,−20,−10, 10, 20, 30, 40, 50, 60, 70, 80, 90, 99 per cent of 2.6 $\times 10^{-2}$ Jy/beam. The masers reported by (265) are indicated by the crosses. Grey scale: HST IR image of IRAS 17347−3139 at 1.1 μm obtained with the NIC1 in the F110W filter.

extended structure elongated in the northwest-southeast direction (P.A. = −30°). Particularly, in the image at 1.3 cm, the extended emission shows a double horn structure in the nortwest-southeast direction with an opening angle of about 30° (see Figure 2). Our high angular resolution images reveal the presence of two structures elongated in more or less perpendicular directions. In fact, a Gaussian fitting to the continuum emission of IRAS 17347−3139 shows that the central compact structure is elongated in the direction with P.A.≃ 50°, while the extended structure is elongated in the direction with P.A.≃ −30°. These directions correspond to those of the dark lane and the bipolar bright lobes observed in the IR images, respectively. This alignment suggests that the radio continuum emission could be arising from two different components: an equatorial ionized torus-like structure (which is evident from the 0.7 cm image), and two ionized bipolar lobes. We have superimposed the water maser emission found by (265) on the radio continuum emission at 0.7 cm from our observations (see Figure 2). In order to do this, we have shifted the positions of the observations of (265), so that the position of the continuum peak emission of their observations coincides with that of our observations at $\lambda \simeq 1.3$ cm. From Figure 2 we find no clear evidence of the presence of a secondary companion associated with the maser emission as suggested by (265), although this possibility cannot be completely ruled out. If we consider that the emission at 0.7 cm is tracing an ionized torus around the central star(s), the relative positions of the maser and the continuum emission suggest that the water masers arise from the outer parts of the ionized torus.

References

Balick, B., & Frank, A. 2002, ARA&A, 40, 439
de Gregorio-Monsalvo, I., Gómez, Y., Anglada, G., Cesaroni, R., Miranda, L. F., Gómez, J. F., & Torrelles, J. M. 2004, ApJ, 601, 921
Miranda, L. F., Gómez, Y., Anglada, G., & Torrelles, J. M. 2001, Nature, 414, 284
Robishaw, T., Quataert, E., & Heiles, C. 2008, ApJ, 680, 981
Vlemmings, W., van Lagevelde, H. J., & Diamond, P. J. 2005, A&A, 434, 1029

Asymmetric Planetary Nebulae V
A. A. Zijlstra, F. Lykou, E. Lagadec and I. McDonald
Jodrell Bank Centre for Astrophysics, Manchester, UK © 2011

Magnetic fields around (post-)AGB stars and (Pre-)Planetary Nebulae

W. H. T. Vlemmings

Argelander-Institut für Astronomie, University of Bonn, Auf dem Hügel 71, D-53121 Bonn, Germany

Abstract. Observational evidence for strong magnetic fields throughout the envelopes of evolved stars is increasing. Many of the instruments coming on line in the near-future will be able to make further contributions to this field. Specifically, maser polarization observations and dust/line polarization in the sub-mm regime has the potential to finally provide a definite picture of the magnetic field strength and configuration from the Asymptotic Giant Branch (AGB) all the way to the Planetary Nebula phase. While current observations are limited in sample size, strong magnetic fields appear ubiquitous at all stages of (post-)AGB evolution. Recent observations also strongly support a field structure that is maintained from close to the star to several thousands of AU distance. While its origin is still unclear, the magnetic field is thus a strong candidate for shaping the stellar outflows on the path to the planetary nebula phase and might even play a role in determining the stellar mass-loss.
Keywords. Planetary Nebulae – Stars: AGB and post-AGB – Magnetic fields

1. Introduction

Strongly asymmetric planetary nebulae (PNe) have been shown to be common. The research into their shaping processes has become a fundamental part of our attempts to further the understanding of the return of processed material into the ISM by low- and intermediate-mass stars at the end of their evolution. Whereas the standard interacting winds scenario (283) can explain a number of the PN properties, an important discovery has been that the collimated outflows of the pre-PNe (P-PNe), where such outflows are common, have a momentum that exceeds that which can be supplied by radiation pressure alone (274). The source of this momentum excess has been heavily debated during the past several years, with the most commonly invoked cause being magnetic fields, binary or disk interaction or a combination of these (e.g. 271). Due to a number of similarities with the jets and outflows produces by young stellar objects, the study of P-PNe outflows provides further research opportunities into a potentially universal mechanism of jet launching.

Here I will review the observational evidence for strong magnetic fields in PNe as well as around their AGB and post-AGB progenitors. I will give an overview of the methods that can be used to study magnetic fields, especially in light of the plethora of new instruments that will be available shortly. Finally, I will discuss a number of questions related this topic that we can expect to be answered with the new instruments in the next few years.

2. Observational Techniques - Polarization

With the exception of observations where the magnetic field strength is estimated assuming forms of energy equilibrium, such as synchrotron observations, the magnetic field strength and structure is typically determined from polarization observations.

2.1. Circular Polarization

Circular polarization, generated through Zeeman splitting, can be used to measure the magnetic field strength. It measures the total field strength when the splitting is large and the line-of-sight component of the field when the splitting is small. The predominant source of magnetic field strength information during the late stages of stellar evolution comes from maser circular polarization observations, and particularly the common SiO, H_2O and OH masers. These can show circular polarization fractions ranging from $\sim 0.1\%$ (H_2O) up to $\sim 100\%$ (OH) and are, because of their compactness and strength, excellent sources to be observed with high angular resolution. Unfortunately, the analysis of maser polarization is not straightforward (For a review, see 291), and it has taken a long time before maser observations were acknowledged to provide accurate magnetic field measurements. More recently, the first attempts have been made to detect the Zeeman splitting of non-maser molecular lines in circumstellar envelopes, such as CN (280). As many of these occur at shorter wavelength in the (sub-)mm regime, the advent of the Atacama Large (sub-)Millimeter Array will further enhance these types of studies.

2.2. Linear Polarization

Linear polarization, probing the structure of the plane-of-the-sky component of the magnetic field, can be observed both in the dust (through aligned grains) and molecular lines (through radiation anisotropy - the Goldreich-Kylafis effect). Typical percentages of linear polarization range from up to a few percent (e.g. dust, CO, H_2O masers) to several tens of percent (OH and SiO masers). Again the interpretation of maser polarization depends on a number of intrinsic maser properties, but in specific instances maser linear polarization can even be used to determine the full 3-dimensional field morphology. In addition to the geometry, the linear polarization of most notably dust, can also be used to obtain a value for the strength of the plane-of-the-sky component of the magnetic field. This is done using the Chandrasekhar-Fermi method, which refers to the relation between the turbulence induced scatter of polarization vectors and the magnetic field strength.

3. Current Status - Evolved Star Magnetic Fields

3.1. AGB Stars

Most AGB magnetic field measurements come from maser polarization observations (SiO, H_2O and OH). These have revealed a strong magnetic field throughout the circumstellar envelope. In Figure 1, I have indicated the magnetic field strength in the regions of the envelope traced by the maser measurements throughout AGB envelopes. While a clear trend with increasing distance from the star is seen, the lack of accurate

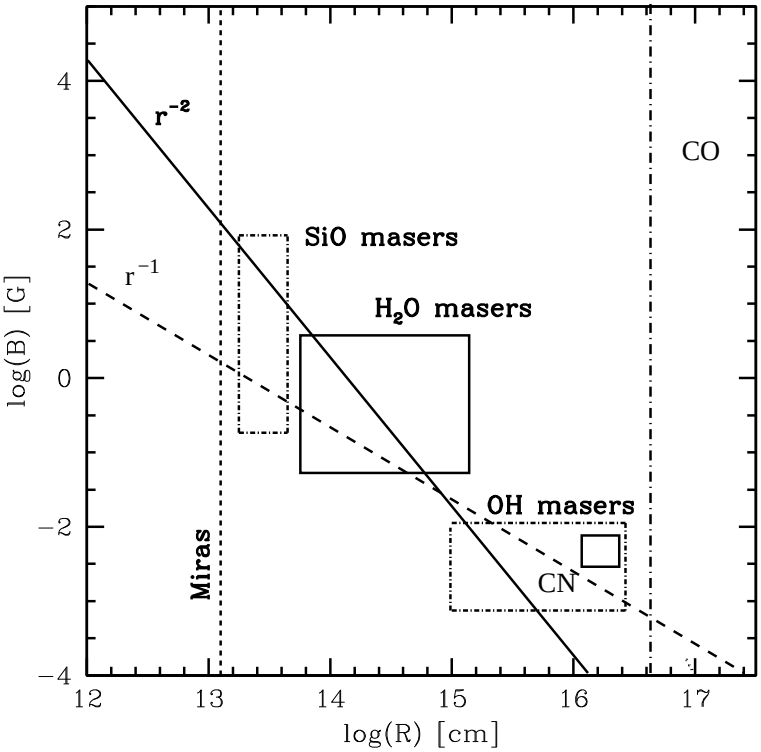

Figure 1. Magnetic field strength vs. radius relation as indicated by current maser polarization observation of a number of Mira stars. The boxes show the range of observed magnetic field strengths derived from the observations of SiO masers (282; 279), H_2O masers (293; 295), OH masers (e.g. 286) and CN (280). The thick solid and dashed lines indicate an r^{-2} solar-type and r^{-1} toroidal magnetic field configuration. The vertical dashed line indicates the stellar surface. CO polarization observations will uniquely probe the outer edge of the envelope (vertical dashed dotted line).

information on the location of the maser with respect to the central stars makes it difficult to constrain this relation beyond stating that it seems to vary between $B \propto R^{-2}$ (solar-type) and $B \propto R^{-1}$ (toroidal). Future observations of CO polarization might be able to provide further constraints.

As the masers used for these studies are mostly found in oxygen-rich AGB stars, it has to be considered that the sample is biased. However, recent CN Zeeman splitting observations (280) seem to indicate that similar strength fields are found around carbon-rich stars.

Beyond determining the magnetic field strength, the large scale structure of the magnetic field is more difficult to determine, predominantly because the maser observations often probe only limited line-of-sights. Even though specifically OH observations seem to indicate a systematic field structure, it has often been suggested that there might not be a large scale component to the field that would be necessary to shape the outflow (289). So far the only shape constraints throughout the envelope have been determined for the field around the supergiant star VX Sgr (Fig.2), where maser obser-

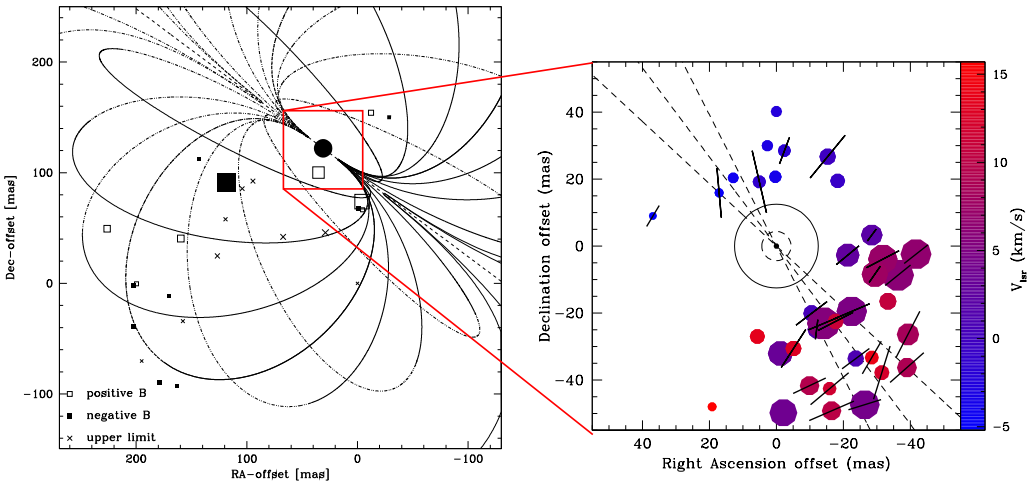

Figure 2. (left) The dipole magnetic field of the supergiant VX Sgr as determined from a fit to the H_2O maser magnetic field observations (295). (right) Positions and polarization of the VX Sgr $v = 0, J = 5 - 4$ ^{29}SiO masers observed with the SMA (294). The masers spots are plotted with respect to the peak of the continuum emission. The black vectors are the observed polarization vectors scaled linearly according to polarization fraction. The long dashed inner circle indicates the star and the solid circle indicates the location of the 43 GHz SiO masers. The short dashed circle indicates the minimum radius of the ^{28}SiO masers. The dashed lines indicate the position angle and its uncertainty of the inferred orientation of the dipole magnetic field of VX Sgr observed using H_2O and OH masers(295; 290).

vations spanning 3 orders of magnitude in distance are all consistent with a large scale, possibly dipole shaped, magnetic field.

3.2. Post-AGB Stars and P-PNe

Similar to the AGB stars, masers are the major source of magnetic field information of post-AGB and P-PNe, with the majority of observations focused on OH masers. These have revealed magnetic field strengths similar to those of AGB stars (few mG) and a clear large scale magnetic field structure (e.g. 270).

The most promising results have come after the detection of the so-called 'water-fountain' sources. These sources exhibit fast and highly collimated H_2O maser jets that often extend beyond even the regular OH maser shell. With the dynamical age of the jet of order 100 years, they potentially are the progenitors of the bipolar (P-)PNe. Although the masers are often too weak for a detection of the magnetic field, observations of the arch-type of the water-fountains, W43A, have revealed a strong toroidal magnetic field that is collimating the jet (Fig. 3 and 292).

3.3. Planetary Nebulae

During the PN phase, masers are rare and weak and until now only the PN K3-35 has had a few mG magnetic field measured in its OH masers (284). Fortunately, there are

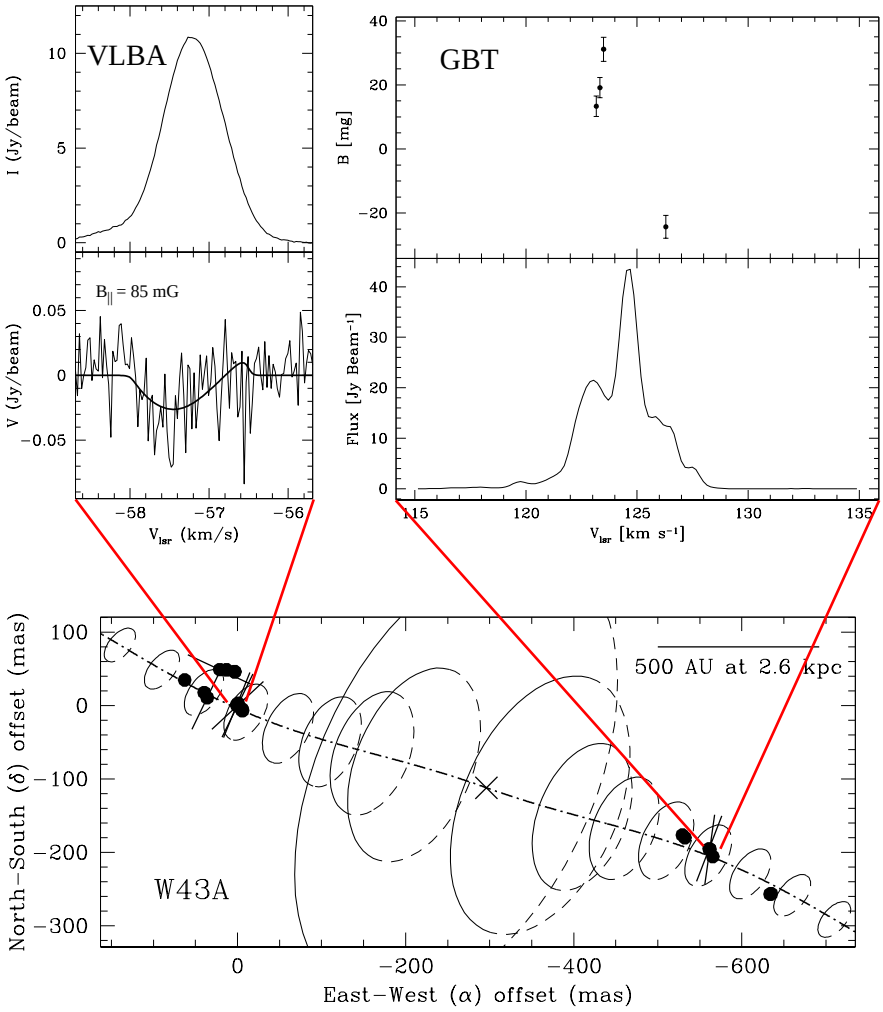

Figure 3. (top left) Total power (I) and V-spectrum for one of the H_2O maser features in red-shifted lobe of the collimated jet of W43A including the best model fit of the V-spectrum corresponding to a magnetic field (292). (top right) Confirmation of the magnetic field from single-dish GBT observations in the blue-shifted side of the lobe. As expected for being toroidal, the magnetic field reverses sign across the blue-shifted masers (269). (bottom) The H_2O masers in the precessing jet (dashed-dotted line) of W43A (indicated by the cross) and the toroidal magnetic field of W43A. The vectors indicate the determined magnetic field direction, perpendicular to the polarization vectors, at the location of the H_2O masers. The ellipses indicate the toroidal field along the jet, scaled with magnetic field strength $\propto r^{-1}$.

a few other methods of measuring PN magnetic fields. The field orientation in the dust of the nebula can be determined using dust continuum polarization observations and current observations seem to indicate toroidal fields, with the dust alignment likely occurring close to the dust formation zone (287). Faraday rotation studies are potentially

also able to study the magnetic field in the interaction region between the interstellar medium and the stellar outflow.

In contrast to AGB stars, the central stars of PNe also show atomic lines that can be used to directly probe the magnetic fields on the surface of these stars. While measurements are still rare, observations of for example the central star of NGC 1360, indicate a field of order several kG (281).

4. Origin of the Magnetic Field

Despite the strong observational evidence for evolved star magnetic fields, the origin of these fields is still unclear. In single stars, differential rotation between the AGB star core and the envelope could potentially result in sufficiently strong magnetic field (273). However, as the energy loss due to a rotating magnetic field drag drains the rotation needed to maintain the field within several tens of years, an additional source of energy is needed (e.g. 285). If AGB stars would be able to have a sun-like convective dynamo, magnetically dominated explosions could indeed result from single stars. Alternatively, the energy could be provided by the interaction with a circumstellar disk, although the origin of the disk is then another puzzle.

Another explanation for maintaining a magnetic field is the interaction between a binary companion or potentially a heavy planet, with common-envelope evolution providing paths to both magnetically as well as thermally driven outflows (285). A companion could be the cause of the precession seen in a number of water-fountain and (P-)PNe jets. However, to date, the majority of the stars with measured magnetic fields do not show any other indication of binarity.

Table 1. Energy densities in AGB envelopes

		Photosphere	SiO	H_2O	OH
B	[G]	~ 50?	~ 3.5	~ 0.3	~ 0.003
R	[AU]	-	~ 3	~ 25	~ 500
		-	$[2-4]$	$[5-50]$	$[100-10.000]$
$V_{\rm exp}$	[km s^{-1}]	~ 5	~ 5	~ 8	~ 10
$n_{\rm H_2}$	[cm^{-3}]	$\sim 10^{14}$	$\sim 10^{10}$	$\sim 10^{8}$	$\sim 10^{6}$
T	[K]	~ 2500	~ 1300	~ 500	~ 300
$B^2/8\pi$	[dyne cm^{-2}]	$\mathbf{10^{+2.0}}$?	$\mathbf{10^{+0.1}}$	$\mathbf{10^{-2.4}}$	$10^{-6.4}$
nKT	[dyne cm^{-2}]	$10^{+1.5}$	$10^{-2.8}$	$10^{-5.2}$	$10^{-7.4}$
$\rho V_{\rm exp}^2$	[dyne cm^{-2}]	$10^{+1.5}$	$10^{-2.5}$	$10^{-4.1}$	$\mathbf{10^{-5.9}}$
V_A	[km s^{-1}]	~ 15	~ 100	~ 300	~ 8

5. Effect of the Magnetic Field

Until a more complete sample of magnetically active AGB stars, post-AGB stars and (P-)PNe is known, it is hard to observationally determine the effect of the magnetic field on these late stages of evolution. Starting with the AGB phase, a number of theoretical works have described the potential of magnetic fields in (at least partly) driving the stellar mass-loss through Alfvén waves(e.g. 276), or through the creation of cool spots on the surface above with dust can form easier (288). As current models of dust and radiation driven winds are still unable to explain especially the mass-loss of oxygen-rich stars, magnetic fields might provide the missing component of this problem, with tentative evidence already pointing to a relation between the magnetic field strength and mass-loss rate.

Other theoretical works have focused on the magnetic shaping of the stellar winds (e.g. 275; 278; 277). But to properly determine the possible effect of the magnetic fields, it is illustrative to study the approximate ratios of the magnetic, thermal and kinematic energies contained in the stellar wind. In Table.1 I list these energies along with the Alfvén velocities and typical temperature, velocity and temperature parameters in the envelope of AGB stars. While many values are quite uncertain, as the masers that are used to probe them can exist in a fairly large range of conditions, it seems that the magnetic energy dominates out to $\sim 50-100$ AU in the circumstellar envelope. This would correspond to the so-called 'launch' region of magneto-hydrodynamic (MHD) outflows, which typically extend to no more than $\sim 50R_i$, with R_i the inner-most radial scale of launch engine (e.g. 272). A rough constraint on R_i thus seems to be $\sim 1-2$ AU, close to the surface of the star.

6. Outlook

While progress in studying the magnetic fields of evolved stars has been significant, a number of crucial questions remain to be answered. Several of these can be addressed with the new and upgraded telescopes in the near future. For example, the upgraded EVLA and eMERLIN will uniquely be able to determine the location of the masers in the envelope with respect to the central star, giving us, together with polarization observations, crucial information on the shape and structure of the magnetic field throughout the envelopes. ALMA will be able to add further probes of magnetic fields with for example high frequency masers and CO polarization observations, significantly expanding our sample of stars with magnetic field measurements. With the ALMA sensitivity, polarization will be easily detectable even in short observations and thus, even if not the primary goal, polarization calibration should be done. The new low-frequency arrays can potentially be used to determine magnetic fields in the interface between the ISM and PNe envelopes through Faraday rotation observations.

With the advances in the search for binaries and the theories of common-envelope evolution and MHD outflow launching, the new observations will address for example:

- Under what conditions does the magnetic field dominate over e.g. binary interaction when shaping outflows?
- Are magnetic fields as widespread in evolved stars as they seem?

- What is the origin of the AGB magnetic field - can we find the binaries/heavy planets that might be needed?
- Is there a relation between AGB mass-loss and magnetic field strength?

Acknowledgments. WV acknowledges the support by the Deutsche Forschungsgemeinschaft (DFG) through the Emmy Noether Research grant VL 61/3-1, and the work by the various researchers that have been crucial in the development of the area of evolved star magnetic field research (including those that I neglected to reference in this review).

References

Amiri, N., Vlemmings, W., & van Langevelde, H. J. 2010, A&A, 509, A26+
Bains, I., Gledhill, T. M., Yates, J. A., & Richards, A. M. S. 2003, MNRAS, 338, 287
Balick, B., & Frank, A. 2002, ARA&A, 40, 439
Blackman, E. G. 2009, in IAU Symposium, vol. 259 of IAU Symposium, 35
Blackman, E. G., Frank, A., Markiel, J. A., Thomas, J. H., & Van Horn, H. M. 2001, Nat, 409, 485
Bujarrabal, V., Castro-Carrizo, A., Alcolea, J., & Sánchez Contreras, C. 2001, A&A, 377, 868
Chevalier, R. A., & Luo, D. 1994, ApJ, 421, 225
Falceta-Gonçalves, D., & Jatenco-Pereira, V. 2002, ApJ, 576, 976
Frank, A., & Blackman, E. G. 2004, ApJ, 614, 737
García-Segura, G., López, J. A., & Franco, J. 2005, ApJ, 618, 919
Herpin, F., Baudry, A., Thum, C., Morris, D., & Wiesemeyer, H. 2006, A&A, 450, 667
Herpin, F., Baudy, A., Josselin, E., Thum, C., & Wiesemeyer, H. 2009, in IAU Symposium, vol. 259 of IAU Symposium, 47
Jordan, S., Werner, K., & O'Toole, S. J. 2005, A&A, 432, 273
Kemball, A. J., Diamond, P. J., Gonidakis, I., Mitra, M., Yim, K., Pan, K., & Chiang, H. 2009, ApJ, 698, 1721
Kwok, S., Purton, C. R., & Fitzgerald, P. M. 1978, ApJ, 219, L125
Miranda, L. F., Gómez, Y., Anglada, G., & Torrelles, J. M. 2001, Nat, 414, 284
Nordhaus, J., & Blackman, E. G. 2006, MNRAS, 370, 2004
Rudnitski, G. M., Pashchenko, M. I., & Colom, P. 2010, Astronomy Reports, 54, 400
Sabin, L., Zijlstra, A. A., & Greaves, J. S. 2007, MNRAS, 376, 378
Soker, N. 1998, MNRAS, 299, 1242
— 2002, MNRAS, 336, 826
Szymczak, M., Cohen, R. J., & Richards, A. M. S. 2001, A&A, 371, 1012
Vlemmings, W. H. T. 2007, in IAU Symposium, edited by J. M. Chapman & W. A. Baan, vol. 242 of IAU Symposium, 37
Vlemmings, W. H. T., Diamond, P. J., & Imai, H. 2006, Nat, 440, 58
Vlemmings, W. H. T., Diamond, P. J., & van Langevelde, H. J. 2002, A&A, 394, 589
Vlemmings, W. H. T., Humphreys. E. M. L., & Franco-Hernández, R. 2010, ApJ, submitted
Vlemmings, W. H. T., van Langevelde, H. J., & Diamond, P. J. 2005, A&A, 434, 1029

Asymmetric Planetary Nebulae V
A. A. Zijlstra, F. Lykou, E. Lagadec and I. McDonald
Jodrell Bank Centre for Astrophysics, Manchester, UK © 2011

Dust at sub-solar metallicity: the case of post-AGB stars in the Large Magellanic Cloud

M. Matsuura[1,2], G. C. Sloan[3], J. Bernard-Salas[3,4], K. Volk[5], and B. J. Hrivnak[6]
[1] *UCL-Institute of Origins, Department of Physics and Astronomy, University College London, Gower Street, London WC1E 6BT, UK*

[2]*UCL-Institute of Origins, Mullard Space Science Laboratory, University College London, Holmbury St. Mary, Dorking, Surrey RH5 6NT, UK*

[3]*Astronomy Department, Cornell University, 610 Space Sciences Building, Ithaca, NY 14853-6801, USA*

[4]*Institut d Astrophysique Spatiale, CNRS/Universite Paris-Sud 11, 91405 Orsay, France*

[5]*Space Telescope Science Institute, 3700 San Martin Drive, Baltimore, MD 21218, USA*

[6]*Department of Physics and Astronomy, Valparaiso University, Valparaiso, IN 46383, USA*

Abstract. Low- and intermediate-mass stars are one of the important dust sources in the interstellar medium (ISM) of galaxies. The compositions of dust ejected from these stars are likely to affect those in the ISM. We investigate dust in post-Asymptotic Giant Branch (AGB) stars, which are in a late evolutionary phase for low- and intermediate-mass stars, and which produce a wide variety of dust grains. We are particularly targeting post-AGB stars in the Large Magellanic Cloud (LMC), which has about half of the solar metallicity, to investigate the effects of sub-solar metallicity on dust compositions. Using the Spitzer Space Telescope, we obtained 5–30 μm spectra of 24 post-AGB candidates in the LMC. Five are C-rich post-AGB stars, and this presentation focuses on spectra of these stars. We found that rare dust features in the Milky Way, such as a 21 μm unidentified feature are commonly found in LMC post-AGB stars. The 6–8 μm spectra are compared with those of Galactic objects. Four spectra match the Galactic templates of polycyclic aromatic hydrocarbon (PAH) features. However, we found the three objects show 7.85 μm feature which have not been found in Galactic post-AGB stars. Low metallicity conditions definitely affect the dust formation process and compositions.
Keywords. Planetary nebulae – Post-AGB stars – LMC

1. Introduction

There are four key aspects regarding dust grains to be investigated in AGB stars, post-AGB stars and planetary nebulae (PNe). First, the dust grains maintain the thermal balance within the nebulae, absorbing UV and optical photons, and sometimes pro-

ducing large infrared excesses (308). Second, dust grains are an important catalyst for molecular formation. In particular, chemical reactions on grains are required to produce molecular hydrogen (304), including in PNe (296; 325). Third, dusty disks and tori might trigger asymmetry in post-AGB stars and PNe. Finally, these evolved stars are one of the important contributors of dust found in the interstellar medium (ISM) of galaxies (300; 313). The importance of dust is reported in the White Paper developed during this conference.

Our work is specifically directed to comparing dust found in circumstellar envelopes (CSEs) of AGB/post-AGB/PNe to the dust in the ISM. As such, we will be able to reveal if dust has been subsequently processed in the ISM. Our main focus is the dust in post-AGB stars, where wide varieties of dust species have been detected.

Our targets are post-AGB stars in the LMC, our neighbouring galaxy. One of the advantages is that the distance of post-AGB stars in this galaxy are independently measured, whereas the distance is an unknown parameter for the Galactic post-AGB stars. This is ideal since it allows one to trace the stellar evolution on an HR diagram. Secondly, the LMC provides a laboratory at sub-solar metallicity. Dust grains contain metals and so the mass and composition of dust might change according to the metallicity. Finally, the close distance is favourable for resolving the constituent stars in the galaxy, and recent advances in observational techniques in the infrared enable us to carry out detailed studies of objects belonging to this galaxy for the first time.

In this paper, we report our observational studies of dust in the LMC, indicating the effects of metallicity on the dust grains in the post-AGB stars.

2. Observations

We have obtained spectra of 24 post-AGB candidates in the LMC, using the Infrared Spectrometer (IRS; 306) on board the Spitzer Space Telescope. We used the low-spectral resolution mode for the majority of targets. The spectral resolution was $\lambda/\Delta\lambda$=60–130. We have chosen the targets largely based on infrared brightness, using the Spitzer imaging survey data of the LMC (SAGE; 315). Matsuura et al. (314) describe the details of the sample selection and provide an observing log.

Mid-infrared spectroscopy is a powerful tool to distinguish object types (AGB, post-AGB, PNe, and R CrB) of infrared-bright evolved stars, as well as chemical types (oxygen-rich or carbon-rich; no obvious S-type stars found). Figure 1 shows the spectra of the 24 targets we observed. We describe the characteristics and categorise post-AGB objects in our paper; we found 5 carbon-rich (hereafter, C-rich) post-AGB stars and 2 oxygen-rich (O-rich) post-AGB stars. Other types we found among our sample were 8 C-rich AGB stars, 2 R CrB candidates, 3 C-rich PNe, 3 young stellar objects (YSOs) and 1 luminous blue variable (LBV). There are no O-rich AGB stars in our sample.

The largest category in our sample is C-rich AGB stars. The stars we detected are special amongst C-rich AGB stars, the so-called 'extremely red objects' (EROs) (303). The spectral energy distributions peak in the 10–20 μm range, often with a SiC dust feature at 11.3 μm in absorption. C-rich stars commonly show C_2H_2 in absorption (311). EROs still show C_2H_2 in absorption, but very weakly. Some of them (e.g. IRAS 05189−7008 in Figure 1) have a secondary peak in the optical, showing that the

central star has partially cleared out its optically-thick circumstellar envelope. It is likely that these stars are transiting from the AGB to the post-AGB phase.

Gielen et al. (301) and van Aarle et al. (324) have studied post-AGB stars in the LMC, and their targets are mostly binary objects. They found more to be O-rich than C-rich. Our targets are not selected based on suspected binarity. Although the samples are small, it is possible that binarity and chemical types may be related.

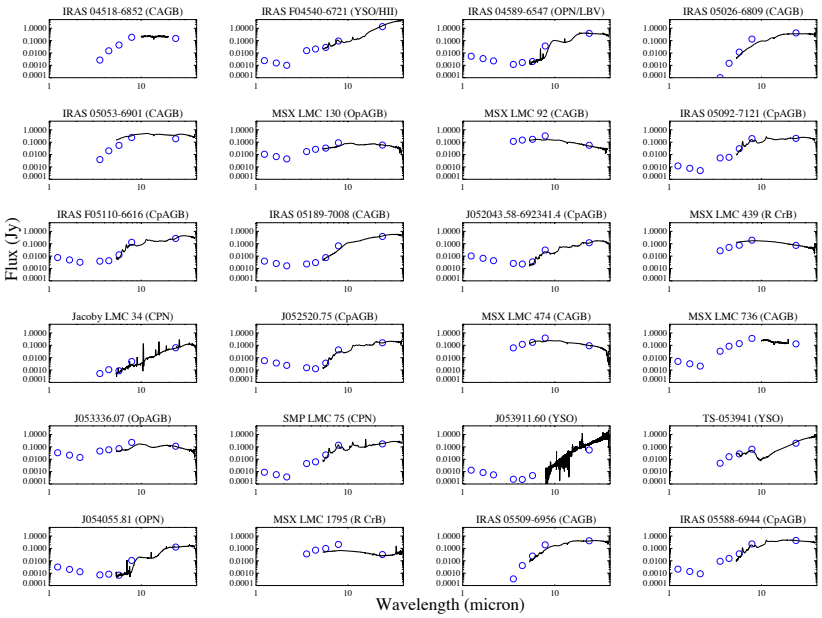

Figure 1. Spitzer IRS spectra of LMC IR bright objects, overlaid on photometric data at 1–24 μm. Object classifications show CAGB (C-rich AGB), CPN (C-rich PN), CpAGB (C-rich post-AGB), LBV (luminous blue variable), OPN (O-rich PN), OpAGB (O-rich post-AGB), R CrB, YSO (young stellar object).

3. Dust features in C-rich post-AGB stars

Figure 2 presents the Spitzer *IRS* spectra of the five C-rich post-AGB stars, showing a variety of emission features. The next section discusses the features related to PAHs, which dominate. The 30 μm feature probably arises from MgS (302). The features at 6.9 μm and 7.3 μm are likely to be from aliphatic carbon (299; 309), although there might be some contributions of PAHs to the 6.9 μm feature (323).

The spectra in Figure 2 also show a feature centred at 15.8 μm (e.g. IRAS 05092 and J052520.70) and the unidentified '21 μm' feature, which actually peaks at 20 μm in these spectra. The carrier of the 21 μm feature remains a point of controversy (e.g.

326; 307). The details of this feature in our sample will be presented by Volk et al. (327). The carrier of the 15.8 μm and 21 μm features may be related (307; 328).

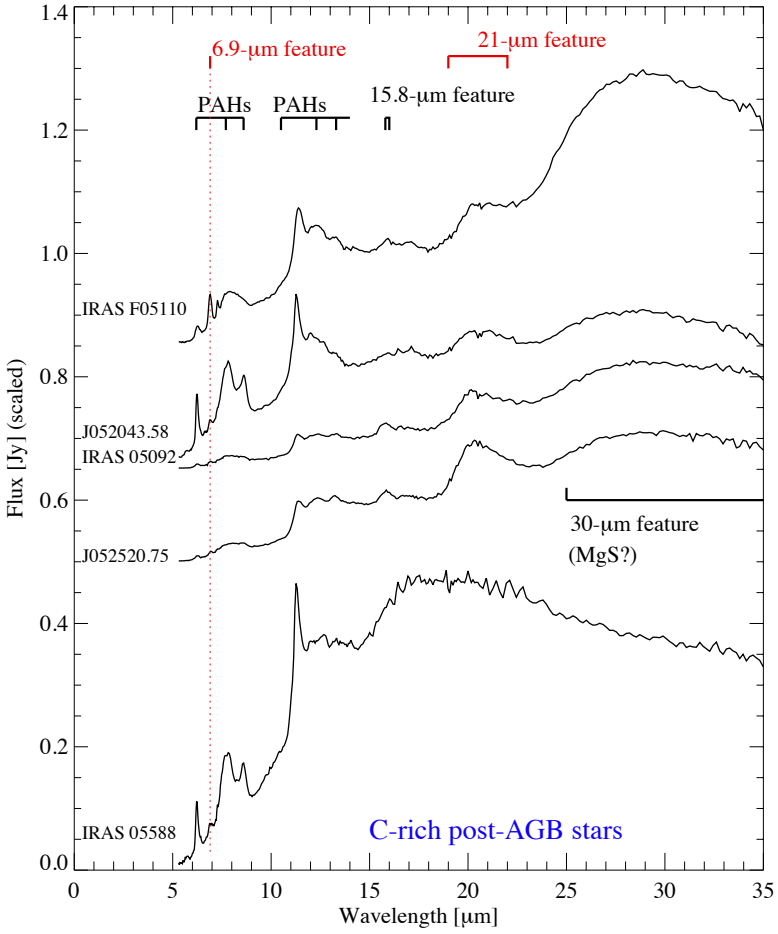

Figure 2. Spectra of C-rich post-AGB stars in the LMC.

4. Polycyclic Aromatic Hydrocarbons (PAHs) and other features at 6–9 μm

To examine the details of PAH and other small features, we subtract 'continua' from the observed spectra. Matsuura et al. (314) provide details of this process. Figure 3 plots the continuum-subtracted spectra. Peeters et al. (317) and Hony et al. (305) have analysed PAHs in Galactic objects, including post-AGB stars, PNe, and HII regions, and these authors classified them into classes, A, B and C. Figure 3 shows their template spectra. The classes can be distinguished by the number of peaks and the peak wavelength, as indicated in the figure. Both classes A and B show features peaking at about 7.65 and 7.85 μm, with the 7.65 μm peak dominating in class A and the 7.85 μm peak dominating in class B. In class C, only a single peak appears at about 8.3 μm.

Among our sample, two spectra can be classified into A, and another two into B. Three further objects show similar profiles to class C, as they have a broad single feature between 7 and 9 μm. However, their peak wavelengths are shorter than those found in class C. These three spectra do not fit within the current A-B-C classification system. We label these three as 'others', having two peaks at about 6.3 and 7.85 μm.

In the spectra of these three 'others', the 6.3 μm feature is due to PAHs. However, that feature is broader than normally observed and much more symmetric. Overall, the behaviour of this feature is analogous to the behaviour of 7-9 μm feature, and together these suggest a carrier that differs in some way from a normal PAH mixture.

The 7.7–7.8 μm feature could arise from PAHs (318; 319) or the vibrational transition of -$(CH_2)_n$- in aliphatic carbon (322). However, the width of the feature probably requires multiple components rather than a solitary aliphatic-carbon band.

Although Galactic class C and LMC objects with the 7.85 μm feature have central stars with similar spectral types (F and G; 317; 320), the wavelength of the feature differs. It could be due to the difference of PAH compositions between LMC and Galactic objects. Whereas in class A and B PAHs, there is no difference between LMC and Galactic objects. The difference is found only in stars with spectral classes of F and G-type.

Among C-rich post-AGB stars, we did not find any difference in the strength of PAHs between Galactic and LMC objects. This is consistent with what Bernard-Salas et al. (298) found in PNe. Among objects with 21 μm features, which are a sub-class of post-AGB stars, PAHs are stronger (327). At lower metallicity, PAHs could be formed reasonably well. This is because C_2H_2, which is a parent molecule for the PAH formation (297), is abundantly found in AGB stars in lower metallicity galaxies (310; 312; 321) since carbon atoms are synthesised within these stars and since the oxygen abundance is low, resulting in a high excess of available carbon.

Acknowledgments. We acknowledge the financial support of NASA grant (JPL-RSA 1378453).

References

Aleman I., & Gruenwald R., 2004, ApJ 607, 865
Allamandola L.J., Tielens A.G.G.M., & Barker, J. R. 1989, ApJS, 71, 733
Bernard-Salas J., Peeters E., Sloan G.C., Gutenkunst S., Matsuura M., Tielens A.G.G.M., Zijlstra A.A., & Houck, J.R., 2009, ApJ 699, 1541

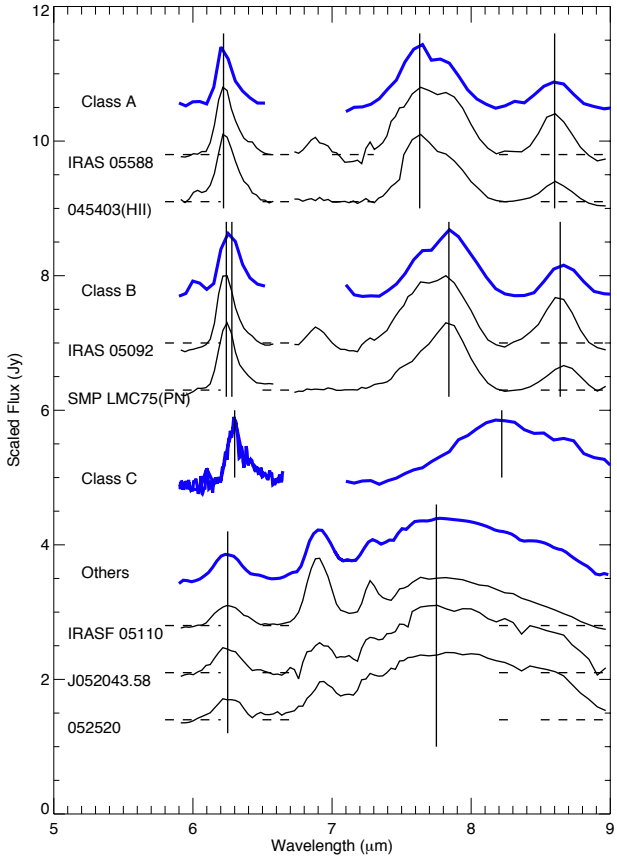

Figure 3. The 6–9 μm spectra in LMC post-AGB stars. As references, PAH spectra of an HII region and planetary nebula in the LMC are plotted. Peeters et al. (317) and Hony et al. (305) have analysed PAHs in Galactic objects and classified them into three classes, A, B and C, and we plot these templates. The spectra of the three LMC objects match any of the Peeters classes. These three are called 'others'.

Duley W.W., & Williams D.A., 1981, MNRAS 196, 269
Gehrz R., 1989, in Allamandola L.J., Tielens A.G.G.M., eds, Proceedings of IAU Symp. 135, 'Interstellar Dust', p. 445
Gielen C., et al., 2009, A&A 508, 1391

Goebel J.H., & Moseley S.H., 1985, ApJ 290, L35
Gruendl R.A., Chu Y.-H., Seale J.P., Matsuura M., Speck A.K., Sloan G.C., & Looney L.W., 2008, ApJ 688, L9
Hollenbach D., & Salpeter E.E., 1971, ApJ 163, 155
Hony S., Waters L.B.F.M., & Tielens A.G.G.M., 2002, A&A 390, 533
Houck J.R., et al., 2004, ApJS 154, 18
Hrivnak B.J., Volk K., & Kwok S., 2009, ApJ 694, 1147
Kwok S., 2000, 'The Origin and Evolution of Planetary Nebulae', Cambridge University Press
Kwok S., Volk K.M., & Bernath P., 2001, ApJ 554, L87
Matsuura M., et al., 2005, A&A 434, 691
Matsuura M., et al., 2006, MNRAS 371, 415
Matsuura M., et al., 2007, MNRAS, 382, 1889
Matsuura M., et al., 2009, MNRAS 396, 918
Matsuura M., et al., to be submitted
Meixner M., et al., 2006, AJ 132, 2268
Moutou C., Verstraete L., Léger A., Sellgren K., & Schmidt W., 2000, A&A 354, L17
Peeters E., Hony S., Van Kerckhoven C., Tielens A.G.G.M., Allamandola L.J., Hudgins D.M., & Bauschlicher C.W., 2002, A&A 390, 1089
Sandford S.A., et al., 1998a, J.Phys.Chem.A, 102, 329-343
Sandford S.A. et al., 1998b, J. Phys. Chem. A, 102, 353-360
Sloan G.C., et al., 2007, ApJ 664, 1144
Sloan G.C., et al., 2009, Science 323, 353
Socrates, G., 2001, 'Infrared and Raman Characteristic Group Frequencies: Tables and Charts', John Wiley & Sons, Ltd, Chichester, England
Tielens A.G.G.M., 2008, ARA&A 46, 289
van Aarle, E., et al., 2009, IAUS 256, 415
van Hoof P.A.M., et al. 2010, A&A 518, L137
Volk K.M., Kwok S., & Hrivnak B.J., 1999, ApJ 516, L99
Volk K.M., et al., to be submitted
Zhang Y., Kwok S., & Hrivnak B.J. 2010, arXiv1010.1327
Zijlstra A.A., et al., 2006, MNRAS 370, 1961

Asymmetric Planetary Nebulae V
A. A. Zijlstra, F. Lykou, E. Lagadec and I. McDonald
Jodrell Bank Centre for Astrophysics, Manchester, UK © 2011

A VISIR/VLT imaging survey of post-AGB stars

Eric Lagadec

European Southern Observatory, Karl Schwarzschildstrasse 2, Garching 85748, Germany

Abstract. We observed 86 evolved stars using the mid-infrared imager VISIR on the VLT, to look for departure from spherical symmetry morphologies in their envelopes. The observations were taken with exceptionally low water vapor at Cerro Paranal, leading to diffraction-limited images for this first 8m class mid-infrared imaging survey of post-AGB stars. We resolved some detached shells or dusty torii in some envelopes. The nebulae with detached shells are all spherical or bipolar,while the nebulae around resolved core are either bipolar or multipolar. Most of the resolved objects appear to be non spherical, which could be a sign of interaction with a binary companion.

Keywords. Planetary nebulae – Stars: AGB to post-AGB stars

1. Introduction

The departure from spherical symmetry during the late stages of the evolution of low and intermediate mass stars occurs in the inner parts of their circumstellar envelopes. To observe the inner part of these envelopes, we need mid-infrared observations, as the dust optical depth is smaller at longer wavelengths. Mid-infrared observations of AGB and post-AGB stars have been made in the past. But the only survey has been made with 3-m class telescopes (335) and present a lack of angular resolution for the morphological study of the observed objects, a selection bias as they observed known bipolar nebulae and consists of only 17 resolved sources. Some work has been done using 8-m class telescope, but always focusing on particular individual bright well-known objects (e.g. 336).

2. Observations and data reduction

We observed 86 evolved stars using VISIR/VLT. The observations presented here come from three ESO programs, two in standard mode (380.D-0630(A), 081.D-0616(A)), and one in burst mode (081.D-0130(A)). All the stars were observed with 3 filters: PAH1 (8.59μm, half band width 0.42μm), SiC (11.85μm, 2.34μm) and NeII (12.81μm, 0.21μm). The burst mode observations were taken during the driest night ever recorded at Cerro Paranal, leading to excellent diffraction-limited images ($\sim$ 0.3 arcsec). We selected all the post-AGB star candidates observable from Paranal with an IRAS 12 μm flux higher than 10 Jy from the Torùn post-AGB star catalog (Szcerba et al., 2007). We also observed the post-AGB stars from the catalogs by Meixner et al. (335) and

Table 1. Log of our VISIR observations. Target shapes are defined as *S, dS, CS, B, El, M, DL, RC*: spherical, detached shell, central source, bipolar, elliptical, multipolar, Dark Lane visible (cold dusty disc) and resolved core respectively. PAGB, RSG and WF refer to Post-AGB, Red Supergiant and Water-fountain respectively.

Source	α(J2000)	δ(J2000)	IRAS$_{12}$(Jy)	shape	type
IRAS07134+1005	07 16 10	+09 59 47	24.51	dS,CS, El	CPAGB
IRAS10197−5750	10 21 33	−58 05 48	200.0	M, RC	C/O PAGB
IRAS15103−5754	15 14 18	−58 05 20	10.8	B, DL?	WF
IRAS15445−5449	15 48 19	−54 58 20	6.8	B, DL?	WF
IRAS16279−4757	16 31 38	−48 04 04	43.0	M,CS	OCPAGB
IRAS16333−4807	16 37 06	−48 13 42	9.3	M,CS	WF
IRAS16342−3814	16 37 40	−38 20 17	16.2	B, DL	WF
IRAS16594−4656	17 03 10	−47 00 27	44.9	B, RC	CPAGB
IRAS17163−3907	17 19 49	−39 10 37	1240	S,dS	PAGB
IRAS17311−4924	17 35 02	−49 26 26	18.3	DL	PAGB
IRAS17347−3139	17 38 01	−31 40 58	18.99	B	OPPN
IRAS17441−2411	17 47 08	−24 12 59	42.8	B	PAGB
IRAS18450−0148	18 47 41	−01 45 11	23.3	CS	WF
IRAS19016−2330	19 04 43	−23 26 08	12.6	El	PAGB
IRAS19114+0002	19 13 58	+00 07 31	31.3	CS, S	OPAGB/RSG
IRAS19244+1115	19 26 48	+11 21 17	1346.0	S	OPAGB/RSG
IRAS19374+2359	19 39 36	+24 06 28	23.62	El	OPAGB
IRAS19386+0155	19 41 08	+02 02 31	17.4	El	PAGB
IRAS19454+2920	19 47 24	+29 28 12	17.27	El	CPAGB
IRAS19500−1709	19 52 52	−17 01 50	27.8	El, dS	CPAGB
IRAS20043+2653	20 06 23	+27 02 09	17.89	El	OPAGB
IRAS23166+1655	23 19 12	+17 11 35	706.0	El	CPAGB

Bujarrabal et al. (330) observable from Cerro Paranal. We added some water fountains and the brightest AGB stars we could observe. Our sample consists of 12 AGB stars, 52 post-AGB, 2 Planetary Nebulae, 2 RCrB, 8 RV Tau and 10 water fountain sources.

3. Observed Morphologies

55 of the stars we observed appeared unresolved even with a 8m-class telescope. Among the 33 resolved targets, we observed 14 elliptical, 7 bipolar, 4 multipolar, 4 spherical, 1 asymmetrical (an HII region) and a squared (a Be star) nebulae. Amongst the 52 post-AGB objects we observed, 34 are point sources, 14 elliptical, 3 spherical, 7 bipolar and 4 multipolar. Most of the post-AGB stars we observed are thus non-spherical. This is also the case for the water fountains that are all bipolar or multipolar.

For five objects (IRAS 07134+1005, IRAS 17163−3907, IRAS 19114+0002, IRAS 19374+2359 and IRAS 19500−1709), we clearly resolved a detached shell, characteristic of the post-AGB phase. All these nebulae are either spherical or elliptical. IRAS 19500−1709 was observed at similar wavelengths with OSCIR on the Gemini South

telescope, but no detached shell was resolved (332). They predicted the presence of a detached shell using a radiative transfer model, with a size similar to the one we observed. This shows that the excellent weather conditions we had during our observing run enabled us to achieve the best possible angular resolution from a ground-based 8m class telescope in the N band. This shell was ejected when the mass-loss phenomenon ceased. We measure a diameter of the inner detached shell of ∼0.4 arcsec. Assuming an expansion velocity of the shell of 11km.s^{-1} and a distance of 4 kpc leads to the conclusion that this shell was ejected ∼1400 years ago.

Four of the observed stars (IRAS10197−5750, IRAS 16594−4656, IRAS 17311−4924 and IRAS 17411−2411) show a clearly resolved central dusty torus. All these nebulae are clearly bipolar or multipolar. The observed torii are perpendicular to the bipolar nebula, and have certainly played an important role in their shaping. Our multi wavelengths observations will bring important constraints on the dust mass and temperature in these torii and a better understanding of their influence in the shaping.

Some of our sources are clearly bipolar or multipolar, with an unresolved core (IRAS 16279−4757, IRAS 17347−3139). These objects will be perfect targets for interferometric observations with the Very Large Telescope Interferometer (VLTI). VLTI/MIDI observations of the planetary nebulae Menzel 3 and M2-9 have enabled us to discover and study dusty discs in the core of these objects (331). Observations of similar structures in the core of post-AGB objects will allow us to study the formation and evolution of discs after the AGB phase.

We finally obtained the first resolved images of the water fountains sources IRAS 15103−5754, IRAS 15445−4449 and W43A. These three objects are clearly bipolar. The edges of the bipolar lobes of IRAS 15445−4449 are terminated by spurs that could be either jets or the projection of a biconical structure on the plane of the sky. The jets are perpendicular to the equatorial plan of the nebula and are certainly due to the jets inferred by the water maser that shaped the bipolar nebula around IRAS 15445−4449. A dark equatorial lane, due to a thick cold dusty disc, is also observed in this nebula. The presence of such a disc and bipolar jets could indicate the presence of a binary system in the core of this nebula, responsible for the shaping of the nebula.

IRAS 16279−4757 and IRAS 10197−5750, classified as bipolar from mid-infrared observations using TIMMI on the ESO 3.6 m telescope (334; 333), appear to be multipolar on our high angular resolution images. This indicates that high angular resolution observations are crucial to understand the morphologies of these objects.

Acknowledgments. This work would not have been possible without the great help from Tijl Verhoelst, Djamel Mékarnia, Olga Suarez and Philippe Bendjoya.

References

Bujarrabal, V., Castro-Carrizo, A., Alcolea, J., & Sánchez Contreras, C. 2001, A&A, 377, 868
Chesneau, O., Lykou, F., Balick, B., Lagadec, E., Matsuura, M., Smith, N., Spang, A., Wolf, S., & Zijlstra, A. A. 2007, A&A, 473, L29
Clube, K. L., & Gledhill, T. M. 2004, MNRAS, 355, L17
Lagadec, E., Mékarnia, D., de Freitas Pacheco, J. A., & Dougados, C. 2005, A&A, 433, 553
Matsuura, M., Zijlstra, A. A., Molster, F. J., Hony, S., Waters, L. B. F. M., Kemper, F., Bowey, J. E., Chihara, H., Koike, C., & Keller, L. P. 2004, ApJ, 604, 791

Meixner, M., Ueta, T., Dayal, A., Hora, J. L., Fazio, G., Hrivnak, B. J., Skinner, C. J., Hoffmann, W. F., & Deutsch, L. K. 1999, ApJS, 122, 221
Miyata, T., Kataza, H., Okamoto, Y. K., Onaka, T., Sako, S., Honda, M., Yamashita, T., & Murakawa, K. 2004, A&A, 415, 179

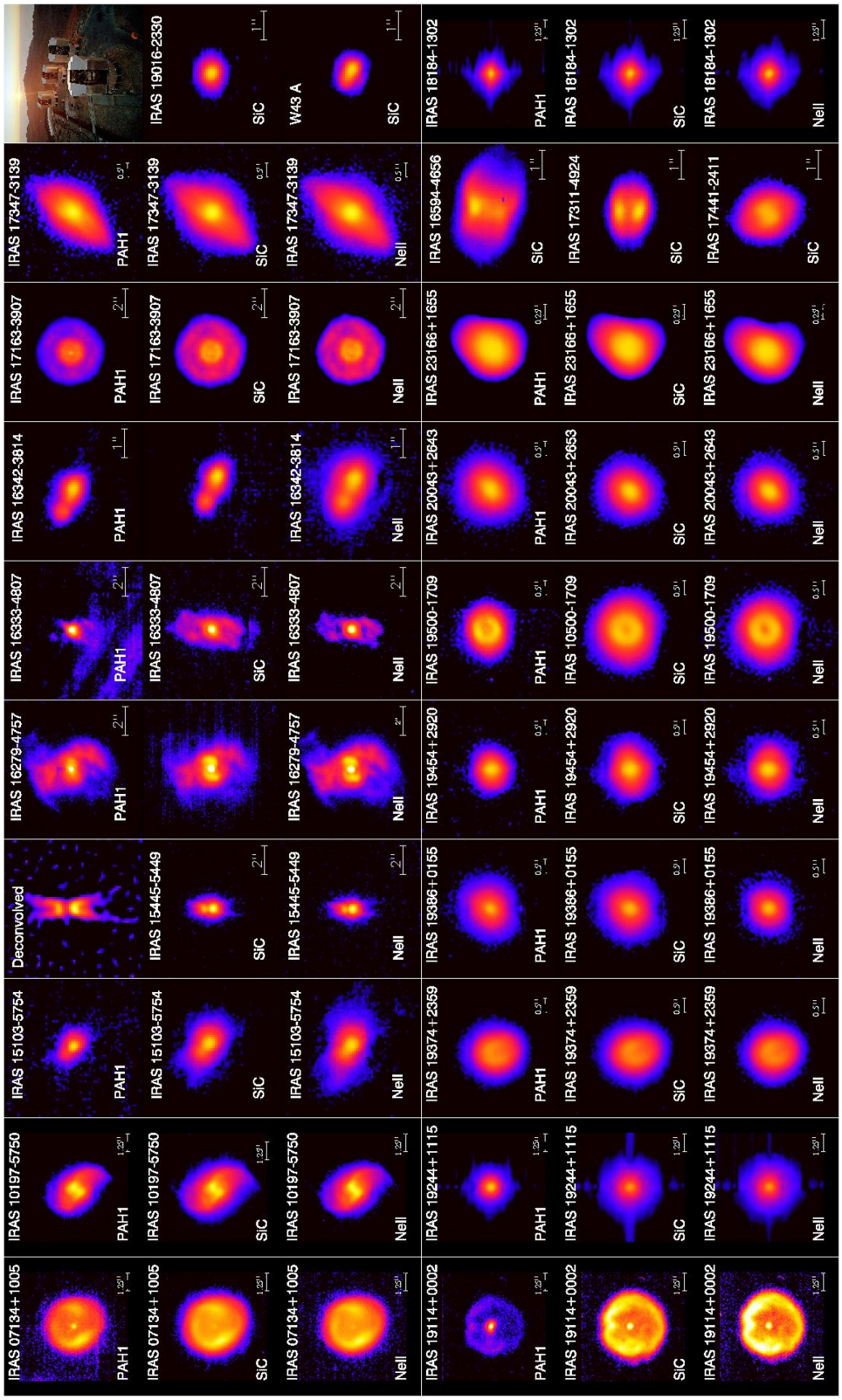

Figure 1. VISIR images of the 23 largest evolved stars we observed in three different filters, centered at 8.59, 11.85 and 12.81μm (PAH1, SiC and NeII respectively).

Asymmetric Planetary Nebulae V
A. A. Zijlstra, F. Lykou, E. Lagadec and I. McDonald
Jodrell Bank Centre for Astrophysics, Manchester, UK © 2011

Point-Symmetry types in Planetary Nebulae

Laurence Sabin[1], Roberto Vázquez[1], Maria Eugenia Contreras[1], Saul Zavala[2], Lorenzo Olguín[3] and Pedro F. Guillen[1]

[1]*Instituto de Astronomía, Universidad Nacional Autónoma de Mexico, C.P.22860, Ensenada, B.C., Mexico*

[2]*Instituto Tecnológico de Ensenada, Av. Transpeninsular 1675, 22835 Ensenada, B.C., Mexico*

[3]*Depto. de Investigación en Física, Universidad de Sonora, Blvd. Rosales Esq. L. D. Colosio, Edif. 3H, 83190 Hermosillo, Sonora, Mexico*

Abstract. Point-Symmetric Planetary Nebulae (PSPNe) are an important part in morphological classification as they exhibit features (e.g. collimated jets, knots) that can directly be associated to physical processes such as precession, binarity or magnetic action. This connection seems more obvious than when it comes to bipolar Planetary Nebulae (PNe) for example, and PSPNe have often been referred to as a proper class. We present a cross-analysis of a group of PSPNe as well as a more detailed physical and kinematical analysis of three cases displaying what we consider to be different type of point-symmetry. The combination of the high resolution spectroscopy with the morpho-kinematical tool *Shape* is giving new insights in the understanding of those complex structures.
Keywords. Planetary Nebulae

1. Introduction

Point-symmetric PNe are characterized by an S-shaped structure with the central star being the point of reflection and collimated outflows apparently tracing successive mass-loss events (e.g. PC 19, IC 4634). The variation in position angles and radial velocities of the symmetric pairs of outflows/jets is likely to be the sign of the occurrence of precession (340). Another important aspect is the absence of waist which makes the difference with bipolar PNe. The origin of PSPNe is generally linked to the presence of a wobbling accretion disk inducing episodic precessing jets (342) or the action of magnetic fields through magnetic collimation around a precessing star (339). In both cases binarity would play a role as the precessing accretion disk would arise from the orbital movement in the (close) binary system (345) and the mass-loss variation would then be due to tidal forces. In the case of magnetic action, by spinning up the primary's envelope, the secondary causes a dynamo effect inducing the jets (343).The systematic analysis of such complex structures is therefore the key to the understanding of the processes responsible for their morphology.

2. PSPNe as a morphological class?

The well defined shapes and patterns exhibited by PSPNe have granted them the denomination of morphological class alongside round, elliptical and bipolar PNe (344). However, we studied a sample of 23 PSPNe specifically answering the description mentioned above and we did not find any particular trend in their location above the plane that would be related to a common progenitor mass, as it has been proven for the other morphological classes (338). Indeed PSPNe are spread at various galactic heights from $|z| \simeq 25$ pc to $|z| \simeq 600$ pc. The analysis of the radial velocity range (from 2 to 161 km s^{-1}) and as well as the expansion velocity range (with a mean value of 29 km s^{-1}) do not reveal any particular tendency. Moreover, point symmetry (via the presence of point-symmetric micro-structures) is found in diverse asymmetrical PNe (e.g. KjPn8, He 3-1475). Therefore, and in agreement with Guerrero et al. (341), PSPNe cannot be established as a proper class based on these grounds alone.

3. Morpho-kinematical analysis

In order to understand the dynamics of point-symmetric PNe we performed high resolution spectroscopic analysis with the echelle spectrometer MEZCAL mounted on the 2.1m telescope of the Observatorio Astronómico Nacional at San Pedro Mártir (Baja California, Mexico). We present 3 PNe showing different aspects of point-symmetry: NGC 7354, NGC 6309 and Pe 1-17. The data obtained were subsequently modelled with the morpho-kinematical software *Shape* (347; 346) which aims at the *reconstruction* of the PNe' 3D morphology.

3.1. NGC 7354

This PN is composed of a set of axisymmetric structures at different position angles and only the jets can be qualified as point symmetric. Contreras et al. (337) gave a detailed description of this planetary nebula and discussed the kinematical characteristics of the four main structures defining the PN (Fig 1): an outer shell expanding at 45 km s^{-1} (de-projected radial velocity), an elliptical inner shell expanding at 35 km s^{-1}, a set of equatorial bright knots with velocities between 25 and 44 km s^{-1} and a pair of jets with an expanding velocity of 60 km s^{-1}, each one.

There is so far no evidence for the presence of a stellar companion in NGC 7354 but a possible scenario, according to the authors, would involve a binary system in common-envelope phase and the presence of a precessing accretion disk.

3.2. NGC 6309

NGC 6309 shows two point-symmetric arms composed of four pairs of symmetric knots around a bright elliptical structure which is in fact a torus expanding at $V_{\rm exp} \simeq 25$ km s^{-1} (348). From the modelling it appears that a simple bipolar system cannot reproduce the observed structure and the best fit is found using a quadrupolar model as we have two lobes at two different position angles (Fig.2). The PN could be the result of the interaction of precessing jets (issued from high velocity bipolar collimated outflows

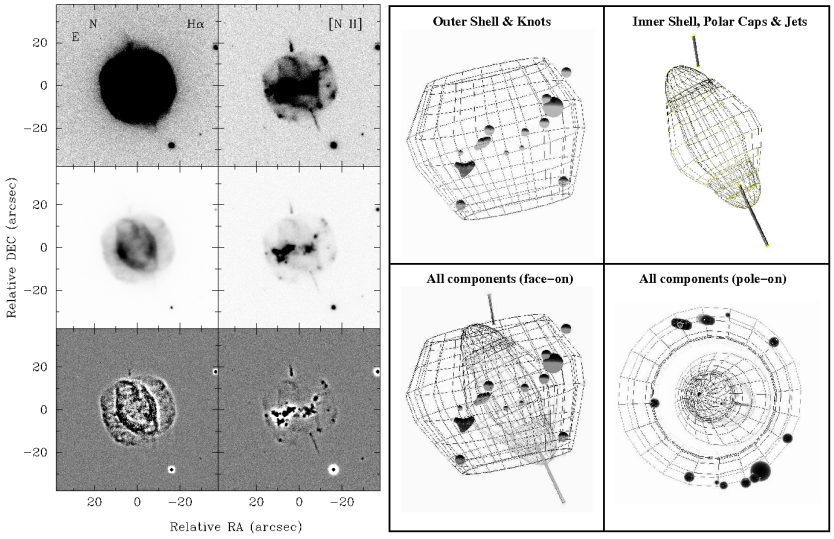

Figure 1. Left panel: Hα and [NII]6584 narrow-band images of NGC 7354 (from the Nordic Optical Telescope, NOT) displayed with different contrast levels and unsharp masking (lower row) to highlight the different structures. Right panel: Results of the Shape reconstruction.

ejected during the proto-PN phase) with the interstellar medium. In the long run the bow shocks/knots merged into a single shock front structure forming the non-homogeneous bipolar lobes which are symmetric respective to the central star.

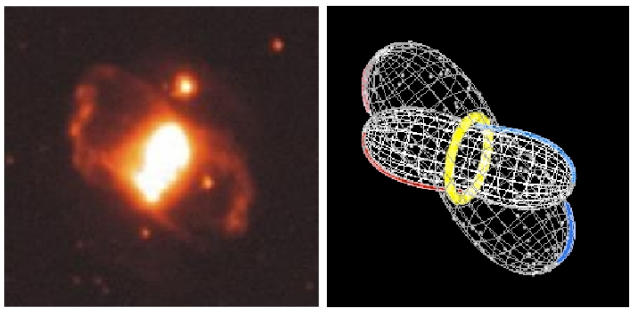

Figure 2. The bipolar lobes in NGC 6309 (left panel) are in fact the result several precessing collimated outflows from a quadrupolar system (right panel).

3.3. Pe1-17

This PN is considered as a very unusual and complex case of point-symmetry (341), indeed there is no visible central star and each opposite pairs of knots indicates a different geometric center. Our recent high resolution spectroscopic observations suggest that Pe1-17 may possess a ring related to its two brightest central structures and the analysis of [OIII] images shows an outer bipolar structure (Fig.3). A full scenario explaining such a structure is still missing nevertheless one should also consider that Pe1-17 may not be a PsPN but a bipolar PN experiencing anisotropic outflows.

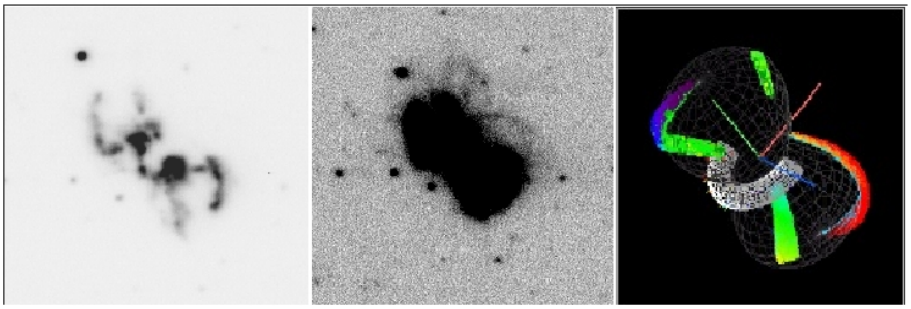

Figure 3. Left and middle panels: Pe1-17 in [NII] and [OIII] emission respectively (NOT images). The high contrast in the [NII] image underlines the knotty morphology of the nebula and the bipolar outer structure is shown in [OIII]. Right panel: Preliminary Shape model with the new ring structure.

4. Conclusion

We presented different types of point-symmetry in three planetary nebulae which are likely to be linked to physical parameters such as binarity and precession. The degree of implication of the latter is however still not clear. Although PSPNe do not seem to form a main morphological class, the analysis of their kinematics and the use of 3D modelling to determine the exact morphology of those objects is one of the keys to constrain the exact role of each physical parameter and (maybe) derive a common ground for PSPNe formation.

Acknowledgments. This project has been supported by PAPIIT-UNAM grant IN109509. LS and LO are in grateful receipt of UNAM and CONACyT postdoctoral fellowships respectively. MEC acknowledges support by CONACyT grant 49002.

References

Contreras, M. E., Vázquez, R., Miranda, L. F., Olguín, L., Zavala, S., & Ayala, S. 2010, AJ, 139, 1426

Corradi, R. L. M., & Schwarz, H. E. 1995, A&A, 293, 871

Garcia-Segura, G. 1997, ApJ, 489, L189

Guerrero, M. A. 2000, in Asymmetrical Planetary Nebulae II: From Origins to Microstructures, edited by J. H. Kastner, N. Soker, & S. Rappaport, vol. 199 of Astronomical Society of the Pacific Conference Series, 371

Guerrero, M. A., Vázquez, R., & López, J. A. 1999, AJ, 117, 967

Livio, M., & Pringle, J. E. 1997, ApJ, 486, 835

Nordhaus, J., & Blackman, E. G. 2006, MNRAS, 370, 2004

Schwarz, H. E. 1993, in European Southern Observatory Conference and Workshop Proceedings, edited by H. E. Schwarz, vol. 46 of European Southern Observatory Conference and Workshop Proceedings, 223

Soker, N., & Rappaport, S. 2000, ApJ, 538, 241

Steffen, W., Koning, N., Wenger, S., Morisset, C., & Magnor, M. 2010, ArXiv e-prints. 1003.2012

Steffen, W., & López, J. A. 2006, RMxAA, 42, 99

Vázquez, R., Miranda, L. F., Olguín, L., Ayala, S., Torrelles, J. M., Contreras, M. E., & Guillén, P. F. 2008, A&A, 481, 107

Asymmetric Planetary Nebulae V
A. A. Zijlstra, F. Lykou, E. Lagadec and I. McDonald
Jodrell Bank Centre for Astrophysics, Manchester, UK © 2011

Planetary Nebula Models: From Core to Outflow

Adam Frank

University of Rochester

Abstract. We review models of Pre-Planetary Nebula (PPN) and Planetary Nebulae (PN). The emphasis in this review is on the role of binary companions and magnetic fields. We first compare models for the direct shaping of the nebula via winds, jets or bullets. While it appears that continuous flows in the form of spherical winds or collimated jets play a role in some systems, there is strong theoretical evidence that explosive releases of mass and energy in the form of bullets are responsible for many PPN flows. We then review the role of binary evolution and PPN/PN shaping. We look at both the ability of the binary to create equatorial density distributions in the AGB wind and the more direct role they may play in creating collimated fast winds via accretion disks. Finally we review the role of magnetic fields in shaping PPN/PN. We emphasize that magnetic fields must both launch and collimate the winds of PPN and this fact restricts possible theoretical accounts of those objects which produce PPN and evolve into PN.
Keywords. Planetary nebulae

1. Introduction

Since the onset of high resolution observational platforms, such as the Hubble Space Telescope, the field of planetary nebula (PN) studies has confronted a growing list of paradoxes or dilemmas which have yet to find coherent resolution. The dominant paradigm of single star evolution coupled with hydrodynamic interacting wind scenarios (e.g., Icke, Balick & Frank 1992, Frank & Mellema 1994) is only able to explain a subset of the total mature PN population and fails entirely to explain the properties of PPN (Sahai & Trauger 1998).

Since the inception of the APN series of conferences the field has seen a variety of new ideas that attempt to explain the formation and shaping of PN together in the context of binary stellar evolution. This so-called "Binary Hypothesis" (DeMarco 2009) relies both on the presence of a companion and the generation of strong magnetic fields. As evidenced by numerous talks at this conference rapid progress is being made in identification of the key players observationally in this paradigm. Binaries with highly bipolar nebula are be discovered as are Keplerian disks and magnetic fields are being observed in a growing number of objects. While these advances mark only the beginning of our ability to directly test the Binary Hypothesis the represent real and compelling progress. This is an exciting time in PN studies as the new mechanisms being explored speak directly to some of the most important unsolved problems in astrophysics such as the nature of dynamo generated magnetic fields, accretion disk

formation processes, collimated stellar explosions, stellar evolution in the context of binary stars and the interaction of jets and outflows with surrounding environments.

Further progress forward, however, requires systematic exploration of both observational and theoretical issues. In this review I look back at theoretical models for PN formation over the last decade or so. I attempt to present a partially systematic outline of how different models address issues related to the nature of the PN central engine, binarity and magnetic fields. I apologize in advance for omissions driven by space concerns. I will not be able to cover many topics such as the interaction of the ISM with PN (Wareing et al 2007, Villaver 2003)

2. Jet Models

The original Generalized Interacting Stellar Winds model explored by Balick, Icke and others (see Balick & Frank 2002 for a review) assumed a spherical fast wind driven from CSPNe expanding into an aspherical AGB wind. While these models were able to produce a wide range of morphologies they could not recover wasp waisted nebula. Also while they were able to generate hot, low density jet flows via shock focusing at the inner shock they were less successful at recovering dense, colder jets like those seen in YSOs. Since many PPN and young PN show evidence for such narrow jets Sahai & Trauger (1998) suggested that collimated PN flows created at, or near, the central engine were the real drivers of early PN morphology. Since that time a number of authors have explored Jet-PN models.

In Soker (2002) the issue of jets driving PN morphologies was explored analytically delimiting different evolutionary pathways based on jet and AGB wind properties. Numerical models of PN jet-driving were first carried forward by Lee & Sahai (2003). In their work a central collimated wind was driven into a spherical AGB wind environment. They characterized the jet by three parameters: opening angle; velocity; mass-loss rate. The angular distribution of ρ_{jet} and V_{jet} where controlled using a $exp[(\theta/\theta_f)^2]$ function as opposed to the top-hat distributions often used in YSO models. Thus these models were not jets but Collimated Fast Winds (CFWs). The resulting models were compared with observations using synthetic observations in various forbidden lines. Comparisons of the model with observations of CRL 618 were generally favorable showing ring-like structures forming as decelerated jet material was shunted into the surrounding cavity. Best fits with the observation were achieved with jet velocities of $V_{jet} = 300 kms^{-1}$, much lower than the typical CSPN winds speeds of $V_{wind} = 1000 kms^{-1}$. The authors concluded that the jet in CRL 618 cannot be radiatively driven and also infer that it is unsteady or episodic.

In Lee & Sahai (2004) the issue of magnetic fields within the jets was explored in a series of simulations meant to model the "naked jet" PN He2-90. Assuming a low AGB mass-loss rate such that the jets appear without a surrounding cavity, the authors found that recovering observations demanded strong $\beta = P_g/P_B \sim 1$ within the jet implying that such fields were likely to play an important role in jet-launching. The authors found that the jets needed periodic variability in the their inflow conditions to match observations which, together with the strong fields, implicated some form of accretion process at work.

The link between jets and accretion disks in producing precession has been noted a number of times by different authors. In Velazquez et al (2004), 3-D simulations were used to study He3-1475 concluding that a precessing jet with a time-dependent ejection velocity, propagating into a pre-existing AGB wind successfully explained both the morphological and the kinematical characteristics. Best fit periods invoked in these models were $\tau_{pre} = 1500y$ and $\tau_{epi} = 120y$. Similar models have been applied to K3-35 (Velazquez et al 2002) finding shorter precession periods $\tau_{pre} = 100y$. Future work should attempt more systematic understanding of the mechanisms generating precession within the assumed disks.

3. Clump Models

While scenarios in which a continuously (though perhaps modulated) outflow from the central engine have proven successful in recovering aspects of PPN morphologies, a number of authors have challenged the jet model. Since many PPN and young PN show evidence for very short nebular acceleration timescales (of order $t_{acc} \sim 100y$; Bujarrabal et al 2001) the possibility that PPN are driven by a single impulsive (explosive) event has gained credibility with increased studies. *Such explosive models may also offer a means for creating multipolar flows if the eruption creates a collimated spray of bullets.* Theoretical support for this scenario comes from MHD models in which a winding toroidal field gains enough energy to breakthrough it overlying atmosphere in a post-AGB star (Matt et al 2004).

Poludnenko et al (2004) explored "radiative bullet" models for both PN and the "strings" of eta Car showing that long cavities are evacuated as the cooling bullet plows through the ambient medium and breaks up. The stronger the cooling that occurs in the bullet at the head of the flow the more the jet fragments into dense knots. These initial 2.5-D studies also demonstrated that bullets naturally produce Hubble-like flows in the cavities they create because the heads of the cavity remain the only place were fast moving material interacts with the ambient medium. In Raga et al (2007, 2008) these results were confirmed and expanded upon. 3-D simulations demonstrated the ongoing fragmentation which occurs as the bullet progresses producing an ensemble of fragments of varying size. The $V \propto R$ behavior still occurred in these higher dimensional studies indicating such kinematics was like to be robust. Shocked cloud and photo-ionized cloud synthetic observations were generated showing a transition from spectra similar to those of shock wave models (for simulations with lower photoionization rates) to spectra similar to those of photo-ionized regions (for simulations with higher photoionization rates). In general observations favored ionization based models however it the authors concluded it was difficult to tell explicitly which situation dominated.

Dennis et al (2009) presented 2.5-D and 3-D hydrodynamic simulations which directly compared jet and bullet models. The simulations drove both jet and bullet into environments appropriate to AGB winds. Bullets were found to account as well or better than jets for PPN morphology in two distinct ways. Firstly, the simulations showed that over the same distance, the frequency of occurrence of ablation events which lead to structures reminiscent of rings seen in observations, is greater for the case of the bullet model than for the jet models. This was particularly evident in synthetic maps of emission. Outflow collimation is also better preserved over the course of the

simulation in the case of the bullets as instabilities at the head of the continuously flowing jet can, in some cases, widen the bow shock beyond what is seen in PPN flows. It is also notable that, in many cases, the jet models produce synthetic emission maps in which the body of the jet is apparent. This is not the case for bullet models and is not the case for most highly collimated PPN flows.

Additionally, kinematical evidence in the form of synthetic position-velocity (PV) diagrams indicate that clumps preserve "Hubble-Flow"-like kinematics better than do jets in spite of the greater frequency of ablation events. Indeed, PV diagrams for the jet indicate a complete absence of any such behavior, while a clear linear trend is evident in the case of the clump when the angle of projection is taken to be non-zero, so that the contribution of the axial component of velocity to the line-of-sight velocity predominates. The authors found that the linear $V \propto R$ behavior could be reasonably recovered with a analytic model of a cylindrically symmetric disk with surface density $\chi(r)$ and velocity $V(R,t)$. The equation of motion for a differential ring of the disk under the ram pressure of the ambient gas of density ρ is given by:

$$\rho v^2(r,t) = -\chi \frac{dV}{dt}. \tag{1}$$

which yields a $V(R)$ curve with small concave curvature for small R while becoming increasingly linear with increasing R implying that a correlation between the kinematical ages of PPN outflows and the extent to which they are observed to exhibit Hubble-flow.

4. The Role of Binaries

The role of binaries in shaping PNe and driving the late stages of evolution for low and intermediate mass stars remains one of the most important, unresolved questions in the field. As Soker, DeMarco, Villaver and others have pointed out the term "binary" must be used with some latitude as numerous lines of evidence indicate that even planetary mass objects can effect the evolution of the central mass loosing star. In terms of the PN shaping models, the most important role of the companion object is to store, and later transfer, angular momentum (and rotational energy) to the central object. Mass transfer is also an important effect that must be considered in terms of the development of accretion disks. The development of dynamo processes driven by angular momentum transfer is also of vital importance as the magnetic fields generated by these dynamos are the likely agent accelerating the flows (see next section). There are a variety of "channels" by which a binary can evolve and produce a bipolar PPN/PN. The articulation of the these various evolutionary pathways remains one of the most important tasks for the community (see Moe & DeMarco 2008 and references therein). To explain the dramatic PPN morphologies and their momentum excess (see below) however more complex outcomes from binary evolution may be required.

Common Envelope evolution is one of the principle channels for binary PN producing evolution. In CE scenarios the secondary spirals into the primary releasing energy through frictional dissipation and blowing off the common envelope. Depending on the initial parameters of the binary a variety of final configurations may result (as has been explored by Soker in a variety of papers). Of particular importance is the dichotomy between a final state consisting of rapidly rotating merged single object that

has ejected much of the original star and a final state consisting of two stars with forming a mass transfer/accretion disk system. The different end states can have profound effects on the type of outflow system that is formed.

In Nordhaus & Blackman (2006) the effect of low-mass ($< 0.3 M_{\odot}$) companions (planets, brown dwarfs and low-mass main-sequence stars) embedded in the envelope of a $3.0 M_{\odot}$ was studied during three epochs of its evolution [red giant branch, asymptotic giant branch, interpulse AGB]. The results showed that common envelope evolution can lead to three qualitatively different consequences: (i) direct ejection of envelope material resulting in a predominately equatorial outflow, (ii) spin-up of the envelope resulting in the possibility of powering an explosive dynamo-driven jet and (iii) tidal shredding of the companion into a disc which facilitates a disc-driven jet.

The actual effect of the binary on nebular shaping comes through the outflows which are generated by the interaction of the two stars. If the primary is simply spun up by the secondary then enhanced equatorial mass loss is to be expected which speaks to GISW models (see Dukestra & Speck 2006). Gravitational focusing by the secondary can lead to more dramatic consequences. This process has been explored via simulations in a number of studies over the last decade beginning with the work of Mastrodemos and Morris (1998, 1999). More recently Gawryszczak et al (2002) explored the creation of both spiral patterns in the AGB wind as well as the development of pole to equator density contrasts. Huggins et al (2009) also explored the links between the results of such simulations and observations of AGB envelopes. These models were then taken as initial conditions for GISW simulations in which a spherical fast wind from the CSPN created bipolar nebula from inertial gradients in the circumstellar medium.

More direct effects from binaries come about when a collimated fast wind (CFW) is driven off of the secondary as it orbits the AGB primary. The CFW is assumed to originate from an accretion disk which forms either via Roche lobe overflow or, more likely, via capture of the AGB wind material. This process and its consequences were explored analytically in Soker & Rappaport (2000). The first 3-D numerical simulations were carried out by Arrendondo-Garcia & Frank 2004 who confirmed the Soker & Rappaport prediction that the critical parameter governing the flow was the ratio of momentum between the AGB wind and the CFW from disk. If $\dot{M}_j V_j / \dot{M}_{agb} V_{agb} > 1$ then the AGB wind can "blow down" the CFW/jet leading to complex morphology. Binaries can also effect shaping via orbital motion of the jet producing star as has been studied by Raga et al 2009.

The role of excretion torii is an area which deserves special note. The relationship between dense equatorial structures and collimated outflows observed in many PPN remains an open question. Huggins et al (2007) offered a cogent analysis of the timing of the torii/jets and found that the equatorial features appear to precede the bipolar outflows by 1000 years or less. Theoretical studies attacking this issue include a series of papers using 2.5-D simulations Akashi & Soker (2009) that explored the consequences of CFWs on the morphology. Their models did not track the full behavior of the orbiting stars but did show how interactions between the CFW and AGB wind could produce features like an equatorial torii that could, in some cases, backflow to perhaps form disks. Also noteworthy are fully 3-D studies by Rijkhorst et al (2005) which demonstrated how warped disks confining an outflow could produce point-symmetric structures.

5. The Role of Magnetic Fields

Interest in the role of magnetic fields in launching and shaping PPN has grown since the recognition of their nearly universal "Momentum Excesses". The momentum excess occurs when linear momentum observed in PPN outflows is higher than can be accounted for by radiation driving from the central star even when multiple scattering is included. These momentum excesses are typically of order 1000 or higher (Bujarrabal et al. 2001). In addition magnetic field measurements, while difficult, have been made in both nebular systems and their central engines. Fields have been observed in 4 central stars as well as in a variety of AGB, pAGB/PPN and PN (Vlemmings: these proceedings).

Models invoking weak magnetic fields, beginning with the analytical work of Luo & Chevalier (1994) have shown that a rich variety of shapes can be produced via hoop stresses in the imposed toroidal fields (Garcia-Segura et al. 1999). These models were critical in demonstrating how magnetic fields can allow theory to recover the extreme bipolarity seen in many PNe. They can not however explain the observed momentum excesses.

To explain both the launching and collimation of PPN models which include the generation of the field at the source are required. Magneto-centrifugal launching (MCL) of magnetic winds (which collimate into jets) have a rich history in other fields such as YSOs and AGN. In a series of papers Blackman, Frank and collaborators have explored the ability of MCL models to be adapted to PPN and PN environments. These studies invoke either a disk around the primary (formed through break-up of the secondary; Blackman et al 2001, Reyes-Ruiz & Franco 1999) or a disk forming around the secondary (Frank & Blackman 2004). A third route for magnetic launching occurs when dynamo processes within the secondary create a strong toroidal field. When the energy in the field exceeds the gravitational energy a kind of "magnetic bomb" occurs which ejects the remaining AGB atmosphere (Blackman et al 2001). Simulations of this process have shown the development of strong bipolar morphologies with characteristic Hubble Flow kinematics.

Assuming far stronger fields embedded in the AGB atmospheres recent studies (Garcia-Segura et al 2005) have also found extreme bipolar morphologies reminiscent of nebula like He3-401. In addition a detailed study of NGC 1360 with magnetic field driven flows was able to recover kinematics and morphologies of NGC 1360 (Garcia-Diaz et al 2008) by following the evolution of the nebula after the magnetized wind was shut off.

Of particular importance in assessing the nature of magnetically driven PPN/PN models is the ability of the central engine to maintain a strong field at the epoch of nebular formation. This has been a point of some contention. As Soker and others have pointed out single stars are unlikely to be capable of maintaining the differential rotation needed for power dynamos (at the level necessary to drive strong flows) across the entire AGB. Thus it is likely that some form of binary interaction will be needed to spin up the AGB envelope and re-power dynamo field generation. Nordhaus et al (2007) explored the creation of fields via dynamos in a number of initial AGB conditions and found that binary interactions were indeed required to create fields of appropriate magnitude to drive high momentum outflows.

Recognition of the importance of magnetic launching of PPN flows opens the potential that the observed morphologies are not driven by kinetic energy dominated winds but by Poynting Flux Dominated Flows (PFDFs: Nakamura & Meier 2004). Such jets, sometimes called magnetic towers because of the dominance of the B_ϕ components have been studied in a number of other contexts such as Gamma Ray Bursts and AGN. These PFDFs have also been studies directly in laboratories plasma experiments. In PFDF flows the electromagnetic energy flux, $\mathbf{F_P} \propto \mathbf{E} \times \mathbf{B}$, overwhelms the kinetic energy flux, $\mathbf{F_K} \propto \rho V^2$. Such flows have the potential to find strong application in PPN environments since the provide a means of driving highly collimated flows even when "wind" densities are quite low. Studies by Huarte-Espinoza et al (in preparation) have articulated morphologies of PFDFs when radiative cooling of the swept up medium is important.

6. Conclusions

As the presentations at this conference demonstrate the PN community has made rapid progress in the last five years in our efforts to test the Binary Hypothesis. It may well be that in another 10 years people will no longer speak of the PN as the "the future of the Sun". On the other hand we may find that there simply are not enough binaries or they have the wrong properties to produce the classes of objects we see and their frequencies. In either case it is an exciting period when new discoveries are challenging us to go beyond accepted assumptions and see our science through fresh eyes.

From this review we can identify a few key questions for future studies

- Are high momentum PPN outflows continuous or explosive events?
- Can we cleanly articulate the different pathways for binary stars to produce outflows?
- Can we cleanly articulate the different pathways by which magnetic fields power outflows?
- How are magnetic fields generated in AGB/PPN/PN systems?
- Thinking long terms how can we simulate the 3-D "multi-physics" of the central engine (Binary + Magnetic Fields)?

Of particular importance in this period is the recognition that PN science has strong ties to many other domains of astrophysics. In many ways the emergence of the Binary Hypothesis with its emphasis on magnetic launching and collimation puts PN into the spectrum of objects from YSOs to Micro-Quasars to AGN which create outflows by processing rotation into outflow through magnetic mediation. These links with other environments should be kept in mind as we both learn from and realize what we can bring back to these other research domains.

References

Akashi, M., & Soker, N. (2008) MNRAS, 391, 1063

Akashi, M., Meiron, Y., & Soker, N. (2008) New Astronomy, 13, 563
Akashi, M., & Soker, N. (2008) New Astronomy, 13, 157
Balick, B., & Frank, A. (2002) ARAA, 40, 439
Blackman, E.G., Frank, A., & Welch, C. (2001) ApJ, 546, 288
Blackman, E. G., Frank, A., Markiel, J. A., Thomas, J. H., & Van Horn, H. M. (2001) Nature, 409, 485
Blandford, R. D., & Payne, D. G. (1982) MNRAS, 199, 883
Bujarrabal, V., Castro-Carrizo, A., Alcolea, J., & Sánchez Contreras, C. (2001) A&A, 377, 868
De Marco, O. (2009) PASP, 121, 316
Dennis, T. J., Frank, A., Blackman, E. G., De Marco, O., Balick, B., & Mitran, S. (2009) ApJ, 707, 1485
Frank A., & Mellema G. (1994) A&A 289, 937
Frank, A., & Blackman, E. G. (2004) ApJ, 614, 737
García-Díaz, M. T., López, J. A., García-Segura, G., Richer, M. G., & Steffen, W. (2008) ApJ, 676, 402
García-Segura G, Langer N, Różyczka, M, Franco J. (1999) ApJ 517, 767
García-Segura, G., López, J.A., & Franco, J. (2005) ApJ, 618, 919
Gawryszczak, C, Miko, J., & Rozyczka, (2002) A&A, 385, 205
Haro-Corzo, S. A. R., Velázquez, P. F., Raga, A. C., Riera, A., & Kajdic, P. (2009) ApJ, 703, L18
Huggins, P. J. (2007) ApJ, 663, 342
Huggins, P. J., Mauron, N., & Wirth, E. A. (2009) MNRAS, 396, 1805
Icke V, Balick B, Frank A. (1992) A&A 253, 224
Jordan, S., Werner, K., & O'Toole, S. J. (2005) A&A, 432, 273
Lee, C.-F., & Sahai, R. (2004) ApJ, 606, 483
Lee, C.-F., & Sahai, R. (2003) ApJ, 586, 319
Luo, D. & Chevalier, R.A. (1994) ApJ 435, 815
Mastrodemos N, Morris M. (1998) ApJ 497, 303
Mastrodemos N, Morris M. (1999) ApJ 523, 357
Matt, S., Frank, A., & Blackman, E.G. (2006) ApJl, 647, L45
Mauron, N., & Huggins, P. J. (2006) A&A, 452, 257
Moe, M. & De Marco, O. (2006) ApJ, 650, 916
Nakamura, M., & Meier, D. L. (2004) ApJ, 617, 123
Nordhaus, J. & Blackman, E.G. (2006) MNRAS, 370, 2004
Nordhaus, J., Blackman, E.G. & Frank, A. (2007) MNRAS, 376, 599
Poludnenko, A.Y., Frank, A., & Mitran, S., (2004) ApJ, 613, 387
Pudritz, R.E., *Accretion discs, jets and high energy phenomena in astrophysics*. Eds. V. Beskin, G. Henri, F Menard, et al (2004) Les Houches Summer School, 78, 187.
Reyes-Ruiz M, López JA. (1999) ApJ 524, 952
Rijkhorst, E.-J., Mellema, G., & Icke, V. (2005) A&A, 444, 849
Sabin, L., Zijlstra, A. A., & Greaves, J. S. (2007) MNRAS, 376, 378
Raga, A. C., Esquivel, A., Riera, A., & Velázquez, P. F. (2007) ApJ, 668, 310
Raga, A. C., Esquivel, A., Velázquez, P. F., Cantó, J., Haro-Corzo, S., Riera, A., & Rodríguez-González, A. (2009) ApJ, 707, L6
Riera, A., Raga, A. C., Velázquez, P. F., Haro-Corzo, S., & Kajdic, P. (2009) Protostellar Jets in Context, 603
Sahai R, Trauger JT. (1998) AJ 116, 1357
Soker, N., & Rappaport, S. (2000) ApJ, 538, 241
Soker, N. (2002) ApJ, 568, 726
Velázquez, P. F., Gómez, Y., Esquivel, A., & Raga, A. C. (2007) MNRAS, 382, 1965
Velázquez, P. F., Riera, A., & Raga, A. C. (2004) A&A, 419, 991
Villaver, E., García-Segura, G., & Manchado, A. (2003) ApJ, 585, L49
Villaver, E., & Livio, M. (2007) ApJ, 661, 1192
Wareing, C. J., Zijlstra, A. A., & O'Brien, T. J. (2007) MNRAS, 382, 1233

Asymmetric Planetary Nebulae V
A. A. Zijlstra, F. Lykou, E. Lagadec and I. McDonald
Jodrell Bank Centre for Astrophysics, Manchester, UK © 2011

Integral field spectroscopy of IRAS 18276-1431 and IRAS 16342-3814

T.M. Gledhill & K.P. Forde
Centre for Astrophysics Research, University of Hertfordshire, Hatfield, AL10 9AB, UK

Abstract. We use integral field spectroscopy to detect the K-band ro-vibrational emission lines of H_2 in IRAS 18276-1431 and IRAS 16342-3814, two post-AGB objects associated with collimated outflows. In IRAS 18276 the H_2 emission arises in shocks within dense, clumpy material in the cavity walls, whereas in IRAS 16342 the emission is seen at the lobe tips and appears to be tracing the working surface of a fast outflow. In both objects we detect the CO bandheads and Na I doublet in emission suggesting hot, low-ionization gas close to the source. These features are also seen in pre-main sequence jet sources and we draw parallels between the two classes of object.
Keywords. Planetary nebulae – post-AGB

1. Introduction

Imaging studies of pre-PN (before the star begins to ionize its environment) have revealed complex structural symmetries (bipolar, multipolar, point symmetric), already present when the environment is still dusty and molecular (e.g. Sahai et al. 2007). The shaping appears to be mediated, at least in the case of more extreme outflows, by the appearance of axial jets which carve out cavities in the molecular envelope (Sahai & Trauger 1998). How the jets are launched or collimated is unknown although they are often accompanied by a circumstellar disc of gas and dust which obscures the star.

The situation is remarkably similar to that in which accretion-driven jets from pre-main sequence stars carve bipolar outflows and interact with their environment to from shock-excited structures such as Herbig-Haro objects. Shock-excited H_2 is detected around both young and evolved stars, tracing the working surfaces of collimated outflows. Pre-main sequence jet sources (e.g. HH34 IRS, HH26 IRS) can also display emission from the first overtone bands of CO as well as atomic lines such as the Na I doublet at 2.2 μm, indicating a hot, low-ionization inner disc (e.g. Antoniucci et al. 2008) close to the star.

Here we use integral field spectroscopy (IFS) with the SINFONI instrument on VLT to map the K-band molecular emission in the bipolar post-AGB objects IRAS 18276-1431 and IRAS 16342-3814, finding evidence for shock-excited H_2, CO overtone and Na I emission.

2. IRAS 18276-1431

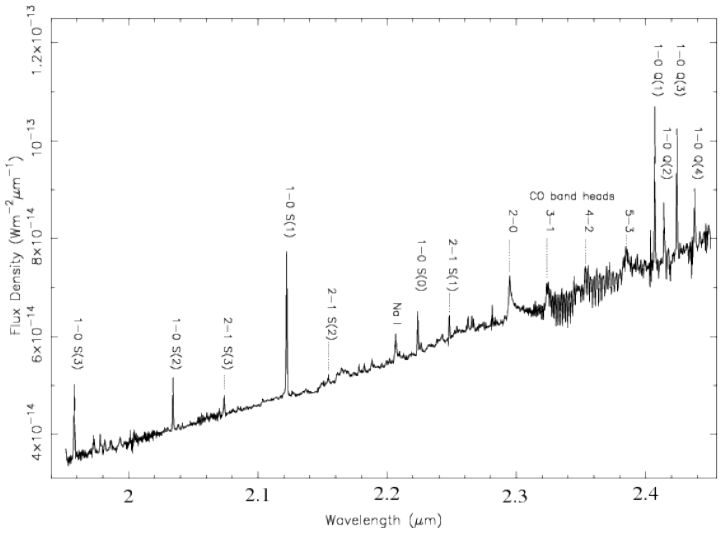

Figure 1. The near-IR spectrum of IRAS 18276-1431 integrated over the object showing the $1-0$ and $2-1$ H_2 ro-vibrational lines, CO first overtone bandheads and Na I lines. Other features result from telluric correction residuals. See Gledhill et al. 2010.

The near-IR spectrum of IRAS 18276 from 1.95 to 2.45 μm is shown in Fig. 1. The continuum rises steeply through the K-band, indicating a very red central source, and is scattered into our line of sight by dust in the bipolar lobes (as indicated by linear polarization of up to 50 per cent; Gledhill 2005). Superimposed on the continuum we see H_2 emission lines corresponding to the $1-0$ S- and Q-branch and $2-1$ S-branch transitions. The diagnostic ratio of the flux in the $1-0$ S(1) and $2-1$ S(1) is 9.3 ± 3.2 integrated over the object, which is typical of shock excited emission. An otho-to-para ratio of 3.02 ± 0.18 and vibrational and rotation temperatures of ≈ 2000 K also indicate shock excitation. A marginal detection of the $3-2$ S(3) line is also consistent with shocks and we find no evidence for UV-pumped fluorescence in this object. Comparison of the observations with shock models (Gledhill et al. 2010) favours C-shocks with either a planar or curved (bow) shock geometry, into high-density gas ($> 10^7$ cm^{-3}) with shock velocities in the range $25-30$ km s^{-1}. These models assume a transverse magnetic field of 4 mG which is consistent with previous polarimetric observation of the OH maser emission (Bains et al. 2003).

The rising continuum is evidence for the presence of warm dust around the star. Using the model of Sánchez Contreras et al. (2007) in which the continuum is composed of 20 per cent star light and 80 per cent dust emission with both traversing an optical depth to the observer of $\tau_{2.12\mu\mathrm{m}} \approx 3.7$, then our K-band continuum slope implies a blackbody temperature of ≈ 450 K for the warm dust.

Our IFU observations show that the first overtone CO bandheads are detected in emission (Fig. 1) and that this emission has the same spatial distribution as the contin-

uum, so that it too originates from an unresolved source in the central region, obscured from direct view, and is scattered into our line of sight by dust grains in the bipolar lobes. The v = 2 – 0 ^{12}CO bandhead peak is red shifted by a LSR-corrected velocity of 156 ± 15 km s^{-1} or 95 ± 15 km s^{-1} relative to the systemic velocity (from OH maser observations; Bains et al. 2003). As the CO emission is seen via scattering by dust in the bipolar lobes, and the same red shift is measured in both lobes, we interpret this shift as the radial velocity from the star of the dust grains responsible for the scattering. This allows us to estimate the axial outflow velocity of the dust as $V_{\rm axial}$ = 95 km s^{-1}.

The detection of CO bandhead emission is very interesting as it signifies the presence of hot (> 2000 K) and dense (> 10^{10} cm^{-3}) molecular gas in a compact central region. The most likely location for this collisionally excited gas is close to the central star, within a few stellar radii, and may be evidence for a circumstellar disc of molecular material. We also note the detection of the Na I doublet in emission, at 2.2 μm, which provides further evidence for high-density low-ionization gas in the central region. The Na I line also has the same spatial distribution as the continuum indicating that it too is scattered.

3. IRAS 16342-3814

The bipolar water maser source IRAS 16342-3814 is known to possess a high speed collimated outflow, with material in the jet head moving at ≈ 155 km s $^{-1}$ (Claussen, Sahai & Morris 2009). Infrared imaging observations show dramatic corkscrew features which have been interpreted in terms of a precessing jet actively carving cavities into the dusty molecular envelope (Sahai et al. 2005).

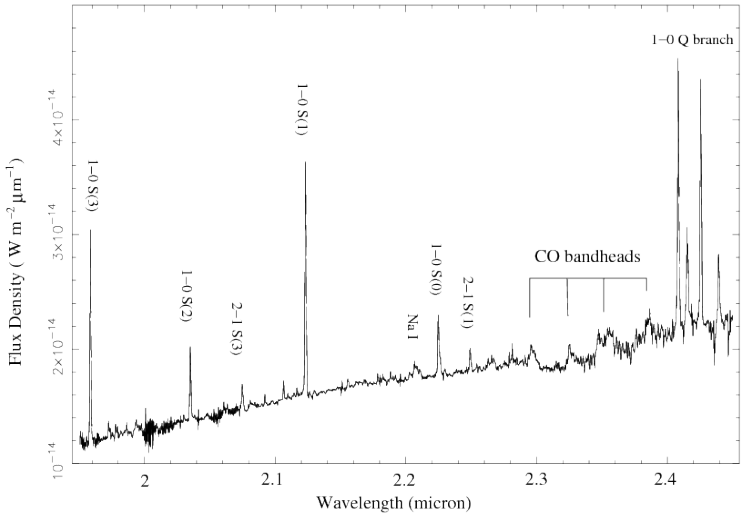

Figure 2. The near-IR spectrum of IRAS 16342-3814 (north-east lobe) showing the 1 – 0 and 2 – 1 H_2 ro-vibrational lines, CO first overtone bandheads and Na I lines. Note the similarity with Fig. 1.

The SINFONI spectrum for this object is shown in Fig. 2 (integrated over the NE lobe) and it bears a strong resemblance to that to IRAS 18276-1431. We detect strong H_2 emission lines, which again bear the hallmarks of shock excitation, with a $1-0S(1)/2-1S(1)$ ratio of 13.7 ± 5.6, averaged over the object. We find no evidence for UV-excited emission. Each H_2 line is seen to be doppler split, with blue-shifted emission arising in the SW lobe and red-shifted emission in the NE lobe. The peaks of the $1-0S(1)$ line are separated by 1.715×10^{-3} μm corresponding to a velocity separation of 242 km s^{-1}. Relative to the systemic velocity of 42 km s^{-1} the emission peaks are shifted by 110 (SW lobe) and 133 km s^{-1} (NE lobe). The tilt of the nebula axis to the plane of the sky as indicated by maser proper motion observations (Claussen et al. 2009) is 44 degrees, so the blue- and red-shifted radial velocities correspond to outflow velocities of 158 and 192 km s^{-1} for the SW and NE lobes respectively. Our IFU data shows that the H_2 emission is concentrated towards the lobe tips, and therefore probably traces the current working surfaces of the jet (Gledhill & Forde 2010, in prep).

CO bandhead emission is seen longward of 2.3 μm as well as the Na I doublet feature at 2.22 μm. These features are again present in the scattered continuum and hence originate from the central obscured region, being scattered into our line of sight by dust in the bipolar lobes.

4. Summary

The similarity of these post-AGB K-band spectra with those of pre-main sequence jet sources associated with Herbig-Haro objects raises the interesting possibility that, in some cases at least, outflows and jets at both ends of the main sequence may share fundamentally similar physical characteristics and may arise under similar conditions. In the case of YSOs, jets are thought to be launched from regions close to the accretion disc, possibly along magnetic field lines. The detection of CO and Na I emission in scattered light indicates that the origin is a compact circumstellar region, rather than photospheric, presumably located close to the jet source. Continued monitoring of these objects will allow us to determine whether these emission features are temporal or associated with longer-lived and more stable configurations such as circumstellar discs.

References

Antoniucci S., Nisini B., Giannini T., Lorenzetti D., 2008, A&A, 479, 503
Bains I., Gledhill T.M., Yates J.A., Richards A.M.S., 2003, MNRAS, 338, 287
Claussen M.J., Sahai R., Morris M.R., 2009, ApJ, 691, 219
Gledhill T.M., 2005, MNRAS, 356, 883
Gledhill T.M., Forde K.P., Lowe K.T.E., Smith, M.D., MNRAS, (arXiv:1009.5608)
Sahai R., Trauger J.T., 1998, A.J., 116, 1357
Sahai R., Le Mignant D., Sánchez Contreras C., Campbell R.D., Chaffee F.H. 2005, ApJ, 622, L56
Sahai R., Morris M., Sánchez Contreras C., Claussen M., 2007, A.J., 134, 2200
Sánchez Contreras C., Le Mignant D., Sahai R., Gil de Paz A., Morris M., 2007, ApJ, 656, 1150

Asymmetric Planetary Nebulae V
A. A. Zijlstra, F. Lykou, E. Lagadec and I. McDonald
Jodrell Bank Centre for Astrophysics, Manchester, UK © 2011

Fast, gusty winds blowing from the core of the pPN M2-56

C. Sánchez Contreras[1], C. Cortijo-Ferrero[2], L.F. Miranda[2], A. Castro-Carrizo[3], and V. Bujarrabal[4]

[1]*Departamento de Astrofísica, Centro de Astrobiología, CSIC-INTA. Postal address: ESAC- LAEFF, P.O. Box 78, E-28691 Villanueva de la Cañada, Madrid, Spain*

[2]*Instituto de Astrofísica de Andalucía-CSIC, C/ Glorieta de la Astronomia s/n E-18008 Granada, Spain*

[3]*Institut de Radioastronomie Millimétrique, 300 Rue de la Piscine, F-38406 Saint M artin d'Hères, France*

[4]*Observatorio Astronómico Nacional, Apartado 112, Alcalá de Henares, E-28803 Madrid, Spain*

Abstract. We report multi-epoch, spectroscopy and imaging of the pPN M 2-56, a unique, key object that enables witnessing the current, variable post-AGB wind activity at its core and tracking the rapid evolution of the circumstellar material shocked by short-lived, post-AGB mass ejections. Some of the results from our work (fully described in 401) include the discovery of: (1) proper motions and other structural changes in the fast, shocked-lobes, (2) an intense burst of Hα emission from the core that had vanished in <3 yr, which we interpret as an indication of a sudden, bipolar mass ejection at high velocity (500 km/s), (3) an equatorial outflow with a linear velocity gradient that suggests simultaneous bipolar and equatorial mass ejections, etc. Our data unveil the complex post-AGB mass-loss history of this object, whose rapid evolution is driven by multiple episodes of mass outflow, not regularly spaced in time, leading to different nebular components. The successive multiple post-AGB winds in M 2-56 are characterized by ejection speeds increasing with time. In contrast, the mass-loss rate and linear momentum show a time decreasing trend.
Keywords. Planetary Nebulae

1. Introduction

In spite of the growing evidence of jet-like ejections in pPNs, their origin, nature (episodic or continuous?), typical mass-loss rates, life-times, etc, are still very poorly known. Detailed studies of pPNs are crucial to obtain information about the properties and dynamics of post-AGB winds and their evolution. Optical spectroscopy is particularly useful for probing the post-AGB winds and their interaction with the CSE formed in the previous AGB phase. This work focuses on M 2-56, a pPN around a B-type central star (398). Its optical spectrum indicates major excitation by shocks (399; 402; 400). Interferometric CO mapping shows an hourglass-like envelope surrounding the optical nebula (397). The East side of the nebula tilted towards us. The

morphology and expansive dynamics of the molecular flow is the result of the interaction between fast, post-AGB jets and the slow AGB CSE. Such an interaction took place approximately 1400 yr ago in a relatively short time, $\lesssim$300 yr.

2. Observations and Results

We report multi-epoch, optical images and long-slit spectra of M2-56. The *R*-band and Hα images were acquired in 2009 with the 2.5m Isaac Newton Telescope (INT, La Palma, Spain). We used *HST* archive images through filters F656N (Hα, observed in 1998) and F606W (*V* band, observed in 2002). Long-slit spectra were obtained with IDS, at INT, and ALFOSC, at the Optical Telescope (NOT, La Palma, Spain), in 1998, 2000, and 2009. Observational details are given in (401).

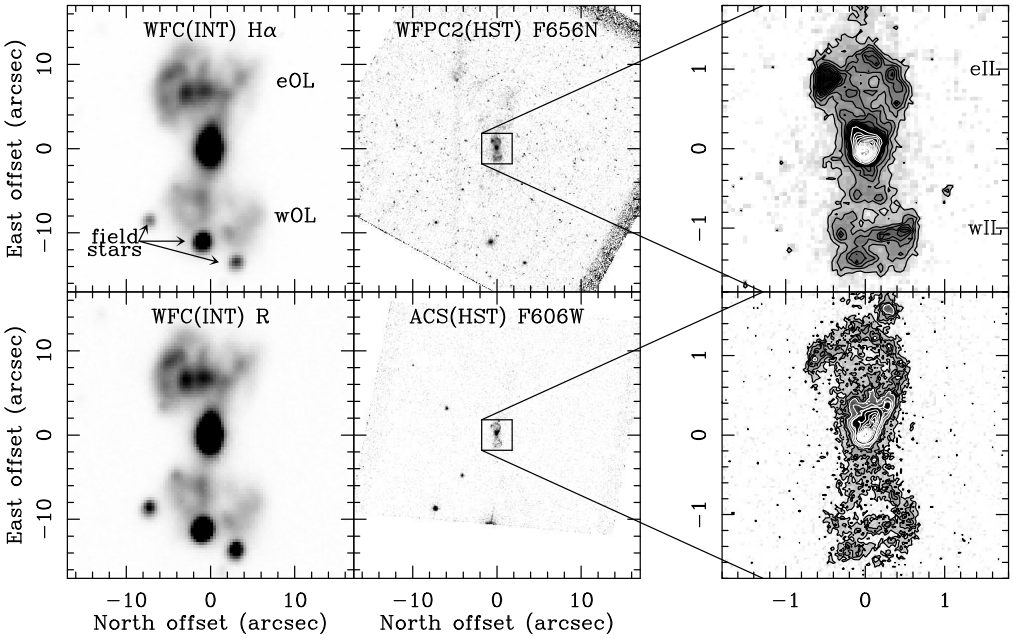

Figure 1. **Left)** Ground-based, Hα and *R*-band images of M 2-56 (top and bottom, respectively). The faint, extended east and west outer lobes (eOL and wOL) and field stars are labeled. **Middle)** F656N (Hα) and F606W *HST* images (top and bottom, respectively). **Right)** Inset of the *HST* images. The bright, compact east and west inner lobes are labeled (eIL and wIL).

We find two pairs of nested lobes similarly oriented but with different sizes and a large contrast in surface brightness (Fig. 1). The bright inner lobes (ILs), which can only be spatially resolved in the *HST* images, display closed, bow-like ends, which very likely represent shock fronts. The faint, more extended outer lobes (OLs), barely detected in the *HST* images, enclose the inner ones. The string of knots at the tips of the ILs in 2002 is located $\approx$0.″13 ahead the same structure as it was observed in 1998.

The Hα spectrum along the lobes has a wide profile with a complex spectral and spatial distribution consistent with an expansive kinematics (Fig. 2). Within the ILs and the OLs the velocity increases with the distance to the center, however, the ILs show

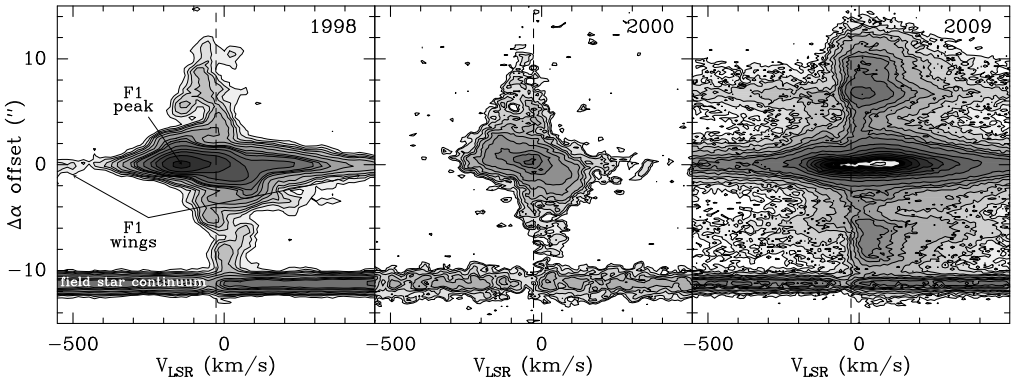

Figure 2. Long-slit Hα spectra along the nebula symmetry axis observed in 1998, 2000, and 2009. The vertical line shows the LSR systemic velocity, −27 km/s. The intense, blue-shifted emission feature F1 and its broad wings observed in 1998 are indicated by arrows.

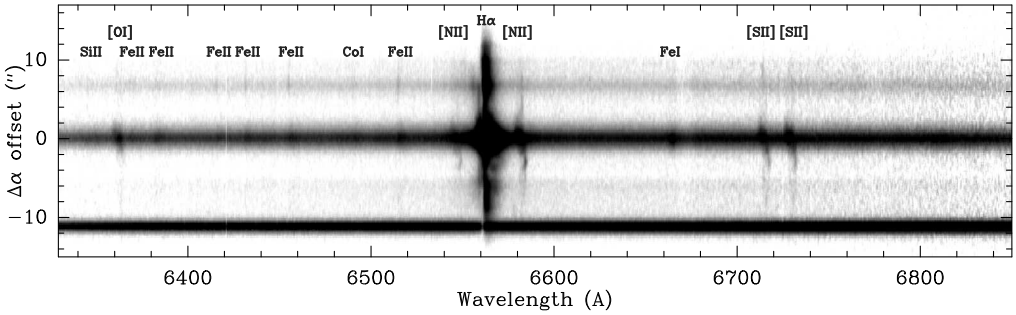

Figure 3. Long-slit spectrum observed in 2009. We report brightening of the scattered continuum and Hα emission, and the emergence of scattered FeII, SiII lines (shock tracers) from the nucleus.

expansion velocities larger than the OLs. Consistent with the large speeds reached by the ILs (of up to ∼350 km/s at the tips), we have measured the expansive proper motions of the knots ($\Delta\theta_t$∼0.″03 yr^{-1}) by comparing the two-epoch *HST* images (Fig. 1). The position-velocity diagram of the [SII]$\lambda\lambda$6716, 6731Å doublet and their intensity ratio (Fig. 10 of 401) unveils a dense equatorial outflow.

We have discovered significant changes with time in the line and continuum emission spectrum of M 2-56. In 1998, we detected a burst of Hα emission (referred to as "feature F1") at the nebula center. Feature F1 displays broad wings (FWZI∼1000 km/s) and has its intensity peak blue-shifted by ∼110 km/s from the systemic velocity. The blue wing is depressed relative to the red one, which is interpreted as a blue-shifted (P-Cygni like) absorption in the profile at V_r∼−430 km/s. Feature F1 was not present neither in the spectrum acquired in 1989 by (399) or in our 2000 and 2009 datasets. We believe that the Hα emission burst observed in 1998 is the consequence of a fast, dense, and short-lived post-AGB wind recently ejected.

In 2009, the Hα emission from both the approaching and receding lobes is on average red-shifted, which indicates that in 2009 a significant fraction of the Hα emission in the lobes is scattered, i.e. is not locally produced in the lobes but rather arises at a

nuclear HII region and is reflected by the nebular dust. At the center, the Hα emission has a broad (FWZI>1300-2500 km/s) asymmetric profile. A number of emission lines have recently emerged, including several FeII, FeI, and SiII permitted transitions. These lines most likely arise at the nebula nucleus and their emission is scattered by circumstellar dust. Finally, in 1998, the continuum emission, dominated by the stellar photospheric continuum scattered off by the nebular dust, arises from a central compact region that is unresolved in our data. In 2009, a relatively faint, red continuum is observed not only at the center but also along the OLs (Fig. 3).

3. Nebular components: formation and evolution of M 2-56

Our data probe several nebular components, namely, two pairs of nested, co-axial lobes with different sizes and a large contrast in surface brightness (the OLs and ILs), a compact bipolar flow (the F1-wind), and an equatorially expanding central structure. A compact circumstellar structure obscuring the star (cocoon?) and a nuclear HII region, both spatially unresolved, are also inferred from our data. Recent brightening of the scattered stellar continuum and scattered Hα emission along the lobes is reported, both results pointing to a decrease of the optical depth of the circumstellar material enshrouding the star.

The kinematical ages of the main nebular components are different from each other: $t_{\rm k}\sim$1400 yr for the molecular bipolar flow, $t_{\rm k}\sim$300-400 yr for the OLs and the equatorial flow, $t_{\rm k}\sim$40 yr for the ILs, $t_{\rm k}\lesssim$10 yr for the F1-wind, and even smaller for the compact cocoon and HII region. The rapid evolution of M 2-56 is driven by multiple episodes of mass ejection, that is, through a gusty or episodic post-AGB wind, that has led to the nested bipolar morphology of the nebula and the younger nuclear components discovered in this work. The detection of FeII lines indicates the presence of shocks at the stellar neighbourhood resulting from current stellar wind activity. The various post-AGB mass ejection events experienced by M 2-56 did not happen at regular time intervals, in particular, the time span between two consecutive post-AGB ejections has shortened with time. The successive multiple post-AGB winds are characterized by ejection speeds increasing with time from 200 to $\gtrsim$ 500 km/s (and possibly >1000 km/s at present). In contrast, the mass-loss rate and linear momentum may show a time decreasing trend. None of the post-AGB ejections probed by our optical data could have transferred its large linear momentum ($\geq$2 $M_\odot$ km/s; 397) to the molecular outflow and, therefore, a primer more energetic post-AGB ejection is necessary to explain the dynamics of the molecular envelope.

Acknowledgments. This work has been supported by the Spanish MICINN through grants AYA2009-07304, and CONSOLIDER INGENIO 2010 (ref.: CSD2009-00038).

References

Castro-Carrizo, A., Bujarrabal, V., Sánchez Contreras, C., Alcolea, J., & Neri, R. 2002, A&A, 386, 633
Cohen, M., & Kuhi, L. V. 1977, PASP, 89, 829
Goodrich, R. W. 1991, ApJ, 376, 654
Riera, A., Binette, L., & Raga, A. C. 2006, A&A, 455, 203

Sánchez Contreras, C., Cortijo-Ferrero, C., Miranda, L. F., Castro-Carrizo, A., & Bujarrabal, V. 2010, ApJ, 715, 143
Trammell, S. R., Dinerstein, H. L., & Goodrich, R. W. 1993, ApJ, 402, 249

Asymmetric Planetary Nebulae V
A. A. Zijlstra, F. Lykou, E. Lagadec and I. McDonald
Jodrell Bank Centre for Astrophysics, Manchester, UK © 2011

3-D Study of the Glowing Eye Nebula, NGC 6751

Clark, D. M., García Díaz, Ma. T., López, J. A., Steffen, W. G., and Richer, M. G.

Instituto de Astronomía, Universidad Nacional Autónoma de México, Apdo Postal 877, Ensenada, Baja California, México

Abstract. In these proceedings we present a detailed, multiwavelength spectral and image analysis of the complex planetary nebula, NGC 6751. This PN consists of multiply shells and a bipolar outflow. Using the Manchester Echelle Spectrometer (MES) at San Pedro Mártir Observatory in Baja California, we acquired optical, high spectral resolution, longslit observations across this nebula, with particular focus on the highly structured inner region near the bipolar outflows. We used the interactive morpho-kinematic reconstruction software Shape to derive the 3-D morpho-kinematic model of the nebula that closely resembles the observed profiles and image of NGC 6751. The inner region consists of a filamentary bubble surrounded by a clumpy ring. The ring is tilted with-respect-to the line-of-sight and is encircled by a disk-like structure. Emanating from the central regions are two, point-symmetric outflows which flow into two lobes seen in a ground based, Gemini image. Farther out are a faint inner halo and a fragmented outer halo. This nebula lies in the galactic plane and appears to be moving through a gas-rich environment. Deep, ground-based images indicate a veil-like structure to the NE, which is most likely nearby ISM. Our spectra indicate a large velocity difference between this gas and NGC 6751, confirming that this structure is indeed ISM material.
Keywords. Planetary Nebulae

1. Introduction

NGC 6751 is an impressive and intricate planetary nebula (PN), that has been given the name the "Glowing Eye Nebula" due to the appearance of the central bubble as seen in high resolution images. This PN has been observed across a wide range of wavelengths from the mid-infrared (*Spitzer*) to the optical (*HST*) and at various levels of spatial resolution. This makes NGC 6751 an ideal target for studying the kinematics of a PN and its environment. The Manchester Echelle Spectrometer at San Pedro Mártir (MES-SPM) is a perfect instrument for this work. Using narrow-band, MES-SPM images we compared these with images taken by *HST*, Gemini and *Spitzer* to get a first pass on the form of this PN. Combining this with the high-resolution spectral capability of this instrument, we made the most detailed study to date of the kinematics and structure of NGC 6751. We also sought to confirm that the emission to the NE of the PN is not associated with the nebula as suggested by Chu et al. (403).

2. Observations

This study is primarily based on high resolution, long slit spectra acquired with MES-SPM at San Pedro Mártir Observatory in Baja California, Mexico. MES-SPM was installed on the 2.1 m telescope using the f/7.5 secondary. We acquired all spectra using a SITE detector consisting of 1024 × 1024 pixels, binned 2 × 2 and observed through a Hα+[NII] filter. We chose 9 slit positions across the field. Slit a passes through the center of the nebula with a position angle (PA) equal to 0°. Previous, spectral observations of this PN indicated an outflow along a line at a positional angle (PA) of ∼ 100° (407). Thus, we chose to position slits b–i parallel to an axis at this PA in order to study the extent of this outflow region. Slit b, to the N, passes through the extended emission and slits c and i pass through the inner halo. All spectra were wavelength calibrated using observations of a ThAr lamp.

Supplemental data included deep Hα+[NII] and [OIII] images taken with MES-SPM (Figure 1). We also included a Gemini, GMOS image taken in three filters, Hα, [SII] and [OIII], for a total observing time of one hour*. This image was provided to us by Christopher Onken from the Australian Gemini Office (Gemini Program II GS-2009A-Q-22, PI Terry Bridges). This image won the 2009 Gemini School Astronomy Contest and was submitted by high school student Daniel Tran. Image credits are Daniel Tran (PAL College), Travis Rector (U. Alaska Anchorage), Terry Bridges (Queen's U.) and the Australian Gemini Office. In addition, we made use of an 8μm, *Spitzer* image taken from the archives†, an image from the Hα composite full sky map (405) and an optical, *HST* image taken from the gallery of the Hubble Heritage Project‡.

3. Morphology and Kinematics

Deep, narrow band images show NGC 6751 to have a detailed, complex structure. A thick, knotty ring surrounding an inner, filamentary bubble is especially evident in the *HST* and Gemini images. The MES-SPM, [OIII] image brings out the inner halo and the bipolar outflow is quite obvious in the MES-SPM, Hα+[NII] image (see Figure 1). The Gemini image further reveals that the outflows are extending into two lobes of material. The MES-SPM images and Gemini image show a filamentary outer halo beyond the central regions of the nebula.

We found that the PN is best described by five components. These include a central bubble, tilted ring (∼ 10°), disk, bipolar outflow and inner halo. Using slits a and g, which pass through the central star, we measured a systemic velocity of V_{sys} = -31.7(±2) km s^{-1}. The central bubble is expanding at V_{exp} = ∼ 42 km s^{-1} (where V_{exp} = V_{hel} - V_{sysl}), which is relatively high for this type of structure (408). Images, such as the *HST* or Gemini images, suggest that there is filamentary material central to the bubble. However, an inspection of our spectra indicate that the filaments are on the surface of the bubble and could be dense material here. Just outside of the central bubble is a

*http://www.gemini.edu/node/11329

†The *Spitzer Space Telescope* is operated by the Jet Propulsion Laboratory, California Institute of Tech

‡*HST* image credit: NASA, ESA, and the Hubble Heritage Team (STScI/Aura)

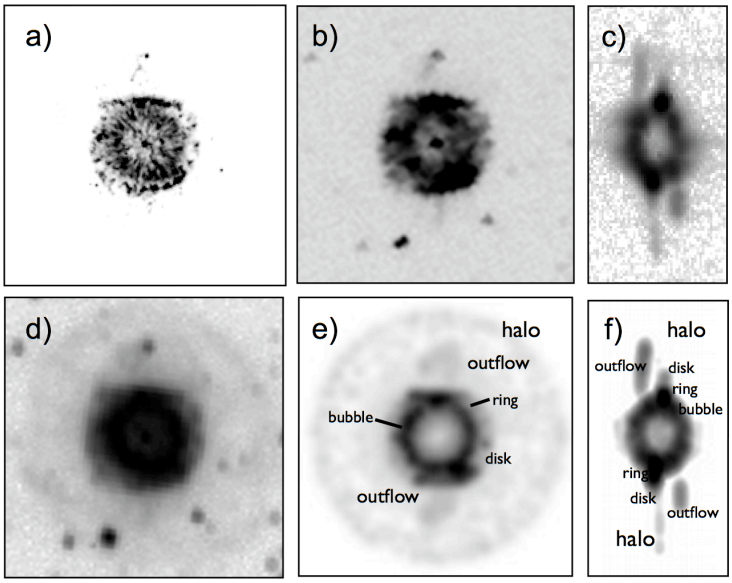

Figure 1. Here we compare various observational views of NGC 6751 with our Shape model. a) *HST* image, b) SPM, Hα+[NII] image, c) [NII] spectra for slit g, d) SPM [OIII] image, e) Shape model, f) model PV diagram.

ring of material. Our spectra indicate the ring is expanding at $V_{exp} \approx 40$ km s^{-1} in the east and $V_{exp} \approx 7$ km s^{-1} in the west. The ring itself is surrounded by a disk of knotty material. This could be gas in the ring that has been swept back and is being photo evaporated by the emission from the central star. The bipolar outflow is expanding at $V_{exp} \sim$79 km s^{-1}. The outer halo is expanding rapidly with $V_{exp} = 16$ km s^{-1}, while the inner halo is expanding more slowly, with $V_{exp} = 2$ km s^{-1}.

We made a 3-dimensional, morpho-kinematic reconstruction of NGC 6751 using the program Shape (409). With this program, various forms can be filled with particles and each particle system can be given a separate velocity law to describe how the nebula is expanding. An artificial slit can then be placed on the 3-D representation of the nebula to make artificial spectra. These spectra can be compared with real, high-resolution spectra to search for the best structural description of a PN. A similar procedure was followed by García-Díaz et al. (406) to model the PN, NGC 6337.

To make our reconstruction of NGC 6751, we used slits a and c–i. In this work, we applied a Hubble flow type velocity law to the particle systems used. This velocity law can be described as $v = k \cdot r/r_0$, where k is a constant, r is the distance from the source and r_0 is the radius at which the velocity k is reached. The central bubble was modelled using a filled sphere and we modelled the inner halo using a thin shell. Tori were used to model the ring and disk surrounding the ring. We found the ring is tilted out of the plane of the sky in the east by $\sim 10^\circ$ and also appears to be slightly warped about the N-S axis. Segments of spheres described the bipolar outflows. Interestingly, we found that the outflow is inclined by $23^\circ \pm 5^\circ$ with-respect-to the plane of the sky, which is not perpendicular to the ring as one might expect.

Aside from our Shape reconstruction, we also explored the nature of the extended emission to the NE. A *Spitzer* 8μm image shows that this emission continues farther to the N. It is also quite evident that NGC 6751 is in a gas rich environment as seen in Hα images from the full sky survey in Hα (405). Our spectra that pass through this region to the NE indicate the emission has a range in heliocentric velocity from 26–34 km s^{-1}. Considering the heliocentric, systemic velocity of this PN is -41($\pm$ 2 km s^{-1}), the velocity of the extended emission is quite different, indicating it is not related to the nebula. This confirmed the observations by Chu et al. (403), which also showed no relation between this emission and the PN.

4. Conclusions

In this work we investigated the 3-dimensional structure and kinematics of the PN, NGC 6751 using high resolution, [NII] spectra taken with MES-SPM. Using the software Shape, we searched for the best structural description of the nebula. We found that this PN consists of a central bubble expanding at ~42 km s^{-1}, a warped ring tilted by 10° out of the plane of the sky, and a clumpy disk just outside of the ring. Two bipolar outflows extend to the east and west side of the nebula, with an expansion velocity of ~79 km s^{-1} and inclined by ~23° to the plane of the sky. These outflows can be seen in Gemini and *HST* images of the PN. Outside of the central region is an inner halo expanding at ~15 km s^{-1} and farther out is a clumpy, outer halo. The inner halo is quite evident in MES-SPM [OIII] images.

To the NE of the PN there appears extended emission. We compared the velocity of this emission with the systemic velocity of NGC 6751 and found they differ by ~70 km s^{-1}. This confirmed the observations by Chu et al. (403) that this emission is not associated with the nebula. *Spitzer* 8 μm and Hα images (405) of the surrounding field of NGC 6751 indicate this nebula is in a gas rich environment.

Details of this work will appear in the October issue of the Astrophysical Journal (404).

Acknowledgments. MTG-D gratefully acknowledges the support of a postdoctoral grant from UNAM. This research has benefited from the financial support of DGAPA-UNAM through grants IN116908, IN108506, IN108406 & IN100410 and CONACYT grants 49447 and 82066. We acknowledge the excellent support of the technical personnel at the OAN-SPM, particularly Gustavo Melgoza and Felipe Montalvo, who were the telescope operators during our observing runs.

References

Chu, Y.-H., Manchado, A., Jacoby, G. H., & Kwitter, K. B. 1991, ApJ, 376, 150
Clark, D. M., García-Díaz, M. T., López, J. A., Steffen, W., & Richer, M. G. 2009, ApJ, accepted
Finkbeiner, D. P. 2003, ApJS, 146, 407
García-Díaz, M. T., Clark, D. M., López, J. A., Steffen, W., & Richer, M. G. 2009, ApJ, 699, 1633
Gieseking, F., & Solf, J. 1986, A&A, 163, 174
Richer, M. G., López, J. A., García-Díaz, M. T., Clark, D. M., Pereyra, M., & Díaz-Méndez, E. 2010, ApJ, 716, 857
Steffen, W., & López, J. A. 2006, Revista Mexicana de Astronomia y Astrofisica, 42, 99

Asymmetric Planetary Nebulae V
A. A. Zijlstra, F. Lykou, E. Lagadec and I. McDonald
Jodrell Bank Centre for Astrophysics, Manchester, UK © 2011

Modelling H_2 Infrared Emission of the Helix Nebula Cometary Knots

Isabel Aleman[1,2], Albert A. Zijlstra[1], Mikako Matsuura[3,4], Ruth Gruenwald[2], and Rafael Kimura[2]

[1]*Jodrell Bank Centre for Astrophysics, The Alan Turing Building, School of Physics and Astronomy, The University of Manchester, Oxford Rd, Manchester, M13 9PL, UK*

[2]*IAG-USP, Universidade de São Paulo, Cidade Universitária, Rua do Matão 1226, São Paulo, SP, 05508-090, Brazil*

[3]*UCL-Institute of Origins, Astrophysics Group, Department of Physics and Astronomy, University College London, Gower Street, London, WC1E 6BT, UK*

[4]*UCL-Institute of Origins, Mullard Space Science Laboratory, University College London, Holmbury St. Mary, Dorking, Surrey, RH5 6NT, UK*

Abstract. In the present work, we use a photoionisation code to study the H_2 emission of the Helix nebula (NGC 7293) cometary knots, particularly that produced in the interface H^+/H^0 of the knot, where a significant fraction of the H_2 1-0 S(1) emission seems to be produced. Our results show that the production of molecular hydrogen in such region may explain several characteristics of the observed emission, particularly the high excitation temperature of the H_2 infrared lines.

Keywords. Planetary Nebulae

1. Introduction

High-resolution images of the Helix nebula (NGC 7293) have shown that the H_2 emission arises from its large population of dense globules embedded in the ionised gas (e.g. 419), the so-called cometary knots (CKs). CKs are structures that resemble comets, particularly in images taken in Hα, [N II] λ6583, and H_2 1-0 S(1) lines. The bright cusp points towards the central star and the tail in the opposite direction, which can indicate that the excitation is connected with the central star (422; 423).

The H_2 emission is intense in a thin layer on the surface of the CKs towards the central star. There is no evidence that this emission is produced by shocks (422; 420). Models of photodissociation regions (PDRs; 414; 423) are unable to reproduce the high excitation temperature of H_2 emission (~900-1800 K) estimated by Cox et al. (414) and Matsuura et al. (420). Recently, Henney et al. (417) showed that advection can cause the ionisation and dissociation front to merge, leading to enhanced heating of the molecular gas.

In this work, we show that the partially ionised region can account for a significant part of the observed H_2 emission and naturally explain its high excitation temperature. Our models are briefly described in Section 2; a more detailed description will be published in a forthcoming paper (412). Results are presented in Section 3.

2. Models

We use the photoionisation code *Aangaba* (415) to simulate the ionising spectrum, physical conditions, density of the species, and line emissivities around and inside the H^+/H^0 interface of the Helix nebula CKs. The H_2 micro-physics is included in the code, as described in Aleman & Gruenwald (410, 411).

We assume that the central star radiates as a blackbody with $T_\star$ = 120,000 K and $L_\star$ = 100 $L_\odot$ (418; 423). We also assume that the density of the diffuse gas is uniform and equal to 50 cm^{-3} (421). The elemental abundances for the Helix were determined by Henry et al. (418) for He, O, C, N, Ne, S, and Ar. For Mg, Si, Cl, and Fe, we adopt averages for PNe from Stasińska & Tylenda (424). We use amorphous carbon dust (with 0.1μm radius) for our calculations, but as discussed in Aleman & Gruenwald (410) the choice of compound among the ones available in the code will not cause significant changes on the results presented below nor will affect our conclusions. The distance to the Helix is assumed to be 219 pc (416). The CKs are simulated as an increase in the density profile of the Helix nebula model at a given distance from the central star. The emissivity along the radial direction (through the CK symmetry axis) is calculated by the photoionisation code. An IDL routine was developed to simulate a three-dimensional CK, allowing the calculation of line surface brightness by the integration of the emissivity in the line of sight inside a CK, which is assumed to be seen edge on. We construct a grid of CK models with different core densities, density profiles, dust-to-gas ratios, and distances from the central star. We assume that the density profile has a density increase from the diffuse gas to the CK core value within a given distance. We call this region the CK interface. We study four types of density increase with distance, but here we only present the results for the exponential increase (more results will be included in 412). Calculation are stopped where the gas temperature, which generally decreases with the distance to the central star, reaches 100 K. In each model, the dust-to-gas ratio and the chemical composition of the CKs are assumed to be the same as in the diffuse gas.

3. Results

3.1. Warm H_2 1-0 S(1) emission

The emissivity of the H_2 1-0 S(1) line, as well as for other rovibrational lines, in the CKs is important in a warm region, where temperatures are between 300 and 7000 K. In the region considered in this work, the peak in the 1-0 S(1) emissivity occurs where the density is around 40% of the core density. The contribution of colder regions should be more important for pure rotational lines of the v = 0 level. This component of the H_2 emission may explain the excitation temperatures around 900-1800 K found by Cox et al. (414) and Matsuura et al. (420).

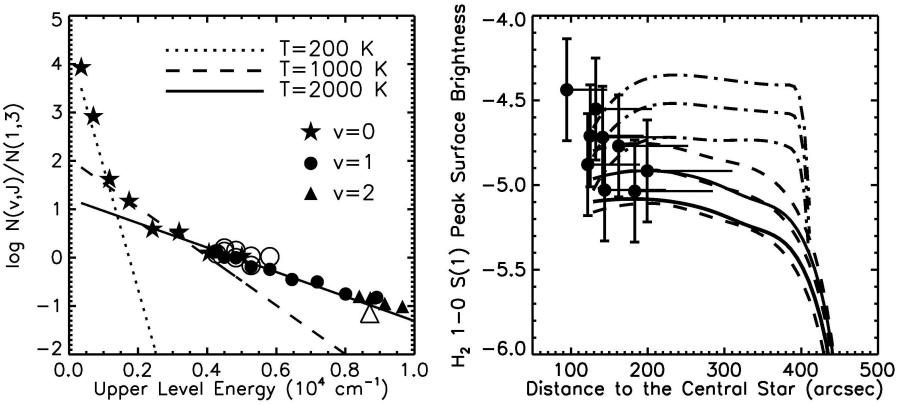

Figure 1. Left Panel: H_2 excitation diagram. The effective column density was calculated where the 1-0 S(1) surface brightness is maximum. Open symbols represents observations and filled symbols models. Lines are Boltzmann distributions for the temperature indicated. Right panel: H_2 1-0 S(1) surface brightness of a cometary knot as a function of its distance to the central star. Sets of solid, dashed, and dot-dashed curves represent models with interface thickness of 0.5, 0.2, and 0.01″, respectively. Different curves within each set represent CK radius of 0.5, 1.0, and 2.0″, with the surface brightness increasing for larger CK radius. Dots represent measured values. The error in the distance is estimated assuming that the Helix symmetry axis is inclined 37° with respect to the line of sight

The left panel in Fig. 1 shows the H_2 excitation diagram. Observational values were obtained by Matsuura et al. (420). Values calculated with an appropriate model are also included. The agreement between the excitation temperatures of the model and the observations is evident. Lines represent Boltzmann distributions for three different temperatures as indicated within the plot. The column densities obtained from the lines of the bands 1-0 and 2-1 are well represented by a excitation temperature of approximately 2000 K. A similar value was obtained by Matsuura et al. (420). The column densities obtained from lines 0-0 S(2) to S(7) are well represented by Boltzmann distribution at a temperature of 1000K, which is close to the excitation temperature of 900K obtained by Cox et al. (414) from ISO observations of the Helix.

3.2. H_2 1-0 S(1) surface brightness

The right panel of Fig. 1 shows the H_2 1-0 S(1) line surface brightness as a function of the CK distance to the central star. Dots represent measurements for some representative CKs of the Helix nebula. We identified 10 isolated CKs commonly detected in Hα and H_2 images. We measured 2.12 μm H_2 intensities from the images obtained by Matsuura et al. (419). To calibrate the data for point sources on the local scale, we use five stars within the observed field to measure the zero-pint. We assume that the 2MASS K'-magnitude of these stars are the same as the magnitudes in H_2-filter. We apply the 25-pixel radius of aperture photometry and take the 35–50 pixel ring as background measurements. The pixel scale is 0.117″.

Curves in the right panel of Fig. 1 show the H_2 1-0 S(1) surface brightness as a function of the distance from the central star for CKs with different interface thickness

and radius. The surface brightness was calculated was averaged over the same aperture as the measurements to allow direct comparison. The surface brightness decreases with the decrease of interface thickness, the increase of the CK radius, and the increase of the distance from the central star. The observed surface brightness also presents a decrease with distance to the central star trend. The interface can account for the whole or a significant part of the observed surface brightness.

An important parameter to the ionization structure of the CKs is the distance from the central star, since the ionising spectrum may change significantly with the optical depth. CKs farther from the central star have smaller ionised zones. If the CK is beyond the Helix ionisation front, there is practically no ionised region and the intensity of 1-0 S(1) drops dramatically, since there is not enough radiation or temperature to excite significantly the upper vibrational levels of the molecule. Our results support that the central star's radiation field plays a major role in the CKs H_2 emission.

We also study the effect of the dust-to-gas ratio and n_K. The 1-0 S(1) peak brightness is slightly higher for models with higher dust-to-gas ratio (the increase caused by changing the dust-to-gas ratio from 10^{-3} to 10^{-2} is about 20%) and higher n_K (the difference between models with $n_K = 10^5$ and 10^6 cm^{-3} is up to 40%).

As pointed out by Burkert & O'Dell (413), the interface between the diffuse gas and the CK core may provide important clues about the mechanisms that shapes and sustain the CKs. Our models show that there are significant differences in the results depending on the assumed density profiles of this region. Images that could resolve the interface of the CK in great detail are then essential to improve or knowledge about the CKs and PNe.

Acknowledgments. We acknowledge the financial support from CNPq PDE grant number 201950/2008-1 (Brazil), The University of Manchester, and STFC (UK).

References

Aleman, I., & Gruenwald, R. 2004, ApJ, 607, 865
— 2010, A&A. Submitted
Aleman, I., Zijlstra, A. A., Matsuura, M., Gruenwald, R., & Kimura, R. 2010, MNRAS. In preparation
Burkert, A., & O'Dell, C. R. 1998, ApJ, 503, 792
Cox, P., Boulanger, F., Huggins, P. J., Tielens, A. G. G. . M., Forveille, T., Bachiller, R., Cesarsky, D., Jones, A. P., Young, K., Roelfsema, P. R., & Cernicharo, J. 1998, ApJ, 495, L23
Gruenwald, R. B., & Viegas, S. M. 1992, AJS, 78, 153
Harris, H. C., Dahn, C. C., Canzian, B., Guetter, H. H., Leggett, S. K., Levine, S. E., Luginbuhl, C. B., Monet, A. K. B., Monet, D. G., Pier, J. R., Stone, R. C., Tilleman, T., Vrba, F. J., & Walker, R. L. 2007, AJ, 133, 631
Henney, W. J., Williams, R. J. R., Ferland, G. J., Shaw, G., & O'Dell, C. R. 2007, ApJ, 671, L137
Henry, R. B. C., Kwitter, K. B., & Dufour, R. J. 1999, ApJ, 517, 782
Matsuura, M., Speck, A. K., McHunu, B. M., Tanaka, I., Wright, N. J., Smith, M. D., Zijlstra, A. A., Viti, S., & Wesson, R. 2009, ApJ, 700, 1067
Matsuura, M., Speck, A. K., Smith, M. D., Zijlstra, A. A., Viti, S., Lowe, K. T. E., Redman, M., Wareing, C. J., & Lagadec, E. 2007, MNRAS, 382, 1447
Meixner, M., McCullough, P., Hartman, J., Son, M., & Speck, A. 2005, AJ, 130, 1784
O'Dell, C. R., Henney, W. J., & Ferland, G. J. 2005, AJ, 130, 172

— 2007, AJ, 133, 2343
Stasińska, G., & Tylenda, R. 1986, A&A, 155, 137

Asymmetric Planetary Nebulae V
A. A. Zijlstra, F. Lykou, E. Lagadec and I. McDonald
Jodrell Bank Centre for Astrophysics, Manchester, UK © 2011

On the construction of a database to search for ICFs that account for asymmetrical nebulae

Denise R. Gonçalves[1], Marcelo L. Leal-Ferreira[1,2], and Hektor Monteiro[3]

[1]*UFRJ - Observatório do Valongo, Ladeira do Pedro Antônio 43, 20080-090 Rio de Janeiro - RJ, Brazil*

[2]*Argelander-Institut für Astronomie, University of Bonn, Auf dem Hügel 71, D-53121 Bonn, Germany*

[3]*Universidade Federal de Itajubá, Av. BPS, 1303 Itajubá - MG, Brazil*

Abstract. In this contribution we analyse the physical and chemical conditions of the planetary nebula NGC 40 through spatially-resolved spectroscopic maps. This parameters were derived by using the 2D_NEB, a new algorithm based on the well-established IRAF *nebular* package, which was developed to enable the use of the spectroscopic maps to easily estimate the astrophysical quantities of ionised nebulae. From these maps, we conclude that T_e[N II] shows only a slight temperature variation from region to region, and that N_e[S II] has a much more prominent spatial variation. Maps of the chemical abundances also show significant variations, suggesting that spatial resolution is crucial for a complete study of the physical and chemical properties of planetary nebulae.

The techniques and results described in this contribution are part of a project we are starting aimed at looking for an ionisation-correction factor (ICF) scheme that properly account for asymmetrical nebulae. This procedure requires good quality spectroscopic data –like those we discuss here– as well detailed 3D photo modelling.

Keywords. Planetary Nebulae

1. Revisiting the ICF scheme and the spectroscopic mapping of NGC 40

Accurate ICFs are the key to determine reliable elemental abundances for ionised nebulae, for which it is usually the case that only one or two ionisation stages of a given element can be observed. The present ICFs used to account for the unseen ionisation fractions of planetary nebulae (PNe) optical spectra were derived using 1D photoionization codes, under the assumption that all the PNe are spherical (e.g., Kingsburgh & Barlow 433). In order to find a set of more reliable equations that can safely be applied to the case of asymmetrical PNe it is mandatory to revisit the ICF formulation. To map the PNe, multiple long-slit (434) and IFU (Integral Field Unit; e.g., Monteiro et al. 2010 in prep., on NGC 3242) spectroscopy are needed. As non-spherical PNe are in focus, the 3D photoionization code MOCASSIN (431) fulfills our proposal in terms of theoretical ionisation structure predictions.

In recent years IFU data are becoming popular for studying PNe (e.g., Monreal-Ibero et al. 437; Sandin et al. 442). In particular, Tsamis et al. (444) used this tool for a few PNe. The latter authors pointed out, from their IFU data, the variation on the discrepancy of the O^{++} abundances obtained from the collisionally excited lines and optical recombination lines, also establishing correlations between the ionisation state of the gas and the O^{++} discrepancies.

Similar kinds of data can be produced by a spectroscopic mapping technique developed by Monteiro et al. (2004), in which multiple parallel long-slit spectra of a nebula are interpolated to create emission-line maps. Both types of data enable better spatially resolved analysis of ionised nebulae than those based on single long-slit spectra. Spatially resolved data are also critical in constraining photoionization models which are now fully 3D and can produce a great number of observable quantities, including projected images for each emission line, sometimes constrained by this kind of data (e.g., Morisset & Georgiev 439).

1.1. Observations and data treatment

Our Hα (30 s exposure) image and optical long-slit spectra were obtained on 2005 October 28^{th}, at the 2.56 m Nordic Optical Telescope (NOT), with ALFOSC, which pixel scale is 0.189″ pixel^{-1}. The 16 (3×300 s) parallel spectra were obtained with a long-slit of 1.3″ in width, a spectral coverage from 3850 Å to 6850 Å, and a reciprocal dispersion of 3.0 Å pixel^{-1}; separated by a fix distance of 3″. Figure 1 (top-left panel) shows our Hα image, and also the relative slit positions across the nebula.

The data reduction was performed using the standard procedures for images and long-slit spectroscopy of IRAF, including flux calibration. The latter were used with the emission-line mapping technique to obtain the spectroscopic maps of NGC 40. These emission-line maps correspond to the $120'' \times 47''$ field of view of Figure 1 (top-right panel). Maps we constructed were corrected for the effects of field rotation due to the Alt-Azimuth nature of the telescope as well as for differential atmospheric refraction, using the tables of (432), and also submitted to signal to noise ratio cut, which avoids pixels with spurious information (more details in Leal-Ferreira et al. 434). To check the accuracy of the technique we compared fluxes measured directly from a single slit and those of the corresponding location in the spectroscopic map. In more than 75% of the cases, the discrepancies are lower than 10%.

2. The 2D_NEB

To perform the usual diagnostic calculations for the emission-line maps, efficiently, we develop a number of IDL routines. The set of routines we built compose the 2D_NEB package (434). The 2D_NEB package was built based on tasks of the IRAF stsdas.analysis *nebular* package –following the recipes given by De Robertis et al. (430) and Shaw & Dufour (443)– adapted to work with 2D images. As such, all the results generated by these tools are 2D maps created in FITS file format.

The routines that compose the first part of the package are based on the Osterbrock & Ferland (440) formalism, and are responsible for calculating the extinction coefficient, c(Hβ), and correcting the data for reddening.

The remaining routines of 2D_NEB were based on the *temden*, *ionic* and *abund* tasks of the IRAF facility. These routines are responsible for solving the equation of statistical equilibrium. The atomic data used in our tools are read from IRAF's atomic data directory. The electron temperatures (T_e) and densities (N_e) are determined from the solution of the equations of statistical equilibrium. This package also calculates chemical abundances (ionic and total). The effective recombination coefficient for the Hβ and the He main transitions, not included in the IRAF's atomic data directory, were taken from Benjamin, Skillman & Smits (1999). Total chemical abundance derivation uses the ICF formalism of Kingsburgh & Barlow (433).

3. Spectroscopic mapping results and discussions

Hα, Hγ and Hδ maps (weighted by their fluxes) and the Cardelli et al. (427) extinction curve were considered in deriving the c(Hβ) map. The variation of c(Hβ) across the nebula can be seen in Figure 1, middle-left panel. It clearly shows that c(Hβ) is not constant throughout NGC 40. The mean value of this map is 0.42. In studying a portion of the nebula Clegg et al. (428) found c(Hβ)=0.70. In our map this region corresponds to an area where c(Hβ) values are higher than average –with minimum and maximum values of ∼0.22 and ∼1.03, respectively– whose median, 0.62, is in agreement with Clegg et al. (428). Pottasch et al. (441) and Aller et al. (425), using data from various regions of the nebula, found c(Hβ)=0.605 and c(Hβ)=0.33, respectively, both in reasonable agreement with our map. As we have access to the spatial variation of c(Hβ), it is clear to us why previous works found so different c(Hβ).

Our T_e[N II] map (Figure 1, bottom-left panel) shows only a slight variation from region to region, from ∼8,000 K up to ∼9,500 K. On the other hand, these variations are much less prominent than those found in the N_e[S II] map (Figure 1, middle-right panel), $1{,}000 \leq N_e[\text{S II}] \leq 3{,}000$ cm^{-3}. This density map also shows that there is a trend to lower density regions on the west side of the nebula, but it does not shows any trend for the outer regions compared to the inner ones. The mean N_e[S II] (1,650 cm^{-3}) and T_e[N II] (8,850 K), from the spectroscopic maps, are in good agreement with other results from the literature (429; 435; 441; 428; 425). And, on the other hand, the maps show spatial variations that were not addressed by previous works.

Concerning the element abundance of helium, He/H (Figure 1, bottom-right panel, not show this map, but the He^+/H^+), we found that 9.32×10^{-2} and 1.18×10^{-1} should correspond to the lower and upper He abundance limits of NGC 40. These values are already corrected by the significant presence of He^0, and are also similar to the previous results found by Liu et al. (436), who adopted the same ICF scheme to account for the unobserved amount of He^0 in the total helium abundance of NGC 40.

We aim at putting together all the 3D model fitting data that already exist for PNe, and those we are getting for PNe with high quality observation constraints. This, as well as the building of a grid of MOCASSIN models spanning a wider range of physical parameters (central star temperature, nebular density distribution, and ionisation parameter) will finally allows to find a new set of ICFs with which to determine elemental abundances of N, O, Ne, S, Ar, and S of asymmetric nebulae.

Acknowledgments. We thank the SOC for the opportunity of giving this talk at the APN5, the LOC so nicely organised. DRG also acknowledge the Brazilian grant of the INCT-Astrofísica (CNPq 573648/2008-5).

References

Aller L., Czyzak S., Buerger E., et al., 1972, ApJ 172, 361
Benjamin R., Skillman E., Smits D., 1999, ApJ 514, 307
Cardelli J., Clayton G., Mathis J., 1989, ApJ 345, 245
Clegg R., Seaton M., Peimbert M., Torres-Peimbert S., 1983, MNRAS 205, 417
Delgado-Inglada G., Rodriguez M., Mampaso A. and Viironen K., 2009, ApJ 694, 1335
De Robertis M., Dufour J., Hunt R., 1987, JRASC 81, 195
Ercolano B., Barlow M. J., Storey P. J., & Liu X.-W., 2003, MNRAS 340, 1136
Filippenko A. V., 1982, PASP 94, 715
Kingsburgh R., Barlow M. J., 1994, MNRAS 271, 257
Leal-Ferreira M. L., Gonçalves D. R., Monteiro H., & Richards J.W., 2010, MNRAS accepted
Liu Y., Liu X.-W., Luo S.-G., Barlow M. J., 2004a, MNRAS 353, 1231-1250
Liu Y., Liu X.-W., Barlow M. J., Luo S.-G., 2004b, MNRAS 353, 1251-1285
Monreal-Ibero A., Roth M. M., Schönberner D. Steffen M., Böhm P., 2005, ApJ 628, L139
Monteiro H., Schwarz H., Gruenwald R., Heathcote S., 2004, ApJ 609, 194
Morisset C., & Georgiev L., 2009, A&A 507, 1517
Osterbrock D., Ferland G., 2006, *Astrophysics of Gaseous Nebulae and Active Galactic Nuclei*, University Science Books
Pottasch S., Bernard-Salas J., Beintema D., Feibelman W., 2003, A&A 409, 599
Sandin C., Schönberner D., Roth M. M., Steffen M., Böhm P., Monreal-Ibero A., 2008, A&A 486, 545
Shaw R. A., Dufour R. J., 1995, PASP 107, 896
Tsamis Y. G., Walsh J. R., Péquignot D., Barlow M. J., Danziger I. J., Liu X.-W., 2008, MNRAS 386, 22

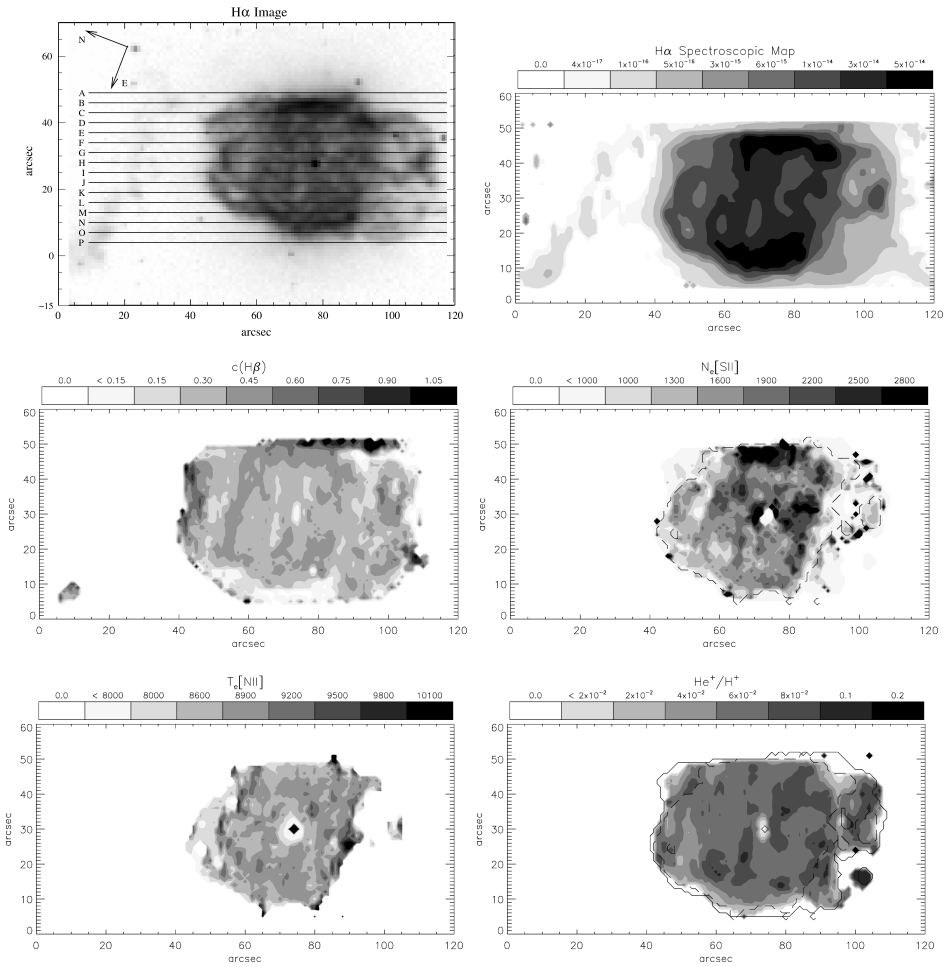

Figure 1. The Hα image and spectroscopic maps of NGC 40. *Top-left*: NOT Hα image, with the parallels slit positions superposed. *Top-right*: The Hα spectroscopic map here computed. *Middle-left*: The c(Hβ) map. *Middle-right*: The N_e[S II] map, in cm^{-3}. *Bottom-left*: The T_e[N II] map, in K. *Bottom-right*: The ionic abundance map of He I, which is the dominant ion in the He/H of this PN.

Asymmetric Planetary Nebulae V
A. A. Zijlstra, F. Lykou, E. Lagadec and I. McDonald
Jodrell Bank Centre for Astrophysics, Manchester, UK © *2011*

Stellar evolution from the main sequence to the post-AGB phase

Amanda I. Karakas
Research School of Astronomy & Astrophysics, Mount Stromlo Observatory, Weston Creek ACT 2611, Australia

Abstract. The evolution of (single) low and intermediate-mass stars from the main sequence to the post-AGB phase is reviewed. These stars evolve through core H and He-burning before entering the asymptotic giant branch (AGB) phase. During the AGB, recurrent mixing events may occur that can significantly change the composition of the envelope, with enrichments in carbon, nitrogen, and heavy elements synthesized by the *slow* neutron capture process observed. The details of dredge-up are still not well understood but likely depend on mass, metallicity, and evolutionary state. The AGB phase is terminated once mass loss has eroded the envelope and envelope ejection occurs. The brief post-AGB phase is characterized by stars evolving at near constant luminosity toward higher effective temperatures. If the ejected envelopes have sufficient time to become ionized by the hot central stars then it will be observed as a planetary nebula (PN). Abundances of post-AGB stars and planetary nebulae can be used as AGB model constraints and as probes of PN evolutionary pathways.
Keywords. Planetary nebulae – Stars: evolution, AGB to post-AGB

1. Introduction

Before stars turn into asymmetrical planetary nebulae (PNe) they first evolve through the *asymptotic giant branch* (AGB) phase of stellar evolution. All stars in the mass range from about $0.8M_{\odot}$ to $\sim 8M_{\odot}$, including our own Sun, will become AGB stars. The AGB is the last nuclear burning phase of stellar evolution for this mass range and is brief, lasting less than 1% of the main sequence lifetime. AGB stars are evolved objects and are found in the high-luminosity, low temperature region of the Hertzsprung-Russell (HR) diagram. AGB stars have evolved through core H and helium (He) burning and are now sustained against gravitational collapse by alternate H-shell and He-shell burning. AGB stars are often observed to be chemically different from their less evolved counterparts and show enrichments in carbon, nitrogen, fluorine, and heavy elements synthesized by the *slow* neutron capture process (the *s* process; see 448; 461, for recent reviews). In particular, AGB stars can become C-rich where C/O ratios ≥ 1.

Many AGB stars are also observed to be losing mass rapidly through slow, dense outflows, where typical mass-loss rates are $\dot{M} \sim 10^{-5} M_{\odot}$ year^{-1} with velocities $\sim$10 km/second. After the AGB phase is terminated, low to intermediate mass stars evolve to become post-AGB stars and possibly planetary nebulae (PNe), if the ejected envelopes have sufficient time to become ionized by the hot central stars before dissipating into the interstellar medium (446; 480). The composition of the bare central star may reveal information about the nuclear burning shells and this information is invaluable to

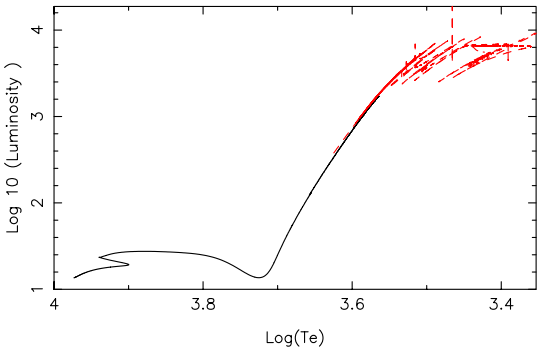

Figure 1. HR diagram for a $1.8M_{\odot}$, $Z = 0.01$ model. The evolutionary track has been plotted from the zero-age main sequence to the tip of the AGB. The x-axis is the effective temperature of the model star, shown in units of $\log_{10} T_{\rm eff}$, whereas the y-axis is the luminosity, in units of $\log_{10}(L/{\rm L}_{\odot})$.

constrain models of AGB stars. Likewise, the illuminated PN is comprised of material from the deep convective envelope, hence nebular abundances reveal information about the efficiency of mixing events and chemical processing that took place during previous evolutionary phases, in addition to the initial composition of the parent star.

In this paper we will use the latest theoretical models to journey from the main sequence through to the post-AGB phase, with a focus on the surface abundance changes caused by stellar evolution. For a more in-depth look at the evolution of these stars we refer to Karakas (464).

2. From the main sequence to the asymptotic giant branch

All stars begin their nuclear-burning life on the main sequence, burning H to He in their cores. In Fig. 1 we show the theoretical evolutionary track of a $1.8M_{\odot}$, $Z = 0.01$ star from the main sequence to the tip of the AGB (using data from 466). This model shows behaviour typical of a *low-mass* star ($\sim 1 - 3M_{\odot}$). *Intermediate-mass stars* have initial masses $\gtrsim 3 - 8M_{\odot}$, depending on metallicity, Z, and evolve in a similar way with a couple of exceptions that we mention below.

The $1.8M_{\odot}$ star begins burning H in a radiative core which quickly becomes convective once the central temperature exceeds $\approx 20 \times 10^6$ K, causing activation of CNO cycle reactions. Following core H exhaustion the core contracts and H burning is established in a shell as the star crosses the Hertzsprung Gap. As the star ascends the first giant branch (FGB), the inward movement of the convective envelope reaches regions where partial H burning occurred during the main sequence. Thus the products of H burning (e.g., ^{3}He, ^{4}He, ^{13}C, and ^{14}N) are mixed to the stellar surface. The most striking change is a reduction in the ^{12}C/^{13}C ratio from its initial value of 89 to $\approx$ 22. The FDU leaves behind a sharp composition discontinuity exterior to the position of the H-burning shell. In the lowest-mass stars the relatively long giant branch lifetime

allows the H-shell to reach the composition discontinuity and erase it. This does not occur in intermediate-mass stars, which leave the FGB before the H-shell can erase the discontinuity.

During the ascent of the FGB, the He core of the $1.8M_{\odot}$ star continues to contract and heat and becomes electron degenerate. Neutrino energy losses from the centre cause the temperature maximum to move outward. The FGB lifetime is terminated when the temperature reaches about 100 million K and the triple alpha reactions are ignited. The temperature and density are essentially decoupled and this leads to a violent helium ignition that is referred to as the *core helium flash*. The maximum initial mass for the core He-flash to occur, is $\approx 2M_{\odot}$ at solar composition. Following the core He flash, the star settles down to a period of quiescent core He-burning for about 100 Myrs.

In intermediate-mass stars, the contracting He cores do not become electron degenerate and the ignition of ^{4}He occurs quiescently in the centre. Note that if overshooting is included in stellar models the core H and He burning lifetimes are longer, because more fuel is added to the core, and the core masses at the base of the AGB are larger (e.g., 481). The properties of the C-O core left after core He-burning depend on a number of factors including the numerical treatment of convection, the inclusion of convective overshoot, and the uncertain rate of the $^{12}C(\alpha,\gamma)^{16}O$ reaction (463).

2.1. Extra mixing on the FGB

Prior to the TP-AGB, the surface composition of a star will be altered by the first and possibly second dredge-up events. Theory predicts that the surface $^{12}C/^{13}C$ ratio increases with decreasing mass after the FDU. These predictions have been found to be inconsistent with observations for low-mass field stars (e.g., 458; 460), as well as for Population II giants in globular clusters, where the deviation between theory and observation is more extreme (459; 451). The observations of low $^{12}C/^{13}C$ and C/N ratios have been interpreted as evidence for non-convective *extra mixing* taking place between the base of the convective envelope and the H-shell. Observations indicate that the conflict between theory and observation does not arise until after the deepest first dredge-up, hence this mixing most likely takes place after the H-shell has erased the composition discontinuity left by the FDU. The physical mechanism that causes the extra mixing is still uncertain and most algorithms used in deep mixing models are parameterized in some way to reproduce the observed data. In recent years thermohaline mixing has received much attention (455; 450; 476) and is currently the most likely candidate for extra mixing on the FGB.

Note that the effects of rotation and magnetic fields are often ignored in stellar models of low and intermediate-mass stars (there are exceptions including 462; 472; 479; 449). Rotation may have an important influence on surface abundances in intermediate-mass stars of $\approx 3M_{\odot}$ (e.g., 449). We discuss this idea below in the context of Type I PNe.

3. During the AGB

Following core He exhaustion the star ascends the giant branch for the second time. The strong expansion of the star caused by the structural re-adjustment to He-shell burning causes the H-shell to be extinguished as the star begins the ascent of the AGB. With

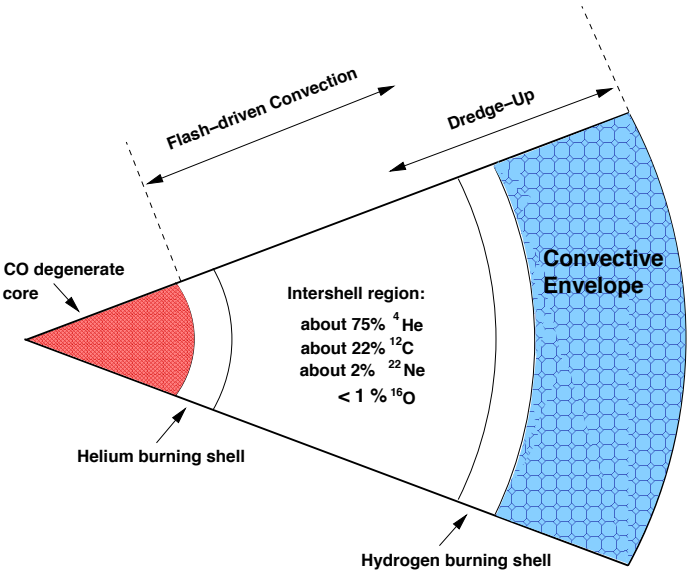

Figure 2. Schematic structure of an AGB star showing the degenerate C-O core surrounded by a He-burning shell above the core, and a H-burning shell below the deep convective envelope. The burning shells are separated by an intershell region rich in helium ($\sim$ 75%) and carbon ($\sim$ 22%), with a few percent each (by mass) of ^{16}O and ^{22}Ne. From (467).

the entropy barrier of the H-shell gone, the convective envelope moves inward. In low-mass stars the envelope does not penetrate as deeply as during the FDU. However in intermediate-mass stars this inward movement results in the second dredge-up (SDU) and large increases in the surface ^{14}N abundance. There is a critical minimum mass below which the SDU does not occur ($\approx 4.5 M_{\odot}$ at $Z = 0.02$). Following the SDU, the H-shell is re-ignited and the first He-shell instability soon follows. The star is now on the TP-AGB, where the structure is qualitatively the same for all masses (Fig. 2).

Briefly, during the TP-AGB phase the He-burning shell becomes thermally unstable every 10^5 years or so, depending on the core mass. The energy from the thermal pulse (TP) drives a convective zone in the He-rich intershell, that mixes the products of He-nucleosynthesis within this region. The energy provided by the TP expands the whole star, pushing the H-shell out to cooler regions where it is almost extinguished and subsequently allowing the convective envelope to move inwards (in mass) to regions previously mixed by the flash-driven convective zone. This inward movement of the convective envelope is known as the third dredge-up (TDU), and is responsible for enriching the surface in ^{12}C and other products of He-burning, as well as heavy elements produced by the *s* process. Following the TDU, the star contracts and the H-shell is re-ignited, providing most of the surface luminosity for the next interpulse period. The cycle of *interpulse–thermal pulse–dredge-up* may occur many times on the AGB, depending on the initial mass and composition, as well as on the mass-loss rate. In the $1.8 M_{\odot}$ example, the star experiences 12 TPs in total and only becomes C-rich at the 9$^{\rm th}$ TP. This model is predicted to leave AGB with a H-exhausted core of $0.585 M_{\odot}$, where this final value greatly depends on the assumptions made about the occurrence of the TDU and the mass-loss rate.

In intermediate-mass AGB stars ($M \gtrsim 4M_{\odot}$) the convective envelope can dip into the top of the H-shell, resulting in nuclear burning at the base of the convective envelope. This phenomena is known as hot bottom burning (HBB) and can also dramatically alter the surface composition. This is because the convective turn-over time of the envelope is $\approx$ 1 year, hence the whole envelope will get processed through the hot region a few thousand times per interpulse period. Note that the TDU still occurs in these stars hence HBB can lead to significant amounts of primary ^{14}N production. Intermediate-mass stars enter the AGB with core masses $\gtrsim 0.8-1.2M_{\odot}$ and will evolve more rapidly than their lower mass counterparts.

The details of AGB nucleosynthesis depends on a number of factors including the efficiency of the third dredge-up, the minimum core mass for thermal pulses, the minimum H-exhausted core mass for the onset of the TDU, and on the minimum mass for the onset of HBB. All of these quantities in turn depend on the stellar mass and/or envelope mass, and these change during evolution along the AGB. HBB for example, will be shut off once the envelope mass drops below some critical value as a result of strong mass loss. The mass-loss rate also determines the total number of thermal pulses and this then sets the level of enrichment in the envelope. All of these quantities depend on large uncertainties related to the stellar modelling. Most of these uncertainties stem from our inability to accurately model convection in stellar interiors (457; 482), although other inputs such as the mass-loss rate and opacities also play an important role (e.g., 483).

The study by Marigo (470) showed that inclusion of C-rich low-temperature opacities was an important addition to the modelling of TP-AGB stars. That is because the C dredged into the envelope forms C-bearing molecules (such as CO, CN) that lead to a strong increase in the opacity. The increase in the opacity cools the star and expands it, leading to an increase in the mass-loss rate which shortens the AGB lifetime. However, most models computed up until about that time used scaled solar low-temperature opacities (e.g., 456) that did not reflect the "true" composition of the outer layers. Most AGB star models now include such low-temperature C-rich opacity tables (453; 484; 483; 466).

4. Post-AGB stars and planetary nebulae

We can now apply our knowledge of AGB evolution to study post-AGB stars and planetary nebulae. Here we discuss PNe; we refer to e.g., Werner & Herwig (486), Bonačić Marinović et al. (447), and Karakas et al. (466) for discussions about post-AGB star abundances.

4.1. The *s*-process in low-metallicity PN

Abundances derived from PN spectra provide a complimentary data set to the abundances derived from the spectra of cool evolved stars. Recent observations have shown that some PNe are enriched in heavy elements that can be produced by the *s*-process including Ge, Se, Kr, Xe, and Ba (474; 478; 473). Sterling & Dinerstein (478) obtained Se and Kr abundances for 120 Galactic PNe and investigated trends between *s*-process enrichments and PN morphology and other nebular and stellar characteristics. It was found that while some PN have large enrichments of Se and Kr (e.g., [Se,Kr/O]

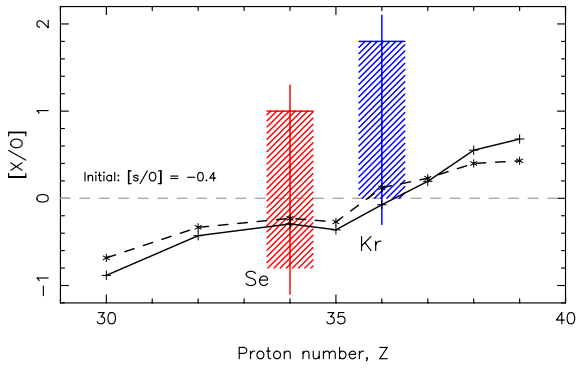

Figure 3. The surface abundances of neutron-capture elements around the first *s*-process peak. The solid lines show results for the $1.25M_{\odot}$, [Fe/H]= −2.3 model (solid line), and the $2M_{\odot}$, [Fe/H]= −2.3 model (dashed line). An α-enhanced initial abundance pattern was used (e.g., [O/Fe] = +0.4), and scaled solar for elements heavier than iron. Abundances are taken at the tip of the TP-AGB after the last computed thermal pulse. The boxes represent the range of observed Se and Kr abundances for the full PN sample from Sterling & Dinerstein (478). Figure from Karakas & Lugaro (468).

> 1), Type I PN have lower *s*-process abundances, on average, than the sample as a whole. In Karakas et al. (469) we compared nucleosynthesis predictions from models of intermediate-mass AGB stars to the results of Sterling & Dinerstein (478), and in Karakas & Lugaro (468) we presented results for lower mass AGB stars. In Karakas & Lugaro (468) we also presented predictions for low metallicity low-mass AGB stars. Recently, Otsuka et al. (473) obtained *s*-process abundances for the metal-poor BoBn1, showing that the PN is highly enriched in Kr, Xe, and Ba.

In Fig. 4 we show the *s*-process abundance distribution for two low-metallicity, low-mass AGB models. For these models we choose an initial α-enhanced abundance pattern (e.g., [O/Fe] = +0.4), which results in initial heavy element abundances with [X/O] = −0.4 when measured relative to oxygen. In Fig. 4 we show the observed Se and Kr abundance distribution from the Sterling & Dinerstein sample, noting that the sample consists of Galactic PNe with higher metallicities than used in the AGB models presented here. From Fig. 4 we see that the relative ratio of Zn/O is sub-solar, with [Zn/O] ~ -1 (starting at [Zn/O] = −0.4) from both models. If we examine the oxygen abundance, we find that a significant amount of this element is dredged to the surface, that is, [O/Fe] = 0.87 for the $1.25M_{\odot}$ model, and [O/Fe]= 1.20 for the $2M_{\odot}$ case. In both cases, Zn is actually produced by the *s*-process but in smaller quantities to oxygen, hence the [X/O] ratios do not reflect the degree of production. For example, the final [Zn/Fe] = 0.45 for both models. Note that in both models the iron abundance remains essentially unchanged.

Our results indicate that for the lowest metallicity PNe, the dredge-up of oxygen implies that this element is no longer a suitable proxy for the initial metallicity of the

progenitor star. Argon is sometimes used in place of oxygen, under the assumption that it remains unchanged by AGB nucleosynthesis which indeed seems to be the case (469). Zinc is also a potentially useful reference element because it does not condense into dust as easily as iron (e.g., 485), and can be observed in PNe (454). However Zn is at the beginning of the *s*-process chain and our results show that it can be produced in observable quantities in low-metallicity AGB stars.

4.2. Type I planetary nebulae

The composition of Type I PNe provides important constraints on nucleosynthesis and mixing in AGB stars. These PNe tend to exhibit bipolar morphologies and have high He/H and N/O ratios characteristic of proton-capture nucleosynthesis, suggesting they are descendants of AGB stars with initial masses ~2.5-8$M_{\odot}$ (477). In the Milky Way, the spatial distribution and kinematics of Type I PNe indicate that they are a young population (e.g., 452).

There is a problem, however, with the idea that most Type I PNe originated from intermediate-mass AGB stars. AGB stars with HBB produce the high He/H and N/O ratios observed in Type I PNe but these stars have massive cores and it is not clear if a $\gtrsim 0.8M_{\odot}$ central star will have time to ionize the surrounding medium to form a PN. Ruling out the most massive AGB stars with HBB leaves the lower end of the mass range, i.e., the 2.5 to 4$M_{\odot}$ objects. These stars do not experience HBB so it is not clear where the high He/H and N/O ratios came from. Note that the 2.5−4$M_{\odot}$ range are also not predicted to experience efficient extra mixing during the giant branches either (e.g., 455).

Some fraction of Type I and bipolar PNe presumably formed via binary evolution (475; 445; 471), although it is unclear how this would lead to the high He/H and N/O ratios observed. One way for the these objects to obtain high He and N would be through rapid rotation during the main sequence. During core H-burning, rotation mixes processed material to layers further out than they would otherwise be found. Hence the FDU would mix material more highly enriched in N than found in models with no rotation (see discussion in 469). Binary evolution would then terminate the AGB before many thermal pulses and dredge-up events have taken place, limiting the enrichment of *s*-process elements as required by observations (478). Rapid rotation may also inhibit the production of *s*-process elements during the AGB phase (462).

5. Conclusions

Before stars turn into planetary nebulae they first evolve through the AGB. It is during the AGB that the richest nucleosynthesis occurs, driven by instabilities of the He-burning shell and brought to the stellar surface by mixing episodes. It is during the AGB when stars shed much of their outer envelopes to the interstellar medium, making these objects important sources of dust and gas in galaxies. The expanding envelope may become a PN if the hot central stars has sufficient time to ionize the gas before it dissipates into the interstellar medium. The PN is comprised of material from the deep convective envelope, hence nebular abundances should reveal information about the efficiency of mixing events and chemical processing that took place during previous evolutionary phases, in addition to the initial composition of the parent star.

We use the latest theoretical models to examine the evolution of stars from the main sequence through to the post-AGB phase, with an emphasis on surface abundances changes caused by stellar evolution. The comparison of stellar models with observations of AGB stars and their progeny have allowed for much progress in our understanding of these fascinating objects. However many model uncertainties still persist, such as our inability to model convection in stellar interiors and uncertainties regarding mass loss. Much work is also to be done in finding the origin of extra mixing, and examining the effects of rotation and magnetic fields on the evolution of low and intermediate-mass stars.

Acknowledgments. I would like to thank the organisers for inviting me to a wonderful meeting!

References

Balick, B., & Frank, A. 2002, ARA&A, 40, 439
Blöcker, T. 2001, Ap&SS, 275, 1
Bonačić Marinović, A., Lugaro, M., Reyniers, M., & van Winckel, H. 2007, A&A, 472, L1
Busso, M., Gallino, R., & Wasserburg, G. J. 1999, ARA&A, 37, 239
Charbonnel, C., & Lagarde, N. 2010, ArXiv e-prints. 1006.5359
Charbonnel, C., & Zahn, J.-P. 2007, A&A, 467, L15
Cohen, J. G., Briley, M. M., & Stetson, P. B. 2005, AJ, 130, 1177
Corradi, R. L. M., & Schwarz, H. E. 1995, A&A, 293, 871
Cristallo, S., et al. 2009, ApJ, 696, 797
Dinerstein, H. L., & Geballe, T. R. 2001, ApJ, 562, 515
Eggleton, P. P., Dearborn, D. S. P., & Lattanzio, J. C. 2008, ApJ, 677, 581
Ferguson, J. W., et al. 2005, ApJ, 623, 585
Frost, C. A., & Lattanzio, J. C. 1996, ApJ, 473, 383
Gilroy, K. K. 1989, ApJ, 347, 835
Gratton, R., Sneden, C., & Carretta, E. 2004, ARA&A, 42, 385
Gratton, R. G., Sneden, C., Carretta, E., & Bragaglia, A. 2000, A&A, 354, 169
Herwig, F. 2005, ARA&A, 43, 435
Herwig, F., Langer, N., & Lugaro, M. 2003, ApJ, 593, 1056
Imbriani, G., et al. 2001, ApJ, 558, 903
Karakas, A. I. 2010, in Principles and Perspectives in Cosmochemistry, edited by A. Goswami & B. E. Reddy, 107
— 2010, MNRAS, 403, 1413
Karakas, A. I., Campbell, S. W., & Stancliffe, R. J. 2010, ApJ, 713, 374
Karakas, A. I., Lattanzio, J. C., & Pols, O. R. 2002, PASA, 19, 515
Karakas, A. I., & Lugaro, M. 2010, PASA, 27, 227
Karakas, A. I., et al. 2009, ApJ, 690, 1130
Marigo, P. 2002, A&A, 387, 507
Moe, M., & De Marco, O. 2006, ApJ, 650, 916
Nordhaus, J., et al. 2008, ApJ, 684, L29
Otsuka, M., Tajitsu, A., Hyung, S., & Izumiura, H. 2010, ArXiv e-prints. 1008.4175
Sharpee, B., et al. 2007, ApJ, 659, 1265
Soker, N. 1997, ApJS, 112, 487
Stancliffe, R. J. 2010, MNRAS, 403, 505
Stanghellini, L., et al. 2006, ApJ, 651, 898
Sterling, N. C., & Dinerstein, H. L. 2008, ApJS, 174, 158
Suijs, M. P. L. et al. 2008, A&A, 481, L87
van Winckel, H. 2003, ARA&A, 41, 391
Ventura, P., Castellani, M., & Straka, C. W. 2005, A&A, 440, 623

Ventura, P., & D'Antona, F. 2005, A&A, 431, 279
Ventura, P., & Marigo, P. 2009, MNRAS, 399, L54
Weiss, A., & Ferguson, J. W. 2009, A&A, 508, 1343
Welty, D. E., et al. 1999, ApJS, 124, 465
Werner, K., & Herwig, F. 2006, Publ. Astron. Soc. Pac., 118, 183

Asymmetric Planetary Nebulae V
A. A. Zijlstra, F. Lykou, E. Lagadec and I. McDonald
Jodrell Bank Centre for Astrophysics, Manchester, UK © 2011

The connection between sequence D and sequence E red giant variables and asymmetric planetary nebulae

C. P. Nicholls and P. R. Wood
Research School of Astronomy & Astrophysics, Mt. Stromlo Observatory, Cotter Road, Weston Creek ACT 2611 AUSTRALIA

Abstract. Red giant stars showing Long Secondary Periods, known as sequence D variables, make up about 30% of all luminous AGB stars. This is similar to the fraction of planetary nebulae that are known to be asymmetric. One of the models for sequence D variables is that they are binaries, a favourite explanation for asymmetric planetary nebulae. However, recent observations of the sequence D stars rule out binarity as an explanation for their behaviour. If there is a connection between sequence D variables and asymmetric planetary nebulae, it is not due to binarity.

Sequence E variables are ellipsoidal red giant binaries, in which a red giant is distorted by its unseen orbiting companion. We have used the observed frequency of sequence E binaries relative to non-variable red giants to estimate the fraction of low mass stars in the LMC that terminate their red giant evolution by a common envelope event, most likely producing a strongly asymmetric planetary nebula.

Keywords. Planetary Nebulae – Stars: AGB and post-AGB – Binaries: close – Stars: oscillations.

1. Introduction

Variable red giants lie on several sequences in the period–luminosity plane (Wood et al. 1999). Most of these sequences represent stars pulsating in different radial modes, but two of these sequences are more enigmatic. Sequence D corresponds to stars which show a Long Secondary Period (LSP) in addition to a radial overtone pulsation, while sequence E is made up of red giant binaries.

Stars on sequence E show regular light variations with periods of 50–400 days and light amplitudes < 0.3 mag in the MACHO red (M_R) band. They populate both the RGB and AGB. Their light curves often display minima of unequal depths, a feature Soszyński et al. (2004) noted is a hallmark of ellipsoidal variation. Ellipsoidal variables are close binaries where one star has evolved to the red giant phase and partially fills its Roche Lobe. This and the small orbital separation means the red giant is distorted into an ellipsoid, or pear-like shape. Therefore while the star's radial velocity curve is dominated by its orbital motion, the light variations are caused by the change in apparent surface area. Because of this, ellipsoidal variables show two cycles in light variation for every single cycle of velocity variation.

We recently presented the first radial velocity curves of sequence E variables (493). These confirmed that sequence E stars are ellipsoidal binaries, as their light curves execute two cycles of variation for every cycle completed by their velocity curves (see fig. 1 of that paper). Additionally, the amplitudes showed by the velocity curves are

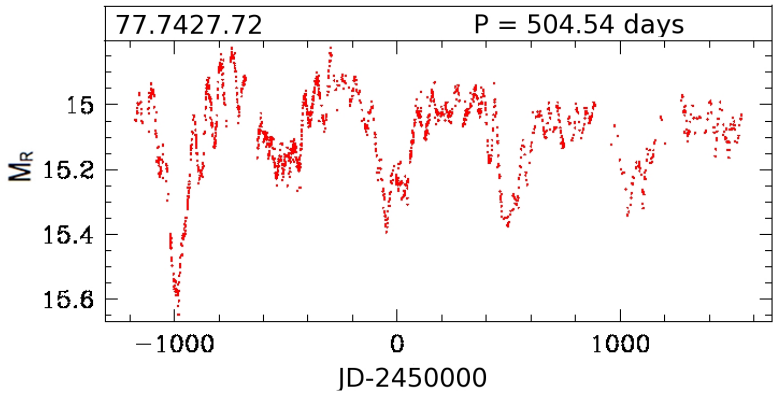

Figure 1. A typical sequence D light curve.

consistent with those expected for close binaries with roughly solar-mass components (mean full velocity amplitude found in the 493, sample is 43.3 km s^{-1}).

Stars on sequence D are nowhere near as easy to interpret. Their primary oscillation is known to be radial pulsation in an overtone mode, but the LSP has defied explanation for over a decade (491; 499; 489; 494, Ita et al. 2004). It is by no means an insignificant variation, with light amplitude up to 1 mag in M_R, periods of 250–1400 days and affecting ~30% of variable AGB stars. Although several models have been proposed to explain LSPs, all have at least one fatal flaw.

Fig. 1 shows a typical sequence D lightcurve, in which both variations are clearly visible. Even a cursory examination reveals the obvious irregularities in LSP period and amplitude, which are shown to greater or lesser degrees by all stars studied. In (494) we showed that sequence D stars have a small radial velocity variation at the period of the LSP.

2. Sequence D stars: connections to APN?

As the LSP has both light and radial velocity variations, one of the most popular models for its cause is an orbiting companion. In (494) we showed sequence D stars have several properties that are at odds with this model.

Fig. 4 of (494) shows a histogram of the velocity amplitudes for sequence D stars. It shows the velocity amplitudes of the LSP variation as small and similar; the median of the distribution is 3.53 km s^{-1}. This is unexpected for a sample of binaries, where a wider distribution and larger values would be more likely.

In a binary, the primary's velocity amplitude, along with the period, dictates the mass of its companion. A back-of-the-envelope calculation with typical sequence D parameters (LSP = 500 days, Δv = 3.5 km s^{-1}, M_{tot} = 1.5 M$_\odot$) yields an orbital separation of ~1.4 AU and a companion mass of ~ 0.09 M$_\odot$. And because velocity amplitudes are remarkably similar across the sequence D sample, so are companion masses. This uncanny similarity is not the sole problem, for (490) show that there is an observational deficit of stars with companions near ~ 0.09 M$_\odot$, as compared to both larger and smaller companions. This is known as the 'Brown Dwarf Desert'. Indeed using their results

we calculate that only 0.86% of main sequence stars should have companions between 0.06–0.12 $M_\odot$. Therefore it is difficult to see how ~30% of all stars could have LSPs caused by brown dwarf sized companions.

Fig. 9 of (494) shows the distribution of angle of periastron for sequence D stars. Angle of periastron, a measure of orbital orientation, should be uniformly distributed for binaries. Our distribution has a median of 227° and is biased towards higher angles. A K–S test gives the probability that our distribution is consistent with the uniform distribution as 1.4×10^{-3}. In other words, it is extremely unlikely that sequence D stars are binaries.

Sequence D stars are now known to show a mid-IR excess compared to stars without LSPs, indicating the presence of dust around these stars (498). This suggests that dust is either a cause or a product of the LSP. In fact, fig. 3 of that paper suggests that the dust around sequence D stars resides in a disk or other asymmetrical distribution. From this evidence it is tempting to suggest that sequence D stars have dusty disks. However, dusty disks are known to be a feature of binary systems, and we have presented convincing evidence above that sequence D stars are not binaries. Although the percentage of red giants with LSPs is similar to the percentage of PN that are asymmetric, if these two objects are related we can categorically state that it is not through binarity (at least if we discount the possibility that AGB stars generate $\sim 0.09\ M_\odot$ companions between the main sequence and the AGB). Perhaps the existence of asymmetric dust around sequence D stars can provide a link.

3. Predicting the fraction of PN that have close binary central stars

If red giants are precursors of planetary nebulae (PN), it follows that close binary red giants – like our sequence E stars – are the precursors of close binary PN. Recently, close binary interaction has been a favourite mechanism for the formation of asymmetric PN (APN) (487). Therefore, using the observed fraction of red giants that are sequence E stars, we can predict what fraction of PN have close binary post-common envelope central stars. By comparing this fraction with the observed fraction of PN that are asymmetric, we can comment on the likelihood of close binary interaction as a means of forming APN.

On the brightest 1 mag of the LMC RGB, Wood et al. (1999) found that 0.5% of stars were sequence E variables with amplitudes $\Delta M_R > 0.05$ mag. Similarly, using the OGLE catalog, (495) found that 1–2% (which we take as 1.5%) of red giants were sequence E variables with amplitudes $\Delta I > 0.025$ mag.

To be an observable ellipsoidal variable, a red giant must substantially fill its Roche Lobe. To find the minimum fractional filling required for a system to be detected as an ellipsoidal variable, we used the program NIGHTFALL to model partial-Roche Lobe filling systems with the same parameters as our sequence E stars. We found that the minimum fractional filling for a detectable variation is ~0.5, and the required filling factor varies with the inclination of the system.

We then made a Monte Carlo simulation of 10^6 binaries in which the larger star had a mass of 1.5 $M_\odot$. The period and mass ratio distributions were taken from (488), and each system was given a random orbital axis alignment. All stars in the simulation were evolved up the giant branches. Stars that filled their Roche Lobes below the RGB tip ($M_{bol} = -3.59$) were assumed to leave the RGB in a common envelope (CE) event

but not to become PN: their central stars would be unable to heat up quickly enough to ionise their ejected envelope before it dispersed. These systems would perhaps become something like RV Tauris. Stars that reached the AGB tip ($M_{bol} = -5.1$) without filling their Roche Lobes were assumed to become PN via the superwind, as single stars would. These became wide binary PN. However stars that filled their Roche Lobes between the RGB tip and the AGB tip were assumed to end their red giant phase in a CE event and become close binary post-CE PN.

In order to calculate the fraction of close binary post-CE PN, we measured the fraction of simulated stars that had detectable ellipsoidal variations in the top 1 magnitude of the RGB. We then added single stars to our simulation until this measured fraction was equal to the observed fraction of ellipsoidal variables in this range (0.5% or 1.5%, for Wood et al. 1999 and 495, respectively). We then divided the number of simulated stars that became binary post-CE PN by the total number of simulated stars that became PN, to get the fraction of post-CE PN.

We found that if we assume Wood's 0.5% sequence E stars, we should expect 7.9% of PN to be post-CE binaries. If we instead assume Soszyński's 1.5%, we calculate that 13.4% of PN should be post-CE binaries. In either case, short-period post-CE binaries are a small fraction of PN central stars.

4. Conclusions

We have used the fraction of red giants that are ellipsoidal variables to predict the fraction of PN that should have close binary post-CE central stars. We find fractions of 7.9% or 13.4%, depending on the observations used. We conclude that short-period post-CE binaries are a small fraction of PN central stars. If close binary interaction is a cause of APN, then not all APN can be caused by close binary interaction.

Our work with sequence D stars has showed that the LSP variation is unlikely to be caused by binarity. Therefore if there is a link between LSPs and APN, it is not due to binarity. Perhaps the presence of asymmetric dust around sequence D stars can provide a link to APN.

Acknowledgments. This paper has made use of the eclipsing binary program NIGHTFALL, written by Rainer Wichmann and available at http://www.hs.uni-hamburg.de/DE/Ins/Per/Wichmann/Nightfall.html.

References

Bond, H. E. 2000, in Asymmetrical Planetary Nebulae II: From Origins to Microstructures, edited by J. H. Kastner, N. Soker, & S. Rappaport, vol. 199 of Astronomical Society of the Pacific Conference Series, 115
Duquennoy, A., & Mayor, M. 1991, A&A, 248, 485
Fraser, O. J., Hawley, S. L., Cook, K. H., & Keller, S. C. 2005, AJ, 129, 768
Grether, D., & Lineweaver, C. H. 2006, ApJ, 640, 1051
Hinkle, K. H., Lebzelter, T., Joyce, R. R., & Fekel, F. C. 2002, AJ, 123, 1002
Ita, Y., & et al. 2004, MNRAS, 347, 720
Nicholls, C. P., Wood, P. R., & Cioni, M. 2010, MNRAS, 405, 1770
Nicholls, C. P., Wood, P. R., Cioni, M., & Soszyński, I. 2009, MNRAS, 399, 2063
Soszyński, I. 2007, ApJ, 660, 1486

Soszyński, I., & et al. 2004, Acta Astronomica, 54, 347
Wood, P. R., & et al. (MACHO Collaboration) 1999, in IAU Symp. 191: Asymptotic Giant Branch Stars, edited by T. Le Bertre, A. Lebre, & C. Waelkens (San Francisco: Astronomical Society of the Pacific), 151
Wood, P. R., & Nicholls, C. P. 2009, ApJ, 707, 573
Wood, P. R., Olivier, E. A., & Kawaler, S. D. 2004, ApJ, 604, 800

Asymmetric Planetary Nebulae V
A. A. Zijlstra, F. Lykou, E. Lagadec and I. McDonald
Jodrell Bank Centre for Astrophysics, Manchester, UK © 2011

The Evolutionary History of the R Coronae Borealis Stars

Geoffrey C. Clayton

Department of Physics & Astronomy, Louisiana State University, Baton Rouge, LA 70803; gclayton@fenway.phys.lsu.edu

Abstract. The RCB stars are hydrogen-deficient carbon stars which undergo large declines in brightness at irregular intervals due to the formation of dust. For about thirty years, there have been two scenarios suggested to explain the evolution of the R Coronae Borealis (RCB) stars. These are a double degenerate white dwarf (WD) merger and a final helium shell flash. The preponderance of observational evidence seems to support the WD merger although a few RCB stars may also be produced through the other channel.
Keywords Planetary nebulae – RCB stars

1. Introduction

The unexpected discovery that the R Coronae Borealis (RCB) stars have isotopic abundances of ^{18}O which are up to 500 times those seen in other stars has increased the likelihood that these rare hydrogen-deficient carbon stars are the result of a double degenerate white dwarf (WD) merger rather than a final helium shell flash (507; 506; 512). The RCB stars and the related hydrogen-deficient carbon (HdC) stars (which do not form dust) are a rare class of extremely interesting transition objects which have the potential to reveal critical details of the late stages of stellar evolution. In particular, both the RCB stars and Type Ia supernova may be the product of a white dwarf (WD) merger. These stars form a small group of carbon-rich supergiants which are defined by extreme hydrogen deficiency and unusual variability, characterized by large declines of up to 8 mag due to the formation of carbon dust at irregular intervals (504). Two scenarios have been proposed for the origin of an RCB star:

1. Double Degenerate WD Mergers (DD): Webbink (523) proposed a model where RCB stars evolve from the merger of a He-WD and a CO-WD. After a common envelope phase the members of the binary system, now on a much shortened period, coalesce through loss of angular momentum from gravitational wave radiation (515; 522). As the two WDs approach one another, the He-WD is disrupted. A fraction of the helium is accreted onto the CO-WD and starts to burn, while the remainder forms an extended envelope around the CO-WD. This structure, a helium-burning shell in the center of a hydrogen-deficient envelope, is believed to be that of an RCB star. WD merging times might not be as long as previously thought which makes the DD scenario a valid and alternative to the FF scenario for the formation of RCB stars (516; 514; 506). This type of merger may result in a Type Ia SN if the total mass of the DD system is greater than the Chandrasekhar limit, or in an RCB star if the mass is too small.

2. Final Helium Shell Flash (FF): An evolving planetary nebula (PN) central star could expand to supergiant size by a FF (510; 521). The possible connection between RCB stars and PNe is compelling, because the central stars of three old PNe (Sakurai's Object, V605 Aql and FG Sge; 509; 505; 513) have had FF outbursts, that transformed them from hot evolved central stars into RCB-like stars that form dust. On the other hand, there is evidence that the star acquires RCB characteristics only for a short time: V605 Aql looked like a cool (~5000 K) RCB star in 1921, but today, less than a century later, it has a T_{eff} ~95,000 K (505; 508). This rate of evolution is too rapid to be consistent with lifetimes suggested for the RCB stars. Sakurai's Object may be evolving quickly to higher temperatures as well (502; 517). This is supported by recent FF stellar models which indicate that the post-FF-RCB stage may only last a few years (518).

2. RCB Star Evolution

During the WD merger, dynamically accreting material may provide a suitable environment for a significant production of ^{18}O. We have found that ^{18}O can be overproduced in an environment of partial He-burning in which the temperature and the duration of nucleosynthesis are consistent with those inferred from our WD merger models (506). A similarly high abundance of ^{19}F has also been found (520). The production of significant amounts of ^{18}O and ^{19}F during a FF is not expected. The CNO abundances in the RCB stars are also more consistent with DD rather than FF evolution (501; 511). On the other hand, five RCB stars, including R CrB itself, show enhanced Li abundances, which favours the FF scenario (501). Hydrogen burning will destroy any Li that was present in a star when it formed. So any Li present in the RCB stars must have been created during the DD or FF event that led to the RCB star. But the temperature and densities required for the production of ^{18}O will destroy any Li present. So Li is not expected to be a product of the WD merger. However, Sakurai's object, which resulted from a FF, and is now in an RCB-like phase, has shown an increasing abundance of Li as well as hydrogen deficiency (500; 502). The obvious conclusion is that there might be (at least) two evolutionary channels leading to the RCB stars, perhaps with the DD being the dominant mechanism.

All of the RCB stars show small amplitude pulsations (519). These pulsations result from the kappa-mechanism and the strange-mode instability. Models of the pulsations are consistent with RCB stars having masses of 0.8–0.9 $M_\odot$ (522). This is significantly more massive than the average for a WD (~0.6 $M_\odot$) (503). In fact, the mass inferred for the RCB stars is consistent with that predicted for the merger of a CO- and a He-WD (~0.8–1.1 $M_\odot$) (514).

References

Asplund, M., Gustafsson, B., Kiselman, D., & Eriksson, K. 1997, A&A, 318, 521
Asplund, M., Gustafsson, B., Lambert, D. L., & Rao, N. K. 2000, A&A, 353, 287
Asplund, M., Lambert, D. L., Kipper, T., Pollacco, D., & Shetrone, M. D. 1999, A&A, 343, 507

Bergeron, P., Gianninas, A., & Boudreault, S. 2007, in 15th European Workshop on White Dwarfs, edited by R. Napiwotzki & M. R. Burleigh, vol. 372 of Astronomical Society of the Pacific Conference Series, 29
Clayton, G. C. 1996, PASP, 108, 225
Clayton, G. C., & De Marco, O. 1997, AJ, 114, 2679
Clayton, G. C., Geballe, T. R., Herwig, F., Fryer, C., & Asplund, M. 2007, ApJ, 662, 1220
Clayton, G. C., Herwig, F., Geballe, T. R., Asplund, M., Tenenbaum, E. D., Engelbracht, C. W., & Gordon, K. D. 2005, ApJ, 623, L141
Clayton, G. C., Kerber, F., Pirzkal, N., De Marco, O., Crowther, P. A., & Fedrow, J. M. 2006, ApJ, 646, L69
Duerbeck, H. W., & Benetti, S. 1996, ApJ, 468, L111
Fujimoto, M. Y. 1977, PASJ, 29, 331
García-Hernández, D. A., Hinkle, K. H., Lambert, D. L., & Eriksson, K. 2009, ApJ, 696, 1733
García-Hernández, D. A., Lambert, D. L., Kameswara Rao, N., Hinkle, K. H., & Eriksson, K. 2010, ApJ, 714, 144
Gonzalez, G., Lambert, D. L., Wallerstein, G., Rao, N. K., Smith, V. V., & McCarthy, J. K. 1998, ApJS, 114, 133
Han, Z. 1998, MNRAS, 296, 1019
Iben, I. J., Tutukov, A. V., & Yungelson, L. R. 1996, ApJ, 456, 750
— 1997, ApJ, 475, 291
Kerber, F., Pirzkal, N., De Marco, O., Asplund, M., Clayton, G. C., & Rosa, M. R. 2002, ApJ, 581, L39
Lawlor, T. M., & MacDonald, J. 2003, ApJ, 583, 913
Lawson, W. A., Cottrell, P. L., Kilmartin, P. M., & Gilmore, A. C. 1990, MNRAS, 247, 91
Pandey, G., Lambert, D. L., & Rao, N. K. 2008, ApJ, 674, 1068
Renzini, A. 1979, in ASSL Vol. 75: Stars and star systems, edited by B. E. Westerlund, 155
Saio, H., & Jeffery, C. S. 2002, MNRAS, 333, 121
Webbink, R. F. 1984, ApJ, 277, 355

Asymmetric Planetary Nebulae V
A. A. Zijlstra, F. Lykou, E. Lagadec and I. McDonald
Jodrell Bank Centre for Astrophysics, Manchester, UK © 2011

Wolf-Rayet Central Stars of Planetary Nebulae: Their Evolution and Properties

K. DePew[1], D.J. Frew[1], Q.A. Parker[1,2] and O. De Marco[1]

[1]*Department of Physics & Astronomy, Macquarie University, Sydney, NSW 2109, Australia*

[2]*Australian Astronomical Observatory, Epping, NSW 1710, Australia*

Abstract. Over the past decade, the number of planetary nebula central stars (CSPN) known to exhibit the Wolf-Rayet (WR) phenomenon has grown substantially. Many of these discoveries have resulted from the Macquarie/AAO/Strasbourg Hα (MASH) PN Survey. While WR CSPN constitute a relatively rare stellar type ($\lesssim$10% of CS), there are indications that the proportion of PN harbouring them may increase as spectroscopy of more central stars is carried out. In addition, with new and better distances from the Hα surface brightness-radius relationship of Frew (2008), we can attempt a dynamical age sequence which may provide insight into the evolution of these stars.
Keywords. Planetary nebulae

1. Introduction

Among central stars of planetary nebulae (CSPN), there exists a class of H-deficient objects that exhibit high mass-loss rates ($\gtrsim 10^{-6}$ $M_\odot$ yr^{-1}) due to strong, fast stellar winds. Their spectra resemble those of massive Wolf-Rayet stars, but these CSPN evolve from low- and intermediate-mass main sequence stars instead of massive O stars. They are designated as [WR] stars to differentiate them (553).

The [WR] class is subdivided into an oxygen sequence (designated [WO]), a carbon sequence ([WC]) and two controversial subclasses, the [WN] and [WN/WC] types. Nitrogen lines are enhanced in the latter two, accompanied in the [WN/WC]s by higher carbon abundances (552). Massive WOs and WCs possess surface abundances that differ from those of WNs. These stars are believed to represent an evolutionary sequence in which progressively deeper layers of the star are exposed through strong wind-driven mass loss (e.g. 524, and references therein). Thus, WCs and WOs possess different surface abundances than WNs. C/He ratios were at one time thought to be less in late-type [WC]s than in early types (e.g. 527), but as noted by Crowther (524), the lack of common diagnostics between late and early types could be a source of error. More recent studies find that chemical abundances appear to be similar across [WC]s and [WO]s (He:C:O $\sim$ 50:40:10 by mass for both; 525), and their subclasses are primarily distinguished by temperature and degree of ionization. PB 8, the lone published [WN/WC] type, has a much higher mass fraction of H (40%) than [WC]s and [WO]s (552).

The first scenario proposed to explain the formation of [WR] CSPN was the so-called "Born-Again Scenario" (e.g. 551; 541), in which a CSPN undergoes a thermal pulse that throws it back into the AGB. Possible [WR] evolutionary paths are differentiated according to the stage at which the thermal pulse occurs: the Asymptotic Giant Branch Final Thermal Pulse (AFTP), which occurs at the end of the AGB phase; a Late Thermal Pulse (LTP), which occurs when the star has left the AGB but has not yet ceased H-burning; or a Very Late Thermal Pulse (VLTP), which occurs when the star is already on the WD cooling track. See Herwig (540) for a more detailed discussion. Formation through a binary interaction has also been proposed (e.g. 528; 526). Hajduk et al. (538) conclude that emission-line stars are less likely than "normal" H-rich PN to be found in binary systems, or else have larger orbital separations. This may suggest that [WR]s result from a binary merger.

A by-product of many searches for [WR]s among the CSPN are weak emission-line stars or WELS, some of which are also H-deficient (543). These objects exhibit weaker emission lines at many of the same high-ionization wavelengths as [WR]s, but are likely less massive, evolutionarily unrelated objects, as evidenced by differences in Galactic scale height z (529). Overall, a near-complete volume-limited 1 kpc sample suggests that 7±3% of CSPN belong to the [WR] class, and ∼20% of CSPN are H-deficient (535).

2. New [WR]/WELS Discoveries

Recently 33 new [WR]/WELS and emission-line star candidates have been discovered in the course of the Macquarie/AAO/Strasbourg Hα (MASH; 547; 544) survey (531). Of these, 19 are objects first found by us within the MASH sample, and 14 are previously known objects whose [WR] or WELS nature was discovered serendipitously by us in the course of spectroscopic follow-up of MASH objects. See DePew et al. (531) for observational details and preliminary analysis. The 17 MASH [WR]s detailed in that paper, added to the 7 previously found in the MASH survey (546; 548; 545), make a contribution of 24 new objects to the list of [WR]s by our group. With the 6 serendipitous discoveries, this represents an increase of ∼40% in known [WR]s. Within the MASH sample, there is also one [WN] subclass object (PM5; 545) and one probable [WN/WC] object (Abell 48; 530).

3. The [WN] Stars

Massive WN stars possess significant amounts of hydrogen that will be lost with the surface nitrogen as they proceed toward the WC and WO phases. The existence of an actual [WN] sequence is open to debate, however. While hot bottom burning (HBB) should strongly enhance nitrogen in the more massive CSPN progenitors ($\gtrsim$ 4 $M_\odot$; 542), there is confusion over whether the two currently designated [WN]s, PM5 for example (545) and LMC-N66 (550) are truly CSPN. The high expansion velocity of the main shell of PM5 (∼165 km s^{-1}) is far higher than the v_{exp} of other known PN, and is more consistent with a massive WR ring nebula. LMC-N66 could be a peculiar binary system (539).

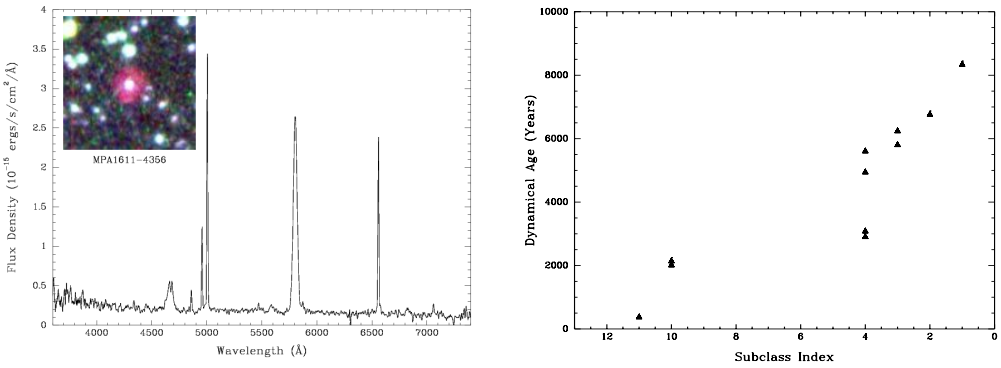

Figure 1. At left, the spectrum and image of MPA1611-4356, a new MASH PN classifiable as [WC/O4]. At right, the preliminary [WR] subclass-dynamical age relationship. Subclass index corresponds to: [WO1]=1, . . . , [WO4]=4, [WC4]=5, . . . , [WC11]=12.

There exists only one published member of the [WN/WC] class, PB 8 (552). The [WN/WC] class exhibits compositions and spectra similar to a massive WR transition type denoted as WN/WC. These objects have strong nitrogen lines, but also possess significant carbon abundances (1.3% by mass, as compared to 2% of nitrogen). Strangely, PB 8 is not a Type I nebula (552), as would normally be expected around a high-mass central star which has undergone HBB. This may not be a completely anomalous result however, as Abell 48 (also not a Type I PN; 530) appears to possess a [WN/WC] CS as well (530).

4. Towards An Evolutionary Subclass Sequence

Distance is one of the most crucial and elusive parameters required for a determination of luminosity, mass and other important properties of a star. The new surface brightness-radius relationship found in Frew & Parker (534) and Frew (533) provides a new, robust method for determining distance to PN. This relation is very easy to use, requiring only the Hα flux, the extinction, and the angular dimensions of the PN.

Between 19-23 April 2010, we observed a selection of PN on the Wide Field Spectrograph (WiFeS; 532) for chemical abundance determinations at Siding Spring Observatory. From these observations we obtained the global $R_{[NII]}$ ratio ($\frac{I(\lambda\lambda 6548,84)}{I(\lambda 6563)}$). We used this value to deconvolve the [N II] contribution and extract the Hα flux using data from the SuperCOSMOS Hα Survey (SHS; 549) and the Southern Hα Sky Survey Atlas (SHASSA; 536). For those PN with nebular v_{exp} in the literature, Hα surface brightness and distance were calculated and a dynamical age derived. A preliminary plot of [WR] subclass versus dynamical age is shown in Figure 1, where a clear trend is evident. More in-depth results will follow (529). While the analysis is not yet complete, it appears as though the late types are significantly younger than the early types, as

previously suspected (e.g. 537). However, more data points are needed to firm up this result.

5. Conclusions

The provenance of [WR] CSPN is still uncertain. However, a larger sample size, arising largely from our new discoveries over the past decade, will enable us to fill in some of the gaps in our understanding. The [WN] and [WN/WC] classes in particular will benefit from new survey data.

In addition, using the SB-r relation of Frew (533), we can determine more accurate distances to PN in our sample, allowing us to establish dynamical ages. The resulting evolutionary sequence, though somewhat crude, may in the future serve to inform stellar models for this rare class of objects.

Acknowledgments. KD thanks Macquarie University for an MQRES PhD scholarship and the Faculty of Science for travel funding for APN V conference attendance.

References

Crowther, P. A. 2007, ARA&A, 45, 177
— 2008, ASPC, 391, 83
De Marco, O. 2008, ASPC, 391, 209
De Marco, O., & Barlow, M. J. 2001, Ap&SS, 275, 53
De Marco, O., & Soker, N. 2002, PASP, 114, 602
DePew, K., Frew, D. J., Parker, Q. A., & De Marco, O. , 2010, in preparation
DePew, K., Frew, D. J., Parker, Q. A., De Marco, O., & Baxter, R. , 2010, in preparation
DePew, K., Parker, Q. A., Miszalski, B., De Marco, O., Frew, D. J., Acker, A., Kovacevic, A., & Sharp, R. , 2010, MNRAS, submitted
Dopita, M., Rhee, J., Farage, C., McGregor, P., Bloxham, G., Green, A., Roberts, B., Neilson, J., Wilson, G., Young, P., Firth, P., Busarello, G., & Merluzzi, P. 2010, Ap&SS, 327, 245
Frew, D. J. 2008, PhD Thesis, Macquarie University
Frew, D. J., & Parker, Q. A. 2006, IAUS, 234, 49
— 2010, in Asymmetric Planetary Nebulae 5, edited by A. A. Zijlstra, F. Lykou, E. Lagadec, & I. McDonald, 33
Gaustad, J. E., McCullough, P. R., Rosing, W., & Van Buren, D. 2001, PASP, 113, 1326
Górny, S. K., & Tylenda, R. 2000, A&A, 362, 1008
Hajduk, M., Zijlstra, A. A., & Gesicki, K. 2010, MNRAS, 406, 626
Hamann, W., Peña, M., Gräfener, G., & Ruiz, M. T. 2003, A&A, 409, 969
Herwig, F. 2001, Ap&SS, 275, 15
Iben, I., Jr., Kaler, J. B., Truran, J. W., & Renzini, A. 1983, ApJ, 264, 605
Lau, H. H. B., Stancliffe, R. J., & Tout, C. A. 2009, MNRAS, 396, 1046
Marcolino, W. L. F., & de Araújo, F. X. 2003, AJ, 126, 887
Miszalski, B., Parker, Q. A., Acker, A., Birkby, J. L., Frew, D. J., & Kovacevic, A. 2008, MNRAS, 384, 525
Morgan, D. H., Parker, Q. A., & Cohen, M. 2003, MNRAS, 346, 719
Morgan, D. H., Parker, Q. A., & Russeil, D. 2001, MNRAS, 322, 877
Parker, Q. A., Acker, A., Frew, D. J., Hartley, M., Peyaud, A. E. J., Ochsenbein, F., Phillipps, S., Russeil, D., Beaulieu, S. F., Cohen, M., Köppen, J., Miszalski, B., Morgan, D. H., Morris, R. A. H., Pierce, M. J., & Vaughan, A. E. 2006, MNRAS, 373, 79
Parker, Q. A., & Morgan, D. H. 2003, MNRAS, 341, 961

Parker, Q. A., Phillipps, S., Pierce, M. J., Hartley, M., Hambly, N. C., Read, M. A., MacGillivray, H. T., Tritton, S. B., Cass, C. P., Cannon, R. D., Cohen, M., Drew, J. E., Frew, D. J., Hopewell, E., Mader, S., Malin, D. F., Masheder, M. R. W., Morgan, D. H., Morris, R. A. H., Russeil, D., Russell, K. S., & Walker, R. N. F. 2005, MNRAS, 362, 689

Peña, M. 1995, RMxAC, 3, 215

Schönberner, D. 1979, A&A, 79, 108

Todt, H., Peña, M., Hamann, W., & Gräfener, G. 2010, A&A, 515, 83

van der Hucht, K. A., Conti, P. S., Lundstrom, I., & Stenholm, B. 1981, Space Sci.Rev., 28, 227

Asymmetric Planetary Nebulae V
A. A. Zijlstra, F. Lykou, E. Lagadec and I. McDonald
Jodrell Bank Centre for Astrophysics, Manchester, UK © 2011

UV Spectroscopy of the Central Star of the Planetary Nebula A 43

Ellen Ringat[1], Felix Friederich[1], Thomas Rauch[1], Klaus Werner[1] and Jeffrey W. Kruk[2]

[1]*Institute for Astronomy and Astrophysics, Kepler Center for Astro and Particle Physics, Eberhard Karls University, Sand 1, 72076 Tübingen, Germany*

[2]*NASA, Goddard Space Flight Center, Greenbelt, MD 20771, USA*

Abstract. About 25% of all post-AGB stars are hydrogen-deficient, e.g. the PG 1159 stars with a typical abundance pattern He:C:O = 33:50:17 (by mass). Only four of about 40 known PG 1159 stars exhibit H in their spectra. The exciting star of the planetary nebula A 43 is one of these so-called hybrid PG 1159 stars. We present preliminary results of an on-going spectral analysis by means of NLTE model-atmosphere techniques based on UV spectra obtained with *FUSE*, *HST*/*GHRS*, and *IUE* as well as on optical observations.
Keywords. Planetary Nebulae – ISM: planetary nebulae: individual: A 43 – Stars: abundances – Stars: atmospheres – Stars: evolution – Stars: individual: WD 1721+106 – Stars: AGB and post-AGB

1. Introduction

PG 1159 stars are hydrogen-deficient post-AGB stars. They have temperatures between 75 000 K and 200 000 K and their surface gravities $\log g$ range between 5.5 and 8.0. They experienced a Final Thermal Pulse (FTP), that mixed the envelope and the intershell (Fig. 1), and became a born-again star (560). Depending on the occurrence of this FTP a maximum remaining hydrogen content of about 20% (by mass) is possible. This maximum value is predicted for the AGB Final Thermal Pulse (AFTP) scenario, where the FTP happens at the end of the AGB phase and the masses of the mixing shells are nearly the same. When the FTP happens later, it is called Late Thermal Pulse (LTP) and the hydrogen content of the star is about 1% due to the smaller envelope mass at the time the FTP happens. An even later FTP (a Very Late Thermal Pulse occurs on the white dwarf cooling sequence) causes a complete burning of the hydrogen. Most PG 1159 stars experienced a LTP or VLTP. Only four stars show hydrogen lines in their spectra which is a hint for an AFTP. Three of these so-called hybrid PG 1159 stars (namely the central stars of Sh 2−68, A 43, and NGC 7094) are surrounded by a planetary nebula. One of these hybrid PG 1159 stars, A 43, is used as an example to introduce the spectral analysis technique in Sect. 3. Then our preliminary results are discussed in Sect. 4. The opportunity to access *TMAP* or already calculated *TMAP* spectra via the VO service *TheoSSA* is described in Sect. 5.

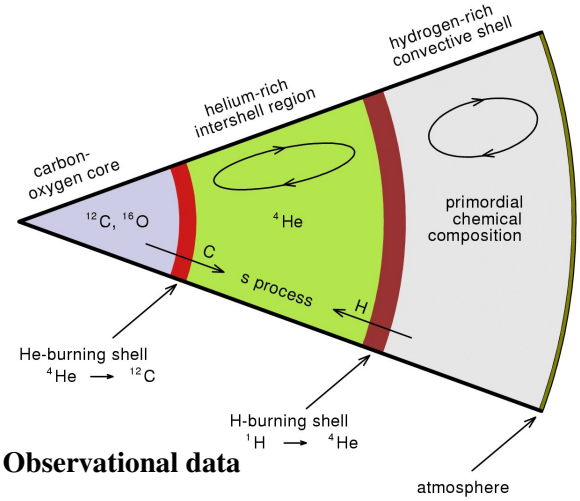

Figure 1. Structure of a post-AGB star. The intershell and the hydrogen-rich shell are mixed by a FTP.

2. Observational data

To perform a precise analysis, observed spectra with a high S/N ratio and resolution are required. Moreover, these spectra should cover a wide wavelength range. Because of the high temperature of PG 1159 stars, their maximum flux is located in the UV. A lot of strategic lines is located in this wavelength range, and thus, these spectra are very important for our analysis. To determine the surface gravity, optical spectra are advantageous. For our analysis, we retrieved *FUSE*, *GHRS*, and *IUE* spectra from MAST (standard pipeline reduction, Table 1). The spectra for the optical wavelength range were obtained with the 3.5 m telescope equipped with the TWIN spectrograph of the German-Spanish Astronomical Center on Calar Alto on April 13-14, 2001. They were reduced with the Image Reduction and Analysis Facility (`IRAF`, http://iraf.noao.edu/). To determine the interstellar extinction we used the UV spectra as well as brightnesses in the optical and infrared wavelength range and considered the Fitzpatrick law (1999). The resulting reddening is $E_{\mathrm{B-V}} = 0.265 \pm 0.035$.

Table 1. Log of our UV observations.

Instrument	Obs ID	Obs Start Time (UT)	Aperture	Exp. Time (sec)
FUSE	B0520201000	2001-07-29 20:41:47	LWRS	11438
FUSE	B0520202000	2001-08-03 22:18:20	LWRS	9528
GHRS	Z3GW0304T	1996-09-08 07:00:34	2.0	4243
IUE	LWR08735	1980-09-06 21:45:21	LARGE	3600
IUE	SWP10245	1980-09-28 21:50:02	LARGE	5100

3. Spectral analysis

The spectral analysis was performed with the Tübingen NLTE Model-Atmosphere Package (*TMAP*) which was developed over the last 25 years. It uses an Accelerated Lambda Iteration (ALI, see e.g. Werner & Dreizler 559; Werner et al. 558; Rauch & Deetjen 557). Hydrostatic and radiative equilibrium and plane-parallel geometry are assumed. About 1000 atomic levels can be considered as NLTE levels and thousands of individual lines can be calculated.

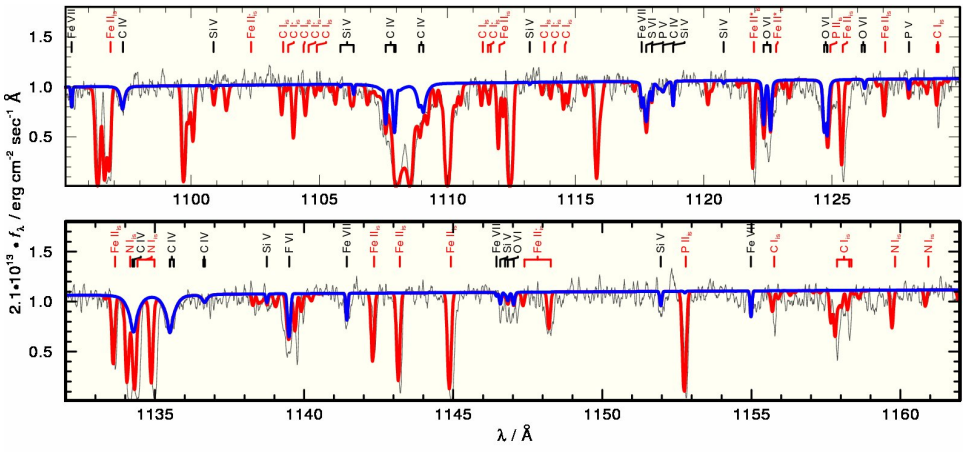

Figure 2. Section of the *FUSE* observations of A 43 compared with a *TMAP* (blue) and *TMAP*/OWENS model (red).

In the UV range numerous interstellar lines overlay the photospheric lines. The program OWENS was used to calculate the interstellar line-absorption spectrum. With OWENS various interstellar clouds, that consider different temperatures, radial and turbulent velocities, chemical compositions, and column densities can be modeled.

We used the parameters determined by Ziegler (priv. comm.) for the so-called spectroscopic twin of A 43, namely NGC 7094, as start values for our analysis ($T_{\rm eff}$ = 105 kK, $\log g$ = 5.4). First, we checked these values with H+He models. Then we calculated more detailed model atmospheres for the newly determined values and included the elements H-Ni. After fitting the effective temperature and surface gravity, the elemental abundances are fine-tuned. In the UV range this is done in an iterative process with *TMAP* and OWENS until the interstellar as well as the photospheric lines reproduce the observed lines (Fig. 2).

4. Preliminary results and discussion

The analysis yields slightly different values $T_{\rm eff}$ = 105 kK ±10 kK, $\log g$ = 5.6 ± 0.3, and different abundances (Table 2). Within the error limits these parameters agree with those of the CSPN of NGC 7094. A mass of 0.53 $M_\odot$ (evolutionary tracks, Miller Bertolami & Althaus 555, 556) and a distance of 2.2 kpc were determined.

Table 2. Abundances of the CSPN of A 43, X is given in mass fractions, [X] denotes $\log \frac{\text{abundance}}{\text{solar abundance}}$. The typical error range is ≈0.3 dex.

	H	He	C	N	O	F	Si	P	S
X	0.24	0.56	0.19	2.4E-4	1.8E-3	2.8E-6	1.8E-3	1.3E-6	1.2E-3
[X]	−0.483	−0.350	1.909	−0.491	−0.516	0.694	−0.560	−0.593	−0.378

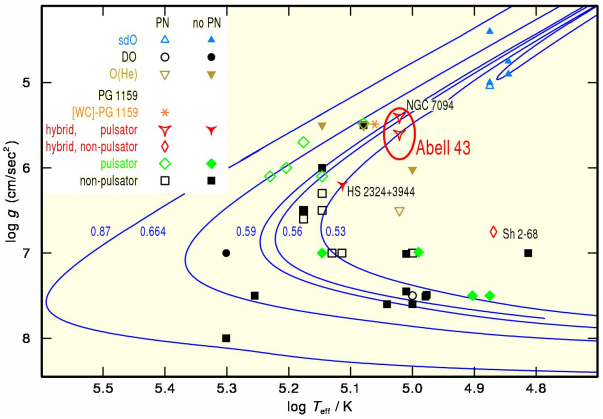

Figure 3. Location of A 43 and related objects in the log $T_{\rm eff}$-log g plane.

4.1. The German Astrophysical Virtual Observatory

The German Astrophysical Virtual Observatory (GAVO) aims to make astronomical data accessible. It is funded by the Federal Ministry for Education and Research (BMBF) and operates within the International Virtual Observatory Alliance (IVOA). In the framework of a GAVO project the model-atmosphere code *TMAP* was made accessible in different ways via *TheoSSA* (Theoretical Simple Spectra Access). It provides:

- SEDs (*TheoSSA*, http://vo.ari.uni-tuebingen.de/ssatr-0.01/TrSpectra.jsp?)
- Simulation Software (*TMAW*, http://astro.uni-tuebingen.de/~TMAW/TMAW.shtml)
- Atomic Data (*TMAD*, http://astro.uni-tuebingen.de/~TMAD/TMAD.html)

It is controlled via a web interface where the fundamental parameters like $T_{\rm eff}$ or log g are entered. As a result a table of already available spectral energy distributions (SEDs) within a parameter range is given which can be downloaded directly. If a requested SED is not available, it can be calculated via *TMAW*, the web interface of *TMAP*. The database is growing in time because newly calculated SEDs are automatically ingested. In this way, the *TMAP* code can easily be used for spectral analysis by everybody. This simplifies getting reliable fluxes of central stars that are e.g. necessary to model planetary nebulae properly.

Acknowledgments. TR is supported by the German Aerospace Center (DLR) under grant 05 OR 0806. ER is supported by the Deutsche Forschungsgemeinschaft (DFG) under grant WE 1312/41-1. This work has been done using the profile fitting procedure OWENS.f developed by M. Lemoine and the *FUSE* French Team.

a

References

Fitzpatrick, E. L. 1999, PASP, 111, 63
Miller Bertolami, M., & Althaus, L. 2006, A&A, 454, 845
— 2007, A&A, 470, 675
Rauch, T., & Deetjen, J. L. 2003, in Stellar Atmosphere Modeling, edited by I. Hubeny, D. Mihalas, & K. Werner, vol. 288 of ASPCS, 103
Werner, K., Deetjen, J. L., Dreizler, S., Nagel, T., Rauch, T., & Schuh, S. L. 2003, in Stellar Atmosphere Modeling, edited by I. Hubeny, D. Mihalas, & K. Werner, vol. 288 of ASPCS, 31

Werner, K., & Dreizler, S. 1999, Journal of Computational and Applied Mathematics, 109, 65
Werner, K., & Herwig, F. 2006, PASP, 118, 183

Asymmetric Planetary Nebulae V
A. A. Zijlstra, F. Lykou, E. Lagadec and I. McDonald
Jodrell Bank Centre for Astrophysics, Manchester, UK © 2011

Modeling Ejecta of Massive Stars

Rich Townsend
Department of Astronomy, University of Wisconsin-Madison, Sterling Hall, 475 N. Charter Street, Madison, WI 53706, USA

Abstract. In this review I describe the various ways in which massive stars can shed matter. At first take, these stars seem to share little in common with the planetary nebula phenomenon. Their mass loss typically takes the form of periods of continuous outflow, rather than the discrete outbursts that form PNe shells. Nevertheless, the ejecta of massive stars tend to be highly structured in space and in time, and it seems likely that some of the mechanisms responsible for this may also explain the diverse morphologies seen in PNe.
Keywords. Planetary nebulae

1. Foreword

Throughout my discussion, I'll be placing deliberate emphasis on four key questions. What causes the structure we see in the ejecta of massive stars? What tools can we use to model this structure? How have these tools so far been applied? And, what problems do we still face?

Due to limitations on page space, and moreover on the boundaries of my own knowledge, I shall cravenly pass over the most extreme forms of massive-star mass loss: binary interactions, giant eruptions and supernovae.

2. Massive-Star Winds

Although making up a small fraction of the mass in galaxies, massive stars* are responsible for a preponderance of the radiant energy generation. This is a reflection of their immense luminosities, which — with a main-sequence scaling $L_*/\mathrm{L}_\odot \sim (M_*/\mathrm{M}_\odot)^3$ — can reach up to a dizzying million-times solar, for the stars at the top end of the mass range ($M_* \sim 100\,\mathrm{M}_\odot$).

These luminosities give rise to strong wind outflows. In contrast to the wimpy ($\dot{M} \sim 10^{-14}\,\mathrm{M}_\odot\,\mathrm{yr}^{-1}$) winds of the Sun and other cool main-sequence stars, which are accelerated by the gas pressure of a hot corona, massive-star winds are driven radiatively by the direct conversion of photon momentum into flow momentum. Mass-loss rates range up to $10^{-5}\,\mathrm{M}_\odot\,\mathrm{yr}^{-1}$, and typical terminal velocities $v_\infty \sim 1,000$ –

*Here, defined loosely as those having spectral types O and B on the main sequence.

$2,000\,\mathrm{km\,s^{-1}}$ are factors of a hundred times the sound speed — that is, the winds are *hypersonic*.

A necessary condition for a radiation-driven wind to arise is that the outward radiative force exceed the inward pull of gravity. This familiar breaching of the Eddington limit is usually framed as $\Gamma_e > 1$, where

$$\Gamma_e = \frac{\kappa_e L_*}{4\pi G M_* c} \tag{1}$$

is the ratio of radiative and gravitational accelerations. However, the presumption in this expression is that the radiative force arises from Thomson scattering of continuum photons (as represented by the opacity κ_e). While such *continuum-driven* winds can occur in extreme cases (for instance, the Great Eruption of η Car; see 597), massive-star winds are more typically driven by line opacity associated with resonance-scattering transitions.

Within the Castor et al. (565, hereafter CAK) formalism for these *line-driven* winds, the Eddington parameter above is replaced by

$$\Gamma_\ell = \frac{1}{1-\alpha}\Gamma_e \bar{Q}\left(\frac{\mathrm{d}v/\mathrm{d}r}{\rho c \bar{Q}\kappa_e}\right)^\alpha \tag{2}$$

where the notation follows Owocki (586), and in particular $\bar{Q}$ is a measure of the total line opacity in the wind, in units of κ_e (see 572). The term in parentheses is the reciprocal of the Sobolev optical depth; through the appearance of the spatial velocity gradient $\mathrm{d}v/\mathrm{d}r$, it represents the degree to which the wind is able to Doppler-shift lines out of their own shadow.

The inverse dependence of the radiative acceleration on the density ρ naturally introduces a negative feedback loop that helps to self-regulate the wind. If too much mass is launched from the surface, the acceleration declines to a point where Γ_ℓ drops below unity; the wind then stalls and falls back to the stellar surface. Accordingly, the mass-loss rate $\dot{M}$ of a radiatively driven wind is not a free parameter, but instead established by this self-regulation process — that is, $\dot{M}$ is an *eigenvalue* of the system. In the idealized point-star case, this eigenvalue is given by CAK theory as

$$\dot{M}_{\mathrm{CAK}} = \frac{L_*}{c^2}\frac{\alpha}{\alpha-1}\left(\frac{\bar{Q}\Gamma_e}{1-\Gamma_e}\right)^{(1-\alpha)/\alpha}, \tag{3}$$

and solution of the equation-of-motion for $\dot{M} = \dot{M}_{\mathrm{CAK}}$ gives a wind terminal velocity that scales with the escape velocity,

$$v_\infty = \sqrt{\frac{\alpha}{1-\alpha}}v_{\mathrm{esc}} = \sqrt{\frac{\alpha}{1-\alpha}\frac{2GM_*}{R_*}}. \tag{4}$$

(586) provides an excellent review of the formalism leading to these various results.

3. Line-Deshadowing Instability

Although the CAK formalism envisages steady, smooth outflows, in reality line-driven winds exhibit significant structure and variability, on scales both small and large, and

with morphologies that can be regular/symmetric or stochastic. As I shall discuss in subsequent sections, the structure in many cases arises via imprinting from an external agent such as pulsation or rotation. However, there is also an intrinsic instability in radiative line driving that leads to the spontaneous generation of structure. The instability reveals itself in a linear perturbation analysis (e.g., 581), indicating a perturbed radiative force that is directly proportional to the perturbed velocity; this simply reflects the amount of additional opacity that is Doppler shifted out of its own shadow at the blue edge of line profiles. The growth timescale of this so-called *line-deshadowing instability* (LDI) is $\tau_{\rm grow} \sim 10^{-2}\,\tau_{\rm wind}$, which — with wind flow timescales $\tau_{\rm wind} = R_*/v_\infty \sim 0.5\,{\rm d}$ — is very short.

The Lucy & Solomon (581) analysis suggests instability at all length scales; but a more-careful investigation (see 591) shows that the LDI operates only for velocity perturbations whose physical length scale is shorter than the Sobolev length $\ell_{\rm Sob} = v_{\rm th}/({\rm d}v/{\rm d}r)$. At larger scales, the perturbed line force is proportional to the perturbed velocity *gradient* (as one might expect from eqn. 2), and the wind is stable. Accordingly, the LDI is primarily responsible for the generation of *small-scale* structure in line-driven winds.

Numerical simulation of the LDI can be computationally expensive, as the Sobolev approximation (which assumes $\ell_{\rm Sob}$ is small compared to any structure in the wind) cannot be used. 1-D hydro simulations by (569) indicate that the instability breaks up a smooth CAK wind solution into a sequence of reverse shocks, where fast, low-density wind material runs into the back of slower-moving, high-density material. These wind shocks are considered a likely source for the soft, broad-lined X-ray emission observed in many single OB stars (e.g., 588, and references therein).

Extending the simulations to 2-D, (567) find that the shell-like shocks produced by the LDI are fragmented by Rayleigh-Taylor instabilities, and the wind structure rapidly becomes incoherent down to angular scales approaching the grid scale. These results are difficult to reconcile with observations of clump-induced stochastic variability in massive-star winds (e.g., 599), suggesting that there's something still missing from the simulations. Lateral forces from side-scattered radiation are a likely candidate, since they will tend to retard the shell fragmentation process (e.g., 586). However, inclusion of these forces will require multi-D radiation hydrodynamics, which for the time being lies beyond our computational grasp.

4. Cyclical Wind Structure

In addition to the stochastic structure caused by the LDI, massive-star winds show evidence for larger-scale structures that recur periodically or episodically. These structures usually manifest themselves as *discrete absorption components* (DACs) that migrate blueward through the absorption troughs of ultraviolet P Cygni line profiles (e.g., 577). Puzzlingly, the typical lifetime of DACs is significantly longer than wind flow times, suggesting that they are caused not by embedded clumps, but instead by patterns in the wind that remain coherent over large spatial scales and long time scales.

The *IUE Megacampaign* observations of the B0.5Ib supergiant HD 64760, spanning almost 16 days, revealed a pair of DACs with lifetimes on the order of $\sim 10\,{\rm d}$ (594). However, superimposed over these DACs is a 1.2 d-periodic modulation in the

depth of UV line profiles, phase-locked over a wide range of blueshift velocities. Because the period is close to one-quarter of the star's rotation period, these *periodic absorption modulations* (PAMs) have been hailed as the indirect evidence of a 'photospheric connection' between surface and wind structure. Support for the existence of this connection has come from a more-recent study of HD 64760 by Kaufer et al. (578), who find that the star's wind-sensitive Hα line is variable on a 6.8 d period, corresponding to the beat period between photospheric non-radial pulsation modes (the issue of pulsation is discussed further in §5). How this 6.8 d period is related to the 1.2 d PAM period is, however, still unclear.

What causes DACs and PAMs? Mullan (582, 583) first suggested that DACs are the signature of co-rotating interaction regions (CIRs) — rotating spiral structures formed by the collision between fast and slow wind streams, which trace back to some kind of inhomogeneity in the photospheric wind-launching. However, based on kinematical models, Fullerton et al. (570) have convincingly argued that it is *PAMs* rather than DACs which are the observational manifestation of CIRs.

5. Rotational Wind Sculpting

Massive stars are systematically rapid rotators: the observational survey by Howarth et al. (576), covering 373 O- and B-type stars, reveals a distribution of equatorial rotation velocities $v_{\rm eq}$ peaking at $\sim 100\,{\rm km\,s^{-1}}$, and extending all the way up to the critical limit $\sim 500\,{\rm km\,s^{-1}}$. What effect does this rapid rotation have on the stars' winds? Physical intuition suggests that the reduction in the effective (Newtonian plus centrifugal) gravity will make it easier to launch a wind from the equator of a rotating star, than from the poles. Thus, we should expect oblate mass loss around more-rapid rotators.

This expectation is at first glance lent support by a simple extension of eqn. (3), giving a latitude-dependent mass flux

$$\dot{m}_{\rm CAK}(\theta) = \frac{F}{c^2}\frac{\alpha}{\alpha-1}\left(\frac{\bar{Q}\Gamma_{\rm e}}{1-\Gamma_{\rm e}}\right)^{(1-\alpha)/\alpha}, \tag{5}$$

where now

$$\Gamma_{\rm e}(\theta) = \frac{\kappa_{\rm e} F}{g_{\rm eff} c}, \tag{6}$$

and F and $g_{\rm eff}$ are the local radiative flux and effective gravity, respectively. These expressions indeed seem to indicate that a lowering of $g_{\rm eff}$ will push Γ_e closer to unity, in turn upping the local mass flux.

However, as Cranmer & Owocki (566) first pointed out, the von Zeipel (608) gravity darkening law — which establishes the proportionality $F \propto g_{\rm eff}$ — means that Γ_e is *constant* over the stellar surface. The elevation of F at the stellar poles (due to the higher effective gravity) then means an enhanced mass flux there, and an overall *prolate* mass-loss morphology. Moreover, the wind terminal velocity v_∞ (cf. eqn. 4) will also be larger over the poles than at the equator, due to the higher escape velocity. Smith et al. (596) presents evidence for both of these effects in the present-day wind of η Car.

6. Rotation and Disks

The preceding section points toward bipolar outflows from rotating massive stars. How, then, do some show the clear signature of equatorial disks — in particular, the enigmatic Be stars, whose disks are revealed in Hα emission lines (e.g., 593)? Bjorkman & Cassinelli (563) proposed that wind streams launched off the surface of rapidly rotating B-type star are focused toward the equatorial plane by angular momentum conservation, where they will collide and form a disk. This kinematical *wind-compressed disk* (WCD) model was initially confirmed in hydrodynamical simulations by Owocki et al. (589). However, when gravity darkening and stellar oblateness were incorporated in the simulations, Cranmer & Owocki (566) found that the polar-enhanced mass loss discussed above tends to reduce the density of the equatorial disk. Moreover, when the simulations were further extended to incorporate non-radial line forces (arising from the velocity gradient between equator and pole via the $\mathrm{d}v/\mathrm{d}r$ term in eqn. 2), Owocki et al. (590) showed that the formation of a WCD is completely inhibited.

Progress in finding an alternative narrative for Be-disk formation was driven by observations constraining the disk velocity structure as Keplerian, with radial outflow speeds on the order of a couple of $\mathrm{km\,s^{-1}}$ or less (e.g., 574). These observations prompted a reevaluation of a seminal paper by Lee et al. (580) advancing a viscous decretion model. Decretion disks operate much like accretion disks, in that they transport angular momentum away from the star; the key difference is that mass is injected at the inner boundary of a decretion disk, and at the outer boundary of an accretion disk. In both cases, the disk velocity structure is Keplerian.

Smooth particle hydrodynamics simulations confirm the viability of the viscous decretion model (e.g., 584). However, a missing component to the model is a prescription of how stellar material is lifted into (Keplerian) orbit at the inner edge of the disk. This process requires angular momentum — and elucidating the mechanism that supplies the angular momentum can be regarded as the key to understanding the Be phenomenon. Radiative driving (as envisaged in the WCD model) is generally unsuited, because it is difficult for photons to impart an azimuthal force (see, however, 573, for an interesting counter-example). Magnetic fields have been considered; however, as discussed below in §7, they appear better-suited to producing *rigid* disks.

This leaves rotation itself as the most promising mechanism for supplying the necessary angular momentum. Of course, if *all* of the angular momentum is to come from rotation, then Be stars must be spinning at their critical velocity — an unlikely scenario. We therefore require an additional agent to supply the velocity boost into orbit. For agents relying on gas pressure to accelerate material, an upper limit on the magnitude of the boost is approximately the photospheric sound speed a; thus, the star's equatorial velocity must be within one to two a of the surface orbital velocity, which in massive stars translates to $90 - 95\%$ of critical. Historically, the consensus had been that Be stars *do not* rotate this close to critical. However, Townsend et al. (602) demonstrate that gravity darkening can cause a significant underestimation of the projected equatorial velocity $v_{\mathrm{eq}} \sin i$ measured from line widths, and that in fact observation of Be stars are consistent with (although do not *prove*) rotation in the required $90 - 95\%$ critical window.

A specific instance of the 'rotation-plus-gas-pressure' mechanism for disk formation was suggested by Osaki (585), who proposed that photospheric g-mode pulsation

waves in a near-critical star can launch equatorial material into orbit. Owocki (587) has supported this *pulsation-driven orbital mass ejection* (PDOME) model using 2-D (equatorial-plane) hydrodynamical simulations, in particular confirming Osaki's stipulation that *prograde*-propagating waves are required for disk formation (since they supply angular momentum in the requisite prograde direction). These theoretical developments tie in nicely with observational work by Rivinius et al. (595) indicating that g-mode pulsation is ubiquitous in early-type Be stars. One remaining puzzle, however, is that the modes detected by these latter authors appear to be universally *retrograde* rather than prograde. My own suspicion is that so-called 'Yanai modes' (e.g., 598), which exhibit retrograde phase propagation but transport angular momentum in the prograde direction, may therefore have some role to play.

The Be stars should not be confused with objects exhibiting the B[e] phenomenon. Although the latter show similar signatures of circumstellar material, they differ by dint of their *forbidden* emission lines and their IR excesses indicative of hot dust. Moreover, B[e] stars are a very heterogeneous group, spanning a broad range of evolutionary phases from pre-main sequence to PN. Within this group, massive stars are represented by the supergiant B[e] stars, characterized by fast polar winds and dense equatorial disks which appear to be outflowing rather than Keplerian (see, e.g., 579, and references therein). One formation mechanism for these disks is rotation-induced bistability (592): the lower effective temperature at the (gravity-darkened) equator produces a higher opacity, which in turn allows a greater line-driven mass flux there (due to the $\bar{Q}$ term in eqn. 5). Since the disks are outflowing, there is not the same angular momentum requirement as with Be-star disks.

7. Magnetically Channeled Winds

Massive stars aren't expected to harbor magnetic fields, owing to the absence of a significant outer convection zone to serve as a field-generating dynamo. Nevertheless, a subset show evidence for strong ($\sim$ kG), ordered (typically, dipole) magnetic fields which are stable over timescales of decades (see, e.g., 609). Because massive-star winds are highly ionized, there is a strong coupling between wind and field, with each competing to determine the morphology of the other. ud-Doula & Owocki (604) investigate this coupling using 2-D magnetohydrodynamical (MHD) simulations of radiation-driven winds in the presence of a dipole field. A key result from these simulations is that the global flow morphology is determined by a single parameter

$$\eta_* = \frac{B_*^2 R_*^2}{\dot{M} v_\infty} \tag{7}$$

representing the ratio between magnetic and wind-kinetic energy densities adjacent to the stellar surface. When $\eta_* \ll 1$, the wind dominates the field, and the latter is stretched out into a split-monopole configuration with radial field lines and an equatorial current sheet. Conversely, in the $\eta_* \gg 1$ limit the field remains relatively unaffected by the wind, with field lines remaining closed out to the Alfvén radius $R_{\rm Alf} \approx \eta_*^{1/4} R_*$.

In the latter 'strong confinement' case, wind streams flowing from opposite footpoints of closed magnetic loops collide near the loop summit. In their seminal *magnetically confined wind shock* (MCWS) paradigm, which foreshadowed the MHD simulations, Babel & Montmerle (562) proposed that the kinetic energy of the colliding

streams is thermalized in shocks, heating the material to temperatures $\sim 10^6 - 10^7$ K where X-ray emission becomes significant. A follow-up paper (561) argues that the hard X-rays of the O6V star θ^1 Ori C arise in this manner (interestingly, this paper pre-dated the actual detection of the star's ~ 1.1 kG field by 568). Subsequent analysis of the star's X-ray emission-line spectrum, coupled with MHD simulations of the wind shocks, has lent strong support to the basic MCWS paradigm (see 571).

More-recent MHD simulations have explored the impact of magnetic-axis-aligned rotation (605; 606). As the post-shock material cools radiatively back to photospheric temperatures, it accumulates in the equatorial plane to form a *rigidly rotating* disk supported against the inward pull of gravity by centrifugal and magnetic forces. Eventually, sufficient material builds up to overwhelm the magnetic field, which then reconnects. During such a centrifugal breakout episode (see 607), material in the disk is flung away from the star and escapes to infinity.

This narrative runs contrary to the *magnetically torqued disk* model introduced by Cassinelli et al. (564), in particular showing that disks formed with the aid of magnetic fields tend to be rigid rather than Keplerian, and are thus unsuited to explaining the Be phenomenon. In fact, the MHD simulations lend support to the alternative *rigidly rotating magnetosphere* (RRM) model developed by Townsend & Owocki (600) to describe the distribution of circumstellar material in the idealized limit $\eta_* \longrightarrow \infty$ where field lines are completely rigid. This limit is effectively realized in the chemically peculiar He-strong stars, whose ~ 10 kG fields and low mass-loss rates combine to produce confinement parameters in the $\eta_* \sim 10^5 - 10^7$ range.

Applied to the B2Vpe star σ Ori E, the RRM model can simultaneously reproduce the observed 1.2-d periodic Hα and photometric variations (601). Building on this success, Townsend et al. (603) have created a *rigid field hydrodynamics* (RFHD) approach for simulating the time-dependent flow along an ensemble of rigid field lines. RFHD models provide a 3-D, dynamical picture of a star's magnetosphere, including the collision shocks anticipated in the MCWS paradigm, at a tiny fraction of the computational cost of equivalent MHD simulations; however, they remain restricted to cases where $\eta_* \gg 1$. An initial application to σ Ori E (575) shows promise in reproducing the star's observed X-ray emission.

Acknowledgments. I gratefully acknowledge support from NASA grant *LTSA*/NNG05GC36G.

References

Babel, J., & Montmerle, T. 1997, ApJ, 485, L29
— 1997, A&A, 323, 121
Bjorkman, J. E., & Cassinelli, J. P. 1993, ApJ, 409, 429
Cassinelli, J. P., Brown, J. C., Maheswaran, M., Miller, N. A., & Telfer, D. C. 2002, ApJ, 578, 951
Castor, J. I., Abbott, D. C., & Klein, R. I. 1975, ApJ, 195, 157
Cranmer, S. R., & Owocki, S. P. 1995, ApJ, 440, 308
Dessart, L., & Owocki, S. P. 2005, A&A, 437, 657
Donati, J., Babel, J., Harries, T. J., Howarth, I. D., Petit, P., & Semel, M. 2002, MNRAS, 333, 55
Feldmeier, A., & Owocki, S. 1998, Ap&SS, 260, 113

Fullerton, A. W., Massa, D. L., Prinja, R. K., Owocki, S. P., & Cranmer, S. R. 1997, A&A, 327, 699
Gagné, M., Oksala, M. E., Cohen, D. H., Tonnesen, S. K., ud-Doula, A., Owocki, S. P., Townsend, R. H. D., & MacFarlane, J. J. 2005, ApJ, 628, 986
Gayley, K. G. 1995, ApJ, 454, 410
Gayley, K. G., & Owocki, S. P. 2000, ApJ, 537, 461
Hanuschik, R. W. 1996, A&A, 308, 170
Hill, N., Townsend, R. H. D., Cohen, D. H., & Gagné, M. 2010, in Proc. IAU Symp. 272: Structure, evolution, mass loss and critical limits, edited by C. Neiner, G. Wade, G. Meynet, & G. Peters. In press
Howarth, I. D., Siebert, K. W., Hussain, G. A. J., & Prinja, R. K. 1997, MNRAS, 284, 265
Kaper, L., & Henrichs, H. F. 1994, Ap&SS, 221, 115
Kaufer, A., Stahl, O., Prinja, R. K., & Witherick, D. 2006, A&A, 447, 325
Lamers, H. J. G. L. M. 2006, in ASP Conf. Series 355: Stars with the B[e] Phenomenon, edited by M. Kraus, & A. S. Miroshnichenko, 371
Lee, U., Osaki, Y., & Saio, H. 1991, MNRAS, 250, 432
Lucy, L. B., & Solomon, P. M. 1970, ApJ, 159, 879
Mullan, D. J. 1984, ApJ, 283, 303
— 1986, A&A, 165, 157
Okazaki, A. T. 2004, in Proc. IAU Symp. 215: Stellar Rotation, edited by A. Maeder, & P. Eenens, 529
Osaki, Y. 1986, PASP, 98, 30
Owocki, S. 2004, in EAS Pub. Ser. 13: Evolution of Massive Stars, Mass Loss and Winds, edited by M. Heydari-Malayeri, P. Stee, & J. P. Zahn, 163
— 2005, in ASP Conf. Ser. 337: The Nature and Evolution of Disks Around Hot Stars, edited by R. Ignace, & K. G. Gayley, vol. 337, 101
Owocki, S. P., & Cohen, D. H. 2006, ApJ, 648, 565
Owocki, S. P., Cranmer, S. R., & Blondin, J. M. 1994, ApJ, 424, 887
Owocki, S. P., Cranmer, S. R., & Gayley, K. G. 1996, ApJ, 472, L115
Owocki, S. P., & Rybicki, G. B. 1984, ApJ, 284, 337
Pelupessy, I., Lamers, H. J. G. L. M., & Vink, J. S. 2000, A&A, 359, 695
Porter, J. M., & Rivinius, T. 2003, PASP, 115, 1153
Prinja, R. K., Massa, D., & Fullerton, A. W. 1995, ApJ, 452, L61
Rivinius, T., Baade, D., & Štefl, S. 2003, A&A, 411, 229
Smith, N., Davidson, K., Gull, T. R., Ishibashi, K., & Hillier, D. J. 2003, ApJ, 586, 432
Smith, N., & Owocki, S. P. 2006, ApJ, 645, L45
Townsend, R. H. D. 2003, MNRAS, 340, 1020
Townsend, R. H. D., & Mast, N. 2010, in Proc. IAU Symp. 272: Structure, evolution, mass loss and critical limits, edited by C. Neiner, G. Wade, G. Meynet, & G. Peters. In press
Townsend, R. H. D., & Owocki, S. P. 2005, MNRAS, 357, 251
Townsend, R. H. D., Owocki, S. P., & Groote, D. 2005, ApJ, 630, L81
Townsend, R. H. D., Owocki, S. P., & Howarth, I. D. 2004, MNRAS, 350, 189
Townsend, R. H. D., Owocki, S. P., & ud-Doula, A. 2007, MNRAS, 382, 139
ud-Doula, A., & Owocki, S. P. 2002, ApJ, 576, 413
ud-Doula, A., Owocki, S. P., & Townsend, R. H. D. 2008, MNRAS, 385, 97
— 2009, MNRAS, 392, 1022
ud-Doula, A., Townsend, R. H. D., & Owocki, S. P. 2006, ApJ, 640, L191
von Zeipel, H. 1924, MNRAS, 84, 665
Wade, G. A., Alecian, E., Bohlender, D. A., Bouret, J., Grunhut, J. H., Henrichs, H., Neiner, C., Petit, V., Louis, N. S., Aurière, M., Kochukhov, O., Silvester, J., & ud-Doula, A. 2009, in Proc. IAU Symp. 259: Cosmic Magnetic Fields, edited by K. G. Strassmeier, A. G. Kosovichev, & J. Beckman, 333

Asymmetric Planetary Nebulae V
A. A. Zijlstra, F. Lykou, E. Lagadec and I. McDonald
Jodrell Bank Centre for Astrophysics, Manchester, UK © 2011

Eta Carinae, Present and Past

Vincent Icke

Sterrewacht Leiden, Postbus 9513, 2300 RA Leiden, The Netherlands

Abstract. Eta Carinae, one of the most extreme and fascinating objects in our Galaxy, is a supermassive interacting binary at the centre of a bipolar nebula, expanding at about 500 km s^{-1}. Finding the mechanisms behind Eta's appearance, behaviour and evolution is the main goal of this investigation. I have constructed a large series of numerical models of dual-wind binary stars, of which I present here one that probably comes close to the Eta Carinae parameters. I presume that the gaseous 'skirt' surrounding Eta is an equatorial 'excretion disk' formed by the interacting binary, that the bipolar 'Homunculus' nebula above and below this plane is due to the collision between the material ejected in the 1840 'Giant Eruption' and the disk, and the 'Little Homunculus' similarly in the smaller 1890 eruption. I have extensively explored the general types of flow pattern expected here. My Theory Group is working towards 3D radiation-hydrodynamics simulations for quantitative comparison with Eta, which many believe to be a key to understanding a variety of hitherto unexplained phenomena in and around massive stars, be they binary or single.
Keywords. Bipolar nebulae: individual: η Car – Stars: binary – Stars: atmospheres – Stars: evolution – Stars: individual: η Car

1. Introduction

The object called Eta Carinae is, astrophysically speaking, one of the most spectacular in our Galaxy. We know that it is a supermassive interacting binary at the centre of a huge bipolar nebula, expanding at 500 km s^{-1}, but for the rest we know rather little for sure. This is all the more embarrassing because Eta is quite close: 2.3 kpc (see e.g. (611), http://etacar.umn.edu/, (616) and (614)).

The bipolar nebula, called 'Homunculus', consists of two cauliflower-shaped bubbles joined in the plane of a fragmented disk-like gas cloud called 'skirt'. The bipolar shape is almost certainly caused by the well established interacting-winds mechanism (612), but the origin of the skirt (which focuses the outflow into its bipolar form) is unclear.

A rough consensus on the observed or inferred properties of Eta Carinae would read as follows. The primary star, η Car A, is the cooler and massive one: 35,000 K at about 90 $M_\odot$, losing $2 - 3 \times 10^{-4}$ $M_\odot$/yr at 550 km s^{-1}. The secondary is hotter and less massive: 41,000 K and 30 $M_\odot$, losing 10^{-5} $M_\odot$/yr at 3000 km s^{-1}. The observed extreme velocities, which should correspond to the terminal velocity of the wind, range from -1000 to +500 km s^{-1}. The speed of sound in the photosphere of the primary would then be about 19 km s^{-1}, giving a Mach number $\mathcal{M} \approx 26$ for the outflow, and

$\mathcal{M} \approx 150$ for η Car B. The binary period is 5.54 yr, with the orbital plane coinciding with the Homunculus 'skirt' and a semimajor axis of 15.4 AU. Because of the evidence that near pericentre the primary star penetrates the wind bubble of the secondary (617), the eccentricity must be large, at least 0.8 and possibly larger.

These numbers are of great importance in simulations, because they determine the density, outflow speed, Mach number and temperature (or pressure) in the flow, and therefore to a large extent the hydrodynamic behaviour. My series of simulations shows that the absolute numbers are less important for the appearance and behaviour of the overall flow patterns than the ratios of these various numbers are. For example, the ratio of the stellar masses and the ratio of their outflow speeds and densities are more important than the actual numbers separately. This allows a ready comparison between various simulations, details of which will be submitted for publication elsewhere. The presumed η Car A Mach number of $\mathcal{M} = 26$ is on the high end of the range I have explored in my binary wind computations. At the ZAMS temperature of 56,000 K, this would be about $\mathcal{M} = 20$; with the more S Dor-type value 20,000K we have $\mathcal{M} = 35$. These three cases would be drastically different from a hydrodynamic point of view, an aspect I will explore in detail later.

Finding the mechanisms behind Eta's appearance and behaviour is the main goal of this investigation, including conjectures about the evolutionary status and history of the binary. I hope that the interaction between Eta's stars will serve as a probe of their properties, thereby helping us to gain insight into the Luminous Blue Variable (LBV) physics and related phenomena.

2. Numerical Model

In the past two years, I have run a large series of hydrodynamical models of stars that both have a substantial stellar wind. With my 2D FCT/LCD code (613) I have investigated the effects of eccentricity, launching temperature, Mach number etc. on the flow patterns, with special attention being paid to the behaviour of the discontinuities and the free-free emission.

Table 1 lists the main properties of the simulation depicted in Figs. 1-4. While the outflow speeds are somewhat smaller than what is usually adopted for Eta, the main features of the flow are robust. In particular, the formation of the S-shaped shock wall during apastron always happens like this, as does the breaking-through at periastron.

Table 1. Parameters of the present simulation.

a	e	P	M_1	M_2	dM_1/dt	dM_2/dt	$\mathcal{M}$	v_1	v_2
15.4 AU	0.8	5.54 yr	90 $M_\odot$	30 $M_\odot$	2.5e-4 M_o/yr	1e-5 M_o/yr	2.0	180 AU/yr	30 AU/yr

The global behaviour of circular binaries is, that in between the stars a triple layer of discontinuities forms, namely a shock around each star, and in between these shocks a contact discontinuity. This sandwich fans out into an Archimedean spiral due to the orbital motion. The stagnation point between the stars, which has a saddle-point flow pattern, swings around the centre of mass. From this saddle point the gas streams

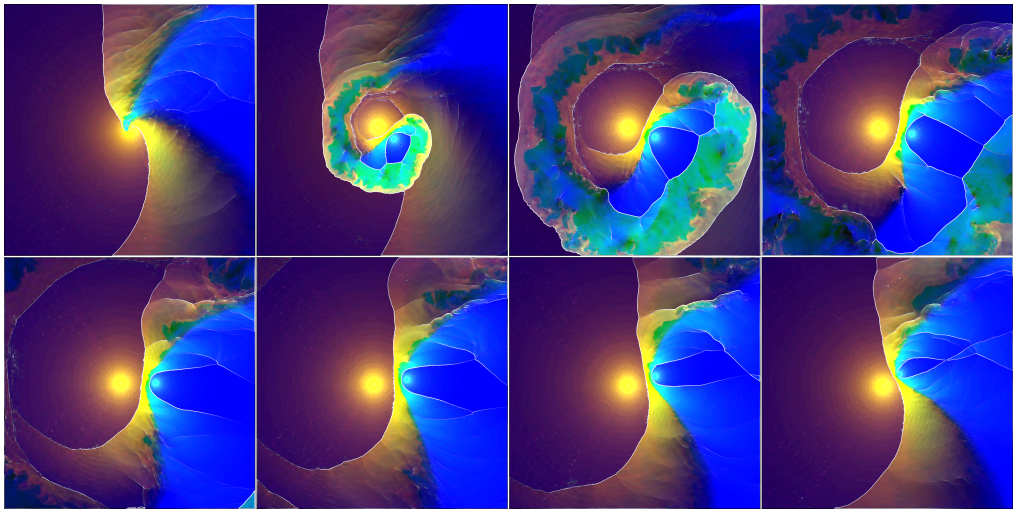

Figure 1. Eight flow pattern snapshots of the Eta simulation with equal time spacing around the orbit. From left to right, top to bottom: orbital phases 0.98, 0.11, 0.23, 0.35, 0.49, 0.60, 0.73 and 0.86. The colours indicate the flow variables: red, mass density; green, gas pressure; blue, absolute value of the velocity.

outward with increasing velocity, making the contact discontinuity extremely unstable so that a long train of partly supersonic eddies propagates along it.

Double-wind binaries with high eccentricity (above 0.4 or 0.5) show a basically similar behaviour, with one important difference: while the stars dwell near their apastron the triple-layer forms as in the circular case, but when the stars approach periastron they slam through this self-made wall, leading to a strong crescent-shaped shock wave that drives mass from the system in a very non-axisymmetric way. Furthermore, the extremely strong shocks that are formed when the stars break through this wall produce strong free-free radiation. Finally, if the mass loss is large (in excess of $1-2\times10^{-4}M_{\odot}$/yr) that radiation is absorbed by the gas compressed between the shocks, and even the stellar ionizing luminosity may be trapped in that layer.

3. A Possible History of the Binary

Eta's remarkable behaviour has been known for a century and a half. Its spectacular properties have revealed themselves gradually during that time. Why then should it be a good subject now? After all, most of the physics and quite a bit of the observations have been in hand for a while.

Fact is, that so far modeling efforts have had limited success. This is partly due to the difficulty of guessing the dominant mechanisms that are responsible for Eta's behaviour, and partly due to the corresponding uncertainty about interpretation of the main observed features. There is not even unanimity about some of its basic properties.

It is not surprising that a full hydrodynamic model of Eta does not yet exist, given the magnitude of the task: a search through a model space of three dimensional

(radiation-) hydrodynamics with a large range of physical parameters of the gas state, mass loss rates, orbital parameters, etc. If, as many investigators suppose and I hope, Eta is closely related to other Luminous Blue Variables and S Doradus stars (e.g. (618)), which are probably precursors to particularly violent classes of super- and hypernovae, these models will have much wider significance.

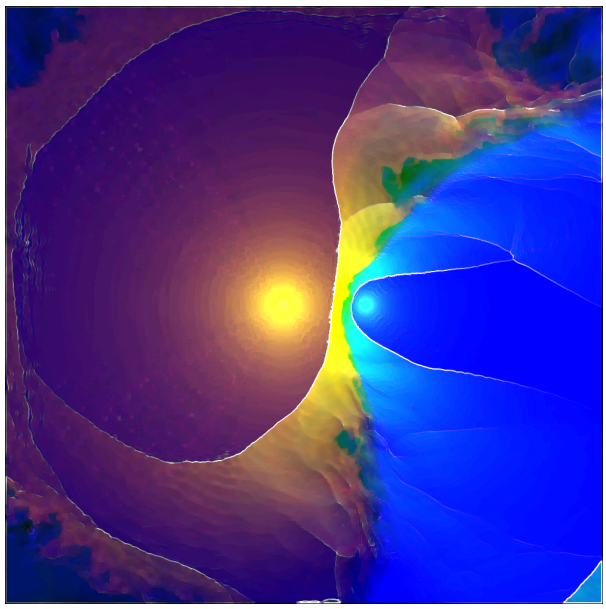

Figure 2. Flow pattern close to apastron, orbital phase 0.49. The white lines accentuate the strongest gradients of the gas pressure, which are mostly those where shocks occur. In models with a faster wind of the secondary, the opening angle of the standoff shock around that star is much closer to 180°.

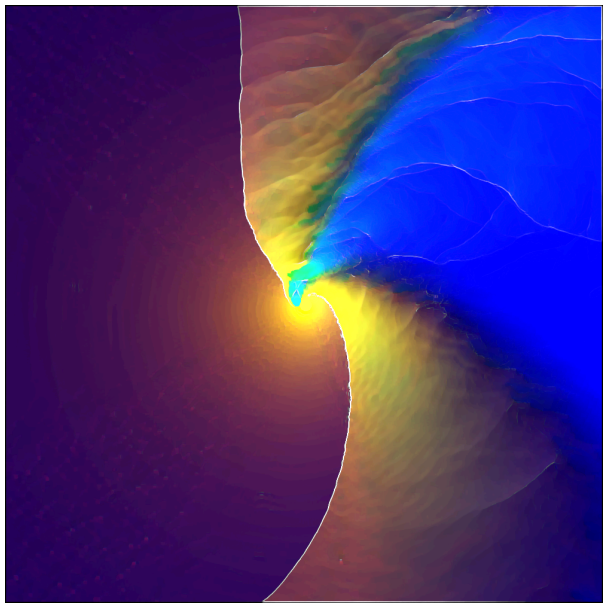

Figure 3. Flow pattern just before periastron, orbital phase 0.98. The breaking-through-the-wall is most dramatic at this point of the orbit. Due to lack of numerical resolution, it is impossible to say what happens exactly at the radius where the winds are launched.

The question then is: how did Eta become what it is? My current working hypothesis is as follows. Eta began as a very close binary star with a circular orbit in which each star had a mass close to the Eddington limit. The stellar winds, which must have been very substantial, collided and formed what we now see as the 'skirt'. One of these

stars expelled a large fraction of its mass in the 1840 event. This mass loss, with the impulsive effects of the blast shell on the companion, produced a very eccentric but still-bound binary. The blast itself was shaped by the skirt into its bipolar shape by the same constrained-outflow mechanism that is common in planetary nebulae (612).

Thus, I find that an enormous amount of mass must have been lost in order to obtain an eccentricity in excess of 0.8, of the order of 70-80 $M_\odot$ or thereabouts. This implies that the star that exploded was the one we now call the 'secondary'. The resulting runaway speed due to the mass-loss kick was of the order of the pre-blast orbital speed which, for a binary consisting of two 100 $M_\odot$ stars separated by 2 AU, should be observable today. Moreover, the direction of this runaway velocity is related to the direction of the major axis, providing a check for my supposition. An eccentricity of 0.9 is practically impossible if, as most authors believe, the present masses of the two stars are similar to those listed in Table 1, unless the smaller 1890 explosion happened at or very near periastron.

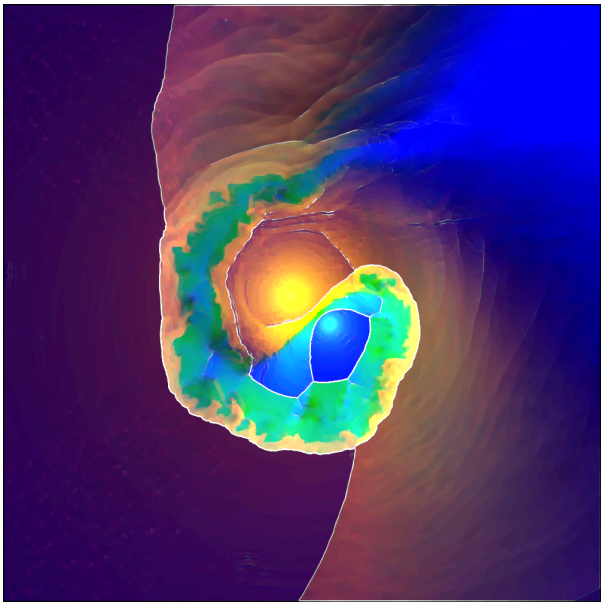

Figure 4. Flow pattern after periastron, orbital phase 0.11. The present numerical resolution (1000 × 1000 grid) is a compromise between resolution, coverage of both peri- and apastron, and computer time. Recent runs by Clementel's parallel FCT/LCD code at four times higher resolution show that the images depicted here are substantially correct.

The equations summarized by Bekenstein (610) for the changes in orbital parameters may be written as follows:

$$\begin{aligned} a^0 &= a(2-\mu^0)(1+\Pi^2)^{-1}, \\ e^2 &= \left[(\mu^0-1)^2+\Pi^2\right](1+\Pi^2)^{-1}, \\ \mu^0 &\equiv M^0/M, \\ \Pi &\equiv p/M_1 V \end{aligned} \tag{1}$$

in which a^0 is the semimajor axis before the 1840 event and a the value thereafter, M^0 is the total mass of the binary before and M the total mass afterwards, M_1 the mass of the present secondary after the event, V the initial orbital speed, and p the momentum deposited on the primary star due to the passage of the blast wave from the present secondary, star 2. If the post-event eccentricity e is larger than about 0.5, the contribution due to p is insignificant unless it is so improbably large that $\Pi \approx 1$.

The properties of the binary in this scenario can be made to fit numerically, but it remains an enigma what caused the exploding star to behave in this way. I am not aware of any phase in the evolution of massive stars in which they eject something like 70 $M_\odot$ and leave 30 $M_\odot$ behind. While near-Eddington stars are fully convective and could be expected to do strange things, I have not found this type of behaviour in the literature. On the other hand, the existence of a pre-supernova bipolar nebula around SN1987A might indicate that Eta is not alone in this respect.

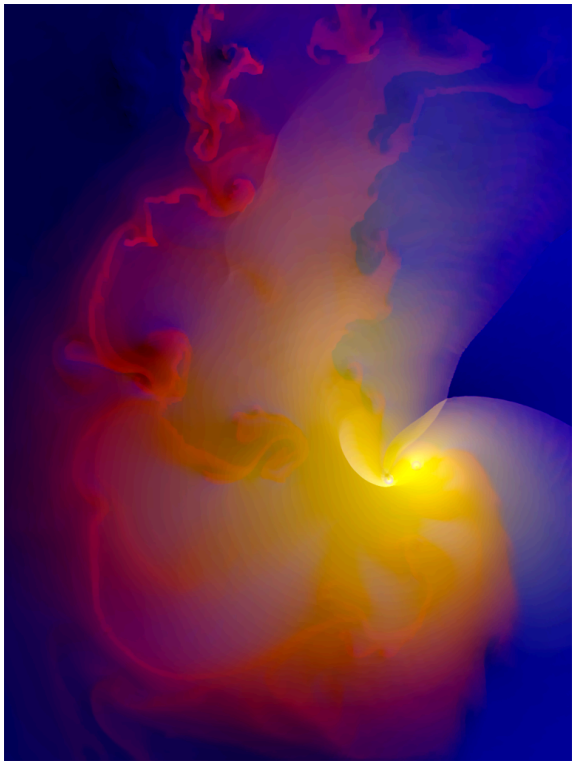

Figure 5. Flow pattern after periastron, orbital phase 0.11, of a simulation with parameters close to those of Figs.1-4 but with a resolution near periastron twice as high. The flow pattern around the two stars is so well resolved that it can be observed how the orbital motion folds the stellar bow shock back so that it intersects itself.

Acknowledgments. I am indebted to the members of the Sterrewacht Leiden Theory Group, in particular Jan-Pieter Paardekooper and Chael Kruip, for their work on radiative transfer, and to Nicola Clementel for his swift and effective parallelization of the FCT/LCD hydrocode and for implementing 3D simulations with the Flash-3 code. While this work was being written up, a paper appeared (615) reporting more or less exactly what we were working on; I congratulate the authors and recommend that the reader consult their work.

References

Bekenstein, J. D. 1976, Astrophys. J., 210, 544
Davidson, K., & Humphreys, R. M. 1997, Ann. Rev. Astron. Astrophys., 35, 1
Icke, V. 1988, Astron. Astrophys., 202, 177
— 1991, Astron. Astrophys., 251, 369
Okazaki, A. T., Owocki, S. P., Russell, C. M., & Corcoran, M. F. 2008, Mon.Not.Roy. astron.Soc., 35, 1

Parkin, E. R., Pittard, J. M., Corcoran, M. F., & Hamaguchi, K. 2010, Astrophys. J., preprint, arXiv:1000.0778v1
Smith, N. 2006, Astrophys. J., 644, 1151
Van Boekel, R., Kervella, P., Scholler, M., Herbst, T., Brandner, W., De Koter, A., Waters, L. B. F. M., Hillier, D. J., Paresce, F., Lenzen, R., & Lagrange, A. M. 2003, Astron. Astrophys., 410, L37
Van Genderen, A. M. 2001, Astron. Astrophys., 366, 508

Asymmetric Planetary Nebulae V
A. A. Zijlstra, F. Lykou, E. Lagadec and I. McDonald
Jodrell Bank Centre for Astrophysics, Manchester, UK © 2011

Jets and winds from binary stars

A. C. Raga[1], J. Cantó[2], A. Esquivel [1], P.J. Huggins[3] and N. Mauron[4]

[1]*Instituto de Ciencias Nucleares, UNAM, Ap. 70-543, 04510 D. F., México*

[2]*Instituto de Astronomía, UNAM, Ap. 70-264, 04510 D. F., México*

[3]*Physics Department, New York University, 4 Washington Place, NewYork, NY 10003, USA*

[4]*Groupe d'Astrophysique, UMR 5024 CNRS, Case CC72, Place Bataillon, 34095 Montpellier Cedex 5, France*

Abstract. This paper discusses the problem of an isotropic wind ejected from a star in orbital motion around a companion. As a result of the orbital motion, a spiral shock structure is formed in the wind. The structures predicted from the models are compared with the remarkable spiral structure of AFGL 3068.
Keywords. Planetary nebulae – Binaries – AFGL3068

1. Introduction

The talk at the meeting covered jets and winds ejected from a stellar source in motion around a binary companion. As the work on jets (prepared for this conference) has already been published (Raga et al. 2009), the present paper is focused on the problem of an isotropic wind ejected by a star in orbital motion.

In this paper we consider the most simple problem in outflows from binary sources : an isotropic, constant velocity wind ejected from one of the components of the binary. This problem was first studied by Soker (1994, formation of caustics on the orbital plane), and then by Mastrodemos & Morris (1999, 3D SPH simulations) and He (2007, 3D momentum conservation model). We present a new analytical model (section 2) and 3D numerical simulations (section 3) of this flow.

This problem has been given new life by the remarkable observation of a spiral structure in the stellar wind envelope of AFGL 3068 (see Mauron & Huggins 2006). In section 4 we present a comparison between our models and the observations of AFGL 3068, through which one obtains estimates of the orbital parameters and masses of the binary that could give rise to this remarkable object. Finally, the results are summarized in section 5.

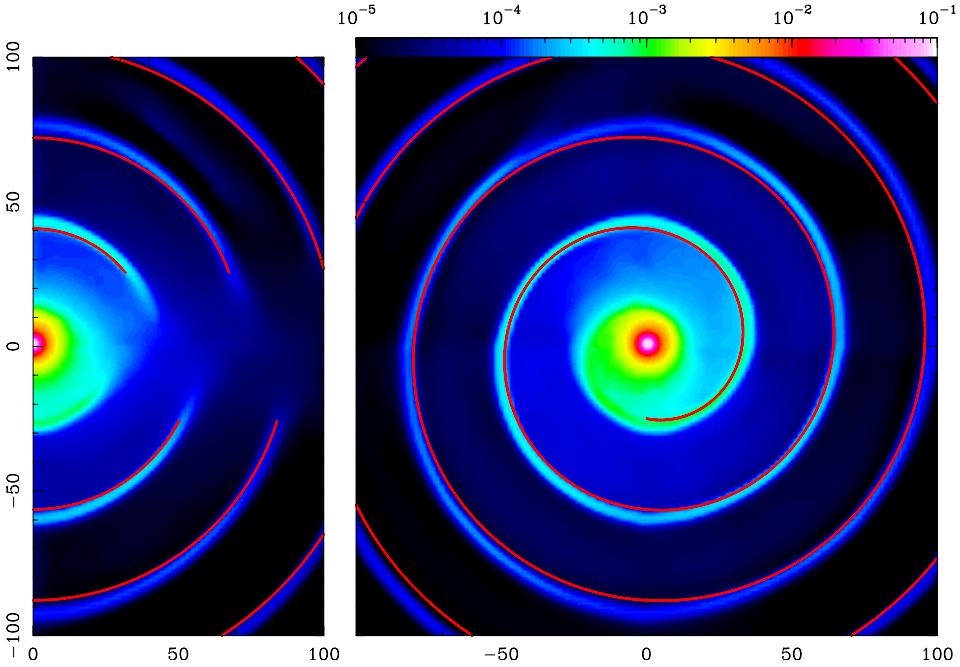

Figure 1. Single time-frame of the density stratification obtained from the circular orbit model described in the text. The right frame shows the density stratification on the orbital plane, and the left frame the stratification on a plane which includes the orbital axis (only the region on one side of the orbital plane is shown). The axes are labeled in units of the orbital radius. The red curves are the analytical solution for the same parameters. In the analytical solution, the dense regions bounded by 2 shocks (found in the numerical simulations) are a single, unresolved thin layer.

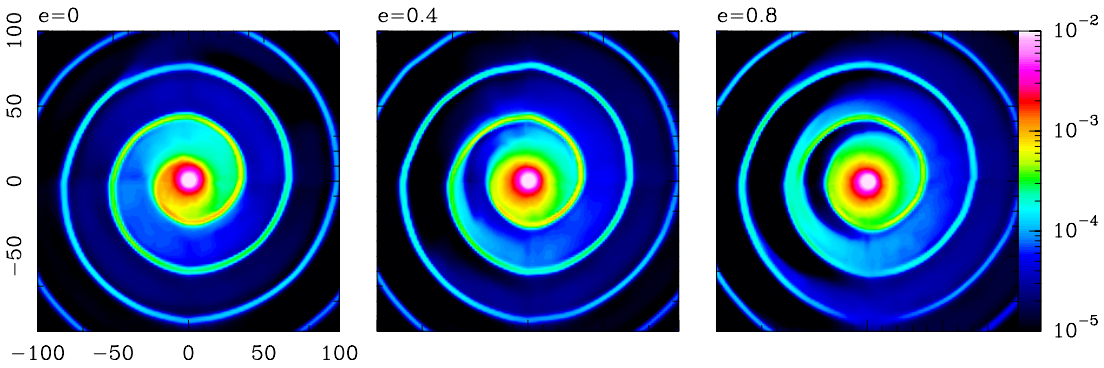

Figure 2. Single time-frame of the orbital plane density stratification obtained from the models with eccentricities $e = 0$ (left), 0.4 (center) and 0.8 (right). The axes are labeled in units of the semi-major axis.

2. The analytical model

Interestingly, it is possible to construct a simple, analytical model for the case of a wind source in a spherical orbit that satisfies the condition $v_{orb} \ll v_w$ (where v_w is the wind velocity and v_{orb} the orbital velocity of the wind source). In this limit, the orbital radius r_{orb} is small compared to the sizes of the shock structures produced in the wind, and the displacement of the wind source can be neglected (the effect of the orbital motion being limited to changing the velocity of the point from which the wind is being ejected). This model was described in a partial way by Cantó et al. (1999).

A two-shock "working surface" rotating spiral structure is formed on the orbital plane, starting at a radius

$$R_0 = r_{orb}\left(\frac{v_w}{v_{orb}}\right)^2 = \frac{\tau_{orb} v_w}{2\pi}\left(\frac{v_w}{v_{orb}}\right), \tag{1}$$

where r_{orb} is the radius and τ_{orb} the period of the circular orbit. The double-shock spiral has a step

$$\Delta r = 2\pi\left(\frac{v_w}{v_{orb}}\right) r_{orb} = \tau_{orb} v_w\,, \tag{2}$$

the second equality having been derived previously by Mauron & Huggins (2006). Combining equations (1-2) we then obtain :

$$\frac{v_w}{v_{orb}} = 2\pi\frac{R_0}{\Delta r}\,. \tag{3}$$

Perpendicular to the orbital plane, the two-shock structure is anchored on the orbital plane spiral, and has a circular shape on planes which include the orbital axis. The two-shock structure is interrupted when it intersects a cylinder of radius $r_{min} = R_0$ (where R_0 is given by equation 1) around the orbital axis. Therefore, a shock-less wind region is left within a cylinder of radius R_0 around the orbital axis.

3. Numerical simulations

Figure 1 shows a comparison between the analytical model described above and a single time-frame obtained from a 3D numerical simulation. The flow has been computed for parameters $v_w = 1$, $\tau_{orb} = 2\pi$ and $r_{orb} = 1$. The simulation is isothermal, with a $c_0 = 10^{-3}$ (isothermal) sound speed, and has been computed on a 5-level binary adaptive grid (with a maximum resolution of $0.78 r_{orb}$ along the three axes) with the `yguazú-a` code (see Raga et al. 2000). From Figure 1 it is clear that the analytical model predicts shock structures that agree well with the numerical results on the orbital plane and in a plane that includes the orbital axis.

We have also computed simulations of winds from a source in an elliptical orbit. We computed models with $v_w = 1$, $\tau_{orb} = 2\pi$, $a = 1$ (a being the semi-major axis of the orbit) and eccentricities $e = 0$, 0.4 and 0.8 (the $e = 0$ model being the same one that has been shown in Figure 1).

The resulting density stratifications on the orbital plane are shown in Figure 2. It is clear that the inner part of the spiral structure becomes progressively more distorted as

the eccentricity increases, but the outer parts of the spiral remain basically unchanged even in the higher eccentricity ($e = 0.8$) model.

Finally, we have taken the $e = 0$, circular orbit model, and calculated predicted intensity maps for observers at angles $i = 0$, 30°, 60° and 90° with respect to the orbital axis. The resulting maps are shown in Figure 3. These maps show that for orientation angles $i \leq 60°$ an almost undistorted spiral structure is observed. Only in our $i = 90°$ map (i. e., with the orbital axis on the plane of the sky) we do obtain an intensity map in which the shock-less axial region (see Figure 1) is evident.

These results show that the spiral shock structure produced as a result of an orbital motion of a wind source is a surprisingly robust feature. Firstly, a clear spiral structure is produced for orbits with eccentricities $e \leq 0.8$. Secondly, even though the shock structure is interrupted close to the orbital axis (see Figure 1), this "orbital axis hole" is evident in the predicted intensity maps (Figure 3) only in the case in which the orbital axis lies very close to the plane of the sky. For other orientations of the orbital axis, the intensity maps show a clear spiral structure.

4. Application to AFGL 3068

Mauron & Huggins (2006) presented an archival HST image of AFGL 3068 (from the HST program 10185, PI R. Sahai, see also Morris et al. 2006). This red (F606W filter) image shows a remarkable spiral structure around the IRAS source, to which Mauron & Huggins (2006) fitted an Archimedes spiral. Both the image and the fit are shown in Figure 4.

Mauron & Huggins (2006) interpret this spiral in terms of the wind from an orbiting source model of Soker (1994). They suggest that the observed emission is due to light from an external source which is reflected by the dusty wind from AFGL 3068. It is clear that the observed spiral has a remarkable similarity to the model predictions (see Figures 3 and 4). In the following, we calculate the parameters of the proposed AFGL 3068 binary that are deduced from an application of the analytical model (of section 2) to the observed spiral structure.

From the spiral fit (and using the distance of 1080 pc to AFGL 3068), one obtains the step of the spiral $\Delta r \approx 2''.29 = 3.71 \times 10^{16}$ cm (see Mauron & Huggins 2006) and from the distance between the center of the spiral and the point (almost directly West from the source) at which the spiral becomes visible one obtains $R_0 \approx 2''.78 = 4.50 \times 10^{16}$ cm.

Considering the $v_w = 14.1$ km s^{-1} outflow velocity from AFGL 3068, one then obtains an orbital period $\tau_{orb} = 835$ yr from equation (2) (see Mauron & Huggins 2006). Using the observed values of v_w, Δr and R_0, we can then use equation (3) to derive an orbital velocity $v_{orb} = 1.85$ km s^{-1} for the primary star of the binary (i. e., the wind source). Therefore, assuming a circular orbit we obtain an orbital radius $r_{orb} = \tau_{orb} v_{orb}/(2\pi) = 52$ AU for the primary.

For an assumed circular orbit, we then have the relation

$$\frac{m}{(1 + M/m)^2} = \frac{v_{orb} r_{orb}}{G} = 0.20 \mathrm{M}_\odot \,, \tag{4}$$

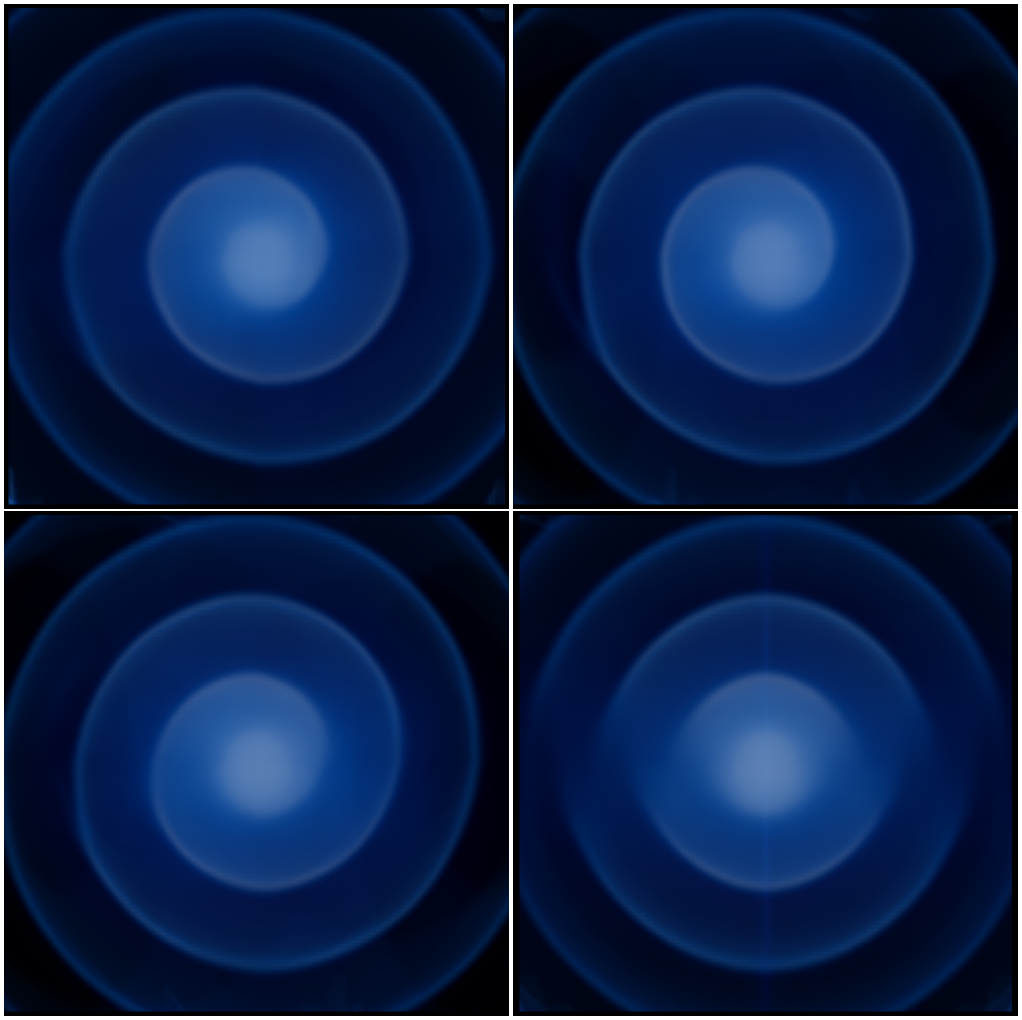

Figure 3. Intensity maps for the $e = 0$ model (circular orbit, see Fig. 1) for inclination angles $i = 0$ (top left), $i = 30°$ (top right), $i = 60°$ (bottom left) and $i = 90°$ (bottom right) between the outflow axis and the plane of the sky. The maps are displayed with a logarithmic scale. The maps were computed assuming that the emission coefficient and the opacity are both proportional to the number density of the flow.

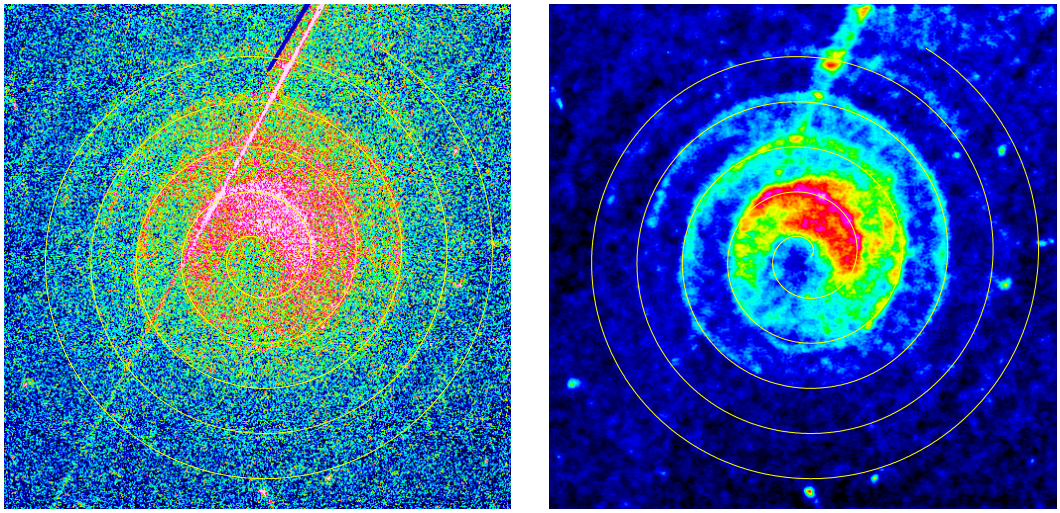

Figure 4. HST image of AFGL 3068 and least squares fit to the spiral structure (see Mauron & Huggins 2006). The original image is shown on the left frame, and a spatially filtered image (in which the diffraction spikes which cross the image were removed by interpolating linearly across the structures, and a wavelet filtering technique was used to smooth structures smaller than ~ 6 pix$\approx 0''.3$ across) on the right. The images have a size of $25''.5$ along the two axes.

where M is the mass of the primary (the wind source), $m \leq M$ is the mass of the secondary and G is the gravitational constant.

We can also use the fact that Morris et al. (2006) detected a companion at a projected distance of 109 AU from the primary. Considering that this is a lower limit for the separation d between the two stars (in an assumed circular orbit), we obtain a mass ratio

$$\frac{M}{m} = \frac{d}{r_{orb}} - 1 \geq 1.1\,. \tag{5}$$

If we take $M/m \sim 1.1$ as an estimate for the mass ratio, from equation (4) we obtain $m = 0.88\mathrm{M}_\odot$ and $M = 0.97\mathrm{M}_\odot$. For a somewhat higher, $M/m = 1.5$ mass ratio we would obtain $m = 1.25\mathrm{M}_\odot$ and $M = 1.9\mathrm{M}_\odot$.

5. Conclusions

In this paper, we have presented an analytical model and 3D gas-dynamic simulations of an isotropic wind ejected from a star in orbital motion around a companion. We find that a spiral structure is produced on the orbital plane, with circular prolongations (on planes that include the orbital axis) that end at a finite distance from the orbital axis. This structure is found for a circular orbit, and is maintained for orbits with eccentricities of up to $e = 0.8$.

Interestingly, when computing predicted intensity maps one finds that they show a spiral morphology for all cases except when the orbital axis lies close to the plane of the sky (in which the axial "holes" in the shock structure are apparent). Therefore, the robustness of the predicted spiral structure (present for a large range of eccentricities

and orientations of the optical axis with respect to the line of sight) indicates that such structures might be observed in binary stellar wind sources.

The evident example of this kind of structure is AFGL 3068, a giant star (whose photosphere is not directly visible at optical wavelengths) which shows an envelope with a remarkable spiral structure (Mauron & Huggins 2006). This structure has a strong resemblance to the predictions from our numerical simulations. We then apply to AFGL 3068 the relations (from our analytical model) giving the starting point and the step of the spiral, and through them obtain the orbital period and radius, as well as a relation involving the masses of the wind source and its binary companion.

The fact that the obtained masses are completely reasonable for a giant star and a somewhat lower mass companion indicates that the proposed interpretation of the spiral structure of AFGL 3068 is likely to be correct. Further possible applications of this model will be studied in the future.

Acknowledgments. AR, JC and AE acknowledge support from the CONACyT grants 61547, 101356 and 101975. PJH acknowledges support from NSF grant AST 08-06910.

References

Cantó, J., Raga, A. C., Koenigsberger, G., Moreno, E., 1999, in IAU Symp. 193, Wolf-Rayet Phenomena in Massive Stars and Starburst Galaxies (ASP Conf. Proc.), p. 338
He, J. H. 2007, A&A, 467, 1081
Mastrodemos, N., Morris, M. 1999, ApJ, 523, 357
Mauron, N., Huggins, P. J., 2006, A&A, 452, 257
Morris, M., Sahai, R., Matthews, K., Cheng, J., Lu, J., Claussen, M., Sánchez-Contreras, C. 2006, in IAU Symp. 234, Planetary Nebulae in our Galaxy and Beyond (ASP Conf. Proc.), p. 469
Raga, A. C., Navarro-González, R., Villagrán-Muniz, M., 2000, RMxAA, 36, 67
Raga, A. C., Esquivel, A., Velázquez, P. F., Cantó, J., Haro-Corzo, S., Riera, A., Rodríguez-González, A. 2009, ApJ, 707, L6
Soker, N. 1994, MNRAS, 270, 774

Asymmetric Planetary Nebulae V
A. A. Zijlstra, F. Lykou, E. Lagadec and I. McDonald
Jodrell Bank Centre for Astrophysics, Manchester, UK © 2011

The Turbulent Destruction of Circumstellar Clouds

J.M. Pittard[1], S.A.E.G. Falle[2], T.W. Hartquist[1], and J.E. Dyson[1]

[1]*School of Physics and Astronomy, The University of Leeds, UK*

[2]*Department of Applied Mathematics, The University of Leeds, UK*

Abstract. The interaction between an astrophysical cloud and a shock has been extensively studied using numerical hydrodynamics. However, the full development of turbulence in what is usually a high Reynolds number interaction is prevented by the numerical viscosity inherent in hydrodynamical simulations. To overcome this limitation we have incorporated a subgrid compressible k-ϵ turbulence model into our numerical code. We first demonstrate its exceptionally good convergence, and then show the results of an investigation into the mass-loss rates and lifetimes of clouds as a function of their density contrasts, χ, and the Mach numbers of the shocks, M. We finish by discussing the formation of tails in shell-cloud interactions.
Keywords. Planetary nebulae

1. Introduction

The multi-phase nature of circumstellar, interstellar and intergalactic environments, together with the high-speed flows which occur in them, lead to ubiquitous interactions between clouds (also referred to as clumps, globules and knots) and shocks, shells, winds and jets. Material stripped off clouds by the passage of a fast wind or shock is frequently manifest as a long tail behind the cloud. Tails also form where the mass-loss is driven by photoevaporation if the clouds are subject also to a strong wind.

The interaction between a wind and individual clouds is perhaps best seen in the stunning observations of planetary nebula (PNe), of which NGC 7293 (the Helix nebula) is a beautiful example. In this source, long molecular tails and bright cresent-rimmed clouds are spectacularly resolved (642; 633; 637). Two different models have been proposed to explain the tails in PNe. In "shadow" models the tail forms due to the shielding of the direct radiation field of the central star (e.g. 636; 642). In contrast, "stream-source" models assume that the tail forms from material photoablated from the cloud (628; 630; 647; 629). The correct model is still disputed (see Dyson et al. 2006 and O'Dell, Henney & Ferland 2007, and references therein). However, observations of the dynamics of the tails favour stream-source models: i) there is no evidence for significant ionized gas velocities perpendicular to the tails (639), in contrast to the shadow model of López-Martin et al. (636); ii) the flow accelerates along the tails (by about $8 - 14\,\mathrm{km\,s^{-1}}$, 638).

In contrast, observational studies of the interaction between a shock and a cloud have typically focused on supernova remnants, and on clouds in the Cygnus loop in

particular (e.g. 631; 627; 635; 646; 640). In some interactions a bowshock is clearly visible, while in others it is not. Possible explanations for the lack of a bowshock are the earliness of the interaction (634), a smooth cloud density profile (641), a high ellipticity of the cloud (640), or the effects of thermal conduction (645), cosmic rays (e.g. 651) or strong turbulence (648).

An extensive literature of numerical hydrodynamic investigations of shock-cloud, wind-cloud and jet-cloud interactions now exists. The effects of radiative cooling, thermal conduction and ordered magnetic fields have all been considered (e.g. 644). Insight into the behaviour and evolution of clouds subject to a variety of internal and external conditions has been obtained. However, existing simulations are for much lower Reynolds numbers than typically occur in astrophysical environments. Therefore, the formation of fully developed turbulence is prevented, the turbulent mixing of cloud material into the surrounding medium is limited and the destruction of a cloud is hindered. The problem is overcome through the use of a subgrid turbulent viscosity model, designed to calculate the properties of the turbulence and the resulting increase in the transport coefficients that the turbulence brings. In this way, a high Reynolds number flow can be emulated. In this contribution we report on simulations of shock-cloud and shell-cloud interactions which include a k-ϵ subgrid turbulence model.

2. The Numerical Setup

Any numerical study must necessarily focus on a limited region of parameter space. We therefore assume that magnetic fields, thermal conduction and self-gravity are unimportant. In our shock-cloud simulations the gas is assumed to behave adiabatically and the cloud is assumed to be small, so that the post-shock quantities are time independent. We assume that the cloud is spherical, and simulate the interaction using a 2D rz-axisymmetric grid. A shock of Mach number M propagates along the z-direction, parallel to the axis of symmetry. The cloud has a smooth edge and an initial radius, $r_{\rm c}$, of one grid unit. The density contrast of the cloud to the ambient medium is χ and the velocity of the shock is $v_{\rm b}$. The grid is large enough to ensure that the cloud is well mixed and dispersed by the flow before the shock encounters the grid edge. All calculations were performed for an ideal gas with $\gamma = 5/3$. The interaction is studied in terms of the "cloud-crushing" time, $t_{\rm cc} = \chi^{1/2} r_{\rm c}/v_{\rm b}$, which is the characteristic time for the cloud to be crushed by the shocks driven into it (634). Further details, including the full set of equations solved, can be found in Pittard et al. (648).

Our shell-cloud simulations incorporate a cooling function and heating term such that the cloud equilibrium temperature is 8 K, while the ambient medium and swept-up shell are maintained at 8000 K. The hotter gas in the bubble interior (which drives the shell) has a temperature in excess of 10^6 K and a cooling time much longer than $t_{\rm cc}$.

3. Shock-cloud Interactions

3.1. Convergence Tests

We first wish to demonstrate that our calculations are performed with sufficiently high spatial resolutions that key features of the interaction are resolved. Previous work has

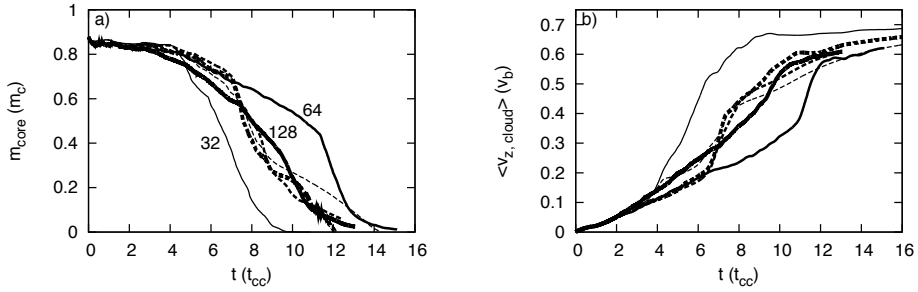

Figure 1. Convergence tests for a shock-cloud interaction with $\chi = 10^3$ and without (solid lines) a k-ϵ model. The time evolution of the core mass (panel a) and the mean velocity of the cloud (panel b) are shown. The results from simulations with a subgrid turbulence model (dashed lines) display much tighter convergence (see 648). The results from the simulations without the subgrid model converge on the subgrid model results.

found that quantities which are sensitive to small scales, such as the mixing rate between cloud and ambient gas, require about 100 cells per cloud radius for convergence (634; 641).

Fig. 1 shows the evolution of the core mass (see Pittard et al. 2009 for the definition of the core mass) and mean cloud velocity as a function of spatial resolution. We find that these quantities are poorly converged in low resolution simulations that do not include a subgrid turbulence model (see also 650). In contrast, including a subgrid turbulence model leads to results which are much less dependent on the spatial resolution (for additional convergence tests see 648). Of particular note is the fact that the results from simulations without the subgrid model approach those with the subgrid model as the resolution of the former models increases. This gives us confidence that the subgrid model results are correct. All of the following results are from simulations that include the subgrid turbulence model.

3.2. Mass-loss Rates and Cloud Lifetime

With the assumptions in Sec. 2 the time evolution of the cloud in units of t_{cc} becomes independent of the shock Mach number at high Mach numbers (this is called "Mach scaling" - see 634). However, significant differences in the interaction occur at lower Mach numbers. For instance, when $M < 2.76$ the post-shock flow is subsonic and a bow wave rather than a bow shock forms upstream of the cloud. The growth of Rayleigh-Taylor (RT) and Kelvin-Helmoltz (KH) instabilities is slower due to the lower velocity shear at the cloud surface, and it takes longer for the cloud to be accelerated and destroyed. Fig. 2(a)-(c) shows the evolution of the core mass of the cloud as a function of M and χ.

The lifetime of the cloud core (defined as the time at which material in the core has sufficiently mixed with ambient material that its concentration is everywhere less than 50%) as a function of M and χ is shown in Fig. 2(d). The numerical results are compared against those from the analytical formula proposed by Hartquist et al. (632). We find good agreement for clouds with density contrasts $\chi \sim 10^3$ hit by shocks with Mach numbers $M < 10$. However, there is a significant and increasing divergence between

the numerical and analytical cloud lifetimes as the shock Mach number increases past $M = 15$. Note that the numerical results are consistent with Mach scaling, whereas the analytical formula is not. There is also serious disagreement at moderate Mach numbers ($1.5 < M < 7$) and low density contrasts ($\chi \sim 10$). The reason for these differences is due to the fact that Hartquist et al. (632) assume that the mass-loss is primarily driven by pressure gradients, whereas in reality mass is lost from the cloud as a result of KH instabilities. We further note that a prominent tail behind the cloud only forms if the cloud density contrast is sufficiently high, with a minimum $\chi \sim 10^3$ needed.

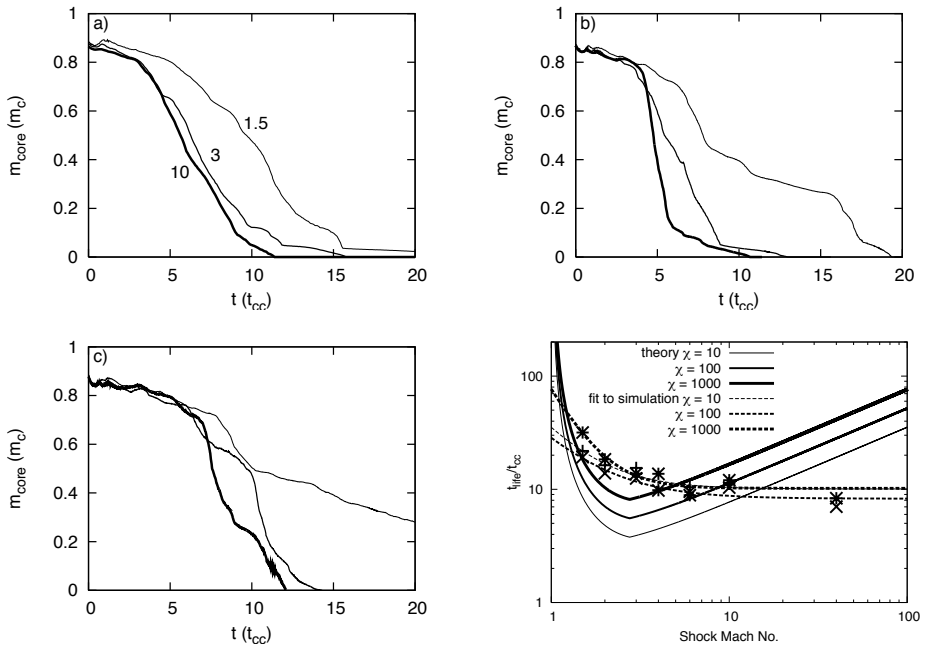

Figure 2. Panels (a)-(c): Time evolution of the core mass, $m_{\rm core}$, for various Mach numbers (1.5, 3, and 10, as indicated) and density contrasts from the numerical simulations with the k-ϵ subgrid model: (a) $\chi = 10$, (b) $\chi = 10^2$, (c) $\chi = 10^3$. Panel (d): Comparison of the cloud lifetime (defined as the time when the "core" disappears) from the numerical simulations with the k-ϵ subgrid model and the lifetime obtained from the analytical result of Hartquist et al. (632), as a function of the shock Mach number, M, and the cloud density contrast, χ. The results from models with $\chi = 10$, 10^2 and 10^3 are shown with pluses, crosses and asterixes, respectively. Adapted from Pittard et al. (649).

4. Shell-cloud Interactions

A recent investigation by us has revealed a totally new mechanism for the formation of tails (Pittard 2011, submitted), which we now discuss. Fig. 3 shows the interaction of an isothermal shell with a dense spherical cloud. The calculation is performed in 2D with rz-axisymmetry and 128 cells per cloud radius on the finest grid. The shell has an adiabatic Mach number of 1.5 with respect to the ambient medium. The pressure

and density jump in the shell is $\gamma M_{\rm a}^2 = M_{\rm i}^2 = 3.75$ (where $M_{\rm i}$ is the isothermal Mach number of the shell).

A key parameter is the ratio of the column density through the shell to that through the centre of the cloud. In Fig. 3 this ratio is $\sigma_{\rm sh}/\sigma_{\rm cl} = 7.5 \times 10^{-3}$. Hence the cloud is relatively unaffected by the initial passage of the shell. However, the jump in the external pressure starts to compress it. This compression is nearly isotropic, due to the low Mach number of the interaction and the high density contrast of the cloud. The cloud then exits through the back surface of the shell to reside in the low density interior of the hot bubble.

The most interesting, and unexpected, aspect of the interaction is the formation of a tail behind the cloud. This is mainly composed of material initially in the shell, with only very small amounts (less than a few percent concentration at $z > 5\,{\rm r_c}$ downstream of the cloud) of material ablated or stripped from the cloud. It appears that part of the shell adjacent to the cloud moves in the lateral direction onto the axis due to the pressure gradient which exists across its face as it sweeps over the cloud. A large eddy forms which causes this material to lose speed relative to the rest of the shell (some material near the axis actually moves back towards the rear of the cloud). This material is subsequently compressed against the axis by the hot, subsonic flow which overtakes it. The pressure gradient across the face of the shell diminishes as the shell moves further downstream, and the focusing becomes more gradual. The focussing doesn't appear to be dependent on the exact shape of the leading edge of the shell, which at various times is either leading or lagging on axis compared to off-axis.

A 3D simulation of this interaction reveals the same features, while an exploration of parameter space reveals that tails can form in this way under a variety of conditions, so this mechanism appears to be relatively robust. The tails exhibit a large length-to-width ratio which can reach nearly 50:1 at late times. The acceleration is approximately constant along the tail. While our models are not specifically of the Helix tails, the linear velocity increase along the tails is similar to observations (Meaburn, private communication). Due to the lack of material being stripped off the cloud, the tail eventually dissipates and detaches from the cloud (by $t \sim 3\,t_{\rm cc}$). The axial velocity profile perpendicular to the tail shows a near constant speed at a given downstream position, which indicates efficient momentum transfer across the tail.

5. Summary

We have presented results of shock-cloud and shell-cloud interactions simulated using a k-ϵ turbulence model. We have determined the lifetime of clouds hit by a shock and have discovered a new mechanism for producing tails behind clouds.

Acknowledgments. We would like to thank the conference organizers for their invitation to present our work. JMP would also like to thank the Royal Society for a University Research Fellowship.

References

Danforth C. W., Blair W. P., Raymond J. C., 2001, AJ, 122, 938
Dyson J. E., Hartquist T. W., Biro S., 1993, MNRAS, 261, 430

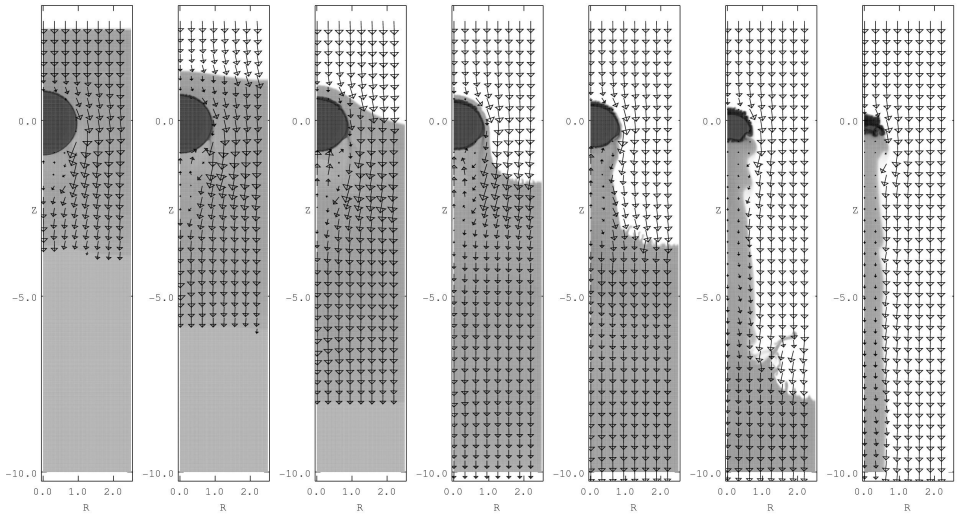

Figure 3. The time evolution of a 2D rz-axisymmetric shell-cloud interaction with $M = 1.5$, $\chi = 10^3$, and an initial shell thickness of $4\,r_c$. The interaction proceeds left to right with $t = 0.098$, 0.162, 0.227, 0.291, 0.355, 0.549, and $0.806\,t_{\rm cc}$. Material in the shell is focussed into a tail as it passes over the cloud which is being compressed by the pressure jump it is experiencing. The density map spans over 5 orders of magnitude. The interior of the bubble has a density 4 dex lower than the original cloud, while the ambient medium, shell and tail have a density about $250 - 1000\times$ lower than the original cloud.

Dyson J. E., Pittard J. M., Meaburn J., Falle S. A. E. G., 2006, A&A, 457, 561
Falle S. A. E. G., Coker R. F., Pittard J. M., Dyson J. E., Hartquist T. W., 2002, MNRAS, 329, 670
Graham J. R., Levenson N. A., Hester J. J., Raymond J. C., Petre R., 1995, ApJ, 444, 787
Hartquist T. W., Dyson J. E., Pettini M., Smith L.J., 1986, MNRAS, 221, 715
Hora J. L., Latter W. B., Smith H. A., Marengo M., 2006, ApJ, 652, 426
Klein R. I., McKee C. F., Colella P., 1994, ApJ, 420, 213
Levenson N. A., Graham J. R., Walters J. L., 2002, ApJ, 576, 798
López-Martin L., Raga A. C., Mellema G., Henney W. J., Cantó J., 2001, ApJ, 548, 288
Matsuura M., et al., 2007, MNRAS, 382, 1447
Meaburn J., Boumis P., 2010, MNRAS, 402, 381
Meaburn J., Clayton C. A., Bryce M., Walsh J. R., Holloway A. J., Steffen W., 1998, MNRAS, 294, 201
Miceli M., Reale F., Orlando S., Bocchino F., 2006, A&A, 458, 213
Nakamura F., McKee C. F., Klein R. I., Fisher R. T., 2006, ApJSS, 164, 477
O'Dell C. R., Henney W. J., Ferland G. J., 2005, AJ, 130, 172
O'Dell C. R., Henney W. J., Ferland G. J., 2007, AJ, 133, 2343
Orlando S., Bocchino F., Reale F., Peres G., Pagano P., 2008, ApJ, 678, 274
Orlando S., Peres G., Reale F., Bocchino F., Rosner R., Plewa T., Siegel A., 2005, A&A, 444, 505
Patnaude D. J., Fesen R. A., Raymond J. C., Levenson N. A., Graham J. R., Wallace D. J., 2002, AJ, 124, 2118
Pittard J. M., Dyson J. E., Falle S. A. E. G., Hartquist, 2005, MNRAS, 361, 1077
Pittard J. M., Falle S. A. E. G., Hartquist T. W., Dyson J. E., 2009, MNRAS, 394, 1351
Pittard J. M., Hartquist T. W., Falle S. A. E. G., 2010, MNRAS, 405, 821
Shin M.-S., Stone J. M., Snyder G. F., 2008, ApJ, 680, 336

Wagner A. Y., Falle S. A. E. G., Hartquist T. W., Pittard J. M., 2006, A&A, 452, 763

Asymmetric Planetary Nebulae V
A. A. Zijlstra, F. Lykou, E. Lagadec and I. McDonald
Jodrell Bank Centre for Astrophysics, Manchester, UK © 2011

Physical conditions and excitation of FLIERs

A. Riera[1], A.C. Raga[2], G. Mellema[3], A. Esquivel[2], and P.F. Velázquez[2]

[1]*Dep. Física i Enginyeria Nuclear. Universitat Politècnica de Catalunya. Spain*

[2]*Instituto de Ciencias Nucleares. Universidad Nacional Autónoma de México, Mexico*

[3]*Department of Astronomy & Oskar Klein Centre, AlbaNova, Stockholm University, Sweden*

Abstract. A fraction of all Planetary nebulae and Proto–Planetary nebulae show high velocity knots (Fast Low Ionization Emission Regions or FLIERs), with line ratios and radial velocities which differ significantly from the surrounding nebular gas. The spectra of these features show evidence of shock excitation. However, the actual physical/dynamical configuration of FLIERs is not clear at all.

We present the results of axisymmetric simulations of an initially spherical cloudlet, moving away from a photoionizing source. These simulations include a detailed calculation of both the transfer of ionizing radiation and the non-equilibrium ionization state of the gas. From these simulations, we predict the spectra of a bow-shock that is illuminated by an ionizing flux from the post-shock direction, which we compare with the observed properties of FLIERs.

Keywords. Planetary Nebulae

1. Introduction

A fraction of Planetary Nebulae show small scale structures that have significantly different line ratios and/or larger radial velocities than their surroundings. Of particular interest are the string of knots which appear as symmetrical pairs, point-symmetrical features or jet structures, which move supersonically with respect to the main body of the nebula, and are often referred to as FLIERs or LIS (Low Ionization Structures).

Balick, Goncalves and coworkers explored the spectroscopic properties of FLIERs (or LIS) in a group of PNe. Balick et al. (1993, 1994), Corradi et al. (1996), and Goncalves et al. (2001, 2004, 2009) found that FLIERs have dimensions of $\sim 10^{16}$ cm, are much lower in ionization, higher in velocity (with Doppler shifts ± 25 to 200 km s^{-1}) and about the same in density and temperature compared with the regions around them. The small sizes and high outflowing velocities of the FLIERs strongly support that these microstructures are associated to outward–flowing bullets or clumps. Consequently, the emission observed at the FLIER would form in a bow shock which

is irradiated by the central star (i.e., the central star is an ionizing photon source that will modify the ionization and excitation structure of the shock).

2. Physical Conditions and excitation of FLIERs

Our characterization of the irradiated shocks is based in three nebulae which have bow shock-like features outside the main body of the nebula and for which images of several emission lines have been obtained with the HST (i.e., IC 4634, NGC 7009, NGC 6543). From the HST images of IC 4634 we obtained the Hα, [O III] 5007Å, and [N II] 6583 Å surface brightness distribution along the axis that passes throught the outer FLIER and the central star of IC 4634 (see figure 7 of Raga et al. (2008)). From these distributions, it is clear that the [O III] and Hα emission extend away from the head of the FLIER towards the central source, and that both differ from the [N II] distribution, which shows a more compact structure. The [N II] distribution peaks at larger distances from the central source than the Hα and [O III] 1-D profiles. Also note that the observed Hα distributions peak at larger distances than the [O III] 5007 Å distributions.

To characterize the spectra of the irradiated shocks in PNe, we present a set of diagnostic diagrams involving several emission line ratios commonly used to discriminate photoionized nebulae from shock-excited objects. In figure 1, we present these diagnostic diagrams including ground-based spectrocopic data (in red) and spectra synthesized from the WFPC2 HST images (in green) of different regions of NGC 6543, NGC 7009, and IC 4634. The open symbols correspond to rims and shells included to trace the locus of normal photoionized gas. The observations of irradiated shocks are plotted as filled symbols. We see that there is a considerable overlap in the values of the [O III]/Hα ratios between photoionized gas and irradiated shocks. From figure 1, we conclude that the spatially integrated emission of irradiated shocks are characterized by a considerable change in [N II]/Hα, [O I]/Hα, and [S II]/Hα emission line ratios, with values in between the values expected for a pure shock-excited objects and photoionized nebulae, and [O III]/Hα values from 1.5 to 6.

3. Numerical simulations

Since the Asymmetrical Planetary Nebulae IV Conference, we have computed a series of axisymmetric numerical simulations of a dense cloudlet moving away from an ionizing source throught a uniform medium (Raga et al. 2008). We use a time-dependent gasdynamic code with an adaptative grid (CORAL) that includes radiative, dielectronic and charge exchange recombination, collisional ionization and photoionization for several species. We include the radiation field from the central star that penetrates the recombination region from the post-shock to the pre-shock region. The version of the CORAL code that we have used is described in detail by Mellema et al. (1998).

In the initial configuration we had a spherical cloudlet of density $n_c = 10^3$ cm^{-3}, temperature $T_c = 10^4$ K, radius $r_c = 10^{16}$ cm, which moved at a velocity $V_c = 40, 70, 100$ and 150 km s^{-1}. The remainder of the computational domain is filled with a uniform , stationary medium of density $n_{env} = 10^2$ cm^{-3} and temperature $T_{env} = 10^4$ K. We adopted the abundances of Kingsburgh and Barlow (1994). For the photoionizing source, we assumed a blackbody source with a luminosity of 5000 L$_\odot$, and effective

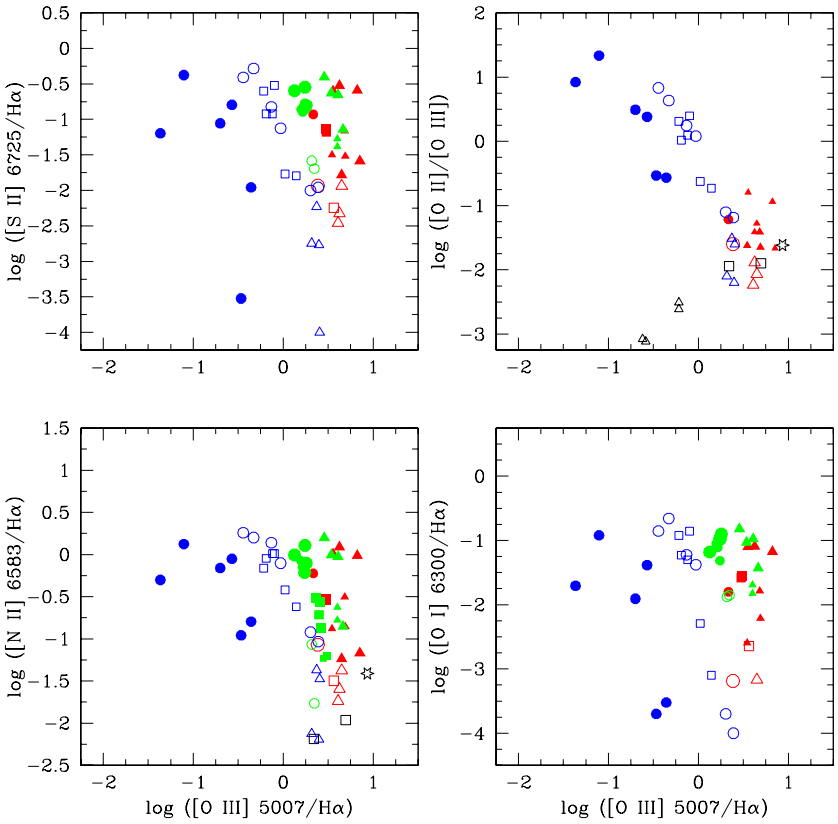

Figure 1. Diagnostic diagrams including several de-reddened and predicted emission-line ratios. The red symbols correspond to ground-based spectroscopic data of NGC 6543 (circles), NGC 7009 (triangles) and IC 4634 (squares). The green symbols are synthesized spectra of different regions of NGC 6543, NGC 7009 and IC 4634 obtained from WFPC2 HST images. The filled symbols correspond to FLIERs, the open symbols correspond to rims and shells. Blue symbols are the predicted emission line ratios from Raga et al. (2008). The models with $n_c = 10^2$ cm^{-3} are shown as black symbols (see text); $V_c = 40, 70$ km s^{-1}, (triangles), 150 km s^{-1} (squares), 200 km s^{-1} (stars).

temperatures of 5x10^4 and 7x10^{4}K. The source was located at a distance D = (0.3, 1, 3) x 10^{18} cm to the left of the computational domain.

We computed 11 simulations with the same values of n_c, T_c, r_c , n_{env} , T_{env} and stellar luminosity, but with different combinations of the initial cloud velocity, stellar effective temperature, and distance D to the ionizing source (values listed above). The choosen parameter combinations results in an ionization parameter μ_c values that range from 10^{-4} to 10^{-2}, where $\mu_c = F_*/n_c c$, F_* is the ionizing photon flux, and c is the light speed. We also computed 4 models with a larger value of the ionization parameter of the undisturbed cloudlet ($\mu_c = 0.10$), with a spherical cloudlet of density $n_c = 10^2$ cm^{-3}, temperature $T_c = 10^4$ K, radius $r_c = 10^{16}$ cm, which moved at a velocity $V_c =$ 40, 70, 150 and 200 km s^{-1}, with a stationary medium of density $n_{env} = 10$ cm^{-3} and temperature $T_{env} = 10^4$ K.

3.1. Results of the Numerical models

From the ionization and temperature stratifications obtained in our simulations, we computed emission line coefficients for Hα (considering the recombination cascade and collisional excitations from n=1 $\rightarrow$ 3), and the [O II] 3726+29, [O III] 5007, [O I] 6300, [N II] 6583, [S II] 6716+30 forbidden lines (solving the appropriate 5-level atom problems). These emission coefficients can be integrated along the line of sight to produce emission line maps. The predicted spectrum of the shocked cloudlet for each of the 15 numerical simulations at two intergration times, have been obtained integrating the computed emission-line coefficients over the entire emitting volume (or, equivalently, integrate the predicted emission maps over the plane of the sky) to compute the emission line luminosities.

3.2. A comparison with observed properties of FLIERs

Figure 7 of Raga et al. (2008) shows the normalized emission-line brightness distributions along the symmetry axis passing through the $t = 400$ years intensity maps obtained for a model with $\mu_c = 10^{-2}$. In this figure, we observe that the [N II] emission-line distribution peaks at larger distances than the other two "1D" profiles. Also note that the Hα and [O III] brightness distributions extend away from the head of the bow shock, in good agreement with the observed behaviour. However, the predicted [O III] distribution peaks at larger distances from the central star than the Hα distribution, which is the opposite to what is observed.

In the diagrams of figure1, we have included the predictions of our models. The predicted emission line ratios are shown in blue (numerical simulations with a high-density cloudlet) and in black (numerical simulations with a low-density cloudlet). From this figure, we see that the predicted line-ratios cover regions of the diagnostic diagrams which are similar to the regions covered by the observed line-ratios. The shocked cloudlet models with $T_{eff} = 50000$ K (shown as solid circles) produce emission line spectra that -specially for those with the lowest ionizing parameters- are similar to that of "pure" shocked spectra. For other values of the initial parameters, i.e. for higher values of the of the incident ionizing photon-flux, the emission line ratios range for typical values of shock-excited spectra to values similar to that of "normal" photoionized nebulae. In these diagnostic diagrams, we see that the models apear to have too low [O III]/Hα line ratios, such that the points corresponding to FLIERs systematically fall just to the right of the predicted points.

Finally, we have computed some models with a low density cloudlet and a high ionizing photon-flux (shown as black symbols) and $V_c = 40, 70, 150$ and 200 km s^{-1}. As shown in figure1, for some parameters, the predicted [O III]/Hα line ratios reproduce the values observed in FLIERs. These models fail to reproduce the [N II]/Hα and [S II]/Hα line ratios observed in some FLIERs (which in many cases are larger than the predicted values).

Acknowledgments. This work was supported by the MICINN grant AYA2008-06189-C03 and AYA2008-04211-C02-01.

References

Balick, B., Rugers, M., Terzian, Y. and Chengalur, J. N. 1993, ApJ, 411, 778
Balick, B., Perinotto, M., Maccioni, A., Terzian, Y. and Hajian, A. 1994, ApJ, 424, 800
Corradi, R. L. M., Manso, R., Mampaso, A. and Schwarz, H. E. 1996, A&A, 313, 913
Goncalves, D.R., Corradi, R.L.M. and Mampaso, A. 2001, ApJ, 547, 302
Goncalves, D.R. 2004, ASP Conference Proceedings 313, 216
Goncalves, D. R., Mampaso, A., Corradi, R. L. M. and Quireza, C. 2009, MNRAS, 398, 2166
Kingsburgh, R.L. and Barlow, M.J. 1994, MNRAS, 271, 275
Mellema, G. et al. 1998, A&A, 331, 335
Raga, A. C., Riera, A., Mellema, G., Esquivel, A. and Velázquez, P. F. 2008, A&A, 489, 1141

Asymmetric Planetary Nebulae V
A. A. Zijlstra, F. Lykou, E. Lagadec and I. McDonald
Jodrell Bank Centre for Astrophysics, Manchester, UK © 2011

Criss-cross mapping BD+30 3639: a new kinematic analysis technique

Wolfgang Steffen[1], Francisco Tamayo[1], and Nico Koning[2]

[1]*Instituto de Astronomía, Universidad Nacional Autónoma de México, C.P. 22860, Ensenada, México*

[2]*Department of Physics and Astronomy, University of Calgary, Calgary, Canada*

Abstract. We present a new analysis of kinematic data of the young planetary nebula BD+30 3639. The data include spectroscopic long-slit and internal proper motion measurements. In this paper we also introduce a new type of mapping of kinematic proper motion data that we name "criss-cross" mapping. It basically consists of finding all points where extended proper motion vectors cross or converge. From the crossing points a map is generated which helps to interpret the kinematic data. From the criss-cross mapping of BD+30 3639, we conclude that the kinematic center is approximately 0.5 arcsec off-set to the South-East from the central star. The mapping does also show evidence for a non-homologous expansion of the nebula that is consistent with a disturbance aligned with the bipolar molecular bullets.

Keywords. Planetary Nebulae

1. Introduction

BD+30 3639 is a young planetary nebula that has been observed in detail with a variety of observational techniques. It shows extended emission in radio up to X-rays. The structure is, however, substantially different in the various wavelength regions. Some of the most striking features are as follows. The basic projected structure is a nearly rectangular ring, with some emission inside. The ring is not uniform along its perimeter, but shows reduced brightness especially in the south-western region. A fainter halo has been observed to go out to at least twice the distance of the ring (Harrington et al., 1997). The infrared continuum emission roughly traces the optical rectangle and its halo. Molecular hydrogen emission is distributed very unevenly in large clumps within the halo (Shupe et al., 1998). The molecular CO lines show a pair of high-speed bullets moving in opposite directions (Bachiller et al., 2000). Extended X-ray emission has been observed inside the optical rectangle with a brightness gradient going roughly from south-west to north-east (Kastner et al., 2000). Figure 1 (left) is a composite image that shows images taken in the different wavelength regions joint within a single frame. Proper motion, combined with Doppler-velocity measurements and an accurate 3D model of the object may help improve the distance determination of the object. Li, Harrington & Borkowski (2002, hereafter LHB) have obtained two HST narrowband images that were observed with a separation of 5.663 years. They determined the

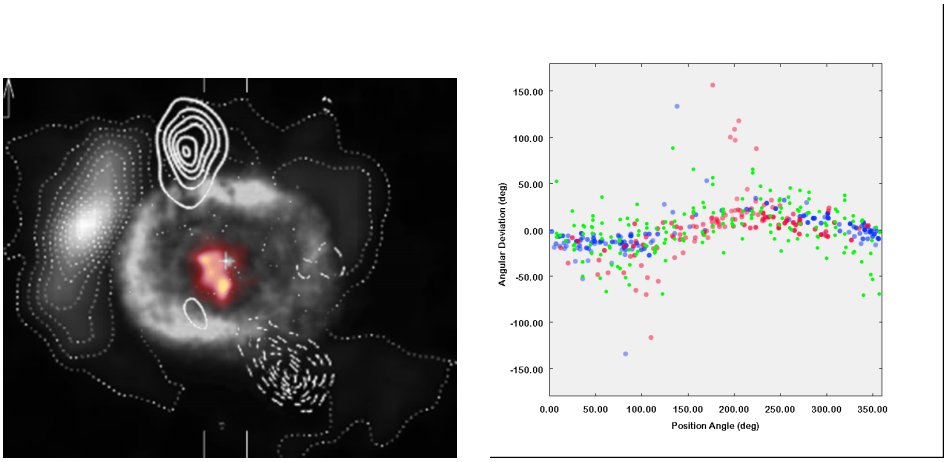

Figure 1. On the left several types of maps have been combined: optical (grey, from LHB), H_2 (contoured grey, from Shupe et al., 1998), CO (contour, from Bachiller et al., 2000) and the criss-cross map (red, this work). On the right the angular deviation from the radial direction of the internal proper motion vectors is plotted against position angle. Data from LHB are in green and model values from this work are in red and blue.

expansion of the nebula along many angular sectors as well as local proper motion vectors of substructure at nearly 200 positions. With their measurements and an ellipsoidal model of BD+30 3639 they determine a distance of 1.2 kpc.

One of their results is that the expansion seems to be somewhat faster along position angles (PA) around 40° and 220°. This coincides approximately with the position angles of the CO outflows. LHB concentrate on the variation of the magnitude of the proper motion vectors as a function of position angle and distance from the central star. In the present paper, in order to further improve the 3D model and the distance determination, we analyze their proper motion vectors with emphasis on the direction, i.e. their deviation from the radial direction, as a function of position angle and distance from the central star. We first describe a new method to visualize and analyze such data in the form of what we call "criss-cross mapping". A detailed 3D model and the distance determination will be presented in a separate paper.

2. Criss-cross mapping

In order to aid in the interpretation of current and future internal proper motion measurements in expanding nebulae we introduce "criss-cross" mapping. The basic idea is to emphasize regions where velocity vectors converge and intersect. Note that a radially expanding nebula will have all its velocity vectors intersect at the position of the central star. If there are systematic deviations from radial expansion, the intersection point might shift or be transformed into some extended pattern. Such a pattern might reveal helpful information. We therefore define the criss-cross mapping in its most basic form as follows:

Replace every proper motion vector with a thin line that extends over the complete

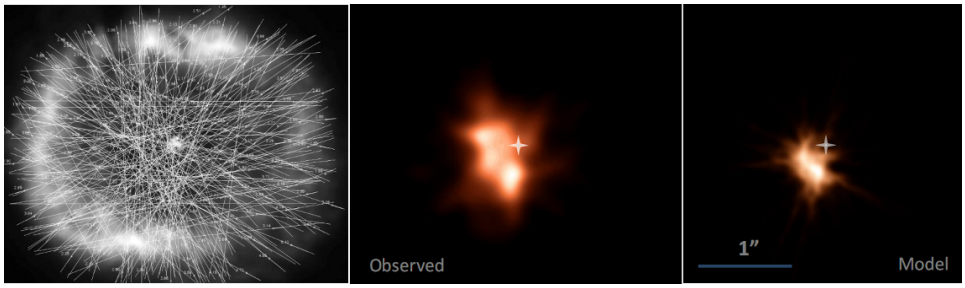

Figure 2. Straight lines have been overlayed on all proper motion vectors of Fig. 3 from LHB (left). The resulting line image has then been convolved with a gaussian kernel to produce the criss-cross map in the middle, which is also shown in red in Figure 1 (left) of this work. On the right is the corresponding criss-cross map from our *Shape* model.

area covered by the nebula. Assign a finite constant brightness to every such line. Generate an image by adding together all lines. Finally, the result is convolved with a suitable kernel, like a gaussian with a width that is larger than the average separation between the vectors. In the regions where vectors converge the resulting image will increase in brightness and prominently reveal the regions where most velocity vectors meet. Details of the mapping theory and extensions to the scheme presented here will be published elsewhere (Steffen & Koning, submitted). We have implemented this simple procedure in the software *Shape*, which allows one to generate criss-cross maps from observations and models for immediate comparison.

3. The direction of proper motion vectors in BD+30 3639

From Figures 3 & 4 of LHB we determined the PAs and deviation δ from the radial direction by direct measurement. We estimate the error in the measurement to be of the order of 2° in PA and δ. The distribution of δ as a function of PA is plotted in Fig. 1 (right). We find that the distribution is not random around zero, as would be expected for a radial expansion with some random measurement errors. Instead, the deviation from radial direction follows approximately a sinusoidal pattern.

4. Modeling

We have used the 3D morpho-kinematic modeling and reconstruction software *Shape* (Steffen et al., 2011) to reconstruct the 3D structure of BD+30 3639 based on the available imaging and internal proper motion from LHB and P-V diagrams from Bryce & Mellema (1999). For this initial reconstruction, we only used the [NII] data as a reference, since they are expected to be more thinshell like in structure, rather than span a significant range in distance for every given direction from the central star. Working with thin shells reduces ambiguities in the reconstructions.

In this paper, we concentrate on explaining the sinusoidal pattern in Fig. 1 (right). We found two quite different explanations. Steffen, García-Segura & Koning (2009, SGK) showed that the hydrodynamics of bipolar planetary nebulae is likely to have a non-homologous expansion with a poloidal velocity component. Since BD+30 3639 has a bipolar molecular ejection, we investigated whether the observations could be explained by a velocity field similar to those found by SGK. We find that the observed deviations from a radial velocity pattern can be explained if a cylindrical component is added to a homologous velocity field starting at some distance from the central star. Furthermore, the cylindrical component on the far side of the nebula is much smaller than on the near side. Alternatively, the observed velocity vectors correspond mainly to structure on the near side. Although there is obscuration in the nebula, we find these solutions rather unlikely.

The second solution was found after introducing the new criss-cross mapping. Fig. 1 (left) shows the criss-cross map for BD+30 3639 superimposed on the observational composite image. There are well defined peaks at approx. 0.5 arcsec from the central star. This map shows that the kinematic center of expanding nebula is not located at the position of the central star. Figure 2 (right) is a model map which includes a 0.5 arcsec shift of the velocity field in the direction as deduced from the observed criss-cross map. In addition to a homologous velocity component, there is a random noise in the velocity vector components of 4 km/s in each cartesian direction, as well as a cylindrical velocity component of 12 km/s along the direction of the molecular outflows. The cylindrical component is suppressed near the equatorial ring. The substructure of the observed and modeled criss-cross maps is similar. However, the model map lacks the northern peak that is present in the observed map.

5. Discussion and Conclusions

The application to BD+30 3639 of our new criss-cross mapping technique leads us to conclude that the kinematic center is offset from the central star. The lines connecting the molecular outflow with the central star and the peaks of the criss-cross map suggests the tails of the outflows might be directed towards the newly deduced kinematic center (Fig. 1). This conclusion does require confirmation, since the elliptical beam of the molecular map is approximately aligned with the direction between the southern outflow and the peak and structure of the criss-cross map. This problem does not, however, occur for the northern component, which shows a similar alignment with the criss-cross structure.

Reasons for the offset of the kinematic center could be motion of the central star within the nebula. There is, however, no evidence for that, since the star appears to be well centered on the optical image of the nebula. Another option is the presence of a secondary object that is responsible for the ejection of the bipolar molecular outflow. The distance of the object would be of 600 AU or more from the central star. The fact that such an object has not been detect so far sets strong constraints on its nature. The molecular outflow might have distorted the velocity field producing the observed offset and deviations from a homologous expansion.

Acknowledgments. This work has been supported by grants from CONACYT 49447 and UNAM PAPIIT IN100410. N.K. received additional support from the Natural Sciences, Alberta Ingenuity Fund and Engineering Research Council of Canada and from the Killam Trust.

References

Bachiller, R., Forveille, T., Huggins, P.J., Cox, P., Maillard, J.P., 2000, A&A, 363, 25
Bryce, M., Mellema, G., 1999, MNRAS, 309, 731-738
Harrington, P., Lame, N.J., White, S., Borkowski, K., 1997, AJ, 113, 2147
Kastner, J.H., Soker, N., Vrtilek, S.D., Dgani, R., 2000, ApJ, 545, L57-L59s
Li, J., Harrington, J.P., Borkowski, K., 2002, ApJ, 123, 2676-2688
Shupe, D. L., Larkin, J. E., Knop, R. A., et al., 1998, ApJ, 498, 267
Steffen, W., García-Segura, Koning, N., 2009, ApJ, 691, 696-704
Steffen, W., Koning, 2010, Criss-cross mapping BD+30 3639: a new kinematic analysis technique, Astronomical Journal, submitted.
Steffen, W., Koning, N., Wenger, S., Morisset, C., Magnor, M., 2011, "Shape: A 3D Modeling Tool for Astrophysics", IEEE Trans. on Visualization & Computer Graphics, in press.

Asymmetric Planetary Nebulae V
A. A. Zijlstra, F. Lykou, E. Lagadec and I. McDonald
Jodrell Bank Centre for Astrophysics, Manchester, UK © 2011

From Bipolar to Elliptical: Morphological Changes in the Temporal Evolution of PN

M. Huarte Espinosa[1,2], A. Frank[1], B. Balick[3], O. De Marco[4], J. H. Kastner[5], R. Sahai[6] and E. G. Blackman[1]

[1]*Department of Physics and Astronomy, University of Rochester, 600 Wilson Boulevard, Rochester, NY, 14627-0171*

[2]*Kavli Institute for Cosmology Cambridge, Madingley Road, Cambridge CB3 0HA, UK*

[3]*Department of Astronomy, University of Washington, Seattle, WA 98195*

[4]*Department of Physics, Macquaurie University, Sydney NSW 2109, Australia*

[5]*Rochester Institute of Technology, 54 Lomb Memorial Drive, Rochester, NY 14623, USA*

[6]*NASA/JPL, 4800 Oak Grove Drive, Pasadena, CA 1109, USA*

Abstract. Proto-planetary nebulae (pPN) and planetary nebulae (PN) seem to be formed by interacting winds from asymptotic giant branch (AGB) stars. The observational issue that most pPN are bipolar but most older PN are elliptical is addressed. We present 2.5D hydrodynamical numerical simulations of episodic cooling interacting winds to investigate the long term evolution of PN morphologies. We track wind acceleration, decrease in mass-loss and episodic change in wind geometry from spherical (AGB) to collimated (pPN) and back to spherical again (PN). This outflow sequence is found to produce realistic PN dynamics and morphological histories. Effects from different AGB distributions and jet duty cycles are also investigated.
Keywords. Planetary Nebulae

1. Introduction

Planetary Nebulae are thick ionized plasma clouds that expand at $\sim 20\,\mathrm{km\,s^{-1}}$ away from an old, hot, intermediate-mass star. The nebulae show bipolar, elliptical, point symmetric, irregular, spherical and quadrupolar morphologies (for a review see 671). The interacting stellar wind model (ISW; 679) suggest that spherical PN form by the collision of the dust slow dense shell around an AGB star and the tenuous fast wind that it blows at the post-AGB phase. As opposed to PN, AGB envelopes are typically spherical, therefore, PN must be shaped as they evolve, by some mechanisms which are not clear yet (671). Generalized ISW models propose that bipolar PN form by the interaction of the post-AGB fast wind and either a toroidal AGN envelope (e.g. 676) or an aspherical AGB wind (e.g. 678). A binary system may cause asymmetries in the AGB wind; where either an AGB interacts with a companion or an AGB and its

companion share a common envelope evolution (for a review see 675). Magnetic fields (e.g. 672), the rotation of the AGB (e.g. 677) and photoionization heating from the central star (e.g. 680) have also been considered in PN shaping.

Jets are evident in high resolution sensitive observations of many pPN and young PN (e.g. 670; 682). The outflows appear to be bipolar, collimated and launched at $\sim 200\,\mathrm{km\,s^{-1}}$ from the vicinities of the central star. Jets are thought to shape PN, to form knots in the nebulae and also to yield point symmetric objects (e.g. 683).

Here we present numerical simulations of episodic interacting winds to address the observational issue that more than 50 % of pPN are bipolar but more than 50% of older PN are elliptical.

2. Model and methodology

Numerical simulations of interacting stellar winds are presented. We track wind acceleration, mass-loss history and episodic change in wind geometry. The equations of radiative hydrodynamics are solved in two-dimensions, with axisymmetry conditions, using the adaptive mesh refinement (AMR) code AstroBEAR (673). We use the tables of Dalgarno & McCray (674) to simulate optically thin cooling, ionization of H and He, and H_2 chemistry too. No gravitational or viscous or magnetic processes are considered.

The computational domain is a square representing $1\,\mathrm{pc}^2$. We use extrapolation boundary conditions in the upper, the lower and the right domain edges, and reflective conditions in the left edge. Cylindrical coordinates are used with the origin at the middle of the left boundary, $r \in (0, \sqrt{2})\,\mathrm{pc}$ and $\theta \in (-\pi/2, \pi/2)\,\mathrm{rad}$. The grid has 128^2 coarse cells and two AMR levels; an effective resolution of $\sim 400\,\mathrm{AU}$. We use BlueHive*, an IBM parallel cluster of the Center for Research Computing of the University of Rochester, to run each simulation for about 20 hrs, using 16 processors.

2.1. Wind episodes

We consider three wind episodes: the isotropic AGB wind, the collimated jet and the isotropic fast (post-AGB) wind. The AGB is the initial condition. Simulation 1 follows the interaction of the AGB wind and the jet, whereas Simulation 2 follows the interaction of the AGB and the fast wind. Simulation 3 tracks the interaction of the AGB wind, the jet which is ejected afterwards and the fast wind which comes after the jet (see Table 1).

The AGB wind is set throughout the domain with an ideal gas equation of state ($\gamma = 5/3$), a temperature of 500 K, a radial velocity of $10\,\mathrm{km\,s^{-1}}$ and a mass-loss of $10^{-5}\,\mathrm{M_\odot\,yr^{-1}}$. The jet is injected for 108 yr, only, in cells where $r < 6000\,\mathrm{AU}$, with a collimated horizontal velocity of $200\,\mathrm{km\,s^{-1}}$, the AGB's temperature and half of the AGB's density. The isotropic fast wind is continuously injected at $r < 6000\,\mathrm{AU}$, with a mass-loss that decreases in time from $5{\times}10^{-7}$ to $5{\times}10^{-9}\,\mathrm{M_\odot\,yr^{-1}}$, following the model

*https://www.rochester.edu/its/web/wiki/crc/index.php/BlueHive_Cluster

of Perinotto et al. (681). The fast wind accelerates from 200 to 2000 km s^{-1}, maintaining a constant ram pressure, and we keep a Mach 20 condition in the injection region.

Additionally, Simulations 4, 5, and 6 follow the interaction between the jet, the fast wind or both, respectively (see Table 1), and an initial AGB with a pole-to-equator density contrast of 1/2. We use the toroidal density distribution in equations (1) and (2) of Frank & Mellema (676)[†]. Finally, in Simulation 7, the fast wind interacts with a spherical AGB wind having a pole-to-equator velocity contrast of 2. This is modeled by multiplying the AGB's radial velocity by $1 + e^{-[\tan^{-1}(|y/x|)/0.3]^2}$ (see Table 1).

Table 1. Simulations and parameters.

Simulation	AGB wind form	Jet duration [×108 yr]	Fast wind duration [×1000 yr]
1	spherical	1	0.0
2	spherical	0	13.0
3	spherical	1	10.7
4	toroidal ρ	1	0.0
5	toroidal ρ	0	3.8
6	toroidal ρ	1	6.0
7	aspherical $\mathbf{v}$	0	13.0

3. Results and discussion

We present a summary of the simulation results, for details see Huarte Espinosa et al. 2010 (in prep.). Figure 1, top row, shows the evolution of Simulation 1. The jet collides with the AGB envelope, drives a bow shock and forms a central elliptical cavity. Jet injection ceases at 108 yr and gas expands passively afterwards. The lobe develops a bipolar morphology with a monotonically increasing aspect ratio (i.e. the ratio of its longer dimension to its shorter dimension) that reaches 4.5 in 13,283 yr. Conversely, Simulation 2 (middle row) follows the ISW model (679) closely. The fast wind quickly overtakes the AGB envelope, drives a bow shock on it, and a hot bubble (10^{7-8} K) forms between the envelope and the working surface of the fast wind. Gas is then pushed supersonically onto the envelope, producing a compressed, spherical and efficiently-cooling shell expanding at ~ 20 km s^{-1}. In Simulation 3 (bottom row), the jet forms a central bipolar cavity which is then blow form within by the isotropic fast wind. A hot bubble forms in the swept up region, bound by a compressed shell that quickly adopts an elliptical morphology and expands at ~ 20 km s^{-1} with a widely constant aspect ratio of 2. Simulation 3 shows how bipolar young PN transform into old larger elliptical nebulae, in agreement with observed PN morphological histories. In Simulations 4, 5 and 6 (not shown), the toroidal AGB envelope funnels any subsequent stellar outflow towards the pole and yields narrow-waisted bi-polar or bi-lobed objects consistently. The long term morphologies correlate with outflow histories. An elliptical rhombus-looking shell forms quickly and slowly expands homogeneously in Simulation 7 (not

[†]We use the referred equations for $\alpha = 1/2$ and $\beta = 1$.

shown), where the radiative hydro evolution occurs as in Sim. 2, but for the differences in the shell shape. In complementary simulations: gas was allowed to expands passive between the jet and the fast wind episodes; Sim. 3 was allowed to expand for longer (up to 26,500 yr); gas temperature was suddenly raised to 10,000 K everywhere, to crudely simulate the effects of photoionization from the central star. We found mild results in these experiments relative to the ones in Table 1.

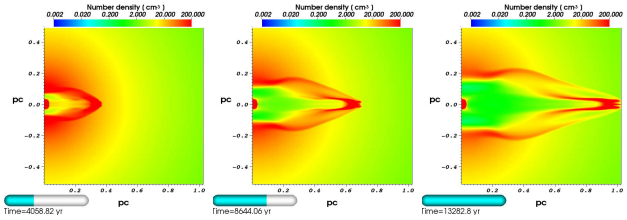

Simulation 1: AGB wind → jet

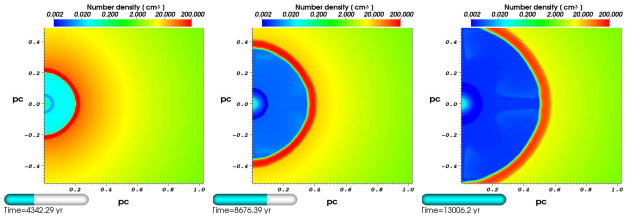

Simulation 2: AGB wind → fast wind

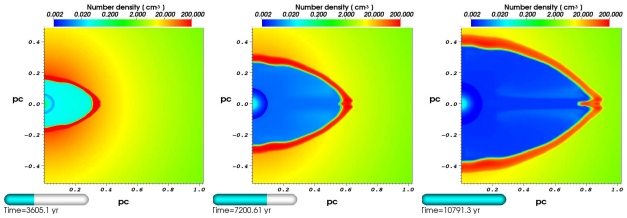

Simulation 3: AGB wind → jet → fast wind

Figure 1. Evolution of the gas density in logarithmic contours. A jet produces a narrow bipolar shell. An isotropic fast wind forms a spherical shell. A jet followed by a fast wind yields an elliptical shell.

Acknowledgments. The authors wish to thank the organizers of the meeting for their work and kindness. MHE thanks Jonathan Carroll for discussions.

References

Balick, B. 2000, in Asymmetrical Planetary Nebulae II: From Origins to Microstructures, edited by J. H. Kastner, N. Soker, & S. Rappaport, vol. 199 of Astronomical Society of the Pacific Conference Series, 41

Balick, B., & Frank, A. 2002, ARA&A, 40, 439

Blackman, E. G., Frank, A., & Welch, C. 2001, ApJ, 546, 288

Cunningham, A. J., Frank, A., Varnière, P., Mitran, S., & Jones, T. W. 2009, ApJS, 182, 519

Dalgarno, A., & McCray, R. A. 1972, ARA&A, 10, 375

de Marco, O. 2009, PASP, 121, 316

Frank, A., & Mellema, G. 1994, ApJ, 430, 800

Garcia-Segura, G. 1997, ApJ, 489, L189
Icke, V., Balick, B., & Frank, A. 1992, A&A, 253, 224
Kwok, S., Purton, C. R., & Fitzgerald, P. M. 1978, ApJ, 219, L125
Mellema, G. 1997, A&A, 321, L29
Perinotto, M., Schönberner, D., Steffen, M., & Calonaci, C. 2004, A&A, 414, 993
Sahai, R. 2000, in Asymmetrical Planetary Nebulae II: From Origins to Microstructures, edited by J. H. Kastner, N. Soker, & S. Rappaport, vol. 199 of Astronomical Society of the Pacific Conference Series, 209
Sahai, R., & Trauger, J. T. 1998, AJ, 116, 1357

Asymmetric Planetary Nebulae V
A. A. Zijlstra, F. Lykou, E. Lagadec and I. McDonald
Jodrell Bank Centre for Astrophysics, Manchester, UK © 2011

Mira: a wonderful prospect

C. J. Wareing

Jodrell Bank Centre for Astrophysics, The University of Manchester, Alan Turing Building, Manchester, M13 9PL, UK; research@cjwareing.net

Abstract. Since being named 'wonderful' in the 17th century for its peculiar brightness variability, Mira A has been the subject of extensive research and become the prototype for a whole class of 'Mira' variables. The primary star in a binary system, Mira A is reaching the end of its life and currently undergoing an extended period of enhanced mass-loss. Recent observations have revealed a surrounding arc-like structure and a stream of material stretching 12 light years away in opposition to the arc. In this conference paper, I will present our recent modelling of this cometary appearance as a bow shock with an accompanying tail of material ram-pressure-stripped from the head of the bow shock and predict the form of the PN which Mira A will eventually produce, drawing parallels with the highly evolved PN Sh 2-68.
Keywords. Planetary Nebulae

1. Introduction

Mira is now known to be the brighter star (Mira A) in a binary system and is the prototype for the class of 'Mira' variables: pulsating variable stars with very red colours and pulsation periods longer than 100 days. Reaching the end of its life, Mira has evolved off the Main Sequence and along the red giant branch. It is currently evolving along the asymptotic giant branch (AGB) on route to becoming a white dwarf before fading to obscurity. On the AGB, the star is losing mass via a relatively slow wind (5 km s^{-1}) which carries away approximately 3×10^{-7} solar masses of material per year, as inferred from CO line observations (Ryde et al. 2000). The second star in the binary system, Mira B, is accreting some of the ejected AGB material, but the orbital distance is so large that only a small fraction of the ejected AGB wind material is accreted. Mira B is usually classed as a white dwarf, but this is now somewhat controversial (Karovska et al. 2005; Ireland et al. 2007). What can be inferred is that any stellar wind from Mira B, whilst potentially fast, is most likely to be insignificant in mass flux and energy terms when compared to that of Mira A and unlikely to illuminate the surrounding structure owing to the small extent of the ionized zone around it (Matthews & Karovska 2006).

2. Recent Observations

During routine inspection of incoming UV images taken with the Galaxy Evolution Explorer satellite (GALEX), Martin et al. (2007) discovered a nebulosity near the location of Mira. Deeper observations revealed an arc-like feature to the South and a

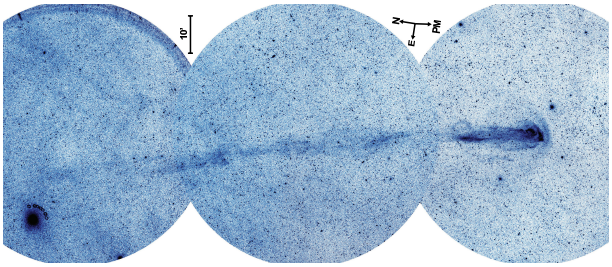

Figure 1. The mosaic'd UV images of the cometary structure surrounding the Mira system taken with GALEX. Note the consistency of the proper motion (PM) with the head of the bow shock. This figure is a reproduction from Wareing et al. (2007b), which is a version of the original observation published by Martin et al. (2007). Please consult these references for full details.

stream of material stretching northward of the location of Mira, extending over a total length of two degrees on the sky. Using the revised Hipparcos-based distance (Knapp et al. 2003) to Mira of 107 pc, Martin et al. estimated the spatial extent of the tail to be approximately 4pc. They found that the direction of the space velocity of 130 km s^{-1} was consistent with the head of the arc-like structure and postulated that the feature is a bow shock caused by motion through the interstellar medium (ISM). The nebulosity in the North is a tail of material ram-pressure stripped from the head of the bow shock. A mosaic of the deeper UV observations is reproduced in figure 1.

Martin et al. estimated the age of the tail to be 30,000 years, based on the time taken for Mira to travel the length of the tail and inferred that features in the tail provide an unprecedented record of Mira's wind-ISM interaction over that period. They suggested that the density variations along the tail reflect changes in the mass-loss rate, in particular reflecting thermal pulsing events (Vassiliadis & Wood 1993). Their search for counterparts at other wavelengths revealed only the knots behind the bow shock show Hα emission, with optical spectroscopy providing evidence that they have been shocked and ionized by the post-bow shock flow. Finally, Martin et al. consider in some depth the mechanism of the far UV emission observed from the tail. Ruling out dust scattered emission and ambient interstellar radiation, they propose that the emission is excited collisionally by the interaction of H_2 in the cool wake with hot electrons in the post-shock gas resulting from the bow shock which also entrains and deccelerates the wind. This they find consistent with the estimated age of the tail of 30,000 years.

3. A bow shock and tail model of Mira

Drawing a parallel between R Hya, the other example of an AGB star with a bow shock, and Mira, the author developed a model tuned to the parameters of Mira and

Figure 2. A slice through the density datacube 185,000 years into the AGB evolution at the position of the central star, parallel to the motion through the ISM.

performed hydrodynamic simulations following the AGB phase of evolution (Wareing et al. 2007b). The simulations fitted the position of the bow shock ahead of Mira A, the width of the bow shock across the position of Mira A and the length of the tail, although required a considerably longer time of approximately 450,000 years to produce the tail. The simulations were unable to reproduce the narrow tail and the author postulated that the first gap seen 1/3 of the way downstream from Mira could be explained by the star's possible recent entry into the Local Bubble, a low-density region of about 100 pc across in which the Sun is also located. An approximate 3D map of the Local Bubble is presented by Lallement et al. (2003): on their maps Mira would be located close to the edge but inside of this shell. This would also explain the narrowness of the tail, which is not reproduced by the author's previous simulation: as Mira moved though interstellar space, a smaller bow shock formed much closer to the star with a narrow tail, as observed beyond the gap under discussion here. Approximately 8pc downstream from its current location, Mira entered the lower density Local Bubble. The bow shock expanded according to the new ram pressure balance, during which time little material was ram-pressure stripped into the tail, directly leading to the gap in the tail. This also supports the low density of n_H=0.03 cm^{-3} of the local medium predicted by the author's previous simulation.

Our recent simulations test this Local Bubble idea. This model has the same parameter values as the models in Wareing et al. 2007b, except the ISM density is initially 25 times higher at n_H=0.75 cm^{-3}. Then, after 190,000 years of AGB evolution, the ISM density drops over the next 10,000 years to the level predicted by the current position of the bow shock, corresponding to Mira entering the Local Bubble. figure 2 above shows a point in the evolution before Mira enters the Local Bubble, demonstrating how the narrowness of the tail comes from the bow shock being much closer to the star. These results are consistent with Raga et al. 2008, who model the effect on the wind of the binary partner, and the poster produced by Raga et al. for this conference elsewhere in this volume, where they also test the idea of Mira entering the Local Bubble.

4. Future evolution of Mira and a comparison to Sh 2-68

The presence of bow shocks ahead of AGB stars was predicted before the observations of R Hya and Mira; simulation of the planetary nebula (PN) Sh 2-188 (Wareing et al. 2006) found that the only way to create the apparent shape of the nebula was to model both the PN phase of evolution and the preceding AGB phase of evolution. It was

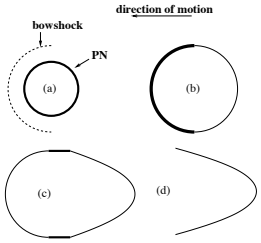

Figure 3. The four stages of PN-ISM interaction, as taken from Wareing et al. 2007a.

during the AGB phase that the shape of the PN was crucially defined by the bow shock which formed against the oncoming ISM. So Mira's planetary nebulae will be similar to Sh 2-188 *with the shape of the nebula already defined by the bow shock and tail we currently observe*.

figure 3 illustrates the probable future of Mira. At the end of the AGB stage, the fast, hot, much lower density wind Mira will start to produce will sweep up the surrounding material into a complex nebula (stage (a)). After the swept up shell has expanded far enough to reach the bow shock, its progress in that direction will effectively be stopped, whilst still expanding unhindered downstream (stage (b)). The interaction with the bow shock will introduce (another) asymmetry to the nebula, restricted to the outer parts of the nebula. Given how close the bow shock is to Mira, it's likely the PNe will reach this stage in a relatively short time of a few thousand years. As the PN-ISM interaction progresses, ram-pressure stripping of material from the head of the bow shock transfers the shell material towards the tail and the highest density regions (naively then also the brightest regions) are around the nebula, rather than at the head of the bow shock (stage (c)). As Mira is moving so quickly though the ISM, the system will evolve quickly through these stages of PN-ISM interaction, reaching the final stage (d) when the shell has been completely disrupted and all that is left is remnants of the structure in the tail. The PN Sh 2-68 (Kerber et al. 2002) is thought to be in this stage of evolution, with PN shell-like remnants in the area of a tail compared to the proper motion of the central star. A paper is in preparation on the structural appearance of this nebula.

On a final note, it is worth remarking the major question over Mira's tail which has not yet been answered. That is, the source of the curvature of the tail. If the tail represents several hundred thousand years of evolution, the simplest interpretation is that the galactic orbital motion of Mira is responsible for this curvature. Further work is in progress to investigate this possibility, although it is difficult to reconcile timescales with orbital motion and it possible that just a general background flow of ISM material is causing the apparent curvature.

Acknowledgments. The author would like to the thank the Scientific Organising Committee of APN5 for the opportunity to give an oral presentation at the conference.

References

Ireland, M. J. et al. 2007, ApJ, 662, 651

Karovska, M., Schlegel, E., Hack, W., Raymond, J. C., Wood, B. E. 2005, ApJ, 623, L137
Kerber, F., Guglielmetti, F., Mignani, R., Roth, M. 2002, A& A, 381, L9
Knapp, G. R., Pourbaix, D., Platais, I., Jorissen, A. 2003, A&A, 403, 993
Lallement, R., Welsh, B.Y., Vergely, J.L., Crifo, F., Sfeir, D. 2003, A&A, 411, 447
Martin, D.C. et al. 2007, Nature, 448, 780
Matthews, L. D., Karovska, M. 2006, ApJ, 637, L49
Raga, A., Cantó, J., De Colle, F., Esquivel, A., Kajdic, P., Rodríguez-González, A., Velázquez, P. F. 2008, ApJ, 680, L45
Ryde, N, Gustafsson, B., Eriksson, K, Hinkle, K. H. 2000, ApJ, 545, 945
Vassiliadis, E., Wood, P.R. 1993, ApJ, 413, 641
Wareing, C. J., et al., 2006a, MNRAS, 366, 387
Wareing, C. J., Zijlstra, A. A., O'Brien, T. J. 2007a, MNRAS, 382, 1233
Wareing, C. J., Zijlstra, A. A., O'Brien, T. J., Seibert, M. 2007b, ApJ, 670, L125

Asymmetric Planetary Nebulae V
A. A. Zijlstra, F. Lykou, E. Lagadec and I. McDonald
Jodrell Bank Centre for Astrophysics, Manchester, UK © 2011

Observations of dusty torii and compact disks around evolved stars: the high spatial resolution infrared view

Olivier Chesneau

H. Fizeau, Univ. Nice Sophia Antipolis, CNRS UMR 6525, Observatoire de la Côte d'Azur, Av. Copernic, F-06130 Grasse, France

Abstract. The recent high angular resolution observations have shown that the transition between a globally symmetrical giant and a source surrounded by a spatially complex environment occurs relatively early, as soon as the external layers of the stars are not tightly bound to the core of the star anymore. In this review, the emphasis will be put on the delineating the differences between the torus and disk classification through the presentation of many examples of near-IR and mid-IR high angular resolution observations. These examples cover the disks discovered in the core of some bipolar nebulae, post-AGB disks, the dusty environment around born-again stars and recent novae, and also the disks encountered around more massive evolved sources. We discuss the broad range of circumstances and time scales for which bipolar nebulae with disks are observed.
Keywords. Planetary Nebulae – Infrared interferometry – Stars: evolution

1. Preamble: Direct detection of binarity with high spatial resolution imaging

A major breakthrough on the study on asymmetrical Planetary Nebulae (PNs) has been the recognition by a large part of our community of the growing importance of binary systems as main shaping agent of the bipolar and asymmetrical PNs. Companions encompassing a large range of mass, from the stellar objects to jovian-mass planets are suspected to deeply influence the ejecta when the star reaches the AGBs or even as early as the RGB (707). This interaction can potentially influence dramatically the fate of the star, leading to poorly known evolutionary paths, influencing deeply the time scales of the different evolutionary stages, eventually bearing only little similarities compared to the time scales involved for the evolution of a single, naked star (720; 759). Nevertheless, it is still far from excluded that a single star may also provide the conditions for the shaping of an asymmetrical nebula, if it expels at one time or another some mass with a significant pole-to-equator density gradient (698).

Many detections of companion of PNs central stars were reported during this conference (699; 742, De Marco, Hrivnak, Hajduk, Miszalski...these proceedings) some based on difficult long-term spectral monitoring, and many on the recent extensive photometric campaigns from automated telescopes. The high spatial resolution techniques may at first sight represent a large potential for detecting some well-separated (2-100 milli-arcsecond, hereafter mas) companions, but they suffer from intrinsic constraints that do not allow them to currently play a significant role in that domain. Adaptive optics on 8m-class telescopes are mostly limited in terms of spatial resolution,

whilst optical interferometry has strong limitations in terms of contrast and imaging capabilities. The brighter the circumstellar environment and the central source, the harder will be the detectability of a small point-like structure in the close vicinity. The best case is the detection of low $Teff$ companions (Δ ~5mag, d~10-100mas) around hot, and preferentially naked sources for which it is easy to separate the SED of the stellar components. For a review of the methods used for detecting companions around low to intermediate mass stars, the reader is referred to Jorissen & Frankowski (731).

2. Defining the different kind of equatorial over-densities

Whatever the origin of the shaping process of an asymmetrical planetary nebula, an equatorial over-density of material is often involved in the models, and a growing number of observations unveil their presence at many stages of the star evolution. A wealth of new high spatial resolution techniques are now routinely available for the observer, namely the adaptive optics techniques, the speckle and lucky imaging techniques (often called the 'burst modes') in the optical and the infrared, and also the interferometry in the optical, infrared, millimetric and radio wavelengths. All these techniques have their own spatial resolution, sensitivity, contrast and astrometric constraints to the point that it is often quite difficult to compare and put into context the outcome of these observations. Hence, the vocabulary can often be somehow misleading. The detection of disks around evolved sources, as in post-AGB stars, may be closely associated with a high probability to see a binary system. However, this claim is highly dependent on the kind of structure encompassed in the 'disk' denotation, and one shall in the following sections precise further the equatorial overdensities, dividing them into the 'torus' (or 'outflowing wind'), and the 'stratified disks' families. The detection of compact, hot, dust-less accretion disks whose SEDs peak in the UV/B and that are hardly detectable by the above mentioned infrared techniques is out of the scope of this review.

2.1. Dusty torii: wind related equatorial overdensities

An equatorial overdensity is a region of higher density and lower expansion speed compared to the polar circumstellar regions. The kinematics of such a structure is dominantly radial, and the total angular momentum carried by the structure is limited. Equatorial overdensities are short-term structures (these are deflected winds), e.g. if the mass-loss ceases, then the fate of the material is to rapidly expand and vanish. The increase of density toward the equatorial plane can be ascribed easily by a dependence on the co-latitude of the star in spherical coordinates, and there is no mass nor energy storage in the structure.

To date, the best examples of such torii originate from millimetric interferometry that associates a good spatial resolution (~1") and an excellent spectral resolution (i.e. $1\,\mathrm{km.s^{-1}}$). One can cite as good example of expanding torii, Dinh-V-Trung et al. (713) or Peretto et al. (750). In the near- or mid-IR, it is more difficult to access the density distribution of the circumstellar material due to opacity effects. Nevertheless, if the scale height of the structure is comparable to its radial extension, without clear sign of marked density increase toward the equatorial plane, the torus hypothesis can be favored (761; 735). Long slit spectroscopy can provide further evidence for this classi-

fication when a significant expansion velocity (i.e. ∼15-40 km.s^{-1}) of the structure can be measured (729; 730).

2.2. Stratified disks

A disk exhibits a clear vertical stratification whose scale height is governed by the gas pressure only. Its aperture angle is very small (i.e. less than ∼10 degrees) and its kinematics is dominated by (quasi) Keplerian velocities, with a small expansion component ($\leq$10 km.s^{-1}). Thus its lifetime is much longer than structures blown within a wind, competing or even exceeding the reference time scale of a PN lifetime of a few tens of thousand years (758).

The density structure of a Keplerian disk is best ascribed in cylindrical coordinates with a radial law in the equatorial plane, and a vertical stratification perpendicular to this plane, for the hydrostatic equilibrium.

Such a model is used in a wealth of astronomical contexts, and in particular for the formation of Young Stellar Objects (YSOs). Some examples of application of a similar model can be found in this list: di Folco et al. (712); Fedele et al. (718); Wolf et al. (763); Dominik et al. (715).

The density law used in this model is

$$\rho\left(r,z\right)=\rho_0\left(\frac{R_*}{r}\right)^{\alpha}\exp\left[-\frac{1}{2}\left(\frac{z}{h\left(r\right)}\right)^2\right] \tag{1}$$

$$h\left(r\right)=h_0\left(\frac{r}{R_*}\right)^{\beta} \tag{2}$$

where r is the radial distance in the disk's mid-plane, R_* is the stellar radius, β defines the flaring of the disk, α defines the density law in the mid-plane and h_0 is the scale height at a reference distance (often 100 AU) from the star. Until recently, such Keplerian disks could only be studied by millimetric interferometry at the highest possible spatial resolution and for the closest targets. One of the best example of such disks is the Red Rectangle (762; 700). Again, the great advantage of such a technique is to provide both the spatial distribution and the kinematics of the source (701).

In absence of any information on the kinematics in the infrared due to the limited spectral resolution of optical interferometric observations, one has to rely on some indirect evidence to claim for the discovery of a stratified dusty disk, namely one has to prove at least that the disk opening angle is small, or better, that the density law follows radially and vertically the model described above. This is a possible task when the disk is seen close to edge-on. In this case, the radial and vertical directions are well separated on the sky. The best example is the discovery of the edge-on disk in the core of Menzel 3, very well fitted by a stratified disk model (704). However, our group has conducted some tests trying to invert the disks parameters from artificial interferometric datasets (Niccolini et al., A&A, accepted). When the disk is seen at low inclination, many degeneracies appear between the parameters of the vertical density law (such as the flaring parameter β), and the parameters of the radial law. Moreover, the size of the dust grains and and their composition affect also critically the fits.

To improve the constraints on the disk temperature law, a good approach is to perform near-IR and mid-IR observations using the AMBER and MIDI instruments of

the VLTI respectively. The post-AGB binary IRAS 08544-4431 was studied this way (710) and the same strategy is used for YSOs (734). It is more difficult to model the near-IR interferometric data due to the potential spatial complexity of the dusty disk's inner rim, and an intense theoretical and observational effort is currently performed, mainly in the YSOs community to better understand the so-called 'puffed-up inner rims' (716; 732; 755). A better determination of the spatial properties and fine chemical content of the dust forming region is a challenge for the future. Other interesting targets are the double-chemistry sources such as BM Gem, in which a companion has recently been discovered (728; 749; 748). These sources seem to harbor systemically an equatorially enhanced circumstellar environment, but there is no firm confirmation yet that the structure is best described by a torus or a disk.

3. Disk evolution

3.1. Stratified disk and binarity

Stratified disks detected in evolved systems are potentially highly correlated with binaries as demonstrated by Van Winckel and collaborators on the environment of binary post-AGBs (722; 759; 760; 708, Gielen et al. these proceedings). Grain growth, settling, radial mixing and crystallization are efficient in such an environment and the circumbinary disc of these sources seems to be governed by the same physical processes that govern the proto-planetary discs around young stellar objects. It seems that another distinctive character of these long-lived stratified disks as seen in the infrared would be their content in highly processed grains (743; 722; 727). The key point for the stabilization of the disk is to provide enough angular momentum (697; 753). A star may (hardly) supply this angular momentum via magnetic fields (719; 757). But even in this case the formation and stabilization of a Keplerian disk remains a challenge. Of course, this argument does not apply to the accretion disks encountered around YSOs, for which the difficulty in the contrary is to understand how the excess of angular momentum is dissipated. The angular momentum provided by a low-mass stellar or even sub-stellar companion may potentially have a dramatic influence on a growing RGB or AGB star (747; 699; 746; 745; 754). The presence of a stratified disk, and the associated Lindblad resonances, seem to be a key ingredient in the orbital evolution of the binary system. Without this ingredient, it is difficult to reproduce the observed morphology of the eccentricity - period diagram (Dermine T. et al., in press)

My personal opinion is that the discovery of a stratified disk with proven Keplerian kinematics is directly connected to the influence of a companion, albeit the few exceptions presented above, namely the Young Stellar Objects or the critical velocity rotating massive sources. This hypothesis must be confirmed by further observations.

3.2. Time scale of formation

When dealing with the theoretical building-up of a disk, time matters, and any constraint on the time-scale on which the observed structures were formed is of importance. An interesting study was presented by Huggins (726) on the close time-scale connection between jets and torii, based on many kinematical studies. π^1 Gruis is a good

example of a recently formed structure (752; 705). OH231.8+4.2 is another example of a similar process caught in the act in IRAS16342-3814 (717; 737; 711).

Some recent examples show how fast may be the building up of an equatorial overdensity. The born-again stars, V605 Aql (724) and the Sakurai's Object are surrounded by an equatorial overdensity with a large scale height that may be described as a torus (703). In the case of the Sakurai's object, the torus was detected in 2007, about 10 years after the dust began to form. A dense equatorial structure was formed even faster, in less than 2yrs, around the slow dust-forming nova V1280 Sco (702, Chesneau et al. in preparation). There is no doubt in this case that the slow ($\sim$500km.s^{-1}) ejecta from the outbursting nova were deeply affected by the common envelope phase that lasted more than tens of orbital period of the companion, leading to the fast formation of a bipolar nebula (see also Evans, these proceedings).

These examples show that as soon as the primary in a binary system gets larger and increases its mass-loss rate when evolving, the influence of a companion can rapidly focus the ejected material onto the equatorial plane of the system, leading to an equatorial overdensity, as already investigated theoretically (736; 756). This physical process depends on many parameters (mass ratio, orbital parameters, mass-loss rate of the primary...), but the efficiency is such that a statistically large number of targets might be deeply affected at one stage or another (699).

3.3. Time scale of dissipation and fate

The observations of the inner circumstellar structures around evolved sources have been to date too scarce to put them into an evolutionary sequence. As written above, the torii are supposed to expand and dissipate much faster than the Keplerian disks. One may even consider the extreme case in which a binary system surrounded by a stable circumbinary disk continuously replenished by the interaction of the stars may remain virtually unchanged for time scale as long as many 10^5-10^6years, as proposed for the Red Rectangle. An attempt of making a unified picture of the evolution of an interacting binary system involving the presence of a torus is presented in Frankowski & Jorissen (720).

What is the fate of a stratified disk? An 'old' dissipating disk can see its density and kinematical structure deeply affected by the fast evolving wind of the central star. Gesicki et al. (721) performed an in-depth kinematical study of the dissipating disk in the core of the M2-29 nebula (723). The torus found around Hen2-113 might also be dissipating under the influence of the fast radiative wind emitted by the Wolf-Rayet star in the core of the nebula (735).

4. Stratified disks around massive stars

There is now a large bunch of evidence that the disks encountered around Be stars and at least some B[e] supergiants are rotating close to Keplerian velocities (739). The Be stars are proven statistically to represent the tail of the fastest rotators among B stars, and their disks of plasma may be explained without invoking the influence of a companion, by a combination of an extreme centrifugal force at the equator and some pulsation properties of the star which leads to erratic ejection of material with high angular momentum (706; 725). By contrast, there is still no consensus for the more

massive supergiant counterparts, the B[e] stars that are surrounded by dense disks of plasma *and* dust. The dust survives much closer to this hot star than expected so far (738; 740; 714).The B[e] supergiant's rotation rate is strongly decreased by the increase of their radius while leaving the main sequence, and the rotation alone is probably far from being sufficient to explain the formation of a disk without invoking the influence of a close companion (741). Note also, that dusty circumbinary disk are commonly encountered around interacting binary systems (744).

The example of the A[e] supergiant HD 62623 is informative in this context (738, Millour, Meilland et al., submitted). HD 62623 is an A supergiant showing the characteristics of the 'B[e]' spectral type, namely a spectrum dominated by strong emission lines and a large infrared excess. Spectrally and spatially resolved observations of AMBER/VLTI in the Brγ line have shown that the supergiant lies in a cavity, and is surrounded by a dense disk of plasma. The Brγ line in the location of the central star is *in absorption* showing that the star is not different from a normal member of its class such as Deneb (A3Ia), albeit with a significantly large v*sini* of about 50km.s^{-1}. By contrast, the Balmer and Bracket lines are wider (*vsini* of about 120km.s^{-1}), and the AMBER observations demonstrated that they originate from a disk of plasma, most probably in Keplerian rotation (Millour, Meilland et al. submitted). In absence of any proof of binarity, it is often difficult to understand how such a dense equatorial disk could have been generated. However, HD62623 is a known binary with a stellar companion that orbits close to the supergiant with a period of about 136 days (751). The mass ratio inferred is very large, and the companion is probably a solar mass star. Plets et al. (751) proposed that an efficient angular momentum transfer occurs near the L2 Lagrangian point of the system, propelling the mass lost from the supergiant by its radiative wind and probably also by strong tides into a stable dense circumbinary disk (709, in the context of an AGB star). A similar idea was proposed by Dermine et al. (709) in relation with radiation pressure acting on the wind of AGB stars and modifying the Roche lobe geometry, therefore probably easing the formation of a circumbinary disk.

The comparison between the disks encountered around low and intermediate mass stars and those observed around the B[e] supergiants, a rare spectral type among the zoo of massive stars might not appear relevant at first sight. Yet, recent Spitzer observations of 9 LMC B[e] stars showed an interesting homogeneity of their spectra, and a great similarity with the spectra of post-AGBs harboring dense dusty disks (733). This tightens further the connection between B[e] stars and binarity.

Acknowledgments. This article benefited from fruitful discussions with many persons, and in particular Alain Jorissen.

References

Akashi, M., & Soker, N. 2008, New Astronomy, 13, 157
Balick, B., & Frank, A. 2002, ARA&A, 40, 439
Bear, E., & Soker, N. 2010, New Astronomy, 15, 483
Bujarrabal, V., Castro-Carrizo, A., Alcolea, J., & Neri, R. 2005, A&A, 441, 1031
Bujarrabal, V., van Winckel, H., Neri, R., Alcolea, J., Castro-Carrizo, A., & Deroo, P. 2007, A&A, 468, L45
Chesneau, O., Banerjee, D. P. K., Millour, F., Nardetto, N., Sacuto, S., Spang, A., Wittkowski, M., Ashok, N. M., Das, R. K., Hummel, C., Kraus, S., Lagadec, E., Morel, S., Petr-Gotzens, M., Rantakyro, F., & Schöller, M. 2008, A&A, 487, 223

Chesneau, O., Clayton, G. C., Lykou, F., de Marco, O., Hummel, C. A., Kerber, F., Lagadec, E., Nordhaus, J., Zijlstra, A. A., & Evans, A. 2009, A&A, 493, L17
Chesneau, O., Lykou, F., Balick, B., Lagadec, E., Matsuura, M., Smith, N., Spang, A., Wolf, S., & Zijlstra, A. A. 2007, A&A, 473, L29
Chiu, P., Hoang, C., Dinh-V-Trung, Lim, J., Kwok, S., Hirano, N., & Muthu, C. 2006, ApJ, 645, 605
Cranmer, S. R. 2009, ApJ, 701, 396
de Marco, O. 2009, PASP, 121, 316
de Ruyter, S., van Winckel, H., Maas, T., Lloyd Evans, T., Waters, L. B. F. M., & Dejonghe, H. 2006, A&A, 448, 641
Dermine, T., Jorissen, A., Siess, L., & Frankowski, A. 2009, A&A, 507, 891
Deroo, P., Acke, B., Verhoelst, T., Dominik, C., Tatulli, E., & van Winckel, H. 2007, A&A, 474, L45
Desmurs, J., Alcolea, J., Bujarrabal, V., Sánchez Contreras, C., & Colomer, F. 2007, A&A, 468, 189
di Folco, E., Dutrey, A., Chesneau, O., Wolf, S., Schegerer, A., Leinert, C., & Lopez, B. 2009, A&A, 500, 1065
Dinh-V-Trung, Bujarrabal, V., Castro-Carrizo, A., Lim, J., & Kwok, S. 2008, ApJ, 673, 934
Domiciano de Souza, A., Driebe, T., Chesneau, O., Hofmann, K., Kraus, S., Miroshnichenko, A. S., Ohnaka, K., Petrov, R. G., Preisbisch, T., Stee, P., Weigelt, G., Lisi, F., Malbet, F., & Richichi, A. 2007, A&A, 464, 81
Dominik, C., Dullemond, C. P., Waters, L. B. F. M., & Walch, S. 2003, A&A, 398, 607
Dullemond, C. P., & Monnier, J. D. 2010, ArXiv e-prints. 1006.3485
Etoka, S., & Diamond, P. J. 2010, ArXiv e-prints. 1004.2659
Fedele, D., van den Ancker, M. E., Acke, B., van der Plas, G., van Boekel, R., Wittkowski, M., Henning, T., Bouwman, J., Meeus, G., & Rafanelli, P. 2008, A&A, 491, 809
Frank, A., & Blackman, E. G. 2004, ApJ, 614, 737
Frankowski, A., & Jorissen, A. 2007, Baltic Astronomy, 16, 104
Gesicki, K., Zijlstra, A. A., Szyszka, C., Hajduk, M., Lagadec, E., & Guzman Ramirez, L. 2010, A&A, 514, A54
Gielen, C., van Winckel, H., Min, M., Waters, L. B. F. M., & Lloyd Evans, T. 2008, A&A, 490, 725
Hajduk, M., Zijlstra, A. A., & Gesicki, K. 2008, A&A, 490, L7
Hinkle, K. H., Lebzelter, T., Joyce, R. R., Ridgway, S., Close, L., Hron, J., & Andre, K. 2008, A&A, 479, 817
Huat, A., Hubert, A., Baudin, F., Floquet, M., Neiner, C., Frémat, Y., Gutiérrez-Soto, J., Andrade, L., de Batz, B., Diago, P. D., Emilio, M., Espinosa Lara, F., Fabregat, J., Janot-Pacheco, E., Leroy, B., Martayan, C., Semaan, T., Suso, J., Auvergne, M., Catala, C., Michel, E., & Samadi, R. 2009, A&A, 506, 95
Huggins, P. J. 2007, ApJ, 663, 342
Isella, A., Testi, L., & Natta, A. 2006, A&A, 451, 951
Izumiura, H., Noguchi, K., Aoki, W., Honda, S., Ando, H., Takada-Hidai, M., Kambe, E., Kawanomoto, S., Sadakane, K., Sato, B., Tajitsu, A., Tanaka, W., Okita, K., Watanabe, E., & Yoshida, M. 2008, ApJ, 682, 499
Jones, D., Lloyd, M., Mitchell, D. L., Pollacco, D. L., O'Brien, T. J., & Vaytet, N. M. H. 2010, MNRAS, 401, 405
Jones, D., Lloyd, M., Santander-García, M., López, J. A., Meaburn, J., Mitchell, D. L., O'Brien, T. J., Pollacco, D., Rubio-Díez, M. M., & Vaytet, N. M. H. 2010, ArXiv e-prints. 1006.5873
Jorissen, A., & Frankowski, A. 2008, in American Institute of Physics Conference Series, edited by P. Pellegrini, S. Daflon, J. S. Alcaniz, & E. Telles, vol. 1057 of American Institute of Physics Conference Series, 1
Kama, M., Min, M., & Dominik, C. 2009, A&A, 506, 1199
Kastner, J. H., Buchanan, C., Sahai, R., Forrest, W. J., & Sargent, B. A. 2010, AJ, 139, 1993
Kraus, S., Preibisch, T., & Ohnaka, K. 2008, ApJ, 676, 490

Lagadec, E., Chesneau, O., Matsuura, M., De Marco, O., de Freitas Pacheco, J. A., Zijlstra, A. A., Acker, A., Clayton, G. C., & Lopez, B. 2006, A&A, 448, 203
Mastrodemos, N., & Morris, M. 1998, ApJ, 497, 303
Matsuura, M., Chesneau, O., Zijlstra, A. A., Jaffe, W., Waters, L. B. F. M., Yates, J. A., Lagadec, E., Gledhill, T., Etoka, S., & Richards, A. M. S. 2006, ApJ, 646, L123
Meilland, A., Kanaan, S., Borges Fernandes, M., Chesneau, O., Millour, F., Stee, P., & Lopez, B. 2010, A&A, 512, A73
Meilland, A., Stee, P., Vannier, M., Millour, F., Domiciano de Souza, A., Malbet, F., Martayan, C., Paresce, F., Petrov, R. G., Richichi, A., & Spang, A. 2007, A&A, 464, 59
Millour, F., Chesneau, O., Borges Fernandes, M., Meilland, A., Mars, G., Benoist, C., Thiébaut, E., Stee, P., Hofmann, K., Baron, F., Young, J., Bendjoya, P., Carciofi, A., Domiciano de Souza, A., Driebe, T., Jankov, S., Kervella, P., Petrov, R. G., Robbe-Dubois, S., Vakili, F., Waters, L. B. F. M., & Weigelt, G. 2009, A&A, 507, 317
Miroshnichenko, A. S. 2007, ApJ, 667, 497
Miszalski, B., Acker, A., Moffat, A. F. J., Parker, Q. A., & Udalski, A. 2009, A&A, 496, 813
Murakawa, K., Ueta, T., & Meixner, M. 2010, A&A, 510, A30
Netolický, M., Bonneau, D., Chesneau, O., Harmanec, P., Koubský, P., Mourard, D., & Stee, P. 2009, A&A, 499, 827
Nordhaus, J., & Blackman, E. G. 2006, MNRAS, 370, 2004
Nordhaus, J., Blackman, E. G., & Frank, A. 2007, MNRAS, 376, 599
Nordhaus, J., Spiegel, D. S., Ibgui, L., Goodman, J., & Burrows, A. 2010, ArXiv e-prints. 1002.2216
Ohnaka, K., Driebe, T., Hofmann, K., Leinert, C., Morel, S., Paresce, F., Preibisch, T., Richichi, A., Schertl, D., Schöller, M., Waters, L. B. F. M., Weigelt, G., & Wittkowski, M. 2006, A&A, 445, 1015
Ohnaka, K., Izumiura, H., Leinert, C., Driebe, T., Weigelt, G., & Wittkowski, M. 2008, A&A, 490, 173
Peretto, N., Fuller, G., Zijlstra, A., & Patel, N. 2007, A&A, 473, 207
Plets, H., Waelkens, C., & Trams, N. R. 1995, A&A, 293, 363
Sacuto, S., Jorissen, A., Cruzalèbes, P., Chesneau, O., Ohnaka, K., Quirrenbach, A., & Lopez, B. 2008, A&A, 482, 561
Soker, N. 1997, ApJS, 112, 487
Soker, N., & Rappaport, S. 2000, ApJ, 538, 241
Tannirkulam, A., Harries, T. J., & Monnier, J. D. 2007, ApJ, 661, 374
Theuns, T., & Jorissen, A. 1993, MNRAS, 265, 946
ud-Doula, A., & Owocki, S. P. 2002, ApJ, 576, 413
van Winckel, H. 2003, ARA&A, 41, 391
Van Winckel, H. 2007, Baltic Astronomy, 16, 112
Van Winckel, H., Lloyd Evans, T., Reyniers, M., Deroo, P., & Gielen, C. 2006, Memorie della Societa Astronomica Italiana, 77, 943
Verhoelst, T., Waters, L. B. F. M., Verhoeff, A., Dijkstra, C., van Winckel, H., Pel, J. W., & Peletier, R. F. 2009, A&A, 503, 837
Witt, A. N., Vijh, U. P., Hobbs, L. M., Aufdenberg, J. P., Thorburn, J. A., & York, D. G. 2009, ApJ, 693, 1946
Wolf, S., Padgett, D. L., & Stapelfeldt, K. R. 2003, ApJ, 588, 373

Asymmetric Planetary Nebulae V
A. A. Zijlstra, F. Lykou, E. Lagadec and I. McDonald
Jodrell Bank Centre for Astrophysics, Manchester, UK © 2011

Stable discs around Galactic and LMC post-AGB binaries

Clio Gielen[1], Hans Van Winckel[1], Michiel Min[2], Rens Waters[3], Carsten Dominik[3,4] Tom Lloyd Evans[5], Mikako Matsuura[6], Pieter Deroo[7], and the SAGE-Spec team[8]

[1]*Instituut voor Sterrenkunde, Katholieke Universiteit Leuven, Celestijnenlaan 200D, B-3001 Leuven, Belgium*

[2]*Astronomisch Instituut Utrecht, Universiteit Utrecht, Princetonplein 5, 3584 CC Utrecht, The Netherlands*

[3]*Sterrenkundig Instituut 'Anton Pannekoek', Universiteit Amsterdam, Kruislaan 403, 1098 Amsterdam, The Netherlands*

[4]*Department of Astrophysics, Radboud University Nijmegen, PO Box 9010, 6500 GL Nijmegen, The Netherlands*

[5]*SUPA, School of Physics and Astronomy, University of St Andrews, North Haugh, St Andrews, Fife KY16 9SS, UK*

[6]*UCL-Institute of Origins, Department of Physics and Astronomy, University College London, Gower Street, London WC1E 6BT, UK*

[7]*Jet Propulsion Laboratory, 4800 Oak Grove Drive, Pasadena, CA 91109, US*

[8]*http://sage.stsci.edu/team_N2.php*

Abstract. In this work we present the results of our study on a particular class of Galactic and extragalactic evolved stars, which are part of a binary system, and surrounded by a stable dusty disc. By combining spectroscopic, photometric and interferometric observations with detailed models describing dust properties and disc structure, we investigate the exact disc composition and structure. With this study we hope to trace the evolution of these evolved binaries and their disc, and determine the impact of the disc on the entire system.
Keywords. Planetary Nebulae – Stars: AGB and post-AGB – Binaries

1. Late phases of stellar evolution

One of the major questions in current research is whether the predominantly symmetrical outflows during the AGB phase can produce the observed wide variety in proto-PNe (PPNe) and PNe shapes and structures, including spherical, point symmetric, axisymmetric and bipolar nebulae. During this short transition time, the star and its circumstellar envelope must be subject to fundamental and rapid changes in structure, mass loss and geometry (765; 779).

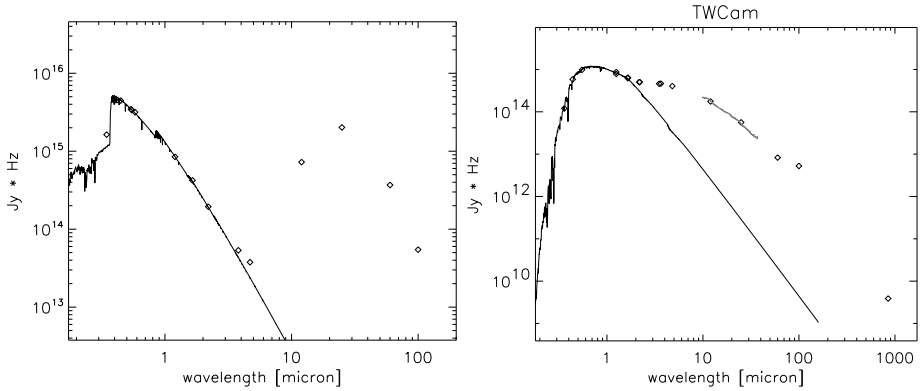

Figure 1. Spectral energy distributions of a typical outflow source (HD 187885, left) and a disc source (TW Cam, right). The outflow source is characterised by a double-peaked SED, dominated by cool dust, which resides at larger distances from the central star. The disc source shows a very broad infrared excess, showing the presence of both hot and cool dust.

There is now growing evidence that the processes in the strongly bipolar PPNe and PNe occur because of strong interactions in a binary system (e.g. 767). Many of these PNe have structures, such as bipolar lobes, jets, rings, dusty discs and tori, which are often explained by common envelope binary interactions, which is a badly understood process by itself.

Direct evidence for the suspected high binary rate in PNe however is still lacking, but this is no longer the case for post-AGB stars (780). Optically-bright post-AGB stars are thus invaluable to study the transition region between the AGB and the PNe phase.

2. Binary post-AGB stars

With the discovery of the first binary post-AGB stars, it became clear that these evolved stars have common observational characteristics, such as a broad infrared excess.

The observed broad IR excess in these binary post-AGB stars points to the presence of both hot and cool dust around the star (Fig. 1). De Ruyter et al. (769) showed that, for all stars, the hot dust is close to sublimation temperature ($\sim$ 1500 K). An outflow model is not adequate to explain the presence of such hot dust, since the near-infrared excess is expected to disappear within years after the cessation of the dusty mass loss. Also, the post-AGB stars are currently too hot to produce a strong dusty outflow. The dust must thus reside in a long-lived, stable reservoir close to the star. This leads us to suspect that these objects are surrounded by a stable Keplerian disc.

The specific observational characteristics allowed for systematic search for these visually bright objects and, so far, more than 70 Galactic objects have been discovered (769). For these stars our group started an extensive multi-wavelength study, including radial velocity monitoring, high-spectral resolution optical and infrared studies, sub-millimetre observations, and high-spatial resolution interferometric studies.

The formation of the disc is still a badly understood process, probably a result of non-conservative Roche Lobe overflow during the evolution in a binary system (see Verhoelst et al., these proceedings). To detect this binary motion, we started an extensive radial velocity monitoring programme, which confirmed the binary hypothesis and gave a typical semi-major axis for the orbit of around 1 AU (780). Given the effective temperature of the central star and its high luminosity, all the discs must be circumbinary, since the orbits all lie well within the sublimation radius of the dust. The mass functions calculated from the orbit indicate that the companion is likely a main-sequence star.

So far we have orbital parameters for about 30 sources, with orbital periods ranging from 100 to 2000 days and high eccentricities, up to 0.6 (see Gorlova et al., these proceedings). This is surprising, since theory predicts efficient circularisation by tidal forces on very short time scales.

All orbits discovered so far are too small to have accommodated a full-grown AGB star. This implies that the system must have been subject to severe binary interaction, while the evolved star was at giant dimension.

2.1. The circumbinary disc

The presence of the circumbinary disc has an impact on several observational characteristics of the post-AGB star:

- The strong infrared excess, $L_{IR}/L_* > 40\%$ for most stars, shows that significant amounts of circumstellar material are present, to reprocess the incoming stellar light. Surprisingly, a very low total reddening towards these stars is observed. This is clear evidence for a non-spherical circumstellar environment (CE).

- The binary disc sources are characterised by a depletion pattern in their photospheres (e.g. 781; 775). Generally, a lack of carbon or s-process enhancement is found. These stars apparently did not undergo a third dredge-up process on the AGB, even though they have initial masses which would theoretically make them evolve to carbon stars. The abundance pattern is the result of gas-dust separation in the CE, followed by a re-accretion of the gas component, which is now poor in refractory elements. Waters et al. (782) already proposed that the most likely circumstance for this process to occur is when the dust is trapped in a disc.

- Recent interferometric studies indeed confirm the very compact nature of the circumstellar material (770; 771). All disc sizes are very similar, with N-band sizes between $30 - 50$ AU, although the geometrical location of different dust components can differ significantly. Some objects show crystalline dust species close to the inner rim, others show strong processing throughout the disc.

- Kinematical information of a few objects detected in CO shows typical rotation velocities instead of outflows (e.g. 766), again confirming the presence of a Keplerian disc.

- Submillimetre measurements (768, Gielen et al. in prep.) indicate the presence of large grains (> cm-size) in the CE. A disc is an ideal environment for grain growth, since it is a long-lived stable reservoir, with relatively high densities.

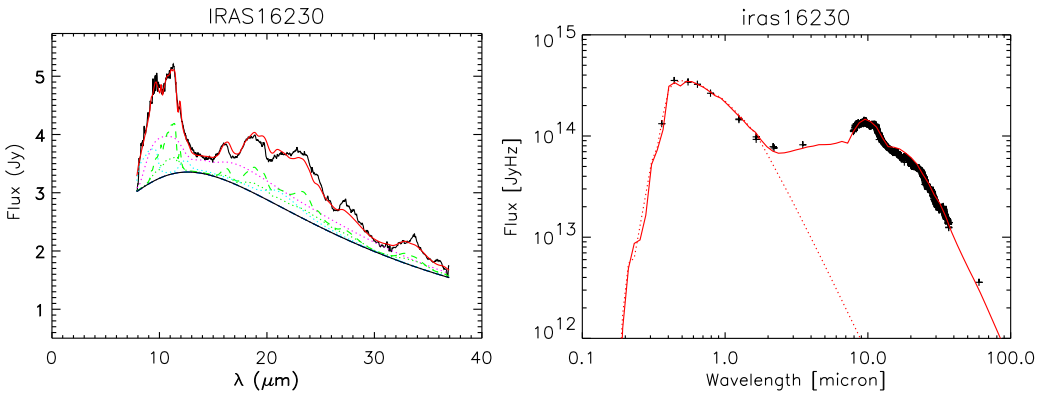

Figure 2. Left: Result from our full-spectrum fitting. The observed spectrum (black) is plotted together with the best model fit (red solid line) and the continuum (black solid line). Right: Result from our 2D disc modelling. Observations are represented by crosses; the underlying Kurucz model is given by the dotted line. The full line represents the SED of the disc model.

These large grains have smaller dust-settling times, causing the disc to be inhomogeneous, consisting of small hot grains in the surface layer of the disc and a cool mid-plane of mainly large grains.

2.2. Similar sources in the LMC

The first extragalactic RV Tauri stars, pulsating post-AGB stars with alternating deep and shallow minima in their lightcurves, in the LMC were discovered by the MACHO experiment (764). Recent chemical studies on a few RV Tauri stars (778; 773), selected from those reported by Alcock et al. (764), show that, like in the Galaxy, the disc candidates display the depletion pattern in their photospheres.

More recently the SAGE (Surveying the Agents of Galaxy Evolution) Spitzer LMC survey (776) observed the LMC, using all photometric bands of Spitzer IRAC/MIPS instruments. Thanks to the release of this database we found that the LMC post-AGB objects have infrared excesses similar to the Galactic sources. Also, a search for other post-AGB disc sources in this survey, based on their location in colour-colour diagrams, resulted in a list of about 650 disc candidates (van Aarle et al., these proceedings). Thanks to the follow-up SAGE-Spec programme we also have Spitzer IRS spectra for the LMC objects (774).

3. Disc composition

To study the mineralogy of the disc, we used Spitzer mid-infrared spectra. So far, we have spectra for 33 Galactic and 24 extragalactic LMC sources. Using a full-spectral fit routine (see Fig.2), we determined the parameters, such as composition and temperature, of the dust responsible for the observed spectra (772).

All sample stars show signatures of oxygen-rich dust species in their infrared spectra, more specifically amorphous and crystalline silicates. Only four stars display evidence for polycyclic aromatic hydrocarbons (PAHs).

The magnesium-rich end members of crystalline silicates seem to prevail in the spectra, with strong emission due to forsterite, and to lesser extent enstatite. From our full spectral fitting we also find that the amorphous dust might be Mg-rich. Detailed chemical studies of these stars (e.g. 775; 773) have shown that the stellar photospheres are devoid of iron, with the iron instead being locked up in the dust of the disc. If no iron is detected in the observed dust species, this could imply that iron is stored in the form of metallic iron or iron oxide, which have no distinct observable dust signatures.

We find that the discs are the ideal environment for strong dust grain processing to occur, both in grain growth and crystallinity. For our sample stars, the mass fraction in crystalline grains ranges from 10 to 70%, which is much higher than what is observed in outflow sources. The observed peak-to-continuum ratio shows that, on average, grain sizes above 0.1 μm prevail. There thus seems to be a removal of the smallest grains in the disc surface layers. Several sources show strong crystalline emission features at longer wavelengths, coming from rather cool crystalline dust grains in the disc. Crystalline dust is typically formed close to the inner rim, where temperatures are high enough for crystallinisation to occur. The presence of cool crystalline grains shows that either radial mixing must be very efficient or that the grains have a crystallinisation process which is already efficient at low temperatures.

So far, no clear difference is found in the disc composition of the Galactic and extragalactic sources. Also, no correlation is found between the observed dust parameters and other characteristics, such as the central star or binary orbit.

4. Disc geometry

To determine the structure of the discs, we performed 2D disc modelling on the observed photometry and spectroscopy of the Galactic and LMC disc sources (see Fig. 2), using the MCMax radiative transfer code (777). We found that a good fit is obtained with a passively irradiated, self-shadowed disc with a puffed-up inner rim. The inner radius of the disc is found slightly below the dust sublimation radius, but the outer radius is unfortunately less-well constrained. Typical values for the inner and outer radius are 2-20 AU and 100-500 AU, respectively. Dust masses range from 10^{-6}-10^{-4}M$_{\odot}$, with a surface density powerlaw > -2, using a gas-to-dust ratio of 100.

5. Conclusions

Our studies show that, both in our Galaxy and beyond, circumbinary discs around evolved stars are clearly present, and are a common by-product of binary evolution.

Both from our mineralogy study and from our disc modelling, we found that the chemical and physical properties of these discs around evolved binaries are very similar to those seen in proto-planetary discs around young stars, which is remarkable since these discs have very different formation histories. All discs are oxygen rich, and thus formed when the star was oxygen rich. In both disc types, dust processing is very

effective: large grain sizes prevail and the crystallinity is very high. The observed correlation between the evolutionary phase and the disc parameters found for young stars, is not yet observed in our limited sample of evolved binary stars.

Clearly, many open questions still remain on the formation, structure and evolution of these circumbinary discs around evolved stars, and the impact the disc has on the evolution of the central binary system. The interaction in the binary system is fundamental in trapping part of the dust in a stable circumbinary environment, and determines the further evolution of the binary star and the disc.

References

Alcock, C., Allsman, R. A., Alves, D. R., Axelrod, T. S., Becker, A., Bennett, D. P., Cook, K. H., Freeman, K. C., Griest, K., Lawson, W. A., Lehner, M. J., Marshall, S. L., Minniti, D., Peterson, B. A., Pollard, K. R., Pratt, M. R., Quinn, P. J., Rodgers, A. W., Sutherland, W., Tomaney, A., & Welch, D. L. 1998, AJ, 115, 1921

Balick, B., & Frank, A. 2002, ARA&A, 40, 439

Bujarrabal, V., Van Winckel, H., Neri, R., Alcolea, J., Castro-Carrizo, A., & Deroo, P. 2007, A&A, 468, L45

De Marco, O., Hillwig, T. C., & Smith, A. J. 2008, AJ, 136, 323

De Ruyter, S., Van Winckel, H., Dominik, C., Waters, L. B. F. M., & Dejonghe, H. 2005, A&A, 435, 161

De Ruyter, S., Van Winckel, H., Maas, T., Lloyd Evans, T., Waters, L. B. F. M., & Dejonghe, H. 2006, A&A, 448, 641

Deroo, P., Acke, B., Verhoelst, T., Dominik, C., Tatulli, E., & van Winckel, H. 2007, A&A, 474, L45

Deroo, P., Van Winckel, H., Verhoelst, T., Min, M., Reyniers, M., & Waters, L. B. F. M. 2007, A&A, 467, 1093

Gielen, C., Van Winckel, H., Min, M., Waters, L. B. F. M., & Lloyd Evans, T. 2008, A&A, 490, 725

Gielen, C., Van Winckel, H., Reyniers, M., Zijlstra, A., Lloyd Evans, T., Gordon, K. D., Kemper, F., Indebetouw, R., Marengo, M., Matsuura, M., Meixner, M., Sloan, G. C., Tielens, A. G. G. M., & Woods, P. M. 2009, A&A, 508, 1391

Kemper, F., Woods, P. M., Antoniou, V., Bernard, J., Blum, R. D., Boyer, M. L., Chan, J., Chen, C., Cohen, M., Dijkstra, C., Engelbracht, C., Galametz, M., Galliano, F., Gielen, C., Gordon, K. D., Gorjian, V., Harris, J., Hony, S., Hora, J. L., Indebetouw, R., Jones, O., Kawamura, A., Lagadec, E., Lawton, B., Leisenring, J. M., Madden, S. C., Marengo, M., Matsuura, M., McDonald, I., McGuire, C., Meixner, M., Mulia, A. J., O'Halloran, B., Oliveira, J. M., Paladini, R., Paradis, D., Reach, W. T., Rubin, D., Sandstrom, K., Sargent, B. A., Sewilo, M., Shiao, B., Sloan, G. C., Speck, A. K., Srinivasan, S., Szczerba, R., Tielens, A. G. G. M., van Aarle, E., Van Dyk, S. D., van Loon, J. T., Van Winckel, H., Vijh, U. P., Volk, K., Whitney, B. A., Wilkins, A. N., & Zijlstra, A. A. 2010, PASP, 122, 683

Maas, T., Van Winckel, H., & Lloyd Evans, T. 2005, A&A, 429, 297

Meixner, M., Gordon, K. D., Indebetouw, R., Hora, J. L., Whitney, B., Blum, R., Reach, W., Bernard, J.-P., Meade, M., Babler, B., Engelbracht, C. W., For, B.-Q., Misselt, K., Vijh, U., Leitherer, C., Cohen, M., Churchwell, E. B., Boulanger, F., Frogel, J. A., Fukui, Y., Gallagher, J., Gorjian, V., Harris, J., Kelly, D., Kawamura, A., Kim, S., Latter, W. B., Madden, S., Markwick-Kemper, C., Mizuno, A., Mizuno, N., Mould, J., Nota, A., Oey, M. S., Olsen, K., Onishi, T., Paladini, R., Panagia, N., Perez-Gonzalez, P., Shibai, H., Sato, S., Smith, L., Staveley-Smith, L., Tielens, A. G. G. M., Ueta, T., Dyk, S. V., Volk, K., Werner, M., & Zaritsky, D. 2006, AJ, 132, 2268

Min, M., Dullemond, C. P., Dominik, C., de Koter, A., & Hovenier, J. W. 2009, A&A, 497, 155

Reyniers, M., & Van Winckel, H. 2007, A&A, 463, L1

Sahai, R., Morris, M., Sánchez Contreras, C., & Claussen, M. 2007, AJ, 134, 2200
Van Winckel, H., Lloyd Evans, T., Briquet, M., De Cat, P., Degroote, P., De Meester, W., De Ridder, J., Deroo, P., Desmet, M., Drummond, R., Eyer, L., Groenewegen, M. A. T., Kolenberg, K., Kilkenny, D., Ladjal, D., Lefever, K., Maas, T., Marang, F., Martinez, P., Østensen, R. H., Raskin, G., Reyniers, M., Royer, P., Saesen, S., Uytterhoeven, K., Vanautgaerden, J., Vandenbussche, B., van Wyk, F., Vučković, M., Waelkens, C., & Zima, W. 2009, A&A, 505, 1221
Van Winckel, H., Waelkens, C., Waters, L. B. F. M., Molster, F. J., Udry, S., & Bakker, E. J. 1998, A&A, 336, L17
Waters, L. B. F. M., Trams, N. R., & Waelkens, C. 1992, A&A, 262, L37

Asymmetric Planetary Nebulae V
A. A. Zijlstra, F. Lykou, E. Lagadec and I. McDonald
Jodrell Bank Centre for Astrophysics, Manchester, UK © *2011*

Dusty discs around evolved stars observed at high angular resolution

F. Lykou[1], A. A. Zijlstra[1], O. Chesneau[2], E. Lagadec[3] and P. G. Tuthill[4]

[1]*Jodrell Bank Centre for Astrophysics, Alan Turing Building, The University of Manchester, Oxford Road, M13 9PL, Manchester, UK*

[2]*Observatoire de la Côte d'Azur, Dept. Fizeau, Avenue Copernic, 06130 Grasse, France*

[3]*European Southern Observatory, Karl Schwarzschild Str. 2, Garching 85748, Germany*

[4]*Sydney Institute for Astronomy, School of Physics, University of Sydney, NSW 2006, Australia*

Abstract. We present the discovery of dusty, edge-on discs around evolved stars at different evolutionary stages. Characterising the dusty discs provides invaluable constraints on the processes that lead to these impressive nebulae. M2-9 and Sakurai's Object were observed with MIDI on the Very Large Telescope Interferometer (VLTI) providing a resolution of 0.01 arcsec in the mid-infrared. The first object contains a disc composed of silicate dust, while the second contains a disc-like structure of carbonaceous material. The dusty discs are aligned with the minor axis of the bipolar nebula (or a density enhancement on the round nebula of Sakurai's Object) and their inner rim radii are less than 100AU. The properties of each disc have been explored with the means of radiative transfer modelling.
Keywords. Planetary nebulae – post-AGB stars – Techniques: interferometry

1. Planetary nebulae shaping and discs

Since APN4 three years ago, it is now well accepted that bipolar planetary nebulae (PNe) are primarily shaped by binaries, whether that is by tidal forces or magnetic field interactions between the components. We are investigating the significance of dusty discs in the cores of PNe, the recurrency of such structures and their importance in the shaping mechanisms. The predictions have shown that they might assist in the collimation of stellar ejecta (787).

2. Infrared interferometry

Dusty structures, such as discs (torii, spirals etc.), are rather small in size (approx. 1/1000) compared to the planetary nebulae that surround them and most cannot be resolved even with the largest of optical telescopes ($\theta \sim 0.1''$).

This restriction can be lifted with the introduction of infrared interferometry. We have used the VLTI and its instrument MIDI (789), a 2-beam recombiner with a maximum baseline of 200m and a spectral resolution of R=230, that produces spectrally dispersed visibilities in the N band (8-13.5μm).

The source's information can be recovered from the visibilities, namely the Fourier Transform of the source's brightness, a complex function with an amplitude's absolute value ranging between $0 < |V^2| < 1$. Sources with amplitude near zero are considered resolved, while those with a value near one are unresolved.

In order to reconstruct a source's image from the interferometric data, one must be able to recover both amplitudes and phases from the Fourier plane. The presence of a disc can be inferred by the decrease in visibility over a clockwise rotation of the projected baselines above the core of a bipolar planetary nebula from the polar axis toward the equatorial plane. Due to atmospheric effects, the phase signals recorded by MIDI are corrupted and image reconstruction is strictly model dependent. For our observations of dusty discs in planetary nebulae, we used MC3D, a Monte Carlo radiative transfer code (792; 791) that enabled us to reproduce the observed visibilities and spectra by assuming the chemical composition of the discs, as well as defining their geometric properties.

3. M2-9

This extremely bipolar planetary nebula with a tight waist was a follow-up observation to its spectrophotometric twin Menzel 3 (784). It is a young PN with a lighthouse beam that indicates a period between 90-120 years for a binary system composed of a red giant (primary) and a white dwarf (secondary) with an approximate separation of 15 AU.

As in the case of Menzel 3, MIDI has detected a disc around the core of M2-9 (Lykou et al., A&A accepted). The disc is composed of amorphous silicates with small traces of forsterite. Its geometric size is 15-900 AU with an enclosed dust mass of 1.5×10^{-5} $M_{\odot}$. We adopted a new distance of 1.3 kpc from our model fitting to the observed visibilities (Fig. 1) in accordance with new estimations (R. Corradi, private communication). The disc is still evolving as it is truncated by the companion, which in turn is expected to be surrounded by an accretion disc.

4. Sakurai's Object

An eruptive event in 1995 gave birth to Sakurai's Object, when a pre-WD star experienced a helium flash and re-ascended the AGB. The star is hidden behind a dusty cloud of carbonaceous material since 2002. Its flux has dropped significantly since then and its blackbody peak has moved towards longer wavelengths, indicating an expanding and cooling cloud (see Fig.1 of Chesneau et al. (783)). MIDI resolved a disc-like structure in 2007 of 65-500 AU, with a dusty component of 6×10^{-5} $M_{\odot}$ of amorphous carbon (783).

The round planetary nebula (~10,000 years old) that engulfs Sakurai's Object was found to have a certain density enhancement in [OIII] (785) at a position angle of ap-

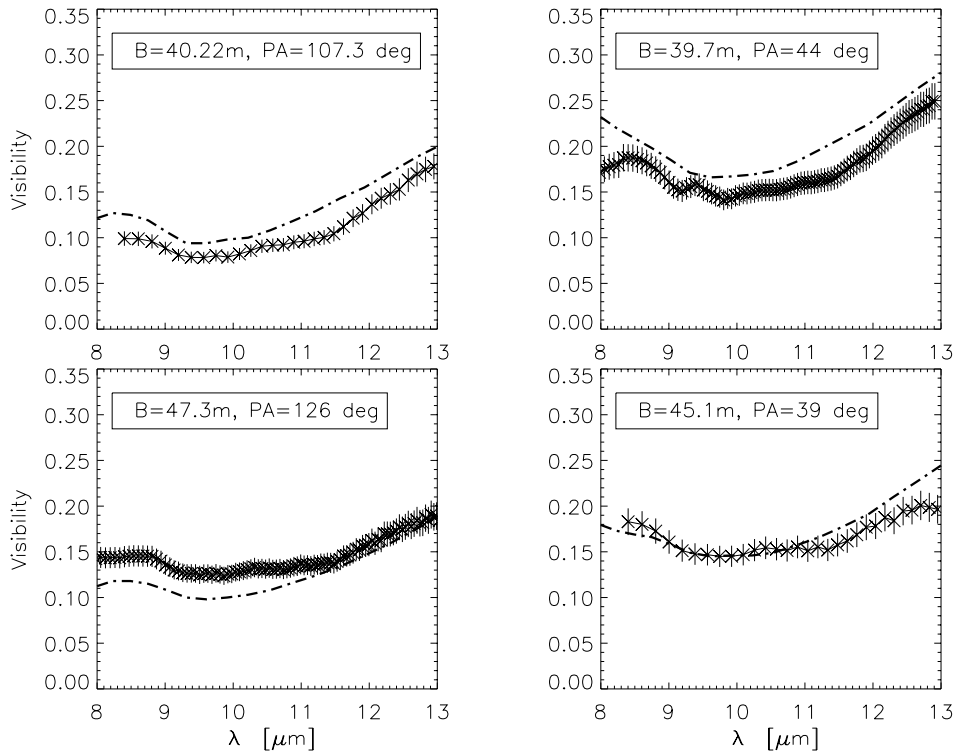

Figure 1. Modeled visibilities (dash-dot) vs. MIDI data in the N band for M2-9. Respective projected baselines are indicated within each plot.

proximately 132^o. Interestingly enough, the modeled disc required an inclination of 132^o to fit the observational data. As such, the disc is aligned to the pre-existing asymmetry of the PN (see Fig.3 & 4 by Chesneau et al. (783)). It is though trivial to define which mechanism initiated the creation of the disc, whether it was a binary companion, a fast-rotating core or accretion from a pre-existing disc.

5. Aperture Masking

A new development in interferometry was introduced during the last two decades: converting a single-dish telescope into an interferometer. The technique is called aperture masking, whereas a mask is incorporated to the telescope optics and speckle patterns are recorded in lieu of images. We have used the Sparse Aperture Masking (SAM) mode on the NACO instrument of the VLT (790) with circular aperture multi-hole masks, which by the use of baselines from 0.5 to 8m, offers optimal Fourier plane coverage, allows the recovery of both amplitudes and closure phases* and thus enables the reconstruction

*That is the sum of phases of each baseline forming a triangle. Deviation from 0^o, or 180^o, in the observed spatial frequency domain is indicative of an asymmetry.

of diffraction limited images. We have observed a plethora of evolved stars at different evolutionary phases, one of those being the variable star V Hya.

V Hya displays a double periodicity with a short period of 529 days ($\Delta m \sim 1.5$) and a long period of 6,300 days ($\Delta m \sim 6$). Radio observations have revealed a CO disc as well as a jet, perpendicular to the disc (786). Lagadec et al. (788) has identified an elongation of dust in the mid-infrared in the direction of the jet. Our observations are expected to provide the first images of the complex dusty structure around the star and results are expected shortly.

Acknowledgments. F. Lykou would like to thank the Royal Astronomical Society for funding the travel expenses and A. Zijlstra for trusting her organisational and photographic skills for this conference.

References

Chesneau, O., Clayton, G. C., Lykou, F., de Marco, O., Hummel, C. A., Kerber, F., Lagadec, E., Nordhaus, J., Zijlstra, A. A., & Evans, A. 2009, A&A, 493, L17

Chesneau, O., Lykou, F., Balick, B., Lagadec, E., Matsuura, M., Smith, N., Spang, A., Wolf, S., & Zijlstra, A. A. 2007, A&A, 473, L29

Hajduk, M., Zijlstra, A. A., Herwig, F., van Hoof, P. A. M., Kerber, F., Kimeswenger, S., Pollacco, D. L., Evans, A., Lopéz, J. A., Bryce, M., Eyres, S. P. S., & Matsuura, M. 2005, Science, 308, 231

Hirano, N., Shinnaga, H., Dinh-V-Trung, Fong, D., Keto, E., Patel, N., Qi, C., Young, K., Zhang, Q., & Zhao, J. 2004, ApJ, 616, L43

Icke, V., Preston, H. L., & Balick, B. 1989, AJ, 97, 462

Lagadec, E., Mékarnia, D., de Freitas Pacheco, J. A., & Dougados, C. 2005, A&A, 433, 553

Leinert, C., Graser, U., Przygodda, F., Waters, L. B. F. M., Perrin, G., Jaffe, W., Lopez, B., Bakker, E. J., Böhm, A., Chesneau, O., Cotton, W. D., Damstra, S., de Jong, J., Glazenborg-Kluttig, A. W., Grimm, B., Hanenburg, H., Laun, W., Lenzen, R., Ligori, S., Mathar, R. J., Meisner, J., Morel, S., Morr, W., Neumann, U., Pel, J., Schuller, P., Rohloff, R., Stecklum, B., Storz, C., von der Lühe, O., & Wagner, K. 2003, Ap&SS, 286, 73

Tuthill, P., Lacour, S., Amico, P., Ireland, M., Norris, B., Stewart, P., Evans, T., Kraus, A., Lidman, C., Pompei, E., & Kornweibel, N. 2010, in Society of Photo-Optical Instrumentation Engineers (SPIE) Conference Series, vol. 7735

Wolf, S. 2003, Computer Physics Communications, 150, 99

Wolf, S., Henning, T., & Stecklum, B. 1999, A&A, 349, 839

Asymmetric Planetary Nebulae V
A. A. Zijlstra, F. Lykou, E. Lagadec and I. McDonald
Jodrell Bank Centre for Astrophysics, Manchester, UK © 2011

A circumbinary dust disc in the making: the semi-detached evolved binary SS Leporis

Tijl Verhoelst, Els van Aarle, and Bram Acke

Instituut voor Sterrenkunde, K.U.Leuven, Celestijnenlaan 200D, B-3001 Leuven, Belgium

Abstract. In the past few years, dusty discs have been observed around several evolved objects. Around post-AGB binaries they appear more often than not, and they have been seen at the center of planetary nebulae. The formation of such discs could, according to theory, occur in different ways, among which a common envelope phase or wind accretion when one component of a binary system ascends a giant branch. However, observational counterparts of these proposed evolutionary events are sparse, and in none of them, a dusty disc has been directly observed. We present a combined interferometric and spectroscopic analysis of the A+M binary SS Leporis, and show it to be forming a circumbinary dust disc through non-conservative mass transfer. We discuss a possible cause for the low detection rate of such systems so far, and we touch upon the characteristics of the disc, with important implications on the theory of dust grain processing.
Keywords. Planetary Nebulae – Infrared interferometry

1. Introduction

In the last editions of this conference series, the role of binarity in the shaping of asymmetrical Planetary Nebulae is becoming more and more accepted. Especially the toroidal or disc-like circumbinary structures that may result from binary interaction can help channel later mass loss into bi- or multi-polar shapes. Although the end products of different kinds of binary interaction are well observed, systems currently undergoing such an interaction event are sparse. Here, we present our results on the Roche-lobe overflowing system SS Leporis.

2. Disentangling the SED with interferometry

In this contribution, we take as starting point our analysis of the A+M binary SS Lep as described in (802), which we briefly summarize below.

Our current view of SS Lep is actually an extension of the scenario proposed by (803) and (794), who put together the composite spectrum (A-type primary with TiO bands in the red, indicating an M-star companion) and the orbital information (P = 260 days, $e = 0.132$, and a mass function $f(M) = 0.24$) with the variable shell spectrum,

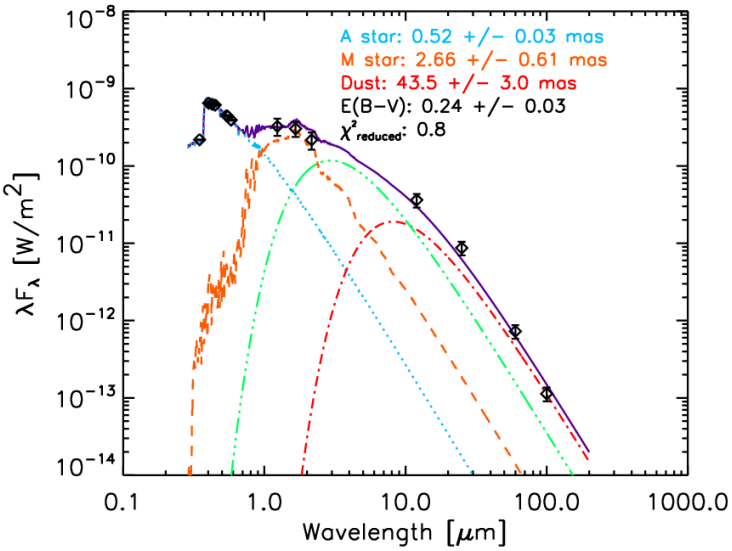

Figure 1. The Spectral Energy Distribution (SED) of SS Lep. The blue dotted line represents the photosphere of the A-type star, the orange dashed line is the contribution of the M giant, the green dash-dot-dot line represents the near-IR excess seen in the interferometry, and the red dash-dot line contains the excess at longer wavelengths. The sum of all these is shown with the solid line.

and proposed a Roche Lobe overflow (at periastron) model as developed by (799) for T CrB.

The exact evolutionary phase, pre- or post-main sequence (MS), was a matter of debate until HIPPARCOS finally put the system at ~ 330 pc, confirming a post-MS status.

Still, with only spatially integrated photometry, it is impossible to derive the stellar parameters of the giant star and the properties of the dusty circumstellar environment detected by (793) with sufficient accuracy to confirm the proposed scenario (Fig. 1). To that end, we used VINCI/VLTI interferometry at 2.2 μm, which put tight constraints on the diameter of the M star and its flux contribution at that wavelength (Fig. 2), confirming it to be filling its Roche lobe. Moreover, the interferometry revealed the presence of a hot circumbinary structure, which must be in a disc-like geometry to be compatible with the low extinction toward the central stars.

3. Discussion

As detailed below, SS Lep is an intriguing target, both in the context of binary interaction after the MS, and in order to study the physical process that come with such mass transfer such as the formation and evolution of circumbinary dust discs.

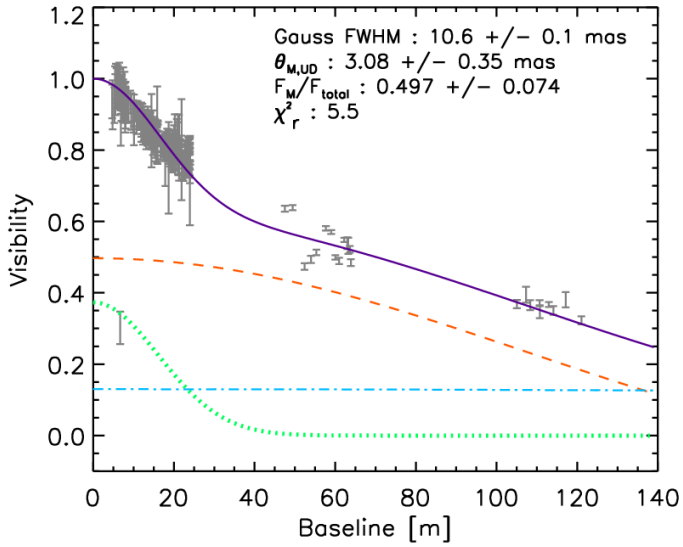

Figure 2. VINCI near-IR interferometry on SS Lep. The green dotted line represents the well resolved component, which we interpret as the inner rim of the circumbinary dust disc. The orange dashed line corresponds to the M giant, and the blue dot-dash line to the A-type star. The sum is shown with a solid line.

3.1. Binary interaction

From a theoretical point of view, it has long been assumed that mass transfer from a convective (giant) star could not be stable, and would lead to a common envelope phase with severe orbit shrinkage on very short time scales. More recently, it was suggested that non-conservative mass-transfer, with the creation of a circumbinary disc, could somehow stabilize the orbit, and this appears to be the case in SS Leporis. Moreover, since the giant in SS Lep is particularly cool, the classic Roche description should probably be replaced with a formalism including the effects of radiation pressure and pulsation as presented by (795), although the relatively stable near-IR light curve speaks against strong pulsational behaviour in SS Lep.

The orbital characteristics (e.g. period and eccentricity) and circumbinary disc resemble very much those of the post-AGB binaries with stable, Keplerian circumbinary dust discs (801). We can therefore postulate that SS Lep is a progenitor to such post-AGB systems, although we have no indications that the giant in SS Lep is on the AGB rather than on the RGB. (798) present an intriguing explanation for the lack of SS Lep analogues: in large surveys, based on colour-magnitude diagrams, SS Lep would appear like its progeny: a luminous A-type giant and a near-IR excess already starting in the near-IR. However, in SS Lep, the luminous A-type giant is a MS star, inflated and overluminous due to the accretion, rather than an actual post-AGB star. It remains to be studied whether this possible confusion between progenitor and progeny is affecting our statistics.

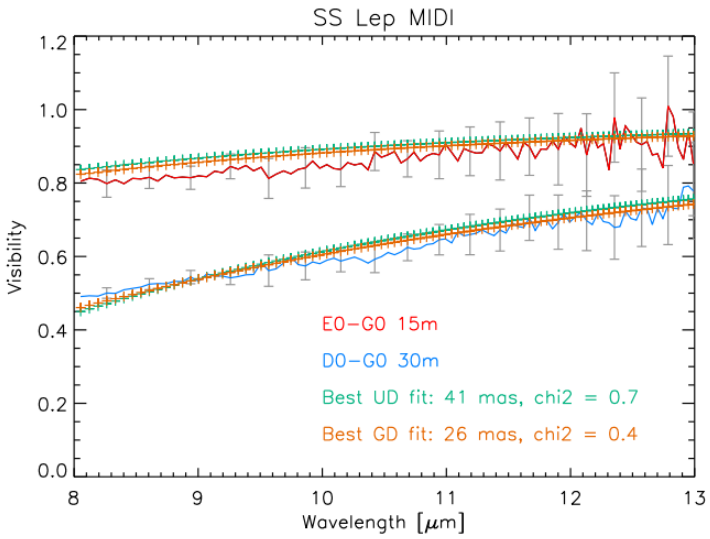

Figure 3. MIDI interferometry of the disc around SS Leporis

3.2. Disc evolution

Hitherto unpublished MIDI interferometry (Fig. 3), can be modelled with a wavelength-independent uniform disc (UD) or gaussian disc (GD), with a diameter or FWHM of 41 mas or 26 mas respectively. The fact that these diameters do not depend on wavelength, although the N-band spectrum shows a clear silicate emission feature, hints at a well developed disc with a puffed-up inner wall and shaded region, as seen in Post-AGB binaries with discs (796). Due to this very steep temperature gradient in the surface layer of the disc, the observed size becomes independent of wavelength. While in those Post-AGB binaries the spectra are rich in crystalline features (797), the spectrum of SS Lep appears entirely amorphous (800). This is strong evidence that the dust in these discs is formed as amorphous grains, and crystallinity appears only with time after long exposure to the stellar or accretion radiation field.

Acknowledgments. TV and BA acknowledge support from the Flemish Fund for Scientific Research (FWO-Vlaanderen).

References

Allen, D. A., & Ney, E. P. 1972, The Observatory, 92, 47
Cowley, A. P. 1967, ApJ, 147, 609
Dermine, T., Jorissen, A., Siess, L., & Frankowski, A. 2009, A&A, 507, 891
Deroo, P., Acke, B., Verhoelst, T., Dominik, C., Tatulli, E., & van Winckel, H. 2007, A&A, 474, L45
Gielen, C., van Winckel, H., Min, M., Waters, L. B. F. M., & Lloyd Evans, T. 2008, A&A, 490, 725
Jorissen, A., Frankowski, A., Famaey, B., & van Eck, S. 2009, A&A, 498, 489
Kraft, R. P. 1958, ApJ, 127, 625

Schütz, O., Meeus, G., & Sterzik, M. F. 2005, A&A, 431, 175
Van Winckel, H. 2003, ARA&A, 41, 391
Verhoelst, T., van Aarle, E., & Acke, B. 2007, A&A, 470, L21
Widing, K. G. 1966, ApJ, 143, 121

Asymmetric Planetary Nebulae V
A. A. Zijlstra, F. Lykou, E. Lagadec and I. McDonald
Jodrell Bank Centre for Astrophysics, Manchester, UK © *2011*

IR Excesses of Central Stars of Planetary Nebulae

Jana Bilikova[1], You-Hua Chu[1], Robert Gruendl[1], Kate Su[2], and Thomas Rauch[3]

[1]*Department of Astronomy, University of Illinois at Urbana-Champaign, 1002 West Green St., Urbana, IL 61801*

[2]*Steward Observatory, University of Arizona, 933 N. Cherry Ave., Tuscon, AZ 85721, USA*

[3]*Institute for Astronomy and Astrophysics, Kepler Center for Astro and Particle Physics, Eberhard Karls University, Tübingen, Germany*

Abstract. *Spitzer Space Telescope* observations of the Helix Nebula's hot ($T_{\rm eff} \approx 110\,000$ K) central star revealed a mid-IR excess consistent with a continuum emission from a dust disk located at 35−150 AU from the central white dwarf (WD), and the dust is most likely produced by collisions among Kuiper Belt-like objects (814). To determine how common such dust disks are, we have carried out a *Spitzer* 24 μm survey of 71 hot WDs, and detected 9 WDs with clear IR excess, 7 of them still surrounded by planetary nebulae (PNe). Inspired by the prevalence of WDs with mid-IR excesses being central stars of planetary nebulae (CSPNs), we have examined archival *Spitzer* IRAC and/or MIPS observations of 66 PNe and found IR excesses for six, and possibly more, CSPNs. We have obtained *Spitzer* IRS, Gemini NIRI and Michelle, and KPNO echelle spectra of some of these CSPNs to determine the nature of the IR emission. We report the results in this paper.

Keywords. Planetary Nebulae

1. Dust Disk around the Central Star of the Helix Nebula

The central star of the Helix Nebula is a hot white dwarf (WD) with an effective temperature of $\sim 110\,000$ K. Its *Spitzer Space Telescope* MIPS 24 and 70 μm observations have revealed a compact source coincident with the central WD. A follow-up Infra-Red Spectrograph (IRS) observation of the central point source has confirmed that the mid-IR emission originates from a dust continuum with a temperature of 90−130 K, and an emitting area of 4−40 AU^2. Only an extended object, such as a dust disk, can explain these properties. The location of the dust, 40−100 AU, corresponds to the location of the Kuiper Belt in the solar system, and the dust disk was suggested to originate from collisionally disrupted Kuiper Belt-like objects (KBOs) dynamically rejuvenated in the AGB and post-AGB evolutionary stages (814).

2. Spitzer MIPS 24 μm Survey of Hot WDs

To search for more dust disks similar to that around the WD in the Helix Nebula, we have carried out a *Spitzer* MIPS 24 μm survey of 71 hot ($\sim$ 100 000 K) WDs. A compact source coincident with the WD is detected in 9 cases; in 7 of these, the star is still surrounded by a PN (Chu et al, 2010, in preparation). We have constructed the SEDs of these WDs using optical and near-IR photometry from the literature. All detections show excess emission at 24 μm. Two example SEDs, along with the follow-up spectra and 24 μm images, are shown in Figure 1, and described below.

Sh 2-216, at a distance of 219 pc (808), is the closest PN. The SED of its central star (CSPN) follows the blackbody curve from optical to IRAC bands, but shows large excess at 24 μm. The *Spitzer* IRS spectrum is dominated by featureless continuum emission, which starts rising at $\sim$10 μm. Such SED is similar to that of the Helix nebula's CSPN.

The *HST* observations of CSPN K1-22 resolved a red companion 0.35″ away from the CSPN (804). The SED in Figure 1 shows V and I magnitudes from each star individually, the remaining magnitudes are for the two stars combined. The two solid curves show contribution of the two components, based on HST photometry from Ciardullo et al. (804), and the dashed curve shows the sum of these two components. The IR flux densities are all higher than the expected photospheric emission of these two stars. The IRS spectrum shows a weak continuum component, as well as a strong [OIV] 25.89 μm emission line component, both of which may be contributing to the observed 24 μm excess. High-resolution mid-IR imaging is necessary to resolve whether the 24 μm source is centered on the CSPN, or its red companion.

3. Spitzer Archival survey of CSPNs

Since most cases of hot WDs exhibiting 24 μm excesses are still surrounded by PNe, we have used archival *Spitzer* IRAC (3.6, 4.5, 5.8, and 8.0 μm) and MIPS (24, 70, and 160 μm) observations of PNe to search for CSPNs with IR excesses. We have examined images of 66 resolved PNe, and selected 18 in which the nebular emission was not too confusing or dominant in the central region, and the CSPN was detected in most IRAC bands. For these 18 cases, we have carried out photometric measurements, and constructed the SEDs. Six of these CSPNs show convincing IR excesses.

In the case of NGC 6804 (Figure 1), prominent IR excess is seen starting from J band throughout all IRAC channels. The SED does not exclude the possible presence of a cool ($T_{\rm eff} \approx 1500$ K) companion; however, a companion alone cannot account for all of the observed IR excess, and furthermore, no companion has been detected around this CSPN (804). Figure 1 presents a follow-up *Spitzer* MIPS 24μm image, which shows a central source coincident with the CSPN. The SED displays a follow-up Gemini NIRI 1–5 μm spectrum, which reveals a rising continuum, as well as a compact emission line source. Furthermore, Gemini Michelle 8–15 μm spectrum exhibits a silicate emission feature at 10 μm.

4. Possible Origins of IR excesses

The differences between the SEDs of our targets imply different properties of the disks, if not even different origins of excess emission. We need to consider origins other than the collisional disruption of KBOs that can produce the observed IR excesses.

4.1. Post-AGB Binary Evolution

It has been suggested from an analysis of broad-band SEDs of 51 post-AGB stars that Keplerian rotating dust disks are common among binary post-AGB stars (807). van Winckel (815) showed that post-AGB stars displaying SEDs of warm dusty disks are all single-lined spectroscopic binaries and the hot dust persists in the system because it is trapped in a stable circumstellar or circumbinary orbit.

Seven out of 9 hot WDs with 24 μm excesses from our survey and the CSPNs with IRAC and/or MIPS excesses found in the *Spitzer* archive are all in PNe and thus represent the youngest WDs that have just evolved past the post-AGB phase. One of them (NGC 2346) has a confirmed binary companion (813) and SED that resembles those of post-AGB binaries; thus, one cannot help asking whether some of these 24 μm and/or IRAC excesses are also related to the IR excesses of binary post-AGB stars reported by de Ruyter et al. (807).

However, it is difficult to identify and confirm the presence of a close companion of a CSPN via direct imaging (804); and irregular spectral variations due to winds hamper the detection of periodic radial velocity variations (806). If a dust disk trapped in a stable orbit around a binary system persists throughout the PN phase, its presence can serve as a powerful diagnostic for the binarity of a CSPN.

4.2. Compact Unresolved Nebulosity

Another possibility is that the observed excess comes from a compact nebulosity with high dust-to-gas ratio, which is seen in the born-again PNe Abell 30 and Abell 78 (805). This central emission enhancement originates from knots seen in [OIII] λ5007 Å and He II λ4686 Å, but undetected in Hα (811; 809). This observed morphological difference implies H depletion in the central region (812), which can occur in born-again PNe (810). We have carried out KPNO echelle spectroscopy of the hot WDs with 24 μm excesses and CSPNs with IRAC excesses, covering both Hα and [OIII] λ5007 Å lines. In all observed cases, each [OIII] feature has its Hα counterpart. Therefore, born-again scenario cannot explain the observed IR excesses of most of our targets.

5. Summary

The discovery of a dust disk around the CSPN of the Helix nebula through its 24 μm excess has inspired us to conduct a *Spitzer* 24 μm survey of hot ($T_{\rm eff} \approx 100\,000$ K) WDs. Out of 71 targets observed, 9 show 24 μm excesses, 7 of them in PNe. To find more cases of CSPNs with IR excess, we have searched the *Spitzer* archive, and found 6 targets with convincing IR excesses. While some SEDs are similar to that of the Helix CSPN and show excess emission only in mid-IR, others show excess starting at shorter wavelength. Similarly, while some mid-IR spectra are dominated by dust

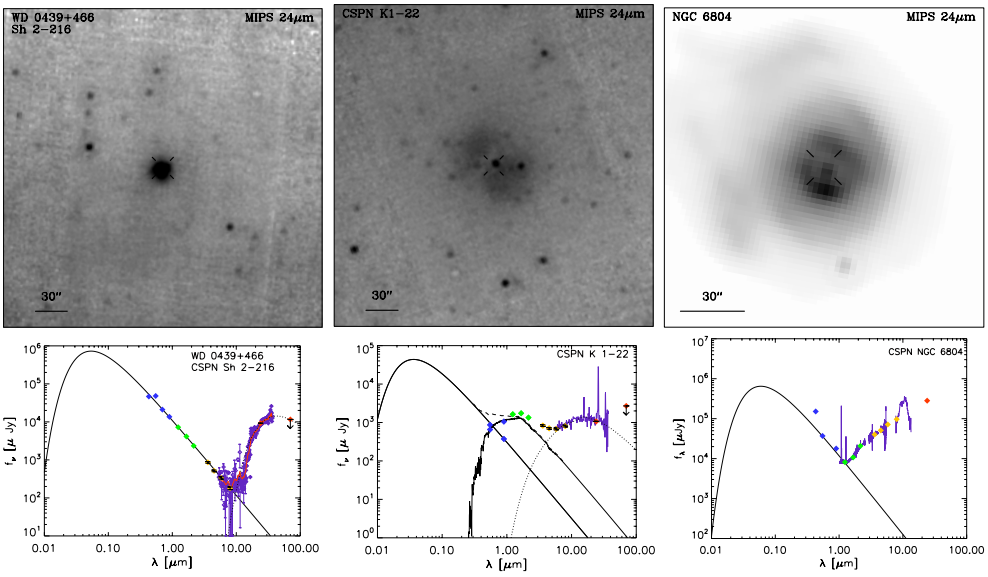

Figure 1. *Spitzer* 24 μm images (top) and SEDs (bottom) of CSPNs Sh 2-216 and K1-22 from *Spitzer* 24μ survey, and NGC 6804 from *Spitzer* archival search. The SEDs are constructed with optical photometry from literature, 2MASS *JHK*, IRAC photometry and *Spitzer* MIPS 24 μm data. The IR spectra from *Spitzer* IRS are shown in purple for CSPN Sh2-216 and K1-22, and Gemini NIRI and Michelle spectra are shown in purple for NGC 6804. For CSPN Sh2-216, the smoothed IRS spectrum is shown in red.

continuum, others show strong emission lines superposed on dust continuum. The dust around the Helix central star was suggested to be produced by collisions among KBOs (814). However, other mechanisms that could produce IR excess, such as binary interactions, need to be considered as well. Future modeling of the mid-IR SEDs is needed to evaluate the origins of the observed excess emission.

References

Ciardullo, R., Bond, H. E., Sipior, M. S., Fullton, L. K., Zhang, C., & Schaefer, K. G. 1999, AJ, 118, 488

Cohen, M., & Barlow, M. J. 1974, ApJ, 193, 401

de Marco, O., Wortel, S., Bond, H. E., & Harmer, D. 2007, in Asymmetrical Planetary Nebulae IV. 0709.1508

de Ruyter, S., van Winckel, H., Maas, T., Lloyd Evans, T., Waters, L. B. F. M., & Dejonghe, H. 2006, A&A, 448, 641

Harris, H. C., Dahn, C. C., Canzian, B., Guetter, H. H., Leggett, S. K., Levine, S. E., Luginbuhl, C. B., Monet, A. K. B., Monet, D. G., Pier, J. R., Stone, R. C., Tilleman, T., Vrba, F. J., & Walker, R. L. 2007, AJ, 133, 631

Hazard, C., Terlevich, R., Ferland, G., Morton, D. C., & Sargent, W. L. W. 1980, Nat, 285, 463

Iben, I., Jr., Kaler, J. B., Truran, J. W., & Renzini, A. 1983, ApJ, 264, 605

Jacoby, G. H. 1979, PASP, 91, 754

Jacoby, G. H., & Ford, H. C. 1983, ApJ, 266, 298

Mendez, R. H., & Niemela, V. S. 1981, ApJ, 250, 240

Su, K. Y. L., Chu, Y., Rieke, G. H., Huggins, P. J., Gruendl, R., Napiwotzki, R., Rauch, T., Latter, W. B., & Volk, K. 2007, ApJ, 657, L41

van Winckel, H. 2003, in Astronomical Society of the Pacific Conference Series, edited by R. L. M. Corradi, J. Mikolajewska, & T. J. Mahoney, vol. 303 of Astronomical Society of the Pacific Conference Series, 294

Asymmetric Planetary Nebulae V
A. A. Zijlstra, F. Lykou, E. Lagadec and I. McDonald
Jodrell Bank Centre for Astrophysics, Manchester, UK © 2011

HERMES Survey of Binarity in Evolved Stars

Nadya Gorlova[1], Hans Van Winckel[1], Alain Jorissen[2], Sophie Van Eck[2], Tyl Dermine[2], Katrina Exter[1], Roy H. Østensen[1], and Griet Van de Steene[3]

[1]*Institute of Astronomy, Celestijnenlaan 200D, 3001, Leuven, Belgium*

[2]*Institut d'Astronomie -ULB, Boulevard du Triomphe, B-1050, Brussels, Belgium*

[3]*Royal Observatory of Belgium, Ringlaan 3, 1180, Brussels, Belgium*

Abstract. We report on our radial velocity monitoring project of a wide range of evolved stars where binarity was proposed to explain some of their peculiarities. Our spectrograph HERMES is a new optical echelle spectrograph mounted on the 1.2m Mercator telescope on La Palma, built by a consortium of Belgian Institutes (KULeuven, ULB, Royal Observatory) with contributions from the Geneva Observatory and Landessternwarte Tautenburg. By combining high S/N single observations with low S/N time-series, we aim at quantifying the orbital and chemical characteristics of every distinct subgroup. The final goal is to gain insight in the diverse binary interaction processes relevant at late stages of stellar evolution. We discuss our project, the unique capabilities of HERMES, and present the first results of our program.
Keywords. Planetary Nebulae – Stars: AGB and post-AGB – Binaries

1. Introduction

One of the reasons that we are now already on the 5th version of the APN series, is that the impact of binarity on our global understanding of the late stellar evolution is still far from clear. A rich zoo of peculiar evolved objects is predicted to be born from the interactions between the loosely bound envelope of a (super)giant, and the gravitational pull of a companion (e.g. 823; 816; 819, and references therein). Unfortunately, the many parameters involved in these models are not well constrained by observations. Here we report on our project to overcome this and bring the different classes of (suspected) evolved binaries into an evolutionary connection.

We started a radial velocity (RV) survey of ~300 post-Main Sequence stars to detect the possible orbital motion and quantify the orbital parameter distributions. The stars were selected based on either of the following criteria: 1) photometric binaries, in particular eclipsing, ellipsoidal, and the RV Tau variables of type "b" (with a long secondary period in addition to the pulsation one); 2) objects with peculiar infrared excesses or molecular outflows; 3) extrinsically polluted chemically-peculiar stars and stars depleted in refractory elements; 4) brighter end of central stars of planetary nebulae, in particular cases of asymmetric nebulae; 5) hot sub-dwarf stars with FGK companions; 6) symbiotic systems.

2. HERMES the New Echelle Spectrograph

Our survey is based on data obtained with our new echelle fiber-fed spectrograph HERMES mounted on the 1.2 m Flemish telescope on La Palma (`www.mercator.iac.es`). The instrument provides a resolution R~80,000, a continuous wavelength coverage of 3800-9000Å and allows the observation of objects down to 12.5 mag in a single exposure. The absolute precision of a single RV measurement is ~200 m/s, which is limited by the pressure fluctuations during the night in the spectrograph room. The internal precision, defined by the accuracy of the arc spectrum calibration, is better than 10 m/s. The instrument is described in Raskin et al. (2010, A&A submitted).

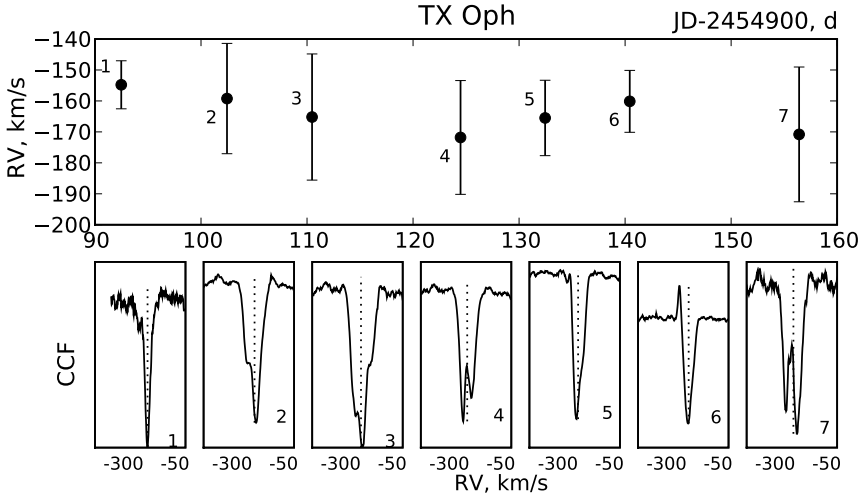

Figure 1. A sample radial velocity curve (top panel) derived from the HERMES spectra by cross-correlating them with a G2 mask. An RV point is obtained by fitting a CCF (bottom panel) with a Gaussian and determining its minimum (dashed vertical lines). The "error bars" here represent the FWHM of the Gaussian fit. TX Oph, an RV Tau star with a photometric P=70/135 d, with its complicated CCFs illustrates the challenges of disentangling the binary motion from pulsations in some of these semi-regular pulsating stars.

A Python-based pipeline extracts a wavelength-calibrated and a cosmic ray cleaned spectrum. A separate routine is provided for measuring RVs, by means of a cross-correlation with the spectral mask corresponding to the spectral type of the star. An example of this procedure is shown in Fig. 1. An S/N=30 in the spectrum is usually sufficient to obtain a cross-correlation function (CCF) with a well pronounced minimum. Higher S/N is needed for hot, metal-poor, and fast rotating stars. In pulsating stars, and stars with circumstellar gas, CCF profiles may show several components. Frequent sampling and a long time-line of our survey (several years) should mitigate these complications. We are in the process of optimising the masks to the spectral peculiarities of all individual objects. The survey started in April 2009. Here we report on a few exciting results based on the data obtained until May 2010.

3. The First Results

3.1. Post-AGB Stars with Disks

There are 39 stars in this subgroup. They were selected, with a few exceptions, based on the locus on the IRAS color-color diagram occupied by the RV Tau stars (821). Abundance analysis of e.g. Giridhar et al. (818), Maas et al. (822) have demonstrated that many of these systems are depleted in refractory elements. Van Winckel et al. (824) demonstrated for the low-amplitude pulsators that they are all binary systems. The current understanding is that these systems went through a mass exchange phase and some mass was trapped into a circumbinary disk (817). In the disk refractory elements condensed into grains and the depleted gas subsequently fell back on the star, creating the observed abundance anomalies.

With 8 spectra per star on average, we detected variability (at the level of >1 km/s) for all stars that had a reasonable coverage, except for HD340949, HD53300 (IRAS flux is confused), and IRAS 17449+2320 (possibly a B[e] star). Further monitoring is needed to verify whether the detected variations are due to orbital motion. The two most obvious cases are shown in Fig. 2. AU Peg has been discussed in the literature, and the ambiguity remains as to whether it is a low-mass Population II Cepheid or a short-period Classical Cepheid. The short orbital period of 53 days points to a sub-AU separation, which must have induced the mass exchange with the companion already on the red giant branch. On the other hand, variability in BD +46 442 has not been reported so far. Based on the large integrated distance and variations in T_{eff} not exceeding 200 K (as measured by us using the line ratios calibrations of Kovtyukh (820)), we conclude that the RV curve of BD +46 442 represents an orbital motion. This star also shows a spectacular double-peak emission in Hα, that changes into a P Cyg profile on the descending part of the RV curve.

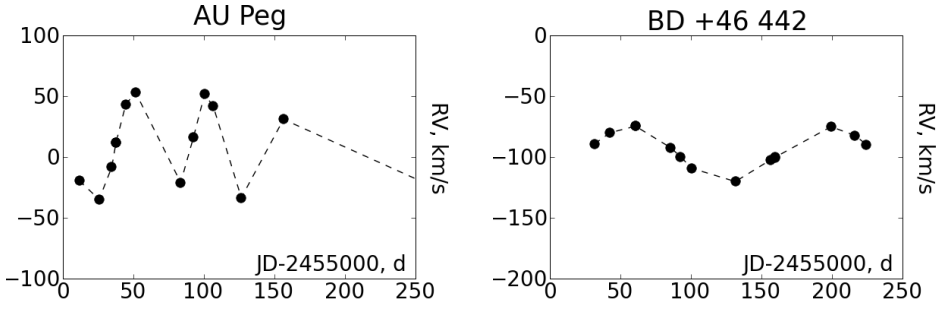

Figure 2. Two examples of the regular RV variations that we uncovered in the course of the first year of our binary survey. AU Peg is a known short-period pulsator (P=2.4 d) and a single-line spectroscopic binary with a P*orb* =53.3 d, as also seen in our RV curve. BD +46 442 is a poorly studied star for which we find RV variations with an amplitude of 47 km/s and a period of 140 d.

Finally, we confirm binarity of non-dusty but strongly depleted star BD +39 4926. It may present an example of the late stage in the evolution of these binary systems when the circumbinary disk has dispersed, or even a missing link with the Barium (Ba) phenomenon discussed in the following section. Combining our observations with the

Utrecht Echelle Spectrograph data, we obtain a new value for the orbital period of 873 d and a non-negligible eccentricity e =0.1 ± 0.05 (Jacobs et al. 2010, in preparation).

3.2. New Orbital Solutions for Barium Stars

Ba giants are thought to have been polluted by the s-process elements from their invisible white dwarf (WD) companions when the latter were AGB stars. The process of mass exchange (either via the wind capture or the Roche lobe overflow) should have circularized the orbits, which disagrees with observations (Fig. 3). WD kicks have been invoked to explain the eccentric orbits (Izzard et al. (2010), astro-ph 1008.3818).

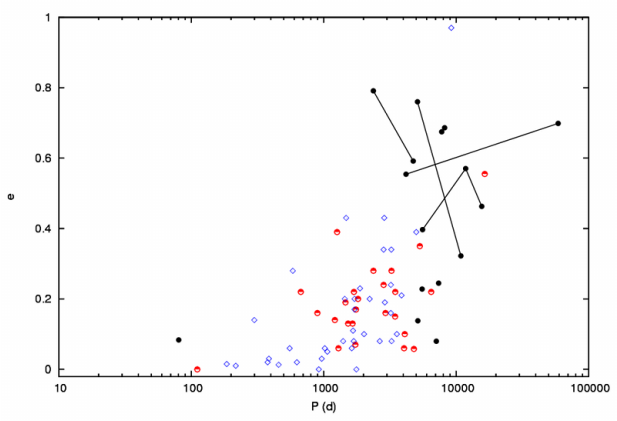

Figure 3. An eccentricity vs. orbital period diagram for Ba stars (strong - blue diamonds, mild - red and black circles). The lines designate multiple possible orbital solutions for mild Ba stars as recently deduced from the HERMES+CORAVEL data. From Dermine & Jorissen et al. (2010), in preparation.

4. Conclusion

The radial velocity monitoring program is scheduled to run for several years. The final observational output will be a better overview of binary rates and the distribution of orbital elements of the different classes. The ultimate goal of the project is to constrain possible evolutionary connections between the different classes and to quantify our understanding of the diverse binary interaction processes.

References

Dermine, T., et al. 2009, A&A, 507, 891
Gielen, C., et al. 2008, A&A, 490, 725
Giridhar, S., et al. 2000, ApJ, 531, 521
Jorissen, A. 2004, in AGB stars, edited by H. Habing, & H. Olofsson (New York: Springer Verlag), A&A Library, 460
Kovtyukh, V. 2007, MNRAS, 378, 617
Lloyd Evans, T. 1999, in Asymptotic Giant Branch Stars, edited by T. Le Bertre, et al. (San Francisco: ASP), vol. 191 of IAU Symp., 453

Maas, T., et al. 2005, A&A, 429, 297
Pols, O. R., & et al. 2003, in Symbiotic Stars Probing Stellar Evolution, edited by R. Corradi, et al. (San Francisco: ASP), vol. 303 of ASP Conf. Proc., 290
Van Winckel, H., et al. 2009, A&A, 505, 1221

Asymmetric Planetary Nebulae V
A. A. Zijlstra, F. Lykou, E. Lagadec and I. McDonald
Jodrell Bank Centre for Astrophysics, Manchester, UK © *2011*

New results on planetary nebula shaping and stellar binarity

Orsola De Marco

Macquarie University

Abstract. The question of what physical mechanisms shape planetary nebulae into their observed morphologies remains open. However, intensified efforts since the last meeting in this series, Asymmetrical Planetary Nebulae IV, in July 2007 have yielded some excellent results. In this review we concentrate on those developments that have taken place in the last three years, with emphasis on results obtained since the review by De Marco (2009).

1. The Problem of Shaping a non-Spherical PN

Approximately 80% of all planetary nebulae (PN) exhibit morphologies that diverge greatly from a spherical shape (867). Despite advancements in the last 10 years, a convincing answer to what the shaping agent might be is still lacking (for a review see 835). Stellar or even sub-stellar companions have the capacity to interact with upper asymptotic giant branch (AGB) stars and shape the ejected envelope either by strong interactions such as common envelopes (866; 871) or wider binary interactions such as wind accretion and gravitational focussing (e.g., 856; 857; 841).

However, the fraction of stellar companions to the progenitors of AGB stars that may interact with them is of the order of 30% (840), so how can the fraction of non spherical PN be as high as 80%? This discrepancy could be explained if not all the 1-8 $M_{\odot}$ stars result in a PN. Moe & De Marco (863) and Moe & De Marco (864) argued, based on population synthesis, that only ~20% of intermediate mass stars make a PN, with the remainder transiting between the AGB and white dwarf (WD) phases with invisible, or under-luminous nebulae.

Soker & Subag (874) predicted that deep searches could find the brightest among these under-luminous PN and that they would be spherical (and of course that spherical PN have no binaries in their centres). This prediction has been partly borne out by the MASH survey (867; 862), the deepest PN survey to date that doubled the fraction of spherical PN from ~10% to ~20% and by the *Deep Sky Hunters* survey, that found a similar fraction in the very faint population (853). These are, in the binary hypothesis, the bright end of the under-luminous, spherical PN formed by single stars and non-interacting binaries.

A main priority established by the community during the *Asymmetrical PN IV* meeting has therefore been to find more binaries in order to relate their parameters to the PN morphology and to determine the PN binary fraction and period distribution. A

great deal of success has been enjoyed in the former search (see § 2), while progress has been slow in the latter (§ 3).

2. The growing (and shrinking) binary list

In Table 1 we present new PN that have a highly probable or confirmed binary central stars (for the list of previously known ones see De Marco et al. 835). Below, we discuss some of them, as well as some that did not make the list, but are likely binaries.

• Hajduk et al. (851) announced the first binary, Wolf-Rayet type ([WC7]) central star. Its PN (PN G221.8-04.2, aka PHR J0652-0951 and PM 1-23) is similar to A 63, showing an edge-on waist of what may have been a bipolar structure. For assumed primary and secondary masses of 0.6 and 0.3 $M_{\odot}$, respectively, the orbital separation would be ∼3 or 5 $R_{\odot}$, depending on whether the variability is from irradiation (P=0.63 days) or ellipsoidal effects (P=1.2 days). The primary Roche lobe radius would be at 1.3 or 2.2 $R_{\odot}$. Although the primary radius would be ∼0.3 $R_{\odot}$ (this is the radius of NGC 40, a slightly hotter [WC8] star (855)), a [WC] stellar atmosphere actually extends past the nominal radius value (see, e.g., 834), so the primary should be filling its Roche lobe. Of the 33 [WC] and "week emission line stars" studied by Hajduk et al. (851), only this PN revealed a periodically-variable central star, from which the authors concluded that the short-period binary fraction among the hydrogen-deficient central stars may be lower than for the hydrogen-normal ones. This may be in line with a predominant merger origin of these stars (831) or indicate that the observational biases that affect the [WC] class are different.

• NGC 6804 and NGC 7139 have a strong IR excess (825) that may be indicative of a companion. We have not included them in Table 1 because a fit to the data imply "secondary" temperatures of only 1500 K, too cool for a late M companion and possibly too bright for a sub-stellar companion. This temperature, however, is at the condensation limit for dust and possibly unbelievable. Better data are needed to constrain the fits.

• Frew & Parker (845) introduced a new class of PN that have a high density, unresolved nebulosity coincidental with the central star. They called this class EGB6-like objects because this PN was the first to have such nebulosity identified. Interestingly, this PN central star was later resolved by the *Hubble Space Telescope (HST)* to have a companion and the nebulosity was found to be around the companion, not the central star (827). Other objects were recently detected to have such high density unresolved nebulae, usually from the fact that the [OIII] line at 4363 Å is stronger than the Hγ line at 4340 Å, indicative of high densities. These include NGC 6804 (De Marco et al., in preparation), Bran 229 (845), M 2-29 (848), PHR J1641-5302 (868; 845), A 57 and PHR J1553-5738 (Miszalski et al., these proceedings), to name a few. Approximately a dozen EGB6-like objects are known today. Both Bond (827) and Gesicki et al. (848) argue that such high density material may be distributed in a disk like structure, or else it would disperse. In the case of EGB6, this disk would be around the companion and would have formed by accretion of AGB primary envelope gas. It is likely that such structures have arisen by binary interactions.

• NGC 2346 (a binary, 858), M 2-29 (a suspected binary, 850; 848) and CPD-56 8032 (a [WC10] with a detected dusty disk; De Marco et al. 832) have lightcurves

showing deep irregular declines, possibly associated with dust emission or a patchy dusty disk.

• Wesson et al. (875) discovered a PN around the V 458 Vul (nova Vul 2007), the second such association after GK Per (826). Rodríguez-Gil et al. (869) determined the period of the binary to be 0.068 days, the shortest period known for a binary central star, and found the binary to be composed of a WD primary and a post-AGB secondary. Another line of evidence associates novae with PN: the high abundance of neon in the hydrogen-deficient ejecta of A30 and A58 (876; 875) interpreted by Lau et al. (854) as the products of a nova explosion that took place shortly after the final helium shell flash (852).

• Santander-Garcia et al. (these proceedings) determined that the secondary star in the binary central star of PN Hen 2-428 is evolved. In agreement with Hillwig (these proceedings), they also determined that about a third of the known central star binary sample (836; 860) has degenerate companions, likely too large compared to the predictions of Moe and De Marco (2010) of ∼5%.

• Hajduk et al. (these proceedings) announced the detection of a 0.2-mag sinusoidal variation with a period of 20.1 days for the central stars of PN G249.8-02.7 (PHR J0755-3346), the longest period irradiated central star binary. The variability amplitude appears too large for such a long period, unless the secondary's radius is quite large and/or the central star very hot. We have not listed this PN in Table 1 because the star may not be associated to the nebula (Miszalski, private communication). The binary in the middle of PN K 1-16 (Table 1) also has a long (21.3 days) photometric period, which may or may not be caused by the binary motion.

• Østensen et al. (865) detected periodic light variability in the central star of the PN DSH J1919.5+4445 (Patchick 5; Jacoby et al. 853) a faint, high excitation, elliptical PN with a hint of bipolarity. The asymmetric lightcurve has a period of 1.1 days and an amplitude of only 0.05 magnitude, the smallest known. The central star is a hot subdwarf. Such small amplitude could only be explained with an almost pole-on viewing angle and/or a small secondary radius.

• A35 was demoted from PN status by Frew (843, see also Frew& Parker 2010). It is more likely to be a Strömgren sphere around a binary star comprising a G subgiant and a hot component that has left the AGB relatively recently. Finally, four PN from the list of De Marco et al. (835) should not be considered binaries until more data is obtained: PHR J1744-3355, PHR J1801-2718, PHR J1804-2645 and PHR J1804-2913 (Miszalski et al. these proceedings).

3. The PN Binary Fraction and Period Distribution

So far we know that 12-21% of all PN have post-common envelope central stars, with periods $\lesssim$3 days (860). This number is not the definitive central star binary fraction for several reasons: (i) The photometric variability technique to detect these binaries is biased to short periods (likely shorter than about 2 weeks; De Marco et al. 836). We still do not know how many binary central stars have periods longer than ∼2 weeks. (ii) The survey of Miszalski et al. (860) was affected by a brightness bias and was carried out only in the Galactic Bulge. (iii) Some of the binaries detected by them have been later questioned (Miszalski et al., these proceedings). (iv) Finally, the period distribution of

Table 1. New or updated binary central stars (update on De Marco et al. 835).

PN name	Type[1]	Period (days)	Morph.[2]	Reference
V 458 Vul	S1	0.068	B:W:	Rodríguez-Gil et al. 869
Te 11	El:	0.12	E	Miszalski et al. these proceedings
NGC 6778	I:	0.15	BPJ	Miszalski et al. these proceedings
He 2-428	El	0.18	RW	Santander-Garcia et al., these proceedings
K 6-34	I	0.20	B:RJ:	revised by Miszalski et al. (861)
Lo 16	EcI	0.49	PJ	Frew 843 and Frew et al., in prep.
ETHOS 1	I	0.53	BJ	Miszalski et al. 2010, submitted
PM 1-23	I:	0.63	W	Hajduk et al. 851
Necklace[3]	I	1.16	RJB	Corradi et al. 829
MPA J1508-6455	I:	12.50	B	Miszalski et al. these proceedings
A 14	Cool,S1:	?	BR	De Marco et al., in preparation
Bran 229	Cool	?	R:P	Frew & Parker (845), Frew et al., in prep.
A 70	Cool,UV	?	R	Miszalski et al., in preparation
K 1-6	Cool,UV	?	E	Frew et al. (846)

[1]Legend: S1: single-lined spectroscopic binaries: El: ellipsoidal variability; I: irradiated; Ec: eclipsing; Cool: only a cool stars is known in the system; UV: a hot component is identified in the UV. ":" means that the designation is uncertain.
[2]Legend: E: elliptical or indistinct; B: clear, bipolar lobes; R: clear ring(s); W: very likely that PN is the edge-on waist of a faded bipolar; J: presence of one or a pair of jets or jet-like structures. P: point symmetry. ":" means that the designation is uncertain.
[3]IPHASXJ194359.5+170901.

the binaries found by Miszalski et al. (860) implies that there is a dearth of binaries in the 3 day to 2 week period range. It is however possible that post-CE binaries with periods in the 3-day to 2 week gap are more plentiful than found by Miszalski et al. (860), but their irradiation properties may be different due, for instance, to the lack of synchronisation of the orbital and spin period of the secondary for these slightly longer period binaries. This would leave the entire secondary irradiated, reducing the contrast between day and night sides. Although this sounds plausible, the period distribution of central stars is similar to that found via radial velocity technique for the WDs by Schreiber et al. (870, see also Hillwig, these proceedings). That technique would not suffer this bias.

Radial velocity surveys of central stars of PN are affected by dramatic wind variability that induces spectral line changes that masks even strong periodic binary signals (833; 839). So the best method to determine the binary fraction with the least number of biases is to test for near-IR excess of a volume-limited sample. With this method we cannot detect periods, although we can get an approximate idea of the companion mass. This method detects unresolved binaries: for a PN at 1 kpc, the orbital separation can be as wide as 500 AU. As a result we will include central star binaries whose separation may be too wide for an interaction having taken place. After detecting the binary fraction in this way, it may not be trivial to account for the fraction of these binaries that has suffered an interaction.

In Fig. 1 (kindly provided by M. Moe) we show the detectability of companions in the *I* and *J* bands. From this figure it is clear that to detect faint companions one has

to use intrinsically faint central stars. Precision photometry is also needed such that the PN has to be faint in order to afford good background subtraction. The *J* band is more sensitive, but logistically problematic (IR and optical photometry of the same targets is needed), such that observing in the *I* band is a more practical approach. Finally, the *H* band can provide some confirmation as well as an idea of the spectral type of the companion. While the *H* band can be contaminated by hot dust the *J* band is unlikely to be.

We have initiated a search using the NOAO 2.1 m telescope in 2007. So far we have found *I*-band excesses indicative of companions brighter than M5V, in 19-42% of the central stars of PN observed (5-11 out of 26) at the 3-1σ level (Passy et al., in preparation). Frew & Parker (844) used the 2MASS and DENIS databases showing that 53% of 34 objects in a volume-limited sample have a *J*-band excess down to ~M6V, at the 2σ level. Combining these results and de-biasing them to include companions down to the M9V limit using the companion mass distribution for the WD population (842), we conclude that (52±10)% of all central stars have a stellar companion closer than ~500 AU. This is tantalisingly higher than predicted by the current PN formation scenario (35%; Duquennoy & Mayor 840). However, with a small sample size we cannot call this a solid result, because small number statistics reject the classical scenario with only 1-2σ confidence.

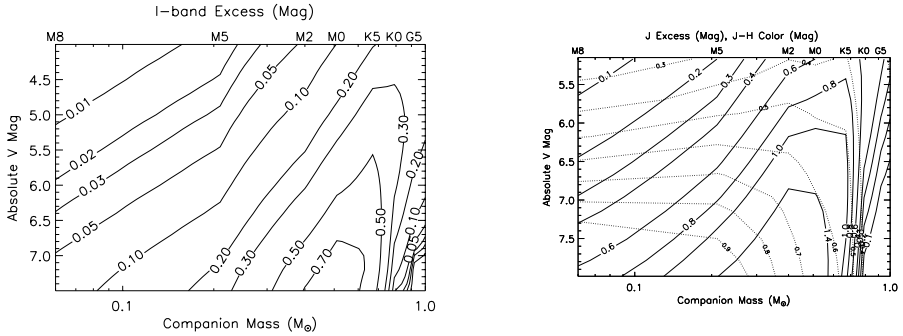

Figure 1. Contour plots of the *I*-band (left) and *J*-band (right, solid) excesses expected for companions of different spectral types and for primaries of different intrinsic *V* brightness (M_V). The *J* band offers increased companion detection sensitivity over the *I* band. The decrease in *I*/*J* excess for earlier companions is due to a contamination of the *V* band by the companion that results in a higher implied reddening resulting in turn in higher predicted (single star) *J* magnitudes and lower excess. The degeneracy in companion spectral type can however be resolved using the $J - H$ colour (dashed contours). *Figure courtesy of M. Moe*

The period distribution of central stars of PN will be very hard to determine. For the short period central star binaries known to date a histogram of the known periods can be found in Miszalski et al. (these proceedings) and Hilliwg (these proceedings). Like the post-CE binary period of WDs (870), the post-CE period for central star of PN peaks at shorter periods than is predicted by any theory of common envelope evolution (e.g., 830).

4. Shaping PN with Planets and Brown Dwarfs

Brown dwarfs and super-Jupiter companions at separations in the range ~2-30 AU may also shape PN (e.g., 872). The actual limits are extremely uncertain. Companions closer than the lower limit will interact on the red giant branch and either be unavailable to interact later on during the AGB evolution or even prevent the AGB ascent altogether. Companions farther than the upper limit have no influence on the AGB star.

We already know that the reservoir of brown dwarfs may be small (also called the brown dwarf desert; Grether & Lineweaver 849) although it is slightly larger for larger separations (~10% 859). However, we do not know how frequently planetary companions at the appropriate orbital separations exist around intermediate mass stars. Bowler et al. (828) determined that (26±9)% of stars having a main sequence mass of $1.5 < M/M_{\odot} < 2.0$ host massive planets at large separations (but still less than 3 AU). The new finding is not only of a larger fraction of planet-hosting stars, but also puts the planets at larger orbital separations, where they can more easily be available to shape winds from AGB stars.

De Marco et al. (835) pointed out that aside from our ignorance of planetary companion frequency, we also did not know what effect, if any, such low mass companions would have on an AGB star. Geier et al. (847) discovered an 8-23-M_J companion in a 2.4-day period orbit around the post-red giant branch subdwarf B star HD149382. This companion must have been in a common envelope with its primary and been able to eject the envelope.

Based on the morphological considerations of Soker (873) and Soker & Subag (874) and the population study of Moe & De Marco (863), as well as from the most recent planetary statistics De Marco & Soker (838) argued that the fraction of PN that have been shaped by planets is of the order of 20%. If we consider that only 20% of all intermediate mass stars make PN, then one would also conclude that the fraction of intermediate mass stars that interact with a planet-mass companion on the AGB is of the order of 4%.

5. What can be achieved by Asymmetrical Planetary Nebula VI

At the current rate of discovery, by the next Asymmetrical PN conference in 2013 we should be able to have:

• Precision (1-2%) photometry of 50-75 central stars of PN in the *B*, *V* and *I*-band as well as accurate *J*-band photometry for one third to one half of them. This will refine considerably the current, extremely imprecise estimate of the overall PN binary fraction.

• A doubling of the sample of central stars binaries form ~50 to ~100. Most of them will be short period binaries as they are easier to detect and will therefore provide only a biased view of the PN binary population. However such a large sample will allow us to draw statistical conclusions regarding the association between binarity and bipolar morphology (see initial results by Miszalski et al. (861))

• At least 20 objects with determined masses and inclinations via radial velocity analysis and stellar atmosphere modelling. There are currently only 6 central stars of

PN for which such parameters are known. A larger sample can help characterise the efficiency of the common envelope ejection (837; 877).

Acknowledgments. David Frew, Brent Miszalski, Marcin Hadjuk, Todd Hillwig, George Jacoby and Geoff Clayton are thanked for helpful comments. Max Moe is thanked for Figure 1.

References

Bilikova, J., Chu, Y., Su, K., Gruendl, R., Rauch, T., De Marco, O., & Volk, K. 2009, Journal of Physics Conference Series, 172, 012055

Bode, M. F., Roberts, J. A., Whittet, D. C. B., Seaquist, E. R., & Frail, D. A. 1987, Nat, 329, 519

Bond, H. E. 2009, Journal of Physics Conference Series, 172, 012029

Bowler, B. P., Johnson, J. A., Marcy, G. W., Henry, G. W., Peek, K. M. G., Fischer, D. A., Clubb, K. I., Liu, M. C., Reffert, S., Schwab, C., & Lowe, T. B. 2010, ApJ, 709, 396. 0912.0518

Corradi, R. L. M., Sabin, L., Miszalski, B., Rodríguez-Gil, P., Santander-García, M., Jones, D., Drew, J., Mampaso, A., Barlow, M., Rubio-Díez, M. M., Casares, J., Viironen, K., Frew, D. J., Giammanco, C., Greimel, R., & Sale, S. 2010, ArXiv e-prints. 1009.1043

Davis, P. J., Kolb, U., & Willems, B. 2010, MNRAS, 403, 179. 0903.4152

De Marco, O. 2008, in Hydrogen-Deficient Stars, edited by A. Werner, & T. Rauch, vol. 391 of Astronomical Society of the Pacific Conference Series, 209

De Marco, O., Barlow, M. J., & Cohen, M. 2002, ApJ, 574, L83. arXiv:astro-ph/0206202

De Marco, O., Bond, H. E., Harmer, D., & Fleming, A. J. 2004, ApJ, 602, L93

De Marco, O., & Crowther, P. A. 1998, MNRAS, 296, 419

De Marco, O., Farihi, J., & Nordhaus, J. 2009, Journal of Physics Conference Series, 172, 012031

De Marco, O., Hillwig, T. C., & Smith, A. J. 2008, AJ, 136, 323

De Marco, O., Passy, J.-C., Moe, M., Herwig, F., Mac Low, M.-M., & Paxton, W. 2010, MNRAS, accepted

De Marco, O., & Soker, N. 2010, PASP, submitted

De Marco, O., Wortel, S., Bond, H. E., & Harmer, D. 2007, in Asymmetrical Planetary Nebulae IV, IAC Elec. Pub. 0709.1508

Duquennoy, A., & Mayor, M. 1991, A&A, 248, 485

Edgar, R. G., Nordhaus, J., Blackman, E. G., & Frank, A. 2008, ApJ, 675, L101. 0709.2292

Farihi, J., Becklin, E. E., & Zuckerman, B. 2005, ApJS, 161, 394. arXiv:astro-ph/0506017

Frew, D. J. 2008, Ph.D. thesis, Department of Physics, Macquarie University.

Frew, D. J., & Parker, Q. A. 2007, in Asymmetric Planetary Nebulae IV, IAC Elec. Pub.

— 2010, PASA, 27, 129. 1002.1525

Frew, D. J., Stanger, J., Fitzgerald, M., Parker, Q., Danaia, L., McKinnon, D., Guerrero, M. A., Hedberg, J., Hollow, R., An, Y., Bor, S. H., Colman, I., Graham-White, C., Li, Q. W., Mai, J., Papadakis, K., Picone-Murray, J., Hoang, M. V., & Yean, V. 2010, ArXiv e-prints. 1009.5914

Geier, S., Edelmann, H., Heber, U., & Morales-Rueda, L. 2009, ApJ, 702, L96. 0908.1025

Gesicki, K., Zijlstra, A. A., Szyszka, C., Hajduk, M., Lagadec, E., & Guzman Ramirez, L. 2010, A&A, 514, A54+. 1001.5387

Grether, D., & Lineweaver, C. H. 2006, ApJ, 640, 1051. arXiv:astro-ph/0412356

Hajduk, M., Zijlstra, A. A., & Gesicki, K. 2008, A&A, 490, L7. 0807.0028

— 2010, MNRAS, 406, 626

Herwig, F. 2001, Ap&SS, 275, 15. arXiv:astro-ph/9912353

Jacoby, G. H., Kronberger, M., Patchick, D., Teutsch, P., Saloranta, J., Howell, M., Crisp, R., Riddle, D., Acker, A., Frew, D. J., & Parker, Q. A. 2010, PASA, 27, 156. 0910.0465

Lau, H. H. B., De Marco, O., & Liu, X. W. 2010, ArXiv e-prints. 1009.3138

Leuenhagen, U., Hamann, W.-R., & Jeffery, C. S. 1996, A&A, 312, 167
Mastrodemos, N., & Morris, M. 1998, ApJ, 497, 303
— 1999, ApJ, 523, 357
Mendez, R. H., & Niemela, V. S. 1981, ApJ, 250, 240
Metchev, S. A., Kirkpatrick, J. D., Berriman, G. B., & Looper, D. 2008, ApJ, 676, 1281. 0710.4157
Miszalski, B., Acker, A., Moffat, A. F. J., Parker, Q. A., & Udalski, A. 2009, A&A, 496, 813. 0901.4419
Miszalski, B., Acker, A., Parker, Q. A., & Moffat, A. F. J. 2009, A&A, 505, 249. 0907.2463
Miszalski, B., Parker, Q. A., Acker, A., Birkby, J. L., Frew, D. J., & Kovacevic, A. 2008, MNRAS, 384, 525. 0711.2923
Moe, M., & De Marco, O. 2006, ApJ, 650, 916. arXiv:astro-ph/0606354
— 2010, in Asymmetric Planetary Nebulae 5, A. A. Zijlstra, F. Lykou, E. Lagadec, and I. McDonald (eds.), published by Ebrary (Palo Alto CA, USA), A107
Østensen, R. H., Silvotti, R., Charpinet, S., Oreiro, R., Handler, G., Green, E. M., Bloemen, S., Heber, U., Gänsicke, B. T., Marsh, T. R., Kurtz, D. W., Telting, J. H., Reed, M. D., Kawaler, S. D., Aerts, C., Rodríguez-López, C., Vučković, M., Ottosen, T. A., Liimets, T., Quint, A. C., Van Grootel, V., Randall, S. K., Gilliland, R. L., Kjeldsen, H., Christensen-Dalsgaard, J., Borucki, W. J., Koch, D., & Quintana, E. V. 2010, ArXiv e-prints. 1007.3170
Paczynski, B. 1976, in Structure and Evolution of Close Binary Systems, edited by P. Eggleton, S. Mitton, & J. Whelan, vol. 73 of IAU Symposium, 75
Parker, Q. A., Acker, A., Frew, D. J., Hartley, M., Peyaud, A. E. J., Ochsenbein, F., Phillipps, S., Russeil, D., Beaulieu, S. F., Cohen, M., Köppen, J., Miszalski, B., Morgan, D. H., Morris, R. A. H., Pierce, M. J., & Vaughan, A. E. 2006, MNRAS, 373, 79
Parker, Q. A., Hartley, M., Russeil, D., Acker, A., Morgan, D. H., Beaulieu, S., Morris, R., Phillipps, S., & Cohen, M. 2003, in IAU Symposium, 25
Rodríguez-Gil, P., Santander-García, M., Knigge, C., Corradi, R. L. M., Gänsicke, B. T., Barlow, M. J., Drake, J. J., Drew, J., Miszalski, B., Napiwotzki, R., Steeghs, D., Wesson, R., Zijlstra, A. A., Jones, D., Liimets, T., Muñoz-Darias, T., Pyrzas, S., & Rubio-Díez, M. M. 2010, MNRAS, 407, L21. 1006.1075
Schreiber, M. R., Gaensicke, B. T., Zorotovic, M., Rebassa-Mansergas, A., Nebot Gomez-Moran, A., Southworth, J., Schwope, A. D., Pyrzas, S., Tappert, C., & Schmidtobreick, L. 2009, Journal of Physics Conference Series, 172, 012024
Soker, N. 1989, ApJ, 340, 927
— 1996, ApJ, 460, L53+
— 1997, ApJS, 112, 487
Soker, N., & Subag, E. 2005, AJ, 130, 2717. arXiv:astro-ph/0503294
Wesson, R., Barlow, M. J., Liu, X.-W., Storey, P. J., Ercolano, B., & de Marco, O. 2008, MNRAS, 383, 1639. arXiv:0711.1139
Wesson, R., Liu, X.-W., & Barlow, M. J. 2003, MNRAS, 340, 253. arXiv:astro-ph/0301119
Zorotovic, M., Schreiber, M. R., Gänsicke, B. T., & Nebot Gómez-Morán, A. 2010, A&A, 520, A86+. 1006.1621

Asymmetric Planetary Nebulae V
A. A. Zijlstra, F. Lykou, E. Lagadec and I. McDonald
Jodrell Bank Centre for Astrophysics, Manchester, UK © 2011

The binary central stars of PNe with the shortest orbital periods

M. Santander-García[1,2,3], P. Rodríguez-Gil[1,2,3], D. Jones[4], R. L. M. Corradi[2,3], B. Miszalski[5], S. Pyrzas[6], and M. M. Rubio-Díez[7]

[1]*Isaac Newton Group of Telescopes, Ap. de Correos 321, E-38700 Sta. Cruz de la Palma, Spain*

[2]*Instituto de Astrofísica de Canarias, E-38200 La Laguna, Tenerife, Spain*

[3]*Departamento de Astrofísica, Universidad de La Laguna, E-38205 La Laguna, Tenerife, Spain*

[4]*Jodrell Bank Centre for Astrophysics, School of Physics and Astronomy, The University of Manchester, Manchester, M13 9PL, UK*

[5]*Centre for Astrophysics Research, STRI, University of Hertfordshire, College Lane Campus, Hatfield AL10 9AB, UK*

[6]*Department of Physics, University of Warwick, Coventry, CV4 7AL, UK*

[7]*Centro de Astrobiología, CSIC-INTA, Ctra de Torrejón a Ajalvir km 4, E-28850 Torrejón de Ardoz, Spain*

Abstract. Close binarity can play a significant role in the shaping of planetary nebulae (PNe) as the system evolves through the common-envelope phase. We present the detection of two of the shortest orbital periods among PN binary central stars. These are Hen 2-428, a bipolar PN, and V458 Vul, a recent nova surrounded by a mildly bipolar planetary nebula. The properties of the central stars of these systems, of their nebulae and their possible fate are discussed.
Keywords. Planetary Nebulae – Binaries

1. Introduction

The link between the shaping of bipolar planetary nebulae and their central stars (CSPN) is still poorly understood. The distinct theoretical approaches to explain their shaping (see the review by 878) fall into two broad categories: *a)* rapid stellar rotation and/or magnetic fields (e.g. 883; 879), and *b)* a close interacting companion to the star (e.g. Nordhaus & Blackman 889, for a review see de Marco 882). This binary hypothesis is currently gaining ground as the number of close binary systems at the cores of bipolar PNe is growing (e.g. Miszalski et al. 2009b).

In this context, our group found several new close-binary CSPNe during recent photometric observing runs at the 1.2-m Mercator telescope (888). One of the main goals of these runs was to test the hypothesis that certain morphological features of

PNe such as rings and/or jets could be related to close binarity. Some of the newly detected binary CSPNe show orbital periods as short as a few hours.

In this work we discuss the extreme case of the shortest orbital periods of binary CSPNe through the examples of Hen 2–428, a bipolar PN, and V458 Vul, a CSPN which recently underwent a nova eruption and shows the shortest orbital period of this kind of object so far.

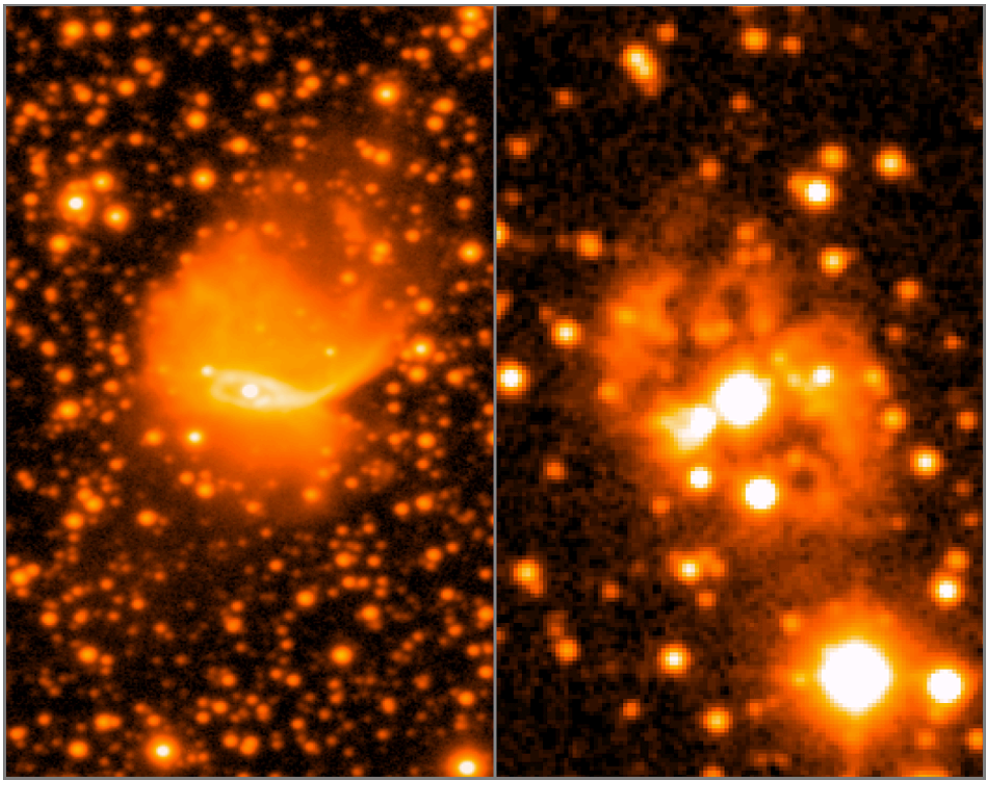

Figure 1. **Left**: Close-up 2 hour-deep image of Hen 2–428 in Hα with the INT/WFC. North is up and East is to the left. There is no apparent trace of ancient polar jets (not even at a larger scale). **Right:** Close-up 36 min image of V458 Vul with the INT/WFC. North is up and East is to the left.

2. Hen 2–428

This nebula consists of a pair of open lobes emerging from a central waist shaped as a ring inclined 68° to the plane of the sky. A 2-hour deep Hα image (see Fig. 1) taken with the Wide Field Camera (WFC) at the 2.5-m Isaac Newton Telescope (INT) reveals no apparent trace of ancient polar jets in the system. Hen 2–428 was studied in detail by (893), who already hinted at the possibility of this system actually hosting a binary core. Among the properties which lead to that suggestion were the extremely low abundance of every element except He (in particular, the oxygen abundance is as low as [O/H]~7.8); the unresolved nebular core with an electron density of n_e=$10^{3.3-6}$

cm^{-3}, indicative of strong mass loss or exchange phenomena taking place; and a central region with $n_e > 10^{10}$ cm^{-3} where the Ca II triplet arises in emission, which could be explained by the presence of an accretion disc.

The following results are preliminary and will be further analysed and discussed in Santander-García (in preparation).

2.1. Observations

We carried out I-band photometry of Hen 2–428 with MEROPE on the Mercator telescope on the nights of August 28 and 30, 2009. Once we detected a photometric variability as large as ∼0.36 mag between different short blocks, we monitored the system for a continuous, 4 hour period on September 2, 2009. Later, on May 1, 2010, we carried out a 2.25 hour spectroscopic monitoring with Intermediate dispersion Spectrograph and Imaging System (ISIS) on the 4.2-m William Herschel Telescope (WHT), with the R600B and the R316R gratings in the blue and red arms, respectively, and a slit width of 1 arcsec. The resolution was, respectively, ∼1.5 and ∼3 Å.

2.2. Results

The light curve of Hen 2–428 in the I-band, folded on the period determined below, is shown in Fig. 2. We performed a period analysis using Schwarzenberg-Czerny's (896) analysis-of-variance (AOV) method as implemented in the `MIDAS/TSA` context. The AOV periodogram shows the strongest peak at ∼11.379 cycles d^{-1}, which corresponds to a period of 0.0879 days, or 2.1 hours. However, the light curve shows a clear ellipsoidal modulation with the two minima showing almost equal depths (in a very similar case to MT Ser, the nucleus of Abell 41, Bruch et al. 880). This, together with the confirmation of the orbital phase given by the spectra (see below), leads us to consider a period twice as large as being the orbital period of the system.

A sine fit to the whole data set results in P∼0.17 d (∼4.2 hours), and an I-band amplitude of ∼0.18 mag. We take the observed CSPN variability as a clear indication of binarity, the brightness modulation being the result of ellipsoidal modulation of one or both stars (i.e. the star is gravitationally distorted, close to or filling its Roche lobe and thus presents the observer at Earth a varying surface along its relative orbital position, and therefore a varying flux). This is supported by the modelling of the light curve presented below.

The spectroscopic monitoring, carried out with the WHT/ISIS for approximately two thirds of a complete orbital period, shows an apparent double S-wave pattern which could be interpreted as two different He II 468.6 nm components in absorption. This would indicate that Hen 2–428 hosts in fact a double-degenerate nucleus with two white dwarves. However, the S/N ratio of the spectra are too low to either unambiguously ascertain the presence of the two absorption components or carry out precise measurements of the Doppler shifts which could lead to mass ratio and orbital parameter constraints, for which an 8-meter class telescope will be needed.

On the other hand, a preliminary modelling of the light curve, made both with `PHOEBE` (Prša & Zwitter 891) and the `LCURVE` code developed by Tom Marsh (Copperwheat et al. 881) provides a fair fit to the data (see Fig.2). Although the lack of constraints such as the orbital velocities and the mass ratio results in a degeneracy of

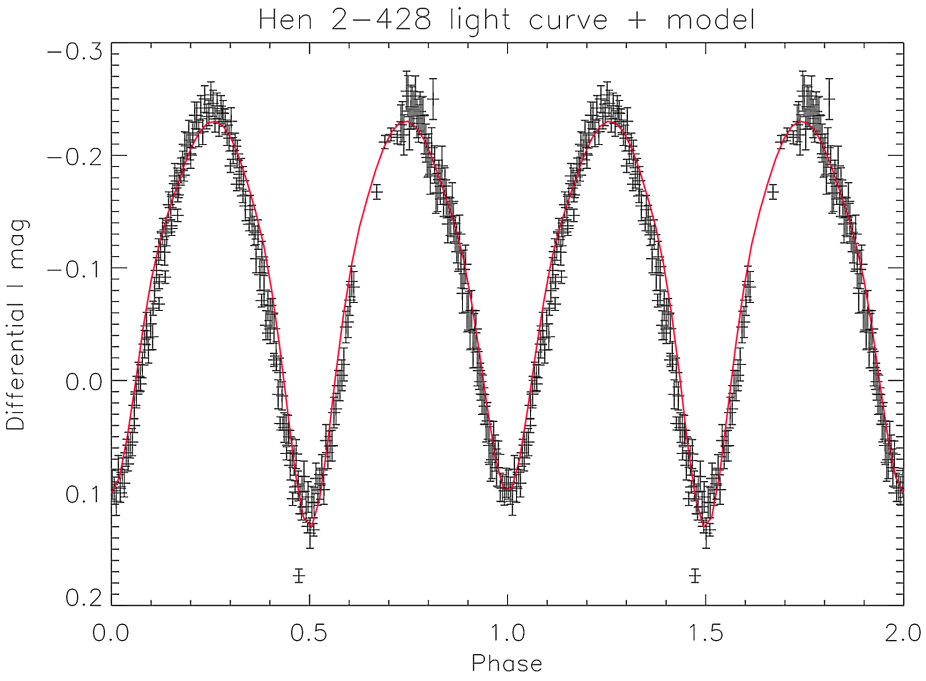

Figure 2. I-band light curve of Hen 2–428, folded on the period of 4.2 hours determined in the text. A preliminary model of the light curve is shown as a thick red line.

most of the model parameters, the following results hold for every possible set of parameters: (a) the light variations are due to ellipsoidal modulation, (b) the system is a contact binary in which both components fill their Roche lobe, (c) the T_{eff} of both stars are similar within a few thousand Kelvin and (d) the inclination of the orbital plane ranges between 40° and 70°, close to the 68°-inclined equatorial ring of the nebula.

3. V458 Vul

V458 Vul (see Fig. 1) is a system which underwent a fast nova eruption on the summer of 2007. It was the subject of a work by (898), in which they reported the discovery of a ~ 14000 year-old, wasp-waisted PN surrounding the nova progenitor. Their photoionisation model revealed that the ionising source must have a temperature of T_{eff} ~90,000 K, a luminosity of L_{bol} ~3000 $L_{\odot}$ and a radius of R~0.23 $R_{\odot}$. These values lead, through the use of H-burning tracks, to a mass for the ionising source of M~0.58 $M_{\odot}$. On the other hand, fast nova theoretical models (e.g. Yaron et al. 899, Prialnik & Kovetz 890), together with some observations (892) point to a mass of M>1 $M_{\odot}$ for the nova progenitor to be able to trigger the thermonuclear runaway, which is clearly at odds with the value found via the H-burning tracks.

3.1. Observations

In an attempt to measure a precise orbital period we started a time-resolved spectroscopic campaign searching for the orbital signature in the radial velocities of the emission lines. The spectroscopic data were obtained with the Intermediate Dispersion Spectrograph (IDS) on the INT and ISIS on the WHT, both on La Palma. The total time on target was 39 hours, over 9 different nights in the period June 4, 2008 – August 31, 2009. The instrumental setup covered a range of gratings and resolutions, for details see (894).

3.2. Results

The average optical spectrum of V458 Vul taken on 2008 June 4 (day 301 after the nova explosion) showed the flat-topped emission line profiles characteristic of this class of objects. However, the round-topped profile of the He II 541.2 nm line attracted our attention during a first visual inspection of the line shapes. We found the Doppler shift of this line to vary between ∼-200 and ∼200 km s^{-1} This radial velocity variation indicated that at least one of the components of the He II 541.2 nm emission forms in a binary system at the core of the planetary nebula. By November 2008, the He II 468.6 nm also showed a clear modulation, once the line thinned out (i.e. shed some nova ejecta emission).

The radial velocity data, combining the measurements from the He II 541.2 nm and He II 468.6 nm lines was subjected to the same AOV period analysis as Hen 2–428. The periodogram exhibits a narrow spike at 14.68 cycles d^{-1}. A sine fit to the whole data set resulted in P = 0.06812255±0.00000017 d (98.1 min). This makes V458 Vul the binary CSPN with the shortest orbital period known so far.

This finding presents us with an intriguing discrepancy: a nova with such a short orbital period must be an old system, of the order of Gyr, much older indeed than the 14000 yr old PN we observe. This discrepancy is easily removed, however, by assuming the observable PN to be the second one of the system (the resulting ejecta after a second common-envelope stage). Furthermore, this is fully consistent with the measurements and modelling presented by 898: we have a double-degenerate nucleus consisting of two white dwarves, one with M∼0.58 $M_\odot$, the present ionising source, and another one, the nova progenitor, with M>1 $M_\odot$.

Hence, the total mass of V458 Vul may well be above 1.6 $M_\odot$, above the critical Chandrasekhar mass, indicating that it may become a Type Ia supernova, if the white dwarf manages to accumulate mass in the presence of nova eruptions.

The aforementioned results are discussed in greater detail in (894).

4. Summary and final thoughts

We have determined the orbital period and nature of the central stars of Hen 2–428 (0.18 days) and V458 Vul (0.068 days), the latter of which is also a SN Ia candidate. V458 Vul is the CSPN with the shortest orbital period known so far, while the period of Hen 2–428 figures among the shortest orbital periods known (after Te 11, 0.12 days, Miszalski et al. 888; Pe 1-9 and BMP 1800-3408, 0.14 days, Miszalski et al. 2009a;

NGC 6778, 0.15 days, Miszalski et al. 888; SBS 1150+599A, 0.16 days, Tovmassian et al. 897 and de Marco 882).

On the other hand, both of the discussed objects appear to be double-degenerate close-binary CSPNe, a class of objects which might indeed be quite common (e.g. MT Ser, Bruch et al. 880; TS 01, Tovmassian et al. 897; NGC 6026, Hillwig et al. 2010a; but see also Hillwig 2010b), amounting up to 33% of the sample in Miszalski et al. (2009a).

Building a larger sample of this class of close-binary CSPN is important, not only to better assess their fraction in the total number of PNe, but also because they can provide us with vital information about the role of the second common-envelope stage and Roche-lobe filling (or contact binarity) in the evolution and shaping of PNe, and because some of them might be SN Ia candidates.

Acknowledgments. MSG thanks Tom Marsh for the use of his code, and the SOC of the APN V conference for the invited talk.

References

Balick, B., & Frank, A. 2002, ARA&A, 40, 439
Blackman, E. G., Frank, A., & Welch, C. 2001, ApJ, 546, 288
Bruch, A., Vaz, L. P. R., & Diaz, M. P. 2001, A&A, 377, 898
Copperwheat, C. M., Marsh, T. R., Dhillon, V. S., Littlefair, S. P., Hickman, R., Gänsicke, B. T., & Southworth, J. 2010, MNRAS, 402, 1824
de Marco, O. 2009, PASP, 121, 316
García-Segura, G., Langer, N., Różyczka, M., & Franco, J. 1999, ApJ, 517, 767
Hillwig, T. 2010b, Asymmetric Planetary Nebulae 5, A. A. Zijlstra, F. Lykou, E. Lagadec and I. McDonald (eds.), published by Ebrary (Palo Alto CA, USA), p. 276
Hillwig, T. C., Bond, H. E., Afşar, M., & De Marco, O. 2010a, AJ, 140, 319
Miszalski, B., Acker, A., Moffat, A. F. J., Parker, Q. A., & Udalski, A. 2009a, A&A, 496, 813
Miszalski, B., Acker, A., Parker, Q. A., & Moffat, A. F. J. 2009b, A&A, 505, 249
Miszalski, B., Corradi, R. L. M., Jones, D., Santander-García, M., Rodríguez-Gil, P., & Rubio-Díez, M. M. 2010, Asymmetric Planetary Nebulae 5, A. A. Zijlstra, F. Lykou, E. Lagadec and I. McDonald (eds.), published by Ebrary (Palo Alto CA, USA), p. 330
Nordhaus, J., & Blackman, E. G. 2006, MNRAS, 370, 2004
Prialnik, D., & Kovetz, A. 1995, ApJ, 445, 789
Prša, A., & Zwitter, T. 2005, ApJ, 628, 426
Ritter, H., & Kolb, U. 2003, A&A, 404, 301
Rodríguez, M., Corradi, R. L. M., & Mampaso, A. 2001, A&A, 377, 1042
Rodríguez-Gil, P., Santander-García, M., Knigge, C., Corradi, R. L. M., Gänsicke, B. T., Barlow, M. J., Drake, J. J., Drew, J., Miszalski, B., Napiwotzki, R., Steeghs, D., Wesson, R., Zijlstra, A. A., Jones, D., Liimets, T., Muñoz-Darias, T., Pyrzas, S., & Rubio-Díez, M. M. 2010, MNRAS, 407, L21
Santander-García, M. in preparation
Schwarzenberg-Czerny, A. 1996, ApJ, 460, L107
Tovmassian, G., Yungelson, L., Rauch, T., Suleimanov, V., Napiwotzki, R., Stasińska, G., Tomsick, J., Wilms, J., Morisset, C., Peña, M., & Richer, M. G. 2010, ApJ, 714, 178
Wesson, R., Barlow, M. J., Corradi, R. L. M., Drew, J. E., Groot, P. J., Knigge, C., Steeghs, D., Gaensicke, B. T., Napiwotzki, R., Rodriguez-Gil, P., Zijlstra, A. A., Bode, M. F., Drake, J. J., Frew, D. J., Gonzalez-Solares, E. A., Greimel, R., Irwin, M. J., Morales-Rueda, L., Nelemans, G., Parker, Q. A., Sale, S. E., Sokoloski, J. L., Somero, A., Uthas, H., Walton, N. A., Warner, B., Watson, C. A., & Wright, N. J. 2008, ApJ, 688, L21
Yaron, O., Prialnik, D., Shara, M. M., & Kovetz, A. 2005, ApJ, 623, 398

Asymmetric Planetary Nebulae V
A. A. Zijlstra, F. Lykou, E. Lagadec and I. McDonald
Jodrell Bank Centre for Astrophysics, Manchester, UK © 2011

Are PPNe Shaped by a Binary? Results of Long-Term Radial Velocity and Light Curve Studies

Bruce J. Hrivnak

Dept. of Physics & Astronomy, Valparaiso University, Valparaiso, IN 46383 USA

Abstract. We have carried out long-term photometric and radial velocity monitoring of a sample of proto-planetary nebulae (PPNe). While pulsational variations are seen in all of them, only one of the seven monitored for radial velocity variations shows evidence of a binary companion (P≈34 years). The high precision and long time scale (18 years) of the velocity monitoring allow us to set significant constraints on any undetected binaries; in general, they must be low mass (< 0.25 $M_{\odot}$) or of long period (> 30 years).
Keywords. Planetary Nebulae – Binaries

1. Why Search for Binaries in PPNe?

The proto-planetary nebula (PPN) and planetary nebula (PN) phases immediately follow the asymptotic giant branch (AGB) phase in the evolution of intermediate- and low-mass stars. During the AGB phase, the star loses a significant fraction of its mass. If the evolution of the central star and the expansion of the nebula have similar time scales, a visible nebula will be seen. Many PNe and PPNe show elliptical or bipolar structures with axial symmetry (900). A leading hypothesis to explain this shape involves a binary companion (905). We are engaged in a long-term photometric and radial velocity study to search for such binaries in PPNe to help clarify the shaping mechanism(s).

2. Photometric Search for Binaries in PPNe

A binary companion can be detected photometrically due to an eclipse, an irradiation of the cooler star by the hotter star, or an ellipticity in the larger star (PPN) caused by the tidal effect of the companion. Such methods have been used successfully by Bond (902), Miszalski et al. (910), and others to identify binary companions to the central stars in ∼40 PNe, with periods ranging from 1 to 8 days. On this basis, they determine that 10−20 % of PNe have close binary companions.

We have carried out photometric monitoring since 1994 of ∼30 PPNe, using the 0.4-m telescope at Valparaiso University. All vary, but this is clearly shown to be due to pulsation. See Hrivnak et al. (907) and Hrivnak (906) for examples of the light curves

and detailed evidence for the pulsational nature of these variations. No photometric evidence for binarity of PPNe has been found.

3. Radial Velocity Search for Binaries in PPNe

Radial velocity variations provide another way to search for binarity in PPNe, particularly those with intermediate periods in the range of a few months to a few decades. Such searches have been carried out for PNe (e.g., 904), but they are complicated by intrinsic variations and winds, and they have not proved to be successful. To illustrate the magnitude of the velocity variation expected, if we assume M_{PPN} = 0.62 $M_{\odot}$, M_{comp} = 0.50 $M_{\odot}$, and a PPN of spectral type G just within its Roche lobe, then the orbital period P = 1.0 year and the orbital velocity is 13 km s^{-1}. If the separation is larger and P = 30 years, then the orbital velocity is 4.5 km s^{-1}. The observed radial velocity will be reduced by sin *i*, where *i* is the inclination with respect to the plane of the sky, but even if $i = 30°$, sin i = 0.5 and thus the effect is not so large.

Our study was carried out at the Dominion Astrophysical Observatory with the 1.2-m telescope. We observed seven bright PPNe (V=7-11 mag) of spectral types F and G; they thus have many sharp lines, an advantage compared to the very hot central stars of PNe. The velocities have a precision of ~0.7 km-s^{-1}. We carried out an initial study from 1991−1995 and then reinitiated the program in 2007, in collaboration with D. Bohlender, A. Woodsworth, S. Morris, and C. Scarfe. The targets are IRAS 07134+1005, 17436+5003, 18095+2704, 19475+3119, 19500−1709, 22223+4327, and 22272+5435. We obtained 35 to 80 observations of each of these targets through the end of 2009. Three of the targets also have substantial data sets in the literature: IRAS 07134+1005 (909; 901), 17436+5003 (903), and 22272+5435 (913),

4. Radial Velocity Results: Perhaps One Binary

All of the PPNe vary in velocity over a range of 10−14 km s^{-1}, and for most of these we could find a period, which in all cases was similar to the photometric period of the target (35−150 days). This can be seen in Figure 1.

Only one object showed clear evidence for a long-term variability that might be interpreted as due to binary motion. That is IRAS 22272+5435, which shows a significant change in average velocity of −2.2 km s^{-1} between its 1991−1995 and its 2005−2009 observations. The data suggest a period of 34±11 years, with a velocity semi-amplitude of K = 1.8±0.5 km s^{-1}. We interpret this as most likely due to the motion of the PPN around the barycenter of a binary star system. This velocity curve is shown in Figure 1. With some reasonable assumptions (M_{PPN}=0.62 $M_{\odot}$, *e*=0.0), and $i = 25°$ determined from the infrared study by Ueta et al. (911), this results in M_{comp} = 0.51 $M_{\odot}$ and a = 11 AU = 2300 $R_{\odot}$.

While the other six do not show evidence of binary motion, *we must consider observational bias in the selection of the targets*. Since they are all bright, then we are unlikely to be observing them edge-on through the torus but at some lower inclination, closer to the plane of the sky. Nevertheless, one can still set useful constraints on the parameters of any undetected binaries. These are shown graphically in Figure 2. For

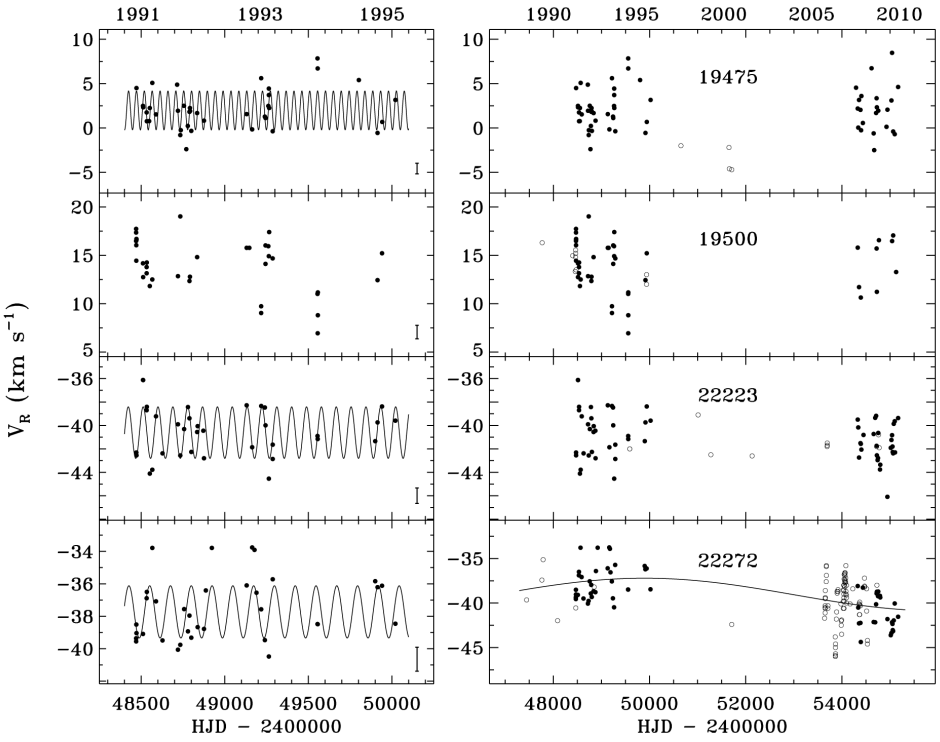

Figure 1. Radial velocity curves for four of the bright targets. On the right are shown the velocities over the entire observing interval (1991−2009) while on the left are shown the velocities during the shorter interval 1991−1995 to better display the pulsational nature of the variations. On the right hand figure of IRAS 22272+5435 is shown the curve of the 34 year period.

example, if M_{comp} = 0.4 $M_\odot$ and assuming a detection limit to K = 2.0 km s^{-1}, then $P_{orbit} \geq 3.5$ years if $i \geq 15°$ and $P_{orbit} \geq 24.5$ years if $i \geq 30°$. In fact, mid-infrared and visible *HST* images of most of these six objects suggest they are at some intermediate orientation rather than pole on, so these provide significant constraints. These results are discussed in more detail by Hrivnak et al. (908).

5. Summary and Future Work

Our photometric observations show clear evidence for pulsation, but no evidence for binarity. The radial velocity observations show evidence for binarity in only one case among the seven studied, with a period of ∼34 years. They also set significant constraints on the properties of any undetected binaries; such binaries must have low mass companions (<0.25 $M_\odot$) or long periods (> 30 years). Thus they do not rule out brown dwarf or planetary companions. However, these results rule out the idea of these PPNe evolving from the post-AGB binaries of the type found by Van Winckel (912), and they rule out their evolving into the short-period central stars of binary PNe.

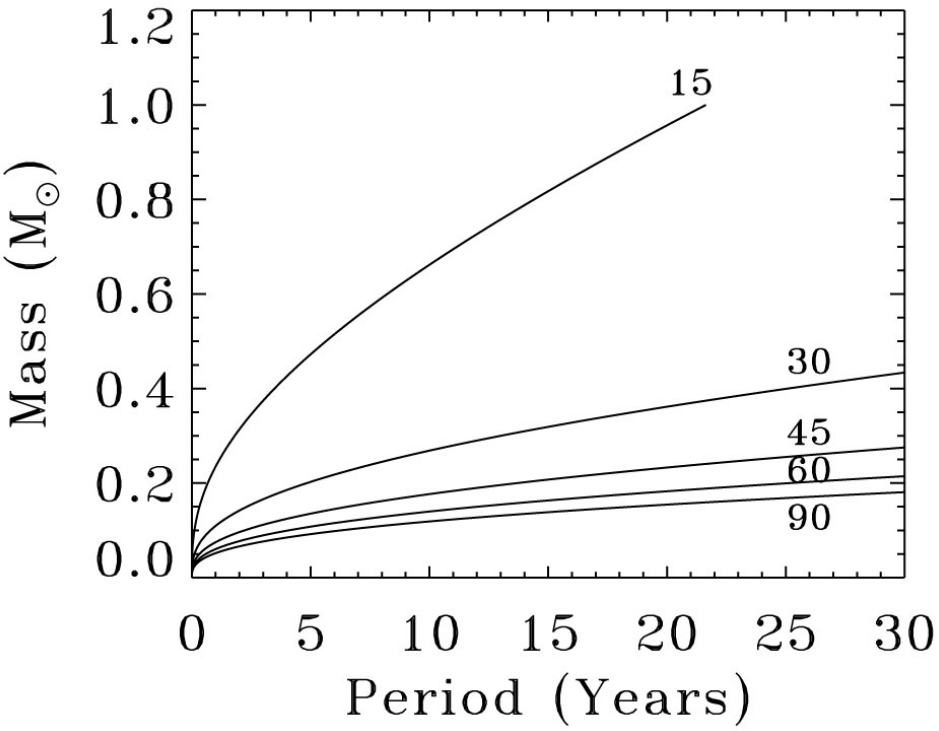

Figure 2. Non-detection constraints on possible binary companions and periods, assuming that $M_{PPN} = 0.62\ M_\odot$ and a detection limit to $K = 2.0$ km s^{-1}. The numbers on the curves represent i in degrees. Non-detections imply that undetected binary companions lie in the parameter space below the curves.

We are continuing the radial velocity monitoring of these seven bright PPNe to search for lower mass or longer period binaries or to further constrain their properties, and to also better determine the properties of the one likely binary. Perhaps more significantly, we have begun a program to monitor the velocity of three edge-on PPNe for which the central stars are seen in the near-infrared. For these there is no ambiguity in i. This is carried out in collaboration with F. Kerber (ESO) and K. Hinkle (Gemini). Hopefully we will have new results to report at APN6!

Acknowledgments. I thank W. Lu, my collaborator in much of this research, and also the many Valparaiso University students who have monitored the light variability of these PPNe since 1994. I also thank my collaborators in the spectroscopic monitoring at the DAO, who are listed above. This research has been partially supported by the NSF (AST-0407087, 1009974).

References

Balick, B., & Frank, A. 2002, ARA&A, 40, 439
Barthés, D., Lébre, A., Gillet, D., & Mauron, N.,2000, A&A, 359, 168
Bond, H.E., 2000, in ASP Conf. Ser. 199: Asymmetic Planetary Nebulae II - From Origins to Microstructures, ed. J. H. Kastner, N. Soker, S. Rappaport (San Francisco: ASP), 115

Burki, G., Mayor, M., & Rufener, F. 1980, A&AS, 42, 383
De Marco, O. 2006, in IAU Symp 234: Planetary Nebulae in our Galaxy and Beyond, ed. by M. J. Barlow, R. H. Méndez (Cambridge University Press, Cambridge 2006), 111
De Marco, O. 2009, PASP, 121, 316
Hrivnak, B.J. 2009, in Stellar Pulsation: Challenges for Theory and Observation, eds. J.A. Guzik, P.A. Bradley (New York, AIP), 597
Hrivnak, B. J., Lu, W., Maupin, R. E. & Spitzbart, B. D. 2010a, ApJ, 709, 1042
Hrivnak, B. J., Lu, W., Wefel, K. L., et al. 2010b, submitted for publication
Lébre, A., Mauron, N., Gillet, D., & Barthés, D. 1996, A&A, 310, 923
Miszalski, B., Acker, A., Moffett, A.F.J., Parker, Q.A., & Udalski, A. 2009, A&A, 496, 813
Ueta, T., Meixner, M., et al. 2001, ApJ, 557, 831
Van Winckel, H. 2007, Baltic Astr, 14, 112
Zăcs, L., Sperauskas, J., Musaev, F.A., et al. 2009, ApJ, 695, L203

Asymmetric Planetary Nebulae V
A. A. Zijlstra, F. Lykou, E. Lagadec and I. McDonald
Jodrell Bank Centre for Astrophysics, Manchester, UK © 2011

Post-AGB stars in the LMC as tracers of (binary) stellar evolution

van Aarle E.[1], Van Winckel H.[1], Lloyd Evans T.[2], Wood P. R.[3], and Ueta T.[4]

[1]*Instituut voor Sterrenkunde, K.U. Leuven, Celestijnenlaan 200D bus 2401, B-3001 Leuven, Belgium*

[2]*School of Physics & Astronomy, University of St Andrews, North Haugh, St Andrews KY16 9SS, Scotland, UK*

[3]*Mount Stromlo Observatory, Cotter Road, Weston Creek, ACT 2611, Australia*

[4]*Department of Physics and Astronomy, University of Denver, 2112 E. Wesley, Denver, CO80208, USA*

Abstract. The rare post-AGB objects in the Galaxy display very diverse observational characteristics. Despite the very detailed studies of many of them, there is no consensus on how the individual objects may be linked by evolutionary channels. With poorly known distances and hence luminosities, it is, however, most difficult to interpret the results on the individual post-AGB stars in the broader theoretical context of (chemical) stellar evolution. In this contribution we will report on our project to overcome this problem by focusing on a large sample of post-AGB stars with known distances: those in the LMC. Via cross-correlation of the SPITZER SAGE catalogue with optical catalogues we selected a sample of 1900 LMC post-AGB candidates based on their [8]-[24] colour index and estimated luminosity. We determined the fundamental properties of the central stars of 90 of these objects using low resolution optical spectra that we obtained at Siding Spring and SAAO. About half of the objects in our sample show an SED that is indicative of a disc rather than an expanding and cooling AGB remnant. Our final catalogue of good candidate post-AGB stars will be presented and evaluated.
Keywords. Planetary Nebulae – Stars: AGB to post-AGB – Binaries

1. Introduction

Our understanding of the evolution of post-AGB stars is limited. The unknown distance and hence luminosity (which is an indication of the initial mass) of the bulk of these objects and the large variety in observed morphologies (e.g. 914, and references therein) as well as in the observed chemical diversity (e.g. 920, and references therein) make it difficult to interpret all results in terms of theoretical post-AGB evolution. This is even more complicated by the fact that we don't know whether the relatively small, Galactic sample of post-AGB stars is representative or dominated by spectacular but very enigmatic examples. We plan on overcoming these problems by performing a systematic study of a significant sample of post-AGB stars at a known distance: those in the LMC. This galaxy is very suitable for this purpose because of its proximity (50 kpc, 917), favourable angle (35°, 922) and low interstellar extinction.

Based on the shape of their SED, post-AGB stars can be subdivided into two major groups. The first group has a double peaked SED where the peak at higher wavelengths corresponds to a freely expanding, detached shell of dust. The central star is visible as a second peak at lower wavelengths if the optical depth in the line of sight is not too large. For the second group of objects, this dust excess already has an onset in the near infrared, which indicates that the dust is still close to the central star. This is indicative of a dusty disc rather than an outflow. It turns out that for Galactic post-AGB stars, objects of the second type are observationally proven to be binaries. The existence of both groups of objects will be mirrored in our selection criteria.

2. Sample selection

To construct our catalogue of post-AGB candidates, we make use of the Surveying the agents of a galaxy's evolution (SAGE) legacy project of Spitzer. SAGE accurately mapped the 7×7 deg^2 central region of the LMC in the photometric filters of IRAC at 3.6, 4.5, 5.8 and 8.0 μm and the 24, 70 and 160 μm MIPS filters. About 6.9 million sources were observed with IRAC and 40 000 with MIPS during two epochs in 2005. We use the SAGE second release data products (september 2009) which combines both visits of the survey and is immediately merged with data from the 2MASS survey in J, H and K.

2.1. Selection

We constructed our own version of the SAGE catalogue by taking only those objects that have an 8 μm detection in the IRAC archive and are measured during at least one epoch at 24 μm in the MIPS catalogue within a search radius of 3" from the IRAC detection. This initial catalogue contains 25 194 objects.

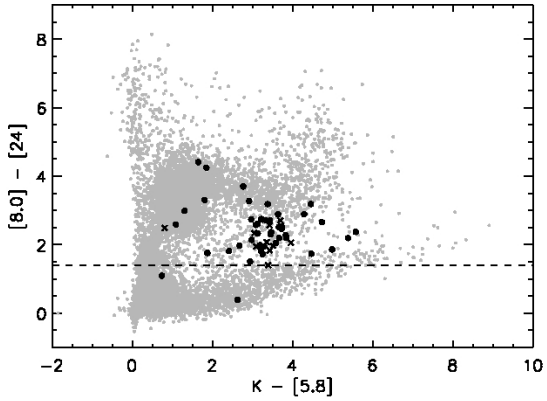

Figure 1. Colour-colour plot of K-[5.8] versus [8]-[24]. The small grey dots are the SAGE catalogue we constructed, the black crosses represent the 11 RV Tauri stars from the OGLE-III catalogue (921) that are detected at 8 and 24 μm and the black dots are the Galactic disc sources from (916) folded on the Spitzer filters. The black dashed line indicates the colour cut we are using to select likely post-AGB candidates.

The selection criteria we use to construct our catalogue of post-AGB candidates are based on what is known about Galactic post-AGB stars. As can be seen in Figure 1, the bulk of the known Galactic post-AGB stars with a circumstellar disc have $F(24) > 0.4 \times F(8)$, with $F(24)$ the flux at 24 μm. This criterion selects both post-AGB sources with a disc and a freely expanding, detached shell as the latter have colder dust in their system and hence live up to $F(24) > F(8)$. 16 570 objects from our catalogue fulfil this criterion.

These objects were cross correlated with three optical catalogues using a search radius of 1.5". We found that 566 objects of our sample have a match in the UBVR CCD survey of the Magellanic clouds (919), 6767 in the LMC stellar catalogue of (924) and 4759 sources are also listed in the Guide Star Catalog version 2.3.2 (GSC2.3) (STScI, 2006) (918). Only the objects with a listed U, B, V, R or I magnitude in at least one of these catalogues were retained. This left 8626 objects in our sample.

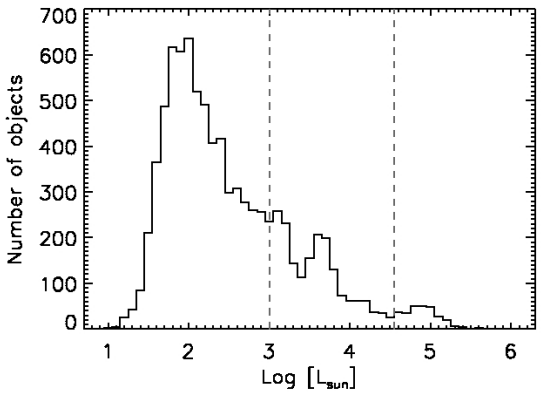

Figure 2. Histogram of the roughly calculated luminosities of all objects in our sample before the luminosity cut. The dashed gray lines indicate a lower and upper limit for the luminosity of post-AGB stars at 1000 and 35 000 $L_\odot$ respectively.

Supergiants and young stellar objects (YSOs) are obvious intruders in our list as they display similar infrared colours, but their characteristic luminosities differ from those of post-AGB stars. We hence estimated the luminosity of all post-AGB candidates by fitting up to three black bodies to the photometry. We did this without dereddening, since the spectral type of the objects is unknown. The histogram of the calculated luminosities (see Figure 2) shows three clearly distinct peaks of which the one in the middle corresponds to the luminosity range of post-AGB stars as is expected from the evolutionary tracks of (915). We get rid of the supergiants by imposing an upper limit of 35 000 $L_\odot$ for the luminosity based on the evolutionary tracks for a 7 $M_\odot$ post-AGB star from (923) or (915). The YSOs are removed from the sample by an arbitrary lower limit of 1000 $L_\odot$. Some luminous YSOs will remain since this is not a strict condition. Our final sample now contains 1892 objects.

2.2. Post-AGB subtypes

To get an idea of the number of post-AGB candidates with a disc and those with a shell, we introduce some additional colour criteria. We already had a lower limit for post-AGB candidates with a disc of $F(24) > 0.4 \times F(8)$ (see Section 2.1) and impose

an upper limit of $F(24) < 3 \times F(8)$. The latter implies that the star emits more flux at 8 than at 24 μm and that the dust is close to the star. Post-AGB stars with a freely expanding, detached shell have cooler dust that is located further away. A lower limit of $F(8) < F(24)$ is hence imposed for these objects. Both limits introduce a grey zone in between where $F(8) < F(24) < 3 \times F(8)$ with objects that live up to all criteria and of which the subtype should hence be confirmed by inspection by eye. According to these colour cuts, our final sample contains 675 objects with a disc, 673 sources with a shell and 538 objects that fall in the grey zone inbetween.

3. Low resolution, optical spectra

Our list of post-AGB candidates is at this point still polluted by many other types of objects with similar colours like background galaxies, compact HII regions, PNe, luminous YSOs and some remaining supergiants. The additional info we need to remove them from the sample can be obtained by taking low resolution, optical spectra of the post-AGB candidates. So far, we obtained spectra for 107 of the 1892 objects at the ANU 2.3m Telescope, Siding Spring Observatory in Australia and the SAAO Radcliffe 1.9 m Telescope. These spectra were used to confirm the membership of the LMC of the different objects and determine their spectral type. 16 objects were discarded and all spectral types from O to M were detected.

4. Conclusions

We constructed a catalogue of 71 high probability and 1780 candidate post-AGB stars in the LMC, while beforehand only about 30 where known. For the bulk of these, spectra are still needed to fully characterise their nature since other types of objects might display similar colours. As in the Galaxy, objects with a disc turn out to be frequent: about half of the objects in our sample have an SED indicative of a disc. The full catalogue will be published shortly.

References

Balick, B., & Frank, A. 2002, ARA&A, 40, 439
Blöcker, T. 1995, A&A, 299, 755
de Ruyter, S., van Winckel, H., Maas, T., Lloyd Evans, T., Waters, L. B. F. M., & Dejonghe, H. 2006, A&A, 448, 641
Feast, M. 1999, in New Views of the Magellanic Clouds, edited by Y.-H. Chu, N. Suntzeff, J. Hesser, & D. Bohlender, vol. 190 of IAU Symposium, 542
Lasker, B. M., Lattanzi, M. G., McLean, B. J., Bucciarelli, B., Drimmel, R., Garcia, J., Greene, G., Guglielmetti, F., Hanley, C., Hawkins, G., Laidler, V. G., Loomis, C., Meakes, M., Mignani, R., Morbidelli, R., Morrison, J., Pannunzio, R., Rosenberg, A., Sarasso, M., Smart, R. L., Spagna, A., Sturch, C. R., Volpicelli, A., White, R. L., Wolfe, D., & Zacchei, A. 2008, AJ, 136, 735
Massey, P. 2002, ApJS, 141, 81
Reyniers, M., Van Winckel, H., Gallino, R., & Straniero, O. 2004, A&A, 417, 269
Soszyński, I., Udalski, A., Szymański, M. K., Kubiak, M., Pietrzyński, G., Wyrzykowski, Ł., Szewczyk, O., Ulaczyk, K., & Poleski, R. 2008, Acta Astronomica, 58, 293
van der Marel, R. P., & Cioni, M. 2001, AJ, 122, 1807

Vassiliadis, E., & Wood, P. R. 1993, ApJ, 413, 641
Zaritsky, D., Harris, J., Thompson, I. B., & Grebel, E. K. 2004, AJ, 128, 1606

Asymmetric Planetary Nebulae V
A. A. Zijlstra, F. Lykou, E. Lagadec and I. McDonald
Jodrell Bank Centre for Astrophysics, Manchester, UK © 2011

The Physical Characteristics of Binary Central Stars of Planetary Nebulae

Todd C. Hillwig

Valparaiso University, Valparaiso, IN 46383 USA

Abstract. A number of efforts are underway to detect close binary stars in planetary nebulae. The primary goal of these studies is to determine the binary fraction of central stars. The next stage is a detailed analysis of the binaries to determine physical parameters for the systems. These analyses can be combined with population synthesis models, common envelope evolution models, and observed properties of nebulae to further understand the impact of binarity on PN formation. I discuss the sample of known close binary central stars in relation to other close binaries with a white dwarf, cataclysmic variables, supernova Ia progenitors, and double degenerate systems.
Keywords. Planetary Nebulae – Binaries

1. Introduction

In our quest to understand the shaping of planetary nebulae (PNe) and how binary stars play a role in that process, it is important to characterize the discovered binary systems. The masses of the component stars, binary separation, evolutionary state of both stars, stellar temperatures and radii, and observed inclination are all important pieces in understanding the connection between binary system and the ejected nebula. In addition to understanding the physical parameters of the binary systems, it is important to know how the observed binary systems compare to what I will call post common envelope binaries (PCEBs) that do *not* have a visible PN. These field binaries can help us to determine if our sample of binary central stars of PNe (CSPNe) represent the overall evolutionary sample, or if they comprise a distinct subset.

Here I discuss the known binary star sample as a set, focusing on close binary CSPNe. The sample of 36 close binary CSPNe comes from De Marco, Hillwig, & Smith (925) and Miszalski et al. (928). I compare the current sample to the known PCEB stars; specifically those with at least one white dwarf (WD) component. I also look more closely at the class of binary stars observed in each case. Below I discuss three distinct classes: 1) WD–main sequence (MS) detached systems, 2) WD–MS semi-detached systems or cataclysmic variables (CVs), and 3) double degenerates (DDs).

2. Comparison to Detached White Dwarf–Main Sequence PCEBs

While a significant amount of work has been done to discover and study MS–WD PCEB systems, there are still only a small number with known orbital periods. The

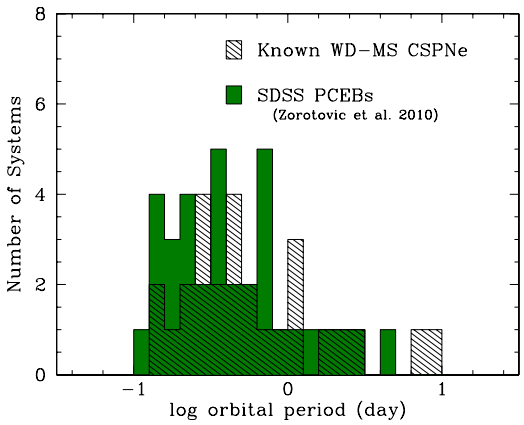

Figure 1. A histogram of the log of the orbital period in days of the known sample from SDSS of detached WD–MS PCEBs (*solid green*) and the CSPNe (*hatched*).

Sloan Digital Sky Survey (SDSS) has provided an excellent source for these PCEBs (936). Figure 1 shows a histogram of the WD–MS PCEB systems with known orbital periods from Zorotovic et al. (936) plotted as a function of the log of the orbital period in days along with the distribution of WD–MS CSPNe with known orbital period. The distributions of field and PN close WD–MS binaries appear to be in good agreement. The two CSPNe with orbital periods close to ten days suggest a possible long orbital period tail, but the total numbers will have to increase significantly before such a difference between the two could be confirmed. If there is a tail, it makes up only a small fraction of the total systems.

Also apparent is that the majority of systems in both distributions have orbital periods < 1 day. In the case of the CSPNe, which have been discovered through photometric variability, it is possible that observational selection effects could play a role and that longer period systems do exist, though De Marco et al. (925) demonstrate that this is unlikely. Such a selection effect is unlikely for the PCEB distribution however, as these systems were discovered via radial velocity variability and the SDSS data are of high enough resolution to allow detection of significantly longer orbital periods.

3. Comparison to Cataclysmic Variables

Recently, the classical nova GK Per (933) and recent nova V458 Vul (931) have had reports of faint PNe surrounding them. Also, observations of the binary CS of Hen 2-428 suggest that it may be a semi-detached system (932).

In Figure 2 we have plotted the complete distribution of close binary CSPNe in a histogram along with the SDSS sample of 137 CVs from Gänsicke et al. (926), which is the best available unbiased sample of CVs (though perhaps with low sensitivity to long period CVs). The two samples show a very small overlap. Furthermore, the period region in which they do overlap is above the CV period gap where a semi-detached state would only occur for relatively high mass secondary stars (typically > 0.5 $M_{\odot}$). Based

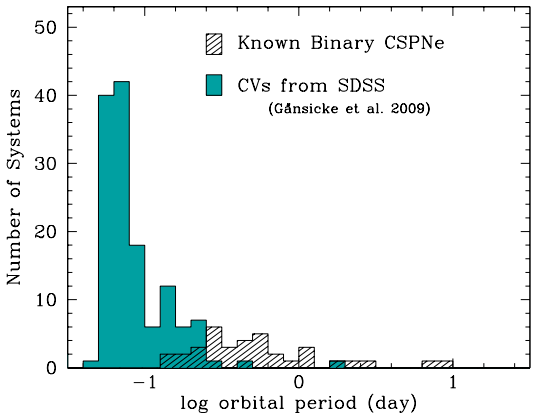

Figure 2. A histogram of the log orbital period in days of the known sample of CVs from SDSS (*solid blue*) and all close binary CSPNe (*hatched*).

on these distributions we expect that very few CSPNe systems would have evolved directly into contact, and that most systems reach a semi-detached state after magnetic or gravitational braking has reduced their orbital period. This result is in agreement with the small number of known CSPNe in semi-detached systems and with the conclusions of Gänsicke et al. (926) for PCEBs in general.

4. Double Degenerate Binary Central Stars

In the context of CSPNe, I will use "double degenerate" to mean a binary system in which the two stars are either WDs or pre-WDs (technically not degenerate yet, but will become so). One reason to understand the fraction and classification of DD binary CSPNe is their possible relationship to type Ia supernovae (SNIa). Another is that the fraction of helium WDs versus carbon-oxygen WDs combined with population synthesis calculations can help us determine typical evolutionary channels for CSPNe.

To date three DD CSPNe have been firmly identified in the literature: the CSs of Abell 41 (934), PN G135.9+55.9 (935), and NGC 6026 (927). To this list we can add the CSs of Hen 2-428 and V458 Vul (932; 931). The calculated masses for each component in all of the systems are too massive to be He WDs (for which M $\lesssim$ 0.46 $M_{\odot}$). A possible exception is the CS of NGC 6026 where the published mass range does include He WD mass values. The dominance of CO WDs contradicts models in which most WDs in DDs will be He WDs (e.g. 930). Therefore, either the four studied systems represent a significant departure from the true sample or CSPNe are intrinsically different than field WDs. If the small sample does not represent the true distribution of WDs in PNe it may either be due to a random selection of only high mass systems or due to an observational bias toward the higher mass CO WDs.

Each of the four known DD CSPNe has a light curve dominated by ellipsoidal variability. These are the only well-studied binary CSPNe showing this type of light curve. Through binary system modeling we find that it is very difficult to have a light

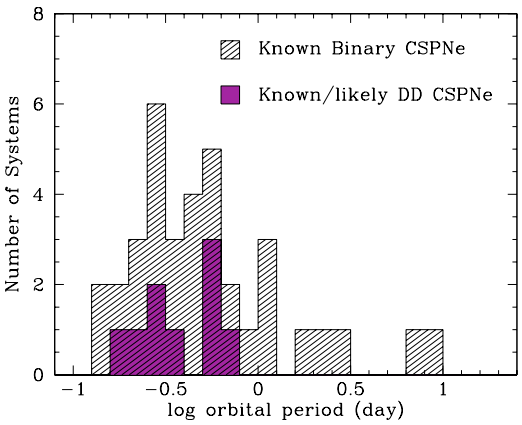

Figure 3. A histogram of in log orbital period of the known sample of CSPNe (*hatched*) with known or suspected DD systems (*solid purple*).

curve dominated by ellipsoidal variability in non-DD systems. Also, light curves with two eclipses of nearly equal depth (nearly equal temperature stars) will also be DD systems. In the sample of known close binary CSPNe (925; 928) we find that nine of the 36 systems have light curves dominated by ellipsoidal variability or show two nearly equal-depth eclipses (see histogram in figure 3). So one-quarter of the known binary CSPNe are known or suspected double-degenerates. From a statistical standpoint this suggests again a possible difference between DDs in CSPNe and those in field stars. The Supernova Ia Progenitor Survey (SPY 929) finds from a radial velocity survey that 15% of *all* field WDs are DDs, whereas for an assumed close binary fraction of 20% we find only 5% of *all* CSPNe to be DDs.

The distribution and classification of DD CSPNe suggests that PNe may harbor a different distribution, with more massive components, than field PCEBs. If after enlarging the sample this still holds, CSPNe would provide a good test ground for SN Ia searches and for exploring DD evolutionary channels in general.

Acknowledgments. This research was supported in part by NASA through the American Astronomical Society's Small Research Grant Program.

References

De Marco, O., Hillwig, T., & Smith, A.J. 2008, AJ, 136, 323
Gänsicke, B. et al. 2009, MNRAS, 397, 2170
Hillwig, T. C., Bond, H. E., Afşar, M., & De Marco, O. 2010, AJ, 140, 319
Miszalski, B., Acker, A., Moffat, A.F.J., Parker, Q.A., & Udalski, A. 2009, A&A, 496, 813
Napiwotzki, R. et al. 2003, *Messenger*, 112, 25
Nelemans, G., Yungelson, L. R. , Portegies Zwart, S. F., & Verbunt, F. 2001 A&A, 365, 491
Rodríguez-Gil, P., et al. 2010, MNRAS, 407, L21
Santander-García, M. et. al. 2010, *Asymmetric Planetary Nebulae 5*, Eds. A. A. Zijlstra, F. Lykou, I. McDonald, and E. Lagadec, p. 260
Scott, A. D., Rawlings, J. M. C., & Evans, A. 1994, MNRAS, 269, 707
Shimanskii, V. V., Borisov, N. V., Sakhibullin, N. A., & Sheveleva, D. V. 2008, ARep, 52, 479

Tovmassian, G., et al. 2010, ApJ, 714, 178
Zorotovic, M., Schreiber, M. R., Gänsicke, B. T., & Nebot Gómez-Morán, A. 2010, arXiv:1006.1621

Asymmetric Planetary Nebulae V
A. A. Zijlstra, F. Lykou, E. Lagadec and I. McDonald
Jodrell Bank Centre for Astrophysics, Manchester, UK © 2011

Variability of Central Stars of Planetary Nebulae in the ASAS survey

M. Hajduk[1], A. A. Zijlstra[2], and K. Gesicki[3]

[1]*Nicolaus Copernicus Astronomical Center, ul. Rabiańska 8, 87-100 Toruń, Poland*

[2]*Jodrell Bank Centre for Astrophysics, School of Physics & Astronomy, University of Manchester, Oxford Road, Manchester M13 9PL, UK*

[3]*Centrum Astronomii UMK, ul. Gagarina 11, PL-87-100 Toruń, Poland*

Abstract. The All Sky Automated Survey (ASAS) survey monitors the brightness of the objects up to 14 magnitude of the southern hemisphere. The collected data allows for analysis of the variability of bright central stars of the planetary nebulae. We present the first results of our research.
Keywords. Planetary Nebulae, Binaries

1. Planetary nebulae in large photometric surveys

Large photometric surveys provide large and consistent data sets for studying all kinds of PNe photometric variability on a timescale from hours to decades. They allow for extensive study of binary nuclei of planetary nebulae, help to eliminate mimics from the PNe sample, or to detect transient events. Up to now, data from MACHO, OGLE, ASAS and WASP has been used (948; 943; 944; 941). We present the first results of our search using the ASAS survey.

2. Data reduction and analysis

The ASAS (All Sky Automated Survey) survey monitors brightness of 10^7 stars brighter than 14 magnitude in two observing stations located in Chile and Hawaii (947). Two wide field instruments observe simultaneously in *V* and *I* bands. The *V* data is available in the ASAS All Star Catalogue. The photometry is given for five different apertures. The images are under-sampled and the image scale is 15 arcsec/pixel.

We have searched for variable central stars using an online ASAS All Star Catalogue in the (only available) *V* band. We used the positions of the planetary nebulae using the SIMBAD database. We searched for data for all Galactic PNe using search radius < 15 arcsec. We used Period04 program (942) and the analysis of variances (AoV) method (945) for the data analysis.

3. Short period binaries

Few known binary central stars have been observed with the ASAS survey. They are listed in Table 1.

LoTr 1 is known to possess a binary nucleus due to its composite spectrum, although its photometric variability was attributed to the starspots on the rotating cool companion (937; 949). Additional variability on the timescale of years may be present in the LoTr 1 and NGC 6026 light curves.

We tentatively classify a bright star near the center of the PN G249.8–02.7 as a true central star (946). The DSS image presents the bright star and the nebula (Fig. 1). The eastern part of the nebula may be brighter due to the interaction with the ISM. If this star is confirmed, it will become the photometric CSPN binary with the longest period known.

SuWt 2 binary (Fig. 2) consists of two eclipsing A-type stars. The hot star is presumed to be the third component of the triple system (940).

Table 1. Short period binary CSPNe observed with the ASAS.

Name	RA	DEC	Period [d]
GLMP 160	06 54 13.43	-10 45 38.2	0.631520 ± 0.000061
LoTr 1	05 55 06.61	-22 54 02.4	6.425 ± 0.001
NGC 6026	16 01 21.13	-34 32 35.8	0.528083 ± 0.000035
PN G249.8–02.7	07 55 55.5	-33 46 00	23.066 ± 0.008
SuWt 2	13 55 43.23	-59 22 39.9	4.909855 ± 0.00008

4. A prolonged minimum in CPD–56°8032

Few CSPNe showing long term brightness variations are within ASAS sensitivity limits, i.e. IC 4997 (Fig. 3), NGC 2346, M 2-29 and CPD–56°8032. CPD–56°8032 is classified as a [WC10] star containing dusty disk (938). Cohen et al. (939) reports three dimmings of the object in the extent of over 10 years, followed by fast recovery, in addition to a slow overall decline. The ASAS data partially overlays with the Cohen et al. (939) lightcurve, starting with the third minimum and providing an evidence for the fourth minimum shortly after the previous one (Fig. 4). The fourth minimum is the longest among all the observed minima and lasts for about 5 years now.

Acknowledgments. This research has made use of the SIMBAD database, operated at CDS, Strasbourg, France. The ASAS online catalogue and the NASA ADS Abstract Service were used to access data and references. This work was financially supported by MNiSW of Poland through grant No. N N203 511838.

References

Bond, H.E., Ciardullo, R., Meakes, M. 1989, BAAS 21, 789
Chesneau, O., et al. 2006, A&A 455, 1009

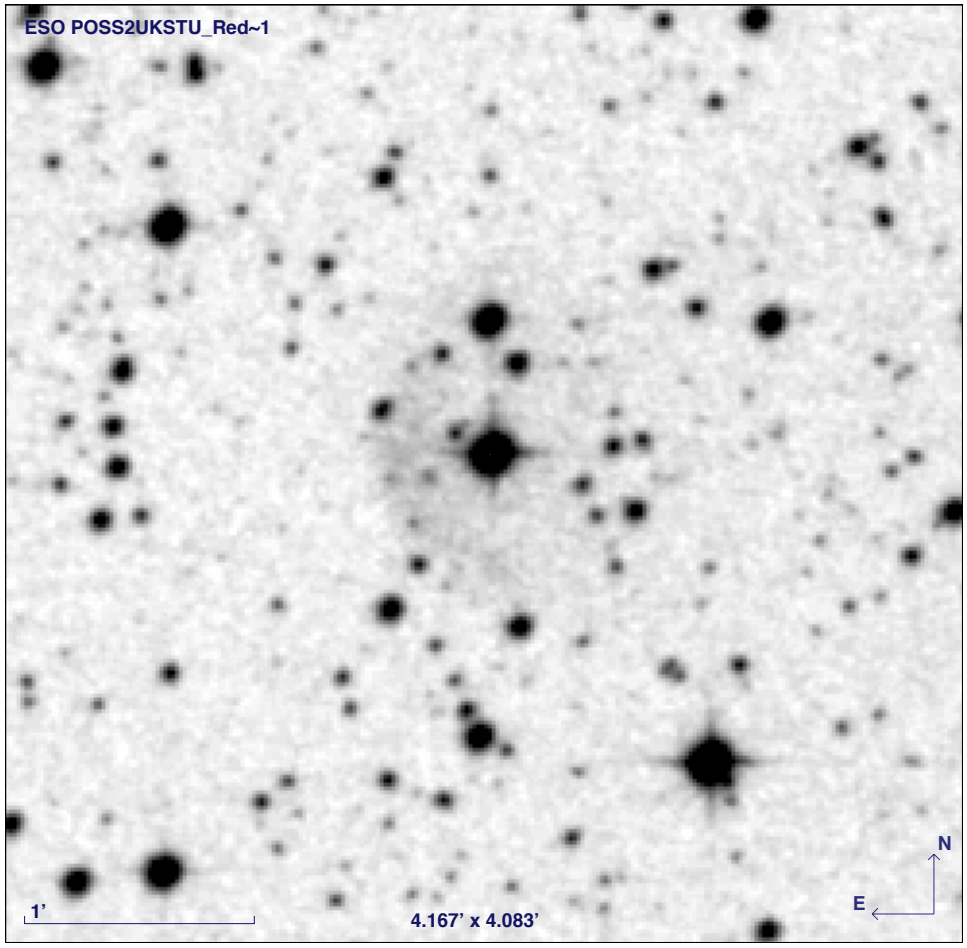

Figure 1. The DSS image of PN G249.8–02.7.

Cohen, M., Barlow, M.J., Liu, X.W., Jones, A.F. 2002, MNRAS 332, 879
De Marco, O. 2009 PASP, 121, 3169
Jones D., Pollacco D., Faedi F., Lloyd M. 2010 *Asymmetrical Planetary Nebulae 5*, Eds. A. A. Zijlstra, F. Lykou, I. McDonald and E. Lagadec, p. A111
Lenz, P., & Breger, M. 2005, Commun. Asteroseismol. 146, 53
Lutz, J., Fraser, O., McKeever, J., Tugaga, D. 2010, PASP 122, 524
Miszalski, B., Acker, A., Moffat, A.F.J., Parker, Q.A., Udalski, A. 2009, A&A 496, 813
Schwarzenberg-Czerny, A. 1989, MNRAS 241, 153
Parker, Q.A. 2006, MNRAS 373, 79
Pojmański, G. 2002, AcA 52, 397
Shaw, R.A., Rest, A., Damke, G., Smith, R.C., Reid, W.A., Parker, Q.A. 2007, ApJ 669L 25
Strassmeier, K.G., Hubl, B., Rice, J.B. 1997, A&A 322, 511

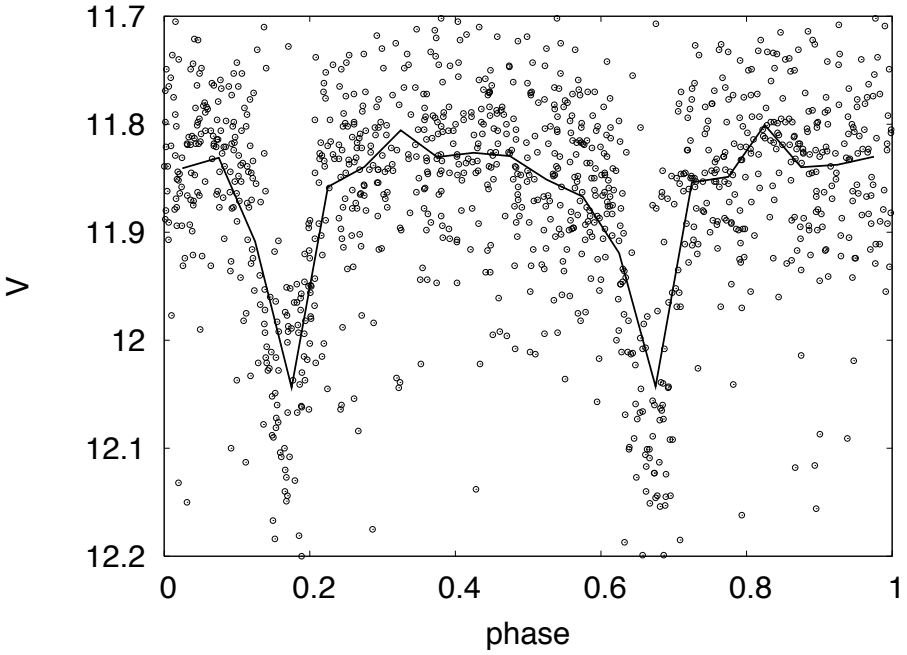

Figure 2. The phased light curve of SuWt 2.

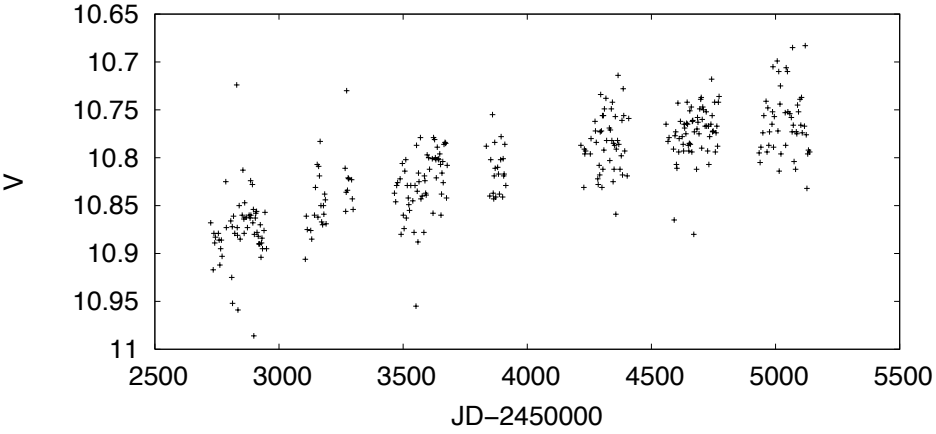

Figure 3. The lightcurve of the central star of the young planetary nebula IC 4997.

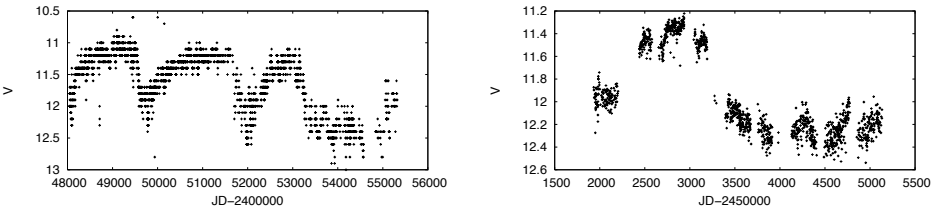

Figure 4. The AAVSO (upper) and ASAS (lower) lightcurve of the central star of CPD–56°8032.

Asymmetric Planetary Nebulae V
A. A. Zijlstra, F. Lykou, E. Lagadec and I. McDonald
Jodrell Bank Centre for Astrophysics, Manchester, UK © 2011

The Rise and Phall of the Barium Stars

Robert G. Izzard[1,2,4], Tyl Dermine[2] and Ross P. Church[3,4]

[1]*Argelander-Institut für Astronomie, University of Bonn, Auf dem Hügel 71, D-53121 Bonn, Germany*

[2]*Institut d'Astronomie et d'Astrophysique, Université Libre de Bruxelles, Boulevard du Triomphe, B-1050 Brussels, Belgium*

[3]*Lund Observatory, Box 43, SE-221 00, Lund, Sweden*

[4]*Centre for Stellar and Planetary Astrophysics, School of Mathematical Sciences, Monash University, VIC 3800, Australia*

Abstract. Barium stars are thought to be formed by accretion of material from the wind of an *s*-process-rich asymptotic giant branch star onto a main sequence star in a binary system. The accretor then evolves up the giant branch and, as it cools, absorption lines of barium are prominent in its spectrum. This is the barium star we see today. Barium stars are excellent probes of binary-star physics because orbital periods and eccentricities are known for nearly all of them, i.e. the sample set is complete. Binary-star theory predicts that barium stars with periods shorter than a few thousand days should circularise by tidal interaction, but the observed stars are often highly eccentric. We investigate a potential source of their eccentricity: white dwarf kicks. We can reproduce the observed period-eccentricity distribution if we introduce a moderate kick speed of a few km/s together with efficient angular momentum loss in stellar winds and efficient common-envelope ejection. Many open questions remain which are key to the wind-accretion mechanism by which barium stars and other chemically-peculiar binaries such as CH and carbon-enhanced metal-poor (CEMP) stars form.
Keywords. Planetary nebulae – Binaries

1. Introduction

The barium stars are a class of chemically peculiar stars which show strong absorption lines of barium in their spectra. They have G and K spectral types and are ascending the giant branch for the first time. They have not made their own barium, rather it accreted from the wind of a companion asymptotic giant branch (AGB) star which is now a white dwarf. The implication is that barium stars are all binaries, a fact borne out by observations (968).

Qualitatively, the barium-star formation mechanism is apparently well understood. Quantitative predictions of the properties of barium stars, such as orbital periods, eccentricities and surface abundances, have been calculated by e.g. Pols et al. (970). These models show that barium-star binaries with periods less than a few thousand days should circularise rapidly because of tidal dissipation. Also, barium stars should have periods in the range of about one hundred days up to several centuries. Fortunately

for theoreticians, observations of barium stars do not agree with the predictions! The data of Jorissen et al. (966), which include almost all barium stars, show that barium stars at *all periods* can be eccentric – some with $e \gtrsim 0.9$ – and the maximum period is at most a few times 10^4 days. More recent data from the HERMES collaboration (Dermine and Jorissen, in preparation) may extend the period maximum slightly, but these stars are still rare when the simulations predict they should be relatively common.

The imagination of stellar modellers knows no bound and hence there are many possible explanations for the discrepancy between theory and observation. Ideas include mass transfer at periastron (971), interaction with a circumbinary disk (956, Dermine et al., in preparation), an improved treatment of mass transfer in binaries (951) and weak tides (Nordhaus, this volume). We investigate a new idea, that of white dwarf kicks. This idea has the support of observations of globular clusters in which young white dwarfs are found to have a systematically larger velocity than old white dwarfs and main sequence stars, the simplest explanation for which is a kick at the birth of the white dwarf (i.e. the end of the AGB) of a few $\mathrm{km\,s^{-1}}$ (954). Kicks also increase the longevity of globular clusters (959; 957). The cause of the kick is unknown, perhaps it is related to asymmetric AGB mass loss, but because the globular cluster binary fraction is small it must occur in both single and binary stars. We show that a natural consequence of the kick is the eccentricity observed in the barium stars but that problems with the models remain.

2. Barium star populations with white-dwarf kicks

We simulate populations of barium stars with the population nucleosynthesis code of Izzard et al. (965, 963, 964) which is based on the stellar evolution prescription of Hurley et al. (960). Our model includes tidal interactions according to Zahn (973) and Hut (961), wind loss from Vassiliadis and Wood (972), wind accretion (952) and an α-λ common-envelope model (960). AGB evolution is fitted to the models of Karakas et al. (967) with *s*-process elements from Busso et al. (953). The initial metallicity is set to $Z = 0.008$ with the scaled solar abundance mixture of Anders and Grevesse (950). Barium stars were selected as G/K spectral-type, post-main sequence stars with $[\mathrm{Ba/Fe}] \geq 0.2$. Full details of the model can be found in Izzard et al. (962). With the default model parameters our results are similar to those of Pols et al. (970), as shown in Fig. 1.

We apply white dwarf kicks in random directions with a fixed speed σ_{WD} at the end of the AGB phase of the primary star. It is difficult to constrain σ_{WD} but values from 2 to 4 $\mathrm{km\,s^{-1}}$ well fit the observed barium-star eccentricities. To remove the period gap at $\sim 10^3$ days because of spiral-in during the common envelope phase we increased the efficiency of common-envelope ejection by allowing a small fraction ($< 10\%$) of the recombination energy of the stellar envelope to contribute to the ejection process.

The remaining problem is the long-period tail predicted to extend out to 10^5 days. We solve this by increasing the efficiency of orbital angular momentum loss during the (non-conservative) wind accretion process. If the specific angular momentum of the wind lost from the system is twice the specific orbital angular momentum then the predicted periods much better agree with the observations, as shown in Fig. 2.

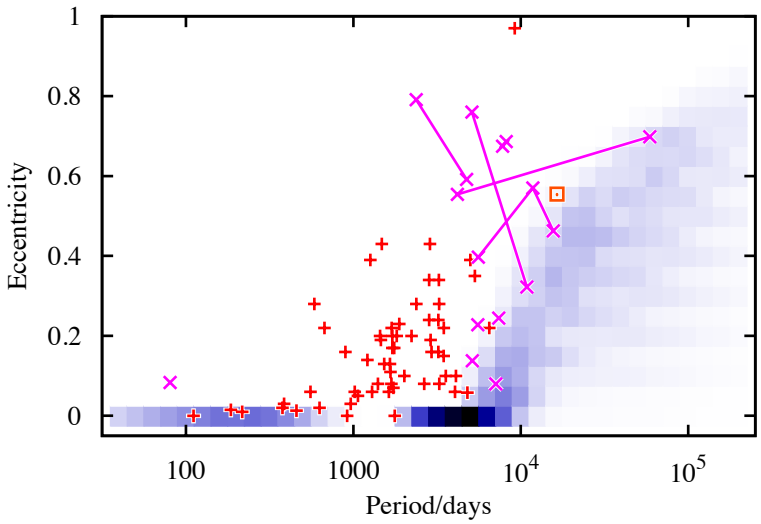

Figure 1. Our canonical barium star population model together with the observations of Jorissen et al. (966, + symbols) and the HERMES collaboration (× symbols, Dermine and Jorissen, in preparation) and 56 Uma (from 958, □ symbol). Note the problems: we predict too many long-period (eccentric) barium stars, all the barium stars with periods less than 4,000 days are circular and there is a period gap because of common-envelope spiral-in at $\sim 10^3$ days.

3. Future work

White dwarf kicks provide a solution to the barium-star eccentricity problem, but open many cans of worms in the process. Several poorly-understood processes contribute to the problem. Each presents its own difficulties but also opportunities for a better physical understanding of binary-star phenomena in general.

The origin of the kick is not obvious because the evidence for kicks is circumstantial and comes only from studies of globular clusters. Field white dwarfs may also be kicked but given the small kick speed (a few $\mathrm{km\,s^{-1}}$) relative to typical field star speeds (tens of $\mathrm{km\,s^{-1}}$) it would be undetectable. Asymmetric mass loss around AGB stars might give some clues as to whether kicks truly occur or not, but it is difficult to disentangle the effect of an asymmetric wind from the interaction of a wind with a non-uniform interstellar medium. AGB winds are generally thought to be spherical, at least at the end of the AGB. This contradicts the effect we seek in the barium stars because we must have the kick at or near the end of the AGB to avoid tidal circularisation. We

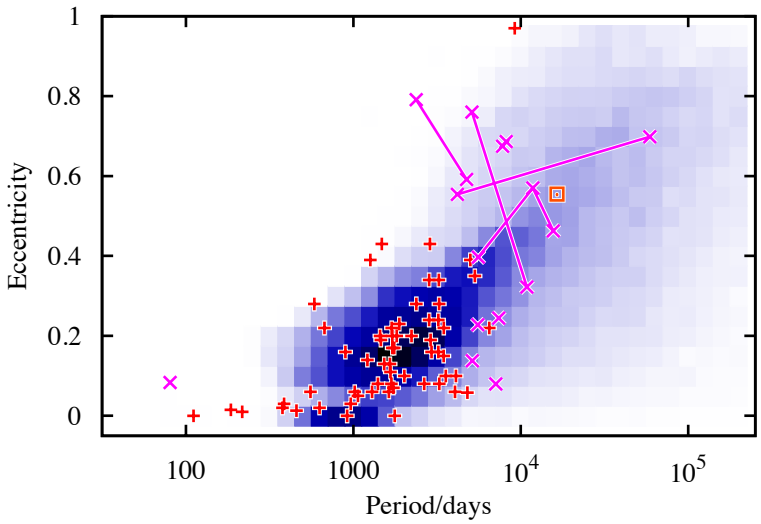

Figure 2. Our barium star population with 4 km s^{-1} white dwarf kicks, efficient common-envelope ejection and efficient orbital angular momentum loss during the non-conservative mass-transfer phase. Observations are as in Fig. 1. The eccentricity distribution much better matches the observations, the period gap at 10^3 days has been closed and the long-period tail largely removed.

have that studies of asymmetric planetary nebulae will lead to some progress on this front.

Our model of AGB wind accretion is wrong! We apply the Bondi and Hoyle (952) formalism for lack of a better alternative, but this is strictly only valid for winds which are fast relative to the orbital speed. In barium stars the orbital speed and wind speed are similar. Three dimensional models such as those of Mohamed and Podsiadlowski (969) and Mohamed (this volume) seem to be the best solution to this problem but it remains to apply these results to population synthesis studies.

Is it valid to extract so much angular momentum from the binary during the mass transfer phase? This may be possible if there is some kind of magnetic locking of material out to a large radius (similar to magnetic braking) or if material is lost from one of the outer Lagrange points. Other possibilities remain, including circumstellar and circumbinary disks. Post-AGB binaries show evidence of such disks (e.g. Van Winckel, this volume) and a similar period-eccentricity distribution to the barium stars, this is probably no coincidence. It may also be that mass loss from AGB binaries is not at all as expected from the Roche potential model (955).

Finally, our dubiously-efficient common-envelope evolution phase solves the problem of the $\sim$ 1000 day period gap, but does not predict eccentric barium stars at periods less than 1000 days. Is it possible that stars can exit the common envelope in an eccentric orbit? If so, a radical rethink of our basic understanding of the physics at work in common envelopes is required.

The results of our study on the barium stars should be of interest to those who study their low-metallicity cousins, the CH and carbon-enhanced metal poor (CEMP) stars. These are thought to form by the same wind-accretion mechanism so any clues we can obtain from the barium stars may be of vital importance in the understanding of these relics of Galactic history.

Acknowledgments. RGI would like to thank the organisers of *APN V* for the opportunity to speak on this subject and the superbly organised conference – he hopes they spend his vegetarian dinner compensation fund wisely. RGI was the recipient of a *Marie Curie-Intra European Fellowship* at ULB and the research leading to these results has received funding from the Seventh Framework Programme of the European Community under grant agreement 220440. TD is *Boursier F.R.I.A.* RPC would like to thank the *Wenner-Gren foundation* for a stipend.

References

Anders, E. and Grevesse, N. (1989). *Geochimica et Cosmochimica Acta*, 53:197–214.

Bonačić Marinović, A. A., Glebbeek, E., and Pols, O. R. (2008). *Astronomy and Astrophysics*, 480:797–805.

Monthly Notices of the Royal Astronomical Society, 104:273.

Busso, M., Gallino, R., Lambert, D. L., Travaglio, C., and Smith, V. V. (2001). *Astrophysical Journal*, 557:802–821.

Davis, D. S., Richer, H. B., King, I. R., Anderson, J., Coffey, J., Fahlman, G. G., Hurley, J., and Kalirai, J. S. (2008). *Monthly Notices of the Royal Astronomical Society*, 383:L20–L24.

Dermine, T., Jorissen, A., Siess, L., and Frankowski, A. (2009). Radiation pressure and pulsation effects on the Roche lobe. *Astronomy and Astrophysics*, 507:891–899.

Frankowski, A. and Jorissen, A. (2007). *Baltic Astronomy*, 16:104–111.

Fregeau, J. M., Richer, H. B., Rasio, F. A., and Hurley, J. R. (2009). *Astrophysical Journal, Letters*, 695:L20–L24.

Griffin, R. F. (2008). *The Observatory*, 128:176–231.

Heyl, J. (2008). *Monthly Notices of the Royal Astronomical Society*, 390:622–624.

Hurley, J. R., Tout, C. A., and Pols, O. R. (2002). *Monthly Notices of the Royal Astronomical Society*, 329:897–928.

Hut, P. (1981). *Astronomy and Astrophysics*, 99:126–140.

Izzard, R. G., Dermine, T., and Church, R. P. (2010). White-Dwarf Kicks and Implications for Barium Stars. *ArXiv e-prints 1008.3818*.

Izzard, R. G., Dray, L. M., Karakas, A. I., Lugaro, M., and Tout, C. A. (2006). *Astronomy and Astrophysics*, 460:565–572.

Izzard, R. G., Glebbeek, E., Stancliffe, R. J., and Pols, O. R. (2009). *Astronomy and Astrophysics*, 508:1359–1374.

Izzard, R. G., Tout, C. A., Karakas, A. I., and Pols, O. R. (2004). *Monthly Notices of the Royal Astronomical Society*, 350:407–426.

Jorissen, A., Van Eck, S., Mayor, M., and Udry, S. (1998). *Astronomy and Astrophysics*, 332:877–903.

Karakas, A. I., Lattanzio, J. C., and Pols, O. R. (2002). *PASA*, 19:515–526.

McClure, R. D. and Woodsworth, A. W. (1990). *Astrophysical Journal*, 352:709–723.

Mohamed, S. and Podsiadlowski, P. (2007). In R. Napiwotzki & M. R. Burleigh, editor, *15th European Workshop on White Dwarfs*, volume 372 of *Astronomical Society of the Pacific Conference Series*, page 397.

Pols, O. R., Karakas, A. I., Lattanzio, J. C., and Tout, C. A. (2003). In Corradi, R. L. M., Mikolajewska, J., and Mahoney, T. J., editors, *Astronomical Society of the Pacific Conference Series*, volume 303 of *Astronomical Society of the Pacific Conference Series*, page 290.

Soker, N. (2000). *Astronomy and Astrophysics*, 357:557–560.

Vassiliadis, E. and Wood, P. R. (1993). *Astrophysical Journal*, 413:641–657.

Zahn, J.-P. (1977). *Astronomy and Astrophysics*, 57:383–394.

Asymmetric Planetary Nebulae V
A. A. Zijlstra, F. Lykou, E. Lagadec and I. McDonald
Jodrell Bank Centre for Astrophysics, Manchester, UK © 2011

Two Populations of Companions around White Dwarfs: The Effect of Tides and Tidal Engulfment

J. Nordhaus
Dept. of Astrophysical Sciences, Princeton University, Princeton, NJ 08544 USA

Abstract. During post-main-sequence evolution, radial expansion of the primary star, accompanied by intense winds, can significantly alter the binary orbit via tidal dissipation and mass loss. The fate of a given binary system is determined by the initial masses of the primary and companion, the initial orbit (taken to be circular), the Reimers mass-loss parameter, and the tidal prescription employed. For a range of these parameters, we determine whether the orbit expands due to mass loss or decays due to tidal torques. Where a common envelope (CE) phase ensues, we estimate the final orbital separation based on the energy required to unbind the envelope. These calculations predict period gaps for planetary and brown dwarf companions to white dwarfs. In particular, the lower end of the gap is the longest period at which companions survive their CE phase while the upper end of the gap is the shortest period at which a CE phase is avoided. For binary systems with 1 $M_\odot$ progenitors, we predict no Jupiter-mass companions with periods $\lesssim$270 days. For binary systems consisting of a 1 $M_\odot$ progenitor with a 10 Jupiter-mass companion, we predict a close, post-CE population with periods $\lesssim$0.1 days and a far population with periods $\gtrsim$380 days. These results are consistent with the detection of a ∼50 M_J brown dwarf in a ∼0.08 day orbit around the white dwarf WD 0137-349 and the tentative detection of a ∼2 M_J planet in a ∼4 year orbit around the white dwarf GD66.
Keywords. Planetary Nebulae – Binaries

1. Introduction

For low-mass stars (initially $\lesssim$8 $M_\odot$), post-main sequence (post-MS) evolution is characterized by expansion via giant phases accompanied by the onset of mass-loss. During the Asymptotic Giant Branch phase (AGB), dust-driven winds expel the stellar envelope as the star transitions to a white dwarf (WD). Before formation of the WD remnant, the spherical outflows observed during the AGB phase undergo a dramatic transition to the highly asymmetric and often bipolar geometries seen in all post-AGB and young planetary nebulae (PNe; Sahai & Trauger 985). This transition is often accompanied by high-speed, collimated outflows. For recent reviews see van Winckel (988) and de Marco (976).

A central hypothesis to explain shaping in post-AGB/PNe is that a close companion is necessary to power and shape bipolarity. This is supported by observations of excess momenta in all post-AGB outflows relative to what isotropic radiation pressure can provide (975). Additionally, maser observations show magnetic jet collimation in AGB and young post-AGB stars (989; 984; 990; 974). Such collimation supports

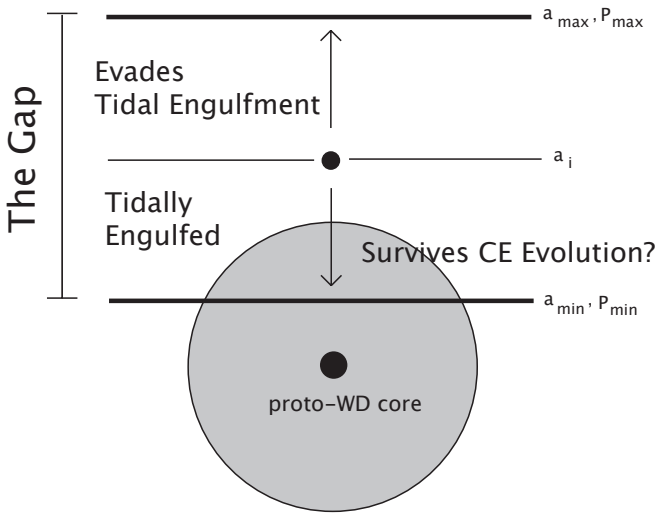

Figure 1. The period gap for low-mass companions around white dwarfs. The orbit of a companion located initially at a_i decays and plunges into the giant star. Depending on the mass of the companion and stellar structure at plunge time, the companion may or may not survive the CE phase. Companions slightly exterior to a_i avoid engulfment and never enter a CE; their orbits expand due to mass-loss. The gap is set by the final maximum semimajor axis which survives CE evolution ($a_{\rm min}$) and the final minimum semimajor axis which avoids tidal engulfment ($a_{\rm max}$).

the binary hypothesis because it is difficult, if not impossible, for single AGB stars to generate the large field strengths needed to power the outflows (980; 981). If a close companion is present, strong interactions can transfer energy and angular momentum from the companion to the primary or outflow. In particular, if the companion is engulfed in a common envelope (CE), rapid in-spiral can cause significant shear inside the CE (979; 982). Coupled with a strong convective envelope, large-scale magnetic fields are amplified and are sufficient to unbind the envelope and power the outflow (980). The recent detection of a white dwarf with an orbiting ~50 $M_{\rm J}$ brown dwarf in a ~2 hour orbit demonstrates that low-mass companions can survive common envelope phases (CEP) (977). The detection of a planetary companion ($M{\rm sin}i$ = 3.2 $M_{\rm J}$) around the extreme horizontal branch star V391 Pegasi in a ~1.7 AU orbit (~3.2 year period; Silvotti et al. 986) and the tentative detection of a ~2 $M_{\rm J}$ planet in a $\gtrsim$2.7 AU orbit ($\gtrsim$4 year period; Mullally et al. 978) around the white dwarf GD66 provide further motivation for studying post-MS orbital dynamics. For more detail on the work summarized in this proceeding, we refer the reader to (983).

2. Tides and Mass-loss

As the binary system evolves, mass-loss and tidal torques are in competition. Mass lost from the system acts to increase the semimajor axis while tidal torques decrease it. For each primary and companion, we compute the evolution of the orbit from the zero-age main sequence through the post-main sequence. If the companion is tidally engulfed

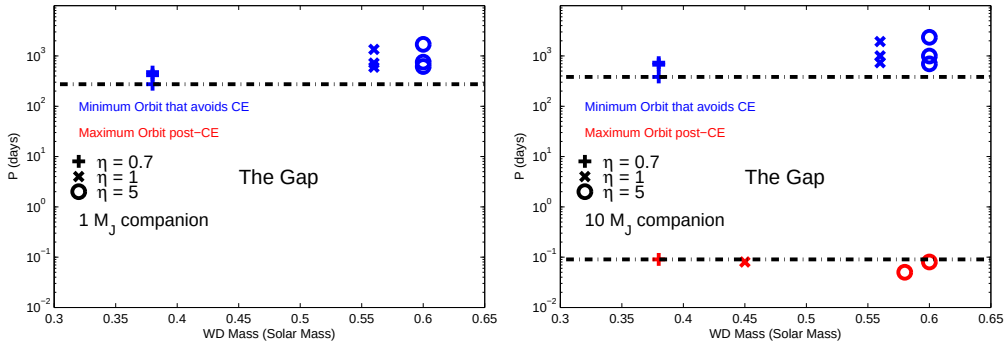

Figure 2. The predicted period gaps for a 1 $M_\odot$ progenitor with 1 M_J (left) and 10 M_J (right) companions. The symbols represent different Remiers η values for the various tidal prescriptions (983). For the 1 M_J system, no companion survives CE evolution. Thus, we predict a paucity of 1 M_J companions with periods $\lesssim$270 days. For the 10 $M_\odot$ system, several companions survive CE evolution and are located in short-period orbits. The predicted period gap occurs between ~0.1 and 380 days.

(i.e. plunges into the primary star), it enters a common envelope with the primary. If the companion evades tidal engulfment, mass-loss continues and the orbit expands until the end of the evolutionary model. We take the companion to be tidally locked to the primary, as is expected; in other contexts, this assumption might be testable (987). For a detailed description of the mass-loss prescriptions, tidal formalisms and orbital assumptions employed see (983).

For each stellar model, companion mass, and tidal theory, we calculate the maximum initial semimajor axis, $a_{\rm i,max}$, that is tidally engulfed (see Fig. 1). Companions initially located exterior to $a_{\rm i,max}$ evade tidal engulfment and move outward while companions located interior to $a_{\rm i,max}$ plunge into their host star. Upon tidal engulfment, the companion enters a common envelope with the primary star (979). The companion inspirals until it is either tidally disrupted or supplies enough orbital energy to overcome the binding energy of the envelope and survive the CE phase.

3. Period Gaps for Planets and Brown Dwarfs Around White Dwarfs

We calculate the minimum period gap expected for a given binary system by assuming that all of the orbital energy released during in-spiral goes toward ejecting the CE. This gives an upper bound on the inner orbital radius at which we would expect to find companions that have survived a CE phase (see Fig. 1). The outer orbital radius is the minimum position for which a companion evades tidal capture but migrates outward due to mass-loss from the primary. These calculations predict period gaps for planetary and brown dwarf companions to white dwarfs.

Our minimum period gaps are presented in Fig. 2. We note that no Jupiter-mass companions survive CE evolution. Thus, we predict a paucity of Jupiter-mass companions with periods $\lesssim$270 days around white dwarfs. Additionally, our results predict

that there should be a paucity of 10 $M_{\rm J}$ companions with periods between 0.1 days and 380 days.

4. Conclusions

By utilizing stellar evolution models from the ZAMS through the post-MS, we have followed the orbital dynamics of binary systems in which the companion is a planet or brown dwarf. Dynamically, the orbital evolution is subject to mass-loss (which acts to increase the separation) and tidal torques (which act to decrease the separation). For various tidal prescriptions and mass-loss rates, we determined the maximum separation for which companions might be tidally engulfed (i.e. plunge into the primary star). These results serve as initial conditions for the onset of the common envelope phase for low-mass companions.

For a binary system consisting of a 1 $M_{\odot}$ primary with a 1 $M_{\rm J}$ companion, we predict a paucity of Jupiter-mass companions with periods below ∼270 days. For a 1 $M_{\odot}$ primary with a 10 $M_{\rm J}$ companion, the gap occurs between ∼0.1 and ∼380 days. Note that our estimated gaps are conservative and are obtained by finding the minimum gap that might be expected for a range of mass-loss rates and a range of assumptions about tidal dissipation. It is unlikely that the true gaps would be narrower than the ranges quoted above, but they easily could be wider. As our knowledge of stellar evolution and tidal dissipation improves, so will our estimates of the ranges for these gaps. Finally, we note that the results of surveys searching for low mass companions to white dwarfs might help to constrain theories of both stellar evolution and tides.

References

Amiri, N., Vlemmings, W., & van Langevelde, H. J. 2010, Astronomy and Astrophysics, 509, A26

Bujarrabal, V., Castro-Carrizo, A., Alcolea, J., & Sánchez Contreras, C. 2001, Astronomy and Astrophysics, 377, 868

de Marco, O. 2009, PASP, 121, 316

Maxted, P. F. L., Napiwotzki, R., Dobbie, P. D., & Burleigh, M. R. 2006, Nature, 442, 543

Mullally, F., Winget, D. E., De Gennaro, S., Jeffery, E., Thompson, S. E., Chandler, D., & Kepler, S. O. 2008, Astrophysical Journal, 676, 573

Nordhaus, J., & Blackman, E. G. 2006, Monthly Notices of the Royal Astronomical Society, 370, 2004

Nordhaus, J., Blackman, E. G., & Frank, A. 2007, Monthly Notices of the Royal Astronomical Society, 376, 599

Nordhaus, J., Busso, M., Wasserburg, G. J., Blackman, E. G., & Palmerini, S. 2008, Astrophysical Journal, Letters, 684, L29

Nordhaus, J., Minchev, I., Sargent, B., Forrest, W., Blackman, E. G., de Marco, O., Kastner, J., Balick, B., & Frank, A. 2008, Monthly Notices of the Royal Astronomical Society, 388, 716

Nordhaus, J., Spiegel, D. S., Ibgui, L., Goodman, J., & Burrows, A. 2010, ArXiv e-prints

Sabin, L., Zijlstra, A. A., & Greaves, J. S. 2007, Monthly Notices of the Royal Astronomical Society, 376, 378

Sahai, R., & Trauger, J. T. 1998, Astronomical Journal, 116, 1357

Silvotti, R., Schuh, S., Janulis, R., Solheim, J., Bernabei, S., Østensen, R., Oswalt, T. D., Bruni, I., Gualandi, R., Bonanno, A., Vauclair, G., Reed, M., Chen, C., Leibowitz, E., Paparo,

M., Baran, A., Charpinet, S., Dolez, N., Kawaler, S., Kurtz, D., Moskalik, P., Riddle, R., & Zola, S. 2007, Nature, 449, 189
Spiegel, D. S., Haiman, Z., & Gaudi, B. S. 2007, Astrophysical Journal, 669, 1324
van Winckel, H. 2003, ARA&A, 41, 391
Vlemmings, W. H. T., Diamond, P. J., & Imai, H. 2006, Nature, 440, 58
Vlemmings, W. H. T., & van Langevelde, H. J. 2008, Astronomy and Astrophysics, 488, 619

Asymmetric Planetary Nebulae V
A. A. Zijlstra, F. Lykou, E. Lagadec and I. McDonald
Jodrell Bank Centre for Astrophysics, Manchester, UK © 2011

Modelling the Asymmetric Outflows of Mira-type Binaries

S. Mohamed[1],[2], and Ph. Podsiadlowski[1]

[1]*Department of Astrophysics, University of Oxford, Oxford OX1 3RH*

[2]*Argelander Institut für Astronomie, Auf dem Hügel, Bonn D-53121, Germany*

Abstract. Detached, symbiotic binaries are generally assumed to interact via Bondi-Hoyle-Littleton (BHL) wind accretion. However, the accretion rates and outflow geometries that result from this mass-transfer mechanism cannot adequately explain the observations of the nearest and best studied symbiotic binary, Mira, or the formation of some post-AGB binaries, e.g. barium stars. We propose a new mass-transfer mode for Mira-type binaries, which we call 'wind Roche-lobe overflow' (wind RLOF), and which we demonstrate utilising 3D Smoothed Particle Hydrodynamics (SPH) simulations. Importantly, we show that the circumstellar outflows which result from wind RLOF tend to be highly aspherical and to be strongly focused towards the binary orbital plane. Furthermore, the subsequent mass-transfer rates are at least an order of magnitude greater than the analogous BHL values. We discuss the implications of these results for the shaping of bipolar (proto)-planetary nebulae and other, related systems.
Keywords. Planetary Nebulae; Binaries: symbiotic; Accretion, accretion disks; hydrodynamics; Stars: mass loss, winds, outflows

1. Introduction

The binary, Mira, consists of a cool but very luminous, pulsating AGB star (o Ceti) and a hot companion thought to be a white dwarf (J. Sokoloski, this volume) with a separation of $a \sim 100$ AU (998). Over the past decade, the system has been both spatially and spectrally resolved from radio to X-ray wavelengths, with some surprising results; e.g. HST and Chandra images have revealed strong asymmetries in Mira's outer atmosphere and the presence of a hook-like extension from Mira A towards Mira B (994; 995). The circumbinary envelope has also been shown to be highly aspherical, with possible dust clumps towards Mira B (996) and evidence for a bipolar outflow (993).

These observations pose a considerable challenge for current mass-transfer theories – given the large binary separation, Bondi-Hoyle-Littleton (BHL) wind accretion cannot account for such a strong binary interaction, and since Mira's radius ($R_* \sim 1$ - 2 AU) is at least of order of magnitude smaller than its Roche-lobe radius ($R_L \gtrsim 30$ AU), the interaction cannot be attributed to standard Roche-lobe overflow (RLOF). In (1000), we proposed a new mass-transfer mode, "wind RLOF", in which the slow Mira wind, rather than the star itself, filled the Roche lobe and then flowed onto the companion through the inner Lagrangian point, L_1. Utilising a simple parametrisation for the Mira wind, we showed that this scenario develops when the wind acceleration zone lies close to, or is a significant fraction of, the primary's Roche-lobe radius, resulting in

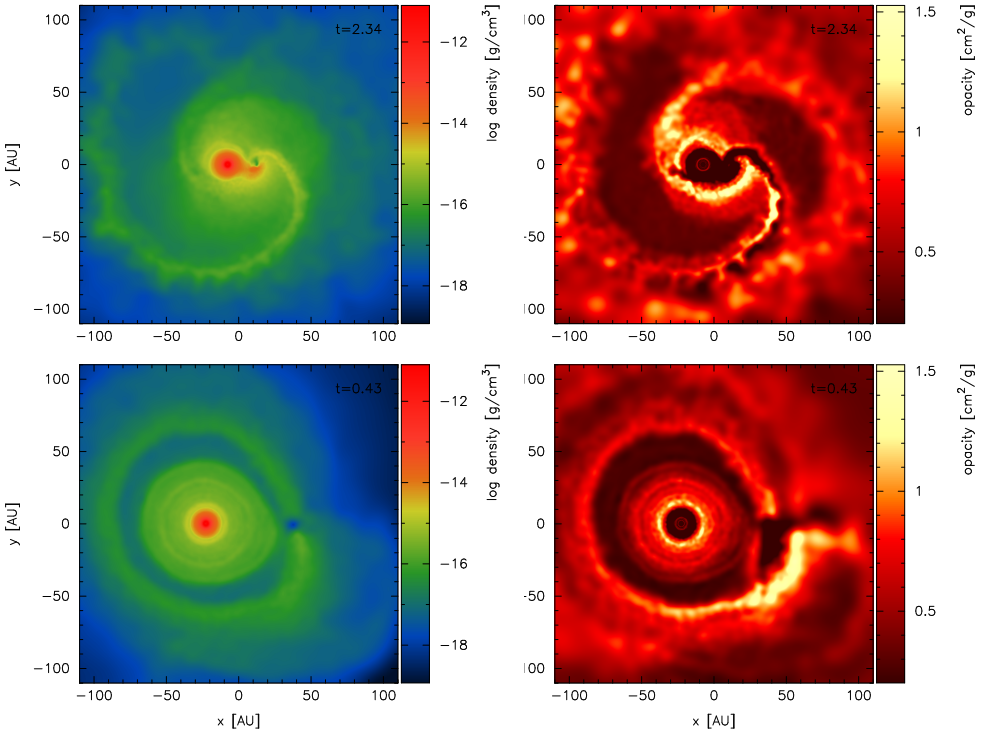

Figure 1. Density [left] and opacity [right] cross-sections in the orbital (*xy*) plane for models M1 and M2, binaries with separations a = 20 AU [top row] and 60 AU [bottom row], respectively. The simulations (each with at least $N \sim 4.5 \times 10^5$ particles) were computed in the co-rotating barycentric frame in which both stars are stationary and the positions of the primary and secondary remain fixed at (-7.5, 0, 0) and (12.5, 0, 0) for the 20 AU model, and (-22.5, 0. 0) and (37.5, 0, 0) for the 60 AU model. Time, t, is in units of $\Pi_{\rm orb}$.

greatly increased accretion rates than typical BHL values, and in an equatorial outflow (i.e. with most of the material in the orbital plane).

2. Wind RLOF: Formation of Arcs, Spirals, Cavities and Detached Shells

To explore the details of wind RLOF, we have now incorporated a wind acceleration prescription (physically motivated by Mira observations and including radial pulsations, radiative cooling and dust formation) into the GADGET2 smoothed particle hydrodynamics code (1002). Each binary model consists of two point masses, a 1 $M_\odot$ Mira and a 0.6 $M_\odot$ white dwarf, in circular e = 0 orbits with separations between a = 5 - 60 AU. A wide range of mass-loss rates and outflow velocities are achieved by injecting the wind particles at the oscillating surface of Mira A with a piston velocity of 2 km s^{-1}, a pulsation period of $\Pi_{\rm puls}$ = 332 days, and various C/O ratios for carbon- and oxygen-rich dust (see (999) for details).

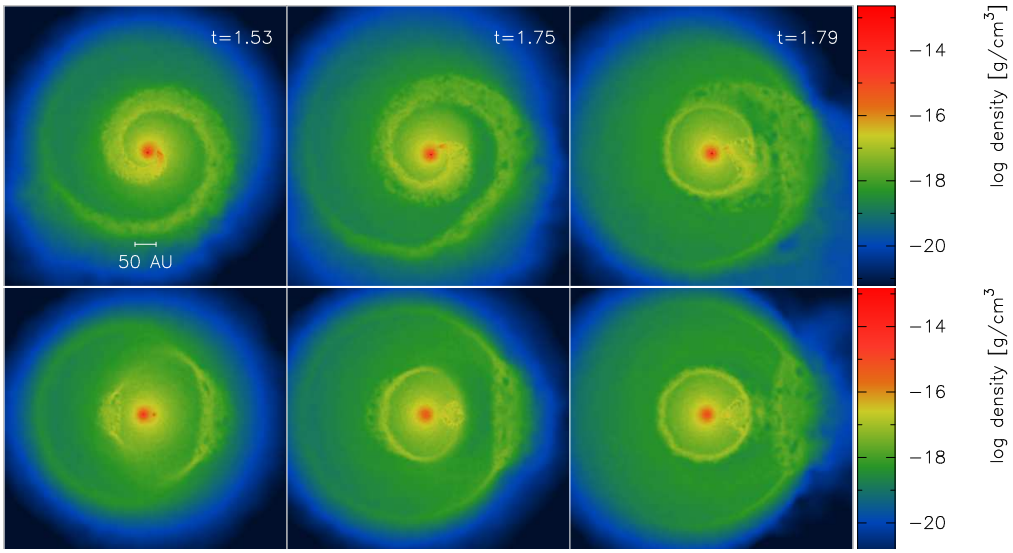

Figure 2. Density profiles in the binary orbital (*xy*) [top] and vertical (*xz*) [bottom] planes for systems with different eccentricities: $e = 0.0$ [left], $e = 0.4$ [middle], and $e = 0.8$ [right], respectively. All models have the same semi-major axis $a = 20$ AU. Time, t, is in units of $\Pi_{\rm orb}$ (70.7 years).

Fig. 1 shows two models of an oxygen-rich Mira losing 10^{-6} $M_{\odot}yr^{-1}$, a dust formation radius at $R_{\rm dust} \sim 6\,R_{*}$, and a slow wind $v_{\rm w} \sim 4$ km s^{-1}, similar to that observed in Mira. The outflow geometries shown are characteristic of two different mass-transfer regimes: model M1 exemplifies systems in which the dust forms beyond the Roche-lobe (i.e. $R_{\rm dust}/R_L \gtrsim 1$) and model M2, those in which $R_{\rm dust}/R_L < 1$.

Model M1 ($a = 20$ AU), with $R_{\rm dust}/R_L \sim 1.18$, demonstrates mass-transfer via wind RLOF. In this case, the majority of the wind does not have sufficient velocity to escape spherically from the primary's Roche lobe, but instead it is first drawn into the potential well of the secondary through L_1 and then onto the surface of this star via an accretion disk. The material which does escape (primarily from disk outflows due to angular momentum transfer) has been gravitationally focused, and forms a highly equatorial outflow traversed by spiral shocks (the density contrast at $r > 50$ AU is $\rho_{\rm equator}/\rho_{\rm pole} \gtrsim 10$). Dust grains condense behind these shocks in the dense, cooling gas, forming dusty, spiral arms and arcs that trace dust-free cavities. The companion accretes $\sim$ 50% of the mass lost by the primary – much more than the typical BHL fraction of a few %.

The outflow geometry of model M2, with $R_{\rm dust}\,/\,R_L \sim 0.4$, is more spherical though still containing asymmetries. Dust shells are ejected periodically ($\sim$ every 50 years) and are distorted as they expand towards the companion. A dusty extension forms beyond the latter as each shell collides with the accretion wake. The mass-transfer rate is an order of magnitude greater than the BHL estimates (although it should be noted that only 0.43 orbital periods have been simulated here) and increases periodically during each passage of a shell.

Detailed studies of the effect of orbital eccentricity on wind-interacting binaries are also currently underway. As shown in the evolution of binaries with a faster 11 $\mathrm{km\,s^{-1}}$ wind (see Fig. 2), the Archimedes spiral which was produced in the circular binaries becomes distorted in models with larger eccentricities, and at $e = 0.6$ the spiral shock wraps back on itself and transitions to an "interrupted" shell structure (this transition occurs as well at smaller e, but only for smaller a). The accretion rate becomes strongly modulated, sharply peaking just after periastron passage and then decreasing non-linearly back to its low state. Both of the above effects are likely to be more pronounced in eccentric Mira-type binaries with slower winds, and where the mass-transfer mode is likely to switch from BHL-type flows to wind RLOF at apastron and periastron, respectively, during each orbit (Mohamed & Podsiadlowski, in preparation).

3. Implications

The physical Mira system appears to exhibit characteristics of both models M1 and M2. While the stream connecting the two stars and the bipolar outflow are both natural consequences of model M1, i.e. wind RLOF, model M2 may additionally explain the enhancement of dust emission beyond the companion and the observed detached, dusty shells (991). The fluctuations in the accretion rate produced by the passage of these shells may account for the mysterious variability (with a $\sim$ 14 year period) exhibited by Mira B (1004; 1003).

Finally, wind RLOF has implications for several related systems; the creation of a highly aspherical mass-loss geometry, previously only thought to be significant in binaries with $a < 10$ AU (997; 992), may be closely related to the origin of the equatorial outflows, disks and dusty torii observed around post-AGB stars and also be important for shaping bipolar (proto)-planetary nebulae. The higher mass-transfer rates of wind RLOF also have far-reaching consequences for a wide range of accretion-dependent phenomena, e.g. for symbiotic binaries as progenitors of supernovae Ia (see (1000) for a discussion about SN 2002ic), and may explain the formation of eccentric barium stars (see (999) and R. Izzard, this volume).

Acknowledgments. S. Mohamed would like to thank the SOC for providing her with financial assistance to attend the conference, and Paul Taylor for helpful comments. All figures were produced with the SPLASH visualisation code (1001).

References

Chandler, A. A., Tatebe, K., Wishnow, E. H., Hale, D. D., & Townes, C. H. 2007, Astrophysical Journal, 670, 1347

Gawryszczak, A. J., Mikołajewska, J., & Różyczka, M. 2002, Astronomy and Astrophysics, 385, 205

Josselin, E., Mauron, N., Planesas, P., & Bachiller, R. 2000, Astronomy and Astrophysics, 362, 255

Karovska, M., Hack, W., Raymond, J., & Guinan, E. 1997, Astrophysical Journal, Letters, 482, L175

Karovska, M., Schlegel, E., Hack, W., Raymond, J. C., & Wood, B. E. 2005, Astrophysical Journal, Letters, 623, L137

Marengo, M., Karovska, M., Fazio, G. G., Hora, J. L., Hoffmann, W. F., Dayal, A., & Deutsch, L. K. 2001, Astrophysical Journal, Letters, 556, L47

Mastrodemos, N., & Morris, M. 1999, Astrophysical Journal, 523, 357
Matthews, L. D., & Karovska, M. 2006, Astrophysical Journal, Letters, 637, L49
Mohamed, S. 2010, Ph.D. thesis, Univ. Oxford
Mohamed, S., & Podsiadlowski, P. 2007, in 15th European Workshop on White Dwarfs, edited by R. Napiwotzki & M. R. Burleigh, vol. 372 of Astronomical Society of the Pacific Conference Series, 397
Price, D. J. 2007, Publications of the Astronomical Society of Australia, 24, 159
Springel, V. 2005, Monthly Notices of the Royal Astronomical Society, 364, 1105
Wood, B. E., & Karovska, M. 2006, Astrophysical Journal, 649, 410
Yamashita, Y., & Maehara, H. 1977, PASJ, 29, 319

Asymmetric Planetary Nebulae V
A. A. Zijlstra, F. Lykou, E. Lagadec and I. McDonald
Jodrell Bank Centre for Astrophysics, Manchester, UK © 2011

Asymmetry in Common Envelope Ejecta

Ben Fitzpatrick and Philipp Podsiadlowski

University of Oxford, Sub-department of Astrophysics, Denys Wilkinson Building, Keble Road, Oxford

Abstract. We have performed a parameter study of common envelope ejecta morphology using the smoothed particle hydrodynamics code `Gadget2`. We use simple single polytrope models to assess the effects of deposition energy, angular momentum and envelope structure on the final ejecta morphology. For small core deposition energies, ejecta is bipolar in both centrally condensed and flatter density profiles (polytropic index 3 and 1.5 respectively). The centrally condensed envelope structure produces ejecta that is strongly peaked at 45 degrees from the rotation axis, given significant angular momentum. The flatter density profile envelope produces double-lobed like ejecta, where the largest mass per solid angle is at the poles. Both envelope structures produce increasingly spherically symmetric ejecta given larger deposition energies. We explore the possibilities that this has for the formation of bipolar planetary nebulae.
Keywords. Planetary nebulae – Circumstellar matter

1. Introduction

The origins of bipolar planetary nebulae are not well constrained; a single star losing mass on the AGB, in the absence of sufficient equatorially enhanced circumstellar material, cannot produce strongly bipolar mass loss without rapid rotation. This requires angular momentum addition, whether by tidal spin-up from a companion or by a merger with a stellar or planetary companion (e.g. Soker 1009; Nordhaus 1006). Significant mass loss from post-main sequence stars can also occur as part of a merger which leads to a common envelope phase, in which a relatively compact companion enters the envelope (1008; 1007). Angular momentum is deposited in the envelope as the companion spirals in, and energy can be released thermally in a dynamically short timescale during the final fast spiral in / core merger phase.

We investigate the ejecta produced by driving shocks into oblate, spun-up envelopes with different density profiles in order to qualitatively study the likelihood of common envelope production of bipolar PNe.

2. Method

We construct two 50 solar mass, 30 solar radii envelopes with polytropic indices $n = 1.5$ and $n = 3$ by solving the Lane-Emden equations. The low index ($n = 1.5$) has a much flatter density profile, whereas the high index has much more mass in the central regions

than in the outer envelope. We then add angular momentum on dynamical timescales to each model as a solid body, following the methodology of Morris & Podsiadlowski (1005). The high index model develops a partially toroidal density distribution at large radii, whereas the low index model becomes more oblate. At given values of angular momentum in the models, we add varying energies $E_{\rm dep}$ to the particles in the inner 5 solar radii as $E_{\rm dep} = \alpha E_{\rm bind}$, where $E_{\rm bind}$ is the gravitational binding energy of the star at the time of energy addition. An adiabatic index of $\gamma = \frac{5}{3}$ is used in the simulations.

3. Results

The following results have on the y-axis descending values of $\alpha = 0.1, 0.15, 0.2, 0.3$ and, on the x-axis, momentum values left to right of $L = 4.4 \times 10^{54}, 5.6 \times 10^{54}, 4.4 \times 10^{54}$, and 5.6×10^{54} g cm^2 s^{-1}. The larger value is approximately half the total amount of angular momentum that can be added to these models in this way. The left two columns are $n = 1.5$ models and the right two $n = 3.0$.

The bipolarity of the ejecta for lower deposition energies can be seen from Figure 2 which displays the mass distribution by altitudinal angle measured from the z-axis. As each bin in the histogram represents equal solid angle, it can be seen that while there is some mass loss near the equatorial plane, the greatest density of ejecta is at or above $\pi/4$ from the rotation axis (z-axis). Figure 2 demonstrates the higher momentum in these regions as well, which would be less suppressed than the slower moving equatorial ejecta by any circumstellar material, and thus enhance bipolarity.

We see the appearance of inner bipolar structures in some ejecta in Figure 1. These are not formed by the initial shock, but by the inflation of the hot gas in the deposition region causing a second mass loss event. Provided that the deposition region is not asymptotically point-like, we expect this to be reasonably robust. Smaller deposition regions will cause stronger shocks for the same deposition energy.

4. Conclusion

We find that distinctly different envelope structures can produce bipolar ejecta under our methodology. Although the model is simplistic and makes no allowance for the gravitational and hydrodynamic influence of the spiralling-in secondary other than in angular momentum addition, it is a qualitative demonstration of the types of ejecta produced by reasonably weak shocks propagating into high angular momentum envelopes. The bipolarity of the ejecta under certain parameters in mass and momentum reinforces the role of common envelope processes as a possible cause of bipolar planetary nebulae. The differing morphology produced by varying envelope structures suggests that given a CE origin for a particular PN, the envelope structure of the PN progenitor could be deduced.

References

Morris, T., & Podsiadlowski, P. 2006, MNRAS, 365, 2
Nordhaus, J. 2008, Ph.D. thesis, University of Rochester

Ostriker, J. 1975, in The Structure and Evolution of Close Binary Systems (Cambridge), IAU Symp. 73rd
Paczynski, B. 1976, in The Structure and Evolution of Close Binary Systems, edited by P. Eggleton, S. Mitton, & J. Whelan (Dordrecht: Reidel), IAU Symp., 75
Soker, N. 2003, in Stars as Suns, edited by A. Dupree, & A. Benz, vol. 20 of IAU Symp., 323

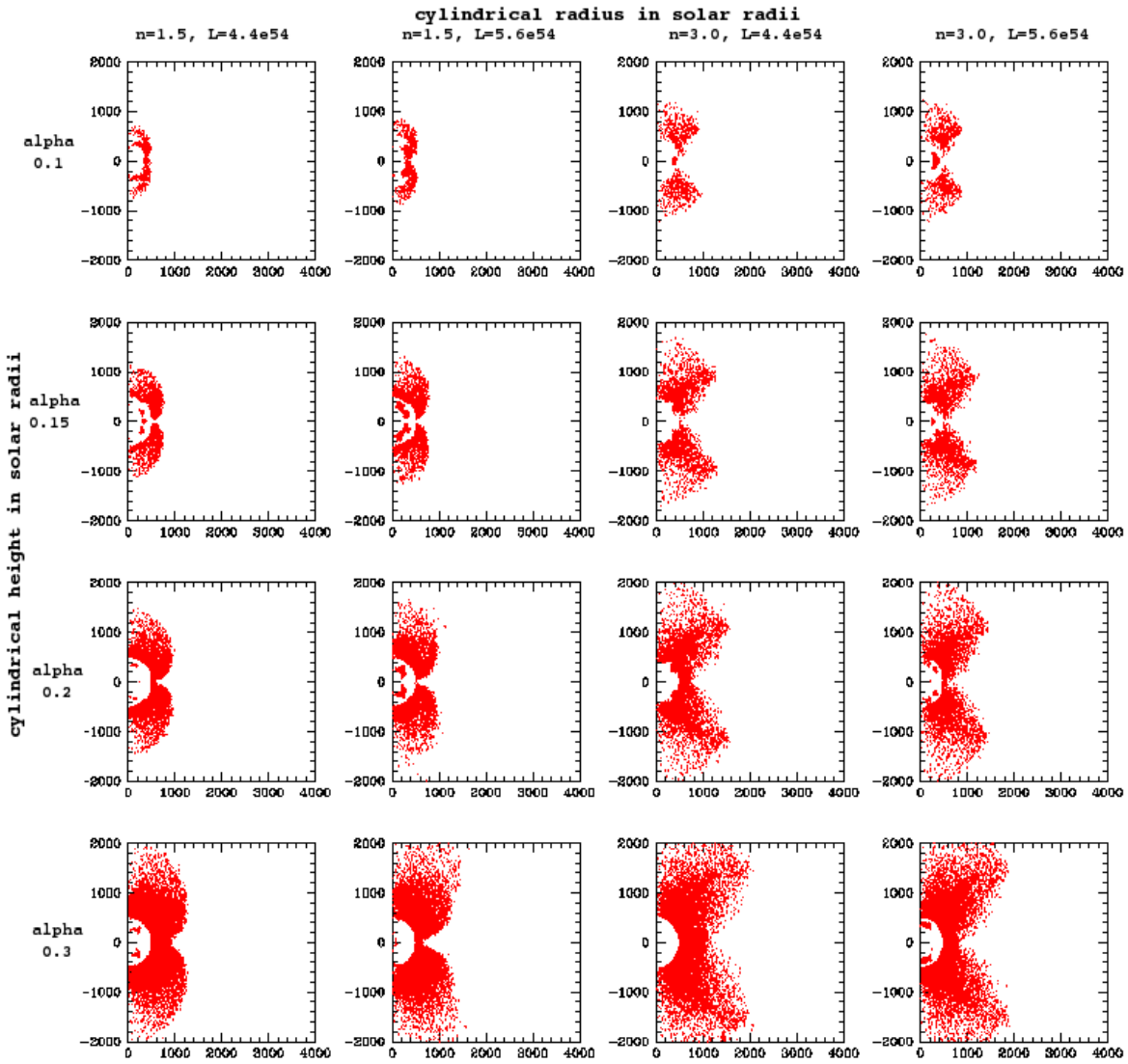

Figure 1. Particle position plots in cylindrical coordinates of unbound ejecta at late times $t \approx 40\, t_{\rm dyn}$. The left two columns have $n = 1.5$ and the right two $n = 3$. Lower deposition energies produce slower moving ejecta, as expected, and there is a clear morphological difference between the two polytropic indices.

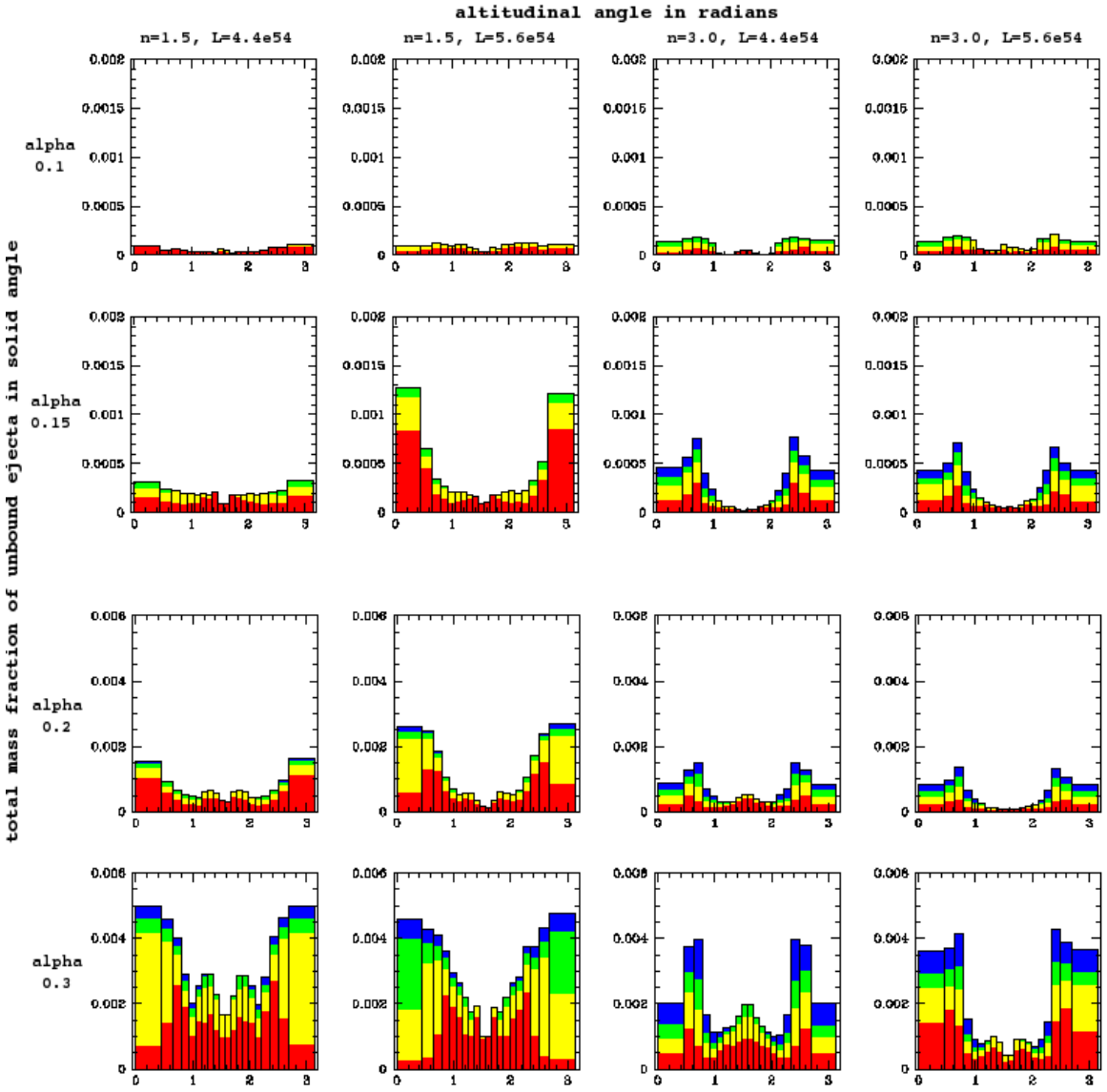

Figure 2. Histograms of mass per solid angle vs altitudinal angle of unbound ejecta at late times $t \approx 40\,t_{\rm dyn}$, colour coded by radial velocity. Velocities less than $300\,{\rm km s^{-1}}$ are in red, less than $450\,{\rm km s^{-1}}$ in yellow, less than $600\,{\rm km s^{-1}}$ in green, and more than $600\,{\rm km s^{-1}}$ in blue. The high index models can produce ejecta strongly peaked at $\pi/4$ from the poles.

Asymmetric Planetary Nebulae V
A. A. Zijlstra, F. Lykou, E. Lagadec and I. McDonald
Jodrell Bank Centre for Astrophysics, Manchester, UK © 2011

Drawing parallels between planetaries and novae

A. Evans

Astrophysics Group, Keele University, Keele, Staffordshire, ST5 5BG, UK

Abstract. We present a brief overview of classical nova eruptions. There is a number of similarites between the evolution and environments of novae and planetaries, and observing and understanding the evolution of nova eruptions may give clues to the formation and evolution of planetary nebulae.
Keywords. Planetary Nebulae – Novae

1. Introduction

Classical novae (CNe) are a subset of the cataclysmic variables (CV; 1047). Their outbursts occur in semi-detached binaries, in which a Roche-lobe-filling secondary transfers matter onto the surface of a white dwarf (WD) via the L1 point. Conditions in the accreted material eventually become suitable for a thermonuclear runaway (TNR) on the WD surface. Following the TNR $\sim 10^{-5} \ldots 10^{-4} M_{\odot}$ of material is ejected at $\sim 300 \ldots 3000\,\mathrm{km\,s^{-1}}$ (1013). Therefore CN nebulae are short-lived compared with, and less of a 'spectacle' than, Planetary Nebulae (PNe).

The WD in a nova binary may be a CO WD ($M_{\rm WD} \lesssim 1.2 M_{\odot}$) or a ONe WD ($M_{\rm WD} \gtrsim 1.2 M_{\odot}$). CN explosions on CO WD result in lower ejected velocities, and tend to be dust-producers; those on ONe WD result in higher velocities, little or no dust, and display coronal emission. In the latter forbidden neon lines (such as [Ne II]12.8 μm, [Ne v]14.32 μm) are often prominent; these are the 'neon novae' (see Fig. 1).

The ejected material is enriched in CNO, Ne, Mg, Al, S, Si (see e.g. 1031). This is partly a consequence of the TNR, but also due to the fact that some of the WD is dredged up into accreted envelope. Determination of the mass ejected in a CN eruption is important for two reasons, of relevance to broader areas of astrophysics: (i) if the ejected mass exceeds that accreted then the WD mass will decrease over time, but this means that CNe may be more significant contributors to Galactic chemical evolution than previously thought; (ii) if the ejected mass is less than that accreted then the WD mass will increase, with implications for a subset of CNe as progenitors of Type Ia supernovae. Observationally, it seems that more mass is ejected than expected on the basis of TNR but the jury is still out on this issue.

Apart from extra-galactic surveys, the discovery of CNe is (currently) somewhat haphazard, and is dominated by the amateur community. However this is likely to change dramatically in the foreseeable future when large-scale surveys such as those proposed with the LSST come on-stream.

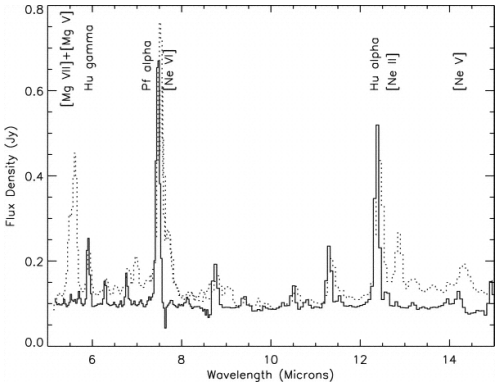

Figure 1. Spitzer IRS spectra of the CO nova V1186 Sco (solid line) and the neon nova V1187 Sco; note the stronger Ne lines in the latter (from 1042).

2. The evolution of a CN eruption

The CN 'cycle' may be summarised as follows (roughly in time order):

- mass transfer from the secondary onto the WD;
- thermonuclear runaway;
- fireball (optically thick) phase as material lifts off the WD;
- common envelope phase, while binary is engulfed by the ejecta;
- the ejecta become optically thin at visible wavelengths;
- free-free phase, during which the ejected mass can be determined (1027);
- nebular phase, during which elemental abundances in the ejecta can be determined (1027; 1044);
- dust phase (for CNe on CO WD) (1027; 1024);
- coronal phase (for CNe on ONe WD);
- fine structure line phase (when abundances may also be determined);
- return to 'quiescent' (inter-outburst) state.

Once the eruption has subsided mass transfer resumes and the cycle starts over again; the system will experience another eruption in $\gtrsim 10^4$ years' time. All novae are recurrent, but those that recur on a human timescale ($\lesssim 100$ years as opposed to $\gtrsim 10^4$ years) are classified as recurrent novae (see 1023, for a recent review).

The energetics of a CN eruption are determined by the 'speed class'; this is characterised by the observational parameter t_n, ($n = 2$ or 3), the time in days for the visual light curve to fall by n magnitudes from maximum (see Fig. 2; see 1041, for a comprehensive discussion of CNe light curves).

Following the nova eruption the stellar remnant emits at $\sim L_{\rm Edd}$ appropriate for the WD mass ($M_{\rm bol} \simeq -6 \ldots -9$), so they are visible out to the Virgo cluster. Furthermore, as the absolute visual magnitude at maximum ($\simeq M_{\rm bol}$) depends in a simple way on t_n (see 1048; 1045, for reviews) CNe are a useful rung on the cosmic distance ladder. During the nova eruption the bolometric luminosity of the stellar remnant is $\sim$ constant, so that as the mass-loss declines, the pseudo-photospheric radius collapses and the effective temperature rises.

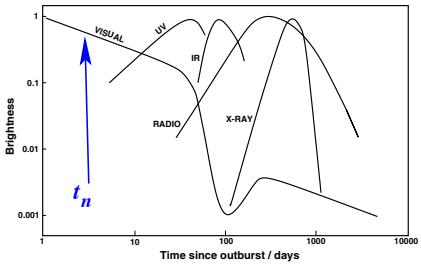

Figure 2. Schematic multi-frequency light curve of a classical nova eruption; the energetics of the eruption is determined by t_n, the time (in days) for the light curve to decline by n (=2 or 3) magnitudes. Adapted from (1014).

It is interesting to compare the evolution of a CN eruption with that of a PN as summarised in the Rochester white paper (1011): "…at this point the star's structure changes as the photospheric radius shrinks and $T_{\rm eff}$ rises, the mass-loss drops while wind speed increases, fast wind ploughs up material ejected during super-wind phase, the resulting gas then ionized by the central star". *A CN eruption therefore resembles in many ways the formation of a PN, but in fast-forward.*

3. The CN progenitor

Unlike recurrent novae, whose inter- and pre-eruption behaviour can in principle be studied in detail, comparatively little is known about the pre-outburst behaviour of CNe; however there do exist a number of observational clues.

3.1. The circumstellar environments of CN progenitors

(1051) have drawn attention to short-lived narrow absorption lines in the post-outburst spectra of CNe. They conclude that the material responsible is unconnected with the eruption, lies well outside the outburst ejecta, and must therefore be located in the circum-binary environment and lost from the binary prior to eruption. Williams et al. suggest that these lines arise in material lost from the secondary star (possibly by 'leakage' through the L1, L2, L3 points), perhaps in mass-transfer events that trigger the CN eruption. There is also a hint that abundances of species such as Sc, Ti, V in this material may be enhanced relative to solar; if confirmed this would imply that CN outbursts may occur in systems containing evolved secondaries.

There is evidence that the CN V445 Pup (see below) had substantial circum-stellar reddening prior to its 2000 eruption.

3.2. Are there CNe with PNe?

The WD (CO/ONe) progenitor in a CN system had mass $\lesssim 8 M_{\odot}$. So clearly a close binary containing a WD means that the WD progenitor in a CV has already shed a PN. Is there any evidence that CNe are associated with PNe? There are two good candidates, but both are oddballs.

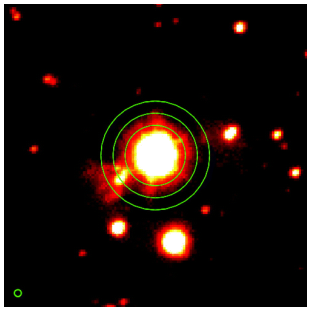

Figure 3. The PN surrounding nova V458 Vul, flash-ionised by the 2007 eruption (see 1049; 1050, for details).

GK Per (1901). GK Per is an Intermediate Polar (see below), and (apropos the above) has an evolved (K2IV) secondary (1010). The 'PN' associated with GK Per was identified in *IRAS* data (1012); it has also been identified at optical (1015) and sub-millimetre (1043) wavelengths. (1020) however argued that the putative PN may not have originated directly from the WD, but is the result of Roche Lobe overflow from an evolved secondary onto the WD, converting the latter into a 'born-again' AGB star.

V458 Vul (2007). This was a 'fast' nova, with ejection velocities in the range 1500 . . . 2000 km s^{-1}. A pre-existing PN was identified from pre-outburst IPHAS images and the 2007 CN eruption flash-ionised the PN (1049). The orbital period (98 min, towards the low end of CN orbital periods; 1048) was determined by (1039). For further discussion see (1040) and (1050).

4. Shaping of nova ejecta

In CNe we know that the stellar component is a binary, the orbital periods (with a few outliers at the high end) ranging from $\sim$ 1.4 . . . 8 hours (1048); compare this with the 3 hours . . . 8 days (likewise with a few outliers) for the 'close' binary components of PNe (1019). While there are clearly strong selection effects it is evident that there is considerable overlap between the orbital periods of CNe and close PN binaries. Novae with long ($\gtrsim$ 100 days) periods are recurrents, the secondary being a red giant; there is also of course a population of PNe central stars with long periods (1018).

The binarity of CNe is an obvious candidate for shaping the nebular remnant, and this property has been foremost in trying to understand the shaping of CN shells. For example, the shaping might take place during the common envelope phase (see 1032, for an early discussion). (1035) have folded in the effect of WD rotation into the common envelope phase, but either way resulting in a prolate nebula.

The dependence of the axial ratio of the nebular remnant on the CN speed class is shown in Fig. 4, in which there is a very strong indication that ellipticity decreases towards 'faster' novae. This can be probably be traced to the fact that slower CNe have lower ejection velocities, allowing greater time for the ejected material to interact with the binary during the common envelope phase (see 1014, for a recent review of CN remnants).

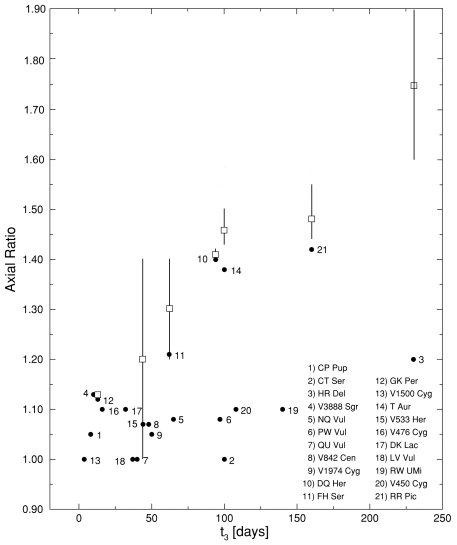

Figure 4. Observed dependence of CN remnants' axial ratio against speed class, t_3; open squares have been corrected for inclination, where known (1014).

In some CV the white dwarf is magnetic. If the field is sufficiently strong ($\gtrsim 10^7$ G; the 'Polars') the accretion flow occurs directly onto the magnetic pole(s) of the WD (see 1047, for details). A weaker field ($10^6 \ldots 10^7$ G) will still disrupt the inner accretion disc (the 'Intermediate Polars', IPs). About a dozen CNe are known or suspected IPs, while only one (V1500 Cyg) is a known Polar. (1033) have suggested that, if the magnetic WDs in CNe are rapid rotators, a consequence is that the ejected shells are asymmetric.

A further cause of asymmetric shells might be the fact that the TNR might be localised, rather than spherically symmetric, subsequently spreading over the WD surface (1034); for a more recent discussion of this see (1028).

Finally we note that little attention seems to have been given to the effect of pre-exisiting material (such as that identified by 1051, see above) on the shaping of ejecta. In particular it would be interesting to follow the evolution of the nebular remnants of the CNe in Williams et al.'s study.

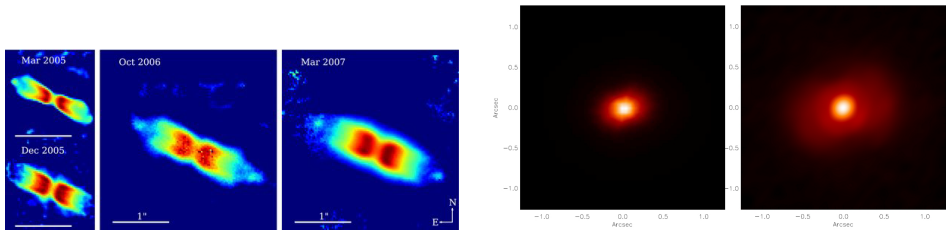

Figure 5. High spatial resolution observations of the early shaping of CN ejecta. Top, 2.2 μm VLT observations of V445 Pup over the period 2005–2007 (1052); bottom, the expansion of V1280 Sco at 2.2 μm as seen with VLTI (1017)

Early shaping

Observational evidence is now beginning to throw light on the shaping of CN ejecta at early times in the eruption (for the shaping of *recurrent* nova ejecta, see (1037) for an observational view, and (1021) for a theoretical view). The exquisite high spatial resolution observations, obtained with VLT/VLTI, are now providing evidence for nebula shaping at very early times in the eruption. Such data are available for two recent CNe, but they tell a very different story.

V445 Pup. This was, uniquely, a 'helium' nova, with apparently a complete absence of hydrogen in the ejecta. It showed a highly collimated bipolar shell (possibly the most highly collimated seen in any CN), reminiscent of PNe and p-PNe (Fig. 5); however the outflow velocities were consistent with a CN rather than a PN (1052). There is an equatorial dust 'waist', with (as already noted) substantial circum-stellar reddening before outburst. Woudt et al. argue that the waist is not the cause of the collimated ouflow, rather a consequence (cf. 1046), and that the real cause of the collimation may become apparent as the dust waist disperses.

V1280 Sco. This CN was discovered 12 days before maximum, and there was a dust-formation event $\sim$ 20 days after visual maximum (1016; 1030). VLTI observations were carried out over the period 11...133 days post-outburst and the diameter of the dust shell at 8 μm, 10 μm and 13 μm increased uniformly over this period (1016, see Fig. 5). Observations of this type, combined with expansion velocities, are clearly valuable in determining CN distances. Furthermore, as emphasised by (1016), the high spatial resolution observations that are now possible have the potential to investigate the earliest stages of the formation of CN nebulae.

5. Dust in CNe

CO novae produce a range of dust types, including silicates, hydrocarbons (or hydrogenated amorphous carbon) and SiC (1026; 1027; 1024). Indeed in view of the overabundances in the ejecta, which are unique to each object, it may be that the dust composition in CNe outflows may be impossible to specify unambiguously, for example silicates may have hydrocarbon and/or N inclusions (1022). See (1038) for an early (observational) discussion of the effect of N inclusions in hydrocarbons on the wavelengths of aromatic features in PNe, and (1036) for a more recent (and general) discussion.

In order for dust to form, the ejected material must go from plasma, to atomic, to molecular, to grains very quickly; for example (see above) the CN V1280 Sco formed dust $\sim$ 20 days after eruption. The key molecule in the chemistry that leads to grain formation is H_2; while this is observationally elusive, there is now ample observational evidence for diatomic molecules (see 1024, for a recent review). Molecule (and dust) formation requires the presence of dense clumps in the ejecta (similar to those famously sported by the Helix Nebula), to shield molecules and nucleation sites from ionizing radiation; indeed there is evidence for clumping in CN shells when they are resolved (see 1014).

CNe often display the 'chemical dichotomy' frequently seen in post-AGB stars etc. Whereas in evolved stars this is likely due to the ejection of material having different

C:O ratios at different stages of the stars' evolution, in CNe it is most likely due to the fact that CO formation does not go to saturation (so the C:O ratio paradigm is irrelevant); in addition clumping and structure in the ejecta are almost certainly a factor in determining the chemistry.

The infra-red spectra of a number of CNe have shown aromatic features (see Fig. 6 and (1029) for examples). These features in CNe resemble those in Peeters et al.'s (2002) 'Class C', which are normally associated with cool ($\lesssim 10^4$ K) post-AGB stars evolving from the AGB to the PN phase; this seems inconsistent with the high ($\sim 10^5$ K) temperatures of the stellar remnants of CNe. This paradox is resolved if the carrier of the aromatic emitter in CNe is still buried in dense clumps, and hence unaffected by the hard radiation field of the stellar remnant.

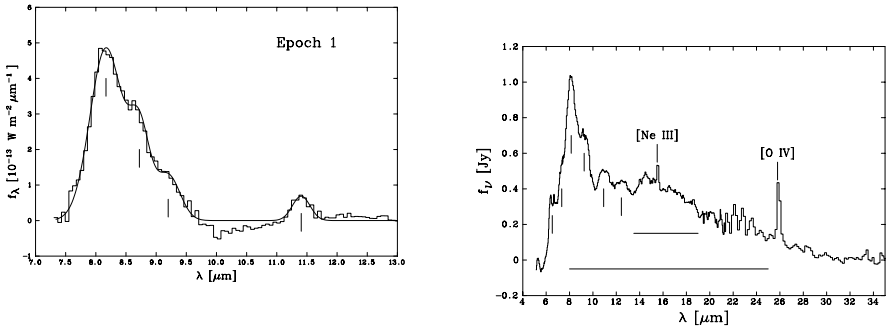

Figure 6. Aromatic features in nova dust. Left, V705 Cas, right, DZ Cru (1022; 1025).

The chemistry that leads to grain formation in CNe is poorly understood, and pushes interstellar chemistry networks to the limit; as these networks evolve to better understand dust nucleation and formation in CNe there will inevitably be a benefit to our understanding of chemistry and dust formation in PN and p-PN.

6. Summary

There is a number of parallels between the evolution and environments of PNe and CNe, and the latter are therefore potential laboratories for studying several phenomena in PNe. These include common envelope evolution, extreme photochemistry with non-solar abundances, dust formation and remnant shaping. In CNe however we can observe many of these phenomena in real time.

A glance at the agenda for the Rochester workshop (1011) highlights a number of key questions and projects to further understand the PN phenomenon; these include both theoretical and observational challenges, with an eye on facilities that will soon come on-stream. With a few obvious exceptions many of these questions and projects not only apply to CNe, but the application of these ideas to CNe themselves could well help to answer some of the questions about PNe. There is considerable opportunity for, and merit in, dialogue between the PN and CN communities.

Acknowledgments. I would like to express my thanks to members of the 'nova consortium', particularly Mike Bode, Olivier Chesneau, Stew Eyres, Bob Gehrz, Andrew Helton, Joachim Krautter, Dave Lynch, Tim O'Brien, Rick Rudy, Sumner Starrfield and Chick Woodward, and to Mike Bode and Olivier Chesneau in particular for comments on a draft of this paper.

References

Anupama, G. C. & Kantharia, N. G., 2005, A&A, 435, 167
Balick, B., et al., 2009, Rochester White Paper
Bode et al., 1987, Nature, 329, 519
Bode, M. F., Evans, A., 2008, eds *Classical Novae*, second edition, Cambridge University Press
Bode, M. F., O'Brien, T. J., 2008, in *Classical Novae*, Chapter 12, eds. M. F. Bode & A. Evans, Cambridge University Press
Bode et al., 2004, ApJ, 600, L63
Chesneau et al., 2008, A&A, 487, 223
Chesneau et al., 2010, private communication; see also these proceedings
Ciardullo, R., et al., 1999, AJ, 118, 488
De Marco, O., 2009, PASP, 121, 316
Dougherty, S. et al., 1996, A&A, 306, 547
Drake, J. J. & Orlando, S., 2010, ApJ, 720, 195
Evans, A., et al., 2005, MNRAS, 360, 1483
Evans, A., et al., 2008, eds, *RS Ophiuchi (2006) and the Recurrent Nova Phenomenon*, ASP Conference Series Vol. 401
Evans, A. & Rawlings, J. M. C., 2008, in *Classical Novae*, Second edition, Chapter 13, eds. M. F. Bode & A. Evans, Cambridge University Press
Evans, A., et al., 2010, MNRAS, 406, L85
Gehrz, R. D., et al., 1998, PASP, 110, 3
Gehrz, R. D., 2008, in *Classical Novae*, Second edition, Chapter 8, eds. M. F. Bode & A. Evans, Cambridge University Press
Glasner, A. & Livne, E., 2002, in *Classical Nova Explosions*, eds M. Hernanz, J. José, API Conference Proceedings Volum 637, p. 124
Helton, L. A., et al., 2010, in *PAHs and the Universe*, ed C. Joblin, EDP Sciences, in press
Hounsell, R., et al., 2010, ApJ, in press, arXiv:1009.1737
José, J., Shore, S. N., 2008, in *Classical Novae*, Second edition, Chapter 6, eds. M. F. Bode & A. Evans, Cambridge University Press
Livio et al., 1990, ApJ, 356, 250
Orio, M., et al., 1992, A&A, 257, 548
Orio, M. & Shaviv, G., 1993, Ap&SpSc, 202, 273
Porter, J. M., et al., 1998, MNRAS, 296, 943
Peeters et al., 2002, A&A, 390, 1089
Ribeiro, V. A. R. M., et al., *in Asymmetric Planetary Nebulae 5* (2010), Eds. A.A. Zijlstra, F. Lykou, E. Lagadec, I. McDonald, p. 315
Roche, P. F., et al., 1996, MNRAS, 280, 924
Rodrígues-Gil, P. et al., 2010, MNRAS, 407, L21
Santander García, M., et al., *in Asymmetric Planetary Nebulae 5* (2010), Eds. A.A. Zijlstra, F. Lykou, E. Lagadec, I. McDonald, p. 260
Schaefer, B., 2010, ApJS, 187, 275
Schwarz, G., et al., 2007, AJ, 134, 516
Scott, A. D., et al., 1994, MNRAS, 269, 707
Shore, S. N., 2008, in *Classical Novae*, Second edition, Chapter 9, eds. M. F. Bode & A. Evans, Cambridge University Press
Shafter, A. W., 2008, in *Classical Novae*, Second edition, Chapter 14, eds. M. F. Bode & A. Evans, Cambridge University Press

Soker, N. & Rappaport, S., 2000, ApJ, 538, 241
Warner, B., 1995, *Cataclysmic Variable Stars*, Cambridge University Press
Warner, B., 2008, in *Classical Novae*, Second edition, Chapter 2, eds. M. F. Bode & A. Evans, Cambridge University Press
Wesson, R., et al., 2008, ApJ, 688, L21
Wesson, R., et al., 2010, these proceedings
Williams et al., 2008, ApJ, 685, 451
Woudt et al., 2009. ApJ, 706, 738

Asymmetric Planetary Nebulae V
A. A. Zijlstra, F. Lykou, E. Lagadec and I. McDonald
Jodrell Bank Centre for Astrophysics, Manchester, UK © 2011

Exploring the Morphology of the Expanding Remnants of Classical and Recurrent Novae

V. A. R. M. Ribeiro[1], M. F. Bode[1], M. J. Darnley[1], U. Munari[2,3], D. J. Harman[1]
[1]*Astrophysics Research Institute, Liverpool John Moores University, Twelve Quays House, Egerton Wharf, Birkenhead, CH41 1LD, UK*

[2]*INAF Astronomical Observatory of Padova, via dell'Osservatorio, 36012 Asiago (VI), Italy*

[3]*ANS Collaboration, c/o Astronomical Observatory, 36012 Asiago (VI), Italy*

Abstract. We report studies of several novae which are known or suspected to be recurrent. We discuss our morpho-kinematical modelling of the evolution of the optical spectra taken early after outburst for two recent novae. In the case of the known RN RS Oph, this is also coupled with *HST* imaging. Results support the hypothesis that remnant shaping occurs very early in a nova outburst and we also derive the structures (including inclination) and velocity field of the remnants. Overall, these results emphasise the need for coordinated imaging and spectrometry, although not always possible, if we are to truly understand remnant shaping in these systems, together with the wider implications for studies of shaping mechanisms in Planetary Nebulae.
Keywords. Planetary Nebulae – Novae

1. Introduction

The classical nova (CN) outburst is due to a thermonuclear runaway on the surface of a white dwarf (WD; see e.g., 1055; 1060, these proceedings) occurring within the matter accreted from a close companion star. A related class of objects are the recurrent novae (RNe), which have high mass WDs, probably close to the Chandrasekhar limit, to account for the short recurrence time-scales, and high accretion rates (e.g., 1075; 1079).

Classical nova remnants show a range of morphologies whose basic origin has been modelled via a combination of a common envelope phase and binary motion (e.g., 1068, and references therein). In the case of RN RS Oph-type remnants, shaping is suggested to be due to interaction of the ejected material with the pre-existing red-giant wind.

This paper will focus on our work with morpho-kinematical modelling, using Shape (see poster 32; 1078; 1077) of three novae to determine their 3D morphology (including inclination) and velocity field with a combination of *Hubble Space Telescope* (*HST*) imaging and ground-based spectrometry for RS Oph (Section 2) and in the case of V2491 Cyg and V2672 Oph using solely Hα line profiles (Section 3). Finally in Section 4 we summarise our findings.

2. The Expanding Nebular Remnant of the 2006 Outburst of RS Ophiuchi

RS Oph is one of the most well studied RNe, with six previous recorded outbursts and two further ones suggested (e.g. 1071; 1072; 1066; 1073; 1059). From its latest outburst, beginning 2006 February 12.83 (1064), RS Oph was quickly followed with a multi-frequency campaign from the radio to X-ray (e.g., 1074; 1065; 1056; 1057).

RS Oph was observed at around 155 days after outburst with *HST* imaging and ground-based spectrometry (1069). These observations were used to derive the physical parameters of the object. Figure 1 shows the results of this modelling, constraining a model with an outer dumbbell and high density inner hour glass structure. The higher density was required to replicate the lower expansion velocities observed in the spectrum. The inclination of the system was derived to be 39^{+1}_{-10} degrees, comparable to estimates of the inclination of the central binary of Dobrzycka & Kenyon (1058). At a distance of 1.6±0.3 kpc (Bode 1054; see also Barry et al. 1053) the implied maximum expansion velocity of the system is 5100^{+1500}_{-100} km s^{-1} (the range in velocity arise from the 1σ errors on the inclination). The observed apparent asymmetry of the ejecta in the ACS/HRC image is suggested to be due to the effect of the finite width and offset from the [O III] line's rest wavelength of the F502N filter. The model was then evolved to 449 days after outburst (the second *HST* epoch). The results implied that the outer dumbbell structure expanded linearly while the inner hour glass structure shows some evidence for deceleration. However, since only lower quality WFPC2 imaging was available at that time, the results are open to over-interpretation.

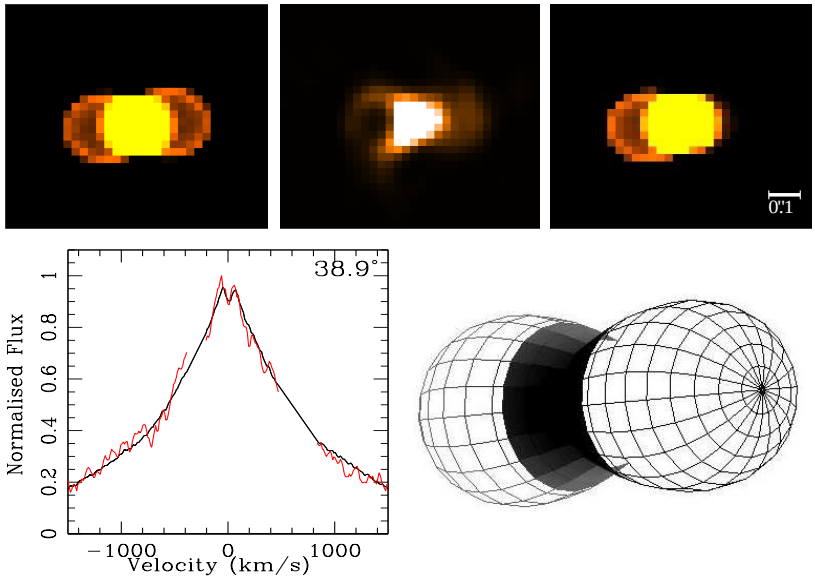

Figure 1. Top: synthetic image without the *HST* F502N ACS/HRC filter profile applied (left), enlarged ACS/HRC image at t = 155 days after outburst (middle) and synthetic image with the ACS/HRC F502N filter profile applied (right). Bottom: best fit synthetic spectrum (black) overlaid with the observed spectrum (red). To the right is the model structure for RS Oph (outer dumbbell and inner hour glass). Images reproduced from Ribeiro et al. (1069).

3. Early Spectrometric Evolution of V2491 Cygni and V2672 Ophiuchi

V2491 Cyg and V2672 Oph are two particularly interesting novae that have been suggested to be RNe candidates and that underwent their outbursts on 2008 April 10.8 (1062) and 2009 August 16.5 (1063) respectively. V2491 Cyg is only the second nova with recorded pre-outburst X-ray observations (after V2487 Oph - a RN; e.g., 1067). V2672 Oph shows very similar characteristics to the RN U Sco. It displayed a photometric plateau phase, a He/N spectrum classification, extreme expansion velocities and triple peaked emission line profiles during the decline phase (1061).

Using the Meaburn Spectrograph on the Liverpool Telescope (1076) we observed V2491 Cyg from 2 to 31 days after outburst and with the Asiago-AFOSC at 108 days after outburst. With the lack of resolved imaging to complement our spectra we first assumed some structures which have been previously observed in CNe (Figure 2). We modelled the Hα emission line at 25 days after outburst and then evolved our models to the later date (day 108). The effects of optical depth were investigated and we found that the line shape did not change considerably. We found that two models produced similar results at 25 days after outburst (polar blobs and equatorial ring and the dumbbell with an hour glass). However, when both models were evolved to day 108 we found that due to the contribution of [N II], which was not detected at the earlier date, the best-fit model was that for the polar blobs and an equatorial ring. We suggest that the inclination angle of the system is 80^{+3}_{-12} degrees and a maximum expansion velocity of 3100^{+200}_{-100} km s^{-1} (see 1070, for further details).

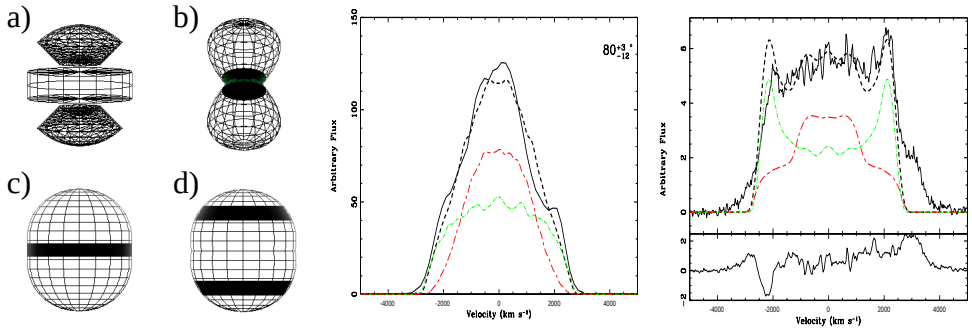

Figure 2. Model fit to V2491 Cyg. Left: model structures used to replicate the emission lines; a) polar blobs with an equatorial ring; b) outer dumbbell with an inner hour glass; c) prolate shell with tropical rings; and d) prolate shell with an equatorial ring. Middle: best fit synthetic spectrum (dashed black) to the observed spectrum (solid black) on day 25 after outburst for the polar blobs (short-dash-long-dash red) and equatorial ring (dot-dashed green) structure. Right: observed spectrum at 108 days after outburst compared with the evolved model spectrum.

Similarly, we applied the techniques above to V2672 Oph and found that the best fit model was for polar blobs and an equatorial ring with an underlying prolate structure whose density appears to decline faster with time than that of the other components. The inclination of the system is suggested to be 0±6 degrees and a maximum expansion velocity of the polar blobs of 4800^{+900}_{-800} km s^{-1} (1061).

4. Conclusions

We have investigated the evolution of three novae to derive their 3D geometry (including inclination) and expansion velocities. We show that the best way to have a true grasp of these parameters is with combined multi-epoch imaging and spectrometry. Caution should be exercised when dealing solely with spectrometric data and any model should ideally have predictions. Useful lessons may be learnt from the study of remnant shaping in novae that may be applied to that in PNe (1060), particularly of course those with binary star nuclei.

Acknowledgments. VARMR would like to thank financial support from the Royal Astronomical Society, STFC, the LOC and the Astrophysics Research Institute, LJMU.

References

Barry, R. K., et al. 2008, in RS Ophiuchi (2006) and the Recurrent Nova Phenomenon, edited by A. Evans, M. F. Bode, T. J. O'Brien, & M. J. Darnley, vol. 401 of Astronomical Society of the Pacific Conference Series, p. 52
Bode, M. F. 1987, in RS Ophiuchi (1985) and the Recurrent Nova Phenomenon, edited by M. F. Bode, VNU Science Press, p. 241
Bode, M. F., & Evans, A. (ed.) 2008, Classical Novae, CUP
Bode, M. F. et al. 2006, Astrophysical Journal, 652, 629
Chesneau, O. et al. 2007, Astronomy and Astrophysics, 464, 119
Dobrzycka, D., & Kenyon, S. J. 1994, Astronomical Journal, 108, 2259
Evans, A. et al. (ed.) 2008, RS Ophiuchi (2006) and the Recurrent Nova Phenomenon, vol. 401 of Astronomical Society of the Pacific Conference Series
Evans, A. 2010, *Asymmetrical Planetary Nebulae 5*, Eds. A. A. Zijlstra, F. Lykou, I. McDonald and E. Lagadec, p. 306
Munari, U. et al. 2010, Monthly Notices of the Royal Astronomical Society, in press, arXiv:1009.0334
Nakano, S. et al. 2008, IAU Circ., 8934
Nakano, S., Yamaoka, H., & Kadota, K. 2009, Central Bureau Electronic Telegrams, 1910
Narumi, H. et al. 2006, IAU Circ., 8671
O'Brien, T. J. et al. 2006, Nature, 442, 279
Oppenheimer, B. D., & Mattei, J. A. 1993, JAAVSO, 22, 105
Page, K. L. et al. 2010, Monthly Notices of the Royal Astronomical Society, 401, 121
Porter, J. M., O'Brien, T. J., & Bode, M. F. 1998, Monthly Notices of the Royal Astronomical Society, 296, 943
Ribeiro, V. A. R. M. et al. 2009, Astrophysical Journal, 703, 1955
Ribeiro, V. A. R. M. et al. 2010, Monthly Notices of the Royal Astronomical Society, submitted
Rosino, L. 1987, in RS Ophiuchi (1985) and the Recurrent Nova Phenomenon, edited by M. F. Bode, VNU Science Press, p. 1
Rosino, L., & Iijima, T. 1987, in RS Ophiuchi (1985) and the Recurrent Nova Phenomenon, edited by M. F. Bode, VNU Science Press, p. 27
Schaefer, B. E. 2004, IAU Circ., 8396
Sokoloski, J. L. et al. 2006, Nature, 442, 276
Starrfield, S., Sparks, W. M., & Truran, J. W. 1985, Astrophysical Journal, 291, 136
Steele, I. A., et al. 2004,
Steffen, W. et al. 2010, IEEE Transactions on Visualization and Computer Graphics, in press
Steffen, W., & López, J. A. 2006, Revista Mexicana de Astronomia y Astrofisica, 42, 99
Yaron, O. et al. 2005, Astrophysical Journal, 623, 398

Asymmetric Planetary Nebulae V
A. A. Zijlstra, F. Lykou, E. Lagadec and I. McDonald
Jodrell Bank Centre for Astrophysics, Manchester, UK © *2011*

Models of interacting winds in the 2006 outburst of RS Ophiuchi

N. Vaytet[1], T. O'Brien[2], K. Page[3], M. Bode[4], M. Lloyd[2], A. Beardmore[3]

[1]*CEA/DSM/IRFU, Service d'Astrophysique, Gif-sur-Yvette, France*
[2]*Jodrell Bank Centre for Astrophysics, The University of Manchester, UK*
[3]*Department of Physics and Astronomy, University of Leicester, UK*
[4]*Astrophysics Research Institute, Liverpool John Moores University, UK*

Abstract. Following the *Swift* X-ray observations of the 2006 outburst of the recurrent nova RS Ophiuchi, we developed hydrodynamical models of wind driven shocks to estimate the ejecta mass and velocity. We present here synthetic X-ray spectra computed from our hydrodynamical calculations which we compare to the *Swift* data. An extensive set of simulations was carried out to find a model which best fits the observations. We find a good fit at high energies but require additional absorption to match the low energy emission. We estimate the ejecta mass to be in the range $(2-5)\times10^{-7}$M$_\odot$and the ejection velocity to be close to 10,000 km s^{-1}. We also find that estimates of shock velocities derived from gas temperatures via standard model fits to the X-ray spectra are much lower than the true shock velocities.
Keywords. Planetary Nebulae

1. Introduction

RS Ophiuchi (RS Oph) is one of the most well-studied recurrent novae (RNe). The central binary system comprises a white dwarf (WD) and a red giant (RG). A nova outburst involves mass transfer from the companion to the WD. The build-up of pressure in the accreted hydrogen leads to a thermonuclear runaway ejecting a shell of material into the circumstellar medium (1091). Novae which have been observed in outburst more than once are called RNe. The shock interaction of the ejecta with the surrounding medium heats the gas to temperatures of $10^7 - 10^9$ K, yielding hard X-ray radiation (Lloyd et al. 1087; O'Brien et al. 1089). RS Oph has undergone six recorded outbursts between 1898 and 2006. The distance to RS Oph is 1.6 kpc (1081; 1080) and the mass of the WD is close to the Chandrasekhar limit. In 2006, RS Oph was detected in X-rays just 3 days after outburst using the *Swift* (1082) and RXTE (1090) telescopes. The *Swift* observations were performed every one or two days during the first 100 days, covering all the phases of the remnant's evolution.

In order to interpret the new observations, we developed hydrodynamical models for RS Oph (1092). We used a 1D Eulerian second order Godunov code with radiative cooling to simulate the outburst where mass-loss in the form of a fast wind from the WD ran into a surrounding slow RG wind. This allowed us to determine that the ejecta had a low mass ($\sim 2\times10^{-7}$M$_\odot$) and a high ejection velocity. We take the study further by calculating full X-ray spectra directly from our hydrodynamical results using the XSPEC software.

2. Synthetic X-ray spectra for RS Oph (2006)

Our hydrodynamical simulations predict the physical conditions of the hot shocked gas at any time during the outburst. We grouped the grid data into 30 logarithmically-divided temperature bins from 10^4 to 10^9 K, weighting each shell's contribution by its emission measure (EM). These were then fed as a 30-component MEKAL plasma into XSPEC to compute the X-ray spectrum. The interstellar hydrogen absorption column is $n_H = (2.4 \pm 0.6) \times 10^{21}$ cm^{-2} (1086). We also included circumstellar absorption due to the RG wind surrounding the hot shocked gas behind the forward shock (FS). Only the unshocked neutral part of the RG wind contributes to absorption. It is however non-trivial to know the ionisation state of the RG wind at all times, and we thus simply used upper and lower extremes; a fully neutral or fully ionised RG wind.

A full exploration of the model parameter space was undertaken with 88 simulations carried out in total. We extracted fluxes from our models (1–10 keV) for direct comparison to the observed *Swift* fluxes between days 3 and 100. We also examined all the spectra by eye to ensure that we had not excluded runs which had the correct spectral shape but were lying either above or below the *Swift* data at all epochs. We find our best fitting model to be run 81 (see Fig. 1). Its main characteristics are its low ejected mass $M_{\rm ej} = 2.7 \times 10^{-7}M_\odot$and high fast wind velocity $V_2 = 10^4$ km s^{-1}.

The majority of the runs produce too many low energy X-rays. In order to naturally increase the absorption, we increased the slow wind mass-loss rate but this has a strong effect on the shock dynamics. With a denser RG wind, high shock velocities (consistent with observations) can only be obtained by vastly increasing V_2. This leads to an overestimate of the soft and medium energy count rates. An alternative solution is to include some additional ad-hoc absorption during the calculation of the spectrum (shown as bold solid lines in Fig. 1). This allows us to produce good agreement between the synthetic spectra and the *Swift* observations. Such additional absorption could be due to the presence of a dense gas torus close to the binary core, as suggested by the observations of Evans et al. (1085); Bode et al. (1083); O'Brien et al. (1088).

3. Shock velocities

Fig. 2 shows the FS velocities (dots) of run 81. These are compared to the shock velocities estimated in Bode et al. (1082) from single-temperature fits to the *Swift* spectra (empty squares with error bars) and to the IR velocities from Das et al. (1084) (triangles) measured from the full width zero intensity (FWZI) of the OI and Paβ emission lines. The model velocities are much higher than the Bode et al. (1082) velocities. The IR velocities are in better agreement with the model. We also show in Fig. 2 the gas velocity just after the reverse shock (stars), which is in very good agreement with the IR velocities at early times. Taking the FWZI of the IR lines probes only the fastest moving material in the system, which suggests that the IR line widths are first dominated by the post reverse shock gas and only later by the post FS gas.

In order to investigate the differences between the simulation shock velocities and the *Swift* X-ray velocities, we fitted MEKAL models to our synthetic spectra for run 81. We then estimated FS velocities using the fit temperatures and these are plotted in Fig. 2 (empty circles). These new velocities are in very good agreement with the

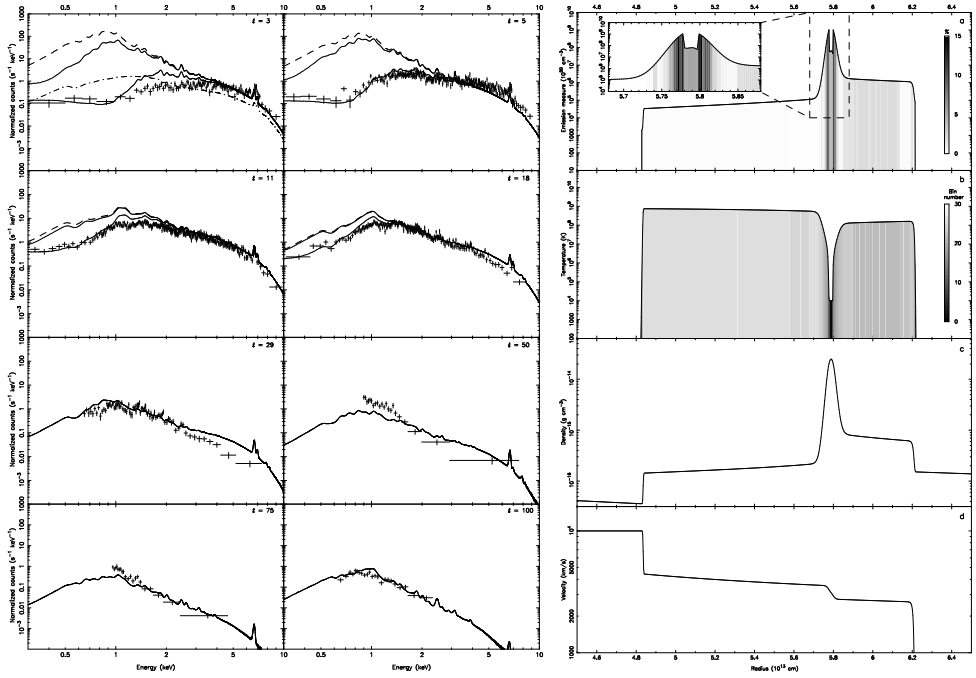

Figure 1. **Left**: Run 81 synthetic X-ray spectra at days 3, 5, 11, 18, 29, 50, 75 and 100. The thin solid and dashed lines represent a fully neutral and ionised RG wind, respectively. The bold solid line is the spectrum including additional absorption. The black crosses are the *Swift* data. The dot-dash line in the top left panel is the post-shock material's contribution to the total spectrum. **Right**: (a) EM as a function of r inside the hot shell for run 81 at day 3. The data are greyscale coded to represent what percentage of the total EM each temperature bin contributes. (b) Gas temperature as a function of r. The data are greyscale coded according to temperature bin. Gas density (c) and velocity (d) as a function of r.

observed *Swift* X-ray velocities at early times ($t < 5$ days) and are much lower than the shock velocities found in the hydrodynamic simulation.

Fig. 1a shows the EM as a function of r inside the remnant for run 81 at day 3. The greyscale represents the percentage of the total EM contained within each temperature bin. The lower panels show the temperature (b), density (c) and velocity (d) of the gas. The major contribution to the total EM is located around the CD, while the broader forward shocked region ($T \sim 10^8$ K) contributes only a few percent. This implies that the total X-ray emission is dominated by CD material at lower temperatures and that the contribution from the hotter shocked gas is small.

The dot-dash line in the top left panel of Fig. 1 shows the X-ray spectrum emitted by the post-FS gas; the contribution to the total X-ray spectrum is small at low energies but is high for energies above 5 keV. The post-FS gas spectrum is much flatter than the total X-ray spectrum; by fitting a single temperature MEKAL model to the post-FS gas spectrum at day 3 we obtain a temperature of 13.5 keV, translating as a shock velocity of 3400 km s^{-1}which is entirely consistent with the real shock velocity measured in the simulation. This flat post-FS spectrum gets drowned by the bright but cooler emission

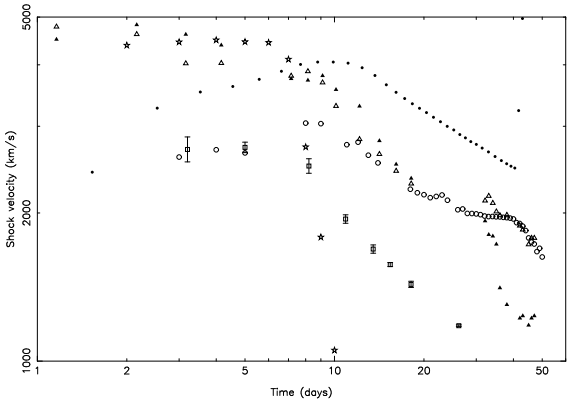

Figure 2. Run 81 FS velocities compared to observations. The empty squares are the *Swift* data, the triangles the IR data (filled = OI; empty = Paβ) and the dots the model. The empty circles are the velocities derived from the T fits to our synthetic spectra. The stars are the gas velocity behind the reverse shock.

from the CD which changes the shape of the X-ray spectrum and therefore changes the fit temperature. Fitting temperatures to the total observed spectra in order to estimate post-shock temperatures and therefore shock velocities is thus unreliable.

4. Conclusions

We have calculated synthetic X-ray spectra of RS Oph from our hydrodynamical models using the XSPEC code and compared them to *Swift* observations. We found the mass ejected in the outburst to be around $(2-5)\times10^{-7}$M$_\odot$. This ejected mass is thought to be lower than the mass accreted between two successive outbursts, which implies that the WD (which is close to 1.4M$_\odot$) is growing in mass, making RS Oph the best SN Ia progenitor candidate ever found to date. Another important conclusion is that the emission from the post-shock material is negligible compared to that of the regions around the CD, and that fitting emission models with single temperatures to X-ray spectra greatly underestimates immediate post-shock temperatures and hence FS velocities.

References

Barry, R. K. et al. 2008, in RS Ophiuchi (2006) and the Recurrent Nova Phenomenon, ASP Conference Series, 401, 52
Bode, M. F. 1987, in RS Oph (1985) and the Recurrent Nova Phenomenon, Utrecht: VNU Science, 241
Bode, M. F. et al. 2006, ApJ, 652, 629
Bode, M. F. et al. 2007, ApJL, 655, L63
Das, R., Banerjee, D. P. K., Ashok N. M. 2006, ApJL, 653, L141
Evans, A. et al. 2007, ApJL, 671, L157
Hjellming, R. M. et al. 1986, ApJL, 305, L71
Lloyd, H. M. et al. 1992, Nature, 356, 222
O'Brien, T. J. et al. 2006, Nature, 442, 279

O'Brien, T. J., Lloyd, H. M., Bode, M. F. 1994, MNRAS, 271, 155
Sokoloski, J. L., Luna, G. J. M., Mukai, K., Kenyon, S. J. 2006, Nature, 442, 276
Starrfield, S. 2008, in Classical Novae, eds Bode M. F. & Evans A., Cambridge University Press
Vaytet, N. M. H., O'Brien, T. J., Bode, M. F., 2007, ApJ, 665, 654

Asymmetric Planetary Nebulae V
A. A. Zijlstra, F. Lykou, E. Lagadec and I. McDonald
Jodrell Bank Centre for Astrophysics, Manchester, UK © 2011

Multiwavelength modeling the SED of stellar explosions

Augustin Skopal

Astronomical Institute, Slovak Academy of Sciences, Tatranská Lomnica

Abstract. In general, the spectrum of exploding objects consists of different components of radiation, whose contributions are a function of the outburst evolution. Extreme conditions that develop during outbursts, can be derived from the spectral energy distribution (SED) throughout a very large range of energies. Here, I illustrate the multiwavelength modeling the X-ray – IR SED of the 'Z And-type' of outbursts, observed in the light curve of the classical symbiotic star AG Dra, and the 'nova-like' outburst produced by the recurrent symbiotic nova RS Oph.
Keywords. Planetary Nebulae

1. Introduction

Stellar explosions represent an important phase of the stellar evolution, during which a significant amount of particles and photons can be injected into the interstellar medium. There are very large number of different types of outbursts, e.g. eruptions of young single stars and those detected in more evolved systems, usually binary or multiple systems. For example, cataclysmic variables can produce classical nova explosions with optical brightening of around 11 mag, while symbiotic stars produce the so-called 'Z And-type' of outbursts, characterized with a 1-3 mag increase of the optical light.

During the outburst event the liberated radiative energy can be transferred throughout the outer layer of material, and thus being converted to lower energies, and/or can ionize directly the circumstellar material, which can re-process it via the recombination and bremsstrahlung acts. Also a conversion of the kinetic energy of particles to radiation due to shocks can be important mainly at the beginning of explosion, having pronounced signatures at the hard X-ray domain. On the other hand, the post-outburst circumstellar material can condense in dust particles, be warmed by the remnant radiation from the exploded object, and thus can re-process it effectively into significantly longer wavelengths. As a result, the observed spectrum will be composed of different components of radiation, whose contributions evolve in time and depend of the type of outburst. Their extraction from the composite spectrum, observed at a given stage of the outburst evolution, can aid us to understand better the nature of outbursts and physical processes giving rise the observed result.

In this contribution I will introduce modeling the X-ray–IR SED for two different types of outbursts. The first one is that of the Z And-type, observed in the light curve of the classical symbiotic star AG Dra, and the second one is the nova-like outburst produced by the recurrent symbiotic nova RS Oph. Both types of outbursts are produced

by the white dwarf (WD) accretor in a symbiotic binary system. The former results most probably from a transient increase in the accretion rate due to an accretion disk instability, while the latter is produced by a thermonuclear runaway, when the pressure at the base of the long-term accreted envelope exceeds a critical value. To point the evolution in the multi-band SED I will present two models for each object corresponding to different levels of their optical brightness.

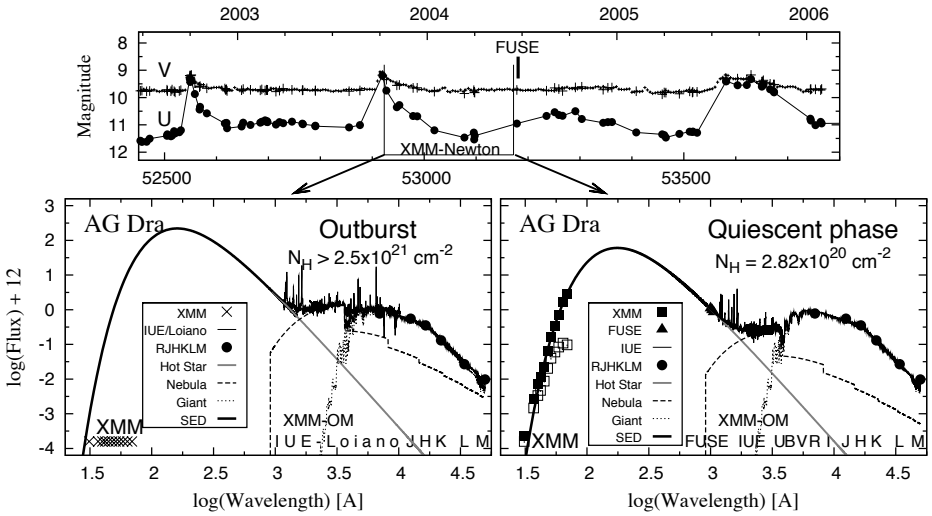

Figure 1. Top: The 'Z And-type' of outbursts in the light curve of AG Dra. The panel shows a detail around the 2003 burst with timing of the *XMM-Newton* (long thin lines) and the *FUSE* (short thick bars) observations. Bottom: Spectral energy distribution during the burst (left) and quiescent phase (right). Open/filled squares are the observed/corrected X-ray fluxes. They are in units of erg cm^{-2} s^{-1} Å^{-1}.

2. Disentangling the composite spectrum

According to the nature of the objects, which outbursts are the subject to our studying, I will assume that their composite spectrum within the supersoft X-ray to infrared region, $F(\lambda)$, can be compared with the radiation from a hot stellar source, $F_{\rm H}(\lambda)$, and that from the irradiated circumstellar matter, $F_{\rm N}(\lambda)$, which is of nebular nature. Because of the presence of a cool giant in these systems, its radiation has also to be included. As a result, their observed spectrum at any stage of their evolution can be expressed as

$$F(\lambda) = F_{\rm H}(\lambda) + F_{\rm N}(\lambda) + F_{\rm G}(\lambda). \quad (1)$$

For the sake of simplicity, I approximate fluxes from the hot stellar source with a blackbody radiation that is attenuated by bound-free absorptions in the X-ray domain (e.g. 1097) and by scattering on the dust grains from the far-UV spectrum to longer wavelengths. To correct the observed X-ray fluxes for absorptions I used the *tbabs* absorption model for ISM composition with abundances given by (1103). To approximate the nebular continuum, it is quite satisfactory to assume that the nebular emission is generated by processes of recombination and thermal bremsstrahlung in the hydrogen plasma, which radiates under conditions of the Case *B*. The stellar radiation from the giant can be estimated by using the optical and near-IR photometric fluxes from quiescent phase. Then a synthetic spectrum, which matches best the photometric fluxes, defines the giant's effective temperature.

Having defined the model SED (Eq. (1)), the measured fluxes, covering the X-ray–IR range, are used to calculate a grid of models. The best model, i.e. the set of fitting parameters given by 2 temperatures, effective radius of the stellar source, emission measure of the nebula and the absorption of the X-ray photons parametrized by the neutral hydrogen column density $N_{\rm H}$, is selected from the grid with the aid of a standard χ^2 function (see 1102, for details).

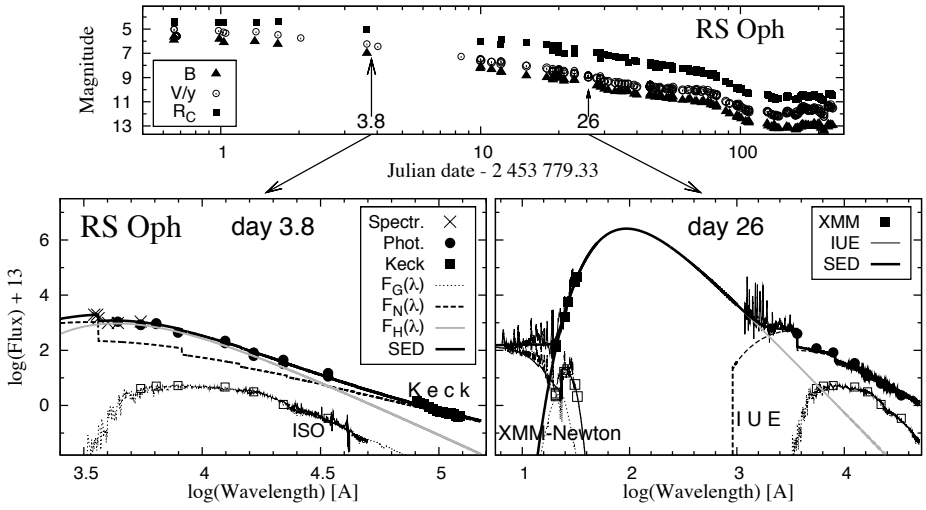

Figure 2. Top: The $BVR_{\rm C}$ light curves of the recurrent symbiotic nova RS Oph covering its recent 'nova-like' explosion, which occurred on 2006 February 12.83. Bottom: Spectral energy distribution as measured at the beginning of the outburst, on day 3.8 (left), and on day 26, when the soft X-rays from the white dwarf penetrated the *CSM* to the observer for the first time from the blast.

3. Z And-type of outbursts

This type of outbursts is observed in light curves of all active symbiotic stars. It is characterized with a 1-3 mag brightening in the optical, accession to the maximum lasting from days to a few months and the return to quiescence on around one order of magnitude longer time-scale. Multiple maxima are often observed. For the purpose of this contribution I selected the case of AG Dra, because this symbiotics produces a strong X-ray emission, which amount varies with the star's brightness. During outbursts it disappears entirely (1100). AG Dra is a yellow S-type symbiotic binary comprising a K2 III giant and a WD on a 549-day orbit (1099).

Results of the modeling the supersoft X-ray to near-IR SED of AG Dra during the maximum of its 2003 burst and the following quiescence are depicted in Fig. 1. The model shows that the optical bursts are associated to an increase in the nebular component of radiation and disappearance of the supersoft X-rays. The effect is caused by the enhanced wind from the hot star, whose particles give rise to the optical bursts by reprocessing high-energy photons from the Lyman continuum to the optical/UV. This process also explains the anti-correlation between the supersoft X-ray and optical/UV fluxes (1102, and references therein).

4. Nova-like outbursts

RS Oph is a recurrent symbiotic nova. Its nova-like outbursts are characterized with the optical brightening by about 7 mag and the recurrence period of about 20 years. The binary comprises a K7 III giant and a WD on a 456-day orbit (e.g. 1099). The WD's mass is very close to the Chandrasekhar limit (e.g. 1096).

Here I modeled the SED of the RS Oph spectrum at the beginning of its 2006 explosion, on day 3.8, and on day 26, when the soft X-ray radiation from the burning WD was detected for the first time (1101). At day 3.8, RS Oph was measured at the Keck Observatory at the N band, from 8 to 12.5 μm (1095). These data were complemented with photometric fluxes from (1098) and (1094), and a low resolution spectrum obtained on day 4 (1093). The model SED revealed the presence of a cool, $T_{\rm h} = 6700 \pm 200$ K, pseudophotosphere with the effective radius, $R_{\rm h}^{\rm eff} = 163 \pm 14\,R_{\odot}$, and a strong H I/He II nebular continuum radiation corresponding to the emission measure of $1.3 \pm 0.2 \times 10^{62}$cm^{-3}. The observed large amount of the nebular emission excludes a spherically symmetric expansion of the WD pseudophotosphere, because its low-temperature radiation is not capable of producing the required flux of the ionizing photons. At day 26, the *XMM-Newton* spectrum from day 26.20 (Hanke, private communication) was complemented with the *IUE* spectra from day 26.0 of the 1985 outburst, and the multicolour photometry from the literature as for day 3.8. The best model SED of the X-ray – IR observed fluxes corresponded to $N_{\rm H} = 7.4 \pm 0.5 \times 10^{21}$ cm^{-2}, $T_{\rm h} = 310 \pm 10$ kK and $R_{\rm h}^{\rm eff} = 0.6 \pm 0.04\,R_{\odot}$. At both days, large quantities of fundamental parameters required highly super-Eddington luminosity for the exploding WD for the distance to RS Oph of 1.6 kpc.

Acknowledgments. This work was supported by the Slovak Academy of Sciences grant VEGA No. 2/0038/10.

References

Anupama, G. C. 2008, in ASP Conf. Ser. 401, RS Ophiuchi (2006) and the Recurrent Nova Phenomenon, ed. A. Evans, M. F. Bode, T. J. O'Brien, & M. J. Darnley (San Francisco, CA: ASP), 251
Banerjee, D. P. K., Das, R. K., & Ashok, N. M. 2009, MNRAS, 399, 357
Barry, R. K., W. C. Danchi, W. A. Traub, et al. 2008, ApJ, 677, 1253
Bode, M. F. 1987, in RS Ophiuchi (1985) and the Recurrent Nova Phenomenon, ed. M. F. Bode (Utrecht: VNU Science Press), 241
Cruddace, R., Paresce, F., Bowyer, S., & Lampton, M. 1974, ApJ, 187, 497
Evans, A., et al. 1988, MNRAS, 234, 755
Fekel, F. C., Hinkle, K. H., Joyce, R. R., & Skrutskie, M. 2000, AJ, 120, 3255
Greiner, J. et al. 1997, A&A, 322, 576
Ness, J.-U., et al. 2009, AJ, 137, 3414
Skopal, A., Sekeráš, M., Gonzíez-Riestra, R., & Viotti, R. F. 2009, A&A, 507, 1531
Wilms, J., Allen, A., & McCray, R. 2000, ApJ, 542, 914

Asymmetric Planetary Nebulae V
A. A. Zijlstra, F. Lykou, E. Lagadec and I. McDonald
Jodrell Bank Centre for Astrophysics, Manchester, UK © *2011*

Prediction of close binarity based on planetary nebula morphology

B. Miszalski[1], R.L.M. Corradi[2,3], D. Jones[4], M. Santander-García[5,2,3], P. Rodríguez-Gil[5,2,3] and M. M. Rubio-Díez[5,6]

[1]*Centre for Astrophysics Research, STRI, University of Hertfordshire, College Lane Campus, Hatfield AL10 9AB, UK*

[2]*Instituto de Astrofísica de Canarias, E-38200 La Laguna, Tenerife, Spain*

[3]*Departamento de Astrofísica, Universidad de La Laguna, E-38205 La Laguna, Tenerife, Spain*

[4]*Jodrell Bank Centre for Astrophysics, School of Physics and Astronomy, University of Manchester, M13 9PL, UK*

[5]*Isaac Newton Group of Telescopes, Apart. de Correos 321, 38700 Santa Cruz de la Palma, Spain*

[6]*Centro de Astrobiologia, CSIC-INTA, Ctra de Torrejón a Ajalvir km 4, E-28850 Torrejón de Ardoz, Spain*

Abstract. A thorough search of the OGLE-III microlensing project has more than doubled the total sample of PNe known to have close binary central stars. These discoveries have enabled close binary induced morphological trends to be revealed for the first time. Canonical bipolar nebulae, low-ionisation structures and polar outflows are all identified within the sample and are provisionally associated with binarity. We have embarked upon a large photometric monitoring program using the Flemish Mercator telescope to simultaneously test the predictive power of these morphological features and to find more close binaries. Early results are very positive with at least five binaries found so far. This suggests our method is an effective means to expedite the construction of a statistically significant sample of close binary shaped nebulae. Such an authoritative sample will be essential to quantify the degree to which close binary nuclei may shape PNe.
Keywords. Planetary Nebulae – Binaries

1. Introduction

The pioneering work of H.E. Bond and collaborators (Bond 2000) clearly established the existence of close binary central stars of planetary nebulae (CSPN). These binaries evolved through a common-envelope (CE) phase (Iben & Livio 1993) to typically consist of a low-mass, main-sequence companion that orbits around a hot pre-white dwarf in less than ∼1 day. Termination of the CE phase is marked by the ejection of the CE to form a short-lived PN ($t \sim 10^4$ years). The presence of a nebula therefore guarantees a post-CE binary is 'fresh out of the oven' and ready for use as an ideal probe of the poorly understood post-CE period distribution (e.g. Miszalski et al. 2009a). Furthermore, the same sample is uniquely placed to scrutinise theoretical predictions that the

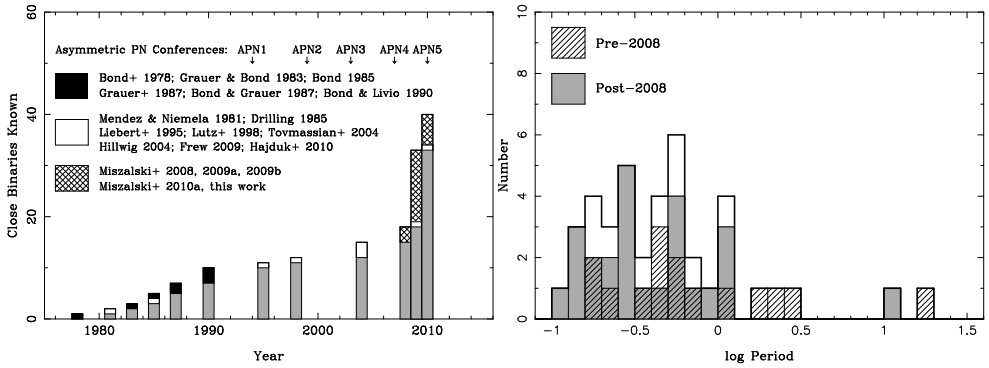

Figure 1. Discovery timeline of the 40 close binary CSPN known (left) and their orbital period distribution (right). We have added objects in Tab. 1 and excluded four objects that require further study: PHR 1744−3355, PHR 1801−2718, PHR 1804−2645 and PHR 1804−2913 (Miszalski et al. 2009a, 2009b).

CE phase produces a density contrast responsible for shaping bipolar nebulae (Bond & Livio 1990; Miszalski et al. 2009b).

The discovery of many new close binary CSPN is *fundamental* to develop the full potential of these powerful probes of CE evolution. A meagre 15 close binary CSPN were known before 2008 (Fig. 1) leaving their period distribution and the Bond (2000) 10–15% binary fraction rather uncertain (De Marco et al. 2008). Morphological trends amongst the sample were also somewhat inconclusive with a surprising lack of bipolar morphologies except for NGC 2346 (Bond & Livio 1990). The paucity of close binaries may be explained by limitations in the discovery technique used to find them as well as a general lack of attention to multi-epoch central star studies in the PN literature (the nebula is the focus of most studies). All of these binaries were discovered by observing periodic photometric variability caused by irradiation effects, ellipsoidal variation or eclipses. The method is straightforward in the absence of bright nebulae and is the only reliable way to find close binaries. Disadvantages include insensitivity to wider binaries (De Marco et al. 2008) and the sometimes slow survey progress due to the quite varied orbital period range of hours to days.

2. Advances from the OGLE-III Microlensing Survey

Microlensing surveys are a revolutionary new means to find close binary CSPN. Their extensive time-series photometry and large areal coverage circumvent most limitations of previous searches for close binaries. Of the 15 known binaries only Hf 2-2 was discovered in this way (Lutz et al. 1998). Miszalski et al. (2008b, 2009a) conducted the first detailed study of PNe in any microlensing survey by investigating ~300 Galactic Bulge PNe in OGLE-III (Udalski et al. 2002). Beneficial to this work was the inclusion of faint MASH and MASH-II PNe well-matched to the OGLE-III survey depth (Parker et al. 2006; Miszalski et al 2008a). An unprecedented haul of 21 new periodic variables were found which gave a close binary fraction of 17±5%. Another major result is the *independent* finding that post-CE population synthesis models overpredict

the observed period distribution in agreement with other studies (Rebassa-Mansergas et al. 2008; Davis et al. 2010). The vast majority of these new variables have since been spectroscopically confirmed as CSPN (Miszalski et al. 2009b).

With the enlarged sample came the opportunity to revisit the previously ambiguous observed morphologies of post-CE PNe. The previous lack of canonical bipolars was altered by the discovery of the first close binary with $P < 1$ day in the canonical bipolar PN M 2-19 (Miszalski et al. 2008b). An implication of this discovery is that the CE phase need not necessarily be avoided to produce a bipolar PN as had been suggested for NGC 2346 (Soker 1997, 1998). With improved images for 30 post-CE PNe Miszalski et al. (2009b) found ~30% of nebulae had canonical bipolar morphologies. If inclination effects are considered, then this may be as high as 60–70%, suggesting that CE evolution has a strong preference for producing bipolar nebulae. In addition to the underlying bipolar shape, Miszalski et al. (2009b) recognised the elevated presence of poorly understood low-ionisation structures (LIS, Gonçalves et al. 2001) in ~30% of the sample and suggested they have a binary origin. Figure 2 portrays the two main types of LIS: (i) a ring or partial ring of knots or filaments (presumably in the orbital plane), and (ii) the shocked tips of polar outflows or jets (presumably collimated and ejected by the binary e.g. Nordhaus & Blackman 2006).

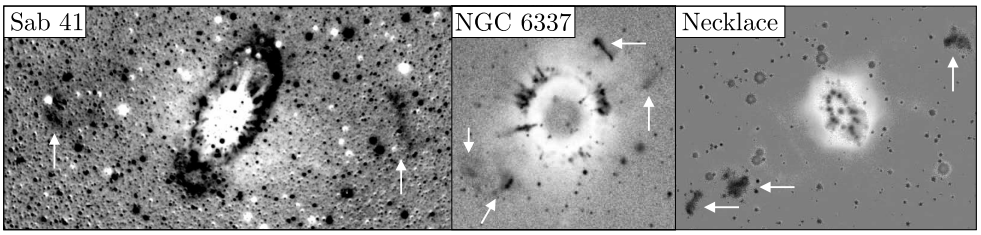

Figure 2. Sab 41, NGC 6337 and the Necklace all share rings of low-ionisation filaments and presumably polar outflows (arrowed). These features are most evident in [NII] emission (black) against the main nebula bodies in [OIII] (white).

The real test for the trends identified by Miszalski et al. (2009b) comes with additional observations. The high bipolar fraction is supported by López et al. (2010) who find the general kinematic signature of a torus in many post-CE PNe. Even though the sample size of post-CE PNe is still very small, we have since made further discoveries that strengthen the trends identified by Miszalski et al. (2009b). Here we describe our work to specifically target PNe befitting these trends for photometric monitoring. In other words, *we are exploring whether we can predict the presence of a close binary based on the nebula morphology alone*. If confirmed this method offers a way to simultaneously (a) test the morphological trends of Miszalski et al. (2009b), and (b) fast-track the discovery of more close binary CSPN!

3. Prediction of close binarity: The case for a morphologically biased survey

With the close binary fraction of 17±5% now well established by the *morphologically unbiased* survey of Miszalski et al. (2009a), it would be counterproductive to repeat this work. Only radically different surveys that target morphologically peculiar sub-samples

have the potential to accelerate the construction of a *statistically significant* sample of close binary CSPN. A significant sample could be drawn from either a volume-limited sample (e.g. 40–50 PNe expected amongst 200 PNe within 2kpc, Frew & Parker 2007) or a much larger magnitude-limited general sample ($\gtrsim$ 200 binaries expected). Building this sample is fundamental to provide the *direct evidence* needed to resolve the debate concerning the shaping of nebula morphologies (Balick & Frank 2002). In the short term the sample may be perceived to be 'biased', but as we already have an unbiased survey in Miszalski et al. (2009a), this is an entirely justified sacrifice to make in order to accumulate enough objects suitable for detailed physical study (e.g. Mitchell et al. 2007; Jones et al. 2010) and to search for other trends (e.g. are nebula or torus dimensions correlated with CE ejection efficiency, mass or orbital period?). As a matter of course non-detections will contribute to an important control sample.

4. Mercator observations

We have applied our survey strategy to Northern PNe accessible from La Palma with the 1.2-m Flemish Mercator telescope. During an 11 night run starting 24 August 2009 we targeted ~20 PNe that fit the trends identified by Miszalski et al. (2009b). Full details of all objects monitored will be published elsewhere pending analysis of additional 2010 data. The results of our survey were overwhelmingly positive with ~70% of targets showing variability of some kind, of which five were found to be periodic proving their binary nature. The basic details of these binaries are given in Tab. 1 and Fig. 3 shows lightcurves of four from 2009. Two of these, the Necklace (Fig. 2) and ETHOS 1, were selected for their impressive jet systems. Hen 2-428 was selected based on its canonical bipolar morphology and suspicions of binarity (Rodríguez et al. 2001), while Te 11 was selected because of its extremely peculiar morphology (Jacoby et al. 2010). A discovery from our 2010 run, NGC 6778, is also mentioned since its underlying bipolar morphology, pair of jets and extensive LIS filaments (Miranda et al. 2010) make it an exemplary supporting case.

Table 1. Recently discovered close binary central stars.

PN G	Name	Period (days)	References
034.5−06.7	NGC 6778	0.15	(1), (2)
049.4+02.4	Hen 2-428	0.18	(1), (3)
054.2−03.4	Necklace	1.16	(1), (4)
068.1+11.0	ETHOS 1	0.53	(1), (5)
203.1−13.4	Te 11	0.12	(1)
221.8−04.2	PHR 0654−1045	0.63	(6)
316.7−05.8	MPA 1508−6455	12.50	(7)
349.3−04.2	Lo 16	0.49	(8)

(1) this work; (2) Miszalski et al. in prep.; (3) Santander-García et al. 2010; (4) Corradi et al. 2010a, 2010b; (5) Miszalski et al. 2010b; (6) Hajduk et al. 2010; (7) Miszalski et al. 2010a; (8) Frew et al. in prep.

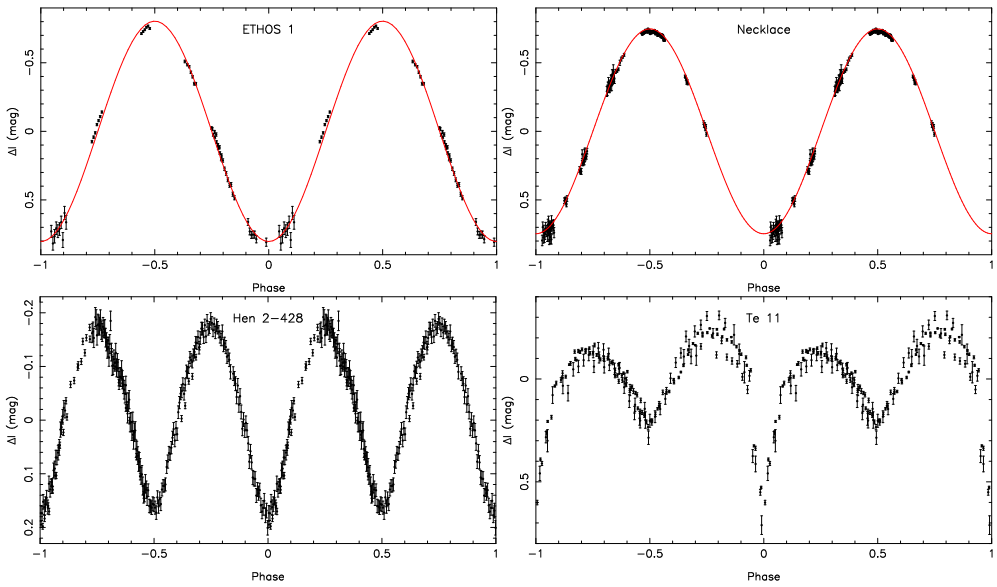

Figure 3. Lightcurves of the 2009 Mercator discoveries. The Necklace and Te 11 lightcurves include some additional photometry from the Isaac Newton Telescope.

The most significant aspect of the Necklace, ETHOS 1 and NGC 6778 is the combination of jets *and* a binary nucleus. These outflows were likely ejected as part of CE interactions that in some cases could be dynamo driven (Nordhaus & Blackman 2006). Emission line ratios of the ETHOS 1 jet tips closely match the FLIERS in NGC 7009 and agree well with predicted ratios of shocks in strongly photoionised environments (Dopita 1997; Raga et al. 2008). Are all FLIERS launched by binaries or could they be produced by other mechanisms? Only with surveys such as ours can we start to answer this longstanding question (Soker & Livio 1994).

Also listed in Tab. 1 are some other pertinent close binary discoveries made recently. PHR 0654−1045 is exceptional since its [WC7] nucleus seems to be the only close binary with a [WR] component (Hajduk et al. 2010). The frequency of close binaries with [WR] components is unknown since the fractions of Hajduk et al. (2010) include very undersampled lightcurves and they did not consider the *indeterminate* binary status of most [WR] sources in OGLE-III as many have very bright nebulae (Miszalski et al. 2009a). We also added MPA 1508−6455 from Miszalski et al. (2008a, 2010a) and Lo 16 whose binary status was announced by D. J. Frew at the MASH workshop (Parker 2010). Together with NGC 6778, Lo 16 fits the pattern of Fig. 2 exceptionally well (Frew & Parker 2007; Frew et al. in prep.).

5. Conclusions

We have begun to test whether the provisional morphological trends identified from a sample of 30 post-CE PNe by Miszalski et al. (2009b) are associated with binarity. These include canonical bipolar nebulae, low-ionisation structures and polar outflows.

Photometric monitoring of a biased sample of Northern Galactic PNe with the Flemish Mercator telescope has found at least 5 new close binary CSPN. New PNe surveys are essential to this effort as 3/5 were only discovered in 2009. All have a bipolar morphology, polar outflows or jet systems appear in 3/5, while 2/5 show low-ionisation filaments. These results are most encouraging and suggest that with further observations we can dramatically increase the known population of post-CE PNe in less time than traditional surveys. Only with a statistically significant sample of post-CE PNe can we begin to assemble the direct evidence needed to resolve the debate surrounding the shaping of PNe (Balick & Frank 2002).

Acknowledgments. BM kindly thanks the SOC for an invited talk. The team wishes to thank Hans Van Winckel for his enthusiastic interest in our project.

References

Balick, B., & Frank, A. 2002, ARA&A, 40, 439
Bond, H. E., Liller, W., & Mannery, E. J. 1978, ApJ, 223, 252
Bond, H. E. 1985, Cataclysmic Variables and Low-Mass X-ray Binaries, 113, 15
Bond, H. E., & Grauer, A. D. 1987, IAUS 95, 221
Bond, H. E., & Livio, M. 1990, ApJ, 355, 568
Bond, H. E. 2000, Asymmetric Planetary Nebulae II, 199, 115
Corradi, R. L. M., et al. 2010a, MNRAS, accepted, arXiv:1009.1043
Corradi, R. L. M., 2011b, *in Asymmetric Planetary Nebulae 5*, Eds. A.A. Zijlstra, F. Lykou, E. Lagadec, I. McDonald, p. 344
Davis, P. J., Kolb, U., & Willems, B. 2010, MNRAS, 403, 179
De Marco, O., Hillwig, T. C., & Smith, A. J. 2008, AJ, 136, 323
De Marco, O. 2009, PASP, 121, 316
Dopita, M. A. 1997, ApJL, 485, L41
Drilling, J. S. 1985, ApJL, 294, L107
Frew, D. J., & Parker, Q. A. 2007, Asymmetric Planetary Nebulae IV
Gonçalves, D. R., Corradi, R. L. M., & Mampaso, A. 2001, ApJ, 547, 302
Grauer, A. D., Bond, H. E., Ciardullo, R., & Fleming, T. A. 1987, BAAS, 19, 643
Hajduk, M., Zijlstra, A. A., & Gesicki, K. 2010, MNRAS, 406, 626
Hillwig, T. C. 2004, Asymmetric Planetary Nebulae III, 313, 529
Iben, I. J., & Livio, M. 1993, PASP, 105, 1373
Jacoby, G. H., et al. 2010, PASA, 27, 156
Jones, D., et al. 2010, MNRAS, accepted, arXiv:1006.5873
Liebert, J., Tweedy, R. W., Napiwotzki, R., & Fulbright, M. S. 1995, ApJ, 441, 424
López, J.A., et al. 2011, *in Asymmetric Planetary Nebulae 5*, Eds. A.A. Zijlstra, F. Lykou, E. Lagadec, I. McDonald, p. 335
Lutz, J., et al. 1998, BAAS, 30, 894
Méndez, R. H., & Niemela, V. S. 1981, ApJ, 250, 240
Miranda, L. F., Ramos-Larios, G., & Guerrero, M. A. 2010, PASA, 27, 180
Miszalski, B., et al. 2008a, MNRAS, 384, 525
Miszalski, B., Acker, A., Moffat, A. F. J., Parker, Q. A., & Udalski, A. 2008b, A&A, 488, L79
Miszalski, B., Acker, A., Moffat, A. F. J., Parker, Q. A., & Udalski, A. 2009a, A&A, 496, 813
Miszalski, B., Acker, A., Parker, Q. A., & Moffat, A. F. J. 2009b, A&A, 505, 249
Miszalski, B., 2011a, *in Asymmetric Planetary Nebulae 5*, Eds. A.A. Zijlstra, F. Lykou, E. Lagadec, I. McDonald, p. A109
Miszalski, B., 2010b, MNRAS, submitted
Mitchell, D. L., et al. 2007, MNRAS, 374, 1404
Nordhaus, J., & Blackman, E. G. 2006, MNRAS, 370, 2004
Parker, Q. A. et al. 2006, MNRAS, 373, 79

Parker, Q. A. 2010, PASA, 27, 125
Raga, A. C., Riera, A., Mellema, G., Esquivel, A., & Velázquez, P. F. 2008, A&A, 489, 1141
Rebassa-Mansergas, A., et al. 2008, MNRAS, 390, 1635
Rodríguez, M., Corradi, R. L. M., & Mampaso, A. 2001, A&A, 377, 1042
Santander-García, M., 2011, *in Asymmetric Planetary Nebulae 5*, Eds. A.A. Zijlstra, F. Lykou, E. Lagadec, I. McDonald, p. 259
Soker, N., & Livio, M. 1994, ApJ, 421, 219
Soker, N. 1997, ApJS, 112, 487
Soker, N. 1998, ApJ, 496, 833
Tovmassian, G. H., et al. 2004, ApJ, 616, 485
Udalski, A. et al. 2002a, Acta Astronomica, 52, 1

Asymmetric Planetary Nebulae V
A. A. Zijlstra, F. Lykou, E. Lagadec and I. McDonald
Jodrell Bank Centre for Astrophysics, Manchester, UK © 2011

The kinematics and morphology of PNe with close binary nuclei

López, J. A.[1], García-Díaz, Ma. T.[1], Richer, M. G[1], Lloyd, M.[2] and Meaburn, J.[2]

[1]*Instituto de Astronomía, Universidad Nacional Autónoma de México, Apdo. Postal 877, Ensenada, Baja California, 22800, México*

[2]*Jodrell Bank Centre for Astrophysics, University of Manchester, Oxford Road, Manchester M 13 9PL, UK*

Abstract. We have obtained images and long-slit, spatially resolved echelle spectra for twenty four planetary nebulae (PNe) that have confirmed close binary nuclei. The sample shows a variety of morphologies, however toroids or dense equatorial density enhancements are identified, both in the imagery and the spectra, as the common structural component. These toroids are thought to be the remnant fingerprints of the post common envelope phase. Based on the characteristics of the present sample we suggest a list of additional PNe that are likely to host close binary nuclei.
Keywords. Planetary nebulae – Binaries

1. Introduction

The presence of fast, collimated, bipolar outflows or jets, and point-symmetric and poly-polar structures in PNe has led for nearly two decades to the suggestion that close binary nuclei should be playing a decisive role in their formation and shaping (e. g. Soker & Livio 1994). Furthermore, evolution paths and population synthesis calculations critically depend on the actual ratio of binary to single core PNe. However, finding these binary systems has proven to be an observational challenge, but after years of dedicated efforts a list of PNe with reasonably confirmed close binary nuclei has been gradually obtained and this has been nicely summarized by De Marco (2009) and references therein. With this group of identified targets available we set out to investigate its detailed morphological and kinematical characteristics.

2. Observations

High-resolution spectroscopic observations and monochromatic images were obtained at the Observatorio Astronómico Nacional at San Pedro Mártir (SPM), Baja California, México and at the Anglo-Australian Observatory. The observations were obtained with the Manchester Echelle Spectrometer (MES-SPM) on the SPM telescope and with UCLES on the AAT for the southernmost targets. In both cases we used a 90 Å bandwidth filter to isolate the 87^{th} order containing the Hα and [N II] $\lambda\lambda$ 6548, 6584 Å,

nebular emission lines. The SPM spectra have a projected slit length of 5′.32 on the sky and those from UCLES approximately one arcmin. In both cases the spectral resolution is $\sim$ 11 km s^{-1}. For the SPM targets we also used MES in its imaging mode to obtain monochromatic images. An additional source of high quality images has been provided by the web based planetary nebulae image catalogue (PNIC) compiled by Bruce Balick (www.astro.washington.edu/users/balick/PNIC/) and its modified version by Brent Miszalski (www.aao.gov.au/local/www/brent/PNIC/).

3. The sample

The twenty four PNe observed in our sample are listed below, grouped by their main large-scale morphology, those marked with an asterisk (*) contain collimated bipolar outflows.

- Ring, Toroid, Cylindrical : NGC 6337*, Hf 2-2, M 3-16, NGC 6026, A 63*, A 46, A 65, Sp 1, SuWt 2, NGC 2438, Ha Tr 4.
- Elliptical with marked equatorial density enhancements: A 41, H 2-29, M 2-19, H 1-33.
- Bipolar: PN G 136, NGC 2346, K 1-2*.
- Irregular, Diffuse, Double Shell, Filamentary Bubble: Ds 1, Lo Tr 5, Lo Tr 1, NGC 1514, HFG 1, A 35.

The first group comprises 46% of the sample, whereas the second group 17%, the third 12% and the fourth 25%. It is clear that this is a mixed sample and prone to the uncertainties of small numbers statistics. Yet this sample seems strongly dominated by rings, toroids, cylindrical shapes and pronounced equatorial density enhancements, somehow in contrast with the expectations for this particular group as described in the introduction. These results agree with those from Frew and Parker (2007) derived from a smaller sample. Long-slit spectra serve as an excellent tool to unveil the presence of collimated outflows and also toroidal or ring-type structures from the additional information provided in the emission line profiles (see Figure 1). The kinematics of these PNe does not show particularly high expansion velocities, they all seem rather standard, with expansion velocities of the order of $V_{exp} = 30 \pm 5$ km s^{-1}. Only three members of this sample are known to host bipolar, collimated outflows, NGC 6337, A 63 and K 1-2, being NGC 6337 the most complex one (García-Díaz et al. 2009). Other examples of this group have been discussed during this meeting, such as Hen 2-428 (Santander-García et al. 2010) and the Necklace nebula, (R. Corradi et al. 2010), both are dominated by toroidal structures at the equator, in the latter a collimated bipolar outflow has also been found.

4. Discussion

From a similar sample, Miszalski et al. (2009) consider that PNe with close binary nuclei show a clear tendency for bipolar shapes once inclination effects are taken into

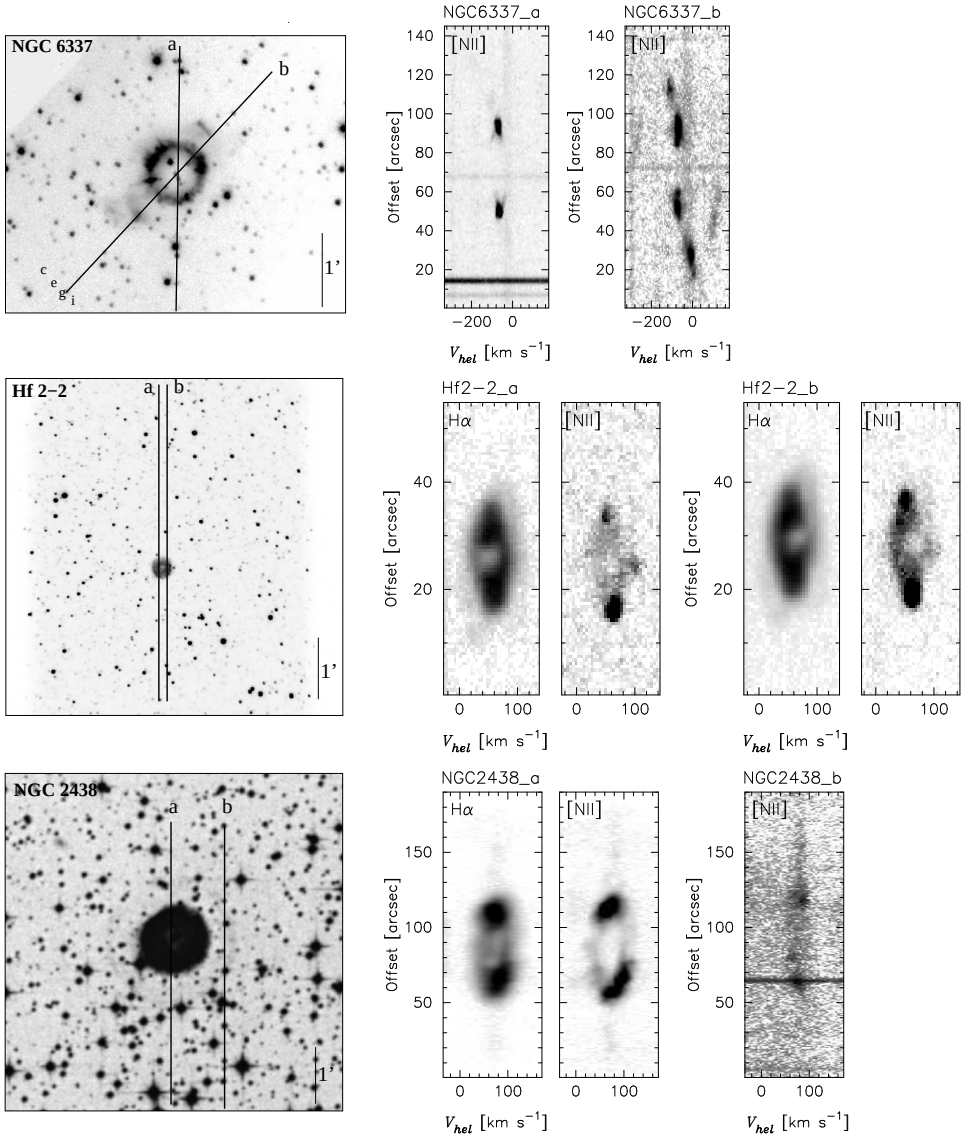

Figure 1. Examples of images and long-slit spectra for three PNe with close binary nuclei. The location of the slits is indicated on the image for each object. NGC 6337 is shown in the top panel. This nebula is dominated by a ring structure which is clearly replicated in the spectra. This object also has a complex collimated outflow. In the middle panel is Hf 2-2 that also shows clearly the toroidal structure in the image and the spectra from both slits. The bottom panel shows NGC 2348 deliberately in an image from the digital sky survey that only shows a filled envelope, this case exemplifies how the ring structure is clearly revealed again in the long-slit spectra.

account. The present sample size does not allow yet to draw firm conclusions on the influence of close binary nuclei on the shaping and evolution of PNe. New members of this group are currently being actively sought with modern techniques and it is anticipated that many more members of this group will be found in the near future. From

the diversity of the members studied in the present sample it can only be expected that more PNe within the categories described above will accumulate until a clearer trend coupled to a better understanding of the binary interaction processes on the shaping mechanisms of the PN can be envisaged.

For the moment, the simplest interpretation to the present results is to assume that PNe with close binary nuclei are post common envelope systems that have predominantly ejected the primary's envelope along the equatorial plane, producing the equatorial density enhancement or toroidal structures observed. Gravitational focusing along the equator from a close low-mass companion can also play an important role, (see e.g. the review by Podsialowski (2007) and Nordhaus, Blackman & Frank (2006)). Once the toroid is formed, at the early stages of PN evolution, the fast isotropic stellar wind is deviated towards the polar regions. Depending on the amount of envelope matter that has been deposited on the equator (i.e. the efficiency of the envelope ejection) the resultant main morphology will appear as toroid-dominated, elliptical with a thick waist or bipolar, with the first two gradually evolving towards the latter as a function of time. It is important to note that under this interpretation the common envelope process is mainly responsible for distributing the isotropic envelope over the equator producing the toroidal structures, not an axisymmetric (e.g. bipolar) nebula *per se*. This large-scale mechanism does not consider the production of fast, bipolar, collimated outflows or point-symmetric and poly-polar structures that must be formed through additional processes, that are also likely related to detailed conditions of the binary nature, its mechanism of interaction and the presence of collimating magnetic fields. Thus for a better evaluation and prediction of the likely effects of binary nuclei on PNe shaping we need a larger sample of confirmed close binary nuclei. Additionally, we need a much better understanding of the detailed outcome of the common envelope process as a function of mass ratio and its dependency on the moment at which this happens during the system's evolution. We also need a better understanding of the shaping effects on the nebula by wider binaries, e.g. Frankowski & Jorissen (2007). For the time being, if the characteristics of the members in the present sample are indeed indicative of the likely presence of close binary nuclei, we suggest to study the following candidates: K 1-9, A 13, Lo 18, SuWt 3, A 47, He 2-70, Hf 4, He 2-163 and Al 1.

Acknowledgments. We gratefully acknowledge the financial support from DGAPA-UNAM through grant IN116908

References

Corradi, R. L. M., Miszalski, B., Santander-García & Rodriguez-Gil, P., 2011, *Asymmetric Planetary Nebulae 5*, Eds. A.A. Zijlstra, F. Lykou, I. MacDonald and E. Lagadec, p. 344

De Marco, O., 2008, PASP 121, 316

Frankowski, A. & Jorissen, A., 2007, Baltic Astronomy, 16, 104

Frew, D. & Parker, Q., 2007, Asymmetric Planetary Nebulae 4, Published online, www.iac.es/proyecto/apn4, Corradi, R.L.M., Manchado, A. & Soker, N. (eds), p. 475

García-Díaz, M. T., Clark, D. M., López, J. A., Steffen, W., & Richer, M. G. 2009, Astrophysical Journal, 699, 1633

Miszalski, B., Acker, A., Parker, Q. & Moffat, A. F. J., 2009, Astronomy and Astrophysics505, 249

Nordhaus, J., Blackman, E. G. & Frank, A., 2007, Monthly Notices of the Royal Astronomical Society376, 599

Podsiadlowski, P., 2007, in Asymmetrical Planetary Nebulae 4, Published online, www.iac.es/proyecto/apn4, Corradi, R.L.M., Manchado, A. & Soker, N.(eds), p. 467
Santander-García, Rodriguez-Gil, P., Corradi, R., Miszalski, B., Jones, D. & Rubio-Dimez, M., 2011, *Asymmetric Planetary Nebulae 5*, Eds. A.A. Zijlstra, F. Lykou, I. MacDonald and E. Lagadec, p. 259
Soker, N. & Livio, M., 1994, Astrophysical Journal, 421, 219

Asymmetric Planetary Nebulae V
A. A. Zijlstra, F. Lykou, E. Lagadec and I. McDonald
Jodrell Bank Centre for Astrophysics, Manchester, UK © *2011*

Abell 41: nebular shaping by a binary central star?

D. Jones[1], M. Lloyd[1], M. Santander-García[2,3,4], J.A. López[5], J. Meaburn[1], D.L. Mitchell[1], T.J. O'Brien[1], D. Pollacco[6], M.M. Rubio-Díez[7,2] and N.M.H. Vaytet[8]

[1]*Jodrell Bank Centre for Astrophysics, University of Manchester, UK*

[2]*Isaac Newton Group of Telescopes, Santa Cruz de La Palma, Spain*

[3]*Instituto de Astrofísica de Canarias, Tenerife, Spain*

[4]*Departamento de Astrofísica, Universidad de La Laguna, Spain*

[5]*Instituto de Astronomía, Universidad Nacional Autónoma de México, México*

[6]*Astrophysics Research Centre, Queen's University Belfast, UK*

[7]*Departamento de Astrofísica, Centro de Astrobiología, CSIC-INTA, Spain*

[8]*Service d'Astrophysique, CEA/DSM/IRFU/SAp, France*

Abstract. We present the first detailed spatio-kinematical analysis and modelling of the planetary nebula Abell 41, which is known to contain the well-studied close-binary system MT Ser. This object represents an important test case in the study of the evolution of planetary nebulae with binary central stars as current evolutionary theories predict that the binary plane should be aligned perpendicular to the symmetry axis of the nebula.

Longslit observations of the [NII]6584 Å emission from Abell 41 were obtained using the Manchester Echelle Spectrometer on the 2.1-m San Pedro Mártir Telescope. These spectra, combined with deep, narrowband imagery acquired using ACAM on the William Herschel Telescope, were used to develop a spatio-kinematical model of [NII]6584 Å emission from Abell 41. The best fitting model reveals Abell 41 to have a waisted, bipolar structure with an expansion velocity of ∼40 km s^{-1} at the waist. The symmetry axis of the model nebula is within 5° of perpendicular to the orbital plane of the central binary system. This provides strong evidence that the close-binary system, MT Ser, has directly affected the shaping of its host nebula, Abell 41.

Keywords. Planetary nebulae – Binaries

1. Introduction

Abell 41 (PN G009.6+10.5, $\alpha = 17^h29^m02.03^s$, $\delta = -15°13'04.4''$ J2000), discovered by (1159), was classified by Bond & Livio (1162) as elliptical under the classification scheme of Balick (1160). However, deeper Hα+[NII]6584 Å imagery reveals "that the

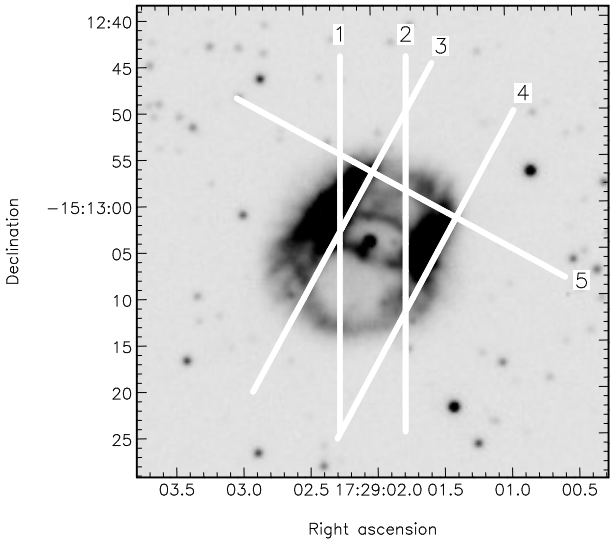

Figure 1. A deep ACAM-WHT image of A 41 in the light of [NII]6584 Å showing the positions of the 5 MES-SPM longslits.

nebular morphology exhibits an 'H' shape with the addition of fainter material forming a continuous loop" (1173).

Photometric analysis of the central star of the planetary nebula (CSPN), MT Ser, revealed it to be a close binary, showing minima at regular intervals of 2^h43^m (1164). Bruch et al. (1163) confirmed the binary nature of MT Ser but were unable to accurately determine its orbital parameters because they found two different models which fit the observed data. (a) The binary consists of a hot sub-dwarf and a less evolved secondary, in which case the period is 2^h43^m and the variations are due to a reflection effect (inclination, $i = 42.52° \pm 1.73°$). (b) The binary consists of two evolved, hot sub-dwarfs with a period of 5^h26^m where the variability results from partial eclipses and ellipsoidal variations ($i = 65.7° \pm 0.9°$). They determined the optimum parameters for each model, but concluded that only radial velocity observations would be able to distinguish between the two. Subsequent observation and modelling by Shimanskii et al. (1174) confirmed the presence of two sub-dwarf components, but gave no independent confirmation of the orbital inclination. Only the second model of Bruch et al. (2001, $i = 65.7° \pm 0.9°$) is consistent with photometric observations and the detection of two hot sub-dwarf central stars, indicating that this is the most reliable model of the CSPN.

In these proceedings we present a spatio-kinematic model, derived from longslit spectroscopy and narrowband imaging, with the aim of understanding the relationship between the nebula and MT Ser. A more complete discussion of this work can be found in (1168).

2. Spatio-kinematic modelling

Spatially-resolved, high spectral-resolution echelle spectroscopy of the [NII]6584 Å line acquired using the Manchester Echelle Spectrograph on the 2.1-m San Pedro Mártir

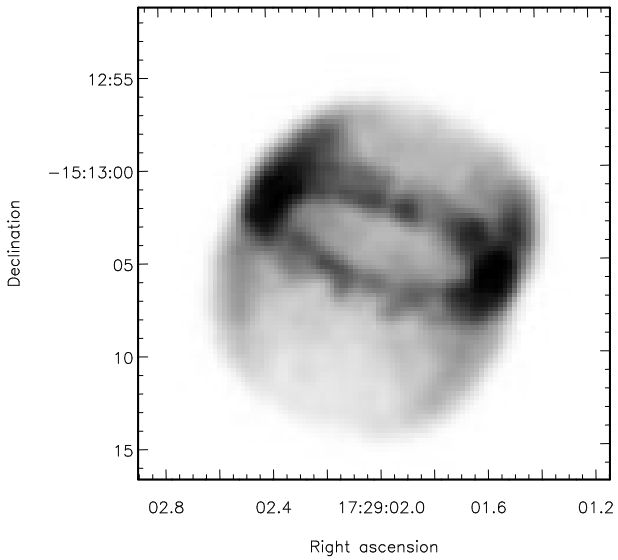

Figure 2. The synthetic SHAPE model for the [NII]6584 Å emission from A 41.

telescope (MES-SPM, Figure 1), in combination with deep narrowband imagery obtained using ACAM on the 4.2-m William Herschel Telescope (WHT-ACAM), have been used to develop a spatio-kinematic model of A 41. The modelling was performed using SHAPE (1175). Further details of the observations and modelling process are found in Jones et al. (1168).

This best fit model comprises a bipolar shell waisted by an equatorial ring with an expansion velocity of ∼40 km s^{-1}. The model nebula is slightly asymmetric in that the northern lobe is shortened by 15%, has a narrower opening angle and has a slight shear with respect to its southern counterpart. No symmetric model could be found which reproduced the observed PV arrays. The nebular inclination angle, as defined by the un-sheared southern lobe, is determined to be 66° ± 5°, in excellent agreement with the inclination of the CSPN (see section 1). The model nebula is shown at the observed orientation in Figure 2. The synthetic position-velocity arrays can be found, along with their observed counterparts, in Jones et al. (1168).

2.1. Systemic velocity and kinematical age

Comparison of synthetic model spectra to their observed counterparts provides an unambiguous measure of the nebular systemic heliocentric radial velocity (V_{sys}), unaffected, for example, by brightness variations or nebular asymmetry (1167). Using our best-fit model, V_{sys} is determined to be 30 ± 5 km s^{-1} in good agreement with the value of 30 km s^{-1} determined by Beaulieu et al. (1161).

The nebular expansion velocity, determined by the kinematical modelling, can be used to calculate a kinematical age for the nebula. This, however, requires the distance to the nebula to be known. The distance to A 41 is a matter of some debate with values in the literature ranging from ∼1 kpc (1164) up to 9.0 ± 0.4 kpc (1174), this probably results from the notorious variation in results from different methods of distance deter-

mination (see e.g., 1165). Therefore, rather than favour one particular distance estimate over another we quote a kinematical age per kiloparsec of ~ 800 years kpc^{-1}.

3. Conclusions

Using high-resolution longslit spectroscopy and deep imaging, a spatio-kinematical model of A 41 has been developed which clearly shows that the nebula is aligned with the binary central system exactly as predicted by current theories of PN shaping by binary CSPN. This is only the second nebula to have this link observationally constrained (after A 63, 1172). The kinematical data confirm A 41 exhibits a waisted, bipolar structure, with some small deviations from perfect axisymmetry. The presence of an equatorial ring is also confirmed, adding further weight to the link between ring structures and central binary stars as commented on by Miszalski et al. (2009, 2010) and López et al. (1169).

Further kinematical investigations, such as this and others presented in these proceedings (e.g. 1166, 1176), coupled with in-depth studies of the CSPN of other PNe with confirmed close-binary CSPN, are necessary to investigate the full extent of the influence of central star binarity on PN nebular shaping. Only once a significant statistical sample has been acquired can generalisations be made about the role of CSPN binarity in PN evolution.

References

Abell, G. O., & Goldreich, P. 1966, PASP, 78, 232
Balick, B. 1987, AJ, 94, 671
Beaulieu, S. F., Dopita, M. A., & Freeman, K. C. 1999, ApJ, 515, 610
Bond, H. E., & Livio, M. 1990, ApJ, 355, 568
Bruch, A., Vaz, L. P. R., & Diaz, M. P. 2001, A&A, 377, 898
Grauer, A. D., & Bond, H. E. 1983, ApJ, 271, 259
Gurzadyan, G. A. 1997, The Physics and Dynamics of Planetary Nebulae (Berlin: Springer-Verlag)
Huckvale, L., Prouse, B., Jones, D., Lloyd, M., & Pollacco, D. L. 2010, in Asymmetric Planetary Nebulae 5: The Shaping of Stellar Ejecta, edited by A.A. Zijlstra, I. McDonald and E. Lagadec (Palo Alto, California, USA: Ebrary)
Jones, D., Lloyd, M., Mitchell, D. L., Pollacco, D. L., O'Brien, T. J., & Vaytet, N. M. H. 2010, MNRAS, 401, 405
Jones, D., Lloyd, M., Santander-García, M., López, J. A., Meaburn, J., Mitchell, D. L., O'Brien, T. J., Pollacco, D., Rubio-Díez, M. M., & Vaytet, N. M. H. 2010, MNRAS, 1353
López, J. A., García-Díaz, M. T., Richer, M., Lloyd, M., & Meaburn, J. 2010, in Asymmetric Planetary Nebulae 5, edited by A.A. Zijlstra, F. Lykou, E. Lagadec and I. McDonald (Palo Alto CA, USA: Ebrary), 337
Miszalski, B., Acker, A., Parker, Q. A., & Moffat, A. F. J. 2009, A&A, 505, 249
Miszalski, B., Corradi, R. L. M., Jones, D., Santander-García, M., Rodríguez-Gil, P., & Rubio-Díez, M. M. 2010, in Asymmetric Planetary Nebulae 5, edited by A.A. Zijlstra, F. Lykou, I. McDonald and E. Lagadec (Palo Alto CA, USA: Ebrary), 330. 1009.2890
Mitchell, D. L., Pollacco, D., O'Brien, T. J., Bryce, M., López, J. A., Meaburn, J., & Vaytet, N. M. H. 2007, MNRAS, 374, 1404
Pollacco, D. L., & Bell, S. A. 1997, MNRAS, 284, 32
Shimanskii, V. V., Borisov, N. V., Sakhibullin, N. A., & Sheveleva, D. V. 2008, Astronomy Reports, 52, 479

Steffen, W., & López, J. A. 2006, RMxAA, 42, 99
Tyndall, A., Jones, D., Lloyd, M., O'Brien, T. J., Pollacco, D. L., & Mitchell, D. L. 2010, in *Asymmetric Planetary Nebulae 5*, edited by A.A. Zijlstra, F. Lykou, I. McDonald and E. Lagadec (Palo Alto CA, USA: Ebrary), A115

Asymmetric Planetary Nebulae V
A. A. Zijlstra, F. Lykou, E. Lagadec and I. McDonald
Jodrell Bank Centre for Astrophysics, Manchester, UK © 2011

The Necklace planetary nebula: equatorial and polar outflows from a post-common-envelope system

R.L.M. Corradi[1,2], L. Sabin[3], B. Miszalski[4], P. Rodríguez–Gil[5,1,2], M. Santander–García[5,1,2], D. Jones[6], J.E. Drew[4], A. Mampaso[1,2], M.J. Barlow[7], M.M. Rubio–Díez[5,8], J. Casares[1,2], K. Viironen[9,10], D.J. Frew[11], C. Giammanco[1,2], R. Greimel[12], S.E. Sale[13,14]

[1]*Instituto de Astrofísica de Canarias, E-38200 La Laguna, Tenerife, Spain*

[2]*Departamento de Astrofísica, Universidad de La Laguna, E-38206 La Laguna, Tenerife, Spain*

[3]*Instituto de Astronomía, Universidad Nacional Autónoma de México, Apdo. Postal 877, 22800 Ensenada, B.C, Mexico*

[4]*Centre for Astrophysics Research, STRI, University of Hertfordshire, College Lane Campus, Hatfield AL10 9AB, UK*

[5]*Isaac Newton Group of Telescopes, Apart. de Correos 321, 38700 Santa Cruz de la Palma, Spain*

[6]*Jodrell Bank Centre for Astrophysics, School of Physics and Astronomy, University of Manchester, M13 9PL, UK*

[7]*Department of Physics and Astronomy, University College London, Gower Street, London WC1E 6BT, UK*

[8]*Centro de Astrobiología, CSIC-INTA, Ctra de Torrejón a Ajalvir km 4, E-28850 Torrejón de Ardoz, Spain*

[9]*Centro Astronómico Hispano Alemán, Calar Alto, C/Jesús Durbán Remón 2-2, E-04004 Almeria, Spain*

[10]*Centro de Estudios de Física del Cosmos de Aragón (CEFCA), C/General Pizarro 1-1, E-44001 Teruel, Spain*

[11]*Department of Physics and Astronomy, Macquarie University, North Ryde, NSW 2109, Australia*

[12]*Institut für Physik, Karl-Franzen Universität Graz, Universitätsplatz 5, 8010 Graz, Austria*

[13]*Dept. de Física y Astronomía, Universidad de Valparaíso, Ave. Gran Bretaña 1111, Playa Ancha, Casilla 53,Valparaíso, Chile*

[14]*Dept. de Astronomía y Astrofísica, Pontificia Universidad Católica de Chile, Av. Vicuña Mackenna 4860, Casilla 306, Santiago 22, Chile*

Abstract. We present the discovery of a new planetary nebula from the IPHAS survey. The remarkable morphology of its inner regions, which display a bright knotty ring surrounded by high excitation gas, led to the object's nickname, the "Necklace nebula". The finding of a binary central star with an orbital period of 1.16 days makes it a new clear example of strongly aspherical mass deposition - both in the form of a slow equatorial outflow and fast polar ejections - resulting from the common-envelope phase.

Keywords. Planetary nebulae – Binaries

1. IPHAS and planetary nebulae

A large number of new planetary nebulae (PNe) are being discovered by the Hα CCD imaging survey of the Northern Galactic Plane (IPHAS, Drew et al. 2005). The IPHAS candidate PNe are selected among other ionized nebulae mainly according to their morphologies and lack of a clear association with star forming regions. As expected, the new IPHAS PNe are generally low surface brightness nebulosities that escaped detection in previous explorations of the Milky Way. This is why one is happily surprised (and often irresistibly captivated) when relatively bright nebulae are found. Examples are the so-called "Princípes de Asturias" PN (IPHASXJ012507.9+635652, Mampaso et al. 2006) and the "Necklace" nebula (IPHASXJ194359.5+170901). Both are bright enough to be easily seen in the sky maps of Google Earth (produced from the DSS plates) with distinctive orange and blue colours, respectively.

The Necklace nebula was found on the IPHAS plates by one of us (LS) in 2006: fascinated by its morphology, we collected over the following years new data aimed at investigating its nature and properties. We present in the following a summary of its most remarkable characteristics, referring the reader to the article by Corradi et al. (2010) for further details.

An image of the Necklace nebula is presented in Fig. 1. The nebula consists of a bright, high-excitation inner body, inside which a well-defined ellipse of knots is located. This ring is most visible in low-ionization [N II] light. Faint lobes extend in the perpendicular directions and culminate in low-ionization caps. Study of the kinematics of the nebula demonstrates that the knotty ellipse ("the necklace") is indeed a circular ring inclined at ∼59 degrees to the plane of the sky, and expanding at a speed of 28 km s^{-1}. The polar caps recede from the central source at a speed of around 100 km s^{-1}. The main nebula is of very high excitation (He II4686 is stronger than Hβ), most of its oxygen being in ionization stages higher than O^{2+}. Abundances are standard for PNe.

2. The binary central star of the Necklace nebula

The morphological characteristics of the Necklace nebula, and in particular the high velocity polar caps and the inner ring, made it a prime target in our morphology-based search for binary central stars of PNe (see Miszalski et al. 2010 and Santander–García et

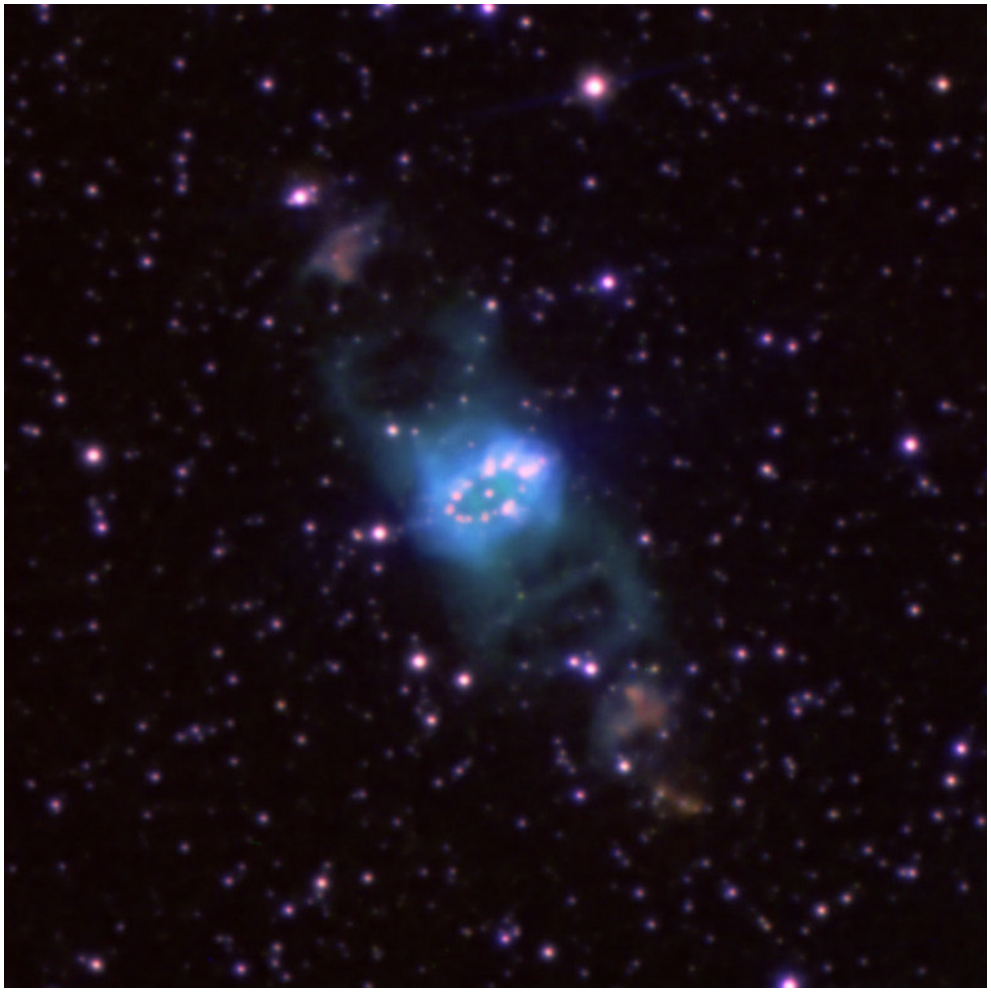

Figure 1. Image of the Necklace nebula from the 2.6m Nordic Optical Telescope (courtesy of Daniel Lopez, IAC). The field of view is 150x150 arcsec^2. North is up and East left. The blue colour is a combination of Hα and [O III]5007 images, the red colour is [N II]6583.

al. 2010). It was then included in our photometric monitoring program at the 1.2m Mercator and other telescopes in the Canary Islands. The *i*-band lightcurve, presented in Fig. 2, shows a clear and ample sinusoidal modulation over a 1.16 days cycle, that we ascribe to strong irradiation by the hot PN core of the facing side of a cool nearby companion. This is confirmed by the spectrum of the central star, which displays typical irradiation features such as narrow C III, C IV, and N III emission lines, as well as broader lines from a flat H I Balmer sequence in emission, over a warm (6000-7000 K) continuum.

Thus, the Necklace nebula is another clear demonstration of the ability of post-common-envelope (CE) binaries to produce highly aspherical nebular geometries. In this case, most of the mass is lost in an equatorial (the orbital?) plane, but fast gas ejections in the polar directions are also produced. It is plausible that the equatorial

outflow forming the ring of knots is the result of the envelope ejection at the end of the short CE phase, while the polar caps are collimated mass loss from an accretion disc around the secondary star prior to the CE phase, but other interpretations are possible (see Corradi et al. 2010). In any case, the well-defined geometry and kinematics of the Necklace nebula make it an excellent target for detailed study of the relationship between central star binarity and PN shaping, one of the main topics of this series of conferences.

Our first next step will be to determine more orbital parameters by means of a radial velocity study of the stellar components. As high-resolution spectroscopy of such faint stars require 8m class telescopes, international collaborations as proposed during the group sessions in the last two days of APN5 might help a lot to accomplish the goal. Thanks to all the organizers, and especially to Orsola De Marco and Bruce Balick, for promoting such a nice experience that we hope will be repeated in the next APN conferences.

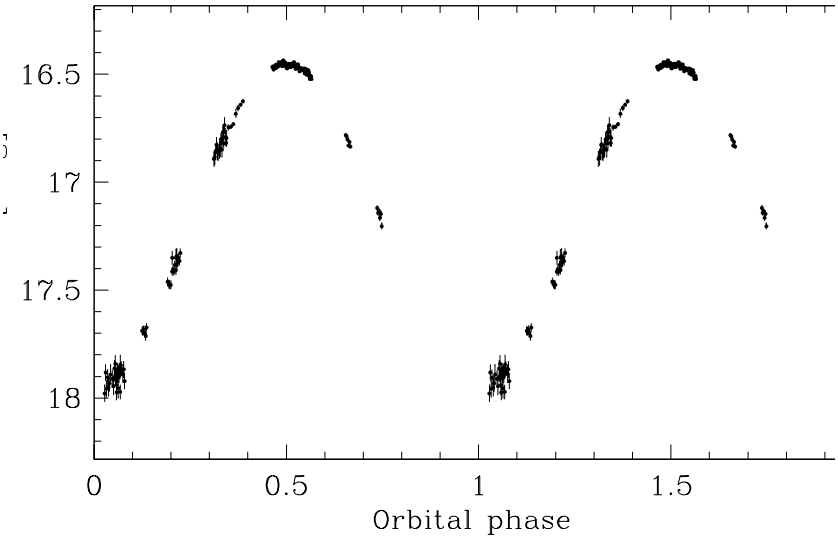

Figure 2. SDSS *i*-band light curve of the Necklace nebula, folded on the computed orbital period of 1.16 days. Figure adapted from Corradi et al. (2010)

Acknowledgments. The work of RLMC, LS, MSG, AMR, and KV has been supported by the Spanish Ministry of Science and Innovation (MICINN) under the grant AYA2007-66804.

References

Corradi, R.L.M., Sabin, L., Miszalski, B., et al. 2010, MNRAS, arXiv:1009.1043
Drew, J., Greimel, R., Irwin, M.J., et al. 2005, MNRAS, 362, 753
Mampaso, A., Corradi, R.L.M.,Viironen, K. et al. 2006, A&A 458, 203
Miszalski, B., et al., *in Asymmetric Planetary Nebulae 5* (2010), A. A. Zijlstra, F. Lykou, E. Lagadec and I. McDonald (eds.), published by Ebrary (Palo Alto CA, USA), p. 330
Santander García, M., et al., *in Asymmetric Planetary Nebulae 5* (2010), A. A. Zijlstra, F. Lykou, E. Lagadec and I. McDonald (eds.), published by Ebrary (Palo Alto CA, USA), p. 260

Asymmetric Planetary Nebulae V
A. A. Zijlstra, F. Lykou, E. Lagadec and I. McDonald
Jodrell Bank Centre for Astrophysics, Manchester, UK © 2011

Watching PrePNe Evolve: 15 Years of HST Observations

Bruce Balick[1], Thomas Gomez[1], Adam Frank[2], Romano Corradi[3], Javier Alcolea[4], and Dejan Vinkovich[5]

[1]*Astronomy Department, University of Washington, Seattle WA 98195 USA*

[2]*Department of Physics and Astronomy, University of Rochester, Rochester NY 14627 USA*

[3]*Instituto de Astrofisica de Canarias, Tenerife, Spain*

[4]*Observatorio Astronomico Nacional (IGN), Alfonso XII N3, 28014 Madrid, Spain*

[5]*Physics Department, University of Split, Nikole Tesle 12, 21000 Split, Croatia*

Abstract. Multi-epoch HST images have been obtained for the pre planetary nebulae CRL618, CRL2688, and Hen3-1475. Each object shows clear and idiosyncratic expansion patterns. CRL618 consists of several well defined fingers with sharp tips. The lengths of the tips have increased by identical factors, ∼7%, over the course of seven years, suggesting a common expansion age of 100 years. The corresponding proper motions range up to ∼400 km s^{-1} assuming a distance of 900 pc. Trailing filaments of starlight-scattering dust expand at a far lower rate, ∼1–2%, in the same time. The bright lobes of CRL2688 expand uniformly at a rate of 2.6% in seven years, suggesting a brief ejection 250 y ago. Surprisingly, the set of concentric and nearly circular arcs that surround the lobes also expand uniformly, but at a third of the rate of the lobes. Thus it appears that the arcs were all formed in a brief event 750 years ago rather than episodically over several hundred years as is commonly believed. Finally, Hen3-1475 shows two expanding components. The first consists of a symmetric pair of two large arcs of dust extending over 5000 AU on opposite sides of the nucleus that expand radially and uniformly at 2% per decade (assuming a distance of 5 kpc). This implies speeds at the leading edge of the arcs as high as 1000 km s^{-1}. The second component is pairs of bright knots seen best in emission-line images. These move along and through the dust arcs at even higher proper motions leaving no disturbances in their wakes. The innermost pair of knots is being launched from the tips of a pair of narrow emission-line cones that straddle the nuclear region and whose base seems anchored to the nucleus.

Keywords. Planetary Nebulae – Stars: evolution

1. Introduction

The partial resolution of the Hubble Space Telescope enables structural changes to be monitored in nearby planetary nebulae ("PNe") and prePNe over the course of a decade. The observable proper motions form a valuable new type of data set that can be used to evaluate the predictions of hydrodynamic models of nebular evolution.

We have repeated previous observations of the prePNe CRL618, CRL2688, and Hen 3-1475 using the same filters and about the same S/N using Wide Field Camera 3 ("WFC3"). Each target shows clear and highly idiosyncratic expansion patterns that are presented here for the first time.

The most recent epoch of observations were obtained in August 2009 using the newly installed Wide Field Camera 3 ("WFC3") in the Hubble Space Telescope. The data are excellent in quality. Our processing of the images was delayed until the most accurate geometric distortion corrections for the camera were released in March 2010 since such corrections are vital for comparing the new images with those from older cameras on HST.

2. Observations and Analysis

Our Cycle 17 observations were patterned after previous images in the HST archives dating back to 1996. We used the same filters and exposed to approximately equal S/N noise levels. OH231.8+04.2 (QX Pup) was a fourth target; however, the S/N of our exposures was not adequate to reliably monitor changes in its structure.

Once high-quality geometric distortions were obtained for WFC3 we worked with Drs. Max Mutchler and Howard Bushouse of STScI to recalibrate all of the images from every epoch using the most recent camera calibration files for WFPC2, ACS, and WFC3. The resulting sets of images were divided into sets, one each for every target and matched filter. The sets of images were spatially aligned. In order to correct for various camera-filter throughput efficiencies, we renormalized the image intensities to match the fluxes of the three brightest field stars. The "signal" of change was generated by subtracting all pairs of images within the set. Changes were obvious in both the nebular structure and the surface brightnesses.

The changes appear, at first glance, to be dominated by radial expansions about the nebular center. Thus we adopted an analysis procedure that makes the initial and very simple assumption that the overall expansion is uniform in which the magnitude of proper motion of every feature scales with the offset of the feature from the nebula center. Deviations from this assumed pattern will be visible in the image residuals after we applied the method of analysis that we describe next.

The earliest of the two epoch was magnified by an amount $1 + M$, where M is the structural scale increase over the time interval between image epochs. M was varied by trial and error until the difference image showed minimal systematic residuals. In a few cases we had to spatially shift one of the images by a small fraction of a pixel to best null the difference image. **This showed that field stars were highly unreliable spatial fiducially** over the course of a few years since their motions were both random and secular, the latter being the possible result of the proper motion of the target. In order to get a flat null difference it was often necessary to multiply the intensities of the earlier image by factors as large as 1.05. These changes are probably real since they differed from object to object but not from filter to filter. All of the results below are new and still subject to critical evaluation. An uncertainty analysis is in progress.

3. Results

3.1. CRL618

The first-epoch images in the HST archives consist of narrow-band F631N, F656N, and F673N images and F547M from 1998-10-23 and a very deep wideband F606W image obtained 2002-07-30 using the high-resolution camera in ACS. F547M is dominated by dust-scattered stellar light. The F606W filter passband includes a series of red emission lines as well as continuum. The new WFC3 images were obtained on 2009-08-07 in F656N, F658N, F673N, F953N, F547M, and F606W. The F953N filter is dominated by light from the central star which is otherwise very faint or undetected in bluer filters. We find that the F658N and F656N (Hα) images are very similar expect that F656N contains bright scattered stellar Hα emission near the center of CRL618.

The overall expansion pattern of CRL618 is best traced using the F656N exposures from 1998 and 2009 and the F606W filter image from 2002. Five thin finger-like features dominate the nebular structure (three on the east side and two on the west). Each of the fingertips increased their radial distance from the nebular center by 7% in seven years. Thus their expansion age is ∼100y. At the distance of 900 pc to CRL618, the tips furthest from the center, 8″ or 7000 AU, have proper motions corresponding to ~ 500 km s^{-1}.

The tips of the fingers are associated with shocks with speeds of 75–200 km s^{-1} (Sánchez-Contreras & Sahai 2004) that are seen as knots of Hα and [NII]. The knots appear to fade and reappear at larger distances when images from 1998, 2002, and 2009 are made into a movie. The timing of fading and reappearance of the tips is different in each finger. [SII] and [OI] form into a network of filaments that fill the fingers behind the fingertips, as expected for post-shock gas. Their recombination times are thus well in excess of 100y, suggesting that their density < 100 cm^{-3}. The network of filaments expands uniformly at a rate of ∼2% in seven years, so the filaments do not keep pace with the knots. This is predicted in the hydrodynamic models of Dennis et al. (2008).

3.2. CRL2688

CRL2688 consists of a pair of bright dusty lobes with an orthogonal lane of deep extinction that hides the central star at visible wavelengths. In H_2 the dark lane is seen to consist of finger-like features that resemble those in CRL618. Outside the lobes and the fingers are a variety of concentric filaments shaped like circle segments with regular separations and often called “rings”. The rings are believed to be the result of episodic mass loss during the AGB ascent, though we shall argue against this interpretation shortly. All of the visible light is dust-scattered starlight. Correspondingly, our images were obtained through the same wide-band filters used for earlier images found in the HST archives, F606W and F814W.

The lobes and the surrounding rings are sharply delineated. Blinking the images from various epochs shows a clear large-scale expansion pattern. We have magnified the deep, high-spatial resolution ACS-HRC F606W images of 2002 and subtracted them from the 2009 WFC3 images through the same filter. The lobes vanish in the difference images when the 2002 image is magnified by factor of 1.026 and its intensities are scaled by 20%. Thus the lobes appear to have been formed 250y ago in a brief event. Similarly, the concentric arcs disappear with a magnification factor of 1.009 and

intensity scaling of 1.15 (a ring of radius of 5″ has a proper motion of 14 km s^{-1}). We will be analyzing the HST data more carefully to see if the standard model of repeated ejections is more consistent with the observations.

WFPC2/WF images of CRL2688 date as far back as 1995. Although a pattern of expansion is plainly visible over 14 years, the poor PSF of the images yields consistent but more uncertain results than those reported here.

3.3. Hen 3-1475

Hen3-1475 is one of the most enigmatic nebulae, and its identification as a pre-PN is not grounded in hard facts. Distance estimates range from 5 kpc (Riera et al. 1995) to 8 kpc (Borkowski & Harrington 2001; "BH01"). BH01 argue that at the far distance Hen3-1475 is located in the bulge where its luminosity is far too large to be a PN precursor with a typical mass. In any case the morphology of the core of the nebula bears a remarkable resemblance to OH231.8+04.2 and M1-92, so the physical processes that collimate the outflow may share similarities other than scale. The outflow from the nucleus consists of an extensive and sinewy ensemble of cloudlets that are very prominent in continuum images suggesting that they are seen in scattered starlight. The outermost of these cloudlets have proper motions of ±500 km s^{-1} relative to the core.

Two sets of small knots identified as I–I′ and M–M′ by BH01 are seen most prominently in emission-line filters. Two thin emission-line thin cones that appear like "wishbones" emanate from the core of Hen3-1475 with their apex pointed outward. The tip of the northwest wishbone is coincident with a compact x-ray source.

After just three years of imaging and despite its distance, Hen3-1475 shows knots with proper motions of ∼0.1 mas y^{-1} (BH01). Our 13-year time baseline reveals a great amount of detail in structural changes within the nebula. For example, the entire ensemble of dust-scattering cloudlets expands uniformly at a rate of 2% per decade, implying a kinematic age of ∼500 y. The pair of inner knots at or near the tips of the wishbones, I and I ′, show no measurable proper motions whatsoever. Instead they brighten and fade in a manner suggesting that some non-radiating form of energy released from the core has traveled outward along or within wishbone, exciting the ambient gas in the process. That is, we may be witnessing the propagation of a disturbance rather than true motions (BH01). On the other hand, studies of the Doppler shifts in the immediate vicinity of I and I ′ show a sudden velocity drop by ∼800 km s^{-1} beyond the tip of the wishbone (BH01), as if mass at high speeds abruptly decelerates, dumping its mechanical energy into heat or light.

The next larger set of knots called M and M′ by BH01, are spatially resolved in all epochs. These knots are clearly changing their shape and size over time. M and M′ move relatively slowly along and through the ensemble of cloudlets. They seem to move relatively slowly the outflowing dust cloudlets at their location, possibly shock-exciting local gas in the process.

Acknowledgments. We are extremely grateful to Drs. Max Mutchler and Howard Bushouse of STScI for their help with the data calibration. BB acknowledges support from NASA grant GO11580. Support for program GO11580 was provided by NASA through a grant from the Space Telescope Science Institute. Some of the data presented in this paper were obtained from the Multimission Archive at the Space Telescope Science Institute (MAST). STScI is operated by the Association of Universities

for Research in Astronomy, Inc., under NASA contract NAS5-26555.

References

Borkowski, K. J., & Harrington, J. P. 2001, Astrophysical Journal, 550, 778
Riera, A., Garcia-Lario, P., Manchado, A., Pottasch, S. R., & Raga, A. C. 1995, Astronomy and Astrophysics, 302, 13
Sánchez Contreras, C., Sahai, R., & Gil de Paz, A. 2002, Astrophysical Journal, 578, 269

Asymmetric Planetary Nebulae V
A. A. Zijlstra, F. Lykou, E. Lagadec and I. McDonald
Jodrell Bank Centre for Astrophysics, Manchester, UK © 2011

The Expanded Very Large Array and Observing AGB Stars, pPNe and PNe

Mark J Claussen
National Radio Astronomy Observatory, 1003 Lopezville Road, Socorro, NM 87801 USA

Abstract. The Expanded Very Large Array (EVLA) is beginning to come on-line, with early science observations begun in March 2010. I describe and extol the characteristics of the EVLA as it pertains to the Asymmetric Planetary Nebulae. In doing this, I will also report on the how the science commissioning of the EVLA is progressing and how the commissioning effort is organized around what we call Open and Resident Shared Risk Observing. The ten times increase in continuum sensitivity of the EVLA over the VLA will enable many new, exciting observations on AGB stars, pre-planetary nebulae, and planetary nebulae. Although the sensitivity of spectroscopy will not be improved by the EVLA over the VLA, many exciting projects will be opened up because of the large simultaneous bandwidths and many spectral channels of the EVLA, as compared with the VLA.
Keywords. Planetary nebulae – Interferometry

1. The EVLA Project

The Expanded Very Large Array (EVLA) is a 90M USD upgrade of the Very Large Array, begun in 2001. It will be completed in 2012, on time, on specifications, and on budget. The EVLA will multiply by orders of magnitude the observational capabilities of the the VLA. The key goals are:

- Full frequency coverage from 1 to 50 GHz.
- Up to 8 GHz (per polarization) instantaneous bandwidth.
- A new correlator with unprecedented capabilities.
- $\sim$3 μJy (1σ, 1 hour) point-source continuum sensitivity over most of the frequency range.
- $\sim$1 mJy (1σ, 1 km s^{-1}, 1 hour) line sensitivity over most of the frequency range.

Figure 1 shows a table of overall performance goals for the EVLA.

Parameter	VLA	EVLA	Factor
Continuum Sensitivity (1-σ, 1 hr.)	30 μJy	3 μJy	**10**
Maximum BW in each polarization	0.1 GHz	8 GHz	**80**
# of frequency channels at max. BW	16	16,384	**1024**
Maximum number of freq. channels	512	4,194,304	**8192**
Coarsest frequency resolution	50 MHz	2 MHz	**25**
Finest frequency resolution	381 Hz	0.12 Hz	**3180**
# of full-polarization spectral windows	2	64	**32**
(Log) Frequency Coverage (1 – 50 GHz)	22%	100%	**5**

Figure 1. The performance goals of the EVLA as compared with the VLA.

2. EVLA Milestones and Growth

As of fall 2010, all twenty-eight antennas have been mechanically and digitally converted to EVLA standards. The final antenna was completed in May 2010. The VLA correlator was shut down on January 11, 2010, and the new EVLA correlator was awakened in mid-February. The new correlator, which makes using the broad bandwidths (and lots of spectral channels) possible, is the Wideband Interferometric Digital Architecture (WIDAR) correlator, which was contributed directly by the EVLA's Canadian partners at HIA/DRAO. Scientific commissioning of correlator modes began in earnest soon after the turn-on, and commissioning began with work on 1 - 2 GHz bandwidths using 8-bit high-speed samplers.

Two "early science" programs called Open Shared Risk Observing (OSRO) and Resident Shared Risk Observing began in March 2010, and will continue through the end of the construction project (end of CY 2012). Further details on these programs will be given below. The full bandwidth of the EVLA (8 GHz per polarization) requires high-speed, 3-bit samplers; prototypes of these samplers are currently (fall 2010) being tested on four antennas of the array. We expect that the production 3-bit samplers will be available on all antennas of the array in mid-to-late 2011. The receiver implementation, which includes wide-band receivers for all frequency bands, and also two completely new receiver systems (2 - 4 GHz and 26.5 - 40 GHz) should be completed by the end of 2012. Figure 2 shows a graphical timeline of the EVLA wideband receiver availability.

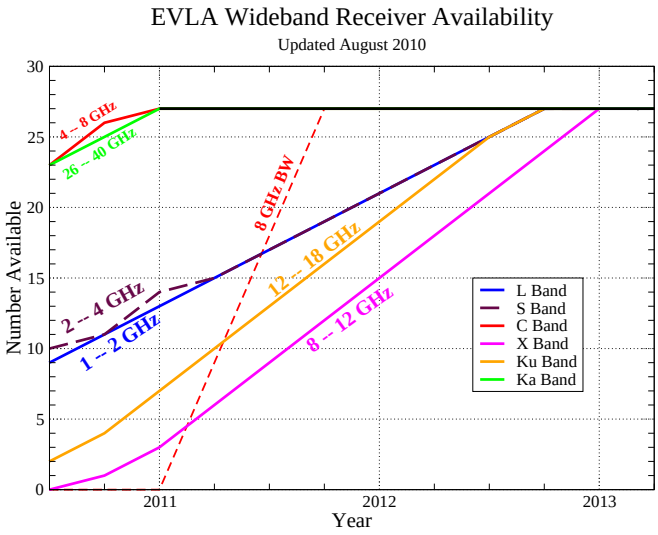

Figure 2. EVLA Wideband Receiver Availability. Note that this plot does not show 18 - 26.5 GHz (K band) or 40 - 50 GHz (Q band) as both those receiver bands were available as soon as the antennas were outfitted as EVLA antennas (i.e. all antennas already have those receivers).

2.1. The WIDAR Correlator

The WIDAR correlator, the heart of the EVLA project, is a 10 petaflop special-purpose computer, and was designed and built by the Canadian HIA/DRAO. The major capabilities of this fantastic machine are:

- 8 GHz instantaneous bandwidth, with full polarization.
- 16384 minimum, 4.2 million maximum frequency channels.
- 64 independently tunable full polarization "spectral windows", each of which effectively forms an independent "sub-correlator"
- Extensive special modes: pulsar gating/binning, phased array, VLBI-ready, burst modes, and more.

The fundamental capabilities of WIDAR will be developed first, with more specialty modes later.

2.2. Early Science Programs

During the scientific commissioning phase, there are two early science programs on the EVLA, which commenced in March 2010 and will continue through December 2012. The first of these is called Open Shared Risk Observing (OSRO), and is essentially a "business as usual" protocol. The observing setups will be very similar to the VLA,

although already an increase in bandwidth up to two spectral windows of 128 MHz (maximum) each is available. Up to 512 spectral channels (total) can be used for spectroscopy with decreasing (from 128 MHz) total bandwidths by factors of two.

The second early science program is called Resident Shared Risk Observing (RSRO). This is a program where observers must be resident in Socorro, NM for at least three months, assisting NRAO staff in testing, commissioning, and expanding the capabilities of the EVLA and WIDAR. The participants in this program will have access to more extensive observing capabilities and their length residency will be proportional to amount of requested observing time.

For further details of these programs, please see the web pages:

http://science.nrao.edu/evla/earlyscience/osro.shtml and

http://science.nrao.edu/evla/earlyscience/rsro.shtml

2.3. WIDAR and Early Science Growth 2010 - 2012

The growth of observational capabilities is expected to be rapid through the end of CY 2012. All initial observations will be with the "fundamental homogeneous correlator setup", with all spectral windows adjacent, each with the same bandwidth and channelization, and arranged, for continuum observations, to maximize the total bandwidth coverage. Resident observers in the RSRO program will have access to 2 GHz bandwidth per polarization, using all antennas by mid-to-late 2010 and 8 GHz bandwidth per polarization, using all antennas, by the end of 2011.

Recirculation in the WIDAR correlator, which will give increased spectral resolution, should be available by early-to-mid 2011, and independent spectral tuning by mid 2011. Flexible resource allocation (i.e. trading spectral windows for even more spectral resolution) should be available by late 2011.

3. EVLA Observations of Asymptotic Giant Branch (AGB) stars, pre-Planetary Nebulae, and Planetary Nebulae

The EVLA will be able to advance the study of AGB stars, pPNe and PNe, as well as using these objects as tracers in the Galaxy, in several ways. These divide into continuum and spectroscopic observations, and in the two sub-sections below I will give some examples of what the EVLA can do for studies of these objects. Note that attendees of this conference will likely think of many more projects that can use the EVLA to advance our knowledge of these sources; the suggestions that I present here are just the tip of the iceberg.

3.1. EVLA Continuum Observations

Because of the great increase in continuum sensitivity, observations using the EVLA should be able to detect radio continuum emission over the entire range of frequencies (wavelengths from 20 to 0.7 cm). This will allow the detection and imaging (for large enough sources) all planetary nebulae throughout the Galaxy in the EVLA sky. Compact PNe could be used as kinematic/dynamic tracers of the Galaxy and the Bulge,

using the high angular resolution of the EVLA in its wider configurations which allows for proper motions to be measured.

Detections of the radio continuum in PNe will allow the study of free-free ionization in PNe and perhaps in some pPNe or transition objects. For PNe, we will be able to determine physical parameters such as n_e and T_e. In some sense this will be a rejuvenation of the radio continuum study of PNe when the VLA first began operation — but with much higher sensitivity, so that many faint PNe can have these physical properties measured. In addition, many PNe in regions of high extinction should be discovered. In pPNe and young PNe, ionized gas from jets (which have an important role in the sculpting of PNe) can be studied, and again at high angular resolution. Continuum emission from dust (i.e. large grain emission) can be studied from central objects of both pPNe and PNe. For well-resolved PNe, the nebular expansion can be measured, and assuming a kinematical model, expansion distances can be estimated. Finally, at high frequencies, the radio photospheres of a large number of AGB stars will be detected, allowing the temperature and perhaps structure of these radio photospheres to be determined with moderate accuracy.

Spectroscopic observations using the EVLA will indeed open up a new vista in AGB stars, pPNe, and PNe molecular line research. Many nearby objects can be observed over a large bandwidth, allowing for many species and transitions to be detected simultaneously, giving input into chemical and ionization models of the circumstellar envelopes. As an example, Figure 3 shows the spectra (made from spectral images) of the SiS J = 2→1 and HC_3N J = 4→3 transitions from the well-known carbon AGB star, IRC+10216. Observations of the emission from these two lines were made simultaneously with the EVLA. Eventually spectral imaging surveys of lines across an entire 8 GHz of bandwidth with 1 km s^{-1} will be able to be made simultaneously. Masers (e.g. OH, H_2O, SiO), as well as thermal lines can be detected and imaged in a large number of sources.

Radio recombination lines from the ionized gas in PNe can be observed. The EVLA doesn't provide increased sensitivity for spectroscopy, but several recombination lines from a given receiver band (e.g. there are six recombination lines in the 2 - 4 GHz band) could be observed simultaneously and stacked, providing an increase in sensitivity. One may observe hydrogen, helium, and possibly radio recombination lines in PNe and use these lines to study the kinematics of the ionized gas.

Depending on the sensitivity required for lines and continuum emission, both could be observed simultaneously.

4. Summary

The EVLA became ready for science observations with all antennas and unprecedented new capabilities in March 2010. Wide-band (full tuning range) receivers are available on all antennas: the highest frequency bands (18 - 50 GHz) will be completely installed in early 2011; the 4 - 8 GHz band receivers will be completely finished by mid 2011, and the remaining four receiver bands will have all receivers installed in 2012.

Early science opportunities from March 2010 through December 2012 include basic modes via the OSRO program where the observer can observe remotely with the EVLA and advanced modes via the RSRO program where the observer comes to

Socorro to participate in EVLA scientific commissioning. The RSRO program includes 2 GHz bandwidth on all antennas by mid-to-late 2010 and 8 GHz bandwidth on all antennas by late 2011. Increasing spectral resolution and tuning flexibility, through the RSRO program will continue through 2011 and 2012, and specialty modes will be implemented using the RSRO program, guided by user interest.

Acknowledgments. I thank the Scientific Organizing Committee of the APN 5 conference for allowing me the opportunity to present this information about a transformational new instrument (the EVLA) for the studies of AGB stars, pre-planetary nebulae, and planetary nebulae, and I hope many of the attendees will be users of the EVLA in the future. The National Radio Astronomy Observatory is a facility of the National Science Foundation operated under cooperative agreement by Associated Universities, Inc.

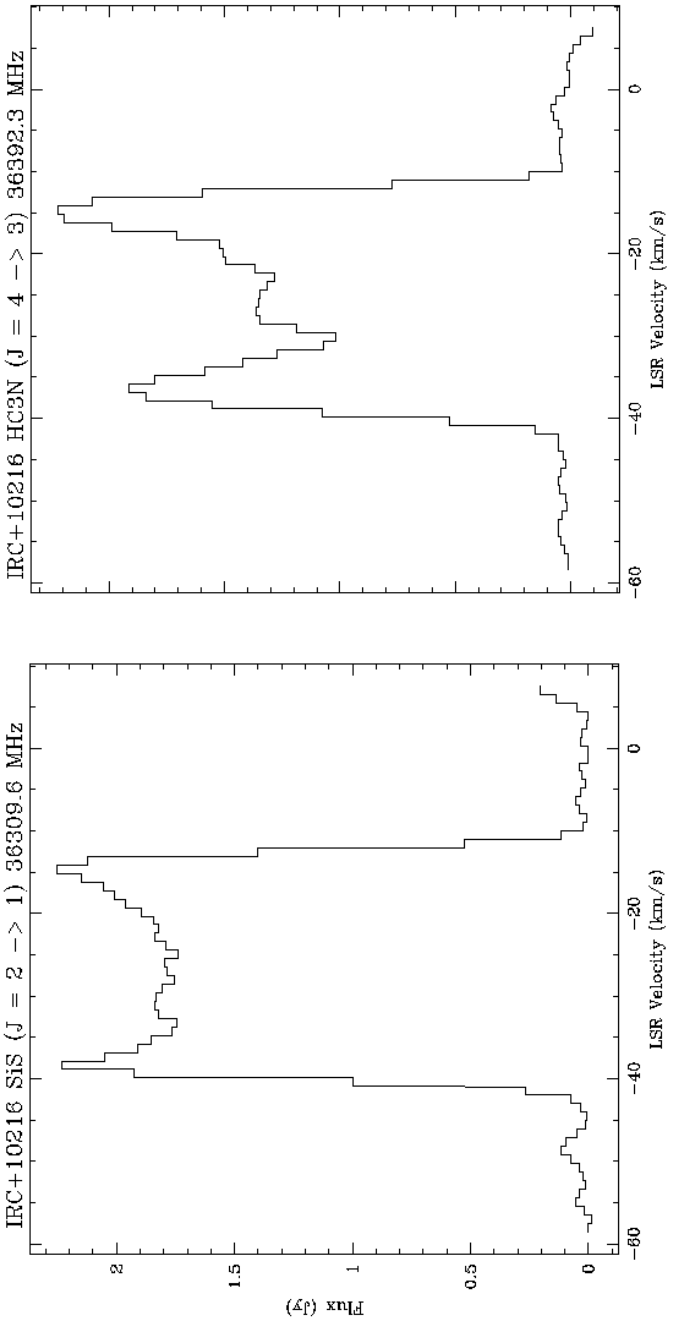

Figure 3. Left: Spectrum of the J = 2→1 transition of the SiS molecule from the carbon star IRC+10°216. Note that the spectrum was made by averaging emission over a given image region through a velocity cube. Right: Simultaneously observed, the J = 4→3 transition of the HC_3N molecule. Note that both these transitions are in the Ka receiver band (26 - 40 GHz), a new receiver system for the EVLA.

Asymmetric Planetary Nebulae V
A. A. Zijlstra, F. Lykou, E. Lagadec and I. McDonald
Jodrell Bank Centre for Astrophysics, Manchester, UK © 2011

Prospects for Asymmetric PNe with ALMA

P. J. Huggins

Physics Department, New York University, New York NY 10003, USA

Abstract. Millimeter and sub-millimeter observations have made fundamental contributions to our current understanding of the transition from AGB stars to white dwarfs. The approaching era of ALMA brings significantly enhanced observing capabilities at these wavelengths and promises to push back the frontiers in a number of ways. We examine the scientific prospects of this new era for PNe, with an emphasis on how developments may contribute to the goals of the asymmetric PNe community.
Keywords. Stars: AGB and post-AGB, Stars: mass-loss, circumstellar matter, planetary nebulae: general

1. Introduction

The Atacama Large Millimeter/sub-millimeter Array (ALMA), is a new, major, international telescope that is currently being built in northern Chile. It will provide significantly enhanced observing capabilities over existing instrumentation in the mm and sub-mm wavebands, and is expected to make important contributions to many areas of astronomy. ALMA's ability to make high quality, high resolution images in lines and the continuum will provide a new tool to probe the structure and origin of asymmetric planetary nebulae (APNe). This paper outlines prospects for APNe with ALMA. Sect. 2 reviews the contributions of mm and sub-mm observations to our current understanding of the field; Sect. 3 describes ALMA's main characteristics; and Sect. 4 considers what it might do for APNe.

2. APNe at mm and sub-mm Wavelengths

The most important contributions of the mm and sub-mm wavebands to our current understanding of APNe have been made using molecular line observations. The low lying rotational transitions of CO, J = 1–0 at 2.6 mm (115 GHz), J = 2–1 at 1.3 mm (230 GHz), and J = 3–2 at 0.87 mm (345 GHz), have been especially useful in probing the kinematics, distribution, and mass of the molecular gas. Numerous lines of other molecular species have been detected in spectral scans of some well-studied objects, e.g., AFGL 618 (1207) and NGC 7027 (1212) and these lines provide valuable diagnostics of physical and chemical conditions. There is an interesting, evolving chemistry in the AGB-PN transition (1187), and the atomic fine structure lines of C I, which are useful probes of photo-dissociation regions, are detectable in the sub-mm (1188; 1210).

The history of APNe observations in the mm and sub-mm can be divided into two phases. In the first phase, the observations were made using single-dish telescopes. The angular resolution for single-dish observations is set by the diffraction of the telescope ($\sim \lambda/D$, where D is the diameter and λ the wavelength) typically ~10–60″; the unit of information is the spectrum; and spatial information is obtained by moving the telescope. One basic contribution of the single-dish work has been in setting the baseline for mass-loss on the AGB. Early detections (e.g., 1199) spawned numerous surveys, so that we now know the expansion velocity and mass-loss rates of many AGB stars. A second contribution of single-dish observations has helped develop one of the central ideas of PN formation: the ejection of neutral gas in the transition from the AGB. The neutral gas can be traced from the AGB, through pre-PNe, to *bona fide* PNe (e.g., 1195), and it makes a direct connection to the ionized nebulae and their asymmetric structures. A good example is the CO distribution in the Helix nebula (1211). A further contribution of single dish observations has been the discovery of high velocity wings in the spectra of pre-PNe and young PNe. This has revealed a new ejection mechanism with a momentum excess which we associate with the launching of jets (1189) but do not fully understand.

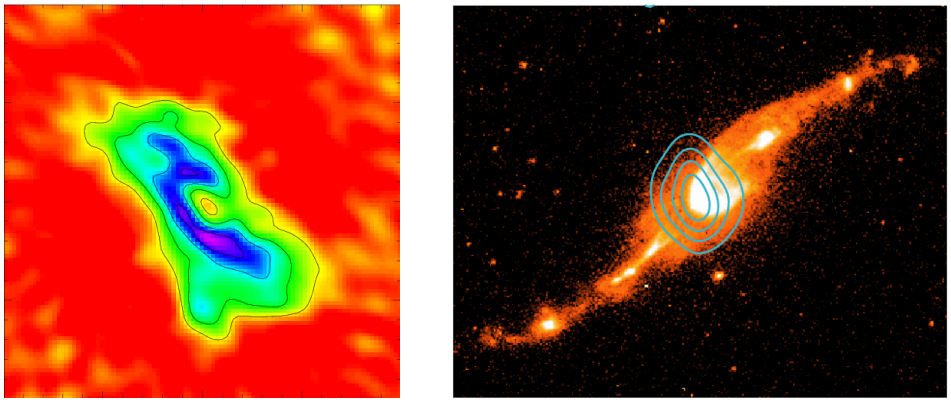

Figure 1. Examples of CO line interferometry of APNe. *Left*: Image in CO (1–0) integrated intensity of the disk in KjPn 8 (1192). *Right*: CO (2–1) intensity contours of the waist in He 3-1475, superposed on optical HST image (1198).

The second phase of mm and sub-mm observations of APNe has involved the use of interferometers (notably BIMA, OVRO, SMA, and the IRAM Plateau de Bure) which provide images/data cubes at higher angular resolution than single-dish telescopes, from ~5″ to as high as ~0.5″. CO line interferometry of the circumstellar envelopes of AGB stars (e.g., Fong et al. 1191, Castro-Carrizo et al. 1190, see also Alcolea, this volume) shows that most (though not all) envelopes are roughly spherically symmetric, but exhibit multiple arcs and other asymmetries. This sub-structure in the envelopes is also seen in images of dust-scattered light at optical wavelengths (e.g., 1202; 1203).

CO line interferometry of pre-PNe and young PNe, especially in conjunction with optical HST imaging, has produced striking results. Two examples, observed with the Plateau de Bure interferometer in the CO (1–0) and CO (2–1) lines, are shown in Fig. 1. Recent examples in other CO lines include: ^{13}CO (2–1) in M1-92 (1185), CO (3–2)

in IRAS 22036+5306 (1208), and CO (6–5) in CRL 618 (1205). These and similar observations provide a common picture of early PN formation consisting of enhanced mass-loss in slowly expanding equatorial tori, with molecular gas entrained in jets along bi-polar or multi-polar axes.

The results to date reveal a rich phenomenology on size scales of 10^{16}–10^{17} cm which is partly explored but not understood. A number of physical processes may be responsible for the outflows that produce the asymmetries. For example, a torus could be produced by rapid rotation, a magnetic explosion, gravitational focusing by a companion, leakage from Roche lobe overflow, or ejection during a common envelope phase. However, there is a lack of quantitative prediction that can clearly discriminate between the various scenarios. The advent of new opportunities to study these phenomena at higher resolution with ALMA offers the possibility of important breakthroughs.

3. ALMA

ALMA is a large, imaging interferometer that will operate in the mm and sub-mm wavebands. It is an international collaboration of North America, Europe, Japan, and Taiwan, in co-operation with Chile. The telescope, which is now being built, will be a significant advance on current mm and sub-mm instrumentation in terms of angular resolution, wavelength coverage, and sensitivity. Part of the array is expected to become available for early science in 2011.

Table 1. Characteristics of ALMA

number of antennas	50 (12 m) + ACA
frequency range	31–950 GHz
maximum baselines	0.2–16.3 km $B_{\rm rms}$ = 0.079–6.6 km
primary beam ($\theta_{\rm p}$)	$21'' \times 300/\nu_{\rm GHz}$
synthesized beam ($\theta_{\rm s}$)	$0.08'' \times 300/\nu_{\rm GHz} \times 1$ km$/B_{\rm rms}$
continuum sensitivity[1]	0.10 mJ
line sensitivity[2]	0.10 K ($\theta_{\rm s} = 1.5''$) – 709 K ($\theta_{\rm s} = 0.018''$)

[1] Band 6 (211–275 GHz), t = 60 s [2] Band 6, t = 60 s, ΔV = 1 km s^{-1}

For technical information about ALMA, a useful introduction for newcomers is the document: *Observing with ALMA – A Primer*, by Doug Johnstone and colleagues. This and other technical information, including an exposure calculator, can be found at the websites of the ALMA Regional Centers. Additional technical information, and many interesting scientific perspectives can be found in the volume: *Science with the Atacama Millimeter Array: A New Era for Astrophysics* edited by Bachiller & Cernicharo (1186).

Some of the principal characteristics of ALMA that determine how it might be used to observe APNe are listed in Table 1. The main array will consist of at least 50 × 12 m antennas, augmented by an additional small array of 7 m and 12 m antennas – the Atacama Compact Array (ACA) – that can be used for wider field observations, and for total power measurements.

ALMA will be equipped with an extensive complement of receivers that will eventually cover almost the entire mm and sub-mm frequency range from 31 to 950 GHz.

The initial receiver development is for wavebands in the range 84 to 720 GHz. The array is located at a high (5,000 m), dry site to minimize atmospheric effects. Even so, the atmospheric transmission at frequencies above about 400 GHz is typically less than 50%, so this needs to be taken into account in planning observations.

The field of view of ALMA (the primary beam, $\theta_{\rm p}$) is determined by the diffraction of the individual 12 m antennas. $\theta_{\rm p} = 21''$ at 300 GHz and varies as ν^{-1}. Thus the field of view is very small by the standards of optical imaging. The field can, of course, be extended by making additional, adjacent observations (mosaicing) at the expense of additional observing time.

The angular resolution of ALMA (the synthesized beam, $\theta_{\rm s}$) is determined by the diffraction of the array (see Table 1). $\theta_{\rm s}$ varies as ν^{-1}, and at a given frequency can be varied by a factor of ∼10 according to the chosen array configuration, which is characterized by the rms baseline $B_{\rm rms}$. Common setups are likely to have a synthesized beam of ∼0.1″, so the impact of the instrument in terms of angular resolution will be somewhat similar to the impact of the HST at optical wavelengths. At the highest frequencies and most extended baselines, the resolution is better than 0.01″, although this is likely to be used only for special applications.

The resolution of the array is not an independent quantity, because it is closely linked to the sensitivity of the observations. In measuring the surface brightness of a spectral line, the noise level (in K) varies according to the expression:

$$\Delta T_{rms} \propto \frac{\theta_{\rm p}^2}{\theta_{\rm s}^2}\,\frac{1}{\eta}\,\frac{1}{\sqrt{N(N-1)}}\,\frac{1}{\sqrt{N_{\rm p}}}\,\frac{T_{\rm s}}{\sqrt{\Delta\nu\, t}}$$

where the first factor on the right hand side is the ratio of the primary beam to the synthesized beam, η lumps together various efficiencies, N is the number of antennas, $N_{\rm p}$ is the number of polarizations, and the last factor is the usual radiometer equation, with $T_{\rm s}$ the system temperature, $\Delta\nu$ the observing bandwidth, and t the observing time. Thus the noise level is proportional to the inverse square of the synthesized beam. For specificity, some numerical examples for the sensitivity in Band 6 (211–275 GHz) are given in Table 1, for an observing time of 60 s, and (for a spectral line observation) an effective resolution of 1 km s^{-1}. The back-end of the ALMA system (the correlator) is extremely flexible and is likely to cover all the spectroscopic requirements of the APN field. The sensitivity in the continuum is particularly high because of the wide (8 GHz) bandwidth available.

From the equation above, it can be seen that the large number of antennas (N = 50) plays an important role in the sensitivity of the array. The corresponding number of baselines, given by $N(N-1)/2$, is even larger (1225). This means that the $u-v$ (Fourier) plane is well sampled, and leads to high quality imaging, even in snapshot (short-exposure) modes. Overall, the gain in sensitivity compared to the state-of-the-art Plateau de Bure interferometer (at ∼ 230 GHz for the same synthesized beam, etc.) is a factor of ∼15–20. The images shown in Fig. 1 could in principle be obtained in observing times ∼1 min. Thus ALMA is indeed a major development in mm and sub-mm instrumentation.

4. Strategies and Projects

There are many ways in which the capabilities of ALMA can be used to study APNe. Strategies range from using the speed of the instrument to carry out snapshot surveys, to exploiting the highest resolution modes to probe details of objects of special interest. Here we outline some of the possibilities, with an emphasis on the scientific objectives.

4.1. AGB Stars

(1206) has reviewed the general prospects for AGB stars with ALMA, and the reader is referred to his paper for details. Important developments will be observations of the dust forming regions, and sensitive studies of the chemistry. For APNe, one interesting aspect is that the photospheres and close environs of the nearest AGB stars will be resolved in the continuum with ALMA in the highest resolution configurations. This is a new type of probe at these wavelengths and may have an important bearing on understanding early APN formation. Low luminosity companion stars will not be directly detected in the glare of the AGB star, but they could generate detectable regions of ionized gas under some circumstances, as in the case of Mira at longer wavelengths (1201).

4.2. AGB Envelopes

As the precursors of APNe, the circumstellar envelopes of AGB stars provide a number of important constraints on the origins of PN asymmetries. First, there is good evidence from optical HST imaging for incipient core activity in some AGB envelopes, as discussed by Sahai (this volume). This activity may be caused by young or weak jets, or some other type of activity which has not yet fully developed. Thus it would be important to determine how widespread this core activity is, and to characterize its structure and kinematics. This could be done using CO line observations of envelope cores at high resolution.

A second perspective on AGB envelopes is directly concerned with probing the presence of a binary companion. If axisymmetry is induced by interaction with a companion, the secondary star must have been present throughout the entire AGB phase and should leave its imprint on the circumstellar envelope, as emphasized by Huggins et al. (1197).

One way the imprint is effected is that the reflex motion of the AGB star induces a spiral pattern in the circumstellar envelope (e.g., Mastrodemos & Morris 1200, see also Raga, this volume). A clear example of the spiral pattern has been seen in the circumstellar envelope of AFGL 3068 (1203; 1204) in dust-scattered light observations. This pattern may also be detectable in CO or some other line affected by the weak spiral shock. The radial wavelength of the spiral is $\lambda \sim VP$ where V is the expansion velocity of the envelope, and P is the period of the binary. For AFGL 3068 $P \sim 800$ yr and $V \sim 14$ km s^{-1}. At a distance of ~ 1 kpc, the angular separation of the arms is $\sim 2''$. Thus the pattern is in principle relatively easy to resolve at high resolution in other nearby systems with intermediate or long periods.

A related signature of a companion star is the degree to which its gravitational field flattens the AGB envelope. This global shaping of the envelope is the simplest characteristic of a binary companion to observe on a large scale. The magnitude of the

effect, which depends on the companion mass and separation and the wind velocity, has been discussed in detail by Huggins et al. (1197). The angular size of an AGB envelope in CO for a mass-loss rate $\gtrsim 10^{-5}$ $M_\odot$ yr^{-1} is $\gtrsim 25''/D_{kpc}$ where D is the distance. Thus envelope shapes can be measured for large numbers of AGB stars to probe this effect.

4.3. Magnetic Fields

The role of magnetic fields in AGB stars and PNe has long been a controversial topic. The problem used to be magnetic fields versus binary companions for shaping PNe, but now that companions seem to be fairly common, and their interactions can generate magnetic fields, the issue has changed focus. There is probably a consensus that MHD is needed to launch and form jets (Frank, this volume). The main issue seems to be: what else do magnetic fields do?

Radio astronomers have long reported the presence of dynamically important magnetic fields in maser spots in AGB envelopes (e.g., Bains, this volume). However, the spots are small, so there is a question whether the strong fields are local or global. Herpin et al. (1193) have recently reported magnetic field measurements using mm CN emission (which is not in spots) at levels equivalent to the fields in the spots. Hence the fields may be globally important. ALMA's ability to measure polarization and thereby to map the magnetic field strength and geometry is likely to be important in sorting out this issue. See Vlemmings (this volume) for more details.

4.4. Shaping in Pre-PNe

One of the most direct applications of ALMA to the problems of APN formation will be in characterizing the early jet shaping in pre-PNe. As explained in Sect. 2, there is already a generic picture (at least for a subset of PNe), based on current interferometry, as shown in the left hand panel of Fig. 2.

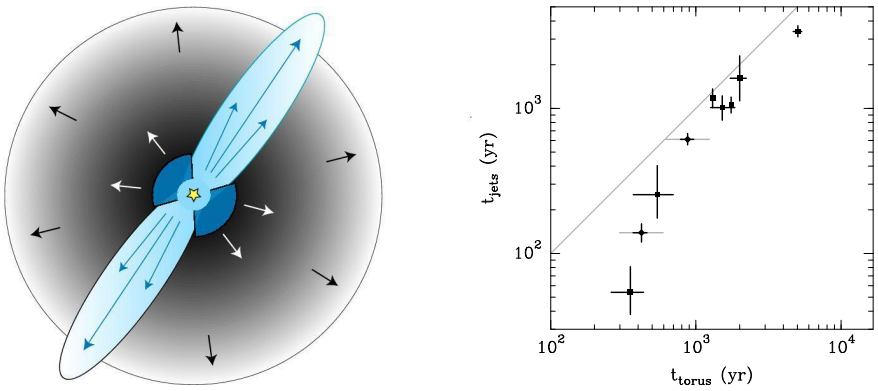

Figure 2. *Left*: Schematic picture of the early shaping of PNe by jets and equatorial outflows. *Right*: Correlation of the kinematic ages of jets and equatorial tori (from 1194).

This picture is only partly explored by current observations. The detailed properties accessible to line observations with ALMA include: the geometry and kinematics

of the jets and equatorial outflows, the energy and momentum budget, and possible connections with extended circumbinary disks, which are common in other classes of post-AGB stars. A systematic investigation of these and related properties is likely to provide important clues on the physics that controls the outflows. For example, one result based on current mm interferometry is that the kinematic ages of jets and tori are correlated (Fig. 2). They have nearly the same ages, and are therefore ejected nearly simultaneously (1194). This points to a fundamental connection between the outflows. It rules out some classes of physical model, and even suggests that slight timing differences between jets and tori can probe the properties of unseen accretion disks that are believed by some to be responsible for launching jets. Much more detailed information along these lines is expected to be very productive.

4.5. Globules and Debris Disks

ALMA also has interesting applications in fully developed PNe. One is probing the excess long wavelength continuum emission from debris disks surrounding the central stars of some PNe. The first of these was detected using Spitzer observations of the Helix nebula (1209). The estimated size is ∼100 AU. Although the dust continuum is expected to be falling in the sub-mm and mm wavebands, the emission from the nearest examples is detectable with ALMA and the structure should be resolved.

A second application to *bona fide* PNe is the small scale structure in the neutral gas – the globules, as exemplified by those in the Helix nebula. The Helix globules are about 1″ in diameter with extended tails, and have already been partially resolved using mm interferometry in CO (1196). A full characterization of the internal structure and kinematics of the globules and their tails is entirely feasible in the Helix and other nearby PNe, and would be an important step in refining our understanding of their origins.

5. Concluding Remarks

ALMA will be a significant advance on current mm and sub-mm instrumentation, and it will have considerable impact in many areas of astronomy. For APNe, there are major unsolved problems, especially with the physical processes that generate the asymmetries. Several aspects of these are well suited to ALMA's capabilities. Some approaches are direct extensions of current interferometric observations to higher resolution and sensitivity (e.g., CO imaging), and some are new types of probes (e.g., line polarization). Overall the prospects are excellent for taking the field of APNe forward to the next level.

Acknowledgments. I thank Pierre Cox for comments on the manuscript. This work is supported in part by NSF grant AST 08-06910.

References

Alcolea, J., Neri, R., & Bujarrabal, V. 2007, Astronomy and Astrophysics, 468, L41

Bachiller, R., & Cernicharo, J. (eds.) 2008, Science With the Atacama Millimeter Array: A New Era for Astrophysics, vol. 313 of Ap&SS (New York: Springer)

Bachiller, R., Forveille, T., Huggins, P. J., & Cox, P. 1997, Astronomy and Astrophysics, 324, 1123
Bachiller, R., Huggins, P. J., Cox, P., & Forveille, T. 1994, Astronomy and Astrophysics, 281, L93
Bujarrabal, V., Castro-Carrizo, A., Alcolea, J., & Sánchez Contreras, C. 2001, Astronomy and Astrophysics, 377, 868
Castro-Carrizo, A., Neri, R., Winters, J. M., Bujarrabal, V., Quintana-Lacaci, G., Alcolea, J., Schïer, F. L., Olofsson, H., & Lindqvist, M. 2007, in Why Galaxies Care About AGB Stars: Their Importance as Actors and Probes, edited by F. Kerschbaum, C. Charbonnel, & R. F. Wing, vol. 378 of ASP Conf. Ser., 199
Fong, D., Meixner, M., Sutton, E. C., Zalucha, A., & Welch, W. J. 2006, Astrophysical Journal, 652, 1626
Forveille, T., Huggins, P. J., Bachiller, R., & Cox, P. 1998, Astrophysical Journal, Letters, 495, L111
Herpin, F., Baudy, A., Josselin, E., Thum, C., & Wiesemeyer, H. 2009, in IAU Symposium, vol. 259 of IAU Symposium, 47
Huggins, P. J. 2007, Astrophysical Journal, 663, 342
Huggins, P. J., Bachiller, R., Cox, P., & Forveille, T. 1996, Astronomy and Astrophysics, 315, 284
Huggins, P. J., Forveille, T., Bachiller, R., Cox, P., Ageorges, N., & Walsh, J. R. 2002, Astrophysical Journal, Letters, 573, L55
Huggins, P. J., Mauron, N., & Wirth, E. A. 2009, Monthly Notices of the Royal Astronomical Society, 396, 1805
Huggins, P. J., Muthu, C., Bachiller, R., Forveille, T., & Cox, P. 2004, Astronomy and Astrophysics, 414, 581
Knapp, G. R., Phillips, T. G., Leighton, R. B., Lo, K. Y., Wannier, P. G., Wootten, H. A., & Huggins, P. J. 1982, Astrophysical Journal, 252, 616
Mastrodemos, N., & Morris, M. 1999, Astrophysical Journal, 523, 357
Matthews, L. D., & Karovska, M. 2006, Astrophysical Journal, Letters, 637, L49
Mauron, N., & Huggins, P. J. 1999, Astronomy and Astrophysics, 349, 203
— 2006, Astronomy and Astrophysics, 452, 257
Morris, M., Sahai, R., Matthews, K., Cheng, J., Lu, J., Claussen, M., & Sánchez-Contreras, C. 2006, in Planetary Nebulae in our Galaxy and Beyond, edited by M. J. Barlow & R. H. Méndez, vol. 234 of IAU Symposium, 469
Nakashima, J., Fong, D., Hasegawa, T., Hirano, N., Koning, N., Kwok, S., Lim, J., Dinh-Van-Trung, & Young, K. 2007, Astronomical Journal, 134, 2035
Olofsson, H. 2008, Ap&SS, 313, 201
Pardo, J. R., Cernicharo, J., Goicoechea, J. R., Guélin, M., & Asensio Ramos, A. 2007, Astrophysical Journal, 661, 250
Sahai, R., Young, K., Patel, N. A., Sánchez Contreras, C., & Morris, M. 2006, Astrophysical Journal, 653, 1241
Su, K. Y. L., Chu, Y., Rieke, G. H., Huggins, P. J., Gruendl, R., Napiwotzki, R., Rauch, T., Latter, W. B., & Volk, K. 2007, Astrophysical Journal, Letters, 657, L41
Young, K., Cox, P., Huggins, P. J., Forveille, T., & Bachiller, R. 1997, Astrophysical Journal, Letters, 482, L101
— 1999, Astrophysical Journal, 522, 387
Zhang, Y., Kwok, S., & Dinh-V-Trung 2008, Astrophysical Journal, 678, 328

Asymmetric Planetary Nebulae V
A. A. Zijlstra, F. Lykou, E. Lagadec and I. McDonald
Jodrell Bank Centre for Astrophysics, Manchester, UK © 2011

APN V: A Highly Skewed and Biased Conference Summary

Joel H. Kastner
Center for Imaging Science, Rochester Institute of Technology, 54 Lomb Memorial Drive, Rochester NY 14623 USA (jhk@cis.rit.edu)

Abstract. I offer a brief retrospective of the *Asymmetrical Planetary Nebulae* (APN) conference series, and present a Highly Skewed and Biased selection of results presented at the fifth meeting in the series. These results highlight clear progress in understanding the roles of stellar binarity, disks, and magnetic fields in shaping planetary nebulae. Looking ahead to APN VI, I present a set of challenges to the community of researchers who study APN and related objects (symbiotic star nebulae, novae ejecta, SN Ia remnants, etc.).

1. Preamble

At the close of this, the fifth meeting in the *Asymmetrical Planetary Nebulae* (APN) series, it was easy to be demoralized by the daunting astrophysical problems still posed by these tremendously photogenic objects. Take the Red Rectangle, for example (Fig. 1). Is the confirmed presence of a binary companion orbiting its progenitor post-asymptotic giant branch (post-AGB) star (1230) both necessary and sufficient to explain its pinched waist and overall, profound degree of axisymmetry? What mechanisms might explain the formation of the long-lived molecular disk that is known to orbit the central binary (1213)? How did the nebula come to have such delicate, sharply defined geometric structures?

Thankfully, this is just a conference summary; I don't have to try to answer these questions. I just get to raise them, and to point out that they (and many other fundamental questions concerning APN) remain unanswered, despite five conferences devoted to the subject. But don't be demoralized. We've actually come a long way in our understanding of APN. To demonstrate this, I first offer some historical context gleaned from previous APN conference summaries (§2), including a review of the nagging questions that emerged from APN IV (thereby necessitating APN V). This is followed by a Highly Skewed and Biased selection of results presented at APN V that I feel go a long way toward answering those nagging questions (§3), including a digression concerning the strange, isolated field star BP Piscium and how its disk/jet system might inform future studies of APN. I finish — alas — by summarizing some new (and old) problems that are apparent as we emerge from APN V and ponder APN VI (§4). I present these in the form of several challenges, including one overarching, Grand Challenge, to the community of APN researchers.

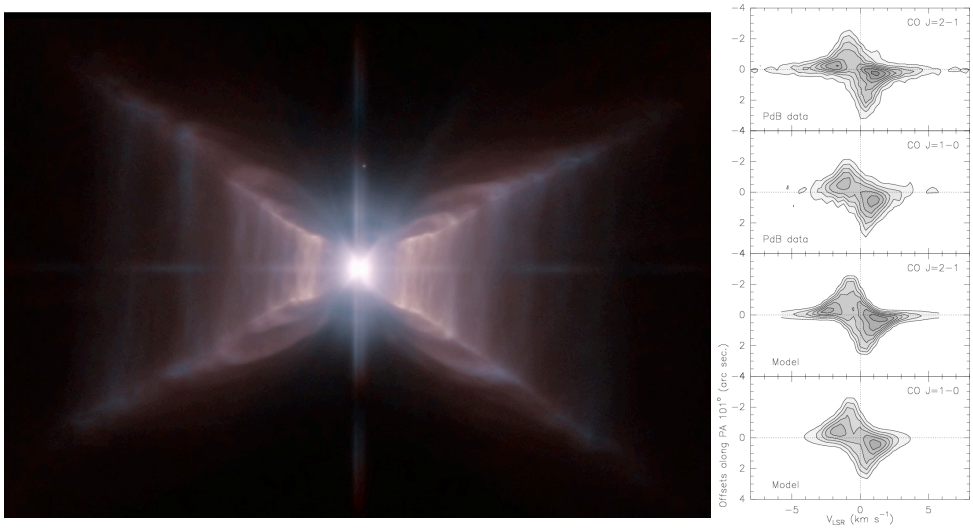

Figure 1. Left: *Hubble Space Telescope* Heritage Project image of the Red Rectangle (from http://heritage.stsci.edu/heic/1007/index.html). According to Noam Soker, no APN meeting would be complete without an image of this object. Right: position-velocity (P-V) maps of the Red Rectangle's pinched waist obtained via radio interferometry of CO emission (top two panels) and simulated CO P-V maps obtained from a model invoking Keplerian rotation (bottom two panels), demonstrating that the post-AGB star within this pre-PN is orbited by a (circumbinary) molecular disk (from 1213)

2. Some Historical Context

The stated aim of the first APN meeting (organized and hosted by APN pioneer Noam Soker in Haifa, Israel in 1994) was "to discuss the physical processes that cause planetary nebulae to acquire non-spherical structures, with emphasis on the role of binarity in the creation of axisymmetric structures." The conference summarizer was none other than F.D. Kahn of Manchester — which, in a sense, brings us full circle to APN V and its gracious Manchester hosts. Prof. Kahn's eloquent, equation-studded summary paper (1217) is dense with concise descriptions of potential mechanisms that might generate axisymmetries in planetary nebulae (PNe) and their proto-PN antecedents. It is well worth a fresh read, 15 years later; the formalism developed therein is straightforward and (to this observer's poorly trained eyes) appears sound.

The summarizer of the second APN meeting — the late, great Hugo Schwarz — shrewdly titled his conference summary paper "Conference Impression" so as to avoid the impression that he was attempting to summarize the entire conference. In that paper (1226), Hugo collects 50 terms used at APN II to describe the dizzying array of PN morphological features that appear in ground-based and *Hubble Space Telescope* imaging. Mercifully, some of this terminology has fallen into disuse (e.g., nipples, SLOBS), while the more useful terms endure (e.g., blobs, knots, FLIERS). Most notably, Hugo wrote, "my overall impression is that binaries are needed for the most extreme bipolars and perhaps for all bipolars..." and he implored the APN community: "We must go out and find those binaries!"

As we will see, I find the subsequent progress in this last (binary) respect to be a prime reason for optimism that we might eventually tackle the Challenges posed in §4. That said, it is important to keep squarely in mind this sage observation by Harm Habing, from his summary of APN III (1214): "The event called 'inspiration' may happen when scientist A gets an idea because of a brilliant or stupid remark she heard when scientist B gave a summary." Harm, like Hugo, was cautioning that the reviews and prognostications in summary talks (and subsequent conference summary papers, like this one) are highly subjective and, hence, should be taken with a very large grain of salt. Well, if summaries by the likes of Habing, Schwarz, Kahn, and Zijlstra (see next) might suffer from this deficiency, then I can only pity the poor reader who does not exercise even more caution in reading this paper. In particular, I offer a blanket apology to all those hard-working researchers whose excellent work was on display at APN V but (through sheer inattentiveness or ignorance on my part) is not mentioned below.

3. Exciting Results at APN V: a Highly Skewed and Biased Selection

In making the following (Highly Skewed and Biased) selection of results that stood out as particularly significant at APN V, I have tried to keep in mind the questions raised by APN V's esteemed lead science organizer and Lake Country tour guide, Albert Zijlstra, in summarizing APN IV (1231). In posing his (four) questions, Albert presciently honed in on a few key areas that were ripe for further investigation (here I paraphrase): (1) Can we find the binaries that are suspected to lurk within (and ultimately determine the shapes of) the vast majority of PNe, and/or can we constrain PN central binary system parameters? (2) Do magnetic fields play an important role in shaping PNe? (3) What are the basic parameters describing the disks evident within certain PNe, and what are the origins and fates of such disks? (4) How might binary companions affect a PN progenitor's mass loss?

3.1. Can We Find Binary Systems within PNe?

Answer: a definitive "yes." Since APN IV, our fearless leader in the relentless pursuit of evidence for binarity among PN central stars (CSPNe) has been Orsola De Marco. Her PLAnetary Nebula Binaries (PlaNB[*]) project is now in full swing, and its influence (direct and indirect) could be found throughout APN V. In addition to the numerous PLaNB-related discoveries of binary CSPNe from photometric and radial velocity monitoring programs (**Santander-Garcia et al.; Hrivnak; Hillwig; Miszalski; Jones; Hajduk et al.**[†]), there were (at least) the following: a successful search for tell-tale FUV excesses (indicative of hot companions) in the spectral energy distributions of AGB stars (**Sahai et al.**); the use of so-called "Sequence E" Large Magellanic Cloud (LMC) variable stars (whose variability can be traced to binarity) to attempt to predict the fraction of bipolar PNe in the LMC (**Nicholls et al.**); the X-ray detection of spun-up, late-type, main sequence (MS) or post-MS companions to PN central stars (**Montez**

[*]http://www.wiyn.org/planb/

[†]Work presented at this meeting and/or in these proceedings is indicated by the lead researchers' names in **boldface**.

et al.); and the ongoing characterizations of post-AGB binaries via their radial velocity variations (**Van Winckel, Gorlova, et al.**).

So it may not be long before we have indeed established that *all* bipolar PNe harbor central binaries, as Noam, Hugo, and others began to assert more than two decades ago. Indeed, one recommendation I would have for attendees of APN VI is that they spend at least one session sitting next to Romano Corradi — and, as images of bipolar PN are paraded on-screen, count the number of times he whispers, "We just found that one's got a central binary, too."

3.2. What Is the Role of Magnetic Fields?

The *presence* of magnetic fields within certain PNe is increasingly well established, and the fields are increasingly well characterized. This was clear from the excellent review by Wouter **Vlemmings**, in which he demonstrated (among other things) how the magnetic field strengths measured thus far for AGB stars and young PNe display a clear trend of decreasing field strength with increasing envelope radius. Such (polarization-based) results unfortunately can be extracted only in cases in which the geometries, temperatures, and densities are conducive to maser emission or to strong far-IR/submm continuum emission from cold dust. The presence of X-ray sources at the cores of some PNe, meanwhile, is likely indicative of energetic magnetic reconnection events near the driving source of the outflowing envelope. On the other hand, in many (if not most) cases it is likely that the X-rays arise not from the mass-losing star but from its companion's accretion of ejected material, either directly (in the case of a white dwarf companion) or indirectly (in the case of a spun-up, late-type companion; see §3.1). Clearly, there is much more to be done in this (magnetic field) realm (§4.1).

3.3. What Is the Structure, Origin, and Fate of Disks?

Just as binary systems are popping up in almost every axisymmetric PN if we look carefully enough, detections and potential detections of disks were a recurrent theme at APN V. High-resolution mid-IR imaging reveals compact sources at the cores of many bipolar and elliptical nebulae associated with post-AGB stars and pre-PNe (**Lagadec et al.**). This suggests there exist unresolved (or at least compact), long-lived, massive reservoirs of warm dust — i.e., disks — in these objects, and therefore that (at least in some cases) the dust may actually orbit the central stars. The evidence for long-lived, orbiting disks seems even more clear-cut in the case of the class of post-AGB stars that *lack* extensive circumstellar nebulosity, many (perhaps all) of which are suspected or confirmed binaries (**Gielen**). The mid-IR spectra of such objects bear striking similarities to those of T Tauri stars, for which the presence of orbiting, dusty disks — in some cases, orbiting *circumbinary* disks — is now well-established (e.g., 1224, and references therein).

Confirming that a post-AGB or pre-PN disk is in fact bound to the central star(s) will require the exceptional velocity and angular resolution that only a facility like ALMA might provide, e.g., in molecular line imaging (**Huggins**). Meanwhile, near-IR interferometry allows us to place constraints on the detailed radial and vertical density structures of disks (**Chesneau**). These results should, in turn, provide indications as to whether or not a given disk is really better described as a torus, and (hence) whether the equatorial density enhancements in post-AGB nebulae are bound or expanding struc-

tures. In this respect, it is noteworthy that evidence (from mid-IR imaging photometry) is now accumulating that certain PN central stars may retain dusty vestiges of Kuiper Belts and Oort Clouds that encircled the stars in their former lives on the MS (**Bilikova et al.**). If this interpretation of mid-IR excesses at PN central stars is correct, it would still remain to establish whether and how such (bound) structures — and/or the planetary systems (or, perhaps, binary interactions; §3.4.1) that likely spawned them — are capable of shaping the evolving star's AGB and post-AGB winds.

3.4. How Do Binary Companions Affect Mass Loss?

Meanwhile, increasingly sophisticated numerical simulations are confirming the extent to which (and manner in which) a *binary companion* can shape AGB and post-AGB mass loss and, in so doing, are clarifying the likely observable consequences. In particular (as predicted more than a decade ago by 1221) it appears that wide binaries likely produce tell-tale "death spiral" patterns in AGB star ejecta, and that such a pattern may hold clues to the central binary's separation **(Raga; Mohamed et al.)**. The generation by binaries of such spiral ejecta patterns, which can appear as multiple thin dust shells (depending on binary separation and viewing geometry), might finally solve the conundrum of the concentric ring systems that are a feature of so many PNe and have been the subject of an enlightening theoretical tussle for more than a decade (e.g., 1229, and references therein).

However, the answer to the question actually posed by Albert at APN IV — "What is the percentage of stars for which the mass loss rate (as opposed to the morphology) is affected by a binary companion?" — remains elusive. New "elapsed time" *Hubble Space Telescope* imagery of complex bipolar pre-PNe like AFGL 2688 and AFGL 618 (**Balick**) dramatically reveals the large proper motions of shrapnel flying outward in Hubble-like flows through slower-moving, quasi-spherical ejecta shells (i.e., the "AGB rings" mentioned above). Certain helpless observers have been wondering for years whether such rapid structural upheaval in a pre-PN or PN might be taken as evidence that we are witnessing the onset of a common envelope phase in the evolution of a binary system (1220). The investment of renewed effort in detailed modeling of common envelope processes — like that which **Fitzpatrick et al.** presented at APN V — would certainly be welcome.

3.4.1. Digression: the Strange, Isolated Field Star BP Psc

This summarizer is always intrigued by objects whose classification as pre-MS vs. post-MS is (at least temporarily) problematic. It seems such objects (e.g., OH231.8+4.2; see discussion in 1223) can help shed light on the APN phenomenon. A case in point is the enigmatic object BP Psc (1232). At first glance, this emission-line field star appears to belong to the rare class of "isolated" classical T Tauri stars (cTTS), i.e., late-type, actively accreting pre-MS stars located degrees away from any known star-forming molecular clouds. Like isolated cTTS (1218, and references therein), BP Psc displays double-peaked CO emission lines in the radio, indicating the star is orbited by a Keplerian molecular disk that is the potential site of giant planet formation. Even more remarkable, the BP Psc star/disk system drives a pair of pc-scale jets of the sort usually associated with very young (age < 1 Myr), deeply embedded young stellar objects (YSOs; Fig. 2). Such a jet system had never before been detected in the case of an isolated cTTS (whose ages are ~ 10 Myr).

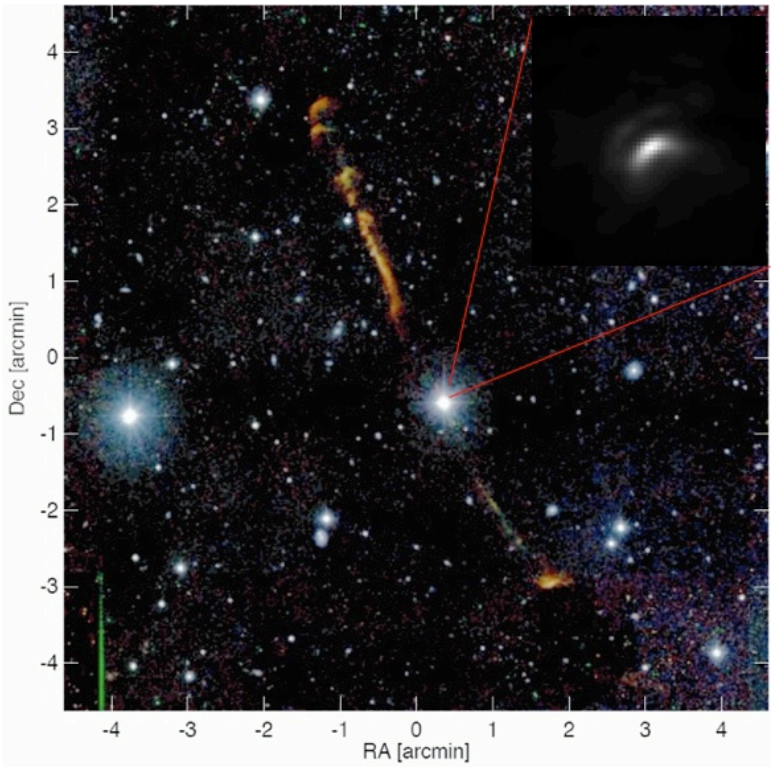

Figure 2. Composite wide-field image of BP Psc, showing its pc-scale jet system. A deconvolved near-IR Keck Telescope adaptive optics image covering a one square arcsec field at the central star is displayed in the inset; the Keck image demonstrates that BP Psc is occulted by a dusty circumstellar disk viewed nearly edge-on. Imaging and spectroscopy of circumstellar CO emission indicates the disk is in Keplerian rotation. Adapted from Zuckerman et al. (1232).

Indeed, the presence of jets actually made us suspicious as to the nature of BP Psc. Looking more closely, it turns out that many characteristics of the star are inconsistent with youth. Unlike isolated cTTS, BP Psc is not associated with any known young stellar association; its weak 6708 Å Li line is suggestive of an age $\gtrsim$ 100 Myr; its photospheric lines are similar to those of evolved G giants; its molecular disk chemistry is anomalous; and, last but not least, its X-ray luminosity is two orders of magnitude smaller than typical of pre-MS stars. These characteristics, combined with evidence for rapid stellar rotation, led us to conclude that BP Psc is most likely a first-ascent giant that has recently engulfed a companion or (perhaps) a giant planet (for the gory details, see 1232; 1219, and references therein).

There are many things that the APN community might take away from the curious case of BP Psc (some of which we already knew). For example:

• Companion engulfment (i.e., the onset of common envelope) has many potentially observable consequences, among other things mass accretion, disk and jet formation, and spin-up of the cannibalistic primary star.

• Some (close) binaries likely interact catastrophically well before the evolving primary arrives on the AGB (a fact that has many interesting implications; see, e.g., 1227).

• Post-MS binary interactions might eventually lead to the formation of "second-generation" planets in the dusty disks generated by such interactions (e.g., 1216; 1222).
• Perhaps most intriguingly, in a highly axisymmetric or asymmetric PN whose central star *appears* to be single, the progenitor may have had a "past life" as a close binary whose catastrophic interactions left behind a disk that eventually influenced the PN's morphology.

4. Looking Ahead

As we look ahead to APN VI, I can identify three Serious Challenges and one Grand Challenge facing the APN community.

4.1. Serious Challenges

4.1.1. Disks and the Disk-jet Connection

Given the rapid rate of discovery of disks around post-AGB stars and within (bipolar) pre-PNe and PNe, one might fairly ask: where are the jets? Here, BP Psc and a few analogs (e.g., Hen 2-90; 1225), as well as YSO disk/jet systems, appear particularly relevant. In BP Psc (as in YSOs and even active galactic nuclei), accretion evidently drives the jet activity. Hence, it would seem prudent to give a closer look to the central stars of PNe in which we suspect jets are actively shaping the nebulae, so as to identify potential stellar accretion signatures. The innermost regions of PNe can present far more complex environments than the inner disk regions of YSOs, however, such that standard young star accretion diagnostics (e.g., circumstellar UV excess, Hα equivalent width, and near-IR excess) will be exceedingly difficult to measure. Therefore we must also continue to work harder to understand (from both theoretical and observational points of view) the detailed structure of circumstellar and circumbinary disks in post-AGB systems and within pre-PNe and PNe, so as to understand whether such structures may in fact constitute long-lived (orbiting) sources of accreting material.

Where jets themselves are concerned, we have much to learn from the YSO community; there are almost as many proposed YSO jet launching and collimation mechanisms as there are YSO jets (i.e., X-wind, disk wind, stellar wind, etc.; see, e.g., reviews in 1228). Then again — given these ongoing, contentious debates in the YSO jet world — we also should have much to teach the YSO community, via insights gained from the identification and study of jets within APNe.

4.1.2. Marrying Big Databases and Big Number Crunching

APN V showcased the recent explosion of high-quality observational databases, both focused/special-purpose (e.g., MASH, SuperWASP, SAGE, GLIMPSE) and generic/multi-mission (e.g., MAST, HEASARC). A parallel explosion of high-fidelity numerical simulation codes and "power tools" — with an equally bewildering array of acronyms (SPH, **Mohamed & Podsiadlowski**; Gadget2 SPH, **Fitzpatrick**; 2.5-MHD & AMR, **Huarte-Espinosa et al.**; SHAPE, **Steffen**) — was also on display. It is therefore quite apparent that the latter should be put to wider use, so as to make predictions that the former can put to the test. As we develop and apply such "brute force" methods to gain

insight into our favorite class(es) of object, we should also be looking toward the Grand Challenge described in §4.2.

4.1.3. What Is the Role of Magnetic Fields?

As previously noted (§3.2), both the uniquity and global strengths of magnetic fields remain poorly established — or simply undetermined — for the vast majority of PNe and their AGB/post-AGB star progenitors. Hence, the role, if any, of magnetic fields in shaping PNe remains quite uncertain. Clearly, this is an area in which both observers and theorists need to focus more attention. And, here again, the star formation community is way ahead of us. Perusing the abstracts from the recent (May 2010) meeting *Magnetic Fields from Core Collapse to Young Stellar Objects*[‡], and reading between the lines, it quickly becomes apparent that cloud core magnetic fields are becoming so well characterized, theoretically and observationally, that those star formation theorists who attempt to include all the relevant magnetic field physics are having severe problems generating stars with circumstellar, proto-planetary disks — thereby denying our very existence. We APN researchers can only hope to be as successful.

4.2. A Grand Challenge

For some time now, Adam Frank has been exhorting the PN community to identify — and then set out to tackle — its next Grand Challenge. I have a suggestion. This suggestion is motivated by the APN community's remarkable progress in honing in on binarity as the primary mechanism ultimately responsible for PN shaping, on the one hand, and by Iben & Tutukov's remarkably thorough treatment of the problem of Supernova (SN) Type I progenitors (1215), on the other. The Iben & Tutukov paper features an ingenious and instructive set of "decision trees" describing the evolutionary paths followed by binary stars for a range of initial masses, mass ratios, and separations (see, e.g., their Figs. 1-4, 6).

Given the tremendous progress in "astroinformatics" and "astronumerics" over the past $\sim$ 25 yrs (§4.1.2), it seems we are now on the verge of being able to construct a far more comprehensive and detailed set of binary star "decision trees." Such trees might resemble the original Iben & Tutukov concept but, at each decision point, their input and output would now be based on high-fidelity, detailed numerical simulations; and the predictions of such simulations should be testable (falsifiable) via present and future generations of large, easily manipulated, self-documenting observational databases. In such a conception, the input to each decision point is a binary system (wherein the secondary could just as well be a massive planet as a low-mass star; **Nordhaus**); the output is a "new" (modified) binary, or perhaps a single (spun-up) star; and the "decision points" are our beloved APN themselves (or, in some cases, their "mimics" [**Parker; Frew**]). The resulting, overarching decision tree might eventually constitute a sort of Binary Star Genome, and APNe and their close cousins (symbiotic star nebulae [**Sokoloski**], novae ejecta [**Evans; Ribeiro**], SN Ia remnants; etc.) would then play the role of phenomes, i.e., the specific, short-lived expressions of binary star evolution.

[‡]http://cc2yso.uwo.ca/abstracts.shtml

False analogy? Perhaps. But recall the words of Harm Habing: a good review is one "that broadens the perspective of at least some people in the audience." If anyone's perspective has been broadened by my remarks, however stupid, then I have done my job — apart from one final, unquestionable assertion (quoting 1217): "There will clearly have to be another conference on this subject."

Acknowledgments. I wish to thank my fellow Rochester (June 2009) "inter-APN workshop" organizers (and Rochester White Paper coauthors) Bruce Balick, Eric Blackman, Orsola De Marco, Adam Frank, and Raghvendra Sahai, as well as Noam Soker, for inspiration and many insights; Albert Zijlstra and his crack team of APN V organizers for their hard work and excellent results; and Rudy Montez for jogging my memory concerning the wonderful "decision trees" of Iben & Tutukov (1215). Support for PN research at Rochester Institute of Technology is provided by *Chandra* X-ray Observatory Center (CXC) awards GO9–0030X and G09–0022X (the CXC is operated by the Smithsonian Astrophysical Observatory for and on behalf of NASA under contract NAS8-03060) and by NASA Astrophysics Data Analysis Program grant NNX08AJ65G.

References

Bujarrabal, V., Castro-Carrizo, A., Alcolea, J., & Neri, R. 2005, Astronomy and Astrophysics, 441, 1031

Habing, H. 2004, in Asymmetrical Planetary Nebulae III: Winds, Structure and the Thunderbird, edited by M. Meixner, J. H. Kastner, B. Balick, & N. Soker, vol. 313 of Astronomical Society of the Pacific Conference Series, 575

Iben, I., Jr., & Tutukov, A. V. 1984, Astrophysical Journal, Supplement, 54, 335

Jura, M., & Kahane, C. 1999, Astrophysical Journal, 521, 302

Kahn, F. D. 1995, in Asymmetrical Planetary Nebulae, edited by A. Harpaz & N. Soker, vol. 11 of Annals of the Israel Physical Society, 282

Kastner, J. H., Hily-Blant, P., Sacco, G. G., Forveille, T., & Zuckerman, B. 2010, ArXiv e-prints. 1010.1174

Kastner, J. H., Montez, R., Rodriguez, D., Grosso, N., Zuckerman, B., Perrin, M. D., Forveille, T., & Graham, J. R. 2010, Astrophysical Journal, Letters, 719, L65

Kastner, J. H., Weintraub, D. A., Gatley, I., & Henn, L. 2001, Astrophysical Journal, 546, 279

Mastrodemos, N., & Morris, M. 1999, Astrophysical Journal, 523, 357

Melis, C., Zuckerman, B., Rhee, J. H., & Song, I. 2010, Astrophysical Journal, Letters, 717, L57

Morris, M., & Bowers, P. F. 1980, Astronomical Journal, 85, 724

Rodriguez, D. R., Kastner, J. H., Wilner, D., & Qi, C. 2010, Astrophysical Journal, 720, 1684

Sahai, R., & Nyman, L. 2000, Astrophysical Journal, Letters, 538, L145

Schwarz, H. E. 2000, in Asymmetrical Planetary Nebulae II: From Origins to Microstructures, edited by J. H. Kastner, N. Soker, & S. Rappaport, vol. 199 of Astronomical Society of the Pacific Conference Series, 457

Soker, N. 1998, Astrophysical Journal, 496, 833

Tsinganos, K., Ray, T., & Stute, M. 2009, Protostellar Jets in Context

Van Horn, H. M., Thomas, J. H., Frank, A., & Blackman, E. G. 2003, Astrophysical Journal, 585, 983

Van Winckel, H., Waelkens, C., & Waters, L. B. F. M. 1995, Astronomy and Astrophysics, 293, L25

Zijlstra, A. A. 2007, in Asymmetrical Planetary Nebulae IV

Zuckerman, B., Melis, C., Song, I., Meier, D. S., Perrin, M. D., Macintosh, B., Marois, C., Weinberger, A. J., Rhee, J. H., Graham, J. R., Kastner, J. H., Palmer, P., Forveille, T.,

Becklin, E. E., Wilner, D. J., Barman, T. S., Marcy, G. W., & Bessell, M. S. 2008, Astrophysical Journal, 683, 1085